THE UNIVERSITY OF HULL

SYNTHESIS AND BIOLOGICAL EVALUATION OF CXCR4 CHEMOKINE RECEPTOR ANTAGONISTS

being a Thesis submitted for the Degree of
Doctor of Philosophy in the University of Hull

by

Kate Louise Nicholson, MChem (Hons)

December 2014

I. ABSTRACT

The CXCR4 chemokine receptor is known to be overexpressed in many types of cancer as well as being involved in several stages of metastasis, which is responsible for the majority of deaths in cancer patients. Molecular imaging techniques, such as positron emission tomography (PET), are being used in the design of early stage CXCR4 expressing cancer diagnosis agents which can be followed by the administration of CXCR4 specific drugs targeting to an individual's specific cancer treatment requirements to prevent the spread of cancer. Incorporation of positron emitting radioisotopes such as ^{18}F and ^{64}Cu into a CXCR4 specific compound allows visualisation of the locations that the drug has accumulated. This can facilitate the diagnosis of a CXCR4 expressing cancer as large volumes of emission signals will be detected in tumours. Following diagnosis, high CXCR4-affinity targeted compounds can be administrated which prevent CXCR4's binding partner, CXCL12, activating the receptor and enabling metastasis. This work focuses on the development of high affinity CXCR4 antagonists which can be used in therapeutic and diagnostic applications.

A series of configurationally restricted complexes of copper(II), zinc(II) and nickel(II), where the metal ion is coordinated to tris-macrocycles, were synthesised. Tris-macrocycles have the potential to show improved affinity for the CXCR4 receptor because the third macrocyclic ring can facilitate more interactions with the CXCR4 receptor than reported bis-macrocycles, due to the extra interactions possible with the aspartate rich receptor surface. Biological studies revealed the tris-macrocyclic series has high affinity for CXCR4. $[Zn_3\mathbf{18}]^{6+}$ showed nanomolar activity with an IC_{50} value of 1 nM, 14 times more potent than the FDA approved drug AMD3100. Another high affinity tris-macrocycle, $[Zn_3\mathbf{19}]^{6+}$ showed an IC_{50} value of 2 nM also significantly lower than ADM3100. The high affinity compounds, $[Zn_3\mathbf{18}]^{6+}$ and $[Zn_3\mathbf{19}]^{6+}$, were radiolabelled with ^{64}Cu via transmetalation. Crude-radiochemical yields (crude-RCY) of 79% and 62% were achieved for $^{64}CuZn_2[\mathbf{18}]$ and $^{64}CuZn_2[\mathbf{19}]$ respectively. The complexes were identified as strongly hydrophilic with calculated LogP values of -3.69 and -2.20 for $^{64}CuZn_2[\mathbf{18}]$ and $^{64}CuZn_2[\mathbf{19}]$ respectively.

A series of rigidified bis-macrocycle copper(II) and zinc(II) complexes were synthesised and explored as imaging agents. Routes to incorporate ^{18}F and ^{68}Ga into the bis-macrocycles for applications in PET imaging were explored. Mono-macrocycles were synthesised and used in a series of test reactions to evaluate a range of pendant arm functionalisations including nitro, amine, azide and alkyne. Subsequently, azide functionalised rigidified bis-macrocycle copper(II) and zinc(II) complexes for use in copper-free click reactions were synthesised which provided an effective route to incorporate ^{18}F into macrocycles. Biological studies identified that the functionalised bis-macrocycle complexes

showed high affinity towards the CXCR4 receptor. The key compound was $[Zn_2\mathbf{32}]^{4+}$ which showed IC_{50} values of 3 nM, more than 3 times lower than AMD3100.

A series of surface plasmon resonance (SPR) experiments were conducted to develop a method to determine the residence time of macrocycles on the CXCR4 receptor. A range of approaches, such as intact cell immobilisation, intact cell capture and receptor capture, were studied but all methods had drawbacks therefore association and dissociation rates of macrocycles and the CXCR4 receptor were not ascertained.

This work highlights important steps towards the diagnosis of CXCR4 expressing cancers with the use of highly stable tris-macroycles. Furthermore, initial steps to incorporate the most readily available radioisotope, ^{18}F, into macrocycles have been identified. Progress towards the development of high affinity, anti-metastatic therapeutic agents, in CXCR4 expressing cancers, has been made with the synthesis and *in vitro* evaluation of configurationally restricted tris-macrocycle metal complexes. Key compounds in this series were $[Zn_3\mathbf{18}]^{6+}$ and $[Zn_3\mathbf{19}]^{6+}$ which showed significantly better affinity for the CXCR4 receptor than AMD3100 and low toxicity.

II. RISK ASSESSMENT

All experiments were carried out in accordance with the University of Hull's Health and Safety guidelines. A full COSHH and risk assessment was carried out for each new experiment, signed by the undertaking student, supervisor (Dr S. J. Archibald) and the departmental safety officer (Dr T. McCreedy) before any practical work started. Copies of each form were provided for reference to the departmental safety officer and supervisor. The COSHH forms carry the reference numbers KLN1-KLN36 and KN01-06.

III. ACKNOWLEDGEMENTS

Firstly, I would like to thank my sponsor Dr Assem Allam for providing me with the Allam Scholarship without which this opportunity would not have been possible. I am sincerely grateful for his kind generosity which has enabled me to conduct my research and attend important conferences. I would also like to thank my supervisors Dr Steve J. Archibald and Prof John Greenman. I would like to especially thank my primary supervisor Steve who guided me through my first year, subsequently enabling me to take ownership of the project and take it down research avenues that were of personal interest. I would like to thank you for making possible many opportunities to diversify my skills. I would like to thank my second supervisor for guidance in Biology and involving me in PR related tasks! These situations have exposed me to new territories and expanded my horizons.

I would like to thank Dr Benjamin Burke, Dr Juozas Domarkas and Dr Francesca Giuntini who have helped me during my project, but special thanks go to Dr Rachel Smith, Dr Francesca Bryden and Louis Allott who have helped me solve problems and given me inspiration and ideas for my project. Lauren Turner, you have always been there to offer kind words of advice so I thank you also. Rachel, Fran, Louis and Lauren - you four have helped me push past the low times and have always been there to celebrate the good times. I have loved having the pleasure of working with you and you have made these last three years the best they could have been.

I wish to thank Bob Knight and Rob Lewis for sorting NMR problems out so quickly and Carol Kennedy for performing all my CHN analysis. I wish to thank the people involved in conducting MS analysis on my samples: EPSRC National Mass Spectrometry Service Centre, Dr Kevin Welham (Hull) and Karl Heaton (York). I would like to thank Dr Leigh Madden for helping me with all my mundane questions in Biology and also Dr Tim Fagge (GE Healthcare) for his training and support with SPR. I would like to acknowledge Prof. Erik De Clercq's and Prof. Dominique Schol's group in Belgium for performing biological assays on my compounds.

Finally, I would like to thank all my other friends, family and fiancé for their encouragement, advice and endless cups of elixir-like tea during my PhD. My fiancé, Rich, you have always been great at cheering me up, taking my mind off stressful situations and supporting me during my write up. I cannot wait to start our lives together once this is all done and dusted – I applaud you for your patience! To my mum and dad, you have always been there for me with open arms at a drop of a hat and given me incredible boosts when I have been at rock bottom. You have always taught me to work hard and I love you so much for all your wise words and the happiness you have brought me. I'd like to thank my brother Simon for making me chuckle and being my personal Maurice Moss on standby ready to deal with all my IT complaints!

IV. ABBREVIATIONS

µg	Microgram
µL	Microlitre
AKT	Activate serine-threonine kinase
Asp	Aspartate
ATCC	American type culture collection
ATR	Attenuated total reflections
BAD	Bcl-2-associated death promoter
BFC	Bifunctional chelator
BOC	Tert-butyloxycarbonyl
BODIPY	Boron dipyrromethenes
BP	Boiling point
br	Broad signal
BSA	Bovine serum albumin
CB	Cross bridge
CC_{50}	Cytotoxic concentration required to reduce a population by 50%
CCD	Charge-coupled device
Chaps	3-[(3-Cholamidopropyl)dimethylammonio]-1-propanesulfonate
Chapso	3-([3-Cholamidopropyl]dimethylammonio)-2-hydroxy-1-propanesulfonate
CHS	Cholesteryl hemisuccinate tris salt
CM	Carboxymethylated
CT	Computed tomography
d	Doublet
dd	Double doublet
d	Day
DAG	Diacyl glycerol
DCM	Dichloromethane
Dep	Diethyl chlorophosphate
DMF	N,N'-Dimethylformamide
DOM	n-dodecyl-β-D-maltopyranoside
DOPC	1,2-dioleoyl-sn-glycero-3-phosphocholine
DOPS	1,2-dioleoyl-sn-glycero-3-phospho-L-serine (sodium salt)
DOTAGA	1-(1-carboxy-3-carboxy-propyl)-4,7, 10(carboxymethyl)-1,4,7,10-tetraazacyclo-dodecane
dt	Double triplet
EC_{50}	Effective concentration required to reduce an effect by 50%
ECCAC	European collection of cell cultures
EDC	1-ethyl-3-(3-dimethylaminopropyl) carbodiimide hydrochloride
EGF	Epidermal growth factor
EGFR	Epidermal growth factor receptor
ER	Endoplasmic reticulum
ESI	Electrospray ionisation
ET	Emission tomography
EWG	Electron withdrawing group
FACS	Fluorescence activated cell sorting
FBS	Foetal bovine serum

FC	Flow cell
FFA	Free fatty acids
FITC	Fluorescein isothiocyanate
FLIPR	Fluorometric imaging plate reader
g	Gram
G-CSF	Granulocyte-colony stimulation factor
GDP	Guanosine diphosphate
Glu	Glutamate
GPCR	G-Protein Coupled Receptor
GTP	Guanosine triphosphate
h	Hour
HBS-P	Hepes-buffered saline with P20
HEPES	4-(2-Hydroxyethyl)-1-piperazineethanesulfonic acid
HIV	Human immunodeficiency virus
HRMS	High resolution mass spectrometry
IC_{50}	Concentration required to inhibit binding by 50%
J	Coupling constant
K_{222}	Kryptofix 222
K_a	Rate of association
K_d	Rate of dissociation
K_D	Langmuir isotherm
LogP	Partition coefficient
m	Multiplet
M	Molar
mAb	Monoclonal antibody
MAPK	Mitogen activated protein kinases
mg	Miligram
MHz	Megahertz
min	Minute
mL	Mililitre
mM	Milimolar
mmol	Milimole
m^o	Millidegrees
MRI	Magnetic resonance imaging
MS	Mass Spectrometry
MTT	3-(4,5-dimethylthiazol-2-yl)-2,5-diphenyltetrazolium bromide
NHS	N-hydroxy succinimide
NIAID	National institute of allergy and infectious diseases
nM	Nanomolar
NMR	Nuclear magnetic resonance
pAb	Polyclonal antibody
PBMC	Peripheral blood mononucleated cell
PBS	Phosphate buffer solution
PE	Phycoerythrin
PEG	Polyethyleneglycol

PET	Positron emission tomography
PHD3	Prolyl hydroxylase 3
PLC	Phospholipase C
PMT	Photomultiplier tubes
POPC	1-Hexadecanoyl-2--(9Z-octadecenoyl)-sn-glycero-3-phosphocholine
ppm	Parts per million
q	Quartet
QSAR	Quantitative structural activity relationship
quin	Quintet
Ras	Rat sarcoma
RBITC	Rhodamine B isothiocyanate
RCY	Radiochemical yield
R_f	Retention factor
RPMI	Roswell park memorial institute
RT	Room temperature
s	Second
s	Singlet
SB	Side bridge
SCID	Severe combined immunodeficent
SIV	Simian immunodeficiency virus
SM	Starting material
S_NAr	Nucleophilic aromatic substitution
SPAAC	Strain-promoted azide alkyne cycloaddition
SPECT	Single photon emission computed tomography
SPR	Surface plasmon resonance
t	Triplet
TBAF	Tetra-n-butyl ammonium fluoride
TCO	Trans cyclooctene
td	Triple doublet
TEA	Triethylamine
THF	Tetrahydrofuran
TLC	Thin layer chromatography
TM	Transmembrane
TMC	Tetramethyl cyclam
TPP-N_3	Azido-tetraphenyl porphyrin
UK	United Kingdom
USA	United States of America
UV	Ultra-Violet
UV-vis	Ultra-Violet-visible
v/v	Volume/volume
v/w	Volume/weight
w/v	Weight/volume
w/w	Weight/weight
β-	Electron
β+	Positron

δ	Chemical Shift
ε	Molar Absorptivity
λ_{em}	Emission wavelength
λ_{ex}	Excitation wavelength
λ_{max}	Maximum wavelength
µM	Micromolar
µmol	Micromole

V. LIST OF FIGURES

VI. LIST OF SCHEMES

VII. LIST OF TABLES

VI. CONTENTS PAGE

CHAPTER ONE

INTRODUCTION

1.1 CHEMOKINES AND CANCER

1.1.1. CXCR4 Chemokine Receptor

1.1.1.1 Chemokines

The word chemokine comes from a combination of the words chemoattractant cytokine.[1] The main role of chemokines is to act as a chemoattractant and guide the movement of cells to regulate cell trafficking. The mediation of cell movement is called chemotaxis.[2] Chemokines are a group of small proteins which have mass of 8-14 kDa.[3] The majority of chemokines are basic and they are all structurally related.[4] Chemokines induce many different effects in a range of cell types in the immune system and central nervous system as well as endothelial cells. Chemokines bind to a widely variant family of seven-transmembrane receptors.[5] A number of chemokines can bind to multiple receptors whilst some receptors can bind to more than one chemokine and this enables many biological effects.[2, 6] Chemokines are located on numerous different chromosomes with larger clusters located on chromosomes 3, 4 and 17.[3] The large clusters of chemokine genes indicate that their function is related to a certain degree, rationalising why many receptors are shared.[4]

There are four families of chemokines: CXC, CC, C and CX_3C which are classified depending on the position of the highly conserved cysteine residues on the N terminus.[7] The X represents the number of residues that separate the cysteine residues, hence, CXC has a single residue between them.[3] Since the late 1980s the knowledge of different chemokines has grown vastly. The first chemokines discovered fell into the CXC and CC chemokine categories. The groups are based on the characteristic feature of the four conserved cysteine residues in chemokines bridged by two disulfide bridges between the first and third cysteine residue and the second and fourth residue. The position of the first two cysteine residues determines the chemokine class which are summarised in Figure 1.

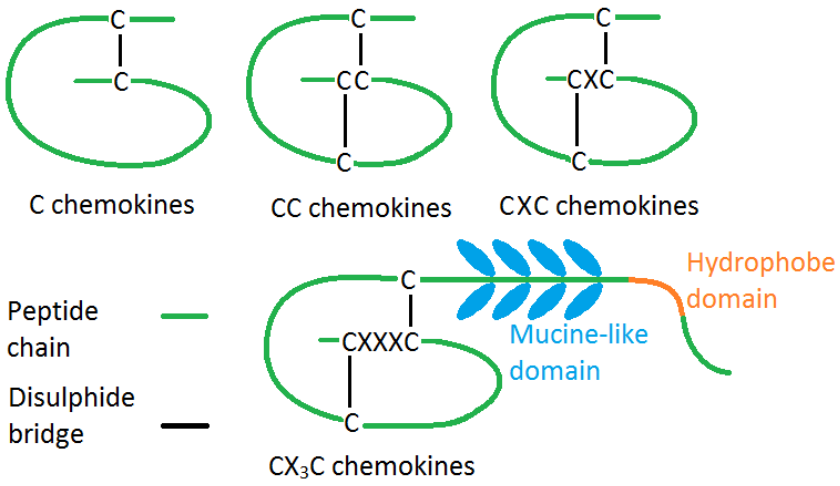

Figure 1 - Classes of chemokines (Adapted from Kohidai)[8]

The C family of chemokines contain only two cysteine residues. C and CX_3C have fewer receptors and ligands.[9] CC chemokine receptors are less specific than CXC receptors as they are able to bind to more chemokine ligands. CC and CXC are the most abundant groups of chemokines.[6] A diagram of the chemokine family showing which receptors they bind to can be seen in Figure 2. There have been more than 40 chemokines and 18 chemokine receptors identified in the human system.[7] Normally, cytokines initiate the high expression of chemokines, though this is not the case for the chemokine CXCL12 which is produced at a constant rate.[7, 9a]

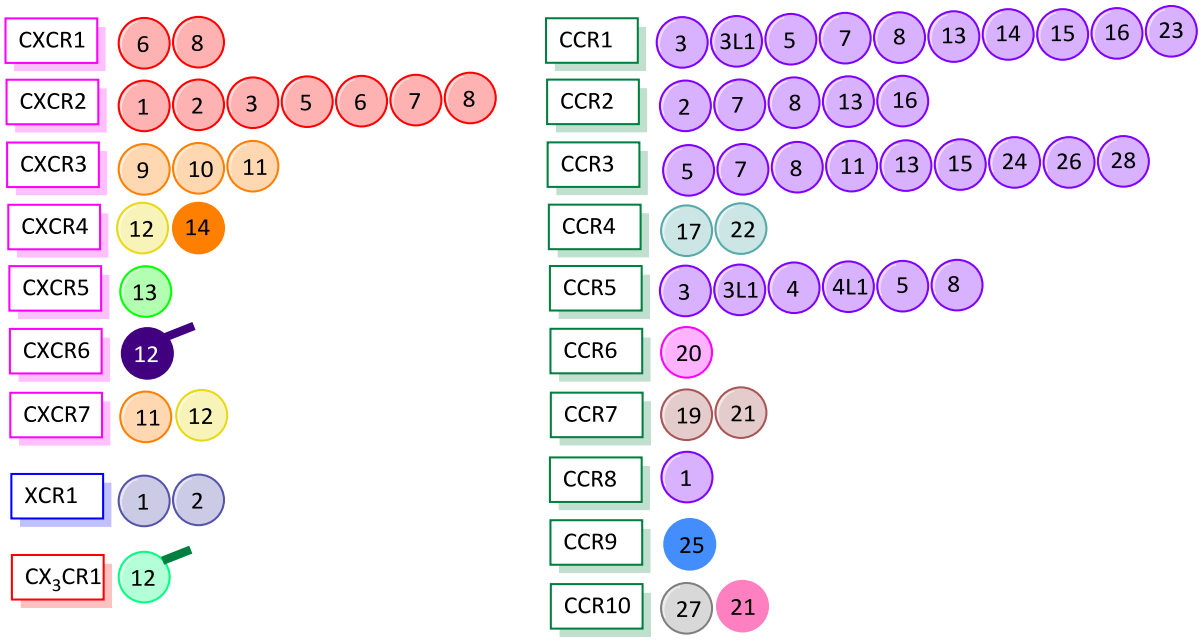

Figure 2 - Superfamily of chemokines and the receptors they bind to (Adapted from Zlotnik *et al.*)[7]
The numbers in circles correspond to chemokines, for example CXCL12 is shown as 12 and is next to CXCR4. The chemokine colours relate to the position of the chemokines on chromosomes, most chemokines from the same location generally bind to the same receptor. The extra lines refer to chemokines that exist as transmembrane proteins.

Chemokines can be divided further into two main classifications: inflammatory and homeostatic, these groups are classified dependant on chemokine function and expression.[10] However, some chemokines show characteristics from both these groups so a third group called dual-function chemokines also exists. Chemokines in the inflammatory group are not constitutively expressed. Their expression relies on an inflammatory stimuli and up-regulation by the local proinflammatory cytokine. Inflammatory chemokines can bind to more than one receptor and their receptors can bind to multiple chemokines. Chemokines in the homeostatic group are involved in the maintenance of the haemopoietic and immune systems. They are constitutively expressed in various cells and tissues. Both homeostatic and dual-function chemokines bind to a single receptor.

1.1.1.2 G-protein coupled receptors (GPCRs)

G-protein coupled receptors (GPCRs) are cell surface receptors which induce a wide range of cellular responses upon activation.[11] GPCRs consist of seven-transmembrane (TM) α-helices with three extracellular loops, three intracellular loops and a C terminus in the cytoplasm; the entire N terminus is outside the cell wall.[12] Each TM is made up of between 20-27 residues although the N-terminus can range from 7-595 residues and the C-terminus between 12-359 residues. GPCRs take on different conformations existing in an equilibrium to one another when the ligand is not bound.[13] In healthy tissue GPCRs regulate almost all physiological processes such as cellular responses to signals from hormones and neurotransmitters.[13-14] GPCRs are also involved in around half of all therapeutic interventions.[14]

GPCR signalling is complicated and a wide range of mechanisms are involved. When the receptor is activated by its ligand it binds to a three-component G-protein complex which sits on the inner surface of the cell membrane. This heterotrimeric G-protein is made up of three subunits: Gα, Gβ and Gγ.[2] The receptor interacts with Gβ and Gγ first, before binding to Gα forming the G-protein. There are four types of Gα: $G\alpha_i$, $G\alpha_q$, $G\alpha_s$ and $G\alpha_{12}$. Each Gα group transmits the GPCR signal through various routes, for instance, $G\alpha_i$, inhibits adenyl cyclase as opposed to $G\alpha_s$ which stimulates it. Once bound to the G-protein exchange of guanosine diphosphate, GDP, for guanosine triphosphate, GTP, changes the G-protein to its active state.[11] Gα-GTP then dissociates from Gβγ which in turn dissociates from the receptor. These subunits are then able to interact with effector enzymes to inhibit or stimulate second messengers and these cause downstream effects such as opening the Ca^{2+} channels or generating other messengers.

Chemokine receptors are rhodopsin-like and members of the class A group of GPCRs.[5] Chemokine receptors contain a generic binding pocket but the receptor specificity is defined by the residues that line the seven helices. Generally, chemokine receptors are $G\alpha_i$ coupled receptors.[2]

1.1.1.3 CXCR4 chemokine receptor

CXCR4 belongs to the CXC group of chemokines and chemokine receptors. It contains 352 amino acid residues and is a GPCR. The CXCR4 gene is located on chromosome 2,[4] and has an overall surface charge of -9, its structure is shown in Figure 3. CXCR4 selectively binds to its basic ligand CXCL12,[15] however, a recently identified natural antagonist for CXCR4 is the chemokine CXCL14.[16] Almost 30% of the CXCR4 amino acids are aspartate, histidine and tyrosine.[15a] There are a number of aspartate residues which face the binding pocket of the receptor. The arrangement of three aspartate residues on transmembrane, TM, –IV, -V and –VI is unique to CXCR4, nonetheless, two of these, Asp^{171} and Asp^{262} are also present in the receptor CXCR3, yet, it is structurally very different.[17]

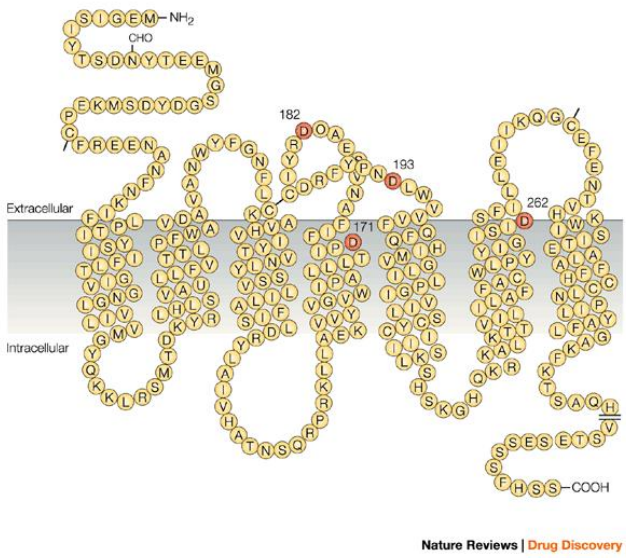

Figure 3 - Structure of the CXCR4 receptor[18]

CXCR4 is commonly expressed on haematopoietic and non-haematopoietic cells[19] in numerous tissues such as the brain, endothelial cells[20] and on a wide range of leukocytes.[21] When bound to its ligand it coordinates the movement of T-lymphocytes around the body. Additionally, CXCR4 is important in immunomodulation and early development.[19] The CXCL12/CXCR4 pathway is involved in organogenesis during normal development and is similar to the process of metastasis.[22] CXCR4 is vital for many processes within the human body, one of which is the vascularisation of the gastrointestinal tract.[20] The expression of CXCR4 is controlled by a number of cytokines.[15a]

1.1.1.4 CXCL12

CXCL12, also known as stromal cell-derived factor-1 or SDF-1, is a CXC chemokine which is able to bind to CXCR4 and CXCR7.[2, 15a] CXCL12 plays a very important role in foetal development which is vividly apparent when the CXCL12 or CXCR4 gene is knocked out.[23] Zou *et al.* reported that CXCR4-knockout mice exhibited haematopoietic and cardiac defects,[24] matching those seen in CXCL12 deficient mice by Nagasawa *et al.*[25] Zou *et al.*'s study used chimaeric mice from three separate embryonic stem cell lines to transmit the mutated CXCR4 gene into the germ line and compared CXCR4-deficient embryos to wild type embryos.[24] This demonstrated that for the first 13.5 d CXCR4 deficient embryos developed normally however after 17.5 d half the CXCR4-deficient embryos had died. What's more, the CXCR4 deficient embryos, alive at 17.5 d, were 26% smaller than their wild-type littermates. CXCL12 is continually present and active and expressed on the majority of tissues. Expression of low levels of CXCL12 is normal for primary endothelial cells.[26] It is expressed in numerous organs such as bone marrow, brain, heart, kidney, lung, liver and skin.[2, 15a] The main role of CXCL12 is to mediate the movement of hematopoietic cells and control the structure of secondary lymphoid tissue.[2] The CXCL12 gene is positioned on chromosome 10 whilst many other CXC

chemokine genes are located on chromosome 4, although the gene for CXCL14 is located on chromosome 5.[4] CXCL12 is a polypeptide consisting of 67 residues and its structure is made up of three anti-parallel β strands with an overlaying α-helix. Just over 20% of CXCL12s residues are arginine, lysine and histidine. The α-helix is generally negatively charged, though the first two β strands are overall positively charged.[15a, 27]

CXCL12 consists of two isoforms: α and β. The difference being four extra residues at the COOH terminus on the β form;[15a] otherwise the isoforms are identical. CXCL12α contains 89 residues whilst the β isoform contains 93. CXCR4 controls the biological effects that CXCL12 has. The first eight residues of the NH_2-terminal have been recognized as being crucial for binding to and activation of CXCR4. Loss of CXCR4 activation was discovered by altering the first two CXCL12 residues. When the entire eight residues were changed CXCL12 was unable to bind to CXCR4 which highlights the importance of these eight residues. Nonetheless, the flexible NH_2-terminus alone is inadequate to facilitate CXCR4 binding and activation; residues 12-17 were depicted as vital for this to occur. As mentioned earlier the binding pocket of the receptor carries a negative charge, as a result of this, four basic residues provide the complementary charge to interact with the region.[26] The positive charges and high basicity of CXCL12 are important properties to consider when designing CXCR4 antagonists.

1.1.1.5 CXCL12/CXCR4 and cancer

Chemokines, along with their receptors, are involved in many important cellular processes, the role of the CXCR4/CXCL12 pathway in adults is to guide and retain hematopoietic stems cells in the bone marrow as well as guide the movement of lymphocytes,[2] however they also partake in the development of pathological diseases such as cancer and the immunodeficiency virus HIV-1 which makes them targets for drug development.[9c] In cancer, a vital step in tumour cell dissemination is chemotaxis. It is through up-regulation of chemokines and receptors which assists the development of cancer.[28] Whilst tumour cells can move without chemoattractants their presence makes the process of migration more effective. This makes targeting chemokines involved with early stage cancer progression an important area. Conversely, it has been argued that targeting biomarkers involved in early cancer progression is futile because prior to a patient presenting with symptoms dissemination from the primary tumour could have already occurred. Nonetheless, these targets are still crucial as even missed circulating metastasising cells are capable of forming a secondary tumour and it is vital that the invading potential of the remaining cells is prevented. It has been shown that inhibiting the CXCR4 receptor significantly hinders the HIV-1 infection as well as metastasis validating the research strategy of targeting CXCR4.[29]

The CXCR4 receptor has been suggested to be involved in the development of more than 23 types of cancer.[30] It has been found to encourage metastasis, angiogenesis, and the growth and survival of tumours.[31] A CXCR4 antagonist prevents cell migration and could be key to preventing the growth and spread of tumours.[15a] The expression of CXCL14 is seen to be supressed in cancer.[16]

Cancer	Chemokine receptors expressed
Breast	CXCR4, CCR7[32]
Ovarian	CXCR4[33]
Prostate	CXCR4[34]
Pancreas	CXCR4[35]
Melanoma	CXCR4[36]
Oesophageal	CXCR4, CCR10, CCR7, CCR9[37]
Lung (NSCLC)	CXCR4[38]
Head and neck	CXCR4, CCR7[36a, 39]
Bladder	CXCR4, CCR7, CXCR5[40]
Colorectal	CXCR4[41]
Osteosarcoma	CXCR4, CCR7[42]
Neuroblastoma	CXCR4[43]
Acute lymphoblastic leukaemia	CXCR4, CXCR3[44]
Chronic myelogenous leukemic	CXCR4, CXCR3, CXCR5[45]

Table 1 – Examples of chemokine receptor expression in cancer

The CXCL12/CXCR4 pathway is involved in numerous stages of tumour development.[2] Metastasis is one of the hallmarks of cancer yet there is limited understanding about the mechanism that regulates it even though it is responsible for the majority of mortalities in cancer patients. The over-expression of chemokine receptors in cancer is not regarded as random indicating that certain chemokine/receptor pairs are involved in metastasis. It was found that breast cancer cells mainly overexpressed CXCR4/CXCL12 and CCR7/CCL21.[22] The CXCR4 receptor is the most commonly overexpressed chemokine receptor in cancers. High expression of CXCL12 is observed in organs where breast cancer metastases are frequently found.[6] The highest expression of CXCL12 is found in the lungs, liver, bone marrow and lymph nodes.[22] A lower expression of CXCL12 is observed in the brain which is also a known metastatic site. CXCL12 expression guides cancer cells to locations of neoangiogenesis assisting the progression of tumour growth.[2] It is known that organs expressing CXCL12 are common sights for metastasis supporting the belief that the CXCL12/CXCR4 pathway heavily influences the locations of secondary tumour sights. This indicates that the CXCL12/CXCR4 pathway is very important in metastasis. Muller *et al.* found that inhibiting CXCR4 receptor in a MDA-MB-231 cell line with CXCR4 specific monoclonal antibody, mAb, prevented metastasis to the lung and lymph nodes.[32a]

In tumours, the CXCL12/CXCR4 pathway is reprogrammed resulting in an up-regulation and spreading of tumour cells. These processes can utilise chemotaxis because, in cancer, the aspects

that control chemotaxis are often mutated. Tumour cells can move randomLy, however, with directed migration the tumour cells are able to invade and disseminate with greater effect.[28] During the progression of metastasis in 11 different types of cancer, CXCR4 and CXCL12 have been identified as initiating directed migration of tumour cells.[23, 28]

The downstream effects generated by the CXCR4/CXCL12 signalling pathway are capable of assisting metastasis, some of the pathways believed to be involved are shown in Figure 4.[2] $G\alpha_{12}$ activates low molecular weight G-proteins like Rho or Ras whose signals can result in cell survival and proliferation.

The enzyme PI3 kinase, shortened to PI3K, manages CXCR4-mediated chemotaxis.[2] PI3K is activated by $G\beta\gamma$ and $G\alpha_i$, which in turn activates serine-threonine kinase, AKT. AKT is crucial in the survival of tumour cells and may assist tumour proliferation. $G\alpha_q$ utilises the enzyme phospholipase C, PLC, to generate diacyl glycerol, DAG, which can induce chemotaxis through mitogen activated protein kinases, MAPK. MAPK, p38 and Erk1/2 are also indicated as playing a role in tumour cell survival. Promotion of cell survival is achieved through PI3K and MAPK resulting in the absence of cell cycle progression. This occurs through two mechanisms, the first involves Bcl-2-associated death promoter, BAD, a protein which initiates apoptosis. BAD is inactivated through stimulation of PI3K preventing cell death. The second mechanism simply involves the up-regulation of genes related to cell survival.

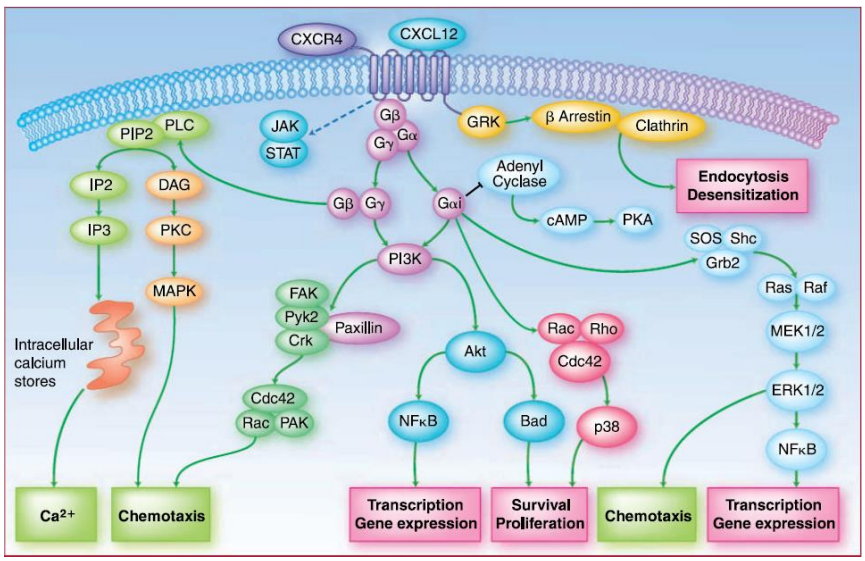

Figure 4 - Signals generated when CXCL12 activates CXCR4[2]

CXCL12 release, by endothelial precursor cells, is linked with tissue damage and inflammation.[2, 15a] It has been suggested that when CXCL12 is secreted in or nearby damaged tissue, it could form a microenvironment homing specific endothelial cell which leads to organ regeneration or tissue

repair.[2] In damaged or hypoxic tissue it has been shown that HIF-1α levels are elevated. Furthermore, CXCL12 expression is increased in HIF-1α expressing endothelial cells, consequently, the elevated CXCL12 levels causes the expression of CXCR4 to increase. As frequently noted in tumours, a vast enhancement of CXCR4 expression is induced by hypoxia suggesting that a regular tumour response to hypoxia is an increase in CXCR4 levels through the HIF-1α pathway.

In the tumour microenvironment, an important process is immune evasion.[23, 35] The chemokine CXCL12 can cause tolerogenic responses. A tolerogenic response is a particular failure of the immune system to react to an antigen, in cancer it refers to the tumour cells stopping the cytotoxic activities induced by the immune system. The tumour uses CXCL12 to accumulate dendritic cells which suppress immune responses specific to tumours. Put simply, the tumour cells move the immune cells into the tumour through chemotaxis and alter the immune microenvironment so that instead of suppressing the tumour dissemination of its cells they are promoted.

Angiogenesis is the process of microvascular endothelial cells branching out from existing cells in the direction of the tumour.[23] This is acheived by the employment of chemokine receptors, such as CXCR4, that are expressed on endothelial cells. The tumour increases the expression of the receptors ligands, in this case CXCL12, which subsequently induces endothelial cell chemotaxis. An invasive response from cancer cells can be aided by CXCR4 expression. Cancer cells expressing CXCR4 migrate towards its ligand CXCL12 expressed in high amounts and once activated CXCR4 can aid invasion. CXCL12 can enhance tumour cell migration towards areas of invasion such as blood vessels and guide metastasising cells to new sites in organs expressing CXCL12.

1.2 CXCR4 ANTAGONISTS

1.2.1. Designing a CXCR4 antagonist

Since the discovery of AMD3100 many groups have investigated macrocycles as therapeutic agents for HIV and cancer and a range of potent CXCR4 antagonists have been synthesised. Antagonists are substances that bind to receptors but which produce no biological response whilst blocking the site; this differs from agonists which activate the receptor when bound.[46] The majority of CXCR4 antagonists have been analysed as anti-HIV agents so much of the published data refers to the anti-HIV activity. However, this data is still relevant because it demonstrates the affinity that compounds have for the receptor. The ability of an antagonist to perform as an anti-cancer agent can be tested with calcium(II) signalling studies because they show how effectively the macrocycle is blocking the signalling pathway. Furthermore, different structural attributes impact the behaviour of macrocycles/antagonists towards the receptor and the results from biological assays help distinguish their suitability as either anti-cancer or anti-HIV agents.

1.2.2. AMD3100 – The Discovery

Research investigating cyclam as an anti HIV agent led to the discovery of AMD3100, see Figure 5.[47] One of the synthesised batches of cyclam, JM1498, see Figure 5, showed anomalously high activity and was therefore evaluated in further detail. During these investigations it was discovered that an impurity was present which was responsible for the increased activity. The impurity was later identified as JM1657 a bis-cyclam connected by a direct C-C link, see Figure 5. Bis-cyclam analogues of JM1657 connected with different aliphatic and aromatic linkers were synthesised. One analogue exhibited a 100 fold increase in potency, JM2987, see Figure 5.

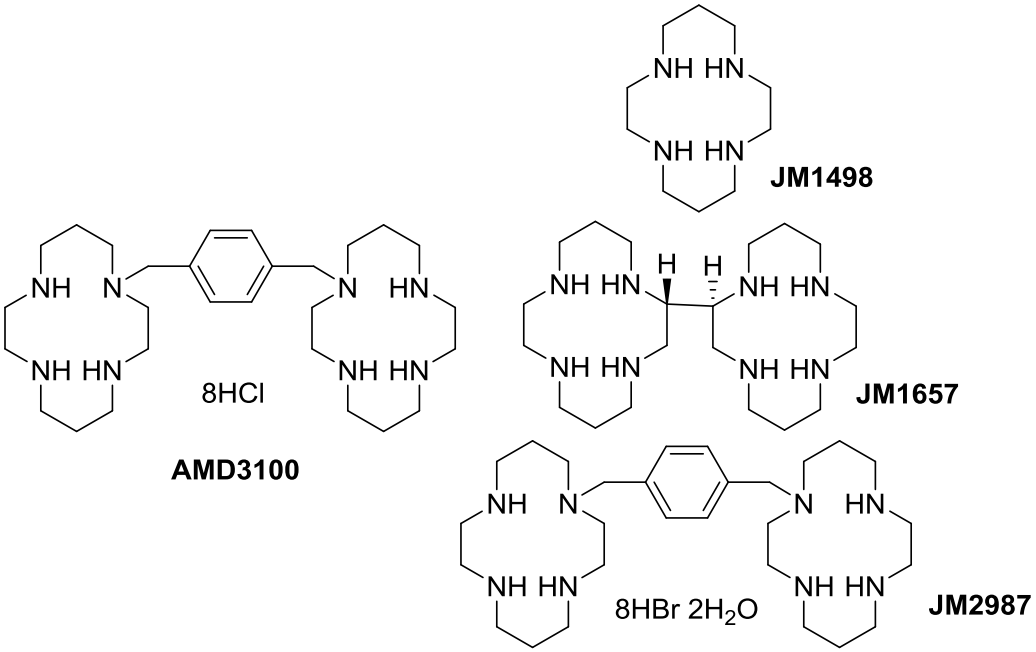

Figure 5 - Important structures in the journey to AMD3100

JM2987 showed a lower effective dose than JM1657 and yet was not toxic at >500 µM.[47] The chloride salt of JM2987, JM3100, was found to be equally as potent as the bromide salt and since that discovery the chloride salt was always used. At this point the name changed from JM3100 to AMD3100 after the company AnorMED which took on the development of the compounds. Both JM2987 and AMD3100 showed specificity for CXCR4 and prevented X4-tropic and dual tropic (X4 and R5) HIV virus strains using CXCR4 from entering cells and replicating. No activity against simian immunodeficiency virus (SIV) strains was observed as SIV was an M-macrophage tropic R5 strain which uses CCR5 as the co-receptor. AMD3100 functions by interfering with the binding of HIV gp120 to the CXCR4 receptor, once the virus is bound to the CD4 receptor. Further work by De Clercq *et al.*, Schols *et al.* and Donzella *et al.* showed AMD3100 to be an active inhibitor of HIV-1 replication, CXCR4 mAb binding and CXCL12 induced Ca^{2+} flux, see Figure 6.[48] Induced Ca^{2+} flux refers to the release of high levels of calcium(II) within the cell from its intra-cellular store which occurs as a result of downstream effects upon CXCR4 receptor activation by CXCL12.[49]

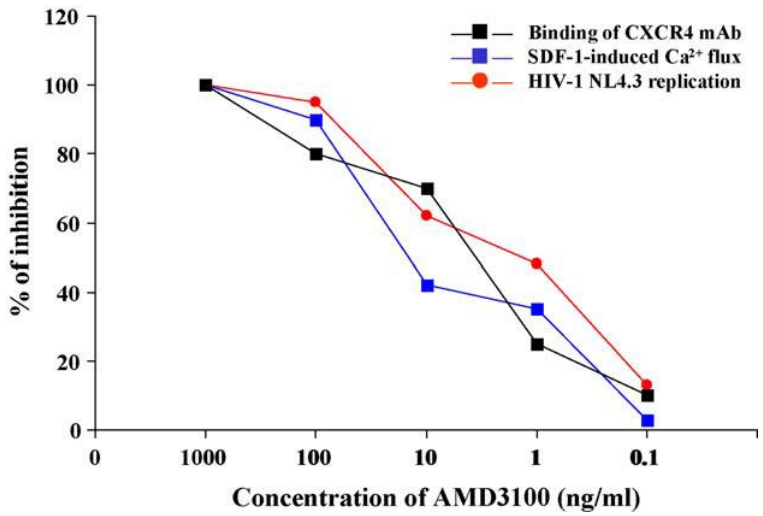

Figure 6 - Correlation between inhibitory effects of AMD3100 on HIV-1 replication, CXCR4 mAb binding and CXCL12 induced Ca^{2+} flux. According to De Clercq[47]

In Phase 1 trials an unexpected side effect of AMD3100 was identified; an increase in the number of white blood cells in circulation. The dose dependant increase in hematopoietic stem cells peaked 6 h subsequent to infusion. An application for this side effect was autologous stem cell transplantation which collects stem cells in sufferers of Hodgkin's disease, non-Hodgkin's lymphoma and multiple myeloma, who produce insufficient amounts of blood cells, and return them when needed. The standard mobilisation agent, granulocyte-colony stimulation factor (G-CSF) is not always sufficiently effective, however in conjunction with a single dose of AMD3100 much higher cell numbers were mobilised. A single subcutaneous injection of AMD3100 was found by Calandra *et al.* to enable two thirds of sufferers of Hodgkin's disease, non-Hodgkin's lymphoma and multiple myeloma to generate enough cells for autologous transplantation.[50] Additional research by Gazitt *et al.*, Flomenberg *et al.*

and Devine *et al.* showed that tumour cells were not mobilised in multiple myeloma and non-Hodgkin's lymphoma patients on administration of AMD3100.[51] AMD3100, now called Plerixafor, was released for haematopoetic stem cell collection in non-Hodgkin's lymphoma and multiple myeloma patients as a Plerixafor injection – Mozobil by Genzyme.[47] Its use was later licensed by the FDA in the USA and Europe in 2009 and it is now used in patients routinely.

AMD3100 has been investigated as an anti-metastatic agent as the over-expression of CXCR4 in breast cancer is well documented. De Falco *et al.* showed that in nude mice inoculated with the rare thyroid cancer anaplastic thyroid carcinoma AMD3100 has shown an effective reduction in tumour growth.[52] Furthermore, Rubin *et al.* discovered that for the development of many malignant brain tumours CXCR4 plays a critical role, suggesting that AMD3100 should be clinically assessed as a treatment.[53] In addition to this, Li *et al.* showed by blocking CXCL12 from activating CXCR4 with AMD3100, in colorectal cancer, a decrease in invasiveness was noted.[54] In summary, targeting the CXCR4 receptor with AMD3100 can prevent invasion and metastasis of multiple cancers. Analogues of AMD3100 could increase the potency further or lead to its use in other applications such as medical imaging.

1.2.3. CXCR4 Antagonists as Therapeutic Agents

1.2.3.1. Introduction

The use of tetraazamacrocycles as CXCR4 antagonists has become a large area of interest following the initial reports on the potent bis-macrocycle AMD3100 by De Clercq *et al.*[47] Derivatives of cyclam have been applied to both cancer diagnosis and therapy.[55] The term macrocycle will be used to refer to derivatives of the class of saturated tetraazamacrocycles based on the 14-membered ring cyclam, see JM1498 Figure 5, and the smaller 12-membered ring cyclen shown in Figure 7.

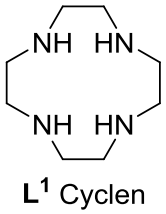

L[1] Cyclen

Figure 7 – Structure of tetraazamacrocycle cyclen, L[1]

CXCR4 antagonists bind to the CXCR4 receptor through interactions with the carboxylate groups of aspartate residues.[56] These carboxylate groups can interact with positively charged 'free' macrocyclic rings as well as with macrocyclic metal complexes through electrostatic interactions, H-bonding, coordination interactions or a combination, as shown in Figure 8. At physiological pH macrocycles are strongly basic due to their 4 primary amines in each macrocyclic ring. Cyclam rings are protonated at physiological pH enabling them to H-bond with the carboxylate groups. Site directed

mutagenesis studies found that Asp^{181}, Asp^{182}, Asp^{187} and Asp^{193} in extracellular loop two and Asp^{171} in TM IV were important for binding whilst Asp^{171} and Asp^{262} on the extracellular part of TM-VI were particularly important.[57] Subsequently, extensive research has been completed to investigate the optimum structure for CXCR4 receptor binding.

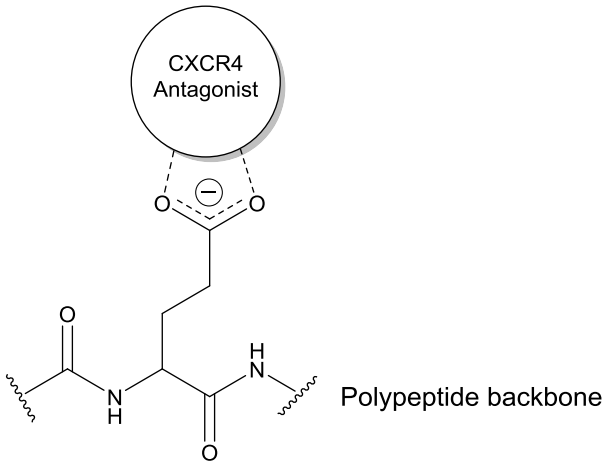

Figure 8 - Diagram of a CXCR4 antagonist bound to an aspartate residue

1.2.3.2. The Chelate and Macrocycle Effect

There have been many reports showing that macrocycles can form highly stable complexes and this stability is largely due to two effects: the chelate effect and the macrocyclic effect. The chelate effect is mainly an entropic factor and relates to the phenomenon that a complex gains more stability when coordinated to a polydentate ligand than when coordinated to multiple monodentate ligands of a similar nature.[58] As a macrocycle is a single tetradentate ligand, macrocyclic complexes are therefore very stable. The macrocyclic effect was first outlined by Cabbiness *et al.* who observed a significant difference in stability between a cyclic mono-macrocycle, **L^2**, copper(II) complex and a number of non-cyclic tetraamine copper(II) complexes. The greater stability observed for the macrocycle copper(II) complex was assigned to the copper(II) ion's natural fit into the macrocyclic cavity as well as the spatial arrangement of macrocyclic ligands.[59]

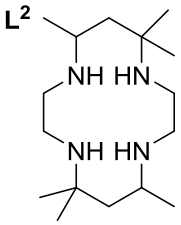

Figure 9 – Curtis' macrocycle which exhibited high stability when coordinated to copper(II) in Cabbiness *et al.*'s study[59]

1.2.3.3. Configurationally Restricted Macrocycles

The incorporation of a bridge into a macrocycle structurally reinforces it. There are two types of bridge: cross bridge (CB), whereby a bridge connects two opposite nitrogen atoms, and side bridge (SB) where adjacent nitrogen atoms are connected by a bridge. Wainwright and Hancock were the first to incorporate an ethylene bridge into mono-macrocycles.[60] Weisman and Wong published cross bridge mono-macrocycles shortly after.[61] Hancock *et al.* synthesised a compound called NE-3,3-DAC which incorporated a propylene bridge between two adjacent nitrogen atoms, see Figure 10.[62] The most common bridge is an ethylene bridge, although there are examples of longer bridges such as propylene bridges, **L**^{5}, synthesised by Pandya *et al.* and butylene bridges,[63] **L**^{6}, synthesised by Pais *et al.,*[64] see Figure 10.

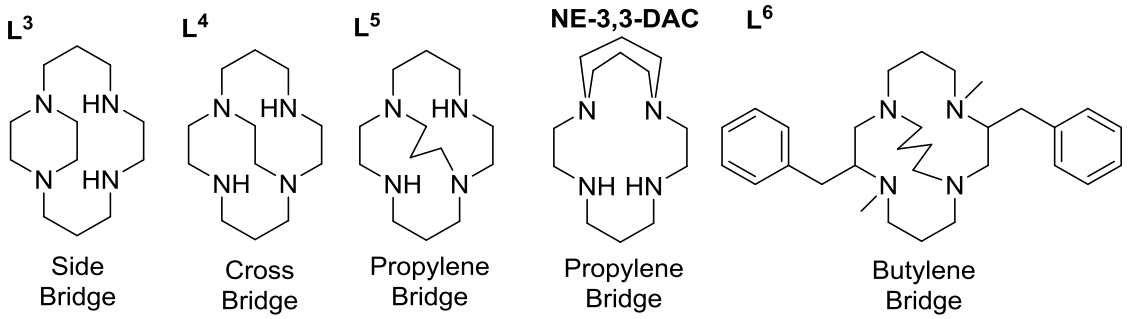

Figure 10 – Structures of mono-macrocycles containing ethylene, propylene and butylene bridges

The incorporation of a bridge is beneficial because it allows the flexibility, ring size, steric strain, configuration and basicity to be controlled. The bridge restricts the macrocycle structure to a single configuration so SB macrocycles are restricted to *trans*-II, see Figure 11, whilst CB macrocycles take on the *cis*-V configuration, see Figure 11, configurations will be discussed in more detail in section 1.2.3.5. Configurational restriction is important because it ensures the macrocycle binds to the receptor in a single configuration so the most biologically active configuration can be used rather than a combination of configurations as seen with cyclam metal complexes.[65] Hunter *et al.* suggested that the most biologically active configuration was *cis*-V as increased binding was observed for *cis*-V configured cyclam-based metal complexes compared to other configurations.[66] Each configuration has the potential to interact differently with the CXCR4 receptor so restricting the configuration may lead to optimised binding and activity. It has been demonstrated that AMD3100 is less efficient than rigidified macrocycles at blocking the CXCR4 signalling pathways, important for anti-cancer agents.[67]

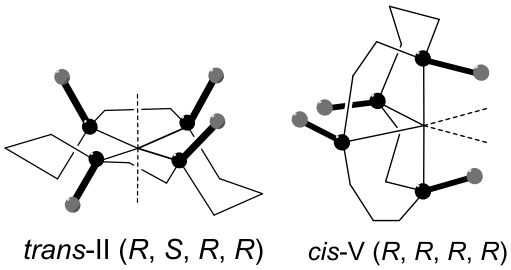

Figure 11 – *Trans*-II and *cis*-V configurations taken on by SB and CB macrocycles respectively

1.2.3.4. Mono-Macrocycles

In the last few years numerous mono-macrocycles have been synthesised, many of which having applications outside the medical field.[68] There has still been extensive work conducted on mono-macrocycles with biological applications. Gano *et al.* synthesised novel macrocyclic complexes with ^{153}Sm and ^{166}Ho in order to develop bone metastasis targeting agents, shown in Figure 12.[69] Cao *et al.* explored macrocycles as HIF prolyl hydroxylase 3 (PHD3) inhibitors for diseases requiring the up-regulation of HIF related genes.[70] It would be interesting to see what affinity these compounds had for the CXCR4 receptor.

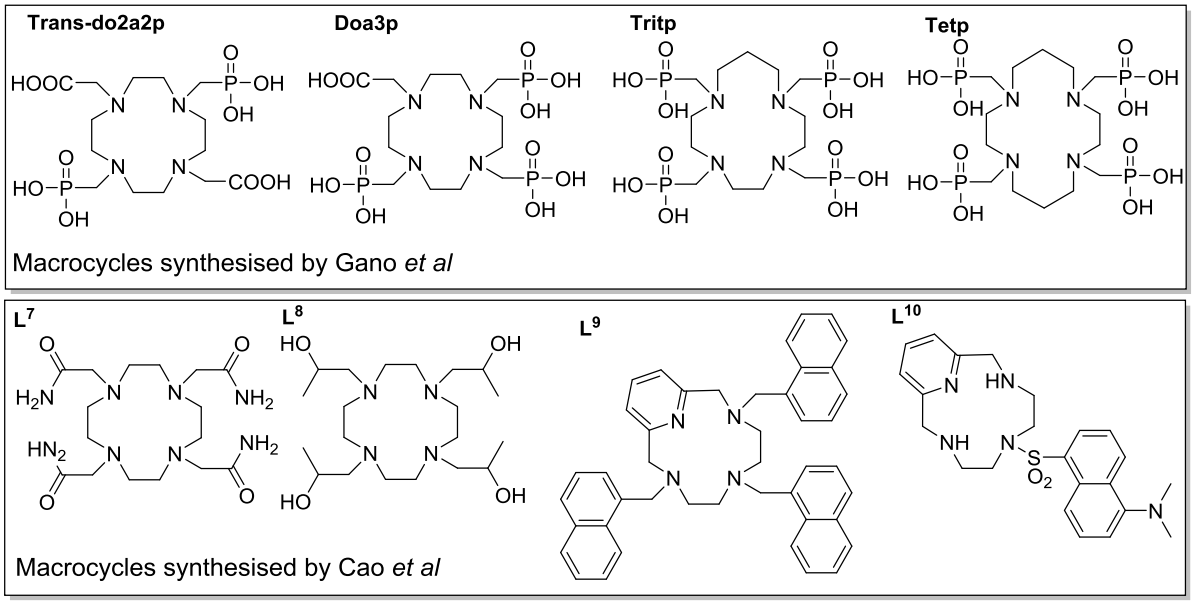

Figure 12 – Tetraazamacroycles synthesised by Gano *et al.* and Cao *et al.*[69-70]

Gerlach *et al.* determined that binding of cyclam to CXCR4 receptor was dependant only on Asp^{171} and mutation of Asp^{262} did not impact binding.[57a] This trend was observed for mono-macrocycle, AMD3465, see Figure 13, which suggests that for mono-macrocycles only one aspartate residue is required for binding.

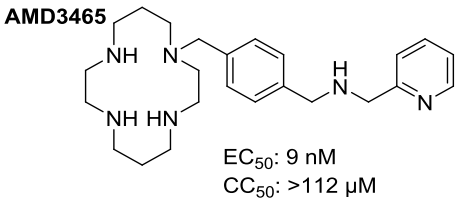

Figure 13 – Structure of mono-macrocycle AMD3465, *in vitro* data from Bridger *et al.* [57d]

In 2010, Bridger *et al.* investigated the minimum structural features required for a potent CXCR4 inhibitor developing a series of mono-macrocycle analogues of AMD3100 based on the scaffolds shown in Figure 14.[57d] They found that replacing one cyclam with benzylamine, **L**[11] in Figure 14, significantly reduced the anti-HIV activity, EC_{50} value of 0.491 µM, which was 100 fold higher than AMD3100, EC_{50}: 4 nM; nonetheless the compound was still active at a micromolar concentration. An EC_{50} value shows the effective concentration of a substance which induces 50% of the maximal response, it is commonly used to measure a drug's potency. *Ortho* and *para* amino-phenyl substituents at R^2, **L**[12] and **L**[13] respectively see Figure 14, did not alter activity, although, the *ortho* amino-phenyl substituent showed a higher degree of toxicity with a CC_{50} value of 24 µM. CC_{50} is the concentration of a substance required to reduce a cell population by 50%, it is a measure of a compounds cytotoxicity. The aromatic group was then substituted for 2-pyridine which resulted in a significant increase in activity, showing an EC_{50} of 9 nM; this led to the development of AMD3465, see Figure 13. Efforts to further improve this value by replacing the proton at R^1 with a methyl group and alternating positioning of the pyridine group only reduced the activity. Alterations were then made to the remaining macrocycle. Replacing both macrocycles with the optimised group, **L**[14], resulted in very poor activity suggesting that the presence of the ring was important. Therefore, to ascertain which parts of the structure were vital Bridger *et al.* replaced amine groups individually by substituting nitrogen in **L**[15] for CH, to give **L**[16], which decreased activity 40 fold indicating that the hydrogen bond acceptor was crucial for activity. Following these findings, the group synthesised more analogues trying different hydrogen bond acceptors but found none that were more active than **L**[15]. The group optimised features for antiviral inhibition whilst also reducing the overall charge.

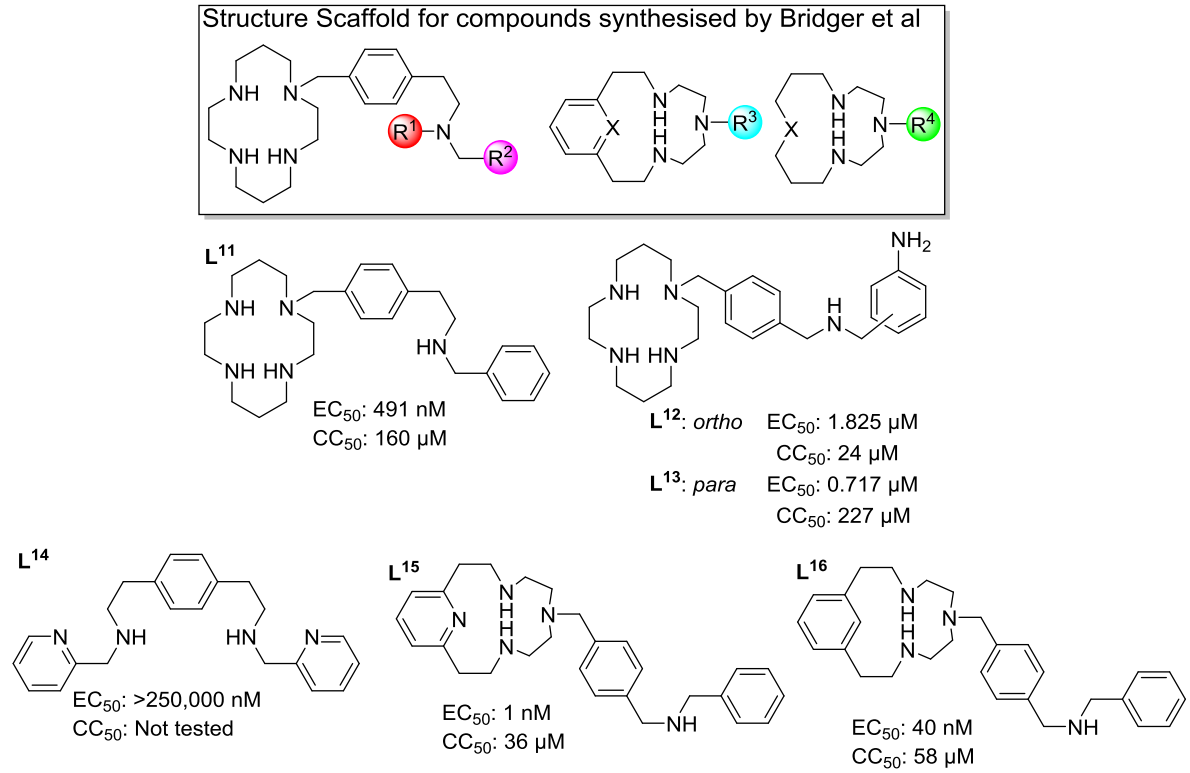

Figure 14 – Scaffold of structures synthesised by Bridger *et al.*[57d]

1.2.3.5. Mono-Macrocycle Metal Complexes

Single macrocycle rings, such as cyclam, are tetradentate ligands, with an ideal cavity size for encompassing d-block metal ions with an ionic radius less than 0.75 Å.[56a, 65b, 71] Cyclam has a very flexible structure and when coordinated to a metal ion all four nitrogen atoms become chiral with each NH bond lying above or below the mean ligand plane in five possible configurations, see Figure 15, part A.[65a, 71d] Six-membered rings within the cyclam complex adopt chair or twist-boat conformations and five-membered rings are either gauche or eclipsed (λ or δ).[65a] The sixth configuration, *cis*-V, is formed by folding *trans*-V, see Figure 15 part A. The four quaternised nitrogen atoms initially deprotonate when cyclam binds to a metal ion, the protons on the amines are easily displaced and all the nitrogen atoms coordinate with the metal ion.[72] The configurations that cyclam metal complexes form depends on which is the most thermodynamically stable.[71d] Cyclam is able to form stable complexes with metal ions and has an elevated affinity for zinc(II), initially a *trans*-III configuration, see Figure 15 part A, is adopted but over a few hours it equilibrates to a mixture of *cis*-V, *trans*-I and *trans*-III, formation of *cis*-V is prevalent with acetate counter ions in zinc(II) coordinated cyclam.[65, 73] Whilst with nickel cyclam *cis*-V is not induced with acetate counter ions but a square planar *trans*-I configuration forms, see Figure 15 part A. The affinity of cyclam metal complexes for the CXCR4 receptor is: $Zn(II)_2$ > AMD3100 > $Ni(II)_2$ > $Cu(II)_2$ >> $Co(III)_2$ >> $Pd(II)_2$ and anti-HIV activity correlates with binding affinity.[66, 74] The most stable configuration is *trans*-III, see Figure 15 part A, and it is the likely shape adopted by free cyclam when bound to CXCR4. However,

there is evidence that the most biologically active configuration is *cis*-V, see Figure 15 part A, therefore configurational restriction could optimise interactions with CXCR4.[66] Free-cyclam interacts with CXCR4 through three hydrogen bonds to the oxygen atoms on the carboxylate group of aspartate residues, see Figure 15 part B. These three bonds are not equivalent and vary from weak to strong, whereas transition metal complexes of cyclam form one hydrogen bond and one metal ion coordination bond, see Figure 15 part B.[56a] There is a high concentration of zinc(II) in the blood plasma, approximately 20 µM which strongly binds to cyclam, log K of around 15, even though levels of free zinc(II) are only 1 nM in blood plasma.[65a, 75] Metal complexes with *cis*-V configuration can bind to carboxylate groups on aspartate residues of CXCR4 in a bidentate manner whereas those in the *trans*-II configuration bind to aspartate residues through an axial coordination to a carboxylate group.[65a, 66]

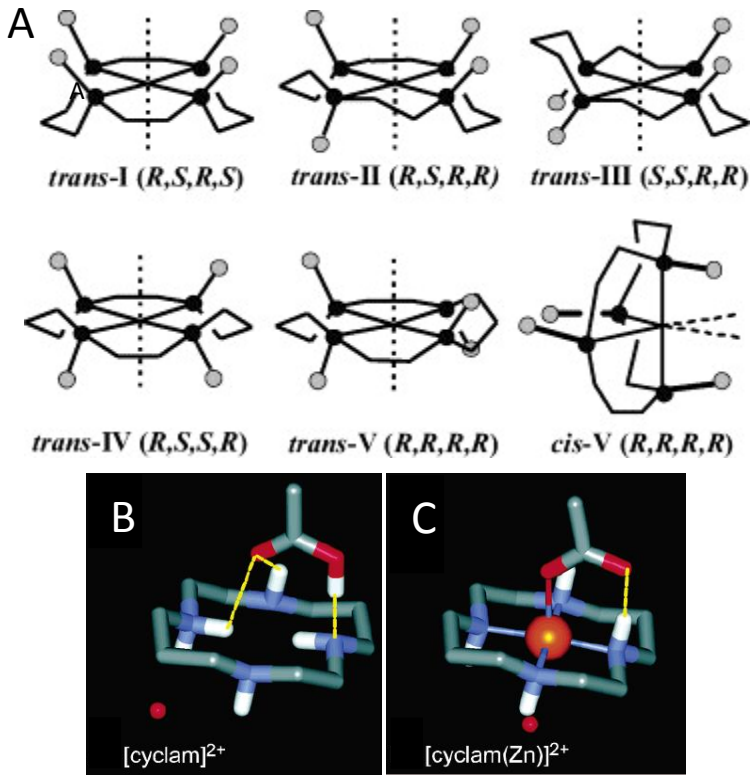

Figure 15 – (A) The six configurations of metal-cyclam complexes (reproduced from Ronconi *et al.*)[73], (B) binding of protonated cyclam and (C) binding of zinc complexed cyclam (reproduced from Gerlach *et al.*)[56a]

Este *et al.* found that binding affinity could be increased up to ten-fold when AMD3100 was complexed to certain transition metals, zinc(II) and nickel(II).[74] Este *et al.* found that there was a close correlation between anti-HIV activity and CXCR4 interaction for the metal complexes, observing an order of activity of Zn>Ni>Cu>Co>Pd. The explanation for the enhancement was explored by Gerlach *et al.*[56a] Theoretically, the metal ion could either strengthen binding to Asp^{171} and Asp^{262} or result in a new interaction with another residue such as histidine, cysteine, aspartate and glutamate. It is believed that incorporating zinc(II) into AMD3100 could result in strong

interactions because zinc(II) coordinates in a square pyramidal or octahedral geometry so there are one or two vacant sites to be filled. Receptor mutagenesis studies indicated that the interaction with Asp[262] was increased. The work supported Este *et al.*'s findings that copper(II) showed the lowest binding but nickel(II) produced the most stable bond which was comparable with zinc(II).[56a, 74] Quantum chemistry docking studies and calculations reveal that cyclam likely binds to aspartate residues through three hydrogen bonds. This differs from Zn(II) bound cyclam which was found to bind with one strong coordinate bond and one hydrogen bond providing an explanation as to why metal complexes show enhanced binding.[56a]

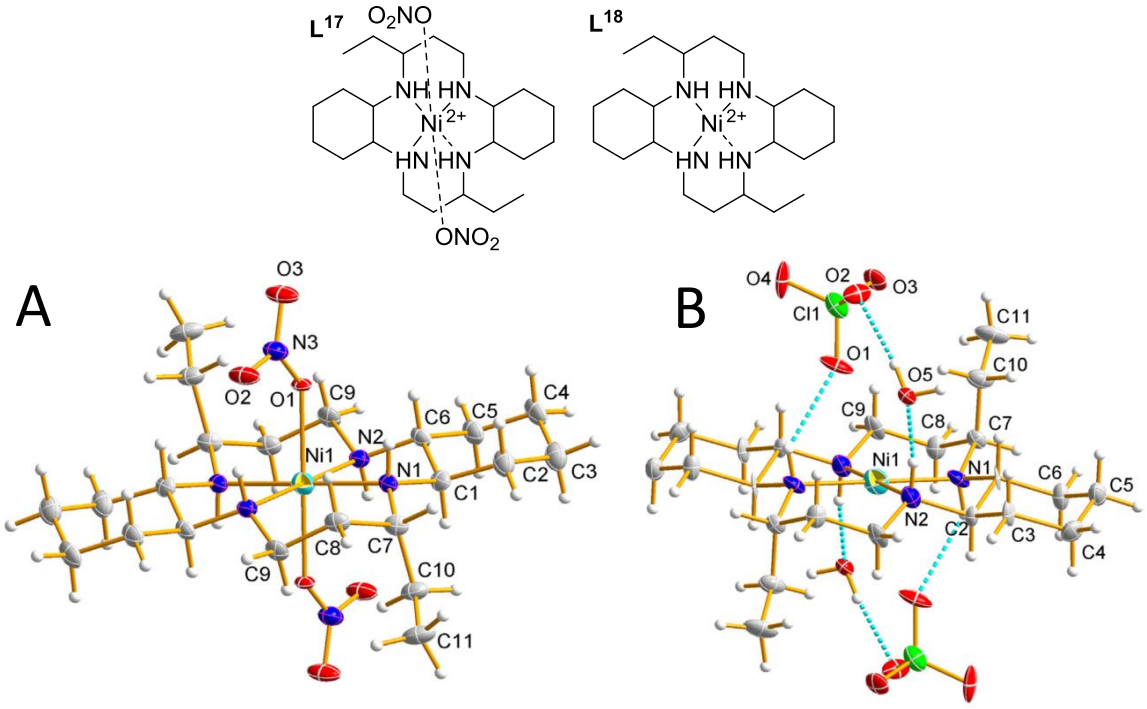

Figure 16 – Nickel(II) complexes of mono-macrocycles synthesised and their crystal structures (Reproduced from Subhan *et al.*)[76]

Subhan *et al.* expanded the knowledge on the coordination behaviour and configuration of cyclam derivatives.[76] Their study involved the synthesis of two cyclam derived nickel(II) complexes, see Figure 16, which were characterised by single crystal X-ray diffraction and infra-red (IR), UV-visible (UV-vis) and photoluminescence (PL) spectroscopies. Ni**L**[17] adopted a distorted octahedral geometry with the cyclam ring in the *trans*-III conformation. The distortion is caused by hydrogen bonding with nitrate groups. The geometry adopted by Ni**L**[18] is square planar. The complexes were not tested in biological assays but this could be an avenue for future work.

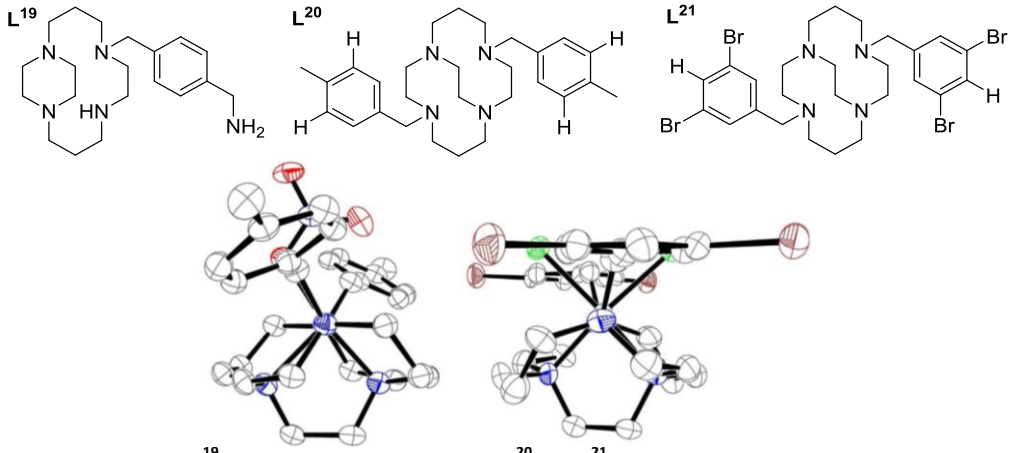

Figure 17 – Structures of SB, L^{19}, and CB mono-macrocycles, L^{20} and L^{21}, with copper complex crystal structures CuL^{20} and CuL^{21} (reproduced from Smith *et al.* and Silversides *et al.*)[67, 77]

Smith *et al.* synthesised a novel SB macrocycle which contains an amine functionalised pendant arm, **L**^{19}.[67] It was believed that this amine group may provide additional interactions with the CXCR4 receptor. Incorporation of the SB meant that the structure was restricted to the *trans*-II configuration, see Figure 15 part A. Calcium(II) signalling assays were conducted to generate an IC_{50} value and compared with AMD3100. The nickel complex $[NiL^{19}]^{2+}$ was assessed as it was anticipated that the free ligand would have low activity due to the lack of hydrogen bond donors in comparison to AMD3100. $[NiL^{19}]^{2+}$ has an IC_{50} of 8.32 µM in the calcium(II) signalling assay. The IC_{50} value means the concentration whereby a reduction of 50% of intracellular calcium(II) release is seen. This is significantly higher than the value obtained for AMD3100 (31 nM) which is as expected for a mono-ring compound. The CC_{50} value for this compound showed low cytotoxicity (> 125 µM). Our group also published **L**^{20} and **L**^{21}, cross bridged mono-macrocycles and their corresponding copper(II) complexes which have the potential to be radiolabelled for PET imaging, see Figure 17.[77] CB macrocycles are restricted to the *cis*-V configuration, see Figure 15 part A. A synthetic route was outlined which led to the isolation of a CB macrocycle via a more rapid and efficient synthetic procedure than the standard methodology. From the crystal structures it was concluded that the copper(II) complexes contained distortion along the N-Cu-N axis which may be due to steric interactions with the two chloride ligands. [77]

1.2.3.6. Bis-Macrocycles

Bis-macrocycles are a highly potent class of CXCR4 antagonists that have shown significantly greater affinity for CXCR4 receptor than mono-macrocycles due to additional interactions with the CXCR4 receptor.[57d] Bis-macrocycles can be joined in three ways; fused, mechanically interlocked or linked, see Figure 18.[78] Rings that are fused together share at least one atom between the different rings. Mechanically interlocked rings are entirely separate rings that are connected like chain links. Linked

rings do not share any atoms within the rings but they are connected by a separate component known as a linker or spacer.

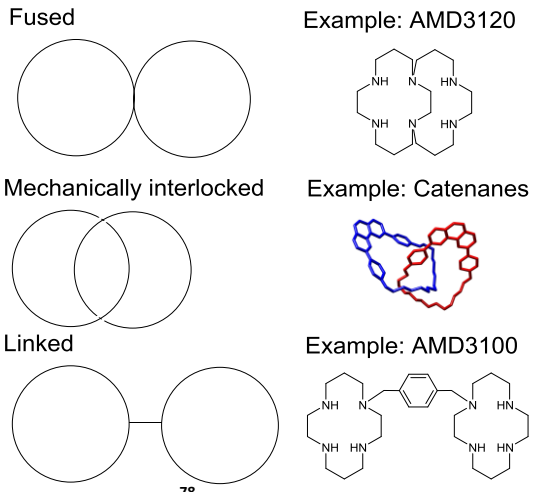

Figure 18 - Types of ways macrocycles can be joined[78]

Aspartate residues are as important for bis-macrocycle binding as they are for mono-macrocycles. Site directed mutagenesis studies revealed that mutations to Asp^{181}, Asp^{182}, Asp^{187} and Asp^{193} in extracellular loop two and Asp^{171} in TM IV caused a dramatic increase in resistance to AMD3100 indicating that these aspartate residues are essential for binding. Gerlach *et al.* proposed that Asp^{171} on TM-IV and Asp^{262} on TM-VI are vital for binding AMD3100.[57a] Binding of AMD3100 is dependant on both residues, see Figure 19, although alterations to the linker group affect the extent of dependence on Asp^{262} with an aliphatic chain causing the compound to behave like two lone cyclam rings. In summary, mutagenesis studies have confirmed that bis-macrocycles can interact with multiple aspartate residues and that Asp^{171} and Asp^{262} are vital for bis-macrocycle binding.[57b, 57c] These findings provide evidence to support the theory that an increase in number of macrocyclic rings facilitates more interactions with aspartate residues explaining why they show greater affinity for CXCR4.

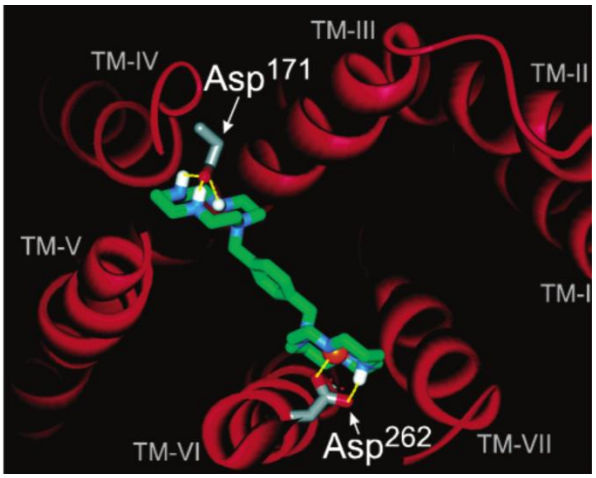

Figure 19 – Docking study of an antagonist with a homology model of the CXCR4 chemokine receptor showing $[Zn_2AMD3100]^{4+}$ bound to Asp^{171} and Asp^{262} (Reproduced from Gerlach *et al.*)[57a]

Este *et al.* investigated numerous analogues of bis-cyclam connected by linkers of different types and lengths, see Figure 20.[74] Fused macrocycles were considered inactive and low activity was observed for macrocycles linked with an aliphatic linker group. Aromatic linkers proved to have increased activity, however the length between the aromatic ring and the macrocycle affected the activity as AMD3390 showed very poor activity, see Figure 20. Therefore, the more aliphatic component to the linker the lower activity obtained. The effect of substituents on the linker groups resulted in lower activity or even inactive compounds with the exception of the 2-(methoxy)-*p*-xylyl linker which exhibited an EC_{50} value of 38 nM. The low activity was likely due to steric hindrance effects by the substituents which reduced the amount of rotation the macrocyclic rings had. None of the bis-macrocycles were more active than AMD3100.

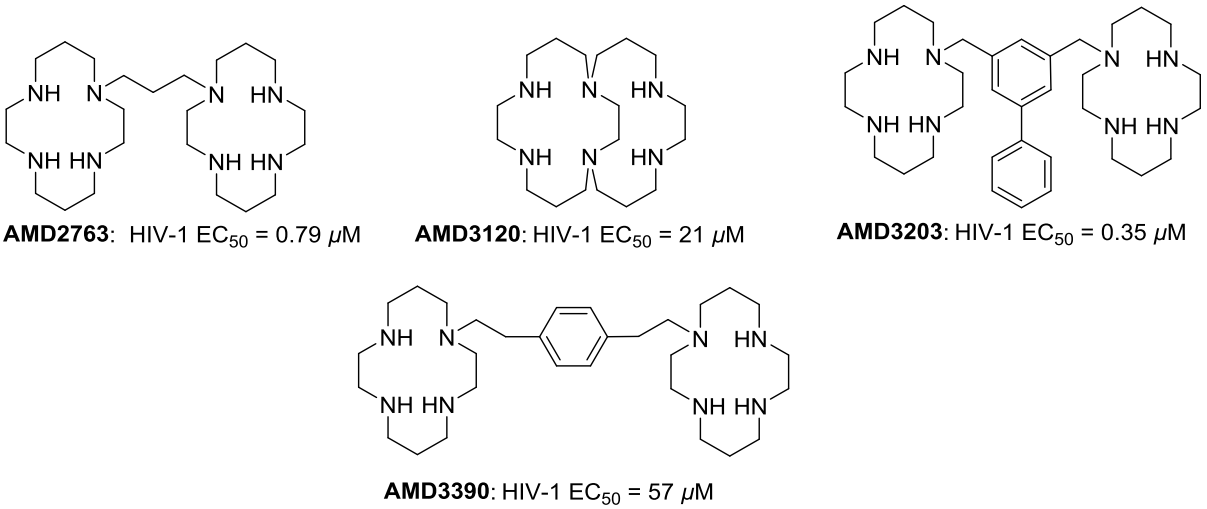

Figure 20 – Structures and EC_{50} values for a selection of the bis-macrocycles synthesised by Este *et al.*[74]

Bridger *et al.* investigated the potency of 12 to 16 membered bis-macrocycles as anti-HIV-1 and HIV-2 agents connected via an aromatic linker with either *meta* or *para* substitution, see Figure 21.[79] They found that for both the *meta* and *para* substituted bis-macrocycles activity increases from 12 membered rings to 14 membered rings although activity decreases for rings larger than this, see Figure 21. Toxicity was seen to decrease from 12 to 14 membered rings and then increase when the rings extended beyond 14 members. Bridger *et al.* also examined the importance of symmetry in bis-macrocycles synthesising bis-macrocycles that contained different macrocycles. The activity of unsymmetrical bis-macrocycles was comparable to that of AMD3100 showing that symmetry was not crucial for activity, although, the macrocyclic ring was important for activity. The highest potency for the 12 and 13 membered rings was seen with the *meta* substitution whilst for the 14 membered rings a *para* substitution was preferable. Further studies revealed that activity of bis-macrocycles was not affected by the presence of electron withdrawing groups or electron donating groups on the *para* linker, nonetheless, the presence of halogens significantly increased macrocycle cytotoxicity,

this could be an important consideration in the development of radiotracers using radioactive fluorine. Moreover, bulky groups substituted on the linker elicited adverse effects on activity; reasoning for this was that the bulky group restricted the position of the cyclam rings. The optimum linker in this study was an aromatic group with methylene groups attaching the two macrocycles to it.

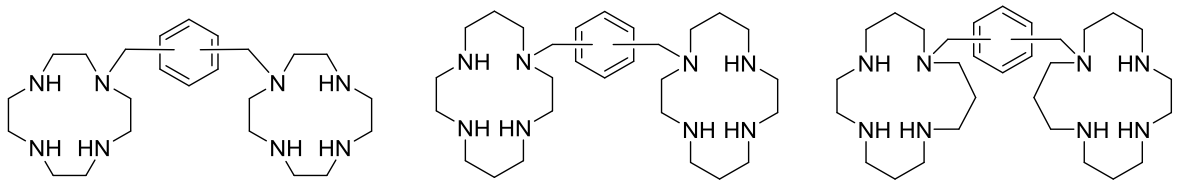

L[22]: *para* HIV-1 EC_{50} = 2.4 μM
CC_{50} = 56 μM
L[23]: *meta* HIV-1 EC_{50} = 0.54 μM
CC_{50} = 20 μM

L[24]: *para* HIV-1 EC_{50} = 0.0042 μM
CC_{50} = >420 μM
L[25]: *meta* HIV-1 EC_{50} = 0.034 μM
CC_{50} = >420 μM

L[26]: *para* HIV-1 EC_{50} = 1.7 μM
CC_{50} = 170 μM
L[27]: *meta* HIV-1 EC_{50} = 2.7 μM
CC_{50} = >190 μM

Figure 21 – A small selection of the bis-macrocycles synthesised by Bridger *et al.*[79]

Tanaka *et al.* produced an extensive collection of bis-macrocycles investigating the relationship between different aza-containing groups, connected with either *para*- or *meta*- xylene, and their activity as CXCR4 antagonists.[80] The aza-containing-groups selected were cyclen, cyclam, homo-cyclam, dipicolylamine, 2-(pyridin-2-yl)ethan-1-amine, 2-(pyridin-2-yl)-N-(pyridin-2-ylmethyl)ethan-1-amine and di(pyridin-2-yl)amine. Percentage inhibitions from a displacement assay were generated whereby compounds competed against [^{125}I]CXCL12 for the CXCR4 receptor on Jurkat cells. Compounds containing solely pyridine-groups or cyclen or one of each showed poor capabilities in competing for the receptor. Furthermore, compounds linked with a *para*-xylyl linker generally showed higher percentage inhibition values than *meta*-xylyl linked compounds. The best inhibitors were **L[30]** and **L[32]**, see Figure 22, with inhibition percentages of 94% and 91% respectively. Interestingly, **L[30]** contained only one macrocycle, cyclam, although cyclam appears vital for binding because when replaced by cyclen the inhibition drops to 32% and 17% for the *para*- and *meta*-linked compounds respectively. The size of the ring was found to impact inhibition as a greater percentage inhibition was identified in compounds containing two 14 and 15 membered rings, although the presence of one 14 membered ring was sufficient to generate a minimum inhibition of 89%. EC_{50} values for **L[28]**-**L[33]** suggest that *meta*-linked compounds are significantly less active than *para*-linked compounds. The most potent compounds were **L[28]** and **L[32]** which achieved EC_{50} values of 38 nM and 36 nM respectively, bis-*para*-cyclen was one of the least active compounds along with **L[31]** obtaining EC_{50} values of 200 nM and 290 nM respectively. The results from this study imply that high inhibition and activity can be achieved with unsymmetrical bis-macrocycles which agrees with the findings by Bridger *et al.*.[79] Tanaka *et al.*'s findings support Este *et al.* who showed that the nature of the linker affects the bis-cyclam macrocycles anti-HIV potency.[74, 80]

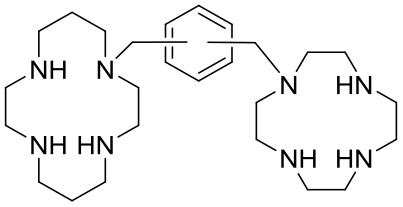

L^{28}: *para* Inhibition = 89 %
HIV-1 EC_{50}: 38 nM
L^{29}: *meta* Inhibition = 89 %
HIV-1 EC_{50}: 50 nM

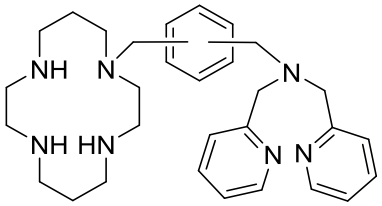

L^{30}: *para* Inhibition = 94 %
HIV-1 EC_{50}: 93 nM
L^{31}: *meta* Inhibition = 58 %
HIV-1 EC_{50}: 290 nM

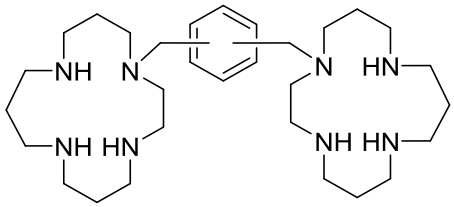

L^{32}: *para* Inhibition = 91 %
HIV-1 EC_{50}: 36 nM
L^{33}: *meta* Inhibition = 87 %
HIV-1 EC_{50}: 130 nM

Figure 22 – Free ligands synthesised by Tanaka *et al.* that exhibited the highest percentage inhibition[80]

1.2.3.7. Bis-Macrocycle Metal Complexes

Bis-macrocycle metal complex activity is highly reliant on the metal complex stability. Furthermore, the affinity of AMD3100 for CXCR4 is increased by complexation to Cu^{2+}, Zn^{2+} and Ni^{2+} by 7, 36 and 50 fold respectively,[56a, 79] although other studies show that copper(II) complex formation decreases the affinity for the receptor.[74, 81] Gerlach *et al.* synthesised mono-Cu^{2+}, Zn^{2+} and Ni^{2+} coordinated AMD3100 and found that they showed equal affinity to the bis-coordinated AMD3100 indicating that only one metal ion was responsible for the increase in binding affinity.[56a] $AMD3100(Ni)_2$ exhibited the strongest M-O(acetate) bond, effectively equivalent to the zinc(II) complex, both were more stable than the copper(II) complex.

Gerlach *et al.* indicated possible geometries of the AMD3100 metal complexes. They suggested that, initially, metal ions coordinate to the macrocycle nitrogens in a planar manner. The zinc(II) complex does not form square planar geometry and so a square pyramidal conformation or an octahedral geometry forms.[56a] This differs from copper(II) complexes which can form square planar structures with cyclen and cyclam macrcocyles, although it is often 5 or 6 coordinate.[80] The binding kinetics and availability of zinc(II) for AMD3100 under physiological conditions allow zinc(II) to compete effectively against copper(II) which has a binding constant approximately 11 fold higher than zinc(II).[82] This indicates AMD3100 is a pro-drug for the active compound $[Zn_2AMD3100]^{4+}$, a substance that reacts *in vivo* to form the active complex.[72, 82a]

Archibald and co-workers found that incorporating nickel(II) or zinc(II) increasingly enhances the binding affinity of SB bis-cyclams for CXCR4 as a result of a further binding site on the molecule provided by configurational restriction. EC_{50} values of 74 nM and 2.5 nM were generated for the nickel(II) and zinc(II) complexes respectively.[67, 83] Valks *et al.* restricted the configuration with ethyl side bridges of a zinc(II) bis-macrocycle, $[Zn_2\mathbf{L^{35}}]^{4+}$ finding that it produced optimised binding to the CXCR4 receptor significantly improving the anti-HIV properties relative to AMD3100 and its metal complexes.[83] Smith *et al.* synthesised a nickel(II) coordinated *meta*-linked CB bis-macrocycle, **L^{34},** to

target the CXCR4 receptor.[67] $[Ni_2\mathbf{L^{34}}]^{4+}$ along with $[Ni_2\mathbf{L^{35}}]^{4+}$, a previously published bis-macrocycle by McRobbie *et al.*, were tested as anti-HIV-1 agents.[84] IC_{50} values were calculated following calcium signalling assays and compared with AMD3100.[67] $[Ni_2\mathbf{L^{35}}]^{4+}$ was found to be the most effective CXCR4 antagonist with an IC_{50} value of 14 nM, this is comparable to AMD3100. Cytotoxicity assays revealed that all the nickel complexes have a CC_{50} of more than 125 µM. Anti-HIV assays were carried out using an X4 strain which utilises the CXCR4 receptor for viral cell entry. The *para*-complex, $[Ni_2\mathbf{L^{35}}]^{4+}$, was more active than $[Ni_2\mathbf{L^{34}}]^{4+}$ but less than AMD3100, EC_{50} values of 74 nM, 398 nM and 11 nM respectively were observed showing that the nickel(II) complexes have high anti-HIV-1 activity and low cytotoxicity.

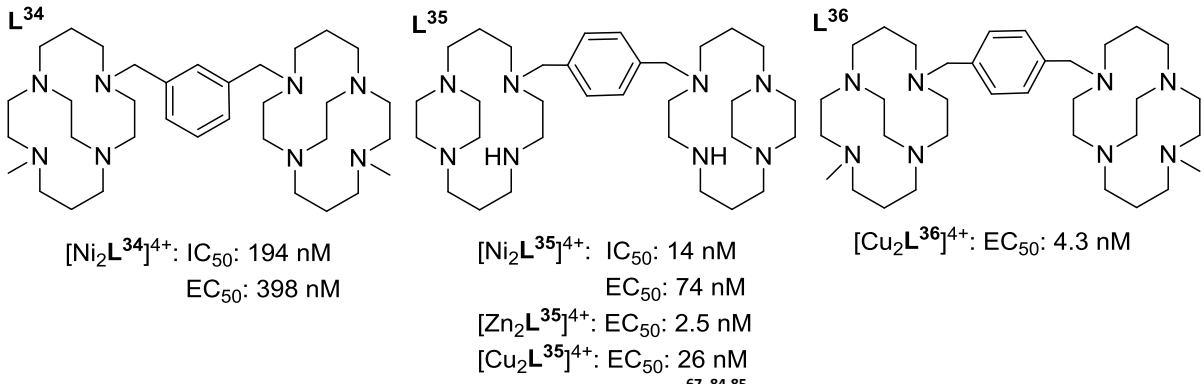

Figure 23 – Bis-macrocycles synthesised by Archibald and co workers[67, 84-85]

Our group synthesised and evaluated $[Cu_2\mathbf{L^{36}}]^{4+}$ as an anti-HIV-1 agent and found it had greater activity than AMD3100 when tested on HIV-1 infected MT-4 cells.[85] The EC_{50} determined for $[Cu_2\mathbf{L^{36}}]^{4+}$ was 4.3 nM. The increase in activity was believed to originate from a longer receptor residence time due to coordinate bonds forming with the copper(II) complex as opposed to weaker hydrogen bonds observed with AMD3100. However, the increase also relates to the optimization of the structure by configuration because simply complexing AMD3100 to copper(II) leads to a decrease in activity. The macrocycle structure favours metal coordination bonds with oxygen atoms from the carboxylate groups on the aspartate residue.

Tanaka *et al.* coordinated a large series of bis-macrocycles to transition metals and found incorporation of zinc(II) enhances the activity of the macrocycles.[80] Percentage inhibition values for all zinc(II) and copper(II) complexes were determined whilst IC_{50} values were only calculated for a small number of the complexes. The percentage inhibitions of *meta*- and *para*- linked zinc(II) complexes are very similar in most cases, although the *para*- linked bis-(bis(pyridin-2-ylmethyl)amine) complexes showed 52% greater inhibition than the *meta*-complex, see $[Zn_2\mathbf{L^{39}}]^{4+}$ and $[Zn_2\mathbf{L^{40}}]^{4+}$ in Figure 24. The free ligands of these compounds showed 0% inhibition for both linkers which demonstrates that chelation to zinc(II) enhances interactions with CXCR4 and is

essential for obtaining competitive binding. This observation was also identified in the equivalent copper(II) complexes, see $[Cu_2\mathbf{L}^{39}]^{4+}$ to $[Cu_2\mathbf{L}^{46}]^{4+}$ in Figure 24, especially when the aza-containing-groups are connected with a *para*-xylyl linker. The non-macrocyclic complexes showed the worst inhibition which highlights the necessity of the macrocycle ring for high affinity. Bis-macrocycles containing cyclam and homo-cyclam exhibited high activity with and without zinc(II) and copper(II) incorporation concluding that metal incorporation is not crucial for high activity. A potential explanation as to why cyclen required metal complexation but cyclam and homo-cyclam did not could be because of the ring size and structure of the macrocycle. The longer carbon chains between nitrogen atoms in cyclam and homo-cyclam may facilitate greater flexibility which enables optimal binding with the CXCR4 receptor. The copper(II) complexes did not bind as well to CXCR4 as the zinc(II) complexes, this was attributed to the fact that the carboxyl groups of the aspartate residues, Asp^{171} and Asp^{262} coordinate strongly with zinc(II) ions but not as well with copper(II) ions in complexes. Interestingly, a combination of cyclen and cyclam with a xylene linker showed high activity, when complexed to zinc(II), compared to other CXCR4 antagonists. It was concluded that the most active compounds were $[Zn_2\mathbf{L}^{37}]^{4+}$ and $[Zn_2\mathbf{L}^{38}]^{4+}$ with IC_{50} values of 11 nM and 8.3 nM respectively, however $[Cu_2\mathbf{L}^{37}]^{4+}$ is still highly active with an IC_{50} value of 16 nM.

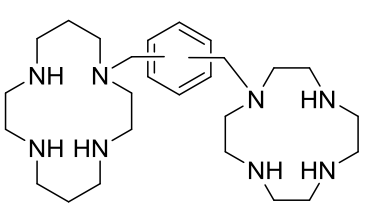

$[Zn_2\mathbf{L}^{37}]^{4+}$: *para* IC_{50} = 11.0 nM
$[Cu_2\mathbf{L}^{37}]^{4+}$: *para* IC_{50} = 16.0 nM
$[Zn_2\mathbf{L}^{38}]^{4+}$: *meta* IC_{50} = 8.3 nM

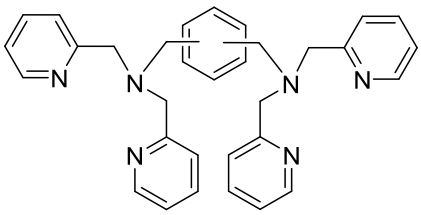

$[Zn_2\mathbf{L}^{39}]^{4+}$: *para* Inhibition = 83%
$[Cu_2\mathbf{L}^{39}]^{4+}$: *para* Inhibition = 10%
$[Zn_2\mathbf{L}^{40}]^{4+}$: *meta* Inhibition = 31%
$[Cu_2\mathbf{L}^{40}]^{4+}$: *meta* Inhibition = 0%

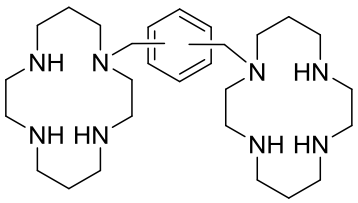

$[Cu_2\mathbf{L}^{41}]^{4+}$: *para* Inhibition = 98%
$[Cu_2\mathbf{L}^{42}]^{4+}$: *meta* Inhibition = 75%

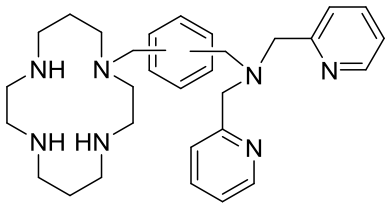

$[Cu_2\mathbf{L}^{43}]^{4+}$: *para* Inhibition = 85%
$[Cu_2\mathbf{L}^{44}]^{4+}$: *meta* Inhibition = 48%

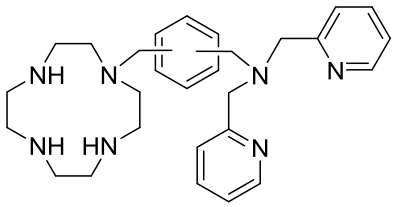

$[Cu_2\mathbf{L}^{45}]^{4+}$: *para* Inhibition = 85%
$[Cu_2\mathbf{L}^{46}]^{4+}$: *meta* Inhibition = 48%

Figure 24 – Zinc(II) and copper(II) complexes of bis-macrocycles synthesised by Tanaka *et al.*[80]

Ross *et al.* synthesised oxovanadium(IV) complexes of bis-cyclam.[86] Unlike the cyclam complexes, $VOCl\mathbf{L}^{47}$ and $VOSO_4\mathbf{L}^{48}$, the bis-cyclam complexes, $V_2O_2Cl_2\mathbf{L}^{49}$ and $V_2O_2(SO_4)_2\mathbf{L}^{50}$ were active. $V_2O_2Cl_2\mathbf{L}^{49}$ was the more active of the two bis-macrocycle complexes with IC_{50} values of 0.116 µM and 0.193 µM against HIV-1 and HIV-2. $V_2O_2(SO_4)_2\mathbf{L}^{50}$ produced average IC_{50} values of 1.365 µM and

3.297 µM respectively; although these are much lower values than have been observed for the other metal complexes presented and AMD3100 (AMD3100, IC_{50}: 0.01 µM, and $[Zn_2AMD3100]^{4+}$, IC_{50}: 0.003-0.009 µM).

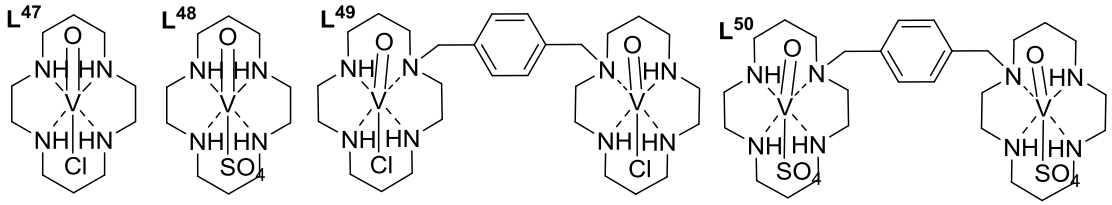

Figure 25 – Bis-macrocycles oxovanadium(IV) complexes synthesised by Ross *et al.*[86]

1.2.3.8. Tris-Macrocycles

There has been a considerable amount of literature published on mono- and bis-macrocycles, but significantly less on tris-macrocycles. Chartres *et al.* reviewed linked macrocycles and their subsequent metal complexes showing macrocycles that could be used as CXCR4 antagonists.[87] One such example is the bis-cyclen macrocycle complexed to zinc linked by a *meta*- and *para*- substituted xylyl group investigated as a receptor for barbiturates in aqueous solutions by Koike *et al.* see Figure 26.[88] Whilst the application was not relevant to this work the macrocycle, with a meta substitution pattern, could show high potency for CXCR4 receptor if Bridger *et al.*'s findings are correct.[79]

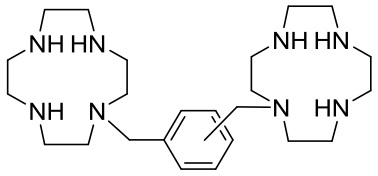

L[51] *para*
L[52] *meta*

Figure 26 – Structures of bis-cyclen macrocycles synthesised by Koike *et al.*[88]

There are few examples of linear tris-macrocycles within the literature; firstly, Kimura *et al.* synthesised a tris-cyclen connected with xylyl linkers,[89] **L[53]**, complexed to zinc see Figure 27. A second cyclen based linear tris-macrocycle was synthesised by Bencini *et al.* **L[55]**.[90] An example of a non-linear tris-macrocycles is the zinc complex of **L[54]** isolated by Sun *et al.*[91] A tris-cyclam equivalent of **L[54]** was also synthesised by this group. The X-ray structure of **L[54]** showed that the geometry of the complex was once again distorted tetragonal-pyramidal as found by Gerlach *et al.*[56a]

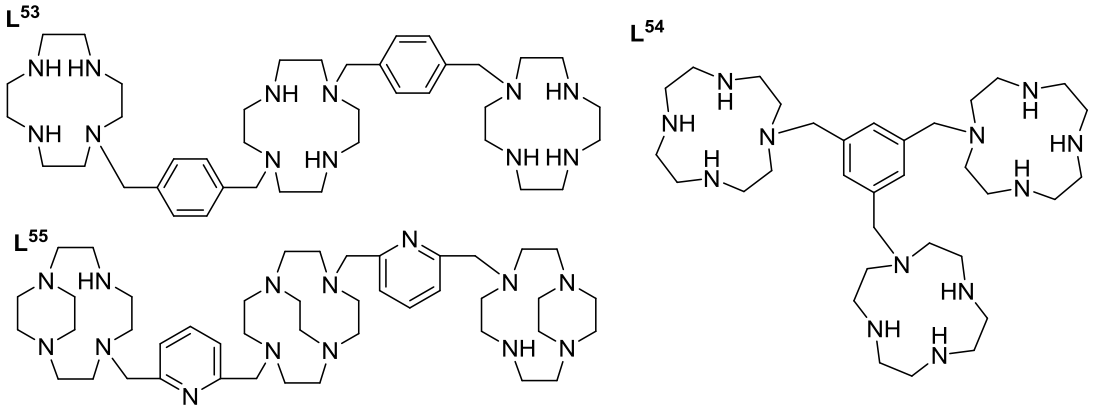

Figure 27 - Structures of tris-tetraazamacrocycles from the literature[89-91]

In conclusion, much work has been conducted into synthesising potent CXCR4 antagonists, yet, an area of research that is underdeveloped is the investigation of compounds with more than two macrocyclic rings and evaluation of CXCR4 chemokine receptor binding. There have been a few larger molecules reported in the literature such as those mentioned in Figure 27 but no tris-macrocyclic compound has been evaluated as a CXCR4 antagonist.

1.3. CXCR4 ANTAGONISTS AS IMAGING AGENTS

1.3.1. Optical CXCR4 Imaging Agents

1.3.1.1. Optical Imaging

Optical imaging provides a cheap, quick and simple imaging alternative to nuclear imaging techniques.[92] The advancement of optical imaging has led to the development of sensitive light detection instruments enabling physiological processes to be observed. Differences in absorption and scatter of light within the tissue enable distinction between healthy and pathological tissue using a non-invasive technique. Advancements in technology have enabled 2D and 3D images to be generated using optical imaging. Mammalian tissue is semi-transparent and photons are absorbed and scattered through the tissue to generate an image.[92] The deeper the signal within a medium, the greater the potential for absorption of the signal or scattering by the tissues which is why the technique has a short penetration depth and imaging humans is challenging.[93]

The general set up of an optical imaging instrument consists of a charge-coupled device (CCD) camera, an excitation light source, lens and filters all enclosed in a light-free chamber.[92-93] CCD cameras detect the signal from the fluorophore. They have very low noise and high sensitivity so that they can pick-up signals a few centimetres deep and can generate macroscopic and microscopic images.[92-93] The excitation light source is usually a laser.[92] A filter is required for fluorescent imaging to remove unwanted wavelengths.

1.3.1.1.1. Fluorescence Optical Imaging

In fluorescent optical imaging a light source excites the fluorophore within the tissue at a specific wavelength, the excitation wavelength, λ_{EX}.[92] The light is absorbed and emitted in the form of lower energy light, the emission wavelength, λ_{EM}, before returning to the ground state. In deeper tissue there is less light to excite the fluorophore because some will have been reflected, scattered and absorbed by other tissue before reaching the fluorophore. To overcome this issue fluorophores with higher emission wavelengths have been designed so that they can pass through more tissue without being lost to absorption.

Examples of commonly used fluorophores in biomedical applications are rhodamine and boron dipyrromethenes, BODIPY, see Figure 28, both of which are taken up by cells. The different structures determine the spectral properties of the dye as well as factors such as photostability, brightness and electrostatic interactions *in vivo*.[94] The major limitations are that there are few dyes approved for clinical use, they have a tendency to cause photobleaching and attaining a high target-to-background ratio is challenging.[93] Peptides and mAb's are most commonly used as targeting agents due to their ease of conjugation to fluorophores.

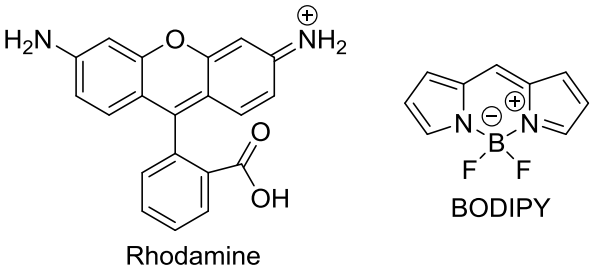

Figure 28 – Commonly used fluorescent dyes in medical imaging applications

1.3.1.1.2. Lanthanide Luminescence Optical Imaging

An alternative type of optical imaging uses lanthanides which again require an excitation wavelength in order to produce an emission wavelength.[95] Lanthanide emission is very specific due to their unfilled $4f^n$ orbital and the well shielded 4f environment. Longer luminescence lifetimes than standard fluorescent probes enables background autofluorescence to be separated from the lanthanide signal.[96] The signal intensity can be reduced by coordination to solvent molecules therefore coordination to a polydentate ligand prevents this.[97] The most common lanthanides used for optical imaging are europium(III) and terbium(III) due to their visible emission wavelengths and long excitation states, 0.6 ms as opposed to 5 ns as observed for BODIPY labelled imaging agents, and there is an analogy with gadolinium(III) which is used extensively in magnetic resonance imaging, MRI.[98]

1.3.1.2. Developing Small Molecule Optical Imaging agents

Kuil *et al.* suggested that fluorescently tagged peptides may have applications in image-guided surgery but there is no evidence to suggest that small molecules cannot be used instead.[99] Relatively few papers report optical imaging of small molecule CXCR4 antagonists, a likely explanation for this is the short penetration depth of the visible wavelengths which limit applications. Nonetheless, a useful role for fluorescent CXCR4 antagonists is during surgery to ascertain the complete removal of a tumour.[100] Previously, fluorescence has been used to gain a greater understanding of the receptor. Dar *et al.* investigated the mechanism of CXCR4 receptor activation using fluorescein-labelled SDF-1.[101]

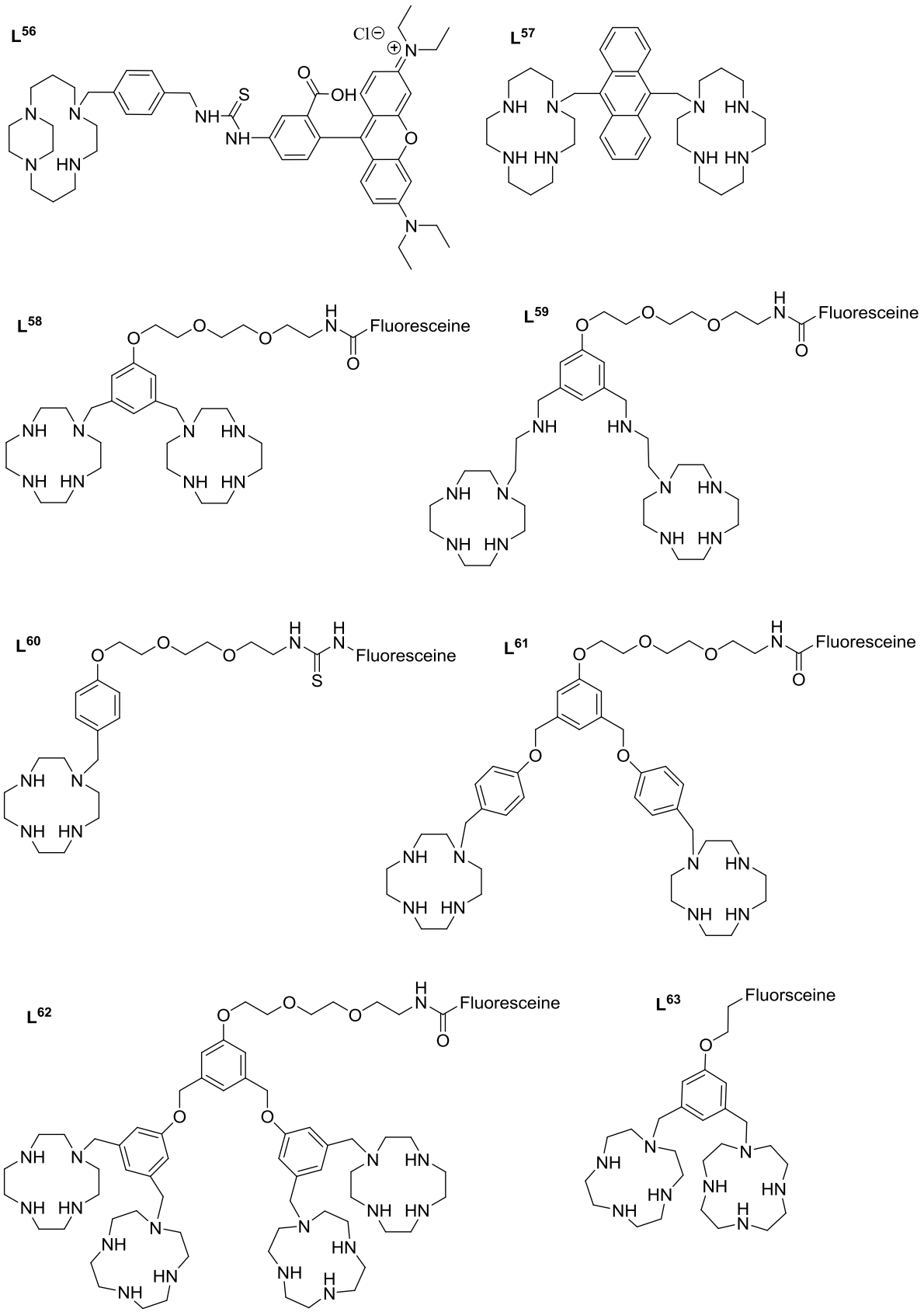

Figure 29 – Macrocyclic CXCR4 optical imaging agents

Our group published rhodamine B isothiocycanate, RBITC, tagged CXCR4 antagonists, **L**[56] and [Cu**L**[56]]$^{2+}$, see Figure 29, and compared their ability to compete with CXCR4 specific antibodies for the

CXCR4 receptor on Jurkat cells.[102] Paramagnetic metal ions, such as Cu^{2+}, have been found to interfere with fluorescence properties so to test this both the free ligand and the copper(II) complex were synthesised and evaluated.[103] Compound $[Cu\mathbf{L^{56}}]^{2+}$ showed some quenching but its activity and ability to compete for the CXCR4 receptor was far greater than $\mathbf{L^{56}}$. However, it was found that the lipophilic rhodamine caused the whole construct to be non-specifically taken up into the cell cytoplasm via active transport. An effective metal complexed fluorescent CXCR4 antagonist was synthesised but futher work is required to prevent non-specific uptake.

Knight *et al.* synthesised a fluorescent analogue of AMD3100 which incorporated anthracene into the linker group, L^{43}, see Figure 29.[104] Molecular modelling suggests that the extra bulk would not lead to unfavourable interactions within the binding pocket. A competition binding assay was conducted to determine the binding affinity of $\mathbf{L^{57}}$ and its metal complexes, $[Ni_2\mathbf{L^{57}}]^{4+}$, $[Cu_2\mathbf{L^{57}}]^{4+}$, $[Zn_2\mathbf{L^{57}}]^{4+}$. $\mathbf{L^{57}}$ was found to inhibit binding of 12G5 to CXCR4 but to a lower extent than AMD3100. A high quantity of non-specific binding was also noted which would reduce its effectiveness. Complexation to nickel(II) did not affect the emission spectra, yet the zinc(II) complex showed a great enhancement in fluorescence intensity.[104] However, as was also reported by Khan *et al.*, fluorescence quenching was observed for the copper(II) complex.[102]

Another group of macrocycle based fluorescent imaging agents were synthesised by Oltmanns *et al.* The group bound fluorescein to six novel bis-cyclen zinc(II) complexes, $\mathbf{L^{58}}$-$\mathbf{L^{63}}$, see Figure 29, and evaluated their ability as apoptosis/necrosis imaging agents. Uptake behaviour in apoptopic/necrotic cells was studied and it was observed that there was significantly greater uptake of the compounds in apoptopic cells and this uptake is reliant on the presence of zinc(II). The intensity of fluorescence is dependant on the number of zinc(II) cyclen groups.[105]

Oishi *et al.* based their fluorescently labelled CXCR4 antagonist on the previously published peptide T140.[106] The group modified the peptide at the α-amino group of the N-terminal Arg1 residue and at the ε-amino group of $_D$-Lys8 to synthesise compounds $\mathbf{L^{64\text{-}73}}$, see Figure 30. The fluorophores tested were Alexa Fluor 488, biotin and carboxyfluorescein and IC_{50} values were obtained using [^{125}I]CXCL12 and the CXCR4 expressing Chinese Hamster Ovary cell line. The affinity of the T140 analogues seemed to be affected by the presence of the fluorophore. $\mathbf{L^{66}}$, which contains fluorescein is almost 5 fold less active than $\mathbf{L^{64}}$, but replacement of $_D$-Lys for $_D$-Glu, $\mathbf{L^{67}}$, decreases the activity by almost 40 fold compared to $\mathbf{L^{67}}$. $\mathbf{L^{68}}$ is over 1000 fold less active than $\mathbf{L^{67}}$, which suggests that fluorescein is the optimum fluorophore for the T140 analogues. Generally, the Ac-TZ14011 analogues show better activity than the T140 analogues. Interestingly the Alexa Fluor 488 analogue, $\mathbf{L^{72}}$, produced an IC_{50} of 8.1 nM which is the most potent of all of the analogues. The fluorescein analogues $\mathbf{L^{66}}$ and $\mathbf{L^{67}}$ are

highly active with IC_{50} values of 16 and 26 nM respectively, but the biotin analogue, **L[71]**, was more potent with an IC_{50} of 11 nM. Compound **L[73]**, was the least active of the Ac-TZ14011 group. It shows a major potency impact on adding an Acp residue between $_D$-Lys and Alexa Fluor 488, decreasing it by almost 33 fold.[106]

Another fluorescent CXCR4 antagonist is the peptide TY14003, L[60] see Figure 30, which was used to image bladder cancer.[107] The depth limitation was averted as the agent bound to urothelial cells in urine. TY14003 also bound to white blood cells, however these are distinctly different from urothelial cells so could be distinguished. The fluorophore in TY14003, **L[74]**, is carboxyfluorescein positioned on the $_D$-lysine group. Whilst CXCR4 is expressed in normal tissue it is at low levels compared to tumour expression in mouse models of invasive bladder cancer and this was visualised through hematoxylin-eosin staining. TY14003 effectively indicated the presence of urothelial cells *in vitro* but the results were not as clear *in vivo*. In addition to this, TY14003 could only be used to detect high-grade and non-muscle invasive cancers as they express high levels of CXCR4. Low-grade bladder cancers express low levels of CXCR4 hence the use of TY14003 is limited. Nonetheless, the authors proposed that TY14003 could be a useful diagnostic agent for detecting bladder cancer at an early stage increasing the chances of patient survival.

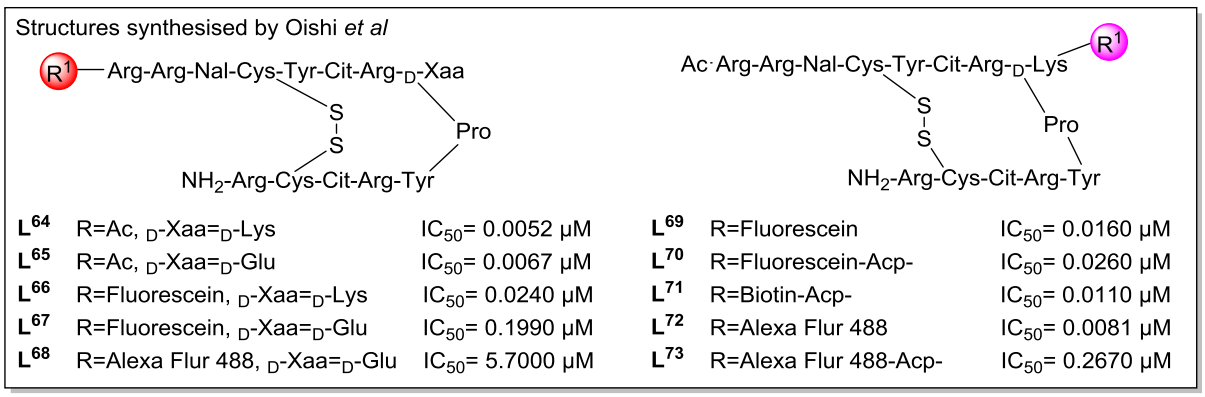

Figure 30 – Fluorescent peptide CXCR4 antagonists synthesised by Nishizawa *et al.* and Oishi *et al.* [106-107]

Overall there has been a limited number of optical imaging CXCR4 antagonists synthesised, this is likely to be due to the short penetration depth that the fluorescent wavelengths have. This causes a problem when the compounds are introduced into humans as there is a greater distance for the wavelengths to travel compared to mice. Perhaps the best application of optical imaging agents is as dual-imaging agents. For example, a radioisotope could be used to determine where the CXCR4 expressing tumour is and the fluorescent imaging agent could be used as an aid during surgery to

ensure all cancerous cells are removed. Alternatively fluorescent agents could be used to analyse bodily fluids such as urine in humans, although this may limit its application and extraction of bodily fluids such as blood would be an invasive procedure which is not ideal.

1.3.2. Nuclear CXCR4 Imaging Agents

Emission tomography (ET) is a medical imaging technique within the nuclear medicine branch of medicine that uses radioactive isotopes to obtain an image.[108] It is a very important diagnostic technique and is regarded as a functional imaging process as it does not just provide structural information like X-ray computed tomography (CT). There are two main types: positron emission tomography (PET) and single-photon emission computed tomography (SPECT). The expression *emission tomography* is a combination of two principles; the first is known as the tracer principle in which gamma-ray emissions are used to create an image. The second principle is the interior volumetric imaging of the body, a process called tomography. The tracer principle utilises materials that participate in an organism's physiological processes but incorporates a radioactive isotope to allow the materials to be tracked. Due to the emission of gamma-rays the flow and distribution of substances vital to the body can be monitored and this altered material is commonly known as a radiotracer. The image obtained from emission tomography is a cross-sectional slice through the body; the word tomography originates from the Greek words for slice and drawing. It is a highly useful technique as it allows the internal visualisation of a patient without the need for any form of surgery. The general process of nuclear imaging is outlined below:[108]

1. Radiopharmaceutical is produced
    - Targeted to a particular queried disease
2. Radiopharmaceutical is administered
    - This is normally injected but sometimes given via inhalation
    - A better image is obtained with a higher concentration of radiopharmaceutical used but radiation of internal organs should be minimised
3. Data is acquired through gamma-ray detection
    - The accumulation time varies with the radiopharmaceutical used
4. Image reconstruction
    - Projection data is obtained via the imaging system and is used to estimate the tomographic image
    - Multiple slices of 2D images are merged into one 3D image
5. Image analysis
    - Normally physicians will interpret images

A disadvantage of ET techniques is that they are limited by the quality of image they can achieve because the data is disrupted by noise. Additionally, they are affected by attenuation; this is where gamma rays are lost due to them being absorbed within the object, this is common when they are emitted from a deep depth. Scattering is another issue and causes a blurred image. It refers to the interactions that occur between the patient's body and the gamma rays, giving an incorrect direction of initial propagation.

The idea of visualising *in vivo* biological processes began in the 1930s when radionuclides carbon, nitrogen and oxygen were first artificially produced.[109] These elements were chosen because they were biologically important. These radionuclides decay by positron emission and were detected by the two 511 keV gamma rays released following anhilation of the positron with an electron in the surrounding environment. The application of PET could only be realised once the instrumentation for measurements, data acquisition and image reconstruction became available which is why its development was only implemented around 40 years ago. Since then significant research into positron-emitting radiopharmaceuticals has been investigated.[108] Most PET radiopharmaceuticals have short half-lives and the most commonly used radionuclides are ^{11}C, ^{13}N, ^{15}O and ^{18}F. [109] PET will be discussed in more depth in section 0. SPECT differs from PET, most obviously, in the type of radiotracers used which produce one gamma ray following radioactive decay and most have long half-lives.[108] Generation of the single gamma ray depends on the radionuclide, for example ^{99m}Tc decays to its ground state by releasing a gamma ray, ^{111}In decays via electron capture emitting a gamma ray, whereas ^{67}Cu produces a gamma ray following beta (β^-) decay.[110] Clinical SPECT has been used for approximately 40 years and can generate two types of image following single-photon emission, planar and tomographic.[108] Planar images portray a single view of radiotracer distribution whereas tomographic images are "slices" generated from many images showing radiotracer distribution throughout the analysed object. Tomographic imaging requires more instrumentation but provides more detailed information. SPECT will be discussed in more depth in section 0.

The development of PET and SPECT CXCR4 imaging agents is an emerging area of research.[111] Nimmagadda *et al.* assessed ^{64}Cu-AMD3100 as an imaging agent for PET,[112] the group also incorporated ^{125}I onto the CXCR4 specific mAb 12G5 as potential SPECT agent.[113] Both imaging agents were tested on U87 tumour xenographs.[112-113] A binuclear ^{99m}Tc complex of AMD3100 for SPECT imaging along with similar ^{64}Cu complexed cyclam analogues for PET imaging have also been reported.[111] Nuclear CXCR4 imaging agents will be discussed in more depth in section 0.

1.4. EVALUATION OF DRUG CANDIDATES

There is a strong interest in analysing the interaction between two biomolecules especially those involved in development of diseases. The effectiveness of antagonists is measured by how its interaction with the receptor affects the natural biological binding process. There are a wide range of techniques available to analyse these interactions and ascertain the extent of antagonism of drug candidates. These techniques often involve using labels to evaluate interactions such as flow cytometry but there is also growing interest in label-free analysis for example using surface plasmon resonance.

1.4.1. Techniques to Evaluate CXCR4 Antagonists

1.4.1.1. Flow Cytometry

Flow cytometry measures cells that are suspended in a stream of liquid.[114] Before analysis the cells are incubated with a fluorophore; depending on the assay type the quantity of fluorescence will lead to different conclusions. A standard flow cytometer consists of three parts: 1) laser light source and sensing system, 2) a hydraulic system to move the cells and 3) a computer system that collates the data and presents it in an understandable format. The cells are taken up into the sensing system and drawn into a stream by a technique called sheath flow. This ensures the cells are analysed individually as they pass through the point of detection. The fluorophore bound to the cells is excited as the cells pass through the light source, which is most commonly a laser. The fluorescence is recorded and converted into readings of electrical pulses which are subsequently changed into numerical signals. The results are then presented in the form of histograms. Figure 31 shows a schematic diagram of a general flow cytometer and all of its components.

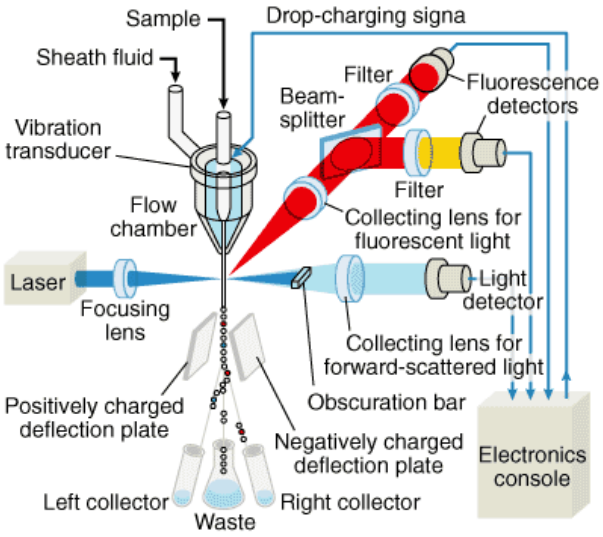

Figure 31 - General setup of a flow cytometer[115]

Flow cytometry has many applications in medicine and biology but because analysed cells are usually discarded after use the analytical potential is restricted.[114] The first restriction is that once a cell has been measured it is unable to be reanalysed with another probe. Secondly, with time-resolved events, like drug uptake, individual cells cannot be examined and thirdly, the analysis of solid tissue needs the cell or nucleus to be isolated which causes information about the tissue structure to be lost. Nonetheless, flow cytometry is particularly good for testing for tumour cells suspended in blood, such as malignant ascites.[116]

1.4.1.1.1. Displacement Assays

The combination of fluorescently labelled molecules with flow cytometry enables the binding of unlabelled compounds to be evaluated.[117] This is achieved by interrogating the capability of a compound to displace a fluorescently tagged molecule. Binding assays using flow cytometry can determine how well a compound competes for its target against a high affinity fluorescently tagged molecule. It is beneficial to choose a high affinity competitor because this will indicate how the compound is likely to behave against the target's natural ligand *in vivo*. The advantage of flow cytometry over methods using radiolabelled ligands is that binding to individual cells can be observed in real time and unbound ligands do not need to be separated from bound ligands. In 1945, Landsteiner laid the foundations for the development of ligand binding assays.[118] Yalow and Berson adapted Landsteiner's work and conducted the first successful ligand binding assay.[118-119] Since these initial ground breaking experiments significant advancements have been made which has enabled a multitude of biological targets to be studied.[118, 120] The development of a competition-based assay was important because both high and low affinity compounds could be efficiently assessed. Low affinity compounds are needed in higher concentrations to match the number of bound receptors as high affinity compounds. However, this results in a higher quantity of free compound which is responsible for high background fluorescence and this causes problems differentiating between bound and unbound compound signals.

Our group has used flow cytometry to determine whether synthesised macrocycles bind to CXCR4 receptors though displacement assays. The assay uses a fluorescently tagged antibody specific to the CXCR4 receptor as the competitor. A higher quantity of fluorescence corresponds to less compound bound to the receptors as the antibody has displaced it. The measurements for this are calculated through the use of a positive and negative control. The positive control represents the highest possible amount of fluorescence and corresponds to the receptors saturated with mAb. The sample for the positive control consists of the CXCR4 specific mAb and cells with no compound added. The negative control consists of cells, a non-CXCR4 specific mAb and phosphate buffer

solution (PBS), it represents 100% binding of the sample compound to the receptors as there is no fluorescence.

1.4.1.2. Cytotoxicity Assays

The purpose of cytotoxicity assays is to ascertain the viability of cells, usually after being exposed to a new compound or condition. The methods for determining whether a compound is toxic towards cells have traditionally been counting living cells after staining them with trypan blue for instance. However, this method is time consuming and lacks precision. An alternative method is to quantify the uptake of radioactive substances by cells such as tritium but this method is also time consuming and involves handling radioactive substances. A preferable method is the MTT assay which does not require physically counting cells.[121] The MTT assay allows for reasonably high-throughput in 96-well plates using a substance called (3-(4,5-dimethylthiazol-2-yl)-2,5-diphenyltetrazolium bromide), MTT. The MTT assay works by monitoring the activity of the mitochondria. Normally the activity is constant therefore this activity is linearly correlated to an increase or decrease in cell viability. The activity is monitored by the conversion of MTT, in living cells the yellow tetrazole is reduced to a purple formazan dye.[122] The intensity of the formazan colour is directly related to the cell activity, the more intense it is the more active and viable the cells are. The intensity of the solution is quantified using a plate reader at 540 and 672 nm.[121] For the assessment of potential drugs, cells are incubated with the drug candidates and the mitochondrial activity is compared to that of standard cells. This is carried out at a range of concentrations to determine the CC_{50} value, 50% of the cytotoxic concentration. This method is simple to perform and has been widely used to determine the toxicity of anti-HIV agents as well as many other drug candidates.[122]

1.4.1.3. Calcium(II) Signalling Assays

When the CXCR4 receptor is activated by its ligand CXCL12 one of the many signalling processes triggered is the release of calcium(II), see Figure 32. When developing CXCR4 antagonists it is important that they do not activate the receptor (agonists). The release of calcium(II) within a cell mediates multiple calcium(II) sensitive pathways.[49] The resting concentration of calcium(II) within a cell is 100 nM but when activated the concentration can increase by up to ten fold. The internal source of calcium is inside the endoplasmic reticulum (ER) membranes and its release is controlled by calcium(II) mobilising second messengers produced when the cell surface receptors are activated.

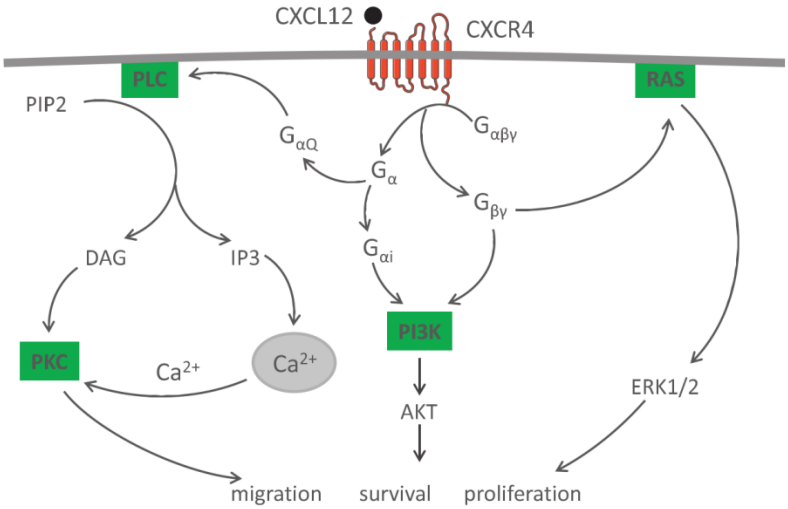

Figure 32 – Downstream affects caused by activation of CXCR4 receptor by CXCL12 (Reproduced from Domaska *et al.*)[123]

The assay used in this work involves incubating a range of antagonist concentrations with U87.CD4.CXCR4 cells, a human glioblastoma cell line that has been transfected with CXCR4 receptors.[124] Firstly, the cells are washed before incubation with the antagonist at a range of concentrations. CXCL12 is then introduced to stimulate the calcium(II) release and the levels of calcium(II) are monitored. A control containing only CXCL12 is run for comparison to the sample. A reduction in calcium(II) release, compared to the control, should be observed when antagonist is present as the receptors are blocked and unable to activate calcium(II) release. The process is monitored by a calcium(II) sensitive dye which binds to calcium(II) and fluoresces. The assay is quantified using fluorometric imaging plate reader, FLIPR. A 96-well plate is used to allow for relatively high-throughput. Use of a range of antagonist concentrations enables the IC_{50} value to be calculated.

1.4.1.4. Surface Plasmon Resonance (SPR)

SPR is a highly advantageous tool because the absence of a label ensures that you are generating data solely from the interaction under study without any interference from a label, as may be the case with the other techniques mentioned. SPR theoretically allows you to determine the binding interactions between any two structures, termed binding partners. One binding partner referred to as the ligand is immobilised onto a surface whilst the second binding partner called the analyte is flowed over the immobilised ligand and the interactions measured. Briefly, the principle of SPR involves the detection of a change in mass near a thin gold film in real time.[125] The detection is recorded in a sensorgram and contains kinetic information relating to the association and dissociation rates of the two binding partners. Information regarding the equilibrium can also be obtained and SPR is one of the few techniques able to produce both sets of data.

Briefly, the principle of SPR involves the detection of a change in mass near a thin gold film in real time.[125] Kinetic information relating to the association and dissociation rates of the two binding partners as well as information regarding the equilibrium can be obtained from SPR measurements and it is one of the few techniques able to produce both sets of data.

In the early 1900s Wood was the first to witness the SPR phenomenon when unusual diffraction patterns were observed after visible polarised light reflected on a metal grating.[126] Although it was not until the 1960s that the SPR phenomenon could be utilised as a technique. Otto and Kretschmann were the first to design an SPR sensor.[127] As the SPR signal is very sensitive to changes in the refractive index and the refractive index is affected by changes in mass close to the gold film, Liedberg *et al.* realised that SPR sensors could be used to analyse binding interactions.[128] There are now six main companies making SPR biosensors: GE Healthcare, Affinity Sensors, Windsor Scientific Limited, BioTul AG, Nippon Laser and Electronics Lab and Texas Instruments. Biacore was the first to release an instrument commercially in 1990.[129]

SPR sensors use the optical excitation of plasmons to generate sensograms. Surface plasmons are generated when light passes through a glass prism onto a thin gold film coating the glass under conditions of attenuated total reflections (ATR).[127] The polarised light irradiates the glass surface with a range of different incident angles but at a certain angle (β), the SPR angle, light penetrates into the gold film meeting the ATR conditions.[125] The intensity of reflected light dips under ATR conditions as energy is transferred from the photons to the free gold electrons exciting them.[128a] The oscillations of the electrons are coupled with an electromagnetic field, from the incident light, forming a highly delocalised state of electrons, the plasmon state.[125] This state causes a plasmon resonant wave, connected to an evanescent electromagnetic field, at the interface of the conducting gold film and a dielectric medium; the glass surface with the immobilised ligand. The wave and evanescent field are often combined and called the evanescent wave field. The evanescent wave field penetrates a short depth into dielectric media with differing refractive indexes; the glass with the immobilised ligand and the solution containing the analyte.[130] The shorter the distance from the gold-glass interface the stronger the evanescent wave field is, decaying exponentially up until the penetration limit of approximately 300 nm.[125] Therefore the closer samples are to the surface the more they will contribute to the SPR signal. The optimum balance between signal and strength and binding capacity is about 100 nm.

The sensor chips available for use in SPR sensors facilitate a wide range of conditions to attach ligands of differing natures to the surface for analysis. Biacore sensor chips contain a hydrogel consisting of a carboxymethylated dextran layer on the gold film surface.[128a] The dextran layer swells

up on contact with water to approximately 100 nm, resulting in a strongly aqueous environment made up of 97% water. This environment ensures that the binding partner interactions take place in a more natural environment as opposed to on the bare, gold surface. The dextran is bound to the gold surface with an alkane thiol linker layer. The dextran matrix is regenerative so low pH buffer can be used to remove analytes from the matrix. Other surfaces are available to attach specific types of molecules enhancing the potential applications of SPR sensors. An overview of Biacore SPR chip surfaces is shown in Table 2.[129]

Chip Type	Chip Surface	Application
CM5	Carboxymethyl dextran	General purpose
SA	Streptavidin	Biotinylated ligand capture
NTA	Nickel chelation	Conjugating His-tagged ligands
HPA	Flat hydrophobic monolayer	Create hybrid lipid mono or bilayers
B1	Low charge	Decreases non-specific binding
C1	Flat carboxymethylated, no dextran	Where dextran is not wanted
C4-3	Range of dextran and carboxymethyl quantities	Low immobilisation or large ligands
Au	Plain gold surface	Custom design chemistry
L1	Lipophilic dextran	Capture liposomes and lipid bilayers

Table 2 - Chip surfaces and applications[129-130]

A further feature of the sensor chip is the microfluidic system which delivers the analyte to the sensing surface.[128a] The system contains channels and valves supported in a plastic casing. The microfluidic channels are pressed against the sensor surface creating a sample cell with a volume of 60 nL, see Figure 33. The 50 µm high by 500 µm wide sample cell facilitates effective and accurate delivery of the analyte to the sensor surface whilst only requiring a very small volume of sample. Light does not penetrate the sample so coloured samples can be used.[130]

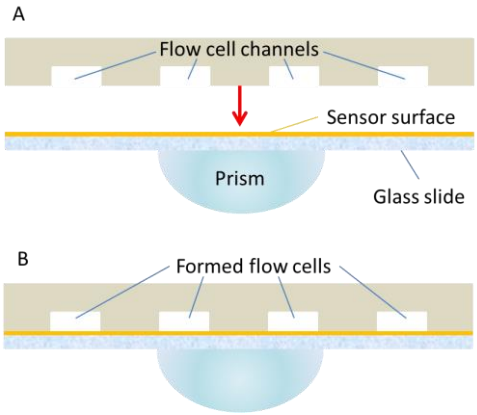

Figure 33 – Formation of flow cells in SPR sensors

The SPR signal can pick up small differences in running buffers and it is this sensitivity the enables the interactions of molecules to be evaluated.[125] The analysis of whole cells can be complicated as generally they are around 10,000 nm, despite this binding can be observed but the relationship

between the SPR signal and bound mass cannot be determined. Every change in the refractive index, the angle at which minimal reflection is observed, is detected as a change in the SPR signal. The SPR signal is expressed in RU on Biacore systems, 1 RU corresponds to 1 pg/mm^2 of mass bound to the surface but this can change depending on the surface type. Other instruments, such as Autolab, express the SPR signal in m^o, millidegrees denoting the change in SPR angle.

A typical sensorgram is depicted in Figure 34, showing the response plotted against time and portrays the interaction between the binding partners.[130] The base line (red) shows the signal generated from the buffer and should be stable, as the analyte is introduced into the system the response increases and shows the 'on' rate or association rate (light blue). Steady state (dark blue) is the point at which the rate of association and dissociation is equal and appears as a plateau on the sensorgram.[125] A decrease in response indicates dissociation of the analyte (purple) and is used to determine the 'off' rate.[130] If the rate of dissociation is extremely slow the remaining analyte can be removed from the surface by carrying out regeneration (green). This process strips the remaining analyte off the surface without damaging the ligand and brings the dissociation curve back to baseline preparing the surface for the next sample.

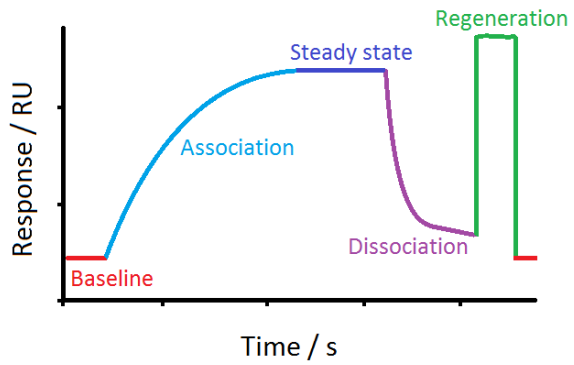

Figure 34 – Typical sensorgram of a molecular interaction

1.4.2. *In Vivo* Evaluation of CXCR4 Antagonists

Once a compound has been established as being an effective antagonist through *in vitro* assays the subsequent step is to move onto *in vivo* studies. Potential CXCR4 imaging and therapeutic agents can be evaluated in a realistic *in vivo* environment through animal models and, if viable, then move into clinical trials.

1.4.2.1. CXCR4 Antagonists in Clinical Trials

Over recent years there have been many clinical trials conducted on medical conditions involving the CXCR4 receptor. AMD3100 was submitted into Phase I trials for myelokathexis in 2012 at a dose below that used to mobilise stem cells and no adverse effects were noted.[131] Currently, volunteers are being recruited for a clinical trial involving AMD3100 in conjunction with bevacizumab to prevent

cancer cells from growing abnormally.[132] In addition to this, a trial combining AMD3100 with bortezomib is underway to test whether this mixture can kill myeloma cells.[133] The non-macrocyclic, orally administered MSX-122 was tested in Phase I trials on patients with refractory metastatic or locally advanced solid tumours however the trial was suspended and the reasons were not disclosed.[134] No further investigations have been published regarding MSX-122 since 2008. More recently, another non-macrocyclic drug tested in Phase I and II trials was AMD070 as an anti-HIV agent. In 2006, a phase I trial aimed to determine the safety of AMD070 in healthy males aged between 18 and 55 was undertaken. The subjects were dosed with different concentrations some in conjunction with a second anti-HIV agent, ritonavir.[135] Additional drug combinations were planned but due to histologic changes to the liver in long-term animal studies these trials were put on hold although there were no indications of this in the human studies.[136] There were no serious adverse effects recorded but diarrhoea was reported in 50% of patients. In 2009, AMD070 completed Phase I and II trials and no clinically significant safety issues were reported, although no follow up studies have been arranged. A CXCR4 peptide antagonist, CTCE-9908, was submitted for Phase I/II trials and administered to patients with solid tumours whereupon it was noted that mild adverse effects were observed, one being phlebitis.[137] Phase II trials were planned, however no progress has since been released. An alternative peptide, POL6326, is currently undergoing Phase II trials as a stem cell mobilising agent in patients with haematological malignancies.[138] POL6326 is also being investigated in Phase I trials in combination with Eribulin as a drug to reduce the invasiveness of metastatic breast cancer.[139] In conclusion, there is currently only one approved drug which targets the CXCR4 receptor and that is AMD3100 but there is significant potential for other drug molecules targeting this receptor to reach the clinic. They could have applications in medical imaging or offer optimised properties for other applications such as cancer treatment.

1.5. RESEARCH AIMS

The aim of this work is to synthesise and evaluate bis- and tris-tetraazamacrocycle compounds as CXCR4 antagonists and display the potential of these compounds as imaging and therapeutic agents. The synthetic design of novel bis- and tris-macrocycles has been optimised for CXCR4 receptor binding and coordination to divalent metals has been carried out to enhance this interaction. All macrocycles have been assessed in biological assays to ascertain their capability to compete for binding to the CXCR4 chemokine receptor against a CXCR4 specific competitor.

A range of terminal functional groups have been investigated for the conjugation of imaging groups to novel bis-macrocycles. Test reactions for conjugations have been conducted on mono-macrocycles as these are easier and quicker to synthesise. The aim is to facilitate non-metal radioisotope conjugation as an alternative to metal radioisotope coordination, although both avenues have been explored so that the macrocycle can be utilised in imaging applications. Methods for labelling the compounds for imaging applications need to be developed.

The synthesis of novel tris-macrocycles may facilitate additional interactions with the CXCR4 receptor and produce a high affinity antagonist. A positive correlation between macrocycle affinity and the number of macrocycle rings was observed for mono- and bis-macrocycles,[57d] the trend is hypothesised to continue for tris-macrocycles. The incorporation of different sized macrocyclic rings may also have an impact on affinity and has been explored.

A novel SPR method for high throughput screening of novel CXCR4 antagonists has been investigated to determine the residence time of macrocycles on the CXCR4 receptor. The use of immobilised and captured intact cells and captured CXCR4 receptor has been investigated in order to develop the most effective evaluation method. Data from this technique can be used to determine the most appropriate application for the individual compounds; either as therapeutic or imaging agents. A longer residence time is beneficial for therapeutic agents because the macrocycle can block the receptor for a longer time and a lower dose can potentially be used. In terms of an imaging agent a shorter residence time is advantageous to ensure that the agent is cleared efficiently from the body.

These approaches facilitate the synthesis and evaluation of novel macrocycles with the potential application as targeted diagnostic and therapeutic agents for CXCR4 expressing tumours.

1.6. SUMMARY

There have been many structurally different compounds tested as CXCR4 antagonists and interest in this research area has dramatically increased over recent years as the drive to develop new anti-cancer agents increases. Currently, there is not a clinically approved imaging agent or therapy specifically for CXCR4 expressing cancers. The CXCR4 receptor plays such an important role in the development of invasive cancers that the demand for a potent and safe CXCR4 antagonist is high. This work investigates the development of high affinity CXCR4 antagonists for diagnostic and therapeutic applications. In chapter 2 the synthesis of novel-tris-macrocycles and their copper(II), nickel(II) and zinc(II) complexes is discussed. Chapter 3 outlines the synthesis of novel bis-macrocycles, their copper(II) and zinc(II) complexes and terminal functional group conjugations. In chapter 4 the range of test reactions to radiolabel macrocycles using mono-macrocycles is discussed. Chapter 5 details the results of biological testing of novel bis- and tris-macrocycles to act as CXCR4 antagonists. The development of an SPR method is also discussed. Chapter 6 describes the radiolabelling of potent novel tris-macrocycles. The work is then summarised and concluded in chapter 7 and potential future work is outlined.

CHAPTER TWO

SYNTHESIS OF NOVEL LINEAR TRIS-MACROCYCLES AND THEIR METAL COMPLEXES

2.2. SYNTHETIC STRATEGY

The synthesis of novel linear tris-macrocycles has been investigated and is reported herein. Structures of the macrocycles were configurationally restricted with an ethylene bridge which formed either CB or SB macrocycles. This restriction has the potential to optimise binding to the CXCR4 receptor. Furthermore, bridges limited the configuration of the divalent metal complexes, copper(II), nickel(II) and zinc(II), which could also enhance binding to the CXCR4 receptor.

2.3. PREVIOUS STRATEGIES

Macrocycles have been utilised in many applications ranging from catalysis to anti-metastatic agents.[65a, 140] Macrocycles are tetradentate ligands and strong transition metal and lanthanide chelators. Tetraazamacrocycles cyclam, a 14-membered ring, and cyclen, a 12-membered ring, have been applied to drug design. The flexibility of their structure enables them to bind strongly to metals, though the carbon skeleton is rigid enough to provide high stability. Stability is extremely important for medical applications because macrocycles must retain the metal for activity as well as preventing toxic side effects.

The addition of pendant arms to macrocycles has resulted in a vast expansion of research and applications of macrocycles over recent years.[65a, 140] Tetraazamacrocycles can be functionalised at carbon or nitrogen atoms and pendant arms for a number of reasons. Firstly, pendant arms can increase the compound stability as well as increase the number of donor atoms for metal coordination. The donor atom can guide the metal into the macrocycle cavity. A further advantage is that the pendant arm can be functionalised to enable conjugation with other molecules for particular applications. Finally, the pendant arm can be synthesised separately to the macrocycle and added at a later stage.

Macrocycles are most commonly linked through nitrogen-nitrogen spacer groups,[78] although problems controlling linkage have been experienced. However this can be achieved by the addition of an ethylene bridge in the macrocycle cavity to form a bisaminal compound.

2.3.1. N-N Linked Tris-Macrocycles

N-N linked macrocycles are linked between a nitrogen atom of an adjoining macrocycle ring and usually through a linker group.[78]

2.3.1.1. Cyclen Based Tris-Macrocycles

Some examples of N-N linked tris-macrocycles are shown in Figure 35 and Figure 36, **L^{75}-L^{83}**. They are structurally related but novel compounds with differing applications. In 2002

Bazzicalupi *et al.* applied **L**[75] and **L**[76], see Figure 35, as hydrolytic agents for catalysis. Synthesis involved forming the macrocycle in the final step which differs from other macrocycle synthesis where the starting point is the macrocycle and substituents are subsequently added to form the compound of interest. For **L**[75] N-[2-[2-[bis[2-[bis[2-[(4-methylphenyl)sulfonylamino] ethyl]amino]ethyl]amino]ethyl-[2-[(4-methylphenyl)sulfonylamino]ethyl]amino]ethyl]-4-methyl-benzenesulfonamide was reacted with sodium ethanolate before adding 4-methyl-N,N-bis[2-[[(4-methylphenyl)sulfonyl] oxy]ethyl]benzene-sulfonamide with potassium carbonate. The 1-sulfonyl-4-methylbenzene groups were then removed with sulfuric acid to form **L**[75], see Figure 35. Synthesis of **L**[76], see Figure 35, was the same except the starting material was 3-(tosyl(3-tosyloxypropyl)amino)propyl tosylate.[141] Synthesis of **L**[77], see Figure 35, began by protecting cyclen with t-BOC at positions 1,4 and 7. A substitution reaction at position 10 with α-α'-di-bromo-*p*-xylene proceeds prior to reaction with 1,7-bis(diethoxyphosphoryl)-cyclen. **L**[77] is then isolated by reaction with sodium carbonate followed by hydrochloric acid. Interaction of the zinc(II) complex of **L**[77] with thymidylylthymidine (TpT) was investigated. The authors noted that it was the first quantitative assessment of stoichiometric and reversible interactions with oligonucleotides.[142] **L**[78], see Figure 35, was synthesised by conjugating 1,7-bis((6-(bromomethyl)pyridin-2-yl)methyl)-glyoxal cyclen bromide salt to glyoxal cyclen. The tris-quaternary salt was then reduced with sodium borohydride to yield **L**[78]. The application for **L**[78] was as a synthetic receptor for phosphate anions to analyse the recognition process in biological systems.[90] This is one of the few tris-macrocycles that incorporates a bridge within the macrocyclic cavity. The addition of a bridge to increase rigidity was first outlined by Wainwright and Hancock *et al.* in the 1980s, to afford SB monomacrocycles.[60, 143] The bridge, seen in the terminal macrocycles of **L**[78], limits flexibility and for the piperidine ring the chair conformation is the most stable. Metal complexes of SB macrocycles are restricted to *trans*-II for monosubstituted species and *trans*-IV for disubstituted species. When the ethylene bridge is bound to opposite nitrogens, as in CB macrocycles seen in the central macrocycle of **L**[78], see Figure 35, the structure is forced into a 'clamshell' type structure, the metal complexes formed are then limited to the *cis*-V configuration. The first published CB macrocycles were by Weisman *et al.* who published 1,8-dimethyl CB cyclam in 1990 and Bencini *et al.* who published 1,7-dimethyl CB cyclen in 1994. [61a, 144]

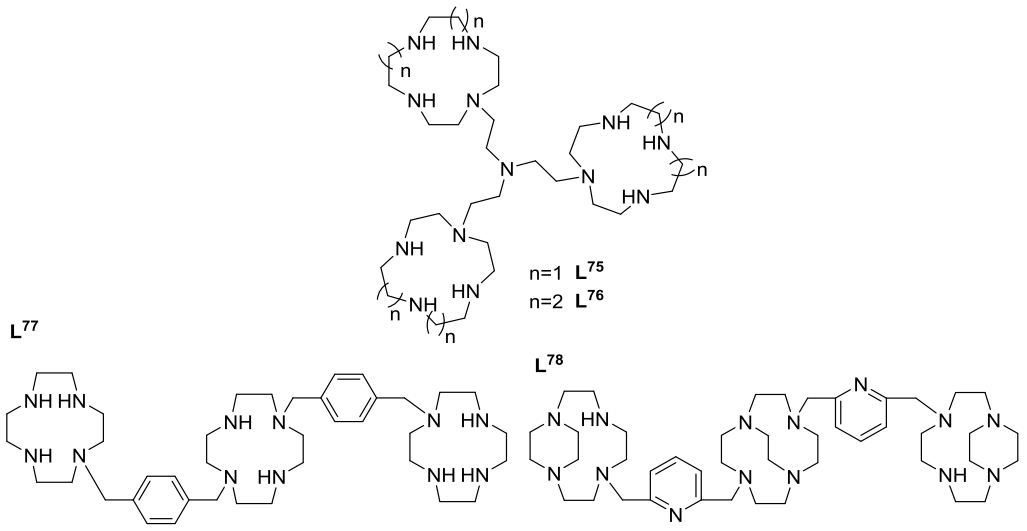

Figure 35 – Structures of cyclen tris-macrocycles, L^{75}-L^{78} [90, 141-142]

2.3.1.2. Cyclam Based Tris-Macrocycles

Luengo *et al.* patented **L^{79}**, see Figure 36, in 2000 as a CXCR4 antagonist for treatment of thrombocytopenia.[145] Dong *et al.* synthesised **L^{79}** a few years later and coordinated it to copper(II), nickel(II), zinc(II) and cadmium(II).[146] The first report of **L^{80}**, see Figure 36, was by Sun *et al.* who synthesised the tris-macrocycle by reacting tri-tosylate cyclam with 1,3,5-tris(bromo-methyl)benzene.[147] Sun *et al.* reported that a mixture of products was obtained upon heating this reaction at reflux. Deprotection to yield **L^{80}** was achieved by heating the crude macrocycle at 70°C for 10 h with HBr-AcOH and purifying by ion-exchange chromatography. Dong *et al.* published an alternative synthetic route to **L^{80}** which involved reacting an excess of 1,4,8-tri-BOC protected cyclam with 1,3,5-benzenetricarbonyl trichloride.[148] Removal of BOC was facilitated by addition of hydrochloric acid and removal of carbonyl groups on the linker group with dimethylsulfide borane complex. **L^{80}** was coordinated to mercury(II) by Sun *et al.* and its interactions with histidine guests were investigated by the group along with Chartres *et al.*[147, 149] The ligand was also coordinated to zinc(II) by Dong *et al.* who studied the ligands coordination behaviour.[150] Comba *et al.* outlined a two-step synthesis to **L^{81}**, see Figure 36, in 2002. It was synthesised from N,N'-bis(2-aminoethyl)-1,3-propanediamine utilising a copper(II) template. The copper(II) complex was reacted with melamine and formaldehyde, in the presence of triethylamine. The mixture of mono-, bis- and tris- complexes formed was separated by column chromatography. The complexes were intended to be hosts for organic and inorganic guest molecules.[151] More recently, RamLi *et al.* published **L^{82}** and **L^{83}**, see Figure 36, which target Tag-72 antigen in ovarian and colorectal cancers when conjugated to B72.3 mAb. **L^{82}** was investigated for use in nuclear imaging through complexation to $^{64}Cu^{2+}$. However, it was noted that the central macrocycle showed weaker binding to $^{64}Cu^{2+}$ resulting in 20% loss of $^{64}Cu^{2+}$ after 24 h.[152] The synthesis involved reacting 1,4,8-tri-BOC protected cyclam

with cyclam containing 4-(chloromethyl)phenyl methanone di-substitution at the 4,8-N position and 4-nitrobenzyl substitution at the 6-C position in the presence of caesium carbonate and potassium iodide.[153]

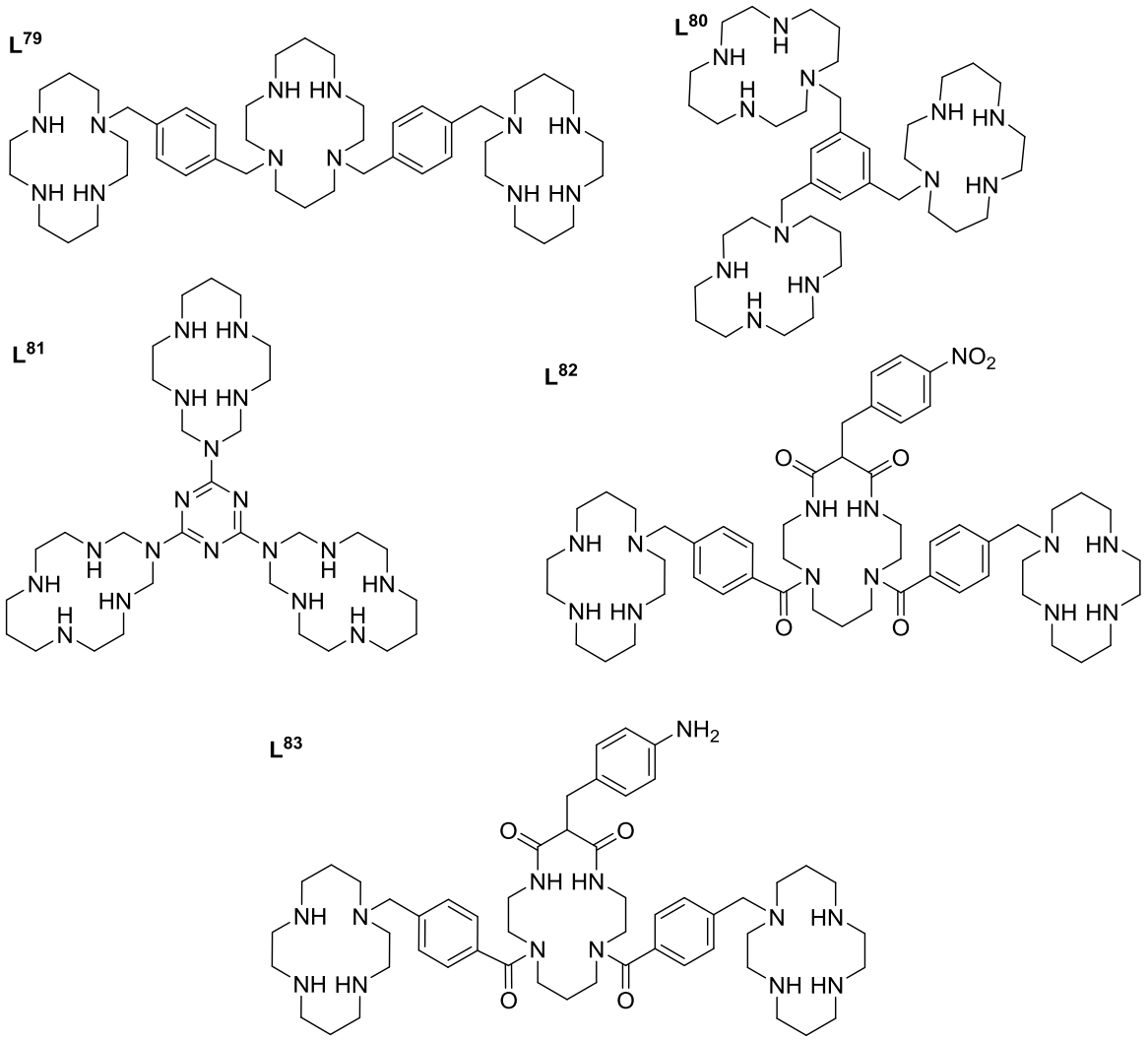

Figure 36 – Cyclam structures of tris-macrocycles, L[79],[145] L[80],[149] L[81],[151] L[82] and L[83] [152-153]

2.4. SYNTHESIS OF TRIS-MACROCYCLES

2.4.1. Synthesis of tris-macrocycles precursors

A vast quantity of work has been published about mono-macrocycles stating the ease of synthesis compared to multi-ring macrocycles, Archibald and co-workers being at the forefront of this research.[67, 102, 154] Validation for synthesising tris-macrocycles comes from the belief that a greater activity towards the CXCR4 receptor will be observed because more interactions are possible with the CXCR4 receptor. Figure 37 outlines the various synthetic routes that can be taken to synthesise tris-macrocyclic compounds, the selected route is highlighted by a dashed line. The most common route to synthesise multi-ring macrocycles is through macrocyclic precursors, therefore precursors were synthesised to provide the basis for the tris-macrocycles, see Figure 38. The synthesis of a tris-macrocycle conducted by Bencini *et al.* (**L**[78], see Figure 35) was adapted to synthesise a range of novel tris-macrocycles.[90]

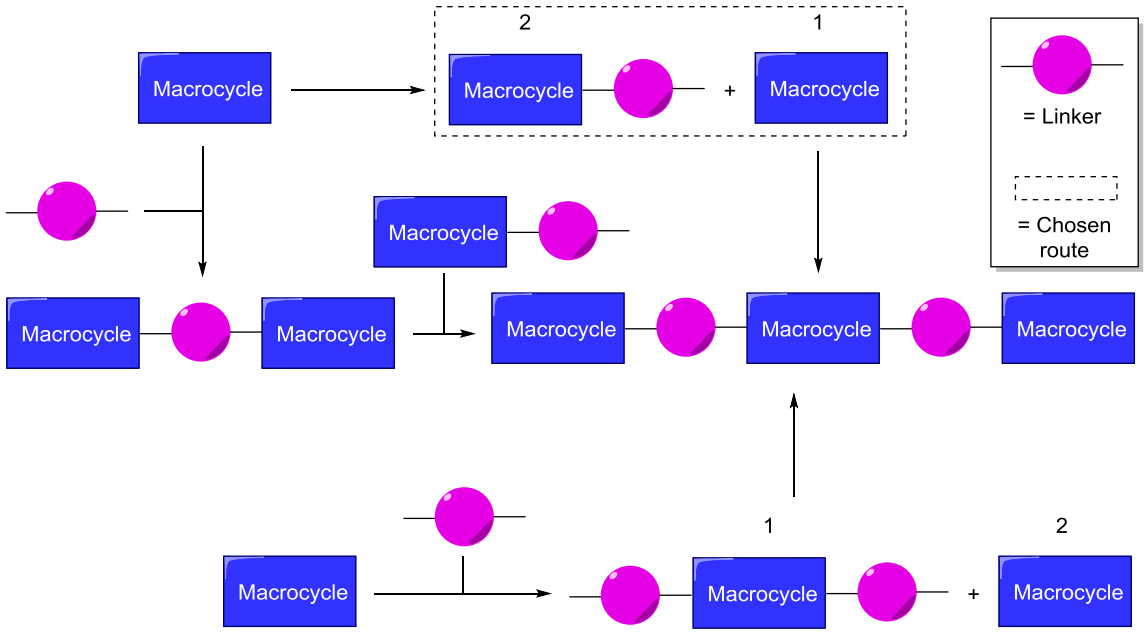

Figure 37 – Schematic of potential synthetic routes to synthesise tris-macrocyclic compounds

Configurationally restricted macrocycles were synthesised from the starting material tetraazadodecane. Cyclam (**1**) was synthesised following a modified method outlined by Barefield, see Scheme 1.[155]

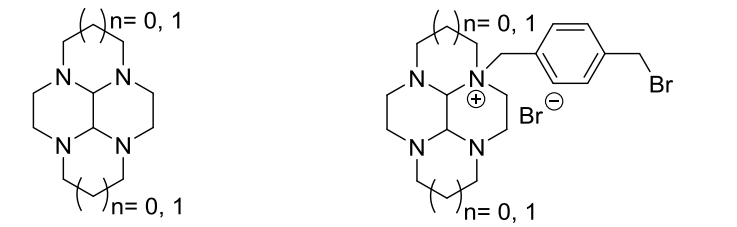

Glyoxal cyclen (n=0)
Glyoxal cyclam (n=1)

Mono-substituted glyoxal cyclam and cyclen

Figure 38- Structures of ethylene bridged precursor macrocycles

A nickel(II) template was used to force the tetraazadodecane into the desired shape so that the closed structure would form. An equimolar amount of glyoxal, tetraazadodecane and nickel(II) perchlorate was added, see Scheme 1. The nickel(II) was then removed with sodium cyanide to leave the uncomplexed cyclam. ^{1}H NMR and ^{13}C NMR corresponded with literature data and CHN confirmed the purity of **1**. Whilst cyclam has been identified as one of the earliest CXCR4 antagonists its structure is not rigid enough to remain in the most active conformation. Consequently, bridges can be added to rigidify the structure, which can then be derivatised to form more active compounds.

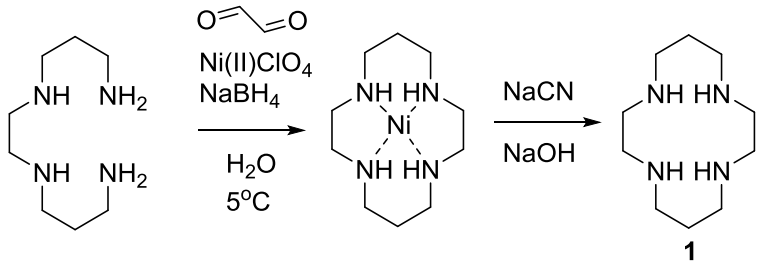

Scheme 1 – Synthesis of cyclam (1)

Glyoxal cyclam, **3**, was synthesised following an adapted method by Le Baccon *et al.*, all batches achieved excellent yields in excess of 80% which was comparable to the literature yield.[156] The reaction was cooled to -10°C and glyoxal was slowly added to avoid polymerisation. The crude product was purified with diethyl ether to separate it from any polymeric material and thoroughly dried to remove water produced during the reaction. **3** was characterised by NMR, in which the characteristic H_{aminal} and C_{aminal} peaks were present, and is supported by MS data. Compound **4**, formaldehyde cyclam, was synthesised by reacting cyclam and aqueous formaldehyde, removing the solvent and then purifying by sublimation, the method was obtained from Alder *et al.*[157] The experiment was conducted multiple times whereby yields of over 80% were obtained. The NMR spectra conclude that compound **4** was isolated as the NH peak was replaced by the characteristic H_{aminal} peak. The synthesis of **3** and **4** is shown in Scheme 2.

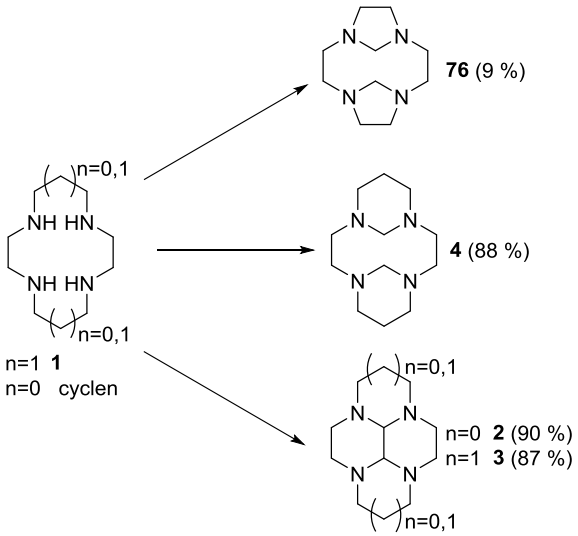

Scheme 2 - Synthesis of formaldehyde cyclam (2), formaldehyde cyclen (76), glyoxal cyclam (3) and glyoxal cyclen (4)

Cyclen derivatives of **3** and **4** were subsequently synthesised. A yield of 90% was achieved for **2**, NMR data confirmed that no polymer was present and adequately characterised the compound. The synthesis of **76** using the method outlined by Alder *et al.* was successful but the product was not able to be purified as it remained an oil even after extensive drying under high vacuum.[157] Consequently, an alternative method by Royal *et al.* was attempted.[158] This involved stirring a solution of cyclen in DCM and 30% aqueous NaOH. Unfortunately, MS analysis revealed that only one methylene bridge had formed. Thus, the reaction was modified and the reaction time was increased to 5 d and heated at 40^{o}C. This resulted in **76** being isolated but in low yield due to loss of product during unsuccessful crystallisation yet **76** was characterised by MS and NMR which showed the distinct H_{aminal} and C_{aminal} peaks. Tris-macrocycles containing **76** were not investigated due to time constraints but this synthesis provides an avenue for future studies.

The incorporation of an ethylene bridge into the macrocycles to form a bisaminal species was important because it mediates the reactivity of the amine groups. This is more clearly seen in the structures of glyoxal cyclam reported previously by Gluzinski *et al.*[159] In Figure 39 it can be seen that the rigid bis-aminal bridge creates a chair configuration causing two of the nitrogens to point onto the fold of the macrocycle, termed *endo* nitrogens, and two to point outwards, termed *exo* nitrogens. The *endo* nitrogens are sterically hindered and therefore do not act as nucleophiles, though the *exo* nitrogens are available, resulting in addition of groups solely on the adjacent nitrogen atoms.

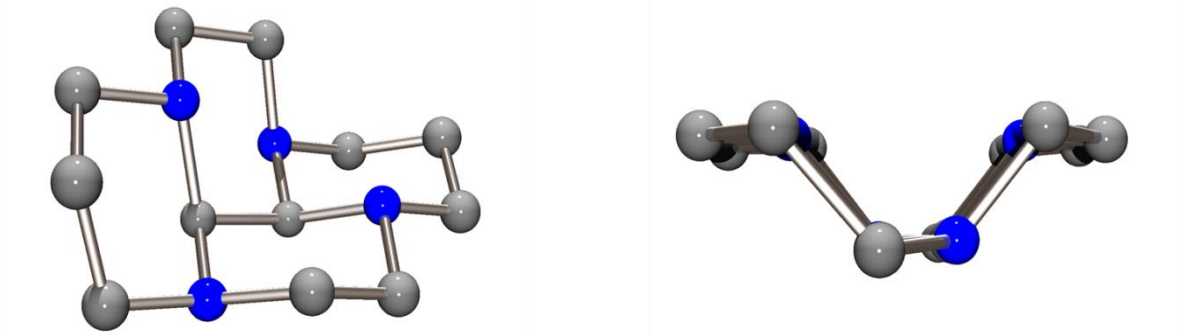

Figure 39 - X-ray crystal structures deduced (reproduced from Gluzinzki *et al.*)[159]. Grey balls represent carbon atoms and blue balls nitrogen atoms, hydrogen atoms have been omitted for clarity.

Addition of a pendant arm to **2** and **3** was performed following a modified method established by Le Baccon *et al.*[156] Whilst Le Baccon *et al.* continued the reaction for 10 d attaining a yield of 87% the yield was not impeded after 3 d and 98% was achieved for **9** in THF, see Scheme 3. The first method for adding pendant arms was established by Kolinski *et al.* in 1995, but since then Archibald and co-workers have lead the research area incorporating novel pendant arms.[77, 81, 102, 154, 160] Del Mundo *et al.*'s modified method produced **5** in an almost quantitative yield which was comparable with the closest comparison in the literature, 1-(biphenyl)methyl−glyoxal cyclen bromide, whereby a yield of 90% was attained.[161] The solubility of **5** was poorer than **9** but NMR and MS data were obtained. The high yield required just a 3 h reaction time and this is most likely due to the high concentration of the solution. The molar equivalence of the pendant arm prevented the formation of di-substituted product (bis-macrocycle).[162] Le Baccon *et al.*'s method was not followed because it resulted in formation of the dis-substituted product.[156] Both compounds were fully characterised.

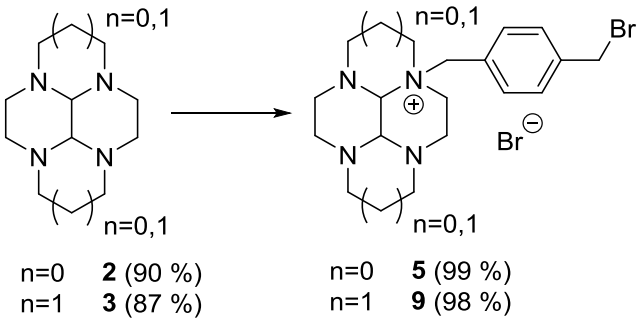

Scheme 3 - Synthesis of mono-substituted tris-macrocycle precursors (6 and 7)

2.4.2. Synthesis of Tris-Macrocycle Quaternary Salts

The synthesis of tris-macrocycle quaternary salts was first conducted by Bencini *et al.* in 2009 who published the structure of **L[78]**, see Figure 35.[90] Since then there have not been any further publications regarding rigidified tris-macrocycles. Work within our group has shown that linear tris-macrocycles could be more effective at inhibiting the CXCR4 receptor, against a conformation specific monoclonal antibody, compared to a non-linear tris-macrocycle whereby three macrocycles were bound to a central linker group.[163] An overview of the synthesis of the tris-macroycle

quaternary salts, **10**-**15**, is shown in Scheme 4. Bridged cyclams (**3**, **4**) and bridged cyclen (**2**) were added to a two molar equivalent excess of mono-substituted bridged cyclam (**9**) or cyclen (**5**), see Scheme 4. To ensure the reaction went to completion the reaction time was increased to 14 d. In general, yields of over 50% were achieved, see Scheme 4. The range of yields may have resulted from the filtration method used to isolate the product which resulted in loss of product during transfer between reaction vessels. An improvement for this could be to reduce the solvent *in vacuo* and then wash the residue to remove impurities. An alternative solvent was tested for the synthesis of **15** inspired by the work of Bernier *et al.* who used a mixture of DMF and MeCN to synthesise di-substituted glyoxal cyclen.[164] An excellent yield, 90%, was achieved for Bernier *et al.*'s di-substituted macrocycles which may have been due to an increased solubility of the macrocycles in DMF. **15** was attained in 94% yield which was comparable with Bernier *et al.* but significantly higher than the yields obtained for **11**-**14**, see Scheme 4. This new method could be repeated for the other macrocycles to determine whether higher yields can be obtained or if **15** was an anomalously high result.

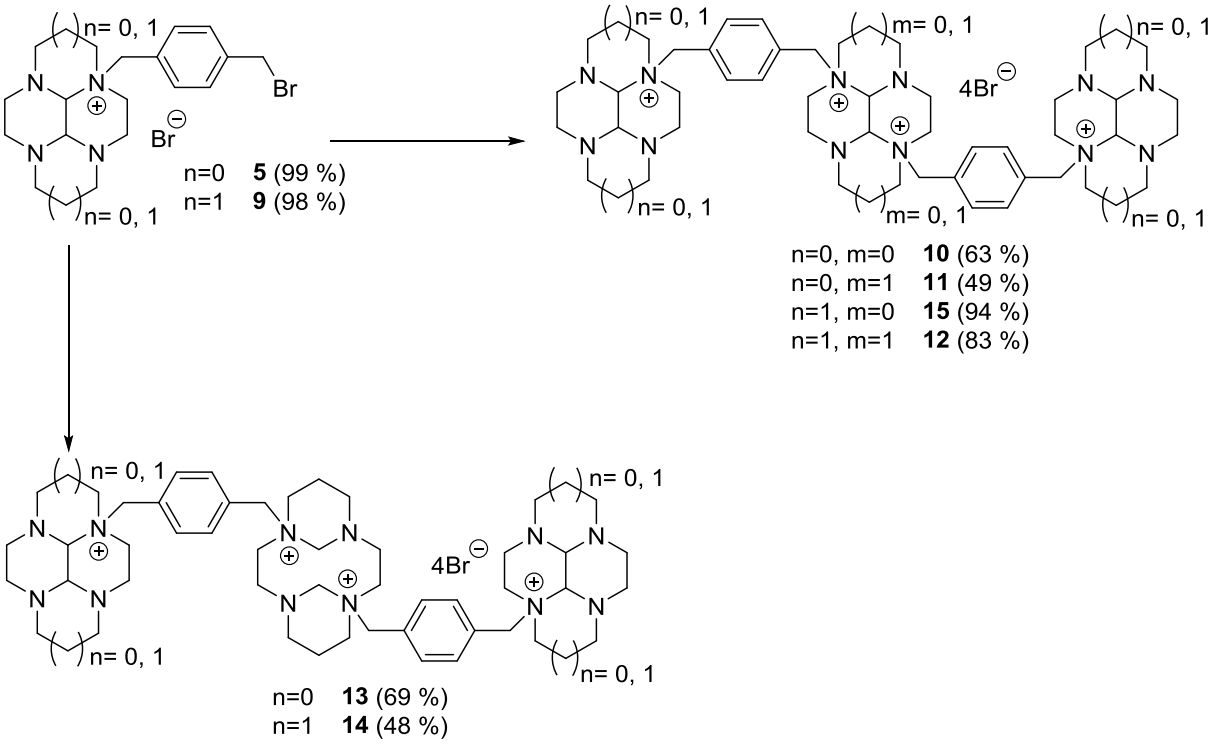

Scheme 4 - Synthesis of tris-macrocycle quaternary salts

An issue experienced during the synthesis of tris-macrocycle quaternary salts was their poor solubility which caused difficulty when obtaining ^{13}C NMR and MS data. Poor solubility was believed to be the reason for the macrocycles flying poorly in the MS instruments. MALDI-TOF MS may assist in characterising the compounds as mass ions of similar reported macrocycles were identified using this technique.[90] The distinctive isotope pattern generated by a bromine containing compound was

used to indicate whether the desired products had been isolated. Its disappearance implies that the nucleophilic substitution reaction, involving the bromine and the nitrogen, has occurred. In all cases, **10**-**15**, were clearly characterised by ^{1}H NMR due to the additional peaks in the aromatic region and the extra H_{aminal} peaks at around 4 ppm with the disappearance of the CH_2-Br peak present in the starting material. It was also possible to obtain ^{13}C NMR for **12**, **14** and **15** as they had greater solubility. Examples of ^{1}H and ^{13}C NMR spectra are shown in Figure 40 and Figure 41 for **12;** the complexity of the ^{1}H NMR spectrum is due to the high number of inequivalent proton environments in the nonplanar macrocyclic structure. Once the macrocycles were reduced their solubility significantly increased and full characterisation could be obtained. Elemental analysis indicated that **10**, **11**, **13** and **15** contained impurities.

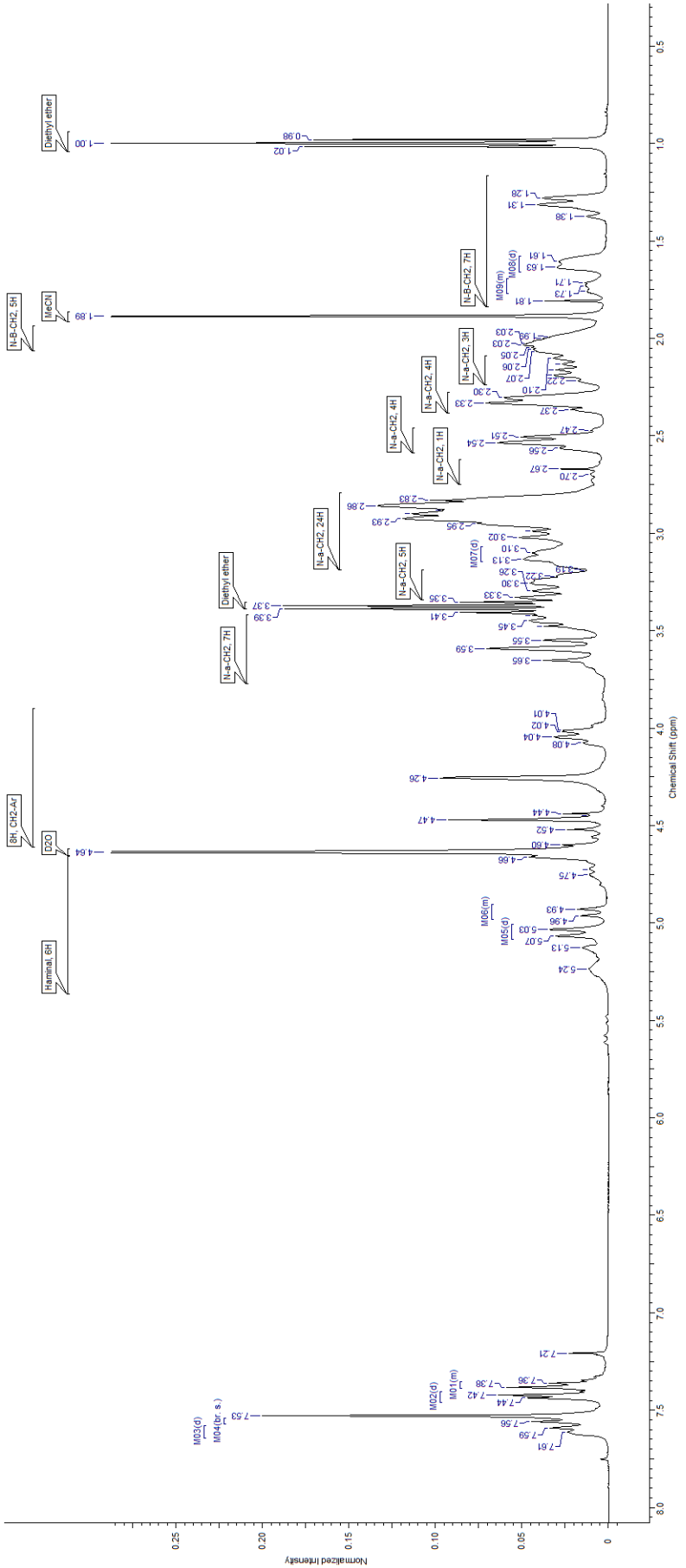

Figure 40 - ^{1}H NMR spectrum of 12

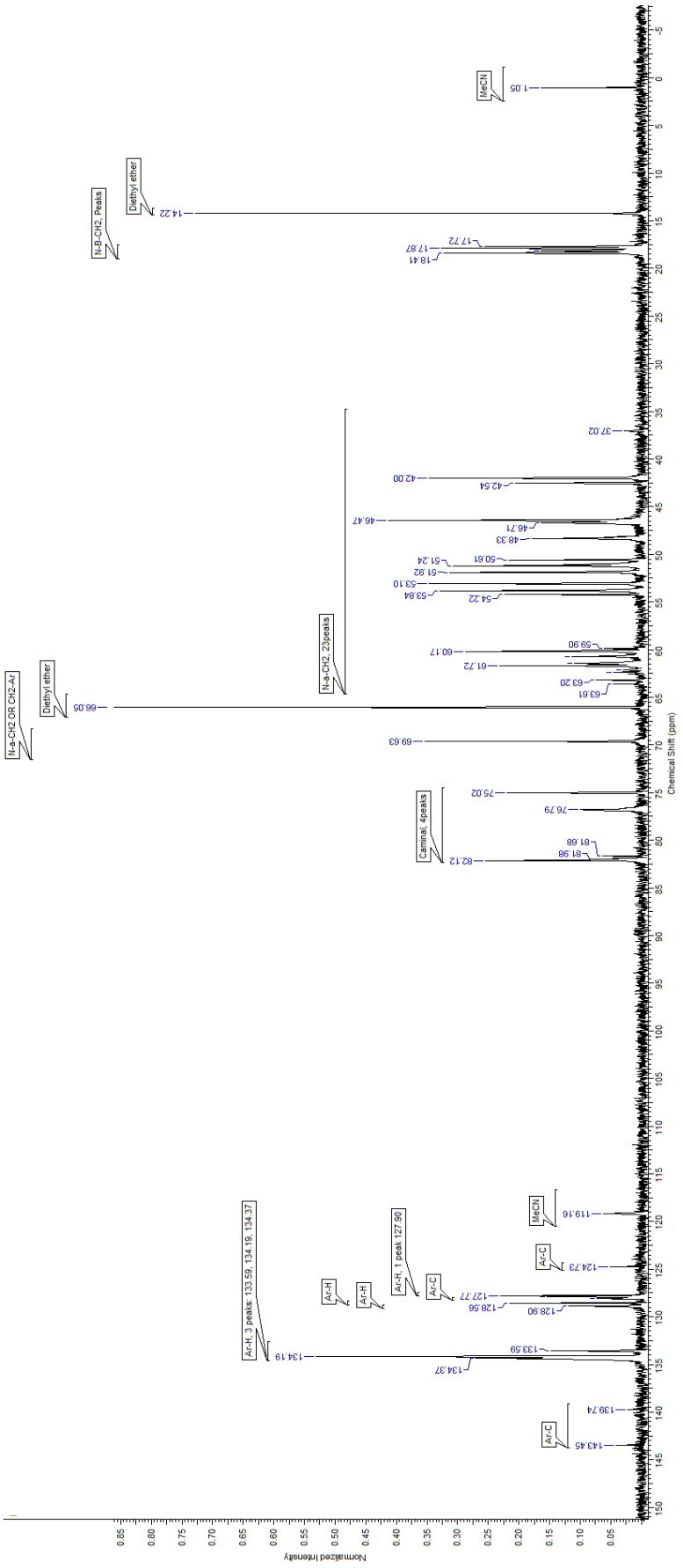

Figure 41 – ^{13}C NMR spectrum of 12

2.4.3. Reduction of Tris-Macrocycle Quaternary Salts

The reductions of **10**-**15** were carried out using sodium borohydride, see Scheme 5.[61b] The reductions of **10**-**12** took longer than **13** and **14**, 10 d *vs*. 1 d because compounds **10**-**12** contain a configurationally restricted CB in the central macrocycle and this takes longer to form than a SB. An extraction in the work-up utilises a strongly basic (pH 14) aqueous layer to deprotonate the macrocycle and facilitate extraction into organic solvent. Overall, good yields were obtained and the compounds were fully characterised, example ^{1}H and ^{13}C NMR spectra of **19** are shown in Figure 41 and Figure 42. Lower yields of 39% and 40% were obtained for **18** and **20** respectively; an explanation for this is that product may not have been extracted efficiently from the aqueous layer during the basic work up. Disappearance of C_{aminal} peaks from ^{13}C NMR spectra for the compounds confirmed a successful reaction. Elemental analysis indicated that **16** and **17** were not pure. Further investigation into the ratio of reagents to optimise the yields is required.

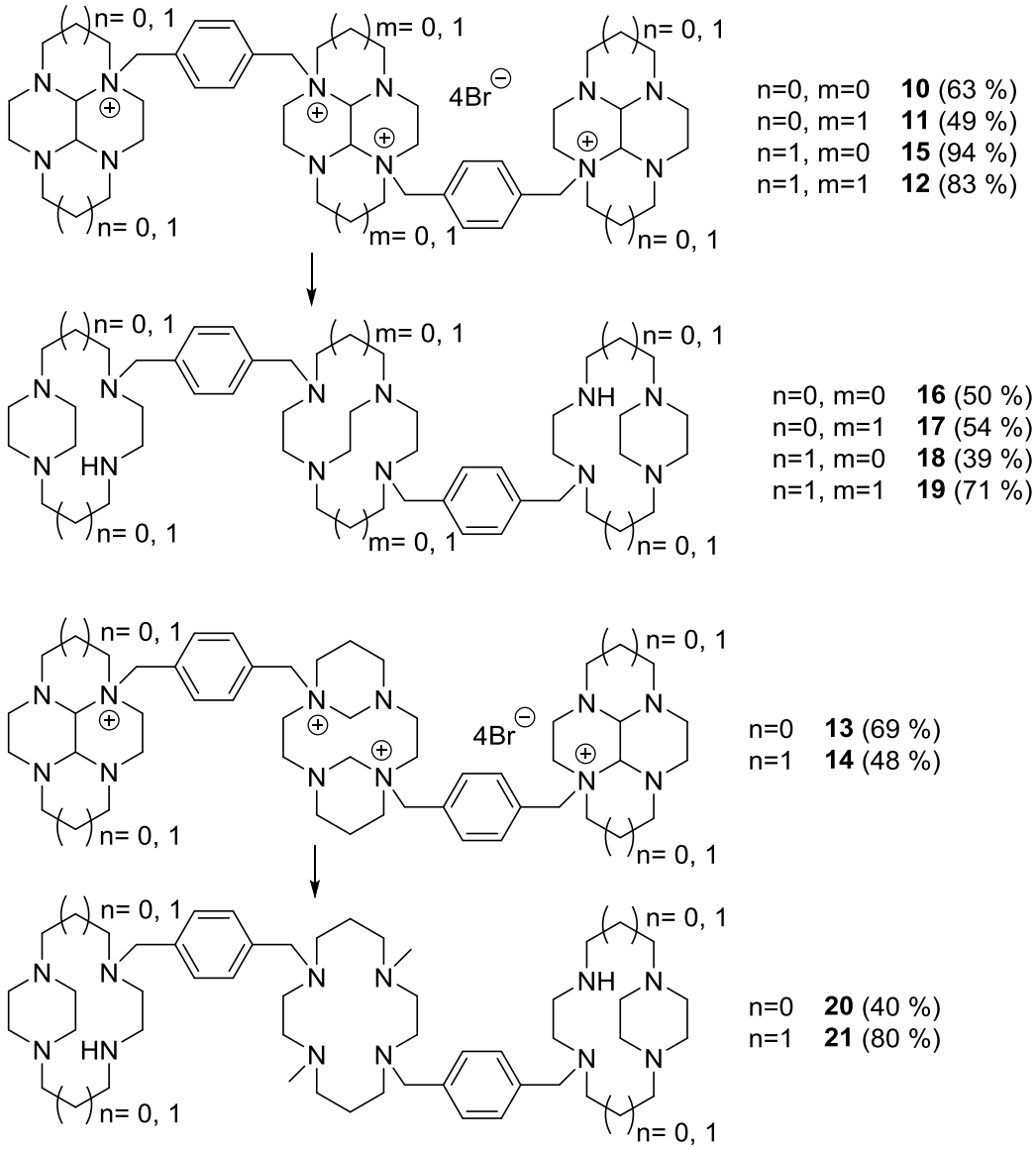

Scheme 5 – Reduction of tris-macrocycles with sodium borohydride (14, 15, 17, 18 and 19)

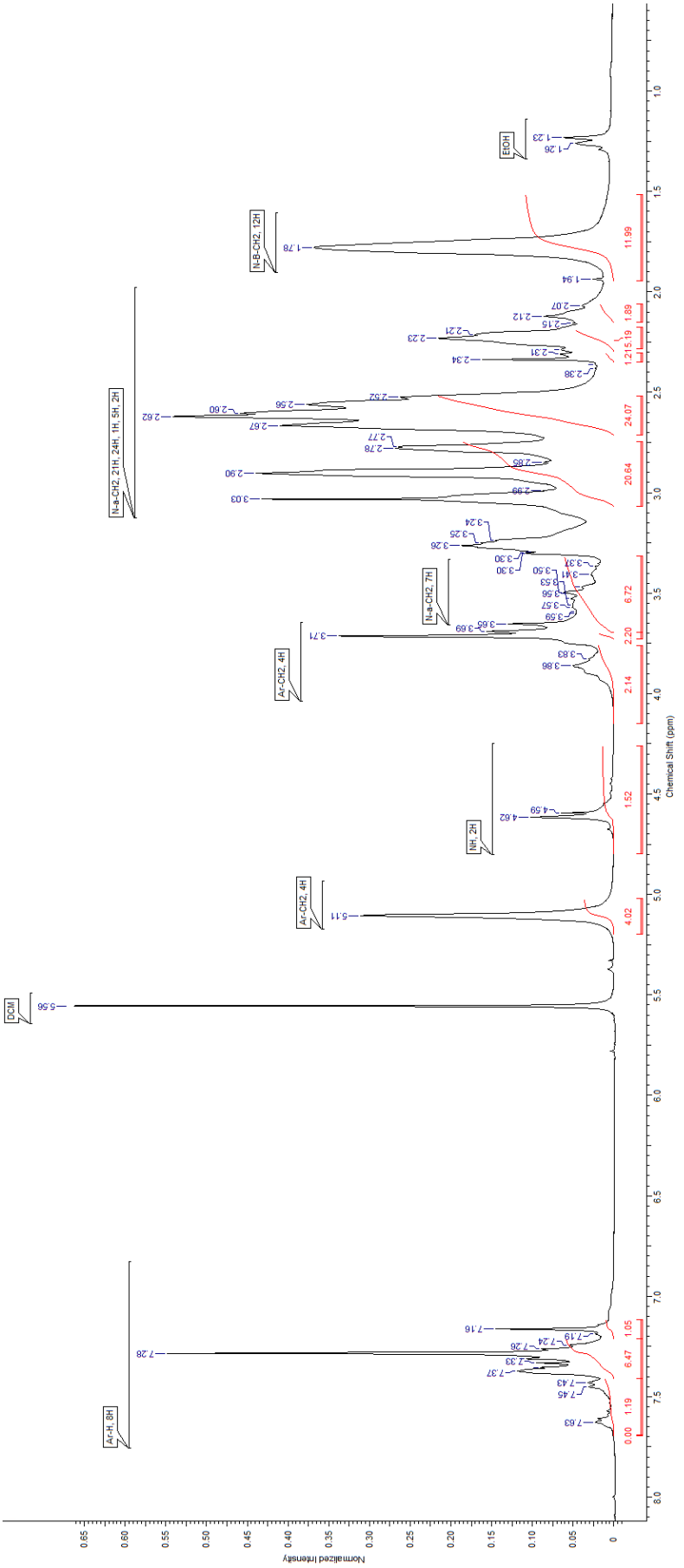

Figure 42 – ^{1}H NMR spectrum of 19

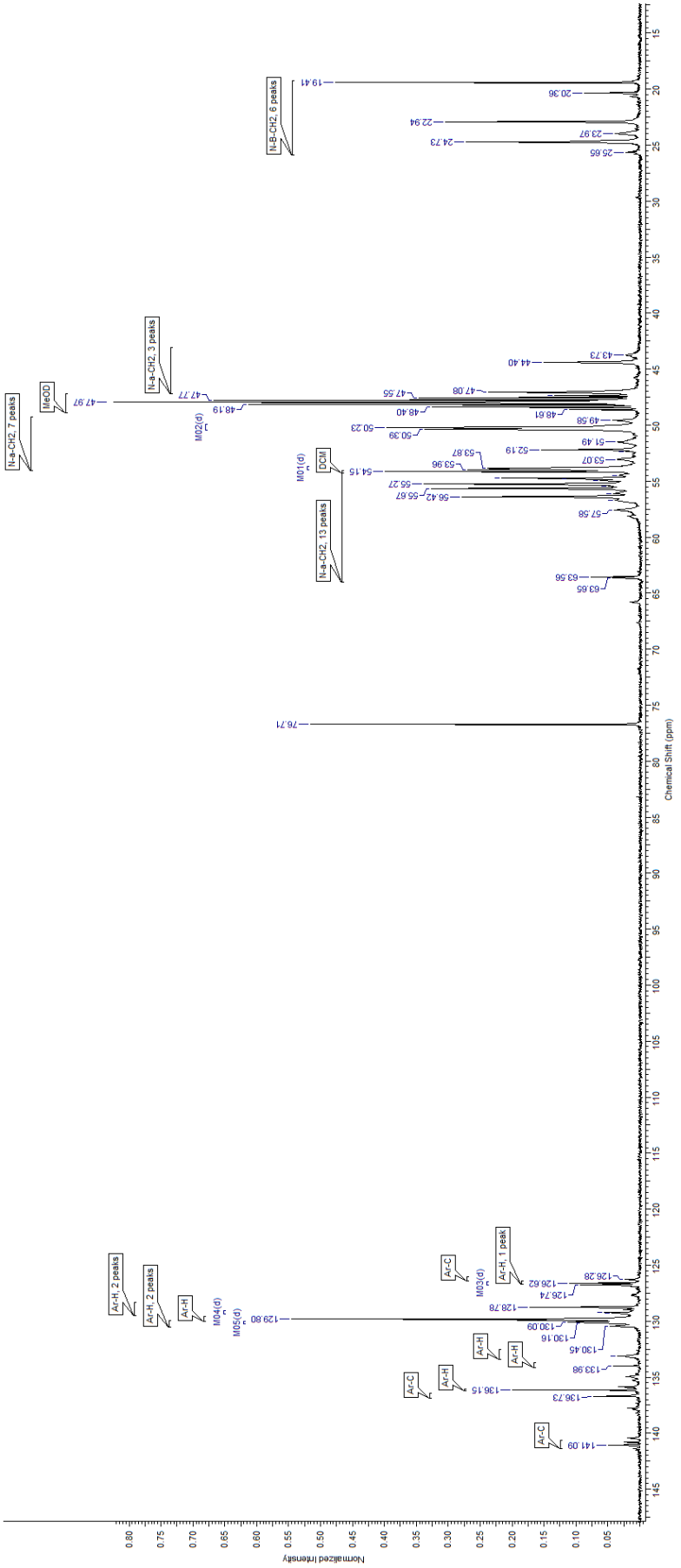

Figure 43 – ^{13}C NMR spectrum of 19

2.4.4. Synthesis of tris-macrocycle metal complexes

The cavity size as well as their tetradentate capability means that macrocycles are ideal for chelating metal ions. Metal ions particularly suited for macrocycles are divalent transition metals with a radius of <0.75 Å.[165] Alcock *et al.* reported the ideal ionic radius ranged between 0.65-0.70 Å to best fit the M-N bond length of 2.06 Å.[166] There are six possible conformations that a cyclam complex can adopt and these were defined by Bosnich *et al.* in 1965, see section 1.2.3.5 Figure 15 part A.[167] Previous research has identified copper(II), nickel(II) and zinc(II) as metals that can dramatically enhance binding to CXCR4 when coordinated to macrocycles and these metals were selected for investigation with tris-macrocycles.[71a, 168] The increase in activity can be explained by the difference in the way free ligands and metal complexes bind to the CXCR4 receptor and would theoretically originate from either an enhancement in bond strength or additional bonds with CXCR4 receptor residues. The residues available for zinc(II) to bind to the CXCR4 receptor are histidine and acidic residues such as glutamate and aspartate.[168] On the extra-cellular TMs of the CXCR4 receptor there are multiple points of interaction for CXCR4 antagonists. It was identified by Gerlach *et al.* that two acidic amino acids were important for binding AMD3100: Asp^{171} and Asp^{262}.[57a] AMD3100 binds through three hydrogen bonds to oxygen atoms on these aspartate residues. In the presence of a transition metal, such as zinc(II), a coordinate bond forms in addition to a hydrogen bond to the aspartate residues. Thus, the reason for increased activity for metal complexes is due to the formation of a stronger bond and this is shown in Figure 40.[168]

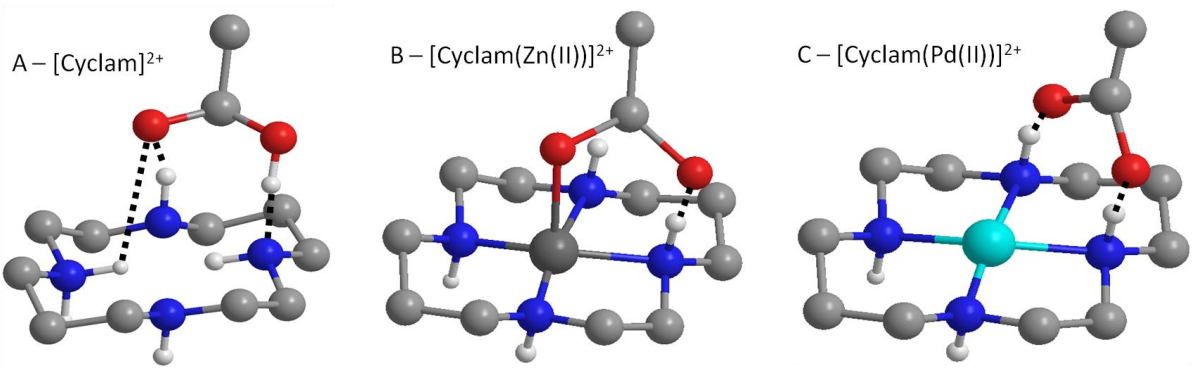

Figure 44 – Crystal structures of cyclam and metal complexed cyclam binding to a carboxylic residue representing binding to aspartate residues on the surface of the CXCR4 receptor (adapted from Gerlach *et al.*)[168]
Blue balls represent nitrogen atoms, grey represent carbon atoms, white are hydrogen atoms, dark grey is a zinc atom and cyan is a palladium atom. Non-polar hydrogen atoms have been omitted for clarity.

AMD3100 can be a pro-drug as it binds to zinc(II) in the blood to produce $[Zn_2AMD3100]^{4+}$ as the active drug. The zinc(II) complex is 6-fold more active than AMD3100 alone, the nickel(II) complex shows slightly higher activity but the copper(II) complex only had a marginal improvement in activity compared to AMD3100.[168] The flexibility of the cyclam structure enables the metal configurations to switch around, the introduction of a side or cross bridge can be used to restrict the configuration of metal complexes to one of six possiblilites, ideal when forcing the macrocycle to take on the most

biologically active configuration, *cis*-V, see Figure 45. Nickel(II) can form different geometries, either square planar or octahedral with additional donors. Its effect on CXCR4 binding with configurationally restricted macrocycles was investigated by Archibald and co-workers.[67] They found that a nickel(II) complexed *para*-SB bis-cyclam was 2 fold more effective at inhibiting CXCR4 than AMD3100 and significantly more active than a nickel(II) complexed *meta*-CB bis-cyclam.[67] The SB complex was highly potent with EC_{50} values as low as 13 nM. Zinc(II) can take on square pyramidal and octahedral geometries but not square planar, therefore there are one or two vacant sites when zinc(II) is coordinated to a tetraazamacrocycle.[169] SB-cyclam zinc(II) complexes have been shown to adopt a *trans*-II configuration, see Figure 45. The crystal structure of bis-SB-cyclam zinc(II) complex was determined by Valks *et al.* and findings showing binding to an acetate group supported those of Gerlach *et al.*[71b, 168] Valks *et al.* observed that zinc(II) binds one acetate group in an anisobidentate manner with bond lengths between zinc(II) and oxygen being 2.112 Å and 2.407 Å in length.[33] The second acetate group associated with the zinc(II) ion is not involved with binding.[71b] This indicates that zinc(II) complexes bind in a octahedral geometry with one acetate group coordinated to two vacant sites. In a SB complex the metal is pushed out of the cavity and this enhances binding by forcing it into the binding pocket of the CXCR4 receptor.[71b] The displacement of copper(II) from the macrocyclic cavity is not as pronounced as zinc(II), 0.19 Å compared to 0.75 Å respectively.[84] As zinc(II) complexes tend to be more active compounds the greater displacement from the cavity could provide an explanation. As the zinc(II) ion is further out of the macrocyclic cavity it is forced into the binding pocket so a better interaction with aspartate residues is potentially possible. Macrocycle copper(II) complexes have been shown to adopt five coordinate geometries. Due to Jahn-Teller distortion the M-N bonds are shorter than equivalent zinc(II) complexes.[84]

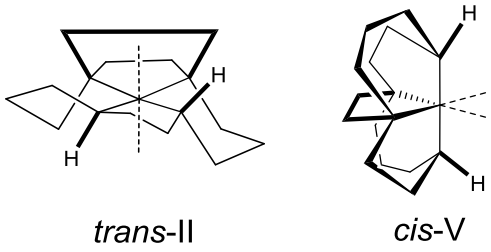

Figure 45 – Select configurations formed by tetraazamacrocycle metal complexes (adapted from Bosnich *et al.*)[167]

The novel tris-macrocyclic compounds synthesised in this work incorporate both SB and CB macrocycles as well as di-methylated macrocycles. Valks *et al.* assessed the activity of bis-SB cyclam and its zinc(II) acetate complex against HIV-1 (III_B) and HIV-2(ROD) virus strains.[33] The compounds were found to be most effective against HIV-1 (III_B), free ligand: 6.98 µM and zinc(II) complex: 2.5 nM, however the zinc(II) complex was also highly active, EC_{50} 4 nM, against HIV-2(ROD). Tetramethyl cyclam has not been investigated as a CXCR4 antagonist so it is difficult to predict the activity of the

structure. Potentially, the less restricted tris-macrocycles, which contain a central macrocycle similar to tetramethyl cyclam, may allow more movement and a stronger interaction with the CXCR4 receptor compared to the extensively restricted tris-macrocycles containing a central CB macrocycle.

The high activity of the reported bis-SB and bis-CB compounds,[67, 71b, 81, 170] in addition to the forced single configuration, was the reason for synthesising rigid tris-macrocycle metal complexes. It was hoped that the three ring structure would enable additional interactions with the CXCR4 compared with bis-macrocycles due to the extra ring and the aspartate-rich receptor surface.[15a]

Metal complexes of tris-macrocycles **16**-**21** were synthesised using copper(II) acetate monohydrate, nickel(II) acetate tetrahydrate, zinc(II) acetate and zinc(II) chloride following the standard preparations, see Figure 46 and Figure 47.[61b, 71b] All complexes were purified via size exclusion chromatography with Sephadex LH20 and characterised by MS and CHN. The complexes were synthesised successfully however the presence of solvent in the CHN was noted, although solvent molecules are often associated with the unit cell in crystallography data. Elemental analysis suggested that $[Ni_3\mathbf{16}]^{6+}$, $[Ni_3\mathbf{18}]^{6+}$, $[Zn_3\mathbf{18}]^{6+}$ and $[Cu_3\mathbf{18}]^{6+}$ were not pure. Zinc(II) complexes were additionally analysed by NMR whilst nickel(II) and copper(II) complexes were analysed using UV-vis spectroscopy. Sephadex LH20 can lead to a loss of product of up to 30% which caused a large range of yields. The low yields of $[Cu_3\mathbf{16}]^{3+}$ and $[Cu_3\mathbf{17}]^{3+}$ were due to an old Sephadex LH20 column being used which appeared to have caused a significant loss of product, subsequently a replenished column afforded significantly higher yields, 84% for $[Cu_3\mathbf{19}]^{3+}$.

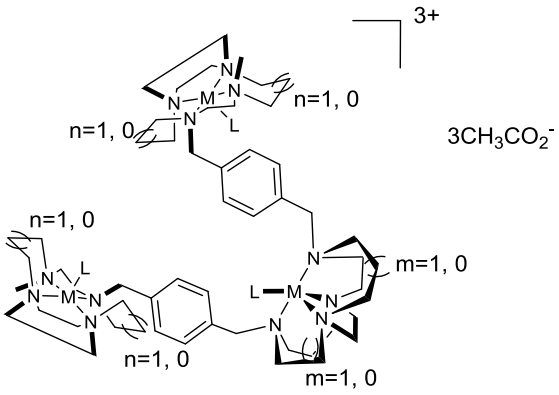

n=0			n=1		
$[Cu_3\mathbf{16}]^{6+}$	m=0,	$M^{2+}=Cu^{2+}$ (22 %)	$[Cu_3\mathbf{18}]^{6+}$	m=0,	$M^{2+}=Cu^{2+}$ (62 %)
$[Zn_3\mathbf{16}]^{6+}$	m=0,	$M^{2+}=Zn^{2+}$ (55 %)	$[Zn_3\mathbf{18}]^{6+}$	m=0,	$M^{2+}=Zn^{2+}$ (81 %)
$[Ni_3\mathbf{16}]^{6+}$	m=0,	$M^{2+}=Ni^{2+}$ (87 %)	$[Ni_3\mathbf{18}]^{6+}$	m=0,	$M^{2+}=Ni^{2+}$ (92 %)
n=0			n=1		
$[Cu_3\mathbf{17}]^{6+}$	m=1,	$M^{2+}=Cu^{2+}$ (14 %)	$[Cu_3\mathbf{19}]^{6+}$	m=1,	$M^{2+}=Cu^{2+}$ (84 %)
$[Zn_3\mathbf{17}]^{6+}$	m=1,	$M^{2+}=Zn^{2+}$ (40 %)	$[Zn_3\mathbf{19}]^{6+}$	m=1,	$M^{2+}=Zn^{2+}$ (89 %)
$[Ni_3\mathbf{17}]^{6+}$	m=1,	$M^{2+}=Ni^{2+}$ (83 %)	$[Ni_3\mathbf{19}]^{6+}$	m=1,	$M^{2+}=Ni^{2+}$ (90 %)

Figure 46 – Structures of metal complexes of tris-macrocycles 16, 17, 18 and 19
Note solvent molecules may coordinate to metal centres

Formation of a CB metal complex is harder to achieve than a SB due its limited structural flexibility, this is the reason for using harsher reaction conditions. In addition to this, protons from water or solvent molecules compete for the CB macrocyclic cavity with nickel(II) and zinc(II) which makes these complexes harder to synthesise. In some cases, with $[Ni_3\mathbf{19}]^{6+}$ for example, problems incorporating a third nickel(II) ion into the CB cavity were experienced therefore it appears that longer reaction times should be carried out to overcome this issue in the future. UV-vis data confirmed nickel(II) chelation into all macrocycle cavities of $[Ni_3\mathbf{19}]^{6+}$ by the presence of a band at around 600 nm, indicative of CB coordination geometry,[67] and a band at around 400 nm characteristic of SB macrocycle metal chelation.[67] Two distinct bands were observed for the nickel(II) complexes of **16**, **17**, **18** and **19** confirming isolation of the desired complexes. Significantly higher bands than expected were noted for $[Ni_3\mathbf{16}]^{6+}$ and $[Ni_3\mathbf{17}]^{6+}$, but higher values have been reported in the literature and attributed to steric restraint caused by distortion of the ideal geometry.[67] Copper(II) complexes of **16**, **17**, **18** and **19** were characterised by UV-vis and MS. SB, five coordinate, copper(II) complexes show absorption at around 600 nm,[81] and CB complexes have also shown bands at approximately 600 nm.[171] The presence of a distinct band at around 600 nm was observed in the UV-vis data of copper(II) complexes of **16**, **17**, **18** and **19** confirming copper(II) coordination within the macrocyclic cavities. As **19** contains the bulkiest macrocycles, of all the tris-macrocycles synthesised, this could explain the distortion. NMR data confirmed the isolation of zinc(II) complexes of **16**, **17**, **18** and **19** by the presence of carbonyl and methyl peaks in the ^{13}C NMR and the distinctive acetate singlet in the ^{1}H NMR at around 2 ppm.

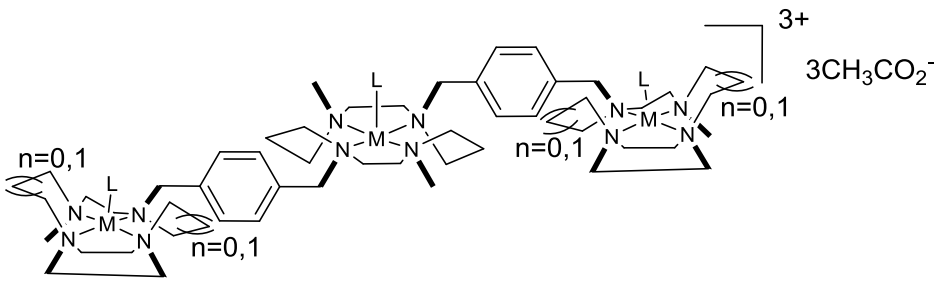

n=0

$[Cu_3\mathbf{20}]^{6+}$	$M^{2+}=Cu^{2+}$ (74 %)
$[Zn_3\mathbf{20}]^{6+}$	$M^{2+}=Zn^{2+}$ (79 %)
$[Ni_3\mathbf{20}]^{6+}$	$M^{2+}=Ni^{2+}$ (77 %)

n=1

$[Cu_3\mathbf{21}]^{6+}$	$M^{2+}=Cu^{2+}$ (75 %)
$[Zn_3\mathbf{21}]^{6+}$	$M^{2+}=Zn^{2+}$ (60 %)
$[Ni_3\mathbf{21}]^{6+}$	$M^{2+}=Ni^{2+}$ (67 %)

Figure 47 – Structures of tris-macrocycle metal complexes of 20 and 21.
Note solvent molecules may coordinate to metal centres

All metals, zinc(II), copper(II) and nickel(II), were chelated successfully to **20** and **21** according to UV-vis data, for copper(II) and nickel(II) complexes, and NMR, for zinc(II) complexes. Characterisation *via* MS proved problematic however, this may be due to the use of metal acetate salts as the zinc(II) complexation of **21** synthesised from zinc(II) chloride showed the expected peaks. Loss of acetate salts and thermal degradation during analysis resulted in poor MS data being ascertained for this series of compounds. Elemental analysis indicated that $[Ni_3\mathbf{21}]^{6+}$, $[Zn_3\mathbf{21}]^{6+}$ and $[Cu_3\mathbf{21}]^{6+}$ contained impurities.

Some consideration was given to the potential configuration of the central macrocycle in **20** and **21** that does not contain an additional ethyl bridge (i.e. SB or CB). TMC, tetramethyl cyclam, has a very similar conformation to the central macrocycle in **20** and **21** and it can been used as a reference to predict the tris-macrocycle structure.[71c] Conversion from *trans*-II to *trans*-I has been reported for TMC nickel(II) complexes,[172] whilst Schönherr *et al.*'s molecular structure of a TMC analogue copper(II) complex identified a *trans*-IV configuration.[173] It is thought that the metal complexes of **20** and **21** contain the *trans*-IV structure for this central ring as this structure is believed to be the most likely due to the steric bulk of the terminal macrocycles.

The variation in shape predicted for the tris-macrocycles, shown in Figure 46 and Figure 47, may result in a different activity due to dissimilar positioning on the surface of the CXCR4 receptor. The activity of the tris-macrocycle metal complexes is predicted to be higher than reported bis-macrocycles due to the additional interactions with the receptor that are possible.

2.5. CONCLUSIONS

This chapter discusses the synthesis of novel configurationally restricted linear tris-tetraazamacrocycles. Tris-macrocycles incorporating CB and SB cyclam and cyclen along with their corresponding copper(II), nickel(II) and zinc(II) complexes were synthesised. Copper(II), nickel(II) and zinc(II) complexes of tris-macrocycles containing SB cyclam and cyclen and TMC were also investigated. The synthesis of unsymmetrical tris-macrocycles has not been previously reported. Some issues were encountered in obtaining a full set of analytical data for all of the compounds.

The advantage tris-macrocycles offer is that they can potentially interact with multiple aspartate residues on the CXCR4 receptor thus enhancing affinity. Furthermore, as opposed to AMD3100 whereby patients suffered cardiotoxic side effects, due to the chelating ability of the secondary amines, the tris-macrocycle complexes will not be able to chelate other metal ions consequently making the compounds more attractive as CXCR4 antagonists. A range of compounds were synthesised to determine what effect, if any, alterations to macrocycle ring size and bridges made to activity towards the CXCR4 receptor. Their ability to act as CXCR4 antagonists is evaluated and discussed in 5.3.4.

2.6. FUTURE WORK

It would be interesting to synthesise a series of tris-macrocycles containing formaldehyde cyclen, **76**. It would be advantageous to compare the activity of these to the activity of the metal complexes of **16**-**21**.

Alternatively, tris-macrocycles containing TMC or tetramethylcyclen in the terminal positions could be explored, although a reduction in affinity may be observed due to lack of configurational restriction. An alternative collection of macrocycles to explore could be tris-CB macrocycles, see Figure 48. Combinations of theses macrocycles could also be studied.

If the general trend of increasing number of rings results in higher CXCR4 affinity then tetrakis-macrocycles and pentakis-macrocycles may be even more active. It would be interesting to synthesise these compounds and explore this theory, however the molecular weight will be higher than those generally accepted in drug design but the advantages of higher activity may overcome this factor. A literature example of this is high molecular weight peptides which have shown potential as anti-metastatic agents.[174]

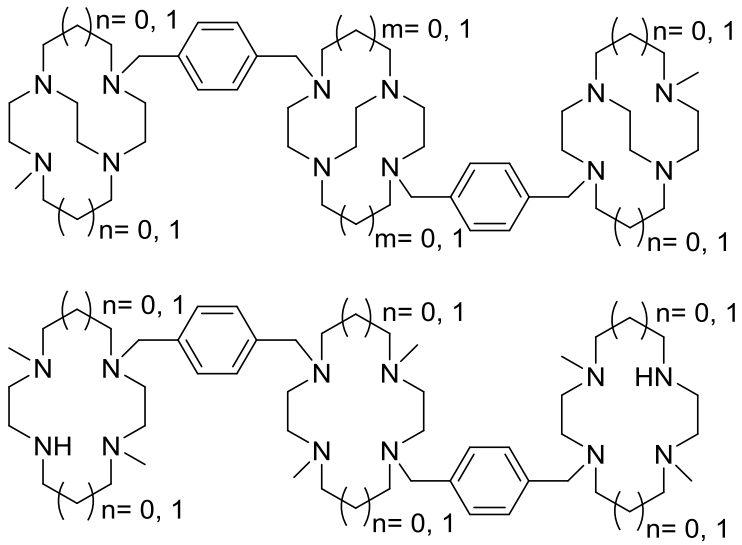

Figure 48 – Structure of potential tris-CB cyclam and tris-CB cyclen macrocycles

CHAPTER THREE

SYNTHESIS OF NOVEL LINEAR BIS-MACROCYCLES AND THEIR METAL COMPLEXES

3.1 SYNTHETIC STRATEGY

The synthesis of novel linear bis-macrocycles was explored. Incorporation of ethylene bridges led to the creation of configurationally restricted CB and SB macrocycles. These novel bis-macrocycles were coordinated to copper(II) and zinc(II) divalent metal ions. Terminal functional groups were modified for the conjugation of imaging groups. Macrocycles containing unconjugated functional groups were complexed to divalent metals copper(II) and zinc(II) to produce a novel library of unsymmetrical bis-macrocycles.

3.2 PAST STRATEGIES

The AMD3100 story was initiated by the Johnson Matthey Technology centre in 1994, since then De Clercq *et al.* and others have synthesised and evaluated a wide variety of bis-macrocycles as CXCR4 antagonists. Many of these bis-macrocycles do not contain configurationally restricting ethylene bridges which are known to stabilise metal complexes.[175]

3.2.1 C-C Linked Bis-Macrocycles

The majority of bis-macrocycles are linked through nitrogen atoms within the macrocycle ring, although there are a couple of examples of carbon-carbon linked bis-macrocycles.[47, 176] The first bis-macrocycle to show high anti-HIV activity was a bis-cyclam macrocycle, **JM1657**, see Figure 5 section 1.2.2. It was synthesised accidently during the synthesis of cyclam and had high anti-HIV activity, EC_{50}: 0.144 µM, and low toxicity, CC_{50}:3 19 µM.[47] An explanation for the lack of C-C linked bis-macrocycles may have originated from the quantitative structural activity relationship (QSAR) study conducted by Joao *et al.* in 1995.[176] Joao *et al.* studied a range of analogues of AMD3100, using QSAR, and generated accurate anti-HIV activity and cytotoxicity predictions. Compounds were built using molecular modelling software based on cryallographic X-ray structure of $[Ni_2[\mathbf{L^{84}}]4ClO_4^-$, see Figure 49, outlined by McAuley *et al.*[177] Predicted values correlated well with experimental data. The bis-cyclam $\mathbf{L^{85}}$, linked through carbon atoms, see Figure 49 $\mathbf{L^{85}}$, was predicted to have low anti-HIV activity compared to many other N-N linked bis-macrocycles.

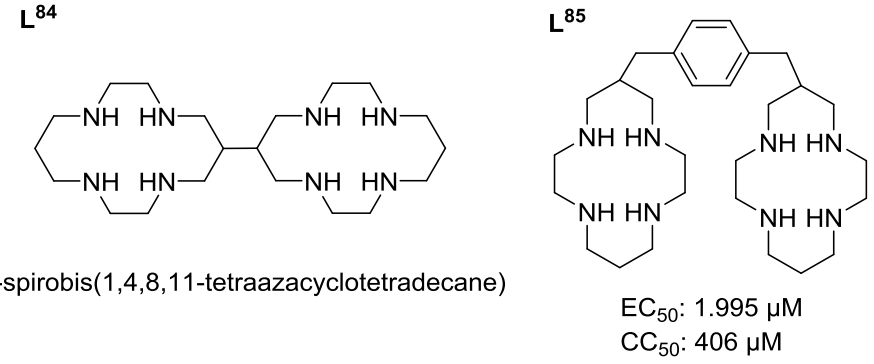

Figure 49 – Structure of C-C linked bis-macrocycles L^{84} by McAuley *et al.*[177] and L^{85} Joao *et al.*[176]

3.2.2 N-N Linked Bis-Macrocycles

A wealth of 12-16 membered N-N linked bis-macrocycles are reported,[79, 178] a large portion of these are not configurationally restricted.[79, 178a] In 1999, Esté *et al.* explored the effect different linker groups and bis-macrocycles had on anti-HIV activity,[74] following synthesis by Bridger *et al.*[79, 178a] To isolate homo-cyclam, 15- and 16-membered macrocycles, a synthetic route outlined by Hediger *et al.* was followed.[178b] Synthesis involved conjugating a bis-sulfonate acyclic precursor to a toluene sulfonamide acyclic precursor. Selective deprotection removed one amine-protecting group and the resulting macrocycle reacted with a dibromo linker group, remaining protecting groups were removed by hydrolysis, **L^{86}-L^{89}** see Figure 50. Synthesis of non-rigidified xylyl linked cyclen, 13-membered and cyclam bis-macrocycles were achieved by reacting tris-N-protected macrocycles with α-α'-dibromo-*p*-xylene,[79] or an alternative dibromo-linker, according to literature procedures.[179] Protective groups were removed with acetic acid:48% aqueous hydrogen bromide mixture (3:2), 18-48 h at 100°C, to afford **L^{90}-L^{95}** see Figure 50.[79] Attempted deprotection of bis-macrocycles containing two 12- or 13-membered rings, **L^{90}-L^{92}** see Figure 50**,** both *meta* and *para* xylyl-linked, led to cleavage of one macrocycle from the benzyl group. Successful deprotonation was achieved using Na/Hg amalgam heated at 100°C for 24-72 h. Overall, reasonable yields were achieved for all bis-macrocycles synthesised with an average bis-macrocycle yield of around 50%.

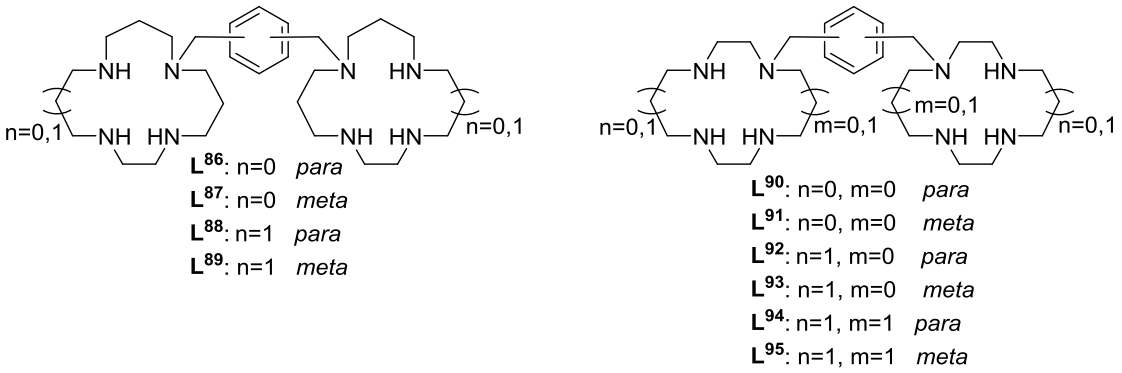

Figure 50 – Bis-macrocycles requiring deprotection with Na/Hg amalgam[79]

Bridger *et al.* synthesised a series of bis-cyclam macrocycles, using synthetic routes outlined previously,[79, 178a] exploring a wide array of linker groups in order to explain why some linkers had a detrimental effect on anti-HIV activity. Anti-HIV activity of bis-cyclam macrocycles, linked with pyridine, strongly correlated with linker substitution. 2,4- and 2,5- linked macrocycles were two times less active and exhibited higher toxicity than 2,6- and 3,5- linked macrocycles and xylyl linked macrocycles, see Figure 51, **L^{99}-L^{102}**. This change in activity was assigned to the pendant arm participating in complexation to available free zinc ions resulting in a macrocyclic configuration not optimum for binding. Alternatively, the pendant arm heteroatom may hydrogen bond to protons in the macrocycle ring in conjunction with other macrocyclic nitrogen atoms also resulting in a

configuration not ideal for binding. The pendant arm heteroatom may also compete for the macrocycle binding site. The overall charge per cyclam ring under physiological conditions is 2+ because the pK_as of the third and fourth protonations are very low, due to repulsion of the positive charges subsequent protonations do not occur.[71c, 180] The pK_a values are 11.5, 10.3, 1.6, and 0.9. Presence of a carboxylate group on the linker, see Figure 51 **L**[96]-**L**[97], resulted in low activity because its negative charge repelled the negatively charged receptor binding site.[178a] Absence of this group led to high activity, see Figure 51 **L**[98]-**L**[99]. A bulky linker group was introduced at the 6-position of the 2,4-pyridine linker, see Figure 51 **L**[104], to prevent any pendant arm conformations and anti-HIV activity was seen to increase, however it was not as active as **L**[100] and **L**[101]. In conclusion, substitution on the linker group had a significant impact on anti-HIV activity. Furthermore, presence of heteroatoms on the linker group can facilitate intramolecular interactions leading to in-active bis-macrocycles.

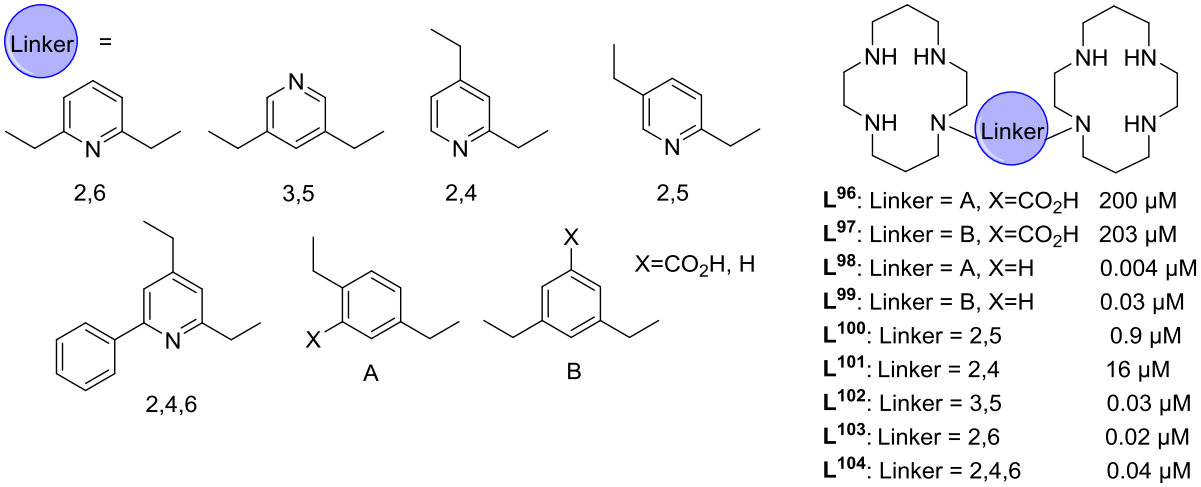

Figure 51 – Bis-macrocycles synthesised by Bridger *et al.*[178a]

A series of 14-membered bis-macrocycles containing alternative heteroatoms were synthesised by Bridger *et al.* in seven steps, macrocycles were connected through nitrogen atoms, see Figure 52.[178e] Precursors were afforded by reacting ethanedithiol and bromopropionitrile to form dithia-dinitrile, reduced nitrile groups were then protected with tosyl groups. Macrocyclisation was achieved by slow addition of ethylene glycol ditosylate to macrocycle precursor in the presence of Cs_2CO_3. Complete deprotection followed by reprotection of one amine group enabled reaction with α-α'-dibromo-*p*-xylene. The remaining protecting group was removed with Na/Hg amalgam, to isolate bis-macrocycles featuring alternative heteroatoms in two of the nitrogen atom positions, see Figure 52, **L**[105]-**L**[106]. Homo-cyclam based bis-macrocycle, **L**[107]-**L**[108], see Figure 52, were synthesised differently and only one nitrogen atom was substituted. Firstly, the amine group in iminodipropionitrile was protected with diethyl chlorophosphate (Dep) prior to nitrile hydrogenation. The resulting amine was protected with tosyl and macrocyclisation achieved by reaction with 2-bromoethyl ether.

Selective deprotection of the Dep group was achieved using hydrogen bromide and acetic acid at RT. This facilitated reaction with α-α'-dibromo-*p*-xylene followed by a final deprotection to yield bis-macrocycles **L**^{107}-**L**^{108}. Incorporation of sulfur, oxygen and carbon had a detrimental effect on anti-HIV activity, see Figure 52. **L**^{105} had over 1500 times greater EC_{50}, 6.84 μM, than AMD3100, EC_{50}: 4.2 nM, and high cytotoxicity, CC_{50}: 6.8 μM. Replacing nitrogen atoms with oxygen atoms, **L**^{106}, resulted in an inactive compound with low cytotoxicity. The optimum replacement was carbon, however anti-HIV activity was still extremely low compared to AMD3100.

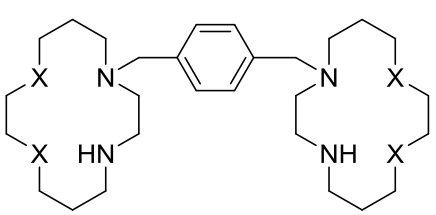

L^{105}**:** X=S, HIV-1(III_B) EC_{50}= >6.8357 μM
CC_{50}= 6.8 μM

L^{106}: X=O, HIV-1(III_B) EC_{50}= >363 μM
CC_{50}= >363 μM

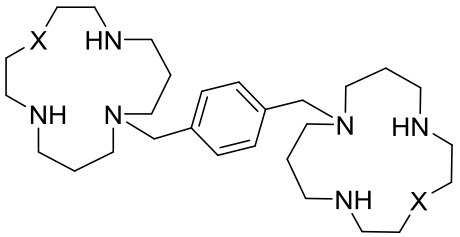

L^{107}: X=O, HIV-1(III_B) EC_{50}= 4.4919 μM
CC_{50}= >244 μM

L^{108}: X=CH, HIV-1(III_B) EC_{50}= 9.6078 μM
CC_{50}= >133 μM

Figure 52 – Bis-macrocycles containing alternative heteroatoms in place of one or more nitrogen atoms[178e]

A prevalent feature in bis-macrocycle synthesis is the use of protecting groups, this feature has been utilised by Faulkner and Gunnlaugsson who isolated bis-cyclen macrocycles using tris-N-protected cyclen.[178c, 178d] Costa *et al.* synthesised *meta*- and *para*-xylyl linked bis-cyclen macrocycles using ethyl bromoacetate groups to protect six of the nitrogen atoms.[181] Ester groups were hydrolysed to give bis-cyclen derivatives and coordinated to gadolinium(III).

The advantage of rigidifying a macrocycle is that protecting groups are not required because there are only two points available for nucleophilic substitution, reaction at these points is controlled with molar excesses of reagents, and reduces the number of synthetic steps. Archibald and co-workers have synthesised bis-macrocycles containing structurally rigidifying bridges, **L**^{34}, **L**^{35} and **L**^{36}, see Figure 23 in section 1.2.3.7.[67, 84-85] Synthesis of **L**^{34} was achieved by the route outlined in Figure 53. Cyclam, glyoxal cyclam and **L**^{34a} were prepared according to literature methods.[156, 182] Modified versions of methods used by Weisman and co-workers were followed to afford **L**^{34b} and **L**^{34} in high yields of 76% and 77% respectively.[61b, 154, 156, 183] Coordination of **L**^{34} to nickel(II) resulted in relatively high anti-HIV activity, in comparison to AMD3100.[67] The restrictive CB forced the macrocycles into a *cis*-V configuration which bound to CXCR4 as demonstrated by Sadler *et al.*[61b, 65a, 66, 167] Khan *et al.* synthesised **L**^{36} using the same methods as **L**^{34}, see Figure 53, but with α-α'-dibromo-*p*-xylene.[170]

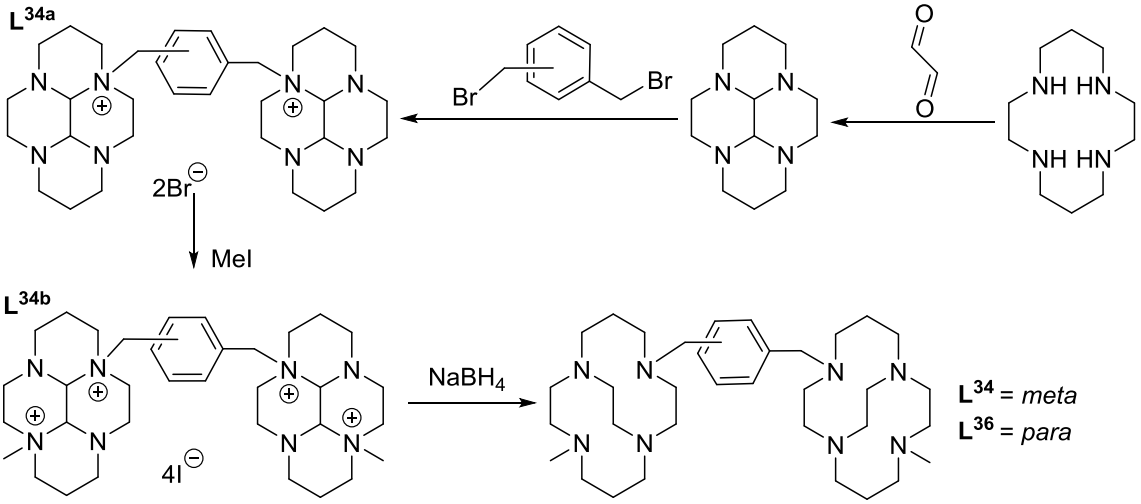

Figure 53 – Synthetic route to L^{32} as outlined by Smith *et al.*[67]

Modified versions of procedures outlined by Kolinski and co-workers were used by Valks *et al.* to prepare **L^{35}**.[71b, 160a] Glyoxal cyclam was reacted with α-α'dibromo-*p*-xylene before reduction with sodium borohydride to cleave the quaternary nitrogen to carbon bonds.[71b] Valks *et al.* found that **L^{35}**, see section 1.2.3.7, exhibited lower anti-HIV activity than AMD3100, EC_{50}:6.98 μM and EC_{50}:0.011 μM respectively.

Bernier *et al.* made a series of CB cyclen bis-macrocycles by an alternative synthetic route to Smith *et al.*[67, 81] A nitrogen atom in glyoxal cyclen, synthesised as reported in the literature,[156] was alkylated with bromoacetate to isolate a mono-macrocycle quaternary salt.[160a, 175a, 184] The bis-macrocycle quaternary salt was then isolated by reacting an excess of mono-macrocycle with either α-α'dibromo-*p*-xylene or α-α'dibromo-*m*-xylene. Quaternary nitrogen-carbon bonds were then reduced with sodium borohydride. An additional step to afford bis-macrocycles **L^{111}** and **L^{112}**, see Figure 54, deprotected the ester groups to carboxylic acid groups using $NaBH_4$ in 95% EtOH.[184a]

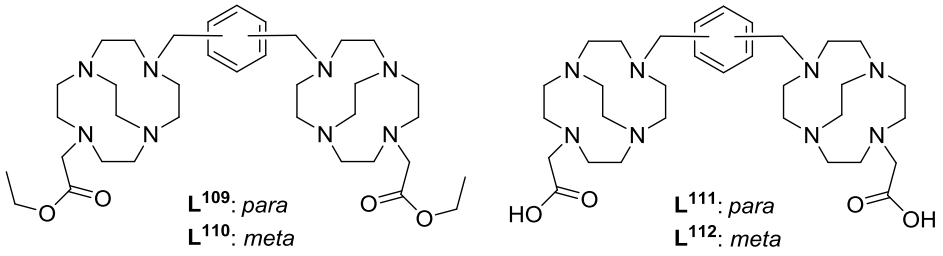

Figure 54 – Structures of bis-macrocycles synthesised by Bernier *et al.*[184a]

3.2.3 Bis-Macrocycle Metal Complexes

Coordination of transition metals into the macrocyclic cavity can significantly increase affinity for the CXCR4 receptor.[56a] The general synthetic procedure for metal coordination requires heating at reflux with a metal salt in a solvent. Wainwright, Hancock and co-workers first investigated SB macrocycles which favour *trans*-II configuration.[60, 62, 143, 185] Weisman, Wong and co-workers explored CB macrocycles which take on a *cis*-V configuration.[61a, 186] Many use complexation conditions outlined

by Wong *et al.* who synthesised the first CB macrocycle copper(II) complexes containing pendant arms, see Figure 55, in methanol or ethanol by heating them at reflux for 2 h before purification by recrystallisation.[61b] Pendant arms can help the kinetics of metal coordination by aiding the capture of a metal ion before the slow encapsulation stage, guiding it into the macrocyclic cavity. The encapsulation stage is slow because the macrocycle undergoes conformational changes to encompass the metal ion.[187] Unlike other restricted macrocycle metal complexes presence of acetate pendant arms can result in a distorted octahedral geometry because the metal is completely enveloped in the macrocyclic cavity.[61b] For copper(II), the octahedral complex exhibited Jahn Teller distortion along the elongated O(1')-Cu(2)-N(8') bond whereby bond lengths were approximately 2.31 Å for Cu-O_{ax} bond and 2.23 Å for Cu-N_{ax} bond, see Figure 55. This is significantly longer than equatorial bond lengths which were 2.00 Å for Cu-O_{eq} and 2.05 Å for Cu-N_{eq}.

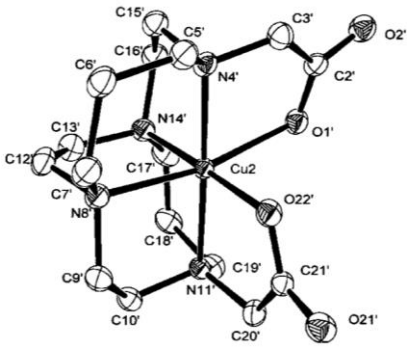

Figure 55 – Distorted octahedral CB copper(II) complex coordinated to two pendant arms (reproduced from Wong *et al*.) [61b]

RamLi *et al.* investigated C-C linked bis-macrocycles containing a pendant arm, see Figure 56 as PET imaging agents for cancer.[152] **L[113]** was coordinated to ^{64}Cu in a range of buffers from pH 3.0-8.0, a 2:1 ratio of metal:ligand was used, and the reactions were heated at 37°C for 30 min. The pendant arm amine group of **L[114]** could facilitate conjugation of antibodies to deliver targeted therapy to a cancer site. In all pH buffers tested coordination of ^{64}Cu did not go to completion, the highest yield obtained was 68% at pHs≥4.0. A flexible structure may not be ideal because the complex is less stable than configurationally restricted macrocycles and may transchelate *in vivo* resulting in toxic side effects. [71b, 175a, 184b, 188]

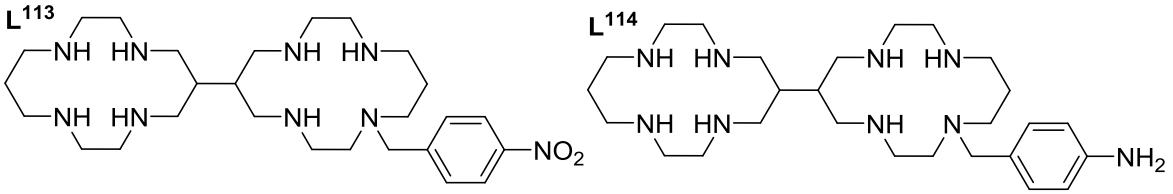

Figure 56 – C-C linked bis-macrocycles synthesised by RamLi *et al.*[152]

Silversides *et al.* afforded SB mono-macrocycle copper(II) complexes by heating at reflux for 2 h before filtration and solvent removal to yield the product.[160c] Smith *et al.* coordinated nickel(II) to a SB mono-macrocycle by heating at 60°C for 30 min under an inert atmosphere and purifying *via* size

exclusion chromatography.[67] CB bis-macrocycle nickel(II) complexes were also synthesised, by heating at 60°C overnight in DMF under an inert atmosphere. Longer reaction times are required because CB-macrocycles are highly basic and bind a proton in the macrocyclic cavity through hydrogen bonds with the nitrogen atoms.[188] This proton competes with a metal ion for the cavity therefore more energy is required to remove it. The slower complexation can be observed by monitoring the colour of the reaction, SB-macrocycles will immediately turn blue on the addition of a copper salt which shows complexation has occurred.[160c] However, on examination of a CB-macrocycle complexation the colour change is much slower.

Archibald and co-workers synthesised a copper(II) complex of **L[36]**, see Figure 23 in section 1.2.3.7, and suggested that the increase in CXCR4 affinity and residence time, compared to the free ligand, originated from a stronger coordination bond, as opposed to weaker H-bonds.[170] As particular configurations are potentially more biologically active it makes sense to add a bridge to restrict the macrocycle to the active *cis*-V configuration.[66] A folded *cis*-V configuration is induced by an ethylene CB, when complexed to a metal ion nitrogen atoms occupy three equatorial sites and one axial site. This is different to *trans*-III, the most stable configuration, where nitrogen atoms occupy all four equatorial sites. This may explain the high activity observed with configurationally restricted copper(II) complexes because copper(II) interacts with an aspartate residue forming a shorter, stronger equatorial coordinate bond rather than a weaker axial bond, seen without a bridge.[167, 170]

Crystal structures of CB macrocycle copper(II) complexes reported by Wong *et al.* showed five-coordinate structures, a hydrogen bond is observed from one axial nitrogen atom to a second counter ion, 0.900 Å.[61b] Axial bond lengths for CB-cyclam copper(II) complex, ca. 1.96 Å, are shorter than equatorial bonds, ca. 2.10 Å.[61b] The structure, between an ideal square pyramid and trigonal bipyramidal, was best described as a distorted square pyramid. The apex of the distorted square pyramid geometry was a longer equatorial bond N(1)-Cu(1), in Figure 57, 2.138 Å.

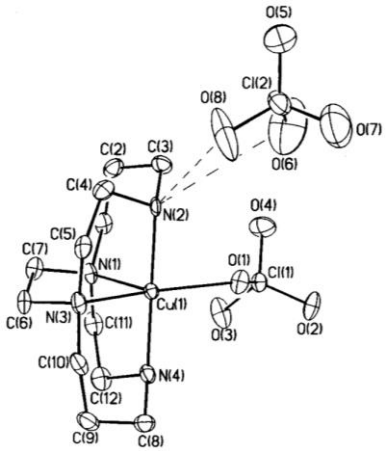

Figure 57 – Crystal structure of CB cyclam copper(II) complex bonding to perchlorate counterions (reproduced from Wong *et al.*)[61b]

3.3 SYNTHESIS OF BIS-MACROCYCLE LIGANDS

The synthetic approach to novel bis-macrocycles was similar to that used by Bernier *et al.*[164] Synthesis of tetraazamacrocycles is well published, most likely due to their interesting properties such as basicity – they are proton sponges, redox behaviour and coordination chemistry, which is especially different when macrocycles are reinforced with an ethylene bridge.[183] Bernier *et al.* synthesised an unsymmetrical di-substituted bridged cyclen to which a crown ether was attached, the bridge was finally removed to yield a novel bis-macrocycle.[164]

3.3.1 Bis-Macrocycles Precursors

Bis-macrocycles synthesised by our group have shown high affinity for the CXCR4 receptor, see Figure 23 in section 1.2.3.7.[67, 71b, 81, 85] These macrocycles do not contain a group which allows additional conjugation. Attachment of pendant arms to bis-macrocycles provides functional groups to allow further conjugation to other molecules, such as fluorescent dyes or radiolabelled groups, and increases applicability of the compounds. A pendant arm can also enhance the compounds overall stability.[189] Addition of a single pendant arm to bis-macrocycles shown in Figure 53 is not viable therefore a new synthetic route was devised to attain the desired compounds, see Scheme 6.

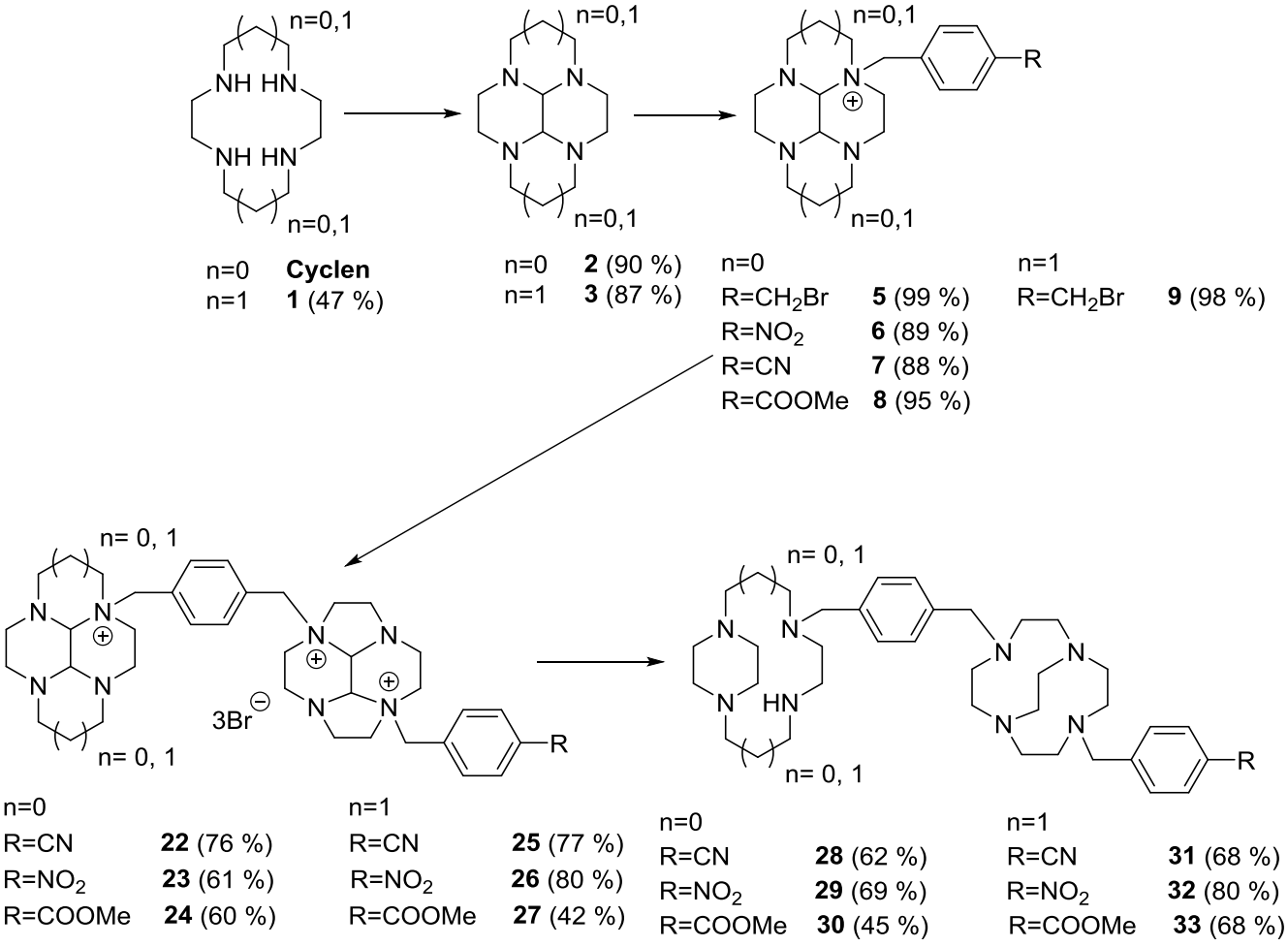

Scheme 6 – Synthetic route to novel functionalised bis-macrocycles

Pendant arm functional groups were modified to enable subsequent conjugation, see Figure 58. Our group previously reported mono-macrocycles containing nitrobenzene, aniline and benzonitrile pendant arms.[67, 102, 190] Compounds containing an aniline pendant arm are notably less reactive than other pendant arm functional groups because the nitrogen atom is bound directly to the aromatic ring, its lone pairs are involved in electron delocalisation which consequently decreases reactivity. Substituting an amine for a nitrile group introduces a carbon between the aromatic ring and nitrogen which, when reduced, ensures that the amine lone pair is not delocalised. Although, as the presence of the nitro group facilitates some alternative synthetic routes, the nitrobenzene pendant arm was still investigated, see Figure 58. Functional groups such as amines and azides facilitate conjugation of fluorescent dyes and radiolabelled groups which enable the synthesis of diagnostic agents for CXCR4 expressing tumours for use in optical and PET imaging.

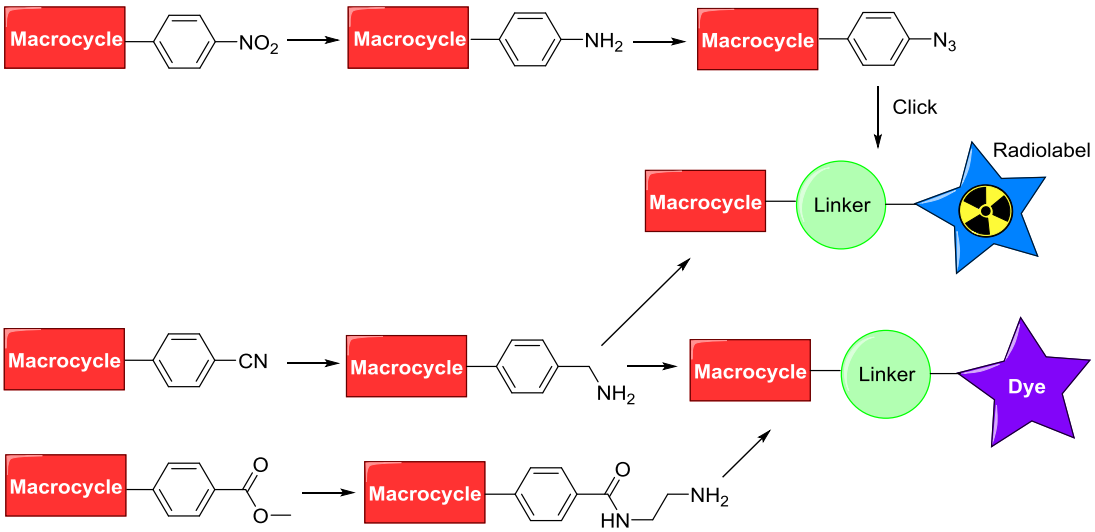

Figure 58 – Pendant arm functionalisation

The work reported in chapter 2 outlines a successful route to isolate **9** based on a modified method by Le Baccon *et al.* therefore this method was applied for the synthesis of **5**, **6**, **7** and **8**, see Scheme 7, with the relevant pendant arm starting material.[156] However, in all cases reacting glyoxal cyclen with excess pendant arm for 3 d led to the di-substituted product forming. In order to combat this, a molar equivalence of pendant arm was tested. Whilst MS and NMR indicated the products had formed they also showed a mixture of mono- and di-substituted macrocycles. As both quaternary salts were not readily soluble or easily purified a different procedure was tested to ensure a mono-substituted product was obtained. The method reported by Del Mundo *et al.* in 2012 was modified and led to successful isolation of **5**, **6**, **7** and **8** with excellent yields ca. 90 % being achieved.[161] Glyoxal cyclen was reacted with an equimolar amount of pendant arm in a small quantity of dry THF. This method was advantageous because the reaction time was reduced to 24 h.

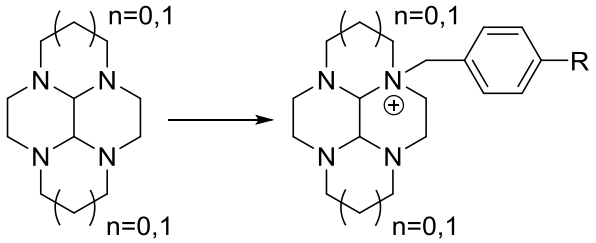

n=0	**2** (90 %)	n=0		n=1	
n=1	**3** (87 %)	$R=CH_2Br$	**5** (99 %)	$R=CH_2Br$	**9** (98 %)
		$R=NO_2$	**6** (89 %)		
		R=CN	**7** (88 %)		
		R=COOMe	**8** (95 %)		

Scheme 7 – Synthesis of mono-macrocycle precursors

5, **6**, **7** and **8**, see Scheme 7, were characterised by NMR, distinguished by peaks in the aromatic region and additional N-α-CH_2 environments due to reduced symmetry within the molecule. The yields of the mono-substituted macrocycles are comparable to similar work by Plutnar *et al.*,[191] 100%, and Khan *et al.*,[102] 87%.

3.3.2 Bis-Macrocycle Quaternary Salts

Synthesis of bis-macrocycle quaternary salts, **22**-**27** see Scheme 8, was achieved using a modified method outlined by Bernier *et al.* and was similar to methods used for synthesising tris-macrocycles,[164] see chapter 2 section 2.4.1, with the exception that both precursors contained a pendant arm. Rationalisation for the long reaction time was to ensure the macrocycles reacted, because unlike Bernier *et al.* an excess of reactive macrocycle could not be used due to the difficult nature of purification. Furthermore the reaction was carried out at RT due to formation of side products at elevated temperatures discussed by Rohovec *et al.*[192] Methods for synthesising quaternary salts had to be adapted from those reported in the literature as there were not any methods reporting addition of a second functionalised macrocycle, highlighting the novelty of this work. Bencini *et al.* used MeCN to form a di-substituted glyoxal cyclen macrocycle which coincides with other literature methods whereby forming a multiply charged species primarily uses MeCN,[90] an example being the work by Silversides *et al.*[154]

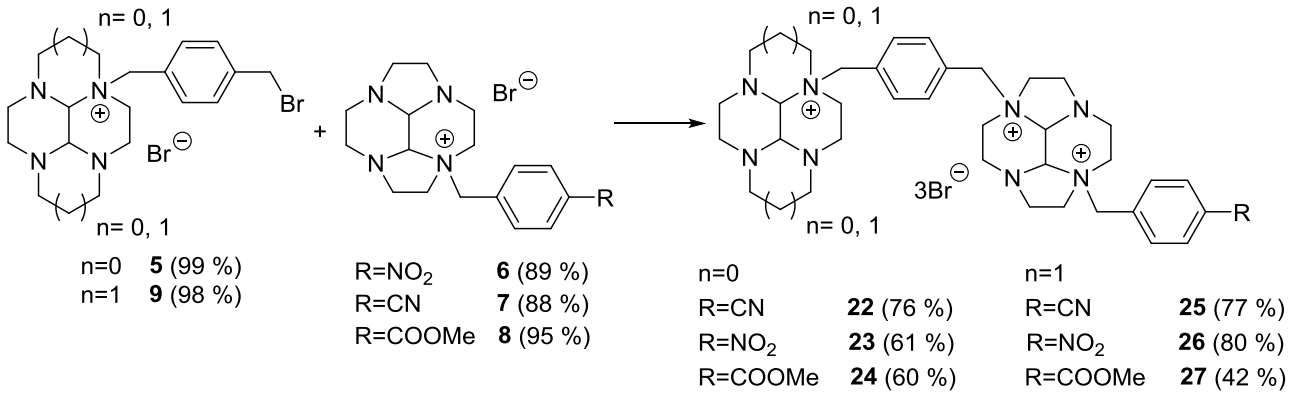

Scheme 8 – Synthesis of bis-macrocycles quaternary salts

When making symmetrical bis-macrocycles literature methods also use MeCN. What is more, the methylation of a mono-substituted single macrocycle to form the doubly charged macrocycle, as outlined by Silversides *et al.,*[154] is carried out by suspending the macrocycle in MeCN and then adding methyl iodide. Rohovec *et al.* explored the synthesis of di-substituted glyoxal cyclen compounds and found that in some cases MeCN was not able to produce the di-substituted product and the addition of MeOH was required.[192] One of those reactions was a di-substitution of a nitro functionalised macrocycle, the same as **6**, however this problem was not observed in this work or by others in the literature.

Two macrocycle suspensions were made with compounds **5** and either **6** or **7** in MeCN. Two analogous suspensions were made using DMF to provide comparative data. Reactions in DMF indicated that by-products and impurities were present, whereas reactions using MeCN gave pure **22** and **23,** see Scheme 8, indicating that MeCN is the solvent of choice for formation of unsymmetrical bis-macrocycles.

The average yield was 66%, see Scheme 8, which is lower than reported literature methods of similar compounds.[164] The lowest yield was obtained with ester functionalised bis-macrocycles, and could possibly be related to the fact that the ester is a bulkier functional group than the nitrile and nitro groups causing the reaction to be sterically hindered. Nonetheless, satisfactory yields of 60% and 42% for **24** and **27**, see Scheme 8, were achieved. Silversides *et al.* for instance achieved a quantitative yield for a di-substituted bridged-cyclam, see Figure 59, yet the second group attached was a methyl group.[154] The methyl group is significantly smaller than compounds **5** or **9**, see Scheme 8, which could explain the lower yields of **24** and **27** if the reaction was sterically hindered. Lower yields were observed when bulkier groups were added, see **L**[116] and **L**[117] in Figure 59.

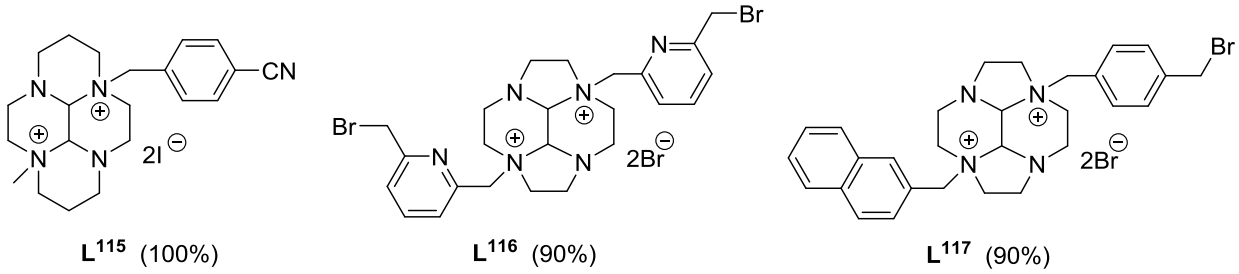

L[115] (100%) **L[116]** (90%) **L[117]** (90%)

Figure 59 – Structure of di-substituted macrocycles from the literature[90, 154, 164]

An issue experienced during the synthesis of the bis-macrocycle quaternary salts was their poor solubility which subsequently caused difficulty when trying to obtain MS data. In all cases **22**-**27** were clearly characterised by NMR due to additional peaks in the aromatic region and extra H_{aminal} peaks at approximately 4 ppm in the ^{1}H NMR spectrum. As was observed in chapter 2, when the macrocycles were reduced their solubility significantly increased and full characterisation was more easily obtained. Impurity was noted for **27** following elemental analysis.

3.3.3 Bis-Macrocycle Reductions

Reduction of macrocycle quaternary salts is an established route to isolate final macrocyclic products.[61a, 160a] Reduction via $NaBH_4$ in an ethanolic solution is slow ca. 14 days but affords a single, desired product and can be used to attain both SB and CB macrocycles effectively. An established procedure was followed for the reduction of **22**-**27**,[61a, 160a] see Scheme 9, and no significant difference in yields was noted, yields of approximately 70% were achieved with the exception of **30** where 45% was attained. These yields were less than those reported by Wong *et al.* and Silversides *et al.* whereby more than 80% was achieved.[61b, 154] An explanation for the lower yields could be the smaller scale of the reactions.

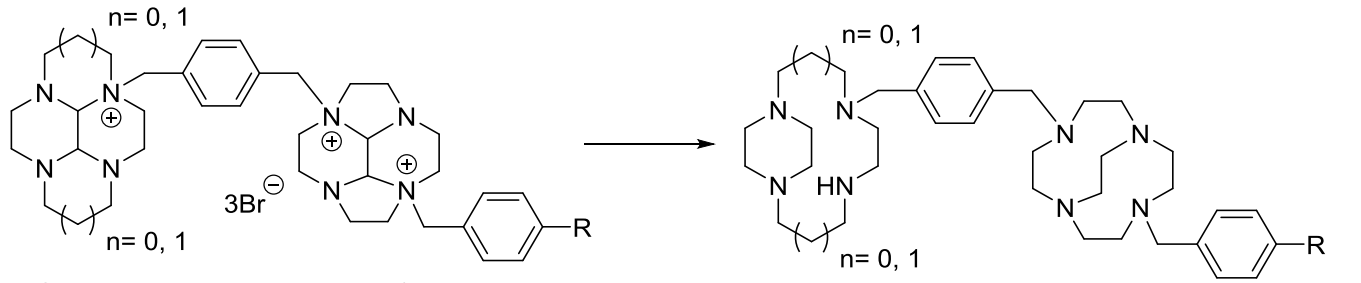

n=0		n=1		n=0		n=1	
R=CN	**22** (76 %)	R=CN	**25** (77 %)	R=CN	**28** (62 %)	R=CN	**31** (68 %)
$R=NO_2$	**23** (61 %)	$R=NO_2$	**26** (80 %)	$R=NO_2$	**29** (69 %)	$R=NO_2$	**32** (80 %)
R=COOMe	**24** (60 %)	R=COOMe	**27** (42 %)	R=COOMe	**30** (45 %)	R=COOMe	**33** (68 %)

Scheme 9 – Reduction of bis-macrocycles with $NaBH_4$

Isolation of the desired products, **28**, **29**, **31** and **32**, see Scheme 9, was confirmed by ^{13}C NMR which showed the disappearance of the C_{aminal} peaks, although slight impurity was introduced during the

reduction (~10 %) for **28**, **29**, **30**, **31** and **32**. The NMR data collected for **33** suggested that the expected product had not been isolated and HRMS identified an additional CH_2 was present. The CH_2 was assigned to an ethyl group on the ester functional group instead of a methyl group.[193] Normally transesterification requires a high temperature and catalysts although a recent publication suggests that transesterfication is possible especially with methyl esters at RT.[193-194] Data confirmed that previous stages had afforded the desired product. Transesterification for **33** was facilitated by the long reaction time and confirmed by ^{1}H NMR, an increase in peak intensity and shift from 3.77 ppm to 5.08 of the O-CH_2 peak. Transesterification during reduction was not observed for **30** confirming it was successfully isolated.

In summary, a range of bis-macrocycles have been effectively reduced using $NaBH_4$, long reaction times are necessary due to the time required to form a CB. Overall, desired products were successfully isolated although an unexpected product was attained following reduction of **27**. Future work could include optimising the yields of **30** and **28**, potentially by performing more extraction cycles.

3.3.4 Modification of Bis-Macrocycle Functional Groups

Smith *et al.* reported an effective method to reduce nitrile groups on SB and CB macrocycles using $LiAlH_4$ in THF and heating at reflux for 3 h, yields of more than 75% were achieved.[67, 195] Following this method **28** and **31** were reduced to afford the methylamine products **34** and **35**, see Scheme 10, in lower yields than reported in the literature for similar compounds.[67, 195] Products were characterised by ^{13}C NMR, showing absence of a nitrile peak, although impurities (<10%) were observed, HRMS confirmed isolation of **34** and **35**. Differentiation between NH_2 and NH proton peaks was determined by comparison of SM and product ^{1}H NMR data and noting the integration when referenced against a known peak.

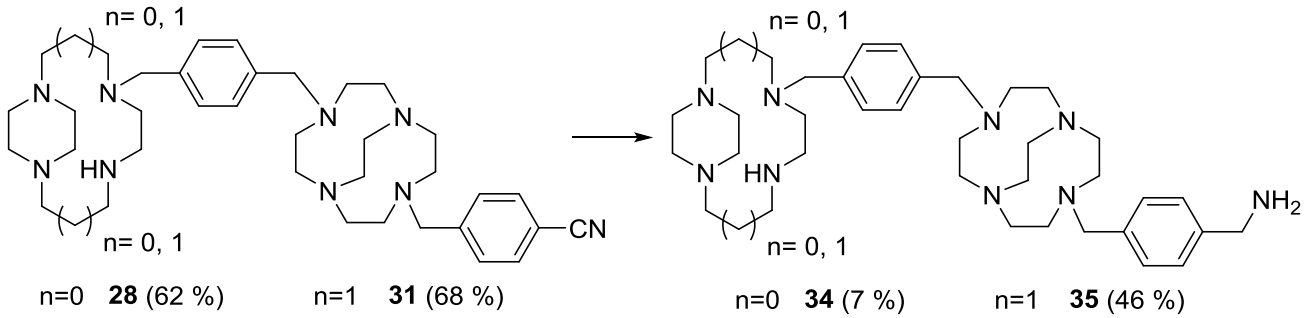

Scheme 10 – Reduction of nitrile group with $LiAlH_4$

Our group previously reported hydrogenation of a nitro group on SB-cyclam using 5% palladium on calcium carbonate, poisoned with lead, in methanol stirred overnight under an atmosphere of hydrogen.[102] An alternative reduction method was conducted by Kaye *et al.* in 1951 to reduce a

nitrobenzene derivative to the aniline deriviative,[196] conditions and reagents were 10% palladium on activated charcoal in ethanol under a hydrogen atmosphere for 1 h. High yields, 80%-96%, were attained by Kaye *et al.* Sun *et al.* used similar conditions with the exception that ethanol was substituted for ethyl acetate and the solution was under an atmosphere of hydrogen for 9 h.[197] This highlights the range of similar reported routes to reduce a nitrobenzene group. There are no reports in the literature reporting reduction of a nitro group on CB-macrocycles or SB-cyclen bearing a nitro pendant arm. The method to reduce **29** and **32** used a poisoned catalyst to control the extent of reduction and prevent debenzylation, see Scheme 11. **32** was successfully reduced after 4 h in ethanol and an almost quantitative yield was achieved. The distinctive shift of peaks in the aromatic region in ^{1}H NMR, from ~8.20 ppm to ~7.30 ppm, is characteristic of a nitro reduction and confirmed isolation of **37**, in addition to HRMS characterisation. Impurity was identified in elemental analysis of **37** and assigned to excess solvent molecules associated with the macrocycle.

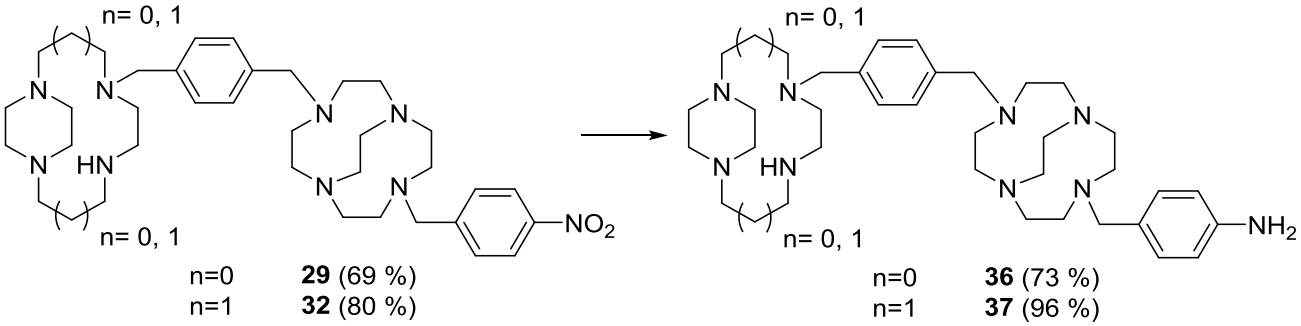

Scheme 11 – Hydrogenation of nitro groups on 29 and 30 with hydrogen and Pd/C catalyst

Following the success of **37** the same method was used to reduce **29** although data suggested debenzylation of the nitro-pendant arm. As conditions and reagents were identical to **37** a rationalisation for this is that the catalyst was insufficiently poisoned therefore reduction was too efficient to prevent debenzylation. Owing to this the reaction was repeated with a lower pressure supply of hydrogen, a hydrogen balloon, to prevent debenzylation. After 4 h the reaction was analysed and the characteristic ^{1}H NMR aromatic peak shift was observed demonstrating the isolation of **36**.

Triazotization reactions are well documented in the literature with a wide variety of reagents being used.[198] Triazotization reactions were conducted on **36** and **37** leading to the azide functionalised bis-macrocycles **38** and **39**, see Scheme 12. Conversions of this type in the literature attain yields ranging from 15%-100% and are commonly conducted on simple aromatic molecules therefore potentially bulky bis-macrocycles may sterically hinder the reaction resulting in low yields. Griffin *et al.* achieved an 81% yield when converting (4-aminophenyl)methanol to (4-azidophenyl)methanol using HCl, sodium nitrite and sodium azide at 0-5^{o}C.[199] The same reaction and method was carried

out by Belkheira *et al.* but an almost quantitative yield was attained, indicating that reaction yields can vary.[200] Other routes to synthesise azidobenzene deriviatives involve replacement of HCl with H_2SO_4, to give an 83% yield.[201] A 6 h reaction with trifluoromethanesulfonyl azide, copper(II) sulfate in methanol, DCM and water, gave 100% and 15% yields,[198, 202] and the use of tertiary-butylnitrite, trimethylsilylazide in MeCN at 0-20°C gave a 95% yield.[203]

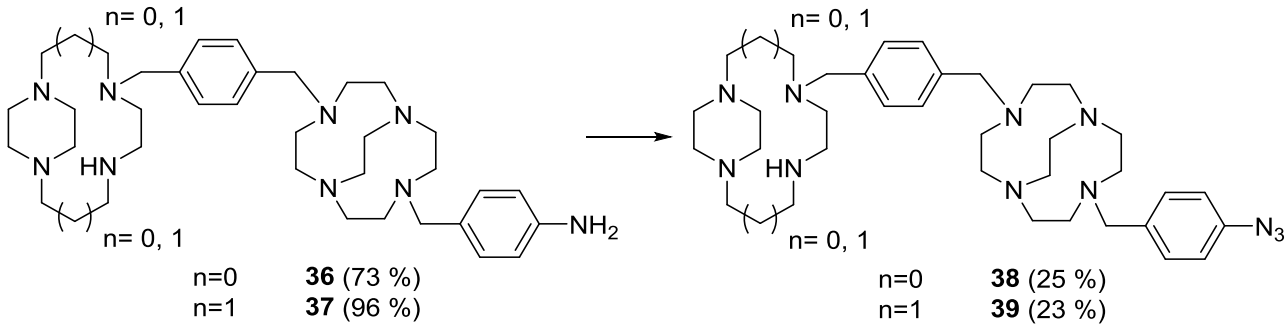

Scheme 12 – Triazotization of amine functionalised bis-macrocycles

The most commonly used method with which highest yields were attained was the deciding factor when it came to selecting a method for triazotization of **36** and **37**, HCl, sodium nitrite and sodium azide were used at 0-5°C. A low reaction temperature is required to isolate the desired product because at higher temperatures the diazonium salt decomposes and is given off as nitrogen gas leaving the aryl cation vulnerable to nucleophilic attack which can result in a mixture of products. Addition of sodium azide enables a controlled nucleophilic aromatic substitution to occur, the diazonium group is given off as nitrogen. The low yield of **38**, 25%, could be attributed to loss of macrocycle in the aqueous layer during extraction because it was not basic enough. **38** and **39** were characterised by HRMS.

3.3.5 Bis-Macrocycle Conjugation Reactions

The term "click chemistry" was first coined by Kolb *et al.* to describe a group of selective,[204] high yielding reactions which occur under mild conditions, for example at room temperature and in benign solvents such as water, using readily available starting materials and reagents, any by-products should be non-toxic and easily removed. The most common "click chemistry" reaction, or "click" reaction, is the azide-alkyne cycloaddition reaction.[205] The azide-alkyne 1,3-dipolar cycloaddition reaction was discovered in 1963 by Huisgen but was ignored because of the high temperatures and pressures required to drive the reaction.[206] It was not until Kolb *et al.* employed copper(I) as a catalyst, see Figure 56, that the reaction received significant interest. The reaction schematic shown in Figure 56 results in the formation of 1,2,3-triazole and is commonly known as the CuAAC reaction which stands for copper(I) catalysed azide alkyne cycloaddition.[205] Since then, its

use in the field of organic chemistry, medicinal chemistry and materials science has been exploited as a result of its lack of reactivity with natural biomolecules and its reliability.[207]

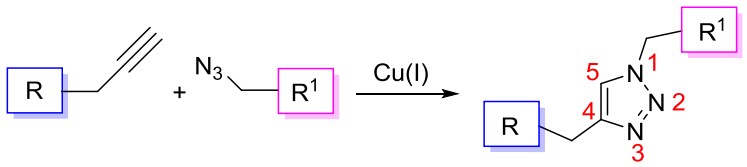

Figure 60 – Components required to perform the azide-alkyne cycloaddition reaction as outlined by Kolb *et al.*[204]

Click reactions, commonly described as "spring-loaded", depend on highly energetic reagents or reactants.[208] Other examples of click reactions are hetero Diels-Alder reactions, nuclophilic ring opening reactions such as epoxides and aziridines, and azide-phosphine coupling also known as the Staudinger ligation. In 2005, Himo *et al.* proposed a mechanism for the popular CuAAC reaction,[209] see Figure 57. The copper(I) catalyst reduces the activation barrier by 11 kcal/mol and rapidly drives the reaction forward with high selectivity.[210] A range of copper(I) catalysts are available such as copper(I) iodide, copper(I) bromide and copper(II) sulfate which is reduced *in situ* with sodium ascorbate. What's more the reaction is not limited to particular solvents, as displayed by Szíjjártó *et al.* and Aucagne *et al.*,[211] but a high number of reactions use aqueous media.[204]

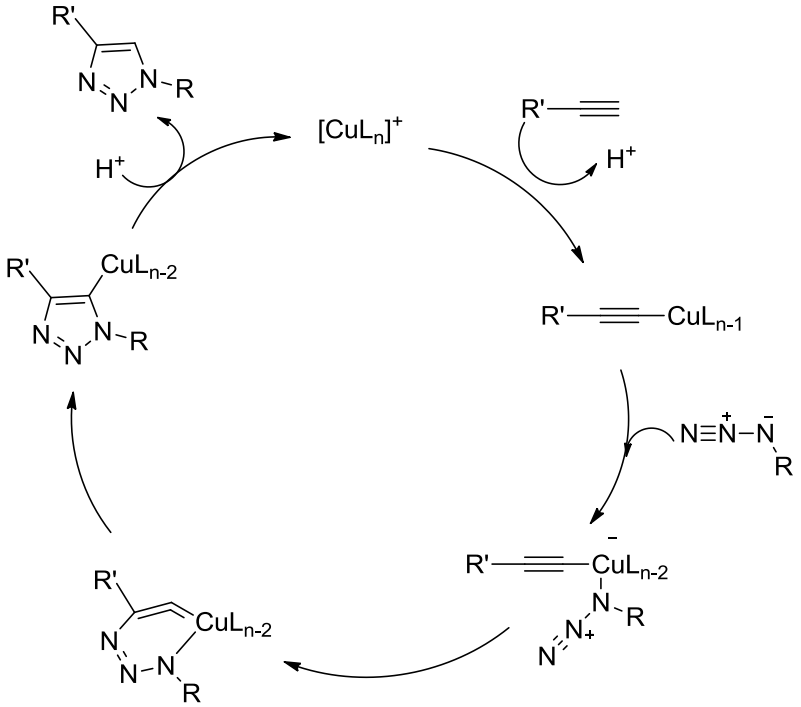

Figure 61 – Proposed mechanism for CuAAC reaction[209]

Preparation of a "click" generated cyclam fluorophore was achieved by Tamanini *et al.*, see **L**[118] in Figure 58.[212] An alkyne functionalised cyclam ring was synthesised by reacting propargyl bromide with triboc-cyclam before reaction with 6-azido-2-ethyl-benzo[de]isoquinoline-1,3-dione, the azide functionalised fluorophore. The protecting groups were then removed to afford **L**[118]. The click reaction was carried out in THF/H_2O (7:3) using copper(II) sulfate pentahydrate in combination with

the reducing agent sodium ascorbate at RT overnight under an atmosphere of nitrogen. The cycloaddition click reaction occurred smoothly and was high yielding, 82%. A different catalyst was used by Szíjjártó *et al.* who synthesised a series of cyclen lanthanide complexes, a selection of which are shown in Figure 58, **L**[119] to **L**[121]. Placement of the clickable groups, either on the macrocycle or on the attached group, did not affect the reaction and high yields for **L**[119] to **L**[121], 98%, 96% and 90% respectively, were achieved. What's more, a range of pendant arms and "clickable" groups were explored and in all cases reasonable yields were attained. All "click" reactions were carried out in a microwave at 100°C for 15 min, for **L**[121], to 30 min, for **L**[119] and **L**[120]. Unlike Tamanini *et al.*, a slight excess, 0.1 excess, of coupling partner was used in the presence of copper(I) iodide catalyst, 5%. The group explored the reaction further by conjugating multiple macrocycles via their disclosed "click" cycloaddition reaction to afford **L**[122], see Figure 58, but a low yield, 34%, was obtained.

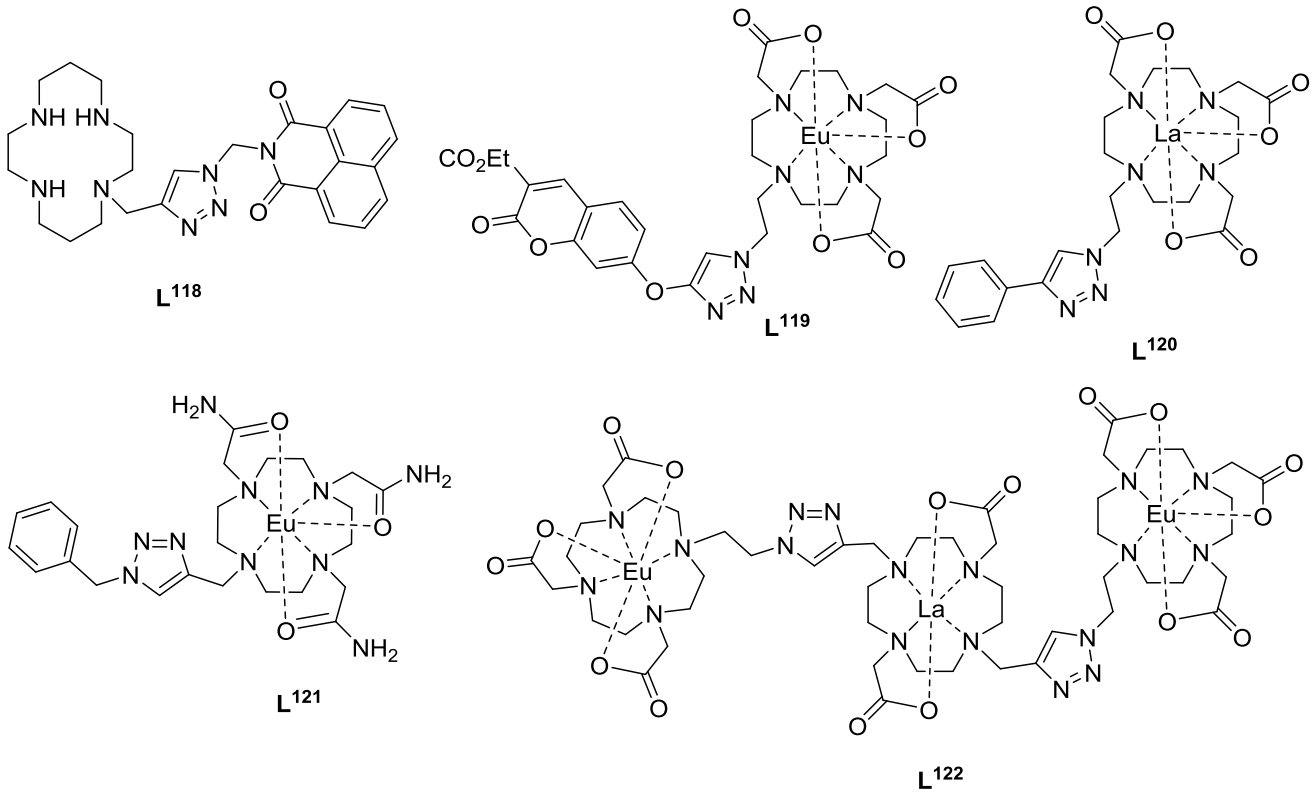

Figure 62 – "Click" generated macrocyclic imaging agents [211a, 212]

Incorporation of a functional group, which enables bioorthogonal chemistry, is highly advantageous because rapid reactions using mild conditions and reagents can effectively label a molecule with an imaging group. The term bioorthogonal chemistry was coined by Bertozzi and refers to chemistry reactions that can occur *in vivo*.[213] The reactions should be rapid, selective, biologically and chemically inert and biocompatible. This area of chemistry is of particular interest because there is no requirement for a copper catalyst which can be problematic when handling macrocycles with excellent chelating properties. A number of bioorthogonal reactions were investigated to test

whether these copper-free click reactions were feasible, groups which facilitated the tetrazine ligation and the cyclooctyne strain promoted azide alkyne cycloaddition (SPAAC) reaction were tested.

A test reaction was conducted on **39** to determine whether the bis-macrocycle would undergo a click reaction with a strained alkyne group tagged with a fluorescent dye, see Scheme 13. The SPAAC reaction was explored due to its high reactivity towards azides and stability. The rhodamine derived fluorescent dye was selected due to its high photostability and pH insensitivity. The reaction outlined by the manufactures, Click Chemistry Tools, was followed but briefly involved incubating the two reagents in a solution of MeOH for 1 h in the dark at RT. EtOH is a frequently used solvent but was not chosen because the dye was not soluble in it. The reaction was carried out on a half mg scale therefore NMR characterisation could not be obtained as the spectra would have been too weak. LRMS indicated that both starting materials were not present in the sample but the product was not identified.This reaction requires further investigation, although the failure of a click reaction with a macrocycle has been previously experienced in this work, see section 4.3.3 and 4.3.4, and in previous unpublished work within the group.

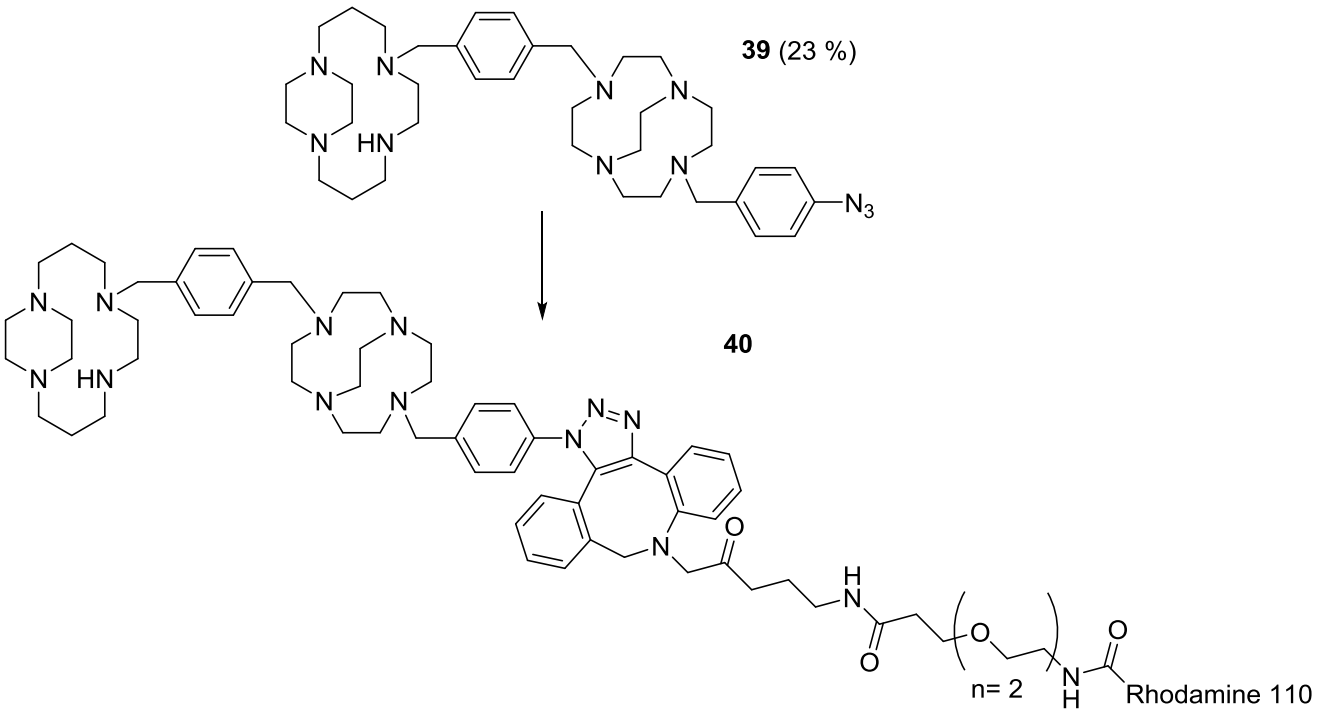

Scheme 13 – Attempted conjugation of an azide functionalised bis-macrocycle to a fluorescent dye

The addition of tetrazine to a macrocycle has not been previously reported but the group facilitates a different copper-free click selective reaction with *trans*-cyclooctene, TCO. Conjugation reactions to form **41** and **42**, see Scheme 14, were carried out using tetrazine-PEG4-NHS in DMSO and extremely small quantities of **34** and **35**, 60 µg, in PBS buffer as outlined by the manufacturers of the tetrazine

reagent. The reaction involved incubating the reagents for 1 h at RT before quenching the reaction with tris-HCl and incubating for a further 5 min. The products were purified through desalting columns packed with Sephadex PD-10. Once again characterisation was limited due to the small scale of the reaction but MS data for **41** and **42** revealed weak mass ion peaks suggesting that the reaction did not go to completion so these reactions require further investigation but SM peaks were not observed so **41** and **42** may not have flown very well in the MS instrument.

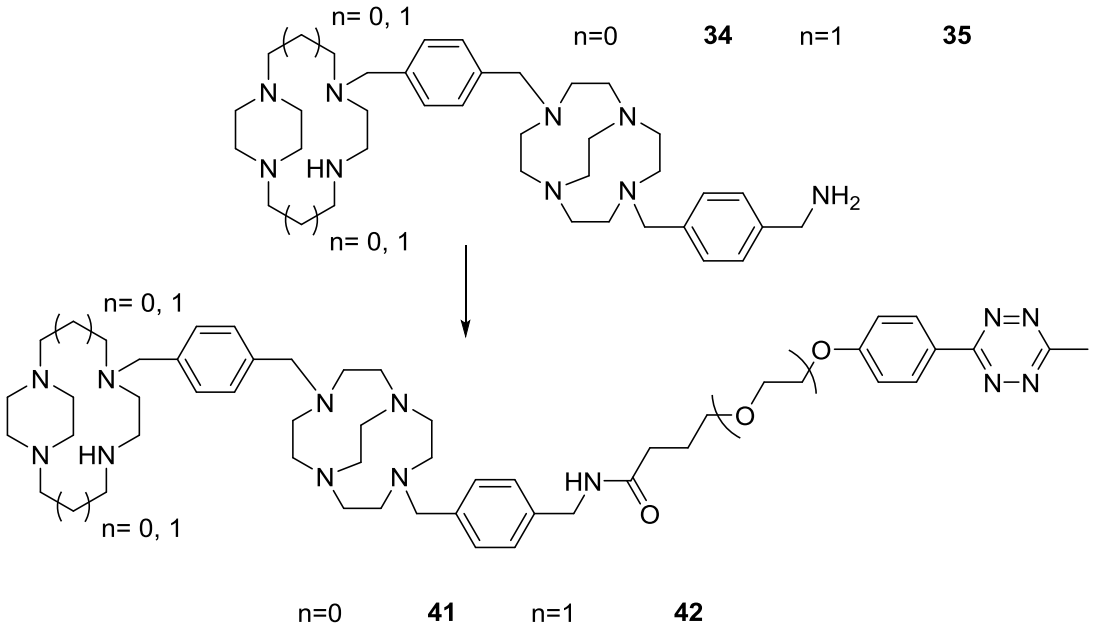

Scheme 14 – Conjugation of amine functionalised bis-macrocycle to tetrazine-PEG-NHS

An alternative method to incorporate an imaging group onto the macrocycle is the conjugation of **35** with DOTAGA-anhydride, see Scheme 15. The resulting product will not undergo bioorthogonal reactions but it does allow the incorporation of ^{68}Ga which can be used in PET imaging.

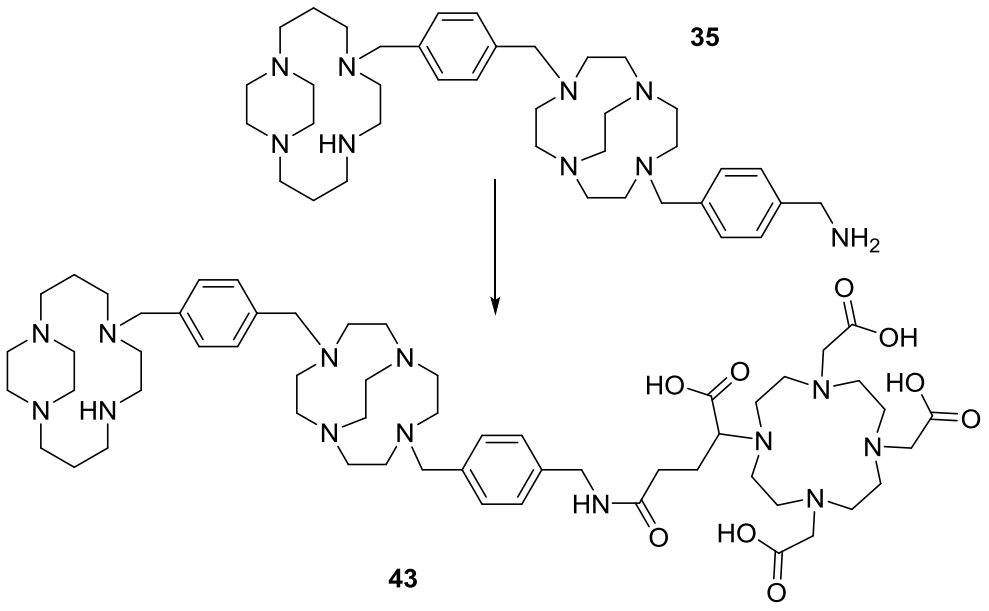

Scheme 15 – Attempted Conjugation of amine functionalised bis-macrocycle to DOTAGA-anhydride

The modified method reported by Sunil *et al.* was followed,[214] the reaction time was increased to ensure the reaction went to completion due to the large steric hindrance created by joining the two bulky starting materials. Isolation of **43** was not clearly characterised by NMR; ^{1}H NMR did not contain the carboxylic acid protons and the potential amide proton was lower than expected. MS data confirmed that **35** was not isolated. As the mono-macrocycle reaction, **75** see Figure 63 and chapter 4 section 4.3.5, was successful a justification for the reaction failure could be that **35** is bulkier than **75** hence steric hindrance is disfavouring the reaction. On the other hand, the test reaction was conducted with a SB macrocycle whereas **35** is CB, this suggests that the folded CB shape could be hindering the reaction, although perhaps the larger 14-membered cyclam ring, of **75**, is more suited to assisting the reaction than 12-membered cyclen, **35**, the longer cyclam carbon chain may facilitate enough movement to favour the reaction with DOTAGA-anhydride. This reaction requires further investigation.

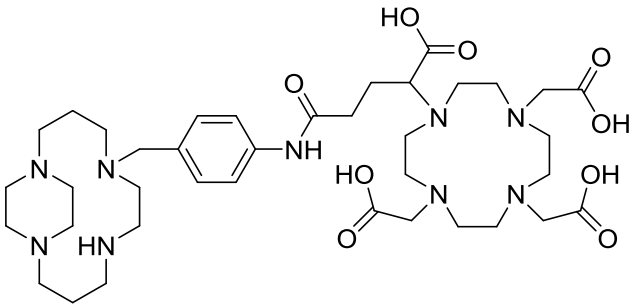

75

Figure 63 – Structure of 75, discussed in section 4.3.5.

3.4 SYNTHESIS OF BIS-MACROCYCLE METAL COMPLEXES

3.4.1 Metal Chelation

Molecules **28** – **37** and **39**, see Figure 64, were coordinated to copper(II) and zinc(II) acetate. The acetate salt was chosen because it is known to have no negative effect on solubility. Further to this, acetate salts have no toxicity effects, our group has previously shown that hexafluorophosphate salts of similar compounds can exhibit high toxicity *in vivo*. Another reason for choosing the acetate salt for all complexes was to ensure that any differences observed between macrocycles in the biological evaluation were due to the macrocycle structure only and not as a result of an alternative metal counter ion.

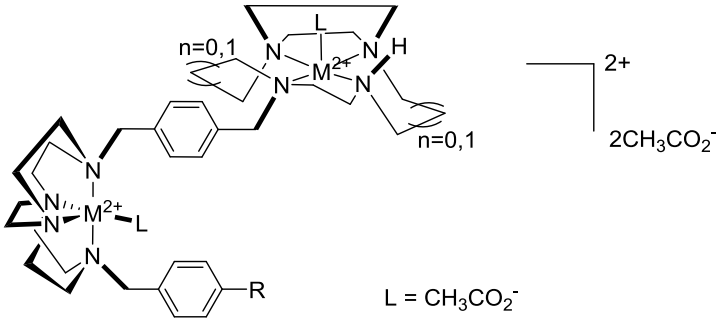

n=0				n=1			
$[Cu_2\mathbf{28}]^{4+}$	R=CN,	$M^{2+}=Cu^{2+}$	(63 %)	$[Cu_2\mathbf{31}]^{4+}$	R=CN,	$M^{2+}=Cu^{2+}$	(86 %)
$[Zn_2\mathbf{28}]^{4+}$	R=CN,	$M^{2+}=Zn^{2+}$	(84 %)	$[Zn_2\mathbf{31}]^{4+}$	R=CN,	$M^{2+}=Zn^{2+}$	(83 %)
$[Cu_2\mathbf{29}]^{4+}$	$R=NO_2$,	$M^{2+}=Cu^{2+}$	(28 %)	$[Cu_2\mathbf{32}]^{4+}$	$R=NO_2$,	$M^{2+}=Cu^{2+}$	(86%)
$[Zn_2\mathbf{29}]^{4+}$	$R=NO_2$,	$M^{2+}=Zn^{2+}$	(70 %)	$[Zn_2\mathbf{32}]^{4+}$	$R=NO_2$,	$M^{2+}=Zn^{2+}$	(86 %)
$[Cu_2\mathbf{30}]^{4+}$	R=COOMe,	$M^{2+}=Cu^{2+}$	(55 %)	$[Cu_2\mathbf{33}]^{4+}$	R=COOMe,	$M^{2+}=Cu^{2+}$	(84 %)
$[Zn_2\mathbf{30}]^{4+}$	R=COOMe,	$M^{2+}=Zn^{2+}$	(54 %)	$[Zn_2\mathbf{33}]^{4+}$	R=COOMe,	$M^{2+}=Zn^{2+}$	(85 %)
$[Cu_2\mathbf{34}]^{4+}$	$R=CH_2NH_2$,	$M^{2+}=Cu^{2+}$	(61 %)	$[Cu_2\mathbf{35}]^{4+}$	$R=CH_2NH_2$,	$M^{2+}=Cu^{2+}$	(85 %)
$[Zn_2\mathbf{34}]^{4+}$	$R=CH_2NH_2$,	$M^{2+}=Zn^{2+}$	(68 %)	$[Zn_2\mathbf{35}]^{4+}$	$R=CH_2NH_2$,	$M^{2+}=Zn^{2+}$	(74 %)
$[Cu_2\mathbf{36}]^{4+}$	$R=NH_2$,	$M^{2+}=Cu^{2+}$	(48 %)	$[Cu_2\mathbf{37}]^{4+}$	$R=NH_2$,	$M^{2+}=Cu^{2+}$	(82 %)
$[Zn_2\mathbf{36}]^{4+}$	$R=NH_2$,	$M^{2+}=Zn^{2+}$	(45 %)	$[Zn_2\mathbf{37}]^{4+}$	$R=NH_2$,	$M^{2+}=Zn^{2+}$	(82 %)
				$[Cu_2\mathbf{39}]^{4+}$	$R=N_3$,	$M^{2+}=Cu^{2+}$	(61 %)
				$[Zn_2\mathbf{39}]^{4+}$	$R=N_3$,	$M^{2+}=Zn^{2+}$	(91 %)

Figure 64 – Structures of bis-macrorcycle copper(II) and zinc(II) complexes

Due to time constraints bis-macrocycles were only coordinated to zinc(II) and copper(II), see Figure 64, although coordination to nickel(II) provides an attractive avenue for future work. NMR characterisation of zinc(II) complexes confirmed successful isolation of all products by the presence of the acetate methyl peaks and distinctive carbonyl peak in the ^{13}C NMR spectra. Isolation is confirmed because un-coordinated metal salts would have been removed during purification *via* size exclusion chromatography (Sephadex LH20) therefore the presence of these peaks in NMR confirm that these counter ions are associated with the macrocycle due to incorporation of a metal ion into the macrocyclic cavity.

Due to reduced flexibility of CB macrocycles longer reaction times were used for metal complexation to guarantee metal ion encapsulation in both SB and CB macrocycles. Overall, high yields were obtained (45-91%) with the exception of $[Cu_2\mathbf{29}]^{4+}$, see Figure 64, which is likely to have a lower yield due to the use of an old Sephadex column, this problem was also observed in previous work, see chapter 2 section 2.4.4. In general, higher yields were obtained for macrocycles containing a terminal SB-cyclam macrocycle, although as the purification process can cause loss of up to 30 % of product this may just be a coincidence and is a likely explanation for the range of yields obtained (28% - 91%). Solvent molecules were noted in the elemental analysis for all complexes however crystallography data often depicts the association of solvent molecules within the unit cell, high impurity was noted in $[Cu_2\mathbf{28}]^{4+}$, $[Cu_2\mathbf{30}]^{4+}$, $[Cu_2\mathbf{36}]^{4+}$ and $[Zn_2\mathbf{36}]^{4+}$ but this may be as a result of insufficient drying. Carbonyl peaks in $[Zn_2\mathbf{30}]^{4+}$ and $[Zn_2\mathbf{33}]^{4+}$ were assigned in ^{13}C NMR by noting the position of the ester carbonyl peak in prior steps and comparing this with metal complex ^{13}C NMR data, the acetate carbonyl peak was lower field in both cases. Due to time constraints the azide functionalised bis-SB-cyclen-CB-cyclen macrocycle zinc(II) and copper(II) complexes were not synthesised but it would be interesting to synthesise these complexes to ascertain their similarity in affinity to the complexes of **29** and **36**.

3.4.2 Conjugation Reactions of Bis-Macrocycle Metal Complexes

Zinc(II) and copper(II) complexes of **39** were conjugated to carboxyrhodamine 110 dibenzocyclooctyl, see Scheme 16, as outlined in section 3.3.5. Isolation of $[Cu_2\mathbf{40}]^{4+}$and $[Zn_2\mathbf{40}]^{4+}$ was not confirmed by MS, although an unidentified peak at 1082.6 could be a fragment of $[Zn_2\mathbf{40}]^{4+}$. Presence of dye SM was observed in the MS of $[Zn_2\mathbf{40}]^{4+}$ so if the reaction did isolate the desired product it contained a mixture of SM and product. No SM peaks were observed in the MS of $[Cu_2\mathbf{40}]^{4+}$ but neither were product mass ions, it is again possible that the complexes did not fly very well in the MS instrument but further work would be required to confirm that these compounds can be synthesised.

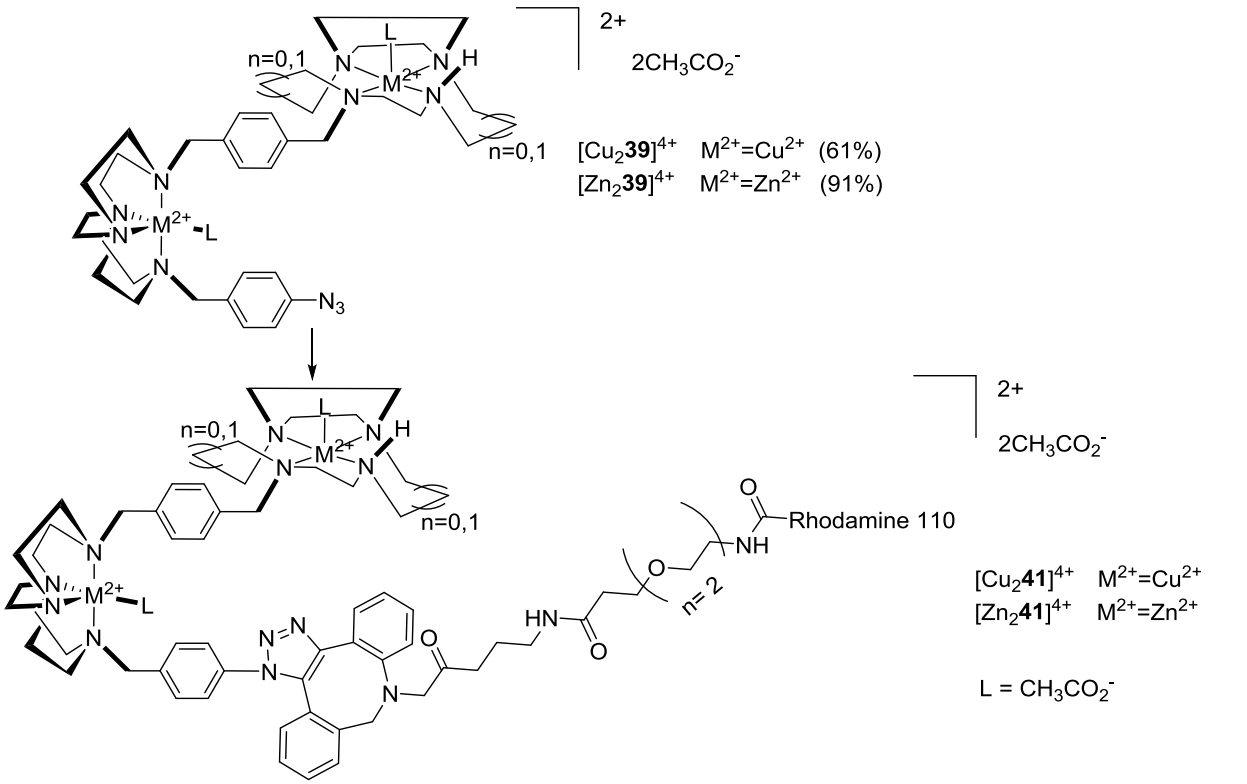

Scheme 16 – Attempted conjugation of amine functionalised bis-macrocycle metal complexes to tetrazine-PEG-NHS

Metal complexes of **34** and **35** were conjugated to tetrazine-PEG-NHS, see Scheme 17, using the same methods as **41**, see section 3.3.5. Characterisation by MS suggested $[Cu_2\mathbf{41}]^{4+}$, $[Cu_2\mathbf{42}]^{4+}$ and $[Zn_2\mathbf{42}]^{4+}$had been isolated, but only weak peaks were observed so the reaction may not have gone to completion, although the compounds may not have flown very well as noted for **41** and **42**. Loss of acetate counterions and zinc(II) ions were observed for $[Zn_2\mathbf{41}]^{4+}$ and may be as a result of decomposition during the MS analysis. Further investigation into these reactions is required.

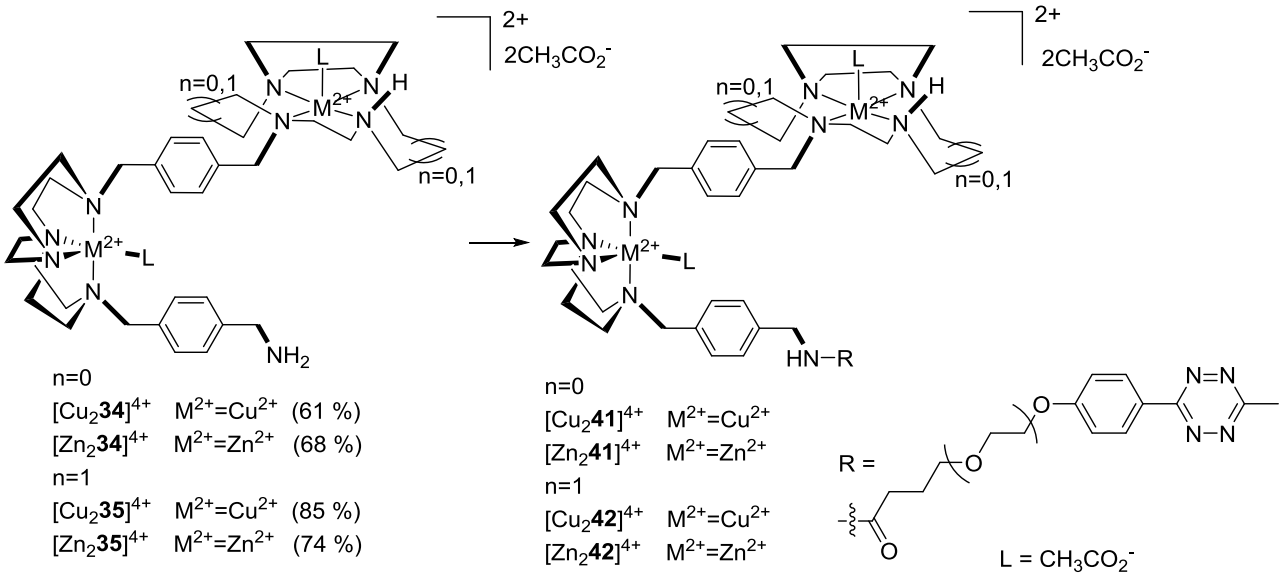

Scheme 17 – Conjugation of amine functionalised bis-macrocycle metal complexes to tetrazine-PEG-NHS

3.5 CONCLUSIONS

This chapter outlines the synthesis of a novel collection of N-functionalised bis-macrocycles for different imaging applications. Zinc(II) and copper(II) complexes have also been synthesised and the biological profile of these complexes was determined and will be discussed in chapter 5 section 5.3.5. Unsymmetrical, configurationally restricted bis-macrocycles may improve interaction with the CXCR4 receptor based on findings by Bridger *et al.* who identified that symmetry was not a requirement for high anti-HIV activity.[79] A novel multi-step synthetic route led to isolation of bis-macrocycles containing both SB and CB macrocycles linked by a *para*-substituted linker group, overall high yields were obtained for **28**-**33**. The terminal linker group was functionalised with nitro, nitrile, amine, azide and ester groups and conjugation to imaging groups for use in PET imaging or optical imaging was explored. Synthesis of macrocycles containing an azide group, **38** and **39**, or an ester group, **30** and **33**, has not been previously reported.

3.6 FUTURE WORK

In order to complete the series of bis-macrocycles it would be worth synthesising zinc(II) and copper(II) complexes of azide functionalised macrocycle **38**. These complexes, in conjunction with $[Zn_2\mathbf{39}]^{4+}$ and $[Cu_2\mathbf{39}]^{4+}$, could then be tested in a series of copper-free click reactions to determine whether they could be labelled with ^{18}F. The complexes could then be tested *in vivo* as PET imaging agents once *in vitro* parameters of cold (^{19}F) derivatives were ascertained.

The series of bis-macrocycles synthesised in this chapter were not coordinated to nickel(II) therefore it would be interesting to determine whether high affinity was observed for these complexes and whether the affinity follows the trends of the tris-macrocycles biological activity profile.

A more in depth investigation into the synthesis of **40** should be conducted in order to determine whether an azide functionalised macrocycle successfully undergoes SPAAC reaction as the initial findings were not conclusive. Furthermore, copper-free click reaction precursor, **42**, requires a more detailed evaluation to ascertain whether the tetrazine group was successfully isolated. Once **42** has been synthesised in high yield its ability to facilitate selective copper-free click reaction with *trans*-cyclooctene, TCO, could be explored. This provides an additional route to radiolabel macrocycles with ^{18}F which would be attached to the TCO group.

Conjugation of DOTAGA-anhydride to **35** requires optimisation because the experimental method established for mono-macrocycle **75**, see chapter 4 section 4.3.5, did not successfully translate to bis-macrocycle, **35**. Once optimised **43** could be radiolabelled with ^{68}Ga(III) following conventional methods. Future studies involving conjugation of multiple bis-macrocycles to the DOTAGA analogue could be completed, see Figure 65. Extra macrocycles could improve affinity as Sano *et al.* experienced increased affinity when multiple CXCR4 targeting peptide groups were bound to DOTA.[215] This idea could be taken further by substituting one acetate arm on DOTAGA-anhydride, for another acid anhydride group, only two acetate arms are needed for ^{68}Ga encapsulation, this would enable conjugation to another bis-macrocycle. It would be interesting to see what difference, one to four bis-macrocycles made to the compounds affinity.

Once these macrocyclic compounds had been isolated they could be conjugated to an imaging group and a biological evaluation could be undertaken to determine if this additional steric bulk has any effect on the ability of the macrocycle to interact with the CXCR4 receptor.

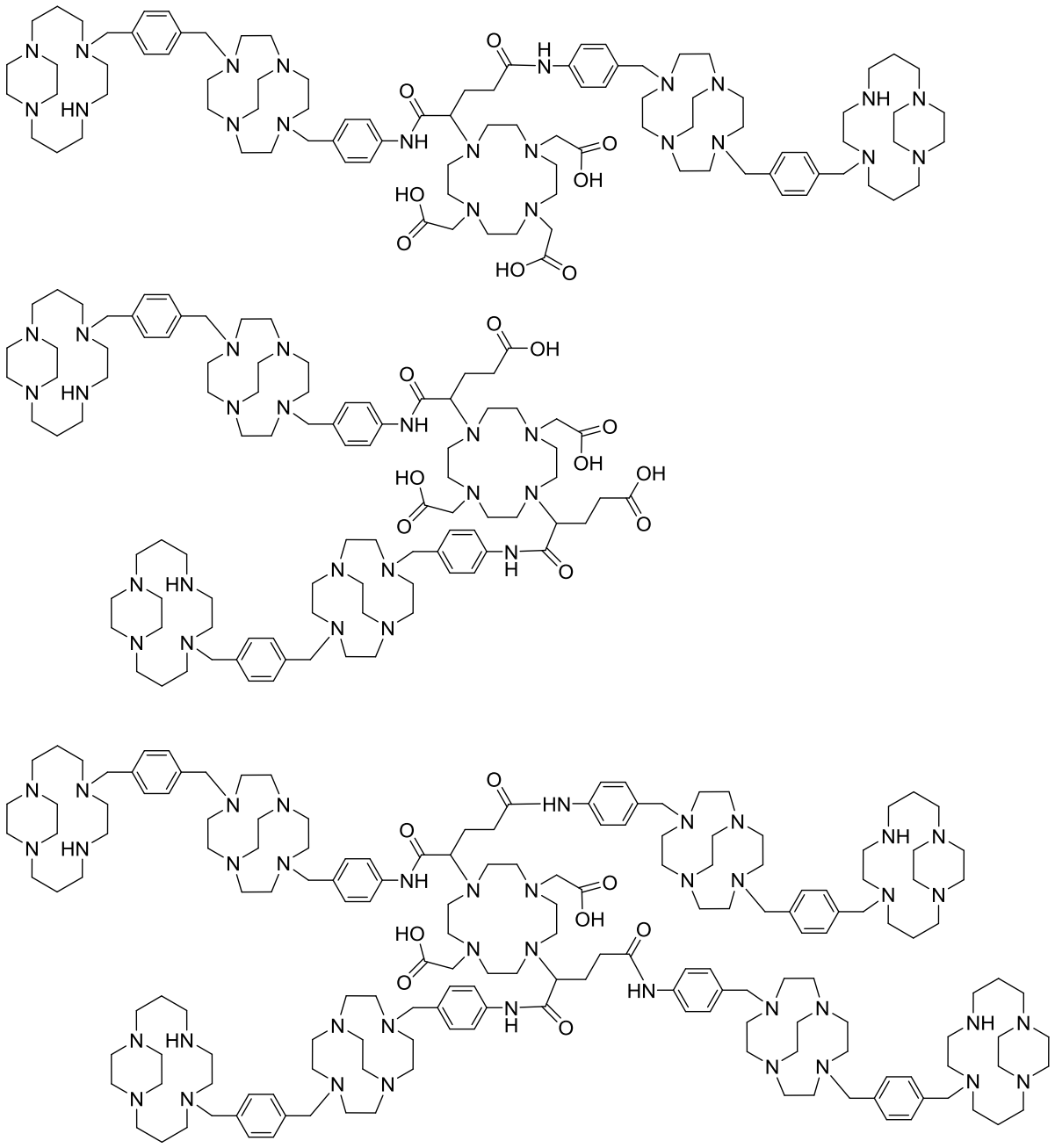

Figure 65 – Potential routes to improve the affinity of DOTAGA conjugated bis-macrocycles

CHAPTER FOUR

SYNTHESIS OF NOVEL MONO-TETRAAZAMACROCYCLES, THEIR METAL COMPLEXES AND TEST REACTIONS

4.1 SYNTHETIC STRATEGY

Novel synthetic routes to isolate previously unreported pendant arms were explored. These pendant arms were attached to mono-macrocycles to obtain a series of novel configurationally restricted CB and SB mono-macrocycles. The ability of these macrocycles to successfully undergo click reactions was subsequently investigated. Alternative pendant arms bearing different functional groups were also studied for conjugation to imaging groups. Conjugation to such groups enables the use of mono-macrocycles in medical imaging to identify CXCR4 expression. Mono-macrocyclic copper(II) and zinc(II) complexes of SB macrocycles were also explored. Mono-macrocycles were synthesised as part of a model system whereby successful synthetic schemes would be extrapolated to bis-macrocycles which have demonstrated higher affinity for the CXCR4 receptor. This chapter discloses a wide range of test reactions using mono-macrocycles due to their ease of synthesis and therefore potential to obtain a large amount of data rapidly.

4.2 PREVIOUS STRATEGIES

In recent years many mono-macrocycles have been synthesised for a wide range of applications such as chemical synthesis, as active catalysts for alkene oxidation, materials with optical and electronic properties but there has also been an extensive amount of work conducted into biological applications.[68] Gano *et al.* synthesised novel tetraazamacrocycles complexed with ^{153}Sm and ^{166}Ho in order to develop bone metastasis targeting agents, shown in Figure 66.[69] Cao *et al.* explored tetraazamacrocycles as HIF prolyl hydroxylase 3 (PHD3) inhibitors for diseases requiring the up-regulation of HIF related genes, this was accomplished through chelating iron(II) generating structures.[70] It would be interesting to see what activity all these compounds had for the CXCR4 receptor.

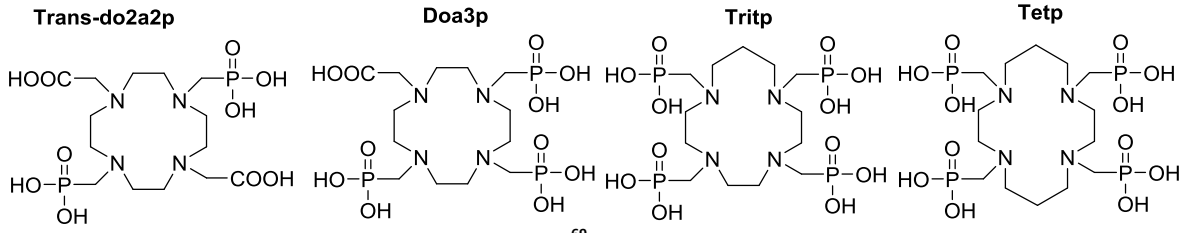

Figure 66 – Tetraazamacroycles synthesised by Gano *et al.*[69]

One of the most commonly investigated mono-macrocycles for CXCR4 antagonism is cyclam. Cyclam is a 14-membered ring and was one of the earliest azamacrocycles tested as an anti-HIV agent.[18] Its activity originated from its ability to target and block the CXCR4 receptor. An impurity in one cyclam batch led to the development of the FDA approved bis-macrocycle AMD3100. Quantum chemistry docking studies revealed that cyclam binds to aspartate residues through three hydrogen bonds. This differs from zinc(II) bound cyclam which was found to bind with one strong coordinate bond

and one hydrogen bond providing an explanation as to why metal complexes show enhanced binding.[168] Like other multi-ring macrocycles mono-macrocycles can be C-functionalised or N-functionalised.

Archibald and co-workers have investigated both C-functionalised and N-functionalised macrocycles.[67, 71b, 81, 102, 160c, 190, 216] Archibald and co-workers have been at the forefront of research into reinforced mono-macrocycles which has resulted in the synthesis of a range of functionalised mono-macrocycles enabling conjugation to molecules such as fluorescent dyes and radiolabelled groups.

4.2.1 C-Functionalised Mono-Macrocycles

In the mid 1990's Edlin *et al.* reported the C-functionalisation of cyclen using an iron(III) template, see Figure 67.[217] The iron(III) template led to the easy isolation of a series of C-functionalised cyclen macrocycles whereas the use of nickel(II) and chromium(II) chloride templates resulted in moisture sensitive intermediate products and de-metalation to isolate the macrocycle proved difficult. The use of iron(III) as a template was preferred because during sodium borohydride reduction of the diimine intermediate the iron(III) centre was also reduced which resulted in successful de-metalation. The group incorporated N-functionalisation into the mono-macrocycles and investigated the photophysical properties of europium(III) and terbium(III) complexes.

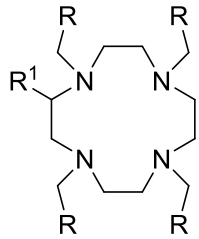

L123 R=COOH, R^1= Ph
L124 R=$PMeO_2H$, R^1= 3-phenanthryl
L125 R=$PMeO_2H$, R^1= *m*-Ph-NO_2
L126 R=$PMeO_2H$, R^1= *2*-fluorenyl
L127 R=$PMeO_2H$, R^1= H

Figure 67 – Cyclen C-functionalised and N-functionalised macrocycles by Edlin *et al.*[217]

Archibald and co-workers reported the synthesis of a mono-macrocycle bearing a nitro functionalised pendant arm on the 6-C position as well as N-functionalisation using a butanedione template,[190b] see Figure 68. They also synthesised a mono-macrocycle containing a 4-nitrobenzyl pendant arm at the 6-C position in addition to benzyl pendant arms on one or two adjacent nitrogen atoms. The synthetic route to C-functionalised macrocycles was very different to standard N-functionalised macrocycle synthesis and involved cyclising the macrocycle ring with 2-(4-nitrobenzyl)-1,3-dibromopropane and a butanedione derived bisaminal to yield the bridged macrocycle, **L128** shown in Figure 68. The bridge facilitated the selective addition of benzyl pendant arms to nitrogen atoms and was then removed to afford **L129** and **L130**, see Figure 68. The application of these molecules was as a bifunctional chelator, BFC. Further work by Archibald and co-workers

led to the synthesis of a configurationally restricted C-functionalised and N-functionalised mono-macrocycle, **L**[131], for use as a BFC.[190a]

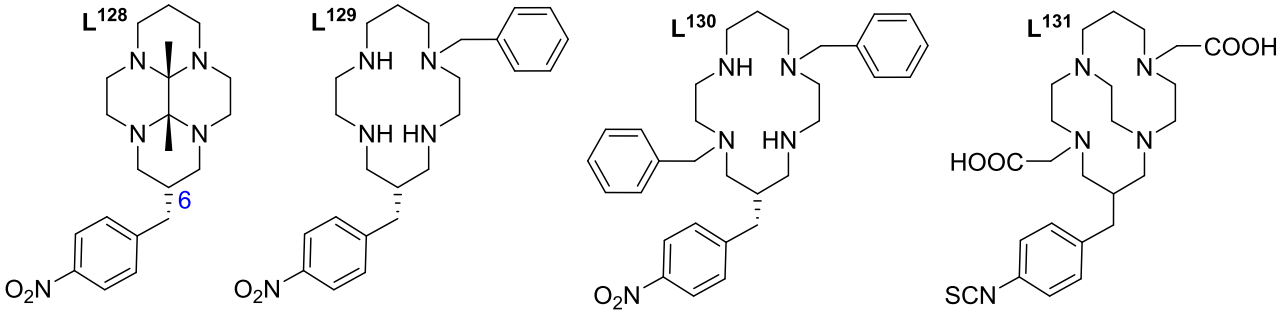

Figure 68 – C-functionalised and N-functionalised macrocycles synthesised by Archibald and co-workers[190]

Boschetti *et al.* investigated C-functionalised mono-macrocycles as BFCs.[218] The benefit of C-functionalisation is that the C-functionalised group can be modified as required but the amine groups remain available for further conjugation to other coordinating groups. The 12-14 membered C-functionalised mono-macrocycles, **L**[132]-**L**[137], were isolated following the bisaminal route using a butanedione template and are shown in Figure 69. The group is currently exploring the N-functionalisation of this series of macrocycles.

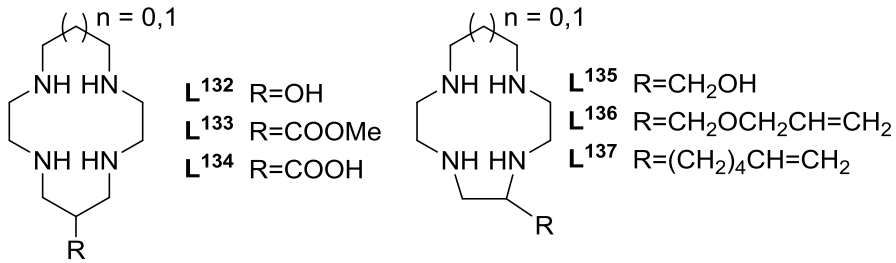

Figure 69 – C-functionalised mono-macrocycles by Boschetti *et al.*[218]

C-functionalised dioxocyclam macrocycles, see Figure 70, have been investigated by multiple groups due to their interesting metal complexing characteristics.[71a, 219] Due to the loss of two amide protons, during metal complexation, metal binding was highly pH sensitive. This property provides a novel application for macrocycles as pH indicators.

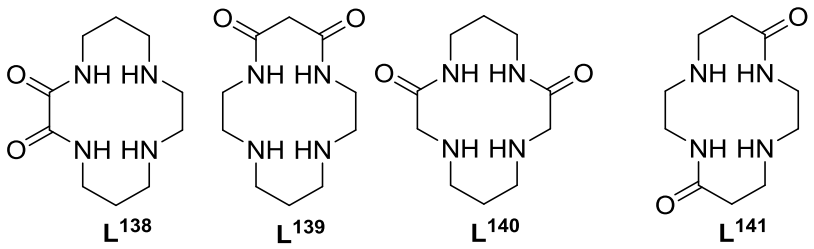

Figure 70 – Dioxocyclam C-functionalised macrocycles[71a, 219]

4.2.2 N-Functionalised Mono-Macrocycles

There is a vast amount of research reporting N-functionalised macrocycles which is not possible to summarise here. A selection of rigidified mono-macrocycles bearing at least one pendant arm will be

discussed to give an idea of the scope of research conducted. Rigidified macrocycles provide selective reaction sights which allow controlled addition of coordinating groups.

Archibald and co-workers have reported many examples of reinforced mono-macrocycles following initial steps taken by Wainwright and Hancock,[60, 62] to isolate SB macrocycles, and Weisman and Wong, to isolate CB macrocycles.[61a] Quaternisation of one of the four tertiary amines in bridged cyclam with an alkyl halide containing pendant arm resulted in the synthesis of this precursor. Smith *et al.* synthesised side-bridged macrocycles, see **L^{142}** and **L^{144}** in Figure 71, functionalised with either a nitrile or amine containing pendant arm, **L^{142}** and **L^{143}**, by simply reducing the macrocyclic precursor in an ethanolic solution of sodium borohydride.[67] Silversides *et al.* synthesised a series of CB mono-macrocycles, see **L^{144}**, **L^{145}** and **L^{146}** in Figure 71, for use as BFCs derived from a mono-substituted mono-macrocycle quaternary salt precursor.[154] Silversides *et al.* went on to quaternerise a second tertiary amine on the adjacent group affording the desired product in approximately 85% yield. Subsequently, reduction with sodium borohydride led to the isolation of the CB macrocycles outlined in Figure 71, **L^{147}** to **L^{150}**. Biological studies have shown these types of compounds to selectively bind to the CXCR4 receptor. These macrocycles are highly attractive as they facilitate conjugation to further groups which improve CXCR4 affinity and can increase the number of applications.

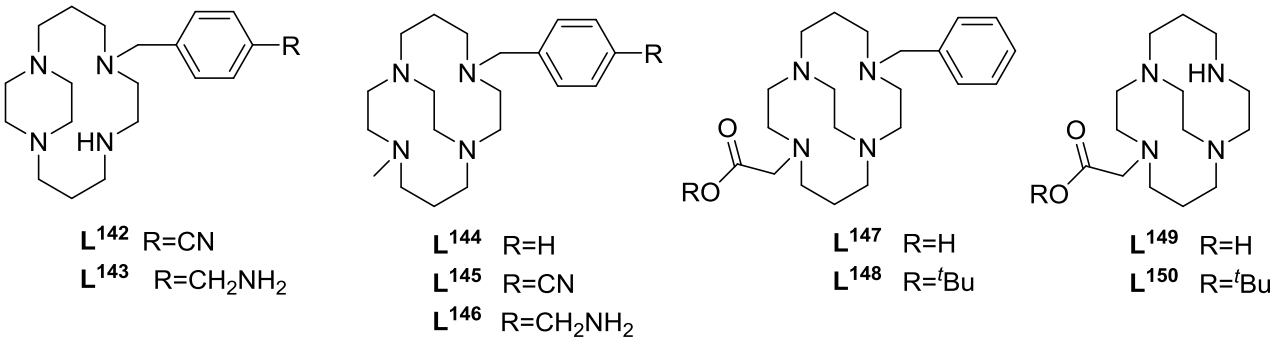

L^{142} R=CN
L^{143} R=CH_2NH_2

L^{144} R=H
L^{145} R=CN
L^{146} R=CH_2NH_2

L^{147} R=H
L^{148} R=^{t}Bu

L^{149} R=H
L^{150} R=^{t}Bu

Figure 71 – Mono-macrocycles synthesised by Archibald and co-workers

Plutnar *et al.* synthesised a series of unsymmetrical mono-macrocycle copper(II) complexes, **L^{151}-L^{154}** with the aim to develop a radiolabelled BFC for *in vivo* applications, see Figure 72.[191] The synthetic route to attain the SB cyclam with a nitro functionalised pendant arm was outlined previously by our group.[102] An unexpected product **L^{151}** was synthesised by reacting $BrCH_2COOH$ with 5-(4-nitrobenzyl)-side-bridged cyclam.[191] Plutnar *et al.* noted that the reaction occurred at N1 either because the twisted boat piperazine conformation means that the nitrogen atom cannot participate in hydrogen bonding thus is available for substitution or that the nitrogen's lone pair is pointing outwards as the piperazine is in the chair conformation. It was found that increasing the polarity of the solvent led to

reaction at N8 and the isolation of **L**[152]. Compounds **L**[153] and **L**[154] were synthesised via Mannich-type reactions in low yields of 27% and 12% respectively. The thermodynamic stability constants of [Cu**L**[151]]$^{2+}$ were ten times higher than **L**[153], however the overall values were lower than expected for constrained tetraazamacrocycles. It was recommended that the macrocycles could be used for copper(II) radiolabelling, although no remarks were made on the binding affinity these compounds would have for the target. The findings detailed by Plutnar *et al.* are important should further conjugation to SB-macrocycles be conducted as they outline specific conditions for reaction at particular nitrogen atoms.

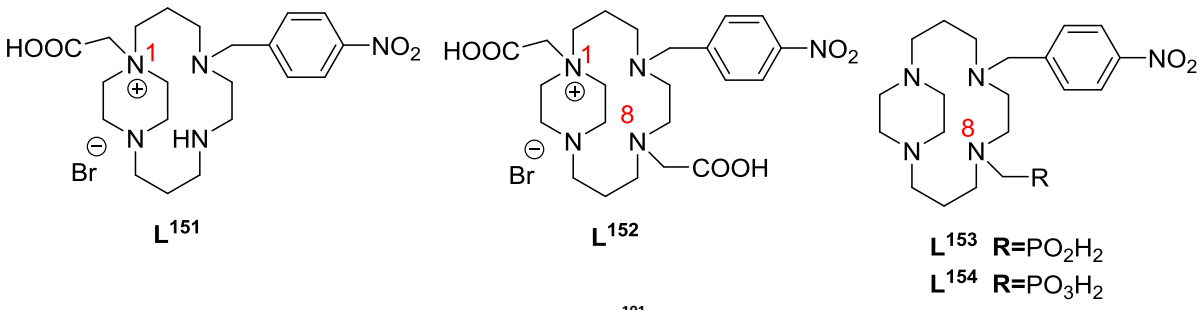

Figure 72 – Plutnar *et al.*'s N-functionalised mono-macrocycles[191]

Weisman, Wong and co-workers have published a series of CB cyclen and cyclam macrocycles with phosphate and carbonyl containing pendant arms as BFCs.[171, 220] Wong and co-workers synthesised **L**[155] and **L**[156], see Figure 73, recently and determined that the corresponding ^{64}Cu complexes showed encouraging kinetic inertness both *in vitro* and *in vivo*.[171] These two compounds were the first examples of CB-cyclam analogues that could be radiolabelled with ^{64}Cu without the need for harsh conditions. The radiochemistry reactions were conducted at RT in 0.4 M ammonium acetate buffer, pH 6.5, and involved shaking for 10 min with $^{64}CuCl_2$ in 2 M HCl. These findings were significant because these conditions provide a rapid route to a highly stable PET imaging agent which means that a greater portion of the half-life can be spent completing multiple tests on the patient. The study is of high relevance to this work and incorporation of ^{64}Cu into a macrocycle using similar conditions is reported in chapter 6 section 0.

Weisman and co-workers synthesised a series of CB cyclen and cyclam macrocycles, see **L**[157] and **L**[158] in Figure 73, and evaluated their potential as BFCs.[220] The longer alkyl chains in **L**[157] and **L**[158] did not negatively impact the stability of the copper(II) complexes however poor clearance of the complexes *in vivo* was noted. This is important to consider when designing novel PET imaging agents as rapid clearance is a desirable property.

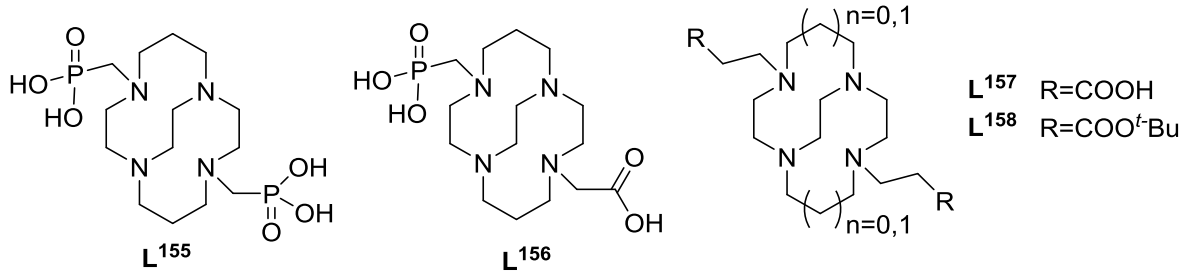

Figure 73 – Structures of CB mono-macrocycles synthesised by Weisman, Wong and co-workers[171, 220]

4.3 SYNTHESIS OF FUNCTIONALISED MONO-MACROCYCLES

Mono-macrocycles have been synthesised by several groups, as described in section 4.2, and shown affinity for the CXCR4 receptor. Mono-macrocycles provide an ideal starting point for the development of new synthetic strategies to afford new endeavours due to their ease and speed of synthesis compared to bis-macrocycles.

The synthesis of novel mono-macrocycles will be outlined in this chapter. Mono-macrocycles were synthesised and utilised as model systems for bis-macrocycles, the synthesis of which is discussed in chapter 3 section 3.3. A model system was chosen because a series of novel reactions could be evaluated rapidly. Mono-macrocycles are also relevant because they can be conjugated to other groups which enhance their applications as well as strengthen their interaction with the CXCR4 receptor through conjugation to a high affinity group.

The schematic shown in Figure 8 highlights the overall aims of the chapter and the large variety of synthetic routes explored. In order to isolate functionalised mono-macrocycles, precursors containing desirable functional groups were synthesised. The synthetic route to glyoxal cyclam and glyoxal cyclen has been discussed earlier in chapter 2 section 2.4.1 therefore this discussion will focus on the synthetic routes after these steps as well as the synthesis of macrocycle pendant arms which resulted in the isolation of a series of novel mono-macrocycles.

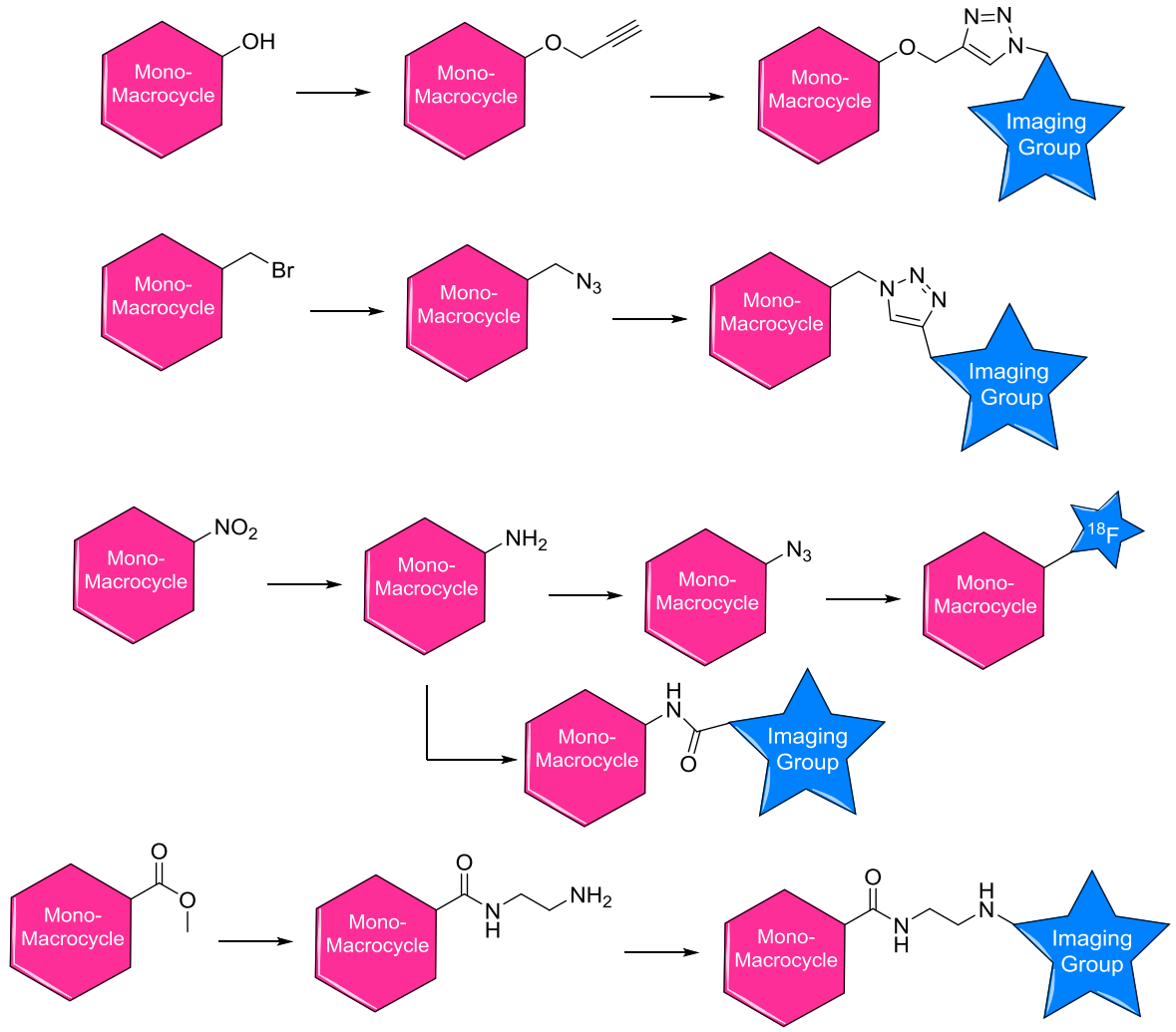

Figure 74 – Schematic of synthetic routes explored incorporating mono-macrocycles

4.3.1 Synthesis of Pendant Arms

Whilst there are an abundance of click chemistry reactions, as discussed in section 3.3.5, the commonly used Cu(I) catalysed azide alkyne Huisgen cycloaddition was selected. The pendant arm was synthesised separately because it meant purification was a lot less problematic as macrocycles are difficult to purify once they contain a bridge. It also meant that the data was much less complicated and easier to interpret which meant isolation of the desired product was quicker. Once functionalised the pendant arm was reacted with the macrocycle and the established synthetic route to isolate a SB and CB macrocycle was followed.

In order to develop macrocycles able to undergo click reactions the incorporation of an azide and alkyne group onto the pendant arm was investigated as part of this work. The advantage of synthesising both variations was that comparisons could be made during click reactions and any differences could be ascertained. The starting point for both pendant arms was α-α'-dibromo-*p*-xylene because it is a readily available reagent and would isolate the product in one synthetic step, although varying degrees of success were experienced during the synthesis of the pendant arms.

The attempted synthesis of an azide containing pendant arm is outlined in Scheme 18. Small azide compounds can be explosive but a general rule outlined by Bräse *et al.* states that if the carbon:nitrogen rule is followed then azide compounds can safely be isolated and handled.[221] If the sum of carbon and oxygen atoms divided by the number of nitrogen atoms is equal to or more than three then the compound is seen as safe. If the number of azide nitrogens is higher than the total number of carbon and oxygen atoms then the compound is very likely to be explosive.

The first synthetic route to synthesise **47** began by reacting α-α'-dibromo-*p*-xylene with a molar equivalent of sodium azide in dry DMF. A mixture of products was expected (**47** and **47b**) and thin layer chromatography (TLC) was used to determine whether the products could be separated. Unfortunately, the products had the same R_f values and therefore could not be separated. Nonetheless, the Staudinger reaction and the ninhydrin stain provided evidence that the reaction had yielded the desired product.

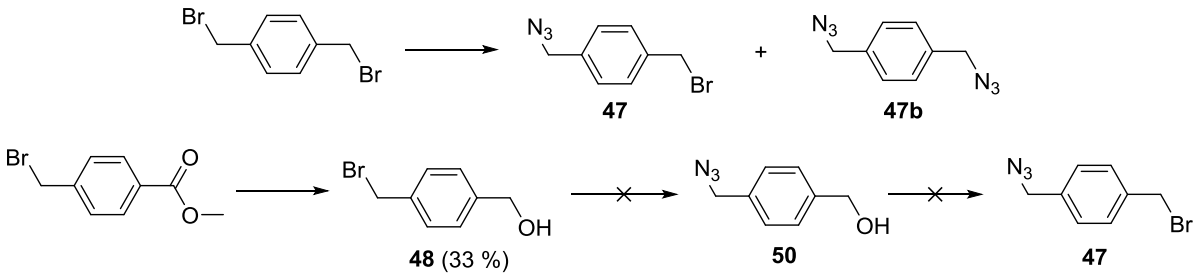

Scheme 18 – Attempted synthesis of an azide containing pendant arm

Consequently, an alternative synthetic route was tested which began with the reduction of methyl-4-(bromomethyl)benzoate with $LiAlH_4$ to afford compound **48** in 33% yield, see Scheme 18. **48**, was characterised by NMR and MS.

Nucleophilic substitution of the bromide to an azide using sodium azide was subsequently conducted to obtain **50**. The reaction was tried in two different solvent systems the first used water, a method obtained from Ju *et al.*,[222] and the second method with DMF. The second method was disclosed by multiple researchers, Luehr *et al.*,[223] Maury *et al.* and Lee *et al.*, who all obtained almost quantitative yields.[224] However, neither reaction resulted in the desired product being isolated. It would be worth testing conditions and solvents, such as THF and DMSO used by other groups, in the future. An alternative rectification could be increasing the heat to drive the reaction. As the product was not isolated the final bromination step with PBr_3 could not proceed.

The alkyne functionalised pendant arm was synthesised according to the synthetic route shown in Scheme 19. The reaction of propargyl alcohol with α-α'-dibromo-*p*-xylene to yield compound **45** has

not been reported, although its reaction with benzyl bromide has been reported.[225] Adapting the method outlined by Farran *et al.*,[225] a 1.1 molar excess of α-α'-dibromo-*p*-xylene was reacted with propargyl alcohol in dry DMF. Analysis concluded that only the di-alkyne product formed, so the synthesis was repeated using a two molar excess of α-α'-dibromo-*p*-xylene, however only the di-alkyne product was isolated. The second attempt produced a greater quantity of material it was just unfortunate it was not the desired product. Due to the consistent acquirement of the di-alkyne product an alternative route was investigated.

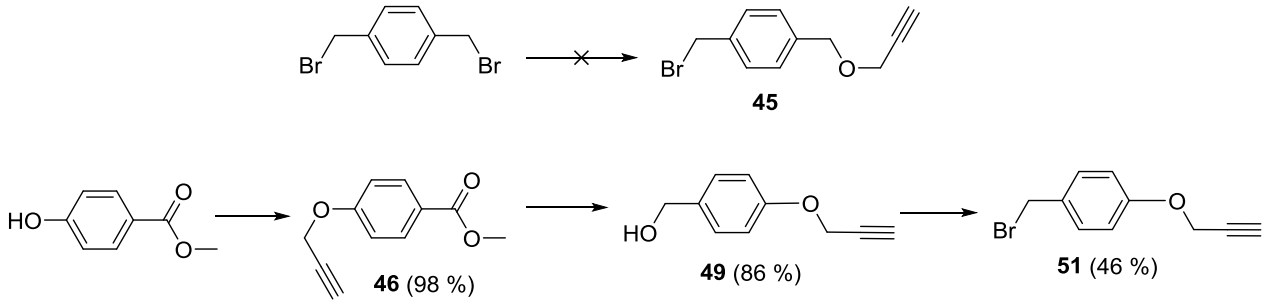

Scheme 19 – Synthetic routes to an alkyne functionalised pendant arm

The second route began with a Williamson-ether reaction with propargylbromide and methyl-4-hydroxylbenzoate to form methyl-4-(prop-2-yn-yloxy)benzoate (**46**) in almost quantitative yield, see Scheme 19, a literature value was not available for comparison. Compound **46** was characterised by HRMS and elemental analysis proved the product was pure. **49** was successfully synthesised by reduction with lithium aluminium hydride in dry THF. The ^{1}H-NMR revealed a trace of starting material which was removed by prep-TLC to yield **49** in 86% yield. The final stage of the reaction scheme was a bromination reaction with phosphorus tribromide in dry DCM to afford **51** via a modified version of the method by Streitwieser *et al.*[226] A crude yield of 4.34 g was obtained, however the reaction contained starting material so plug column chromatography was carried out. This reduced the yield to 46% which was low compared with literature yields for the equivalent benzyl bromide reaction of around 80%.[226] A longer reaction time may have been required to drive the reaction to completion. TLC indicated that only a small amount of the starting material was present therefore some product may have remained with the starting material and not all travelled down the column. CHN data confirmed the impurity of **51** (<10%). A solution to this would be to carry out full column chromatography, but this is more time consuming and an increase in yield may not be guaranteed, it is nonetheless a route worth pursuing.

4.3.2 Synthesis of Alkyne Functionalised Mono-Macrocycle

Following the successful formation of the alkyne functionalised pendant arm **51**, a series of test reactions were completed to determine whether CB and SB alkyne functionalised macrocycles could

be isolated. In the interest of time, the test reactions were conducted with mono-macrocycles glyoxal cyclam (**2**) and glyoxal cyclen (**3**), the synthesis of which is shown in Scheme 20. Quaternisation of a tertiary amine was achieved by reacting **2** or **3** with a molar equivalence or 2x excess of **51** respectively. The reaction time to isolate **57** was significantly shorter than for **58** to prevent the formation of the disubstituted product as observed in other work, see chapter 3 section 3.3.1. Impurity was noted in the elemental analysis of **57**, which is likely to have been due to impure starting material, **51**. Excellent yields of 75% and 100% were achieved for **57** and **58** respectively and both were characterised. Yields reported in the literature for mono-substituted bridged cyclen macrocycles varied between 40% -100%.[161, 192, 227] Isolation of **58** was initially tested on a smaller scale whereby a yield of 77% was attained. A quantitative yield was attained on a larger scale, comparable to similar reported literature values,[191] therefore this scale may be favoured.

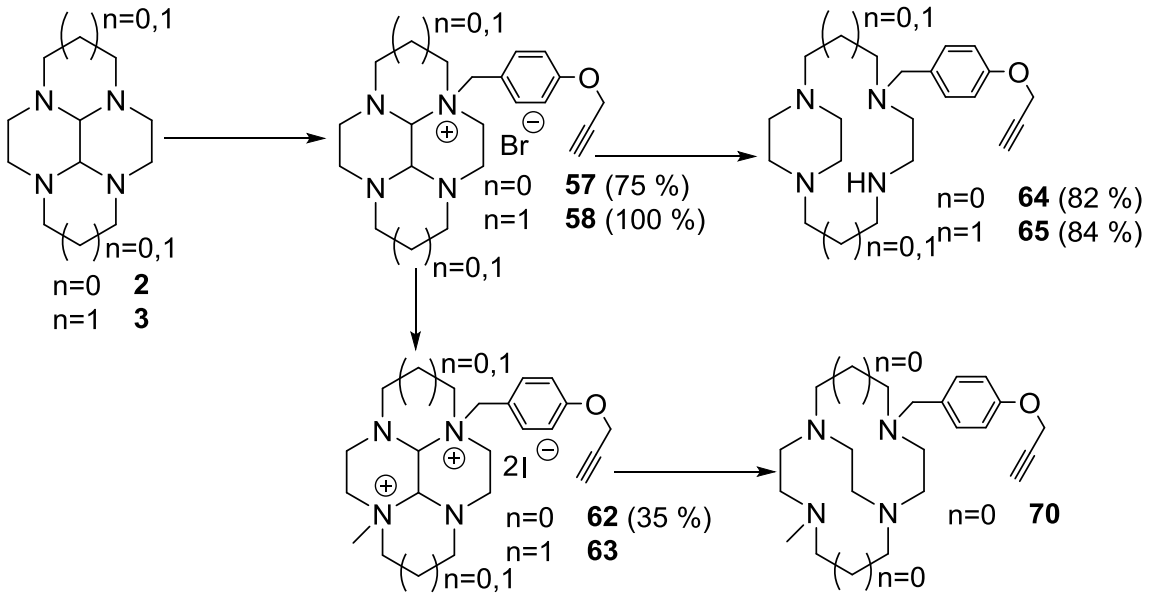

Scheme 20 – Synthesis of SB and CB alkyne functionalised mono-macrocycles

Reduction of **57** and **58** was carried out according to established literature methods[67, 102, 160a, 191] with sodium borohydride to produce the characterised SB macrocycles **64** and **65** in excellent yields of 82% and 84% respectively. ^{13}C NMR confirmed isolation of the products due to disappearance of the distinctive C_{aminal} peaks. Impurity was noted in **65** and is most likely due to salt contamination, removed by a desalting Sephadex LH20 column after metal complexation. **65** was coordinated to copper(II) in methanol to isolate $[Cu\mathbf{65}]^{2+}$, see Scheme 21, in excellent yield and characterised by HRMS and elemental analysis.

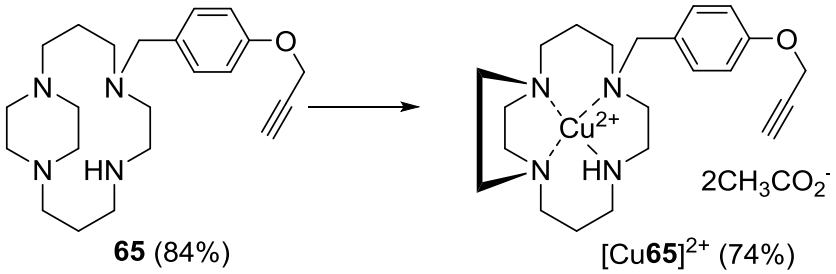

Scheme 21 – Coordination of SB alkyne functionalised mono-macrocycles to copper(II)

Alkylation of the N8 tertiary amine with methyl iodide led to the CB macrocycle precursors **62** and **63**, completed as described by Silversides *et al.*[154] A large excess of methyl iodide and a long reaction time of 10 d, was used to ensure methylation. The compound was characterised and shown to be pure. Reduction of **62** with $NaBH_4$ in an ethanolic solution, as outlined previously in chapter 2 section 2.4.3, was successful and the isolation of **70** was confirmed by HRMS and NMR.

The ^{1}H and ^{13}C NMR spectra of **63** revealed an absence of peaks in the aromatic region. This was firstly attributed to the NMR sample being too weak; however loss of an aromatic pendant arm was confirmed upon increasing sample concentration. Loss of an aromatic group during alkylation was a phenomenon that has never been reported previously for macrocycles and the addition of a methyl group to form a CB macrocycle is a well-established method. The massive excess of methyl iodide results in dimethyl glyoxal cyclam following pendant arm displacement. One explanation for this observation is that the propargyl oxo group is facilitating removal of the pendant arm and relates to the stability and electron density associated with terminal alkynes. Alkyne pendant arm loss has been experienced with porphyrins in unpublished work and caused an aliphatic alkyne chain to be cleaved under mild conditions.[228] Compared with other alkynes, terminal alkynes are the least stable, have high electron density and they are quite acidic but alkyne addition reactions are slow. However, the long 10 d reaction with readily available iodide ions and the drive to become more stable may have caused the unexpected product. Conversely, **62**, see Scheme 20, was sucessfuly isolated and characterised, therefore the larger cyclam ring may play a role. This area of work requires further investigation in order to achieve a CB cyclam macrocycle functionalised with an alkyne pendant arm. Bryden found that replacing propargyl bromide with 4-bromo-1-butyne prevented the removal of the alkyne chain in subsequent reactions because it hindered resonance.[228] In light of this, a new synthetic route to synthesise **52** was attempted, see Scheme 22.

Scheme 22 – Atempted alternative synthesis of an alkyne functionalised pendant arm and macrocycle

52 was synthesised by the same method as **46**, however after 24 h the desired product was not isolated. The reaction time was increased but despite this the product was not isolated. Rationalisation for this could be that the temperature was not high enough to drive the reaction, switching to a solvent with a higher boiling point may resolve this. In an attempt to functionalise a macrocycle with an alkyne, 4-bromo-1-butyne was reacted directly with glyoxal cyclam (**3**) as described by Archibald and co-workers to attain **61**, see Scheme 22.[154] Due to the lack of precipitate after 3 d the reaction was to reacted for a further 10 d as outlined by Le Baccon *et al.*[156] A negligible amount of precipitate had formed but the long reaction time afforded the di-substituted product. The absence of precipitate was observed by Silversides *et al.* who conducted a similar reaction with *tert*-butyl bromoacetate and glyoxal cyclam.[160c] The alkyl pendant arm appears to react faster than the standard aromatic pendant arms because Silversides *et al.*'s achieved a 93% yield following removal of solvent *in vacuo* after 16 h at RT,[160c] as opposed to filtration of product precipitate after 3 d. It would be recommended to repeat this reaction using Silversides *et al.*'s method in the future.

An alternative reaction scheme was devised using well reported literature methods, see Scheme 23. Tosyl chloride was reacted with 3-butyne-1-ol in DCM in the presence of TEA to afford **53** in 72% yield. Distinct alkyne peaks in ^{13}C NMR and additional alkyl peaks confirmed isolation. The modified method by Battenberg *et al.* led to **54**, heating the solution at reflux for 16 h attained a yield comparable to the literature.[229] An aldehyde proton and low field CH_2-C=O protons in place of a high field methyl proton peak in ^{1}H NMR confirmed the isolation of **54**. The presence of a carbonyl peak in place of a methyl peak in the ^{13}C NMR supported this. Characterisation by MS and NMR confirmed reduction of the carbonyl with $NaBH_4$ to obtain **55**, as outlined by Battenberg *et al.*[229] Elemental analysis was not obtained as traces of SM remained therefore the product was acknowledged as impure, purification was to be conducted at the final step *via* column chromatography. The final bromination step with PBr_3 to afford **56** was not achieved due to experimental error. Due to time constraints the repetition of **56** was not pursued, this would be an ideal avenue for future work.

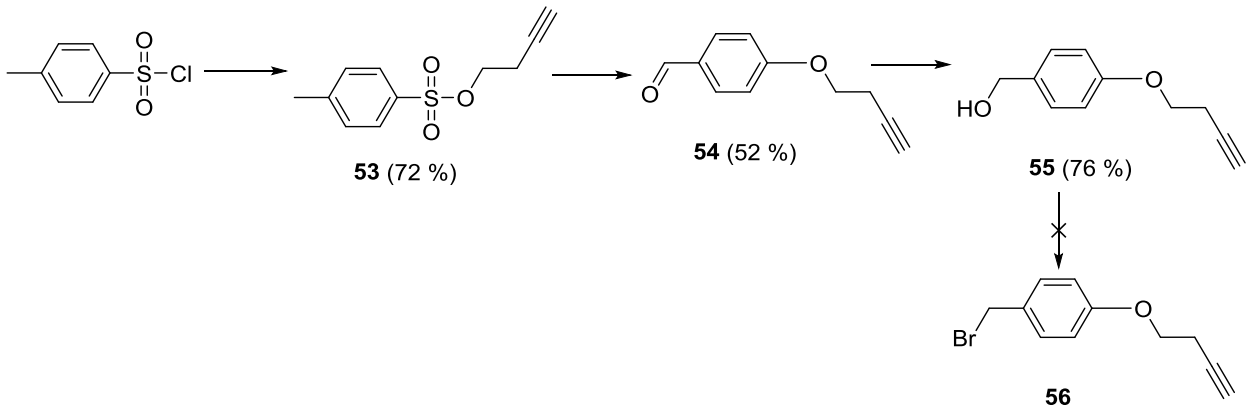

Scheme 23 – Novel synthesis of an alkyne functionalised pendant arm

4.3.3 Click Reactions with Alkyne Functionalised Macrocycles

The SB cyclam macrocycle functionalised with an alkyne pendant arm (**65**) was reacted with azide functionalised compounds, see Scheme 24 and Scheme 25. A copper(I) catalysed click reaction using copper(II) sulfate pentahydrate was selected as these conditions had been optimised for porphyrins **83** and **84**, synthesised by Francesca Bryden. The copper(II) ion was reduced *in situ* by sodium-L-ascorbate to afford the copper(I) catalyst. Conjugation of **83** to **65** was conducted at 45^{o}C in a microwave for 20 min but TLC revealed the reaction was unsucessful. Microwave reactions are advantageous because microwaves facilitate quick and efficient heating which has been extensively reported in the literature to enhance the speed of reactions.[202, 222, 230] As the overall aim of this study was to attach a radiolabelled group to the macrocycle quickly it was essential that the reaction be rapid due to the short lived half-lives of radioisotopes.

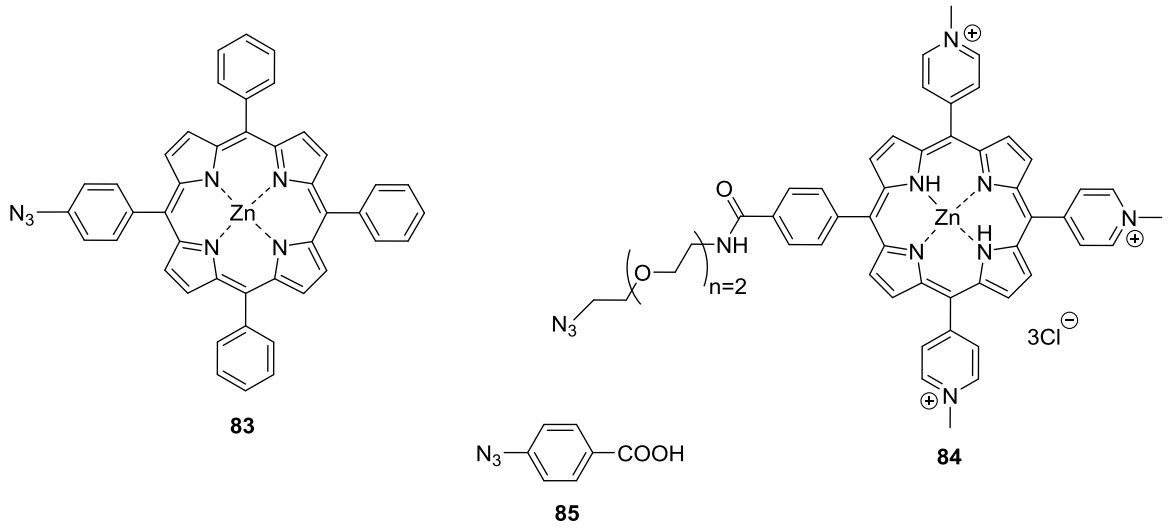

Scheme 24 – Donated Compounds: 83 and 84 were synthesised by Dr Francesca Bryden, compound 85 was synthesised by Dr Louis Allott

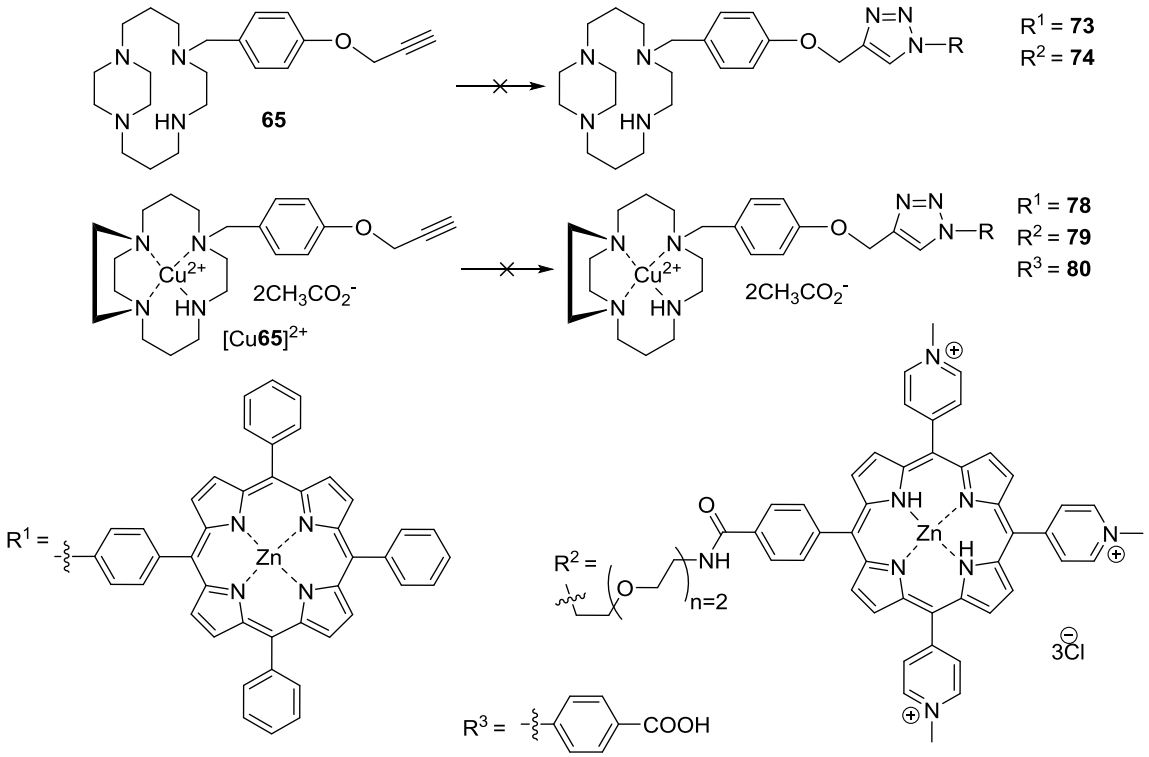

Scheme 25 – Click reactions with 1-(4-(prop-2-yn-1-yloxy)benzyl)-1,4,8,11-tetraazabicyclo[10.2.2]hexadecane (65)

To test whether an increase in temperature would drive the click reaction an alternative porphyrin, **84**, which could tolerate higher temperatures, was tested. Porphyrin (**84**) and macrocycle (**65**) were heated to 80°C for 40 min in the microwave but the desired product was not isolated. A possible explanation for the failure of the click reactions could be related to the macrocycle. It seemed highly likely that the macrocycle was chelating copper(II) ions quicker than the sodium-L-ascorbate could reduce them therefore no catalyst was generated to drive the reaction. On the other hand, Tamanini *et al.* successfully "clicked" a fluorophore to a non-complexed cyclam, using a lower molar ratio of catalyst and reducing agent than click reagents, and made no mention of copper(II) chelation affecting the reaction. Therefore, the macrocycle rigidity, enforced by the ethylene bridge, may be responsible for the failure of the click reaction. In order to test this theory [Cu**65**]$^{2+}$ was substituted into reactions in place of **65** and the click reactions were repeated but were also unsuccessful. This suggests that the catalyst may not be hindering the click reaction. The attempted synthesis of **79** generated a deep red product and was attributed to a transmetalation reaction, porphyrin is green when coordinated to zinc(II) ion but deep red with copper(II). The strong chelating abilities of **65** must have been responsible. This observation is extremely unusual as it is well reported that copper(II) coordinated, reinforced macrocycles show high stability even in physiological conditions when zinc(II) ions are available so it is hard to rationalise. If a CB macrocycle had been tested it would have been interesting to see if this more robust structure could have prevented the transmetalation reaction and provides opportunity for future investigation.

The unsuccessful click reaction could be due to steric bulk of **65** and **83**/**84** causing the reaction to be sterically hindered. This hypothesis was tested by reacting [Cu**65**]$^{2+}$ with a smaller azide functionalised compound, **85**, synthesised by Dr Louis Allott. Conditions reported by Szíjjártó *et al.* were followed and are the only reported click reactions with macrocycles.[211a] A fresh batch of Cu(I)I was used to catalyse the reaction, specifically chosen to rule out any problems caused by oxidised catalyst which is common with old reagent due to exposure to light and moisture. No reactions involving Cu(I)I were successful and copper(I) catalysed click reactions were not explored further.

4.3.4 Synthesis of Alternatively Functionalised Mono-Macrocycles

Nucleophillic aromatic substitution has generated high interest for the synthesis of ^{18}F-labelled molecules because of the excellent availability of [^{18}F]fluoride from cyclotrons. The only report of [^{18}F]fluorinated macrocycles was by Oltmanns *et al.,* whilst there have been many groups radiolabeling macrocycles the majority have utilised their excellent chelating ability to encapsulate positron emitting radioisotopes such as ^{68}Ga and ^{64}Cu.[105, 231] Oltmanns *et al.* generated the PET image shown in Figure 75 with their [^{18}F]fluorinated Zn_2bis-cyclen compound which shows significant uptake of macrocycle in the tumour in comparison to the control.[105] This research proved that the development of [^{18}F]fluorinated macrocycles was viable and that they have strong potential as PET imaging agents for *in vivo* studies.

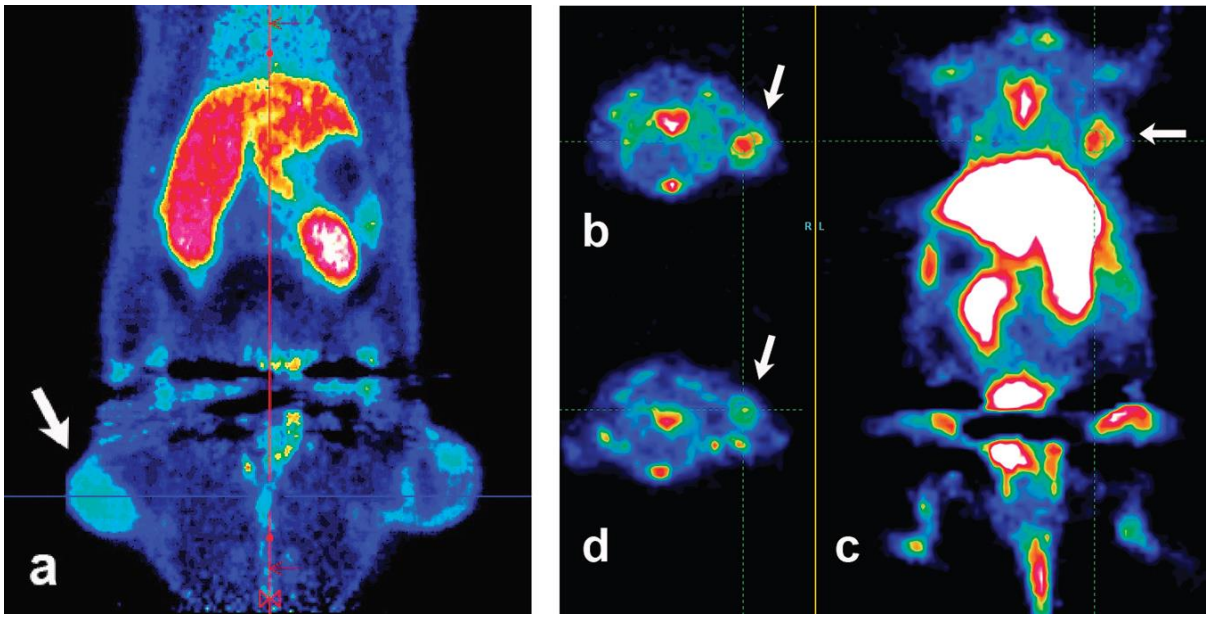

Figure 75 – PET images of [^{18}F]-fluorinated Zn_2bis-cyclen[105]
a) 1 hour coronal PET image of a rat with a bilaterally transplanted Dunning prostate adenocarcinoma 6 d after 50 Gy radiation therapy, the irradiated tumour is indicated by the arrow. b,c,d) 1 hour PET image of a mouse with HelaMatu tumors (arrows). b,c) two days after treatment with taxol, b) transaxial slice, c) coronal slice. d) transaxial slice of the untreated control after two days.

The frequently reported method of [^{18}F]fluorination via nucleophilic aromatic substitution, S_NAr, was investigated, see Figure 76.[232] Aromatic rings, activated by electron withdrawing groups, EWG, such

as nitrile, nitro and halides at the *ortho* or *para* position, are often used in S_NAr in combination with good leaving groups, for example nitro or halide.[232a] Good radiochemical yields, RCYs, with isotopic exchange, $^{18}F/^{19}F$, and substitution of nitro have been reported.[233] [^{18}F]fluoride is produced by irradiating enriched [^{18}O]water, via the $^{18}O(p,n)^{18}F$ nuclear reaction.[234] [^{18}F]fluoride ions are subsequently trapped on an anion-exchange resin cartridge and eluted with Kryptofix solution, K_{222} shown in Figure 76, potassium carbonate or caesium carbonate in water or acetonitrile. Solvent is removed under vacuum for 10 min by azeotropic drying at 110°C with a stream of nitrogen. Once completely dry the desired precursor dissolved in reaction solvent is added and the mixture is heated for a short period of time, for example 50-70°C for 5-15 min. HPLC is normally used to confirm the reaction outcome and purify the product.

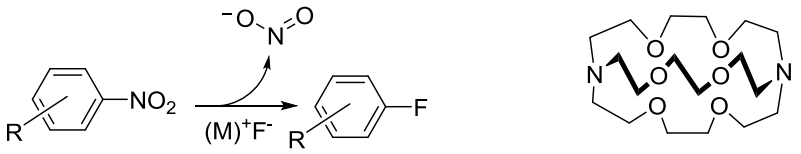

Figure 76 – Fluorination pathways via nucleophilic aromatic substitution

Using the published method by Khan *et al.* quaternerisation of the N1 tertiary amine in glyoxal cyclam with 1-bromomethyl-4-nitro-benzene led to isolation of **59** in almost quantitative yield.[102] Full characterisation of **59** confirmed that the desired product had been attained which allowed the next synthetic step to be carried out, although impurity was noted in the elemental analysis. An overview of the synthesis is shown in Scheme 26.

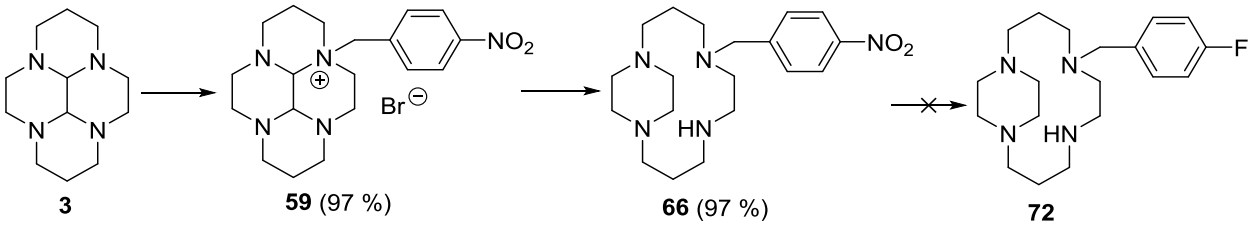

Scheme 26 – Attempted synthetic route to the fluorinated SB mono-macrocycle, 72

The reduction method outlined by Khan *et al.* was followed to obtain **66** in 97% yield,[102] which was significantly higher than Khan *et al.*'s yield, ca. 56%, and similar to Plutnar *et al.*, ca. 95%.[102, 191] The method involved heating an ethanolic solution of $NaBH_4$ and macrocycle at reflux for 2 h before quenching the reaction with HCl and isolating the product with a basic work up. Disappearance of C_{aminal} peaks in the ^{13}C NMR confirmed isolation of **66**. Elemental analysis indicated that **66** was impure (>10%).

Multiple fluorination reactions with **66** were conducted in the microwave, see Table 3. This route to introduce a fluoride, using ^{19}F as a model for incorporation of radioisotope ^{18}F, into the macrocycle is highly advantageous as it removes the need for copper(I) catalysts which had previously caused

problems, see section 4.3.3. Potassium fluoride and TBAF were selected because they are commonly used as [^{18}F]fluorinating agents in the literature.[230a, 234-235] None of the reactions led to the successful isolation of **72**. Test number 3, see Table 3, was conducted for a shorter period of time because previous work noted that multi-ring macrocycles degraded when heated at 130°C for 30 min.[236] Whilst this series of test reactions were conducted on mono-macrocycles it was seen as logical to only investigate optimum conditions that could then be extrapolated to desired multi-ring macrocycles. Even under the harsh conditions outlined in Table 3 the desired product was not obtained. These unsuccessful findings were supported by the work of Shen *et al.* who conducted ^{18}F-fluorination reaction on nitrobenzene and obtained an extremely low 1% RCY.[232a] Whilst this was the first report of a fluorination reaction without the presence of an EWG in the *ortho* or *para* position it is certainly not an optimised radiochemistry reaction. A significantly greater RCY, ca. 84%, was achieved with the introduction of an electron withdrawing carbonyl group, in the *ortho* position by Shen *et al.*[232a] This work suggests that the pendant arm requires the presence of an EWG to viably radiolabel a macrocycle with ^{18}F.

Test Number	Reagent	Solvent	Temperature / °C	Time / min
1	KF	MeCN	85	30
2			100	30
3			130	15
4		DMSO	130	10
5			130	15
6	TBAF	THF/MeCN	100	5
7		THF/DMSO	130	10
8			160	10

Table 3 – Reagents, solvents, temperatures and times tested to fluorinate 66 – Attempted

Another synthetic pathway investigated the incorporation of an azide group directly to a macrocycle, see Scheme 27. Test reactions were conducted on mono-macrocycles as they were quicker to make than bis-macrocycles.

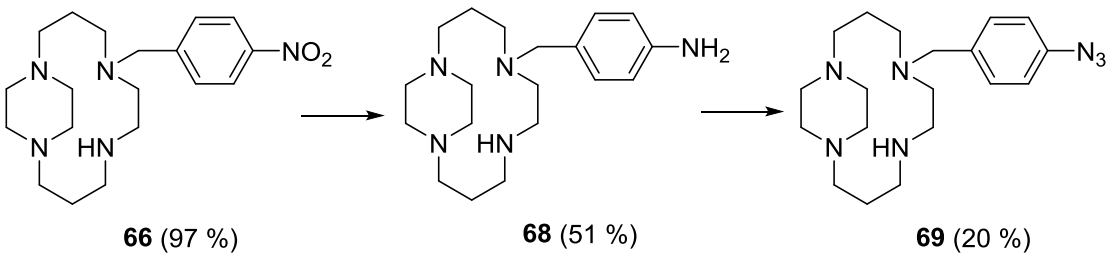

66 (97 %) **68** (51 %) **69** (20 %)

Scheme 27 – Synthesis of azide functionalised macrocycle, 69

The nitro-group was reduced using the same method outlined for the bis-macrocycles in section 3.3.4. Modified methods from the literature by Kaye *et al.* and Sun *et al.* using 10% Pd/C to catalyse the hydrogenation reaction resulted in the isolation of **68** in good yield.[196-197] The distinguishing high field shift of the aromatic peaks in the ^{1}H NMR spectrum confirmed the reduction of the nitro group. The triazotization reaction is discussed in detail in chapter 3 section 3.3.4 but Griffin *et al.*'s and Belkheira *et al.*'s modified methods were followed.[199-200] The low yield obtained may be the optimum yield possible because across a range of reaction scales and macrocycle types the yield was reproducible. Optimisation may be achieved with more concentrated solutions, but the low yield could be due to loss during the reaction work up. Despite this, azide functionalised macrocycles had been successfully isolated which provided proof of concept for direct azide incorporation for use in rapid copper-free click reactions.

4.3.5 Conjugation reactions

An additional macrocycle functionality, incorporating a carboxylate group, was explored for reaction with amines attached to fluorescent dyes. Our group has previously synthesised **60**, see Scheme 28, but the method is not reported in the literature. A modified method by Silversides *et al.* was followed to yield the characterised product in excellent yield, 13% higher than the yield reported by Silversides *et al.*, 76%.[154] Reduction of **60** has not previously been reported but modified literature methods by Khan *et al.*, Plutnar *et al.* along with a patent held by our group were used to produce the desired product (**67**) with $NaBH_4$ in 99% yield.[102, 162, 191]

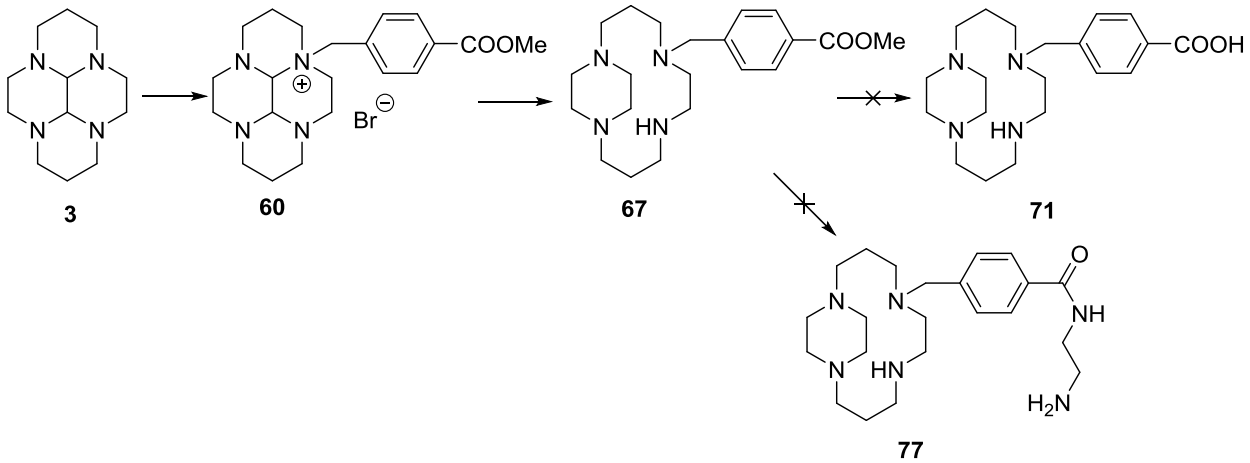

Scheme 28 – Synthesis of ester functionalised macrocycle, 67

Disappearance of the C_{aminal} peaks in the ^{13}C NMR confirmed the successful production of **67** although the presence of water was noted in the ^{1}H NMR therefore the product was dried under high vacuum to remove it. Interestingly the transesterification noted with the ester functionalised bis-macrocycles, see section 3.3.3, was not observed for **67** which strengthens the argument that a long reaction time facilitates transesterification. Hydrolysis of the ester group was conducted using

aqueous NaOH to produce the sodium salt, this was converted to the desired carboxylic acid by treatment with hydrochloric acid although the crude product could not be purified by recrystallisation due to lack of solubility of the product.

Another approach to utilise the ester functionalised macrocycle was investigated. An amide group was synthesised by reacting **67** with excess ethylene diamine, see Scheme 28, to enable conjugation of a fluorescent dye for an optical imaging application. The longer chain provided by ethylene diamine could reduce steric hindrance generated by a bulky dye group. In addition to this, the spacer group may prevent interference with macrocycle interactions with the CXCR4 receptor as noted by Khan *et al*.[102] Khan *et al.* observed that a copper(II) complexed mono-macrocycle affected the photophysical properties of the fluorescent dye when directly conjugated to the macrocycle pendant arm.[102] MS revealed that a dimer of **77** had formed even though a four times excess of ethylene diamine was used to prevent this from occurring. A larger excess of ethylene diamine may prevent the dimer from forming, but its high boiling point ca. 116°C makes it difficult to remove. It may be better to protect one of the amine groups and deprotect it after reaction with the macrocycle. This investigation was taken no further but avenues for future development are apparent.

The successful amine functionalisation of a SB mono-macrocycle inspired conjugation of **68** to DOTAGA anhydride for application in PET imaging with the incorporation of ^{68}Ga as shown in Scheme 29. Test reactions were initiated by the synthesis of **75** following the method by Lopez-Prados.[237] Whilst isolation of the product was confirmed by HRMS a mixture of products was revealed which suggested that the procedure required optimisation however this test reaction was conducted primarily to ascertain the viability of the reaction. As purification of rigidified macrocycles can be complex it would be ideal to develop a reaction that goes to completion. However, due to the mass difference of the product and SM, size exclusion chromatography may be a viable purification method if a quantitative reaction could not be achieved. An alternative method was outlined by Collman *et al.* who reacted glutaric anhydride with aniline in DCM in the presence of triethylamine and achieved an 88% yield after 4 h.[238]

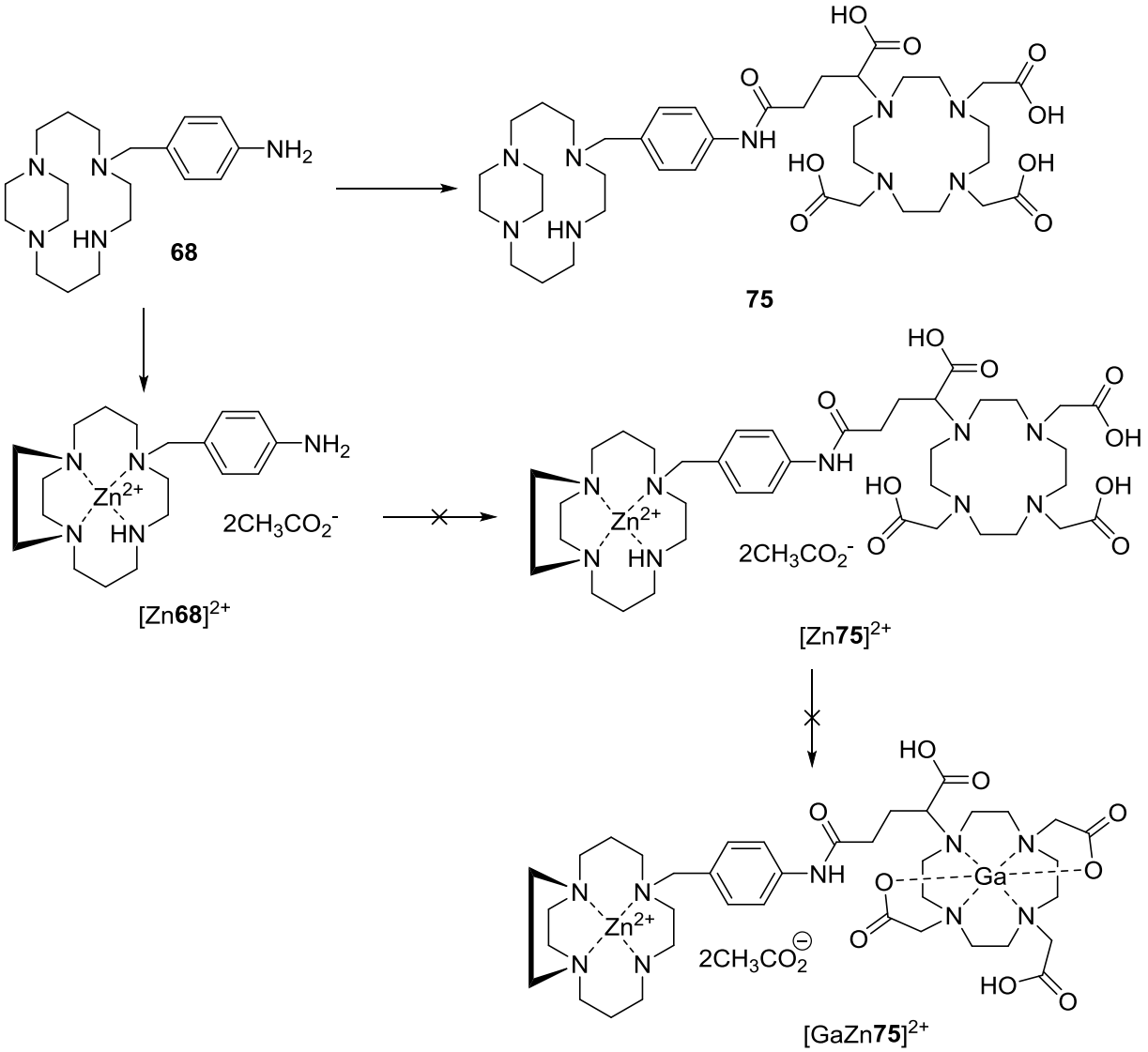

Scheme 29 – Attempted synthesis of gallium(III) conjugated mono-macrocycle

A second attempt to synthesise **75** was carried out in dry THF with TEA following a modified method outlined by Fumio *et al.*, similar to the method outlined by Ito *et al.*[239] Ito *et al.* conducted condensation reactions of acid anhydrides with primary amines and achieved yields of 59%-98%.[239b] Isolation of **75** was confirmed by MS but the peak was very weak. The acid anhydride group on DOTAGA anhydride is moisture sensitive and may have degraded over time hindering the reaction. Another route taken to isolate the DOTAGA conjugated macrocycle was via the zinc(II) complex of **68**, isolated using the literature method reported by our group.[71b] Subsequently, the zinc(II) complex was reacted with DOTAGA anhydride following the same procedure as for **75** but isolation of the product was not confirmed therefore incorporation of gallium(III) could not be studied. The synthesis of **75** requires optimisation which could be achieved by changing solvents, Collman *et al.* replaced THF with DCM to achieve the desired product in high yields.[238]

4.4 CONCLUSIONS

In conclusion, a novel route to synthesise a pendant arm capable of undergoing click chemistry has been developed (**51**). The alkyne pendant arm was achieved in good yield and was successfully conjugated to SB-cyclam (**65**), SB-cyclen (**64**) and CB-cyclen (**70**), although synthesis of a CB-cyclam (**63**) derivative was unsuccessful. The synthesis of a separate azide pendant arm was not successful (**47**) in isolating the desired product but this would be meaningful to revisit. The N:C ratio calculation ((number of carbon atoms + number of oxygen atoms)/number of nitrogen atoms ≥ 3)[221] generates a value that implies the product is unlikely to be explosive. On the other hand, the alkyne pendant arm does not pose any explosive potential so it may be more advantageous to pursue this route. Nonetheless, functionalisation of an azide pendant arm was achieved through hydrogenation of a nitro group followed by triazotisation which overcomes any explosive potential due to the larger N:C ratio (**69**). This synthesis provided a relatively quick pathway to generate good yields of macrocycles able to conjugate to a variety of different molecules enabling additional applications. The synthetic routes discussed resulted in the isolation of alkyne and azide functionalised macrocycles which are readily available for subsequent reactions. Unfortunately, all copper(I) catalysed reactions, **73**, **74**, **78**-**80**, with the alkyne functionalised macrocycle were unsuccessful but it would be worth investigating alternative copper-free click reactions.

The nucleophilic aromatic substitution of the nitro group (**72**) on a mono-macrocycle was explored as a means of fluorination to expand the application of macrocycles as PET imaging agents, but lack of an EWG on the aromatic ring prevented these reactions being successful. An alternative route to incorporate a PET radioisotope was explored through the conjugation of DOTAGA anhydride to an amine functionalised macrocycle (**75**), whilst the product was isolated the reaction requires optimisation to drive the reaction to completion. Efforts to utilise an ester functionalised macrocycle (**71**, **77**) proved ineffective however, these test reactions provided insight as to the direction that future work could explore.

4.5 FUTURE WORK

This chapter contains a wide range of test reactions conducted to expand the scope of macrocycle functionality. In many cases there were not specific literature protocols available which meant that many novel synthetic routes had to be devised. As a result of this there were many cases of non-optimised reactions therefore the opportunities for development are vast, a selection of the potential routes for progression will be discussed but this is certainly not a comprehensive list.

4.5.1 Pendant Arm Development

There were multiple stages of pendant arm development that did not achieve the desired product so there are a number of areas for development. The synthesis of an azide containing pendant arm compound number **47** was unsuccessful so it would be worth repeating the nucleophilic substitution step for the azide in place of the bromide, **50**. Routes to achieve this could include substituting the solvent and driving the reaction by heating it.

Nucleophilic aromatic substitution of **70** did not work because there was not an EWG activating the aromatic ring, development of a pendant arm that incorporates this vital group could facilitate the reaction. Scheme 30 outlines some potential synthetic routes to devise a pendant arm capable of reacting successfully to produce a fluorinated pendant arm. Test reactions would be conducted with the pendant arm attached to mono-macrocycles first before proceeding to analogous bis-macrocycles. This proposed scheme offers an efficient solution to overcome the fluorination problems encountered in this work.

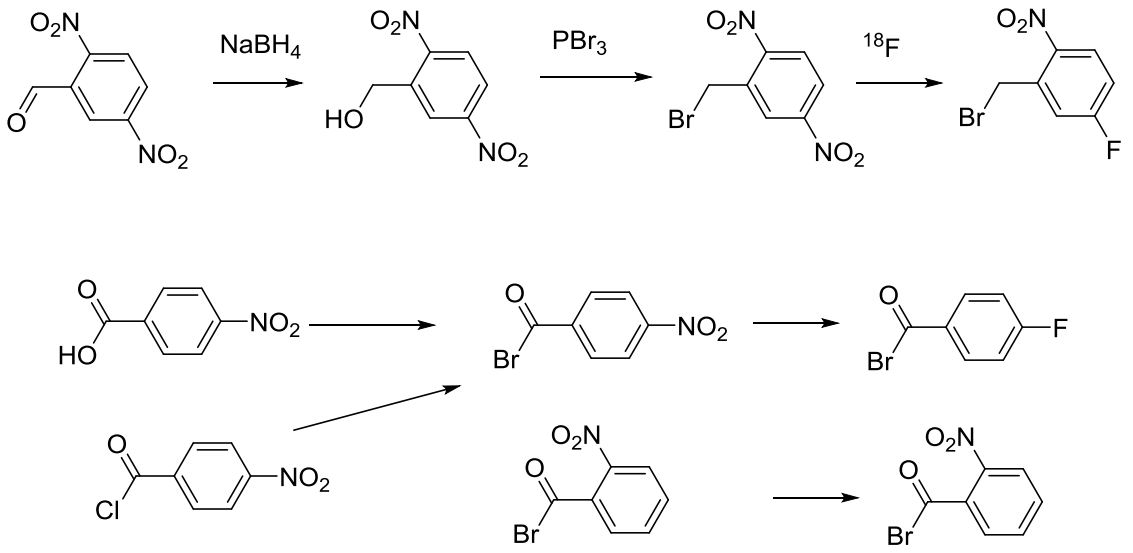

Scheme 30 – Proposed synthetic route to fluorinated pendant arms containing EWG in *ortho* or *para* position

4.5.2 Alkyne Functionalised CB Cyclam

Due to the interesting displacement of the pendant arm observed with **63** it would be advantageous to repeat the synthetic scheme outlined below, see Scheme 31, to determine whether a longer alkyl

chain between the aromatic group and the alkyne would hinder resonance and prevent pendant arm cleavage for the alkyne functionalised CB cyclam. Another reaction to repeat would be the synthesis of **61** as it provides a quick route to functionalising the macrocycle with an alkyne, though the method by Silversides *et al.* should be followed because a similar product to **61** was synthesised which did not precipitate out of solution.[160c] It would be logical to follow the different work up disclosed by Silversides *et al.* to isolate **61** as it does not precipitate out of solution.

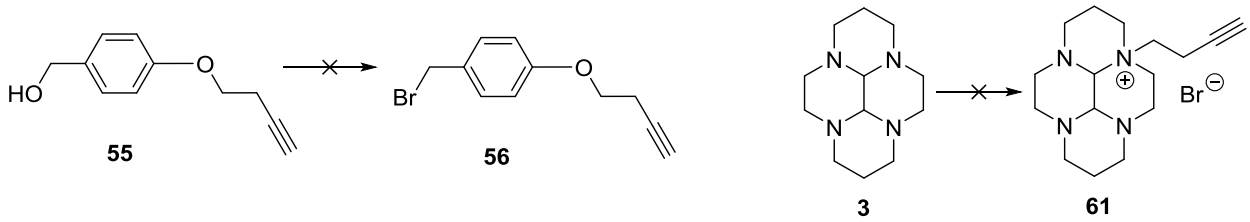

61

Scheme 31 – Synthesis to alkyne functionalised CB-cyclam

4.5.3 Conjugation Reactions

The conjugation of ethylene diamine to **67** is strongly worth further investigation because it would require very little work to successfully isolate **77** as the conditions would only need fine-tuning. A potential plan would be to BOC protect one amine group controlled by molar ratios. The resultant product could then be reacted with **67** before deprotection with HCl to yield the desired product. It would be interesting to investigate a range of chain lengths using the same synthetic routes so that, once labelled with fluorescent dye, the photophysical and biological properties could be evaluated to see if a longer chain length has an impact on these properties. The macrocycles would require copper(II) complexation beforehand as it is the paramagnetic metal ions that cause the quenching of photophysical properties.

A final recommendation for future work would be to repeat the conjugation of DOTAGA anhydride to **68** because this would then provide an additional route to radiolabelling a macrocycle with a well-established, stable, PET imaging group. In order to do this a fresh batch of DOTAGA anhydride should be used and a range of solvents and time scales should be studied to ascertain the optimum conditions for the reaction. Once this was established the incorporation of the zinc(II) ion could be tested which would then produce a molecule ready for radiolabelling with ^{68}Ga.

CHAPTER FIVE

BIOLOGICAL EVALUATION OF MULTI-RING MACROCYCLES AND THEIR METAL COMPLEXES

5.1. STRATEGY

This aims of this chapter are to explore the ability of novel compounds synthesised in chapters 2 and 3 to act as CXCR4 antagonists. Bis-macrocycles and tris-macrocycles were evaluated to assess how effectively they interacted with the CXCR4 receptor. Optimisation of the macrocycles was achieved through structural configuration by introducing an ethylene bridge into the macrocyclic cavity to generate CB and SB macrocycles known to constrict macrocycles to a single configuration. Configurational restriction in macrocycles has previously exhibited high biological activity. Free-ligands, metal-free macrocycles, along with corresponding copper(II), zinc(II) and, in the case of the tris-macrocycles, nickel(II) coordinated macrocycles were initially evaluated before further assays were conducted with the metal complexes. A range of biological assays were used to determine this and data will be presented from displacement assays, anti-HIV assays, cytotoxicity assays and calcium signalling studies. The clinically licenced drug AMD3100 was used for comparison in anti-HIV assays, cytotoxicity assays and calcium signalling studies. From this data the effect of structure on potency will be evaluated. This chapter also aims to investigate the best SPR method for screening novel CXCR4 antagonists. A range of tested SPR methods will be presented as well as sensorgrams generated from these experiments.

5.2. PREVIOUS STUDIES

5.2.1. Biological Assays

In comparison to the quantity of work exploring the design and synthesis of macrocyclic ligands, there is a limited volume of work in the literature discussing the ability of these ligands to act as CXCR4 antagonists. The majority of reports evaluate macrocycle anti-HIV activity rather than anti-metastatic activity.

The forerunners in this field are De Clercq and co-workers who first analysed the anti-HIV activity of a collection of bis-macrocycles in 1992, see Figure 77 and Table 4.[240] Subsequently conducting an in depth bis-macrocycle study into the structure and affinity relationship in MT-4 cells shortly after.[79] It was concluded that anti-HIV potency was dependant on the linker group connecting 12-14 membered macrocycles. Slight differences in structure also had an effect on the cytotoxicity. Some examples of the structures and results from De Clercq and co-workers are shown in Figure 77 and Table 4. The data strongly implied that an *ortho*-substituted xylyl linker is detrimental to the potency of bis-cyclam, the optimum linker being the *para*-substitution. 12- and 13-membered macrocycles however showed the highest potency with a *meta*-substitution although the toxicity of the 12-membered compounds was greater than other macrocycles tested, see Table 4.

Compound	IC_{50} HIV-1(III_B) (μM)	CC_{50} (μM)
JM1498	399	1248
JM1657	0.144	319
JM2763	0.248	>622
	EC_{50} (μM)	
L^{161}	0.075	20
L^{162}	0.322	55
L^{163}	0.041	>184
L^{164}	0.167	>208
L^{165}	0.034	>421
L^{166}	1.357	>168
AMD3100	0.004	>421

Table 4 – Anti-HIV potency of selected tetraazamacrocycles by De Clercq and co-workers, JM1498, 1657, 2763 values from De Clercq 1992[240], L^{161}-L^{166} and AMD3100 values from Bridger 1995.[79]

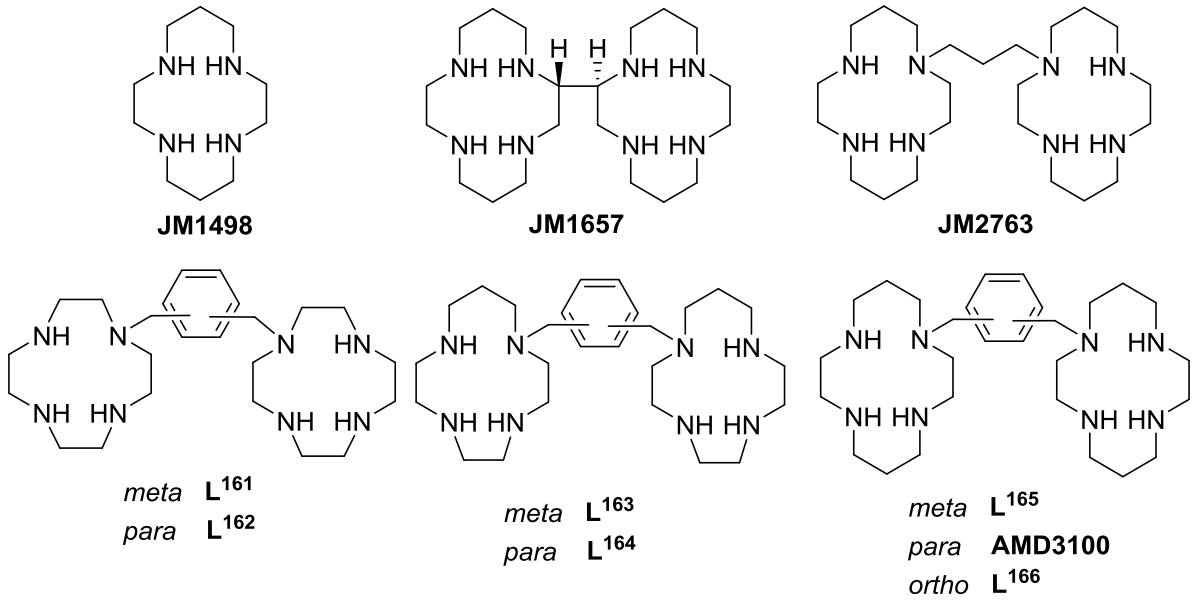

Figure 77 – Some 12-14 membered tetraazamacrocycles structures as described by De Clercq and co-workers[79, 240-241]

A study by Bridger *et al.*, discussed in section 3.2.2, investigated the affect that incorporating a pyridine and pyrazine linker into bis-cyclam had on the anti-HIV activity in MT-4 cells.[79] It was concluded that whilst the linker nitrogen atom facilitated an interaction with the adjacent macrocycle it impeded anti-HIV activity by altering the macrocycle into a shape not as suited to binding to the target. Anti-HIV activity was found to depend greatly on the substitution pattern of the linker group with 2,4- pyridyl substitution, **L^{101}** see Figure 51 section 3.2.2, showing low potency and high toxicity. Optimum pyridine linkers were 2,6- and 3,5-, **L^{102}** and **L^{103}**, which showed comparable anti-HIV activity, see Figure 51 section 3.2.2.

More recently, De Clercq and co-workers investigated the structure:activity relationship further and concluded that not all nitrogen atoms in AMD3100 were required for high anti-HIV potency.[242] This led to the development and evaluation of analogues containing one macrocycle; selected structures can be seen in Figure 78. Replacing one cyclam with benzylamine significantly reduced potency, its

EC_{50} value was 100 fold higher than AMD3100. *Ortho* and *para* amino-phenyl substituents, **L**[167] and **L**[168] see Figure 78, decreased potency to EC_{50} values of 1.825 μM compared to 0.717 μM respectively and **L**[167] showed high toxicity with a CC_{50} value of 24 μM. Changing the aromatic group for 2-pyridine, AMD3645, resulted in a significantly increased anti-HIV activity of 9 nM. Replacing both macrocycles with the optimised group, **L**[169] see Figure 78, resulted in very poor activity suggesting that the presence of the ring is of great importance. To ascertain which parts of the structure were vital each amine group was replaced individually. Substituting the amine in **L**[170] for CH, **L**[171] see Figure 78, decreased activity 40 fold indicating that the hydrogen bond acceptor is crucial for activity. A series of potent compounds had been synthesised with superior or comparable activity to AMD3100; optimum features for antiviral inhibition and oral administration had been recognised.

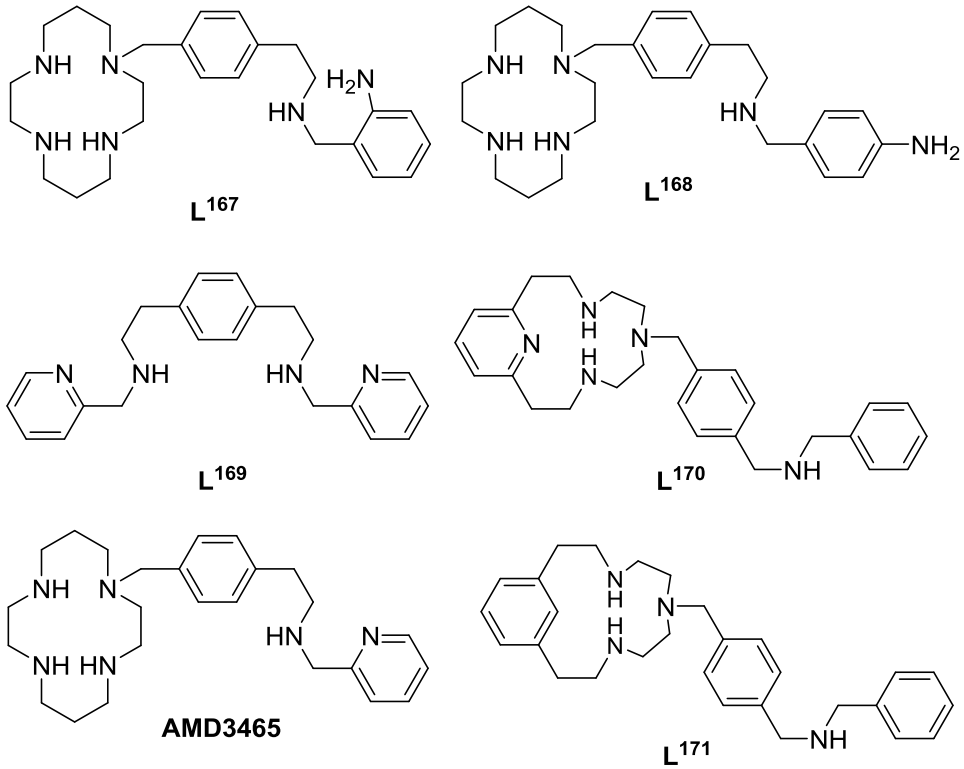

Figure 78 – Selected structures of AMD3100 analogues by Bridger *et al.*[242]

Archibald and co-workers have incorporated configurational restriction into mono- and bis-macrocycles and evaluated the affect this had on CXCR4 inhibition.[67, 71b, 81, 170] Anti-HIV activity assays on AMD3100 and **L**[35], see Figure 23 in section 1.2.3.7, showed that restricting the macrocycle with a SB significantly decreased anti-HIV activity due to the reduction in possible H-bonding interactions. On complexation to certain transition metals the antagonistic ability and anti-HIV potency was greater than AMD3100, this difference was greater when zinc(II) was incorporated. Ni_2[**L**[35]] exhibited around half the IC_{50} concentration than AMD3100 and Zn_2[**L**[35]], see Table 5, achieved approximately 4 fold greater anti-HIV activity than AMD3100 and Zn_2AMD3100 when tested in MT-4 cells infected

with HIV-1(III_B). Rigidifying the macrocycle structure of $\mathbf{L^{34}}$, see Figure 23 in section 1.2.3.7, ensured that the copper(II) complex would favour metal coordination bonds with oxygen atoms from the carboxylate groups on the aspartate residue of the CXCR4 receptor. The cross-bridged copper(II) complex showed 2.5 fold greater activity than AMD3100 when tested on HIV-1(III_B) infected MT-4 cells. It was concluded that the increase in activity originated from the coordinate bonds forming with the copper(II) complex as opposed to weaker hydrogen bonds as observed in AMD3100. However, the increase also related to the optimisation of the structure by configuration because simply complexing AMD3100 to copper(II) leads to a decrease in activity. This trend was also observed in zinc(II) complexes and validates the strategy of configurational restriction in addition to highlighting the importance of metal incorporation. The six fold increase in anti-HIV activity from SB $Cu_2[\mathbf{L^{35}}]$ to CB $Cu_2[\mathbf{L^{35}}]$, see Table 5, suggests that the CB configuration could be optimum for binding. The SB complex is confined to the *trans*-II configuration whereas the CB is forced into the folded *cis*-V configuration. This is because the incorporation of the bridge prevents the macrocycle from switching between configurations. Restriction of the configuration facilitates coordinate bond formation leading to enhanced potency.

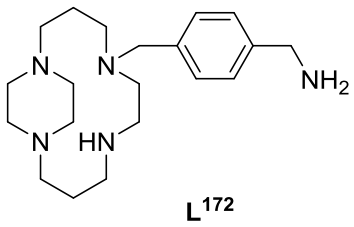

$\mathbf{L^{172}}$

Figure 79 – Structures of ligands synthesised by Archibald and co-workers.[67]

Compound	IC_{50} HIV-1(III_B) (μM)	EC_{50} HIV-1(III_B) (μM)	CC_{50} (μM)
$\mathbf{Ni[L^{172}]}$	8.32	N/A	N/A
$\mathbf{L^{35}}$	N/A	6.980	>225
$\mathbf{Zn_2[L^{35}]}$	N/A	0.0025	60.6
$\mathbf{Cu_2[L^{35}]}$	N/A	0.026	>150
$\mathbf{Ni_2[L^{35}]}$	0.014	0.074	N/A
$\mathbf{Cu_2[L^{34}]}$	N/A	0.004	N/A
$\mathbf{Ni_2[L^{34}]}$	0.194	0.398	N/A
AMD3100	0.031	0.011	>225
$\mathbf{Zn_2}$**AMD3100**	N/A	0.008	>225
$\mathbf{Cu_2}$**AMD3100**	N/A	0.047	>225

Table 5 – Biological evaluation of configurationally restricted macrocycles and their metal complexes by Archibald and co-workers[67, 71b, 81, 170]

Tanaka *et al.* synthesied a collection of bis-macrocycles as discussed earlier,[79-80, 178a] see section 1.2.3.6. The percentage inhibition against [^{125}I]CXCL12, and IC_{50} were determined for the free ligand as well as the corresponding zinc(II) and copper(II) complexes. It was concluded that the most active compounds were $Zn_2[\mathbf{L^{173}}]$ and $Zn_2[\mathbf{L^{174}}]$, see Figure 80, with IC_{50} values of 11 nM and 8.3 nM respectively and these were comparable to AMD3100 and Zn_2AMD3100 IC_{50} values of 11 nM and 8

nM respectively. The high potency of Zn_2[**L**^{173}] and Zn_2[**L**^{174}] validates the strategy of evaluating unsymmetrical bis-macrocycles, furthermore, potency may be enhanced by configurational restriction.

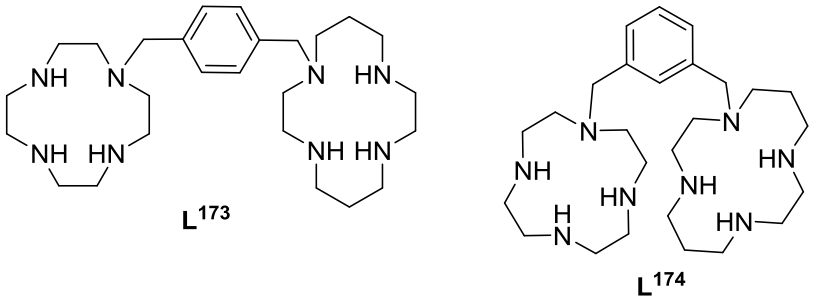

Figure 80 – Most active compounds as established by Tanaka *et al.*[80]

5.2.2. Surface Plasmon Resonance (SPR)

There are many different methods used to generate SPR biosensor data although the amount of literature outlining GPCRs in SPR is rather limited work. The study of GPCRs with SPR has encountered numerous problems mainly because the receptor requires a lipophilic environment to maintain its natural conformation. In order to help with solubility detergents are often used, however this alters the receptor conformation which could change how ligands bind.[243] A further problem is that the process of purification and reconstitution of membrane proteins is time consuming and complex. To overcome this issue some ligand binding SPR assays are conducted on intact cells, however in general there is a limited amount of work in the literature about GPCRs SPR procedures.[243-244] The advantage of SPR biosensor assays is that a label is not required which removes possible interference which may alter binding to the receptor.[245] One group to conduct SPR assays on membrane receptors was Mizuguchi *et al.* who used SA sensor chips to immobilise a biotinylated spacer group followed by amine coupling to capture cells.[246] Whilst they successfully generated ligand-receptor binding interactions the sensorgrams fluctuated significantly more than when the extracellular domain of the receptor was used. This suggested that using intact cells was not ideal to produce reproducible, accurate kinetic data for instance.

An alternative method to study GPCRs is with virus particles. Hoffman *et al.* exploited the retrovirus characteristic of incorporating proteins on the cell surface during budding.[244] The group investigated HIV co-receptors CCR5 and CXCR4. The group were able to produce cells that expressed more than 100,000 CCR5 and CXCR4 receptors. What's more, the receptors were in their natural conformation and the retroviral pseudotypes were universally the same size, stable and purified easily providing benefits over the use of detergents. Conclusively, virus particles were immobilised and produced a response of around 6000 RU ensuring that analyte binding, in this case specific antibodies, could generate responses of many hundreds of RU so that reliable kinetic data could be generated. A more

recent publication of virus particle use in SPR biosensor assays was by Vega *et al.* The group investigated binding between CXCL12 and CXCR4 with lentiviral particles X4LP.[243] The group commented on the ease that virus particles can be purified and immobilised on the sensor chip surface and that CXCR4 expressing virus particles showed specific binding to CXCL12 compared to other chemokines, as shown in Figure 81 A. The group showed an expected reduction in CXCL12 binding following treatment with AMD3100, Figure 81 B indicating that virus cells behaved in a similar fashion to normal cells.

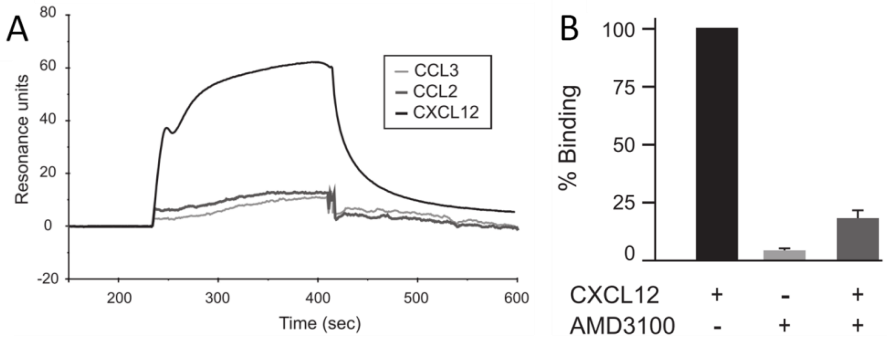

Figure 81 - Sensorgram showing specific binding of CXCR4 to CXCL12 against other chemokines with virus particles (A), Effect on binding in the presence of AMD3100 (B), reproduced from Vega at al.[243]

Vega *et al.* went on to develop a virus particle method which allowed urine samples from rheumatoid arthritis patients to be analysed by SPR directly without sample preparation.[247] Rheumatoid arthritis patients have high levels of CXC12 in synovial fluid and plasma so the group investigated whether SPR could provide a sensitive and reproducible diagnosis tool for autoimmune disorders. The method used CXCR4 lentiviral particles, as previously outlined,[243] and the urine was injected over the chip. The results showed higher levels of CXCL12 in the patients with rheumatoid arthritis compared to healthy patients. Ultimately, this proof of concept highlights that SPR biosensor assays could have many applications in disease diagnosis.

An alternative SPR biosensor method was conducted by Stenlund *et al.* who investigated the immobilisation of GPCRs on an L1 sensor chip by first immobilising a 1D4 antibody and then capturing the receptor.[248] Stenlund *et al.* chose CXCR4 and CCR5 receptors to develop a model system and aimed to solve the problems previously associated with direct receptor immobilisation. The method, visualised in Figure 82, provided a better-orientated-antibody-surface by aldehyde coupling whereby an immobilisation of 10000 RU was achieved (1). Subsequently, the detergent solubilised receptors were captured by a peptide tag recognised by the antibody (2). Responses of just under 4000 RU were achieved. A mixture of lipid and detergent micelles were then injected so a lipid bilayer could form (3). The detergent was removed by washing with buffer (4). The surface was then tested by injecting conformational dependant antibodies which indicated the receptor was in

its natural conformation (5) which then allows ligands binding interactions to be carried out (6). The captured CXCR4 was shown to bind CXCL12 reproducibly and without non-specific binding to the reference flow cell. In conclusion, Stenlund *et al.* provided evidence that the reconstitution of a GPCR to a sensor chip surface does not have to be overly complex and has the potential to produce valuable data.

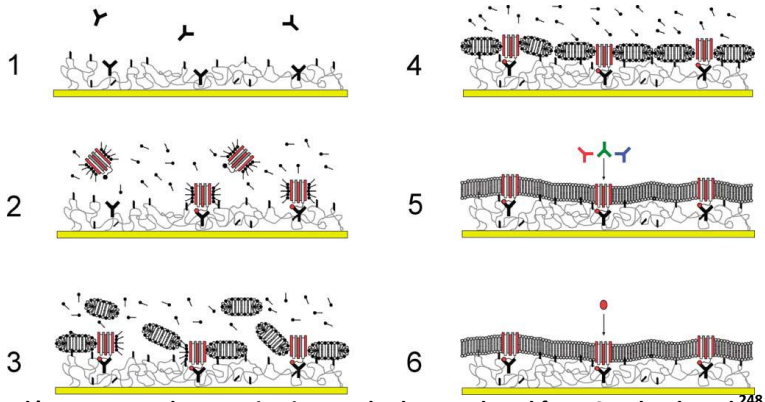

Figure 82 - Stenlund *et al.*'s capture and reconstitution method, reproduced from Stenlund *et al.*[248]

Further work using the 1D4 antibody to capture the peptide tag was performed by Navratilova *et al.* who investigated the receptors CXCR4 and CCR5.[245] They obtained a CXCR4 receptor capture of 2000-2300 RU on a CM4 sensor chip, which was almost half that achieved by Stenlund *et al.*,[248] although the difference in sensor chip, coupling chemistry and different detergent and lipid mixture could account for this difference. The group did not experience binding to the reference cell and the response attained was still high thus reliable data was generated. CXCR4 conformation dependant antibodies, solubilised in the same detergent-lipid mix as the receptor, showed significant binding. Though when solubilised in a detergent known to disrupt the receptor structure, Triton X-100, the binding of the conformation dependant antibodies drastically dropped. Results for the CCR5 receptor where somewhat different; both the detergent-lipid mix and Triton X-100 antibody solutions showed comparably low binding. This shows how sensitive the receptors are and how accurate the conformation dependant antibodies are at detecting those changes. By changing the detergent mix for the CCR5 receptor the group found that binding increased. They concluded that the right lipids and detergents resulted in the natural receptor environment ensuring the natural conformation was stable across a long time period.[249] The group disclosed a protocol for high throughput screening of GPCRs in 2011 mainly focusing on CCR5.[250]

Briefly, another SPR biosensor assay utilising detergents and lipids to explore GPCR interactions was Rich *et al.* who published work on detergent stabilised GPCRs on an NTA sensor chip assessing b1 adrenergic and A2A adenosine G-protein-coupled receptor antagonist kinetics.[251] In conclusion, it can be seen that ensuring the receptor activity is high is essential for ligand binding assays and there

is not a single detergent-lipid mixture for all GPCRs. Nonetheless, once the conditions were determined the use of detergents and lipids in SPR biosensor assays produces possibly superior results compared to other SPR biosensor methods. High and reproducible responses allow valuable and accurate kinetic data to be ascertained. Now that their use has been simplified the capture procedure could be applied to many other GPCRs.

5.3. BIOLOGICAL ASSAYS

Biological assays were used to determine the affinity of macrocycles for the CXCR4 receptor as well as potency in cell lines known to express high levels of the receptor.

5.3.1. Displacement Assay

Displacement assays were used to initially screen the macrocycles before more in depth assays were conducted. The assay was carried out using cultured Jurkat cells which overexpress the CXCR4 receptor, normally cells express about 10,000 copies of the CXCR4 receptor whereas Jurkat cells express 140,000 copies. The macrocycle competes for the CXCR4 receptor against a CXCR4 specific mAb containing a fluorescent label; the label is detected and a percentage of inhibition is generated. A high percentage corresponds to low displacement of macrocycle by the mAb and means that the macrocycle has competed efficiently for the CXCR4 receptor. A high fluorescence reading results in a low percentage because a high degree of mAb has displaced the macrocycle from the CXCR4 receptor. The assay involves incubating the macrocycle with Jurkat cells first before excess macrocycle is removed and mAb added. A second incubation is conducted and the excess mAb is then removed. Analysis via flow cytometry detects the amount of fluorescently labelled mAb there is bound to each cell, of which 10,000 are counted per sample, and from this data inhibition percentages can be calculated. Negative and positive controls are used to establish the assay limits. The negative control contains a mAb that will not bind to the CXCR4 receptor and contains zero fluorescence; the positive control contains only CXCR4 specific mAb producing a reading for 100 % fluorescence.

5.3.2. Anti-HIV Assay

Anti-HIV assays are used to determine the ability of a compound to prevent infection of HIV. All assays were conducted by BD Biosciences Europe, Erembodegem, Belgium. Different cell cultures can be used but the main ones are U87.CD4.CXCR4, a human glioblastoma cell line cell line transfected with high levels of CXCR4 receptor, and MT-4 cells, a human T cell leukaemia cell line. An AMD3100 resistant MT-4 cell line is also available and provides a tougher test for macrocycles as the Asp residues normally used for binding are altered. The assay determines anti-HIV activity and cytoxicity measurements by assessing the viability of the cells against different concentrations of

macrocycles in cells that have or have not been infected with HIV-1, HIV-2 or SIV.[252] The X4 virus strain was used because it replicates through the CXCR4 receptor as opposed to CCR5. The process involves culturing the cells for 5 d and quantifying the number of viable cells using the tetrazolium-based colourimetric method outlined by Pauwels *et al.*[122, 253] The cells were infected with HIV as described by Schols *et al.*[254]

5.3.3. Calcium Signalling Assay

Calcium signalling studies determine whether the macrocycles are having an antagonistic or agonistic effect utilising the calcium(II) flux downstream effect. On activation of CXCR4 by its ligand CXCL12 many downstream effects occur, one of which is the flux in intracellular calcium(II). Calcium(II) signalling studies investigate how effectively macrocycles are blocking the natural signalling. All assays were conducted by BD Biosciences Europe, Erembodegem, Belgium. A series of concentrations of macrocycle are incubated with CXCR4 expressing U87.CD4.CXCR4 cells and on addition of CXCL12 the amount of calcium(II) release should be lower than normal because the receptors are blocked. A calcium sensitive fluorescent label is used to quantify the amount of calcium(II) released and a lower fluorescence relates to a lower calcium(II) flux. IC_{50} values were generated from this data which is defined as the concentration required to block half of the calcium(II) flux.[255]

5.3.4. Tris-Macrocycles as CXCR4 Antagonists

The collection of tris-macrocycles synthesised in chapter 2 were assessed as CXCR4 antagonists initially using the displacement assay, this data is summarised in Table 6. The first point to note regarding the percentage inhibitions is that free ligands, non-metal containing macrocycles, are significantly poorer at competing for the receptor than the metal complexes. This validates the strategy to incorporate a metal ion into the macrocyclic cavities. Furthermore, in general metal complexes of **20**, **17** and **16** do not compete for the receptor as effectively as those of **18, 21** and **19**, this is especially the case for the nickel(II) complexes. When this trend is related to the macrocycle structure a higher percentage inhibition is seen when the terminal macrocycles are SB cyclam, **18, 21** and **19**, as opposed to SB cyclen, **20**, **17** and **16**. The central macrocycle does not appear to have too much of an impact on inhibition, copper(II) and zinc(II) complexes of **20**, **17** and **16** exhibted more than 80 %. A lower inhibition is seen for Cu_3[**21**], 52 %, which can be rationalised by the configuration of the metal complex. The absence of a bridge in the central macrocycle results in a more flexible structure which may lead to a poorer configuration for binding forming. Studies into tetra-methyl cyclam first row transition metal complexes, which the macrocycle strongly resembles, imply the configuration to be *trans*-IV which is not ideal for binding.[166] As copper(II) complexes

experience Jahn Teller distortion, in the *trans*-IV configuration, the equatorial site is elongated, making interaction with the carboxylate group on the receptor surface longer and weaker, therefore the macrocycle is easily displaced. An explanation for the lower inhibition percentages of nickel(II) complexes of **20**, **17** and **16**, 39%, 56%, 69% respectively, may be that the terminal SB cyclen macrocycles do not facilitate optimum binding, this finding coincides with the literature because *para*-linked SB cyclen macrocycles show lower activity which may be due to their poor ability to compete for the receptor.[170] Low inhibition values of nickel(II) complexes have also been observed in our group with bis-macrocycles.[81] Evidence suggests that a *cis*-V configuration is the optimum configuration for binding to aspartate residues on the surface of CXCR4.[256] It was concluded from this that the macrocycles providing optimum inhibition were the metal complexes of **18** and **19**, whereby 100% inhibition was achieved. However, displacement assay data is not as reliable as calcium(II) signalling data so precise conclusions cannot be drawn from this data alone.

The most potent anti-HIV metal complexes were Zn_3[**19**], Zn_3[**21**] and Zn_3[**18**] which showed up to 13 fold greater affinity than AMD3100 (IC_{50}: 1.86, 2.16 and 0.86 nM respectively *vs*. 11.93 nM). The general trend of anti-HIV activity in terms of the metal complexes was zinc(II)>nickel(II)>copper(II). A rational for the highly potent zinc(II) complexes could be that zinc(II) forms stronger interactions with the receptor in comparison to copper(II) and nickel(II). A reason for this is that a d^{10} metal ion exhibits more flexibility in preferences of coordination. The copper(II) complexes showed lower affinity than AMD3100, but some of the nickel(II) complexes exhibited greater affinity such as Ni_3[**21**] with an IC_{50} of 7.79 nM which was 1.5 fold better than AMD3100. The higher potency of the metal complexes of "unsymmetrical" macrocycle **18** compared to "symmetrical" tris-macrocycles **19** and **16** has been observed in the literature,[80] although interestingly the opposite macrocycle arrangement seen in **17** is significantly less potent. This may be because the bulk of the binding interactions are facilitated by SB cyclen, cyclen has been identified as showing inferior affinity compared to cyclam.[79] Poorer anti-HIV activity was observed for all tris-macrocycle metal complexes bearing terminal SB-cyclen macrocycles, **16**, **17** and **20**. All complexes were less toxic than AMD3100.

Calcium(II) signalling studies were conducted on the metal complexes of **19** and **21**. The metal complexes trend in potency observed in the anti-HIV activity data was repeated in this assay, zinc(II)>nickel(II)>copper(II). Zn_3[**19**] and Zn_3[**21**] were the most potent complexes, IC_{50}: 2.90 and 1.55 nM, roughly three to six fold greater than AMD3100, IC_{50}: 9.94 nM.

Sample	Av[a] % inhibition Jurkat	Anti-HIV activity IC_{50}[b]/nM U87.CD4.CXCR4, *MT-4	Cytotoxcity CC_{50}[c]/μM U87.CD4.CXCR4	Calcium signalling IC_{50}[b]/nM U87.CD4.CXCR4
16	27			
Cu_3[16]	100	140	-	-
Ni_3[16]	69	713	-	-
Zn_3[16]	100	533	-	-
17	7			
Cu_3[17]	84	729	-	-
Ni_3[17]	56	368	-	-
Zn_3[17]	93	392*	26*	771*
18	12			
Cu_3[18]	100	28	-	-
Ni_3[18]	100	8	-	-
Zn_3[18]	100	1	-	-
$CuZn_2$[18]	100	21*	8*	9*
19	32			
Cu_3[19]	100	1420	27	1,932
Ni_3[19]	100	12	17	8
Zn_3[19]	100	2	34	3
20	23			
Cu_3[20]	99	387*	32*	187*
Ni_3[20]	39	736*	5*	1130*
Zn_3[20]	92	297*	35*	506*
21	33			
Cu_3[21]	52	-	-	-
Ni_3[21]	100	8	31	21
Zn_3[21]	100	20	11	2
AMD3100		12	2	10

Table 6 – Summary of biological assay data generated for tris-macrocycles and metal complexes
[a] Experiments were run in either duplicate or triplicate and the results averaged. [b] Concentration required to reduce the level of Ca^{2+} ions observed during a 'normal' signalling process by 50% (IC_{50}) in U87.CD4.CXCR4 cells. [c] Concentration required to reduce cell viability by 50% (CC_{50}) in U87.CD4.CXCR4 cells. – Represents compounds awaiting data.

The difference in potency between the metal complexes of **21** and **19** may be explained by their overall shapes. The long, straight shape of **21** may cover more of the receptor surface preventing CXCL12 from binding better than the folded shape of **19**. In conclusion, zinc(II) tris-macrocycles were seen to perform the best as CXCR4 antagonists with multiple macrocycles outperforming AMD3100. The most active anti-HIV agent was Zn_3[**18**] which showed 13-fold better activity and lower toxicity than AMD3100.

5.3.5. Bis-Macrocycles as CXCR4 Antagonists

Zinc(II) and copper(II) coordinated bis-macrocycles were evaluated as CXCR4 antagonists, along with the corresponding free ligand in displacement assays against a CXCR4 specific mAb. A summary of the findings from these assays are shown in Table 7. Free ligands, **28** - **39**, show significantly lower percentage inhibition than all the metal complexes. In general, free ligands containing two bridged

cyclen macrocycles showed lower inhibition than bis-macrocycles containing a bridged cyclam macrocycle. **29**, **37** and **39** showed more than 50% inhibition and were significantly better at inhibiting CXCR4 than any tris-macrocycle free ligands, **16**-**21** see section 5.3.4. Functional groups appeared to impact percentage inhibition for the free ligands with a general trend being: $-N_3$>$-NH_2$>-CH_2NH_2=NO_2>-COOMe>-CN, an anomaly in this trend is **29**(-NO_2) which shows higher inhibition. Our group has observed higher inhibition from an amine functionalised macrocycle,[67] but this was not seen. Inhibition of CXCR4 by copper(II) and zinc(II) complexes of bis-macrocycles **28**-**39** were comparable, all showed more than 90% inhibition see Table 7 and suggests that terminal functional groups or ring size had no impact on inhibition and does not agree with macrocycle complex trends in the literature which show zinc(II) complexes as superior to copper(II) complexes.[67, 71b, 81, 195]

Inhibition data does not indicate whether macrocycles are efficient CXCR4 antagonists therefore additional assays are conducted to determine this. Zinc(II) complexes are significantly more active than copper complexes in general, see Table 7, these findings are supported by the literature.[67, 71b, 81, 195] The most potent bis-macrocyclic metal complexes were $[Zn_2\mathbf{32}]^{4+}$, $[Zn_2\mathbf{37}]^{4+}$ and $[Zn_2\mathbf{39}]^{4+}$, all showed lower IC_{50} values than AMD3100, 3 nM, 10 nM and 10 nM vs 12 nM respectively. These complexes all contained a terminal SB-cyclam macrocycle and a central CB-cyclen macrocycle suggesting this is the optimum structure for CXCR4 interaction.

Sample	Av[a] % inhibition Jurkat	Anti-HIV activity IC_{50}[b]/nM *U87.CD4.CXCR4 MT-4	Cytotoxcity CC_{50}[c]/μM U87.CD4.CXCR4	Calcium signalling IC_{50}[b]/μM U87.CD4.CXCR4
28	0			
Cu_2[28]	-	2569	46	1.5
Zn_2[28]	-	734	43	1.1
31	23			
Cu_2[31]	100	447	42	0.8
Zn_2[31]	-	961	11	0.3
29	53			
Cu_2[29]	-	1003*	-	-
Zn_2[29]	-	500*	-	-
32	29			
Cu_2[32]	96	34*	-	-
Zn_2[32]	100	3*	-	-
30	8			
Cu_2[30]	100	436	67	0.2
Zn_2[30]	92	365	35	0.1
33	28			
Cu_2[33]	98	67	>96	0.1
Zn_2[33]	96	48	>96	0.1
34	14			
Cu_2[34]	98	459	50	0.6
Zn_2[34]	100	274	63	1.0
35	29			
Cu_2[35]	100	525	54	1.0
Zn_2[35]	-	59	32	0.1
36	22			
Cu_2[36]	98	290	44	0.1
Zn_2[36]	-	1030	42	0.1
37	54			
Cu_2[37]	96	322	56	0.2
Zn_2[37]	94	10	50	0.1
38	39			
Zn_2[38]	-	50	37	0.1
39	58			
Cu_2[39]	100	78	52	0.8
Zn_2[39]	-	10	39	0.1
AMD3100		12	2	0.1

Table 7 - Summary of biological assay data generated for bis-macrocycles and metal complexes
[a] Experiments were run in either duplicate or triplicate and the results averaged. [b] Concentration required to reduce the level of Ca^{2+} ions observed during a 'normal' signalling process by 50% (IC_{50}) in U87.CD4.CXCR4 cells. [c] Concentration required to reduce cell viability by 50% (CC_{50}) in U87.CD4.CXCR4 cells. – Represents compounds awaiting data.

5.4. SPR METHOD DEVELOPMENT

In order to obtain the optimum SPR method a range of methods were tested. Important factors for changing the method were reproducibility and the sensorgram level of response.

5.4.1 Intact Cell Immobilisation

This method involved immobilising whole cells onto the surface of a CM5 chip via aldehyde coupling. The cells used were Jurkat cells, a human leukaemia cell line, which over expresses the CXCR4 receptor by 14 fold compared to normal cells. There has been one publication whereby Jurkat cells were used in SPR. Jin *et al.* clarified the ability of SPR to identify specific interactions between Jurkat cells and certain mAb immobilised on the sensor chip surface.[257] Since then very little work has incorporated intact cells into SPR methods, one example though is Mizuguchi *et al.* who used epidermal carcinoma A431 cells overexpressing their receptor of choice, epidermal growth factor receptor (EGFR) to investigate receptor interactions.[246] A significant difference between this work and that of Mizuguchi *et al.* was that they immobilised the receptor ligand onto the surface of the sensor chip and analysed binding between the ligand and the intact cells as opposed to directly attaching the cells to the chip and observing the interactions with the ligand. An interesting finding was that there was more fluctuation in the sensorgrams when using intact cells as opposed to isolated extracellular domains of the EGFR.

In this work, Jurkat cells were cultured and once the cell line was established the cells were washed and re-suspended in PBS/10 mM sodium acetate buffer pH 4.0 (1:1). The surface of the sensor chip was activated before introduction of the cells and the assay ran at 37^{o}C. Slow flow rates were used when injecting cells because the diffusion rates are slower so it takes longer to interact with the immobilised ligand.[258] On all occasions Jurkat cells were immobilised, however, whilst conditions remained the same the response varied significantly between experiments. On one occasion approximately 10,000 RU was reached but on another approximately half that was reached. This is shown in the sensorgram below in Figure 83**.** It was concluded that the experiment was not reproducible and so the method was altered even though a high response was achieved.

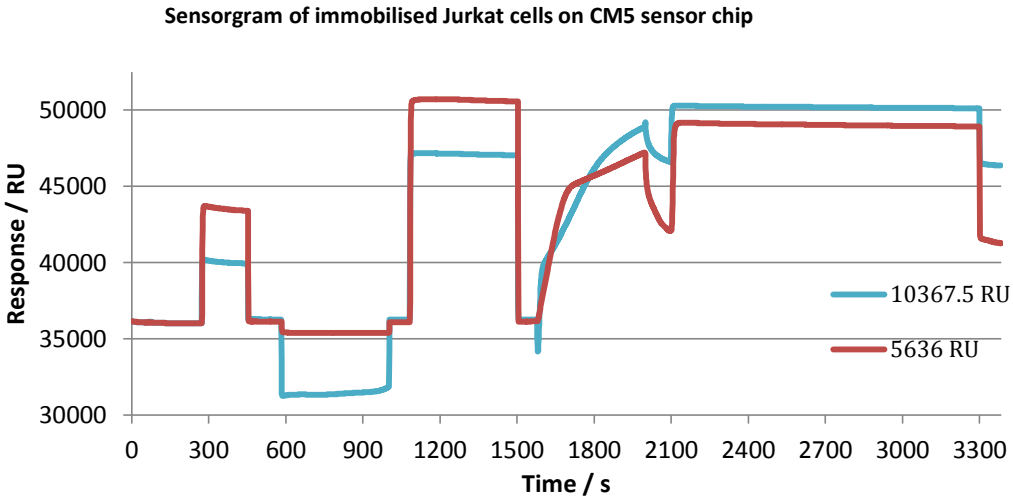

Figure 83 - Sensorgram of immobilised Jurkat cells on CM5 sensor chip

5.4.2 Intact Cell Capture

The intact cell capture method involved immobilising a CXCR4 specific monoclonal antibody to the surface of a CM5 sensor chip via amine coupling followed by capture of the Jurkat cells. The use of an immobilised mAb to capture the item of interest is well documented in the literature for many applications but the use with GPCRs is limited due to the lipophilic nature of the protein.[245, 248]

Optimum conditions for antibody binding were ascertained by carrying out an immobilisation pH scouting assay which tested antibody binding over a range of pHs. The precise nature of antibody binding can be seen in Figure 84 which shows the optimum pH for binding was 4.5. Following sensor chip surface activation by EDC and NHS the target for antibody immobilisation of 10,000 RU was reached on both the reference and test FCs. Compared to mAb immobilisation examples from the literature,[248], the mAB surface density was excellent. A comparable density of 10,000 RU was achieved with mAb 1D4 on an L1 sensor chip,[248] though a lower density of 7000 RU was achieved by Navratilova *et al.* on a CM4 chip.[259] However, as the CM4 chip has a lower amount of carboxymethylated dextran strands on the surface than the CM5 this would explain the difference.[259] Cell capture was conducted at 37°C to ensure the cells were exposed to conditions as mild as possible. The flow rate was very slow to enable the cells chance to bind to the antibody.

Whilst the sensorgram indicated cell capture the response was low, Figure 85 A, a more important feature it showed was that the baseline was unstable. This can be concluded because the baseline is not flat. As a result of this, the temperature was reduced to room temperature and the experiment was repeated. The response achieved for cell capture remained low, though the baseline was very stable as can be seen in Figure 85 B. Cell capture was repeated three times but the response did not significantly improve. Conclusively, cell capture was not high enough for valuable data to be generated therefore an alternative approach was investigated. Levels of capture described in the

literature whereby binding data was generated ranges from 2000-3000 RU which is considerably higher than that achieved in this work.[248-249]

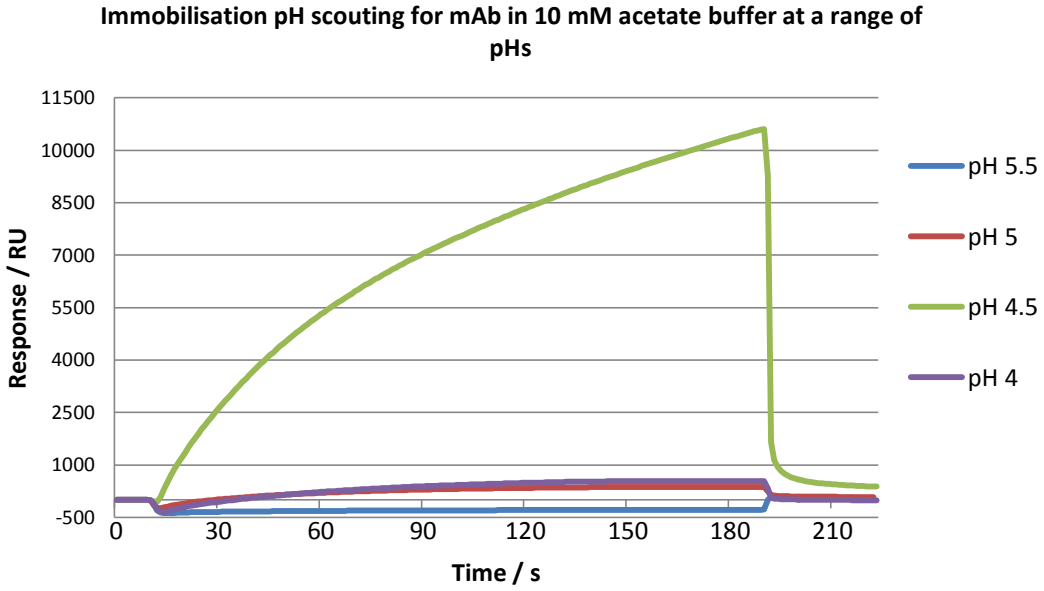

Figure 84 - Immobilisation pH scouting for mAb in 10 mM acetate buffer at a range of pHs

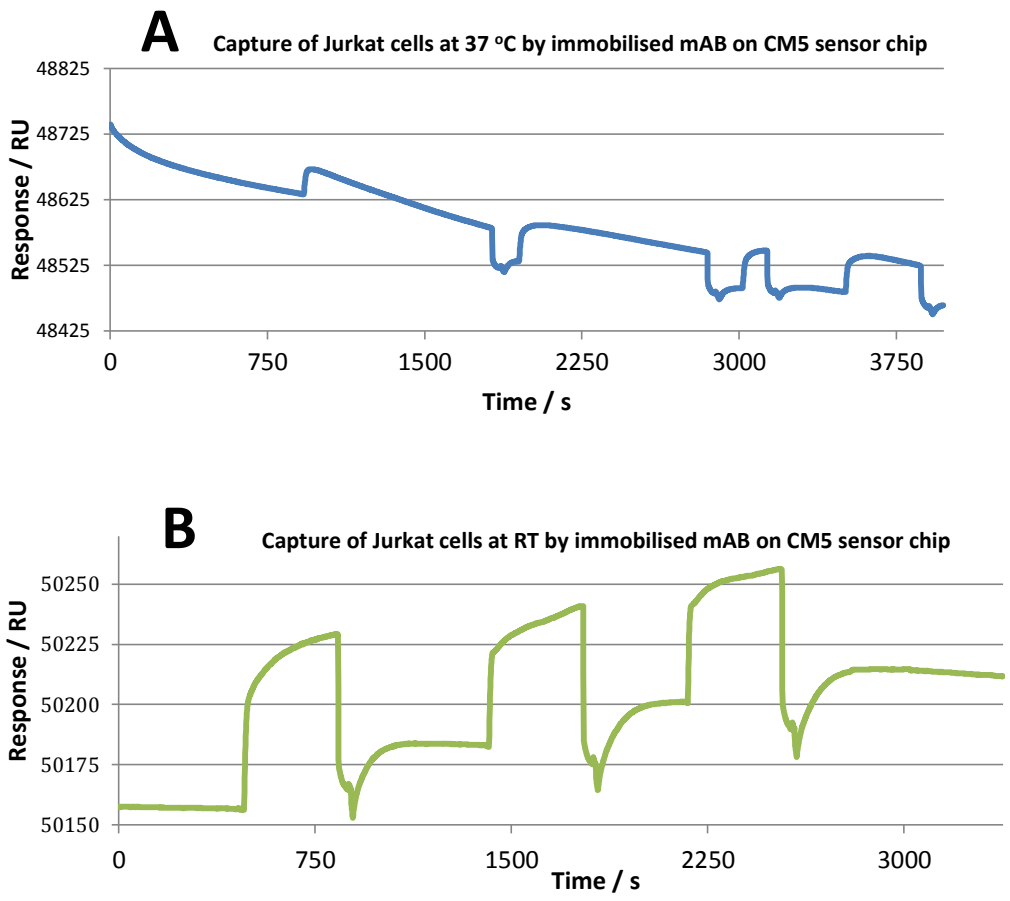

Figure 85 - Sensorgrams showing cell capture at 37°C (A) and at RT (B) by immobilised mAb

5.4.3 Receptor Capture

The literature focuses heavily on using C-terminal linear C9 peptide (TETSQVAPA) tags to capture GPCRs which is recognised by the 1D4 mAb. This work investigated the use of alternately tagged receptors focusing specifically on the GST tagged CXCR4 receptor which would be captured by an anti-GST antibody.

Immobilisation of the anti-GST antibody via amine coupling was straight forward with high mAb surface densities being attained. The values of approximately 7000 RU were slightly less than the expected value outlined by the capture kit manufactures.[260] However the stated value of 7500 RU was observed with a CM5 sensor chip therefore a lower density is predicted for the CM4 sensor chip as mentioned in section 5.4.2. The CXCR4 receptor was reconstituted in a buffer that had shown promising results with the capture of C-terminal linear C9 peptide tagged CXCR4 receptor.[245] Initially a low capture density of around 800 RU was observed which is much lower than the accepted literature values,[248-249] but this was overcome by increasing the contact time whereby an excellent density of 1800 RU was achieved. However, on testing the surface with a conformation specific CXCR4 mAb no binding was observed. Thus, believing that the lack of binding was due to the lipids and detergents not correctly supporting the receptor into the correct conformation an alternative buffer was investigated. This buffer was taken from a different group who had achieved success with analysing binding interactions of CXCR4.[248] Instead of having a mixture of detergents and lipids in the buffer only one detergent is present. An injection of lipid and detergent solution immediately after receptor injection stabilises the receptor into the correct conformation. The capture density of CXCR4 receptor was approximately 700 RU which was significantly less than Stenlund *et al.*, but the different sensor chip is likely to be responsible for this. Following the lipid/detergent injection no binding was observed to the sensor chip surface which was a major problem as it meant that the receptor was not being stabilised into its natural conformation, although this issue could be due to machine differences. The instrument used by Stenlund *et al.* enables a subsequent injection instantaneously however the instrument used in this work inputs a 60 s wait command in between injections and cannot be over ridden. This small difference may have caused the problem. In an attempt to increase the capture density the length of contact time was increased from 600 s to 900 s and this yielded a density of 669 RU. Nonetheless, no increase in response was observed following the injection of lipd/detergent therefore no binding was able to be seen either. Consequently, no binding data between novel CXCR4 antagonists and the CXCR4 receptor were able to be generated.

5.4.4 Biotinylated macrocycle binding assay

The binding of a biotinylated bis-macrocycle to a streptavidin coated sensor chip was analysed. Compounds **81** and **82**, see Figure 86**,** were synthesised and kindly donated by Dr Rachel Smith. Previous flow cytometry data on **82** had produced inconsistent binding data therefore to confirm that the macrocycle was not interfering with the biotin-streptavidin binding an SPR method was developed. As the biotin-streptavidin bond is the strongest non-covalent interaction known the surface could not be regenerated so this was the reason for the layout of the experiment. **81** was injected first to establish the response of zero binding on both FCs. This was followed by either **82** or the positive control. The response was divided by the molecular weights of the compounds to generate binding per molecule. It was established that **82** bound to streptavidin to the same extent as the positive control thus the macrocycle was not affecting binding to streptavidin.

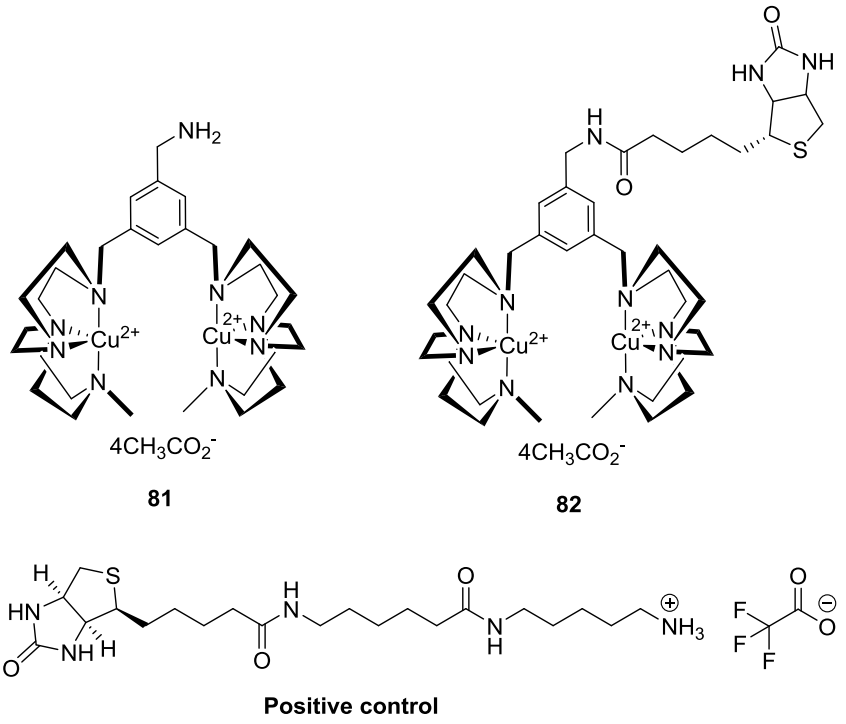

6

Figure 86 – Donated compounds 81 and 82 synthesised by Dr Rachel Smith and the commercially available positive control: (5-([(N-(Biotinoyl)amino)hexanoyl]-amino)pentylamine trifluoroacetate salt

5.5. CONCLUSIONS

A range of synthesised tris- and bis-macrocycles was biologically evaluated in a number of assays with the aim to determine the optimum structure for CXCR4 antagonism. The macrocycles and their metal complexes presented in chapter 2 and 3 were tested through displacement assays, anti-HIV assays, cytotoxicity assays and calcium(II) signalling assays.

Tris-macrocycles have the potential to display more interactions with the CXCR4 receptor than bis- or mono-macrocycles due to the third macrocycle which could lead to a longer residence time on the receptor which is preferable for use in therapeutic applications. A novel collection of tris-macrocycle metal complexes all exhibited micromolar affinity with most complexes being potent at a nanomolar concentration. Both the free ligands and metal complexes showed a measurable inhibitory percentage although the metal complexes were significantly higher. Overall, the metal complexes of **20**, **17** and **16** did not compete for the receptor as well as those of **18, 21** and **19**, in particular the nickel(II) complexes. Higher inhibition percentage was seen when SB cyclam was in the terminal position, as for **18, 21** and **19**. Lower inhibition percentages were seen for the nickel(II) complexes of **20**, **17** and **16**, 39%, 56%, 69% respectively. The macrocycles which showed optimum inhibition were the metal complexes of **18** and **19** whereby 100% inhibition was achieved by all. The most potent anti-HIV tris-macrocycle metal complexes were Zn_3[**19**], Zn_3[**21**] and Zn_3[**18**] which were up to 13 fold more potent than AMD3100 (IC_{50}: 1.86, 2.16 and 0.86 nM respectively *vs*. 11.93 nM). The general trend of anti-HIV activity in terms of the metal complexes was zinc(II)>nickel(II)>copper(II). Copper(II) complexes showed lower affinity than AMD3100, but Ni_3[**21**], IC_{50} of 7.79 nM, exhibited 1.5 fold greater affinity than AMD3100. Higher potency was observed in the metal complexes of "unsymmetrical" macrocycle **18**. All complexes were less toxic than AMD3100. Calcium(II) signalling studies conducted on metal complexes of **19** and **21** revealed that Zn_3[**19**] and Zn_3[**21**] were the most potent complexes, IC_{50}: 2.90 nM and 1.55 nM, and were approximately three to six fold greater than AMD3100, IC_{50}: 9.94 nM. In conclusion, zinc(II) tris-macrocycles were seen to perform the best as CXCR4 antagonists and multiple tris-macrocycles outperformed AMD3100.

Functionalised bis-macrocycles could potentially be used in different imaging applications depending on the imaging group attached. A variety of functionalities were evaluated to assess whether this would have an impact on the pharmacological properties of the macrocycle. Zinc(II) and copper(II) coordinated bis-macrocycles, **28**-**39,** were evaluated as CXCR4 antagonists. Free ligands **28**-**39** showed significantly lower percentage inhibition than all the metal complexes, and generally those consisting of two bridged cyclen macrocycles showed lower inhibition than bridged cyclam

containing bis macrocycles. **29**, **37** and **39** showed more than 50% inhibition and were significantly better at inhibiting CXCR4 than tris-macrocycle free ligands, **16**-**21**. Functional groups made a difference to percentage inhibition for the free ligands a general trend, regardless of macrocycle ring size, was -N_3>-NH_2>-CH_2NH_2=NO_2>-COOMe>-CN. More than 90% inhibition of CXCR4 was achieved with copper(II) and zinc(II) complexes of bis-macrocycles **28**-**39** and suggests that terminal functional groups or ring size did not affect inhibition. This finding does not agree with macrocycle complex trends in the literature which show zinc(II) complexes as superior to copper(II) complexes.[67, 71b, 81, 195] $[Zn_2\mathbf{32}]^{4+}$ showed more than three times greater anti-HIV activity than AMD3100 and was identified as the most potent compound. The findings imply that the optimum bis-macrocyclic metal complex contained a terminal SB-cyclam and a central CB-cyclen. Further studies need conducting to support this hypothesis.

The aim of the SPR method development was to use the kinetic data generated from SPR experiments to determine which application the antagonists were most suitable for either as imaging agents for cancer diagnosis or therapeutic agents for CXCR4 metastatic cancers. Whilst many methods and modifications were tested this outcome was not achieved. High levels of receptor capture were achieved which strongly suggests that GST capture is a valid method for further development. The use of lyophilised CXCR4 receptor may have been the cause of the problems because the E- coli cells used to produce the receptor may not have been able to correctly fold the protein into its active conformation. The use of lysed receptor, as used by Stenlund *et al.* and Navratilova *et al.* may have been the key to their successful method because the differing capture method is unlikely to have been the cause of the problem as GST capture is a frequently used method that does not interfere with capture.[245, 248] Future developments for the method would be to use freshly lysed GST-tagged-CXCR4 receptor transfected cells on the lipophilic L1 sensor chip. This may overcome the problem with lipid association as well as ensure the receptor remains in its active conformation.

5.6. FUTURE WORK

Detailed biological evaluation of leading compounds, Zn_3[**19**], Zn_3[**21**] and $[Zn_2$**32**$]^{4+}$ should be conducted in order to establish which residues on the binding cleft of CXCR the macrocycles are interacting with and can be achieved through mutagenesis studies as outlined by Gerlach *et al.*[56a, 57a] The findings from this study would be especially interesting for tris-macrocycles as key binding residues are currently only hypothesised. Further biological studies that could be conducted are downstream signalling assays to ascertain whether downstream effects are inhibited and whether receptor internalisation *via* endosomal compartments is initiated by macrocycle binding, as observed in previous work within the group.[195]

A series of SPR experiments were conducted in this work but the binding kinetics of the synthesised macrocycles were unable to be ascertained. In order to develop a route to accomplish this, the work in this chapter suggests that, a fresh production of CXCR4 receptor directly from cultured cells would lead to a successful method being developed. In the literature, a C9 tagged CXCR4 receptor expressing Cf2Th dog thymocyte cell line was created by Babcock *et al.*[261] The C9 tagged CXCR4 receptor was separated from the remainder of the cell by Navratilova *et al.* and incorporated onto the surface on a CM4 sensor chip *via* capture by immobilised 1D4 Ab which recognises the C9 tag.[245, 249] It would be interesting to see whether a GST tagged CXCR4 receptor could be produced in a similar way to be recognised by an anti-GST Ab immobilised onto the surface of a sensor chip. The development of this would lead to a novel method which could be applied to other GPCRs such as CCR5 to evaluate anti-HIV agents. This method would hopefully overcome the drawbacks of the methods discussed in this work as it would ensure that the receptor remained folded in its active conformation by solubilisation in correct buffer. A suitable buffer to use could be a 20mM Tris (pH 7.0) buffer supplemented with 0.1M $(NH_4)_2SO_4$, 10% glycerol, 1 protease inhibitor tablet per 50mL buffer and approximately 1% lipid/detergent mixture outlined by Navratilova *et al.*[249]

CHAPTER SIX

RADIOLABELLED CXCR4 ANTAGONISTS

6.1 SYNTHETIC STRATERGY

This chapter reports the synthesis of radiolabelled tris-macrocycle zinc(II) complexes which have potential applications as PET imaging agents. Two high affinity configurationally restricted tris-macrocycles reported in chapter 2 section 2.4.4 were coordinated to ^{64}Cu(II) via transmetalation.

6.2 PREVIOUS STRATEGIES

6.2.1 Nuclear CXCR4 Imaging Agents

6.2.1.1 Positron Emission Tomography (PET)

As mentioned briefly in section 1.3.2, PET is an imaging technique which measures the tissue concentration of a radiotracer to generate images of biological processes *in vivo*.[262] PET is superior compared to other techniques such as MRI, X-ray and ultrasound as they cannot provide information on metabolic or molecular events which PET can.[235] A disadvantage of PET is the short half-lives of the radioisotopes commonly used, which mean that radiolabelling of target biological sites must by rapid. However, a strong advantage of PET is that an image can be generated quickly, the complete process can take between 5-10 min, therefore multiple PET investigations can be conducted on a patient. In addition to this, the atomic weight of PET radioisotopes tends to be low, for example C, N, O, F, therefore the "label" does not interfere with the biological process whereas a bulky fluorescent label might.

PET predominantly differs from SPECT due to its use of positron emitting radioisotopes as opposed to single-photon emitters.[108-109] A PET image is generated by the detection of two 511 keV gamma rays emitted following positron decay.[262a] When the nucleus of a positron-emitting isotope decays it emits a positron which travels a short distance, of between 0.5-2.0 cm, until it collides with an electron in the nearby tissue and undergoes positron annihilation. [235, 262a] This causes the release of two gamma rays at approximately 180^{o} to each other which are detected by the gamma-ray detectors surrounding the patient. As the rays are emitted at around 180^{o} the isotope decay can be traced back along the line connecting the two detectors, termed the line of coincidence, see Figure 87. Ideally, when a patient is injected with a radiotracer the material would be shown to move rapidly around the blood stream until it accumulates in the desired tissue. This accumulation would then be seen as a more intense portion of the image in comparison to other tissue.[108-109]

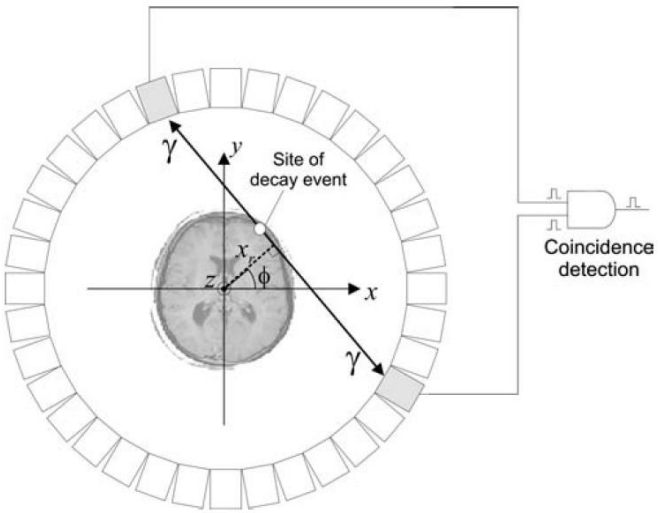

Figure 87 - Diagram showing coincidence detection in PET when two gamma rays are emitted, reproduced from Aarsvold *et al.*[108]

6.2.1.2 Single Photon Emission Computed Tomography (SPECT)

SPECT is more widely used than PET, this could be because SPECT radiotracers are easier to make and obtaining an image is cheaper because the radiotracers and equipment cost less than for PET.[108] In addition to this, SPECT isotopes have longer half-lives and a greater range of isotopes and tracer compounds are available. Despite this, a better image is generally obtained with PET as it's more sensitive because the site of decay and point of annihilation can be identified. More recently, PET is gaining popularity and is the preferred technique in research.

SPECT uses a radiotracer labelled with a single-photon emitter, in other words a radioisotope that emits one gamma-ray photon with each radioactive decay event.[108] The amount of radiotracer that can be administered is limited due to safety therefore gamma-ray emission is quite low. Consequently, gathering data can be time consuming; a SPECT cardiac study takes 15-20 minutes as opposed to an X-ray CT which can be done in seconds.

A collimator is used to create an image in SPECT, see Figure 88. An image is created by selecting the gamma-rays travelling in the direction that the channels are orientated. The other rays are either blocked or completely miss the collimator. Successful gamma rays will strike the scintillator which then utilises the high energy from the rays to produce numerous optical wavelength photons. Photomultiplier tubes (PMT) detect the photons and computers subsequently decipher the data and organise it into a histogram which portrays the object as a projection image.[108]

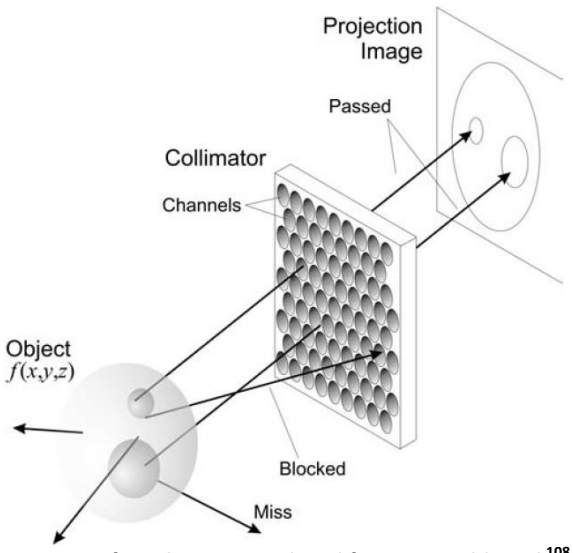

Figure 88 - A collimator forming an image of an object, reproduced from Aarsvold *et al.*[108]

6.2.1.3 Radioisotopes

The first thing to consider when imaging a target area is that you need a radiopharmaceutical that will interact with the body, accumulate in the desired location and produce a valuable image. A radiopharmaceutical has two components: the tracer, to target the specific area of the body, and the radioactive label, the part that is used to generate an image.[108] There are two types of radioactive labels: positron emitters and single-photon emitters. Positron emitters are used in PET, the most common are ^{18}F, ^{82}Rb, ^{11}C, ^{15}O and ^{13}N. Single-photon emitters are those used in SPECT, the most widespread ones are ^{99m}Tc, ^{201}Tl, ^{123}I, ^{111}In and ^{67}Ga. Table 8 shows the half-lives of the commonly used isotopes. Many radioisotopes are made using a cyclotron by bombarding the chosen substance with beams of protons. An alternative method is through isotope generators the method in which ^{68}Ga and ^{99m}Tc are produced. The positron emitting isotope is extracted from another specific decaying isotope, in the case of ^{68}Ga, decaying ^{68}Ge is used.

Positron Emitters	
Isotope	**Half-Life ($t_{1/2}$)**
^{11}C	20.4 min
^{13}N	9.96 min
^{15}O	124 s
^{18}F	110 min
^{82}Rb	1.25 min
^{68}Ga	68 min
^{64}Cu	12.7 h

Single Photon Emitters	
Isotope	**Half-Life ($t_{1/2}$)**
^{67}Ga	78.3 h
^{99m}Tc	6.02 h
^{111}In	2.83 d
^{201}Tl	68 min
^{123}I	13.2 h

Table 8 - Half-life values of some frequently used radioisotopes[108]

An advantage of using radioactive tracers is that they can efficiently target particular processes which allow valuable information to be acquired.[108] This is useful as there are multiple processes

involved in cancer progression and PET is a versatile technique when it comes to oncology. One of the applications is characterising the tumour, detailing what type it is, what quantity it uptakes, and the location of the tumour. PET can be used to determine all these factors as well as deliver targeted tumour therapies. Fluorodeoxyglucose or ^{18}F-FDG, is the most commonly used PET radiopharmaceutical used for characterising a tumour. ^{18}F is often used to replace a hydrogen atom or hydroxyl group.[262a] ^{18}F-FDG is an analogue of glucose whereby ^{18}F replaces one of the hydroxyl groups.[108-109] FDG gets taken up by the cells like standard glucose, however once inside the cell FDG cannot be metabolised like glucose due to the 'missing' OH group so it gets trapped and the concentration builds in correlation with the cell's glucose metabolic rate. An image is then formed showing the cell's glucose metabolism which is especially useful for cancer imaging as tumour cells have higher glucose uptake than normal cells and therefore show up as brighter sections on a PET image. FDG is regularly used in clinical applications. There are many other PET radiopharmaceuticals but very few are in use clinically.[108]

6.2.1.4 Nuclear Imaging Agents

The use of macrocycles as PET imaging agents has been a popular area of research in recent years. Jacobson *et al.* first radiolabelled AMD3100 using ^{64}Cu and tested it in C57BL/6 mice.[263] High uptake was observed in the liver (41%), and immune related organs (37%) (spleen (13%), bone marrow (14%) and lymph nodes (10%) after 1 h. After 2 h there was very little difference in accumulation except in the liver which increased to 47%. Nimmagabba *et al.* showed the potential for radiolabelled AMD3100 by demonstrating that different levels of CXCR4 expression could be differentiated.[112] The ability of ^{64}Cu-AMD3100 to visualise metastasis was also validated, see Figure 89. The accumulation in the liver and immune system was rationalised by target-specific binding as CXCR4 is expressed there. However, transchelation of ^{64}Cu from AMD3100 results in higher accumulation in the liver and increased liver uptake can also be attributed to the positive charge carried by AMD3100. These results have been confirmed by other groups.[112, 175b, 264] A limitation of AMD3100 as a PET imaging agent is that its structure does not easily facilitate radiolabelling with ^{18}F.[112] An alternative macrocycle that has shown higher selectivity in PET imaging is AMD3465, see Figure 90.[265] Furthermore, the pyridine group could allow the addition of alternative radioisotopes. An example which uses an alternative radioisotope is M508Cl, the non-macrocyclic analogue of AMD3100. M508Cl was radiolabelled with ^{18}F to produce ^{18}F-M508F, see Figure 90.[266] Radiolabelling caused the IC_{50} to significantly increase by more than 200 fold, 185 nM compared to 0.8 nM suggesting that optimisation of this compound is required.

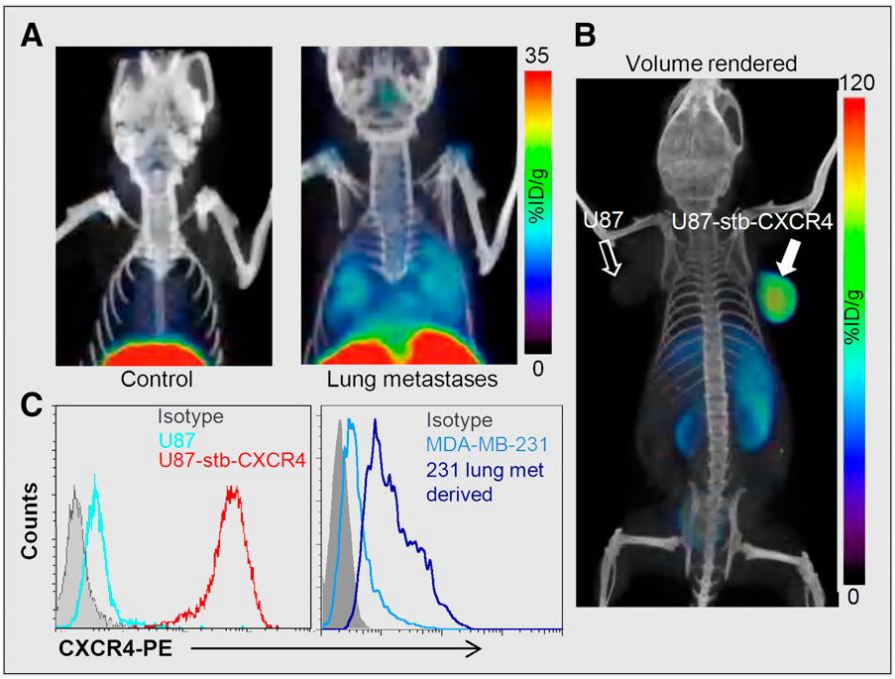

Figure 89 – PET/CT of CXCR4 expression in lung metastasis with ^{64}Cu-AMD3100 (A and B) and histogram showing the surface expression of CXCR4 in various cell lines (C)[112]

^{99m}Tc has been incorporated into AMD3100 for imaging Hep-G2 cell line tumours in BALB/C nude mice.[267] A high radiochemical yield was achieved for ^{99m}Tc-AMD3100 of 99 %. High radiochemical purity of 98 % after 1 h and 99 % after 6 h was recorded using TLPC. SPECT imaging demonstrated that ^{99m}Tc-AMD3100 was taken up by the tumour 1 h prior to injection. High accumulation of ^{99m}Tc-AMD3100 was observed in organs expressing CXCR4 such as the liver and kidney.

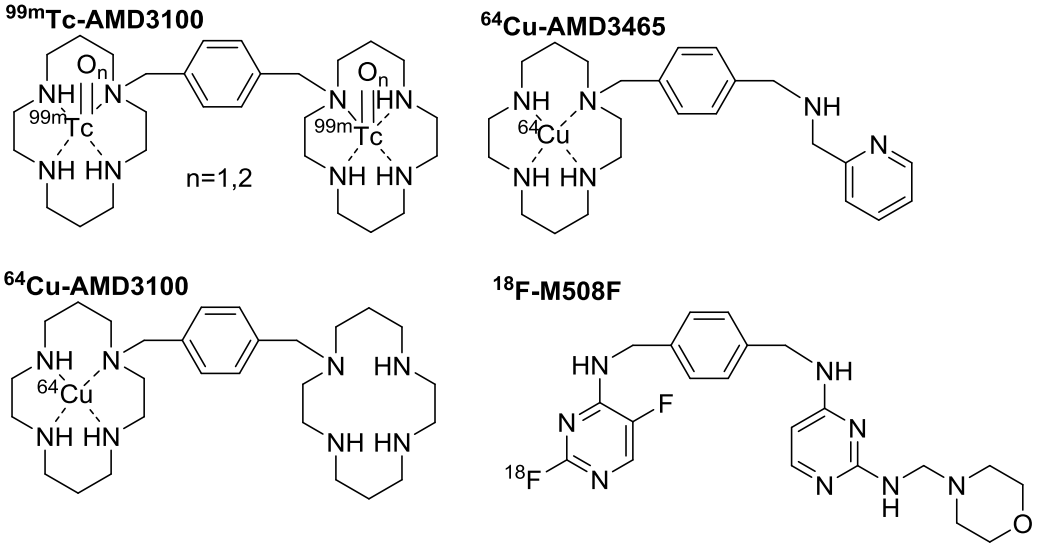

Figure 90 – Structures of CXCR4 nuclear imaging agents

The ^{64}Cu-radiolabelling of many mono-macrocycles has been explored some of these are shown in Figure 91.[175b, 184b, 268] Frequently used radiochemistry conditions, see Table 9, generally show that macrocycles without a bridge require lower temperatures and shorter reaction times for high purity

^{64}Cu-complexation to occur. SB-cyclam showed 90% conversion at RT after just 20 min, however more rigid CB-macrocycles required significantly higher temperatures, commonly 75^{o}C, for quantitative conversion. Reaction times for CB-macrocycles were not excessively higher than other radiochemistry reactions, an exception being Sun *et al.* whereby a 4 h reaction time was used to isolate ^{64}Cu CB-TE2A.[184b] The majority of reactions shown in Table 9 resulted in high purity, ≥95%, but two reactions involving **L^{177}** and CB-TE2A, see Figure 91, both CB macrocycles, produced lower purity values of 76% and 87% respectively. High purity, >95%, of CB-TE2A was subsequently achieved upon increasing the reaction time. Introduction of a 30 min pre-incubation period, followed by heating for a further 30 min at 75^{o}C lead to high purity (ca. 100%) CB-macrocycles, CB-DO2A and CBTE2A, see Figure 91.

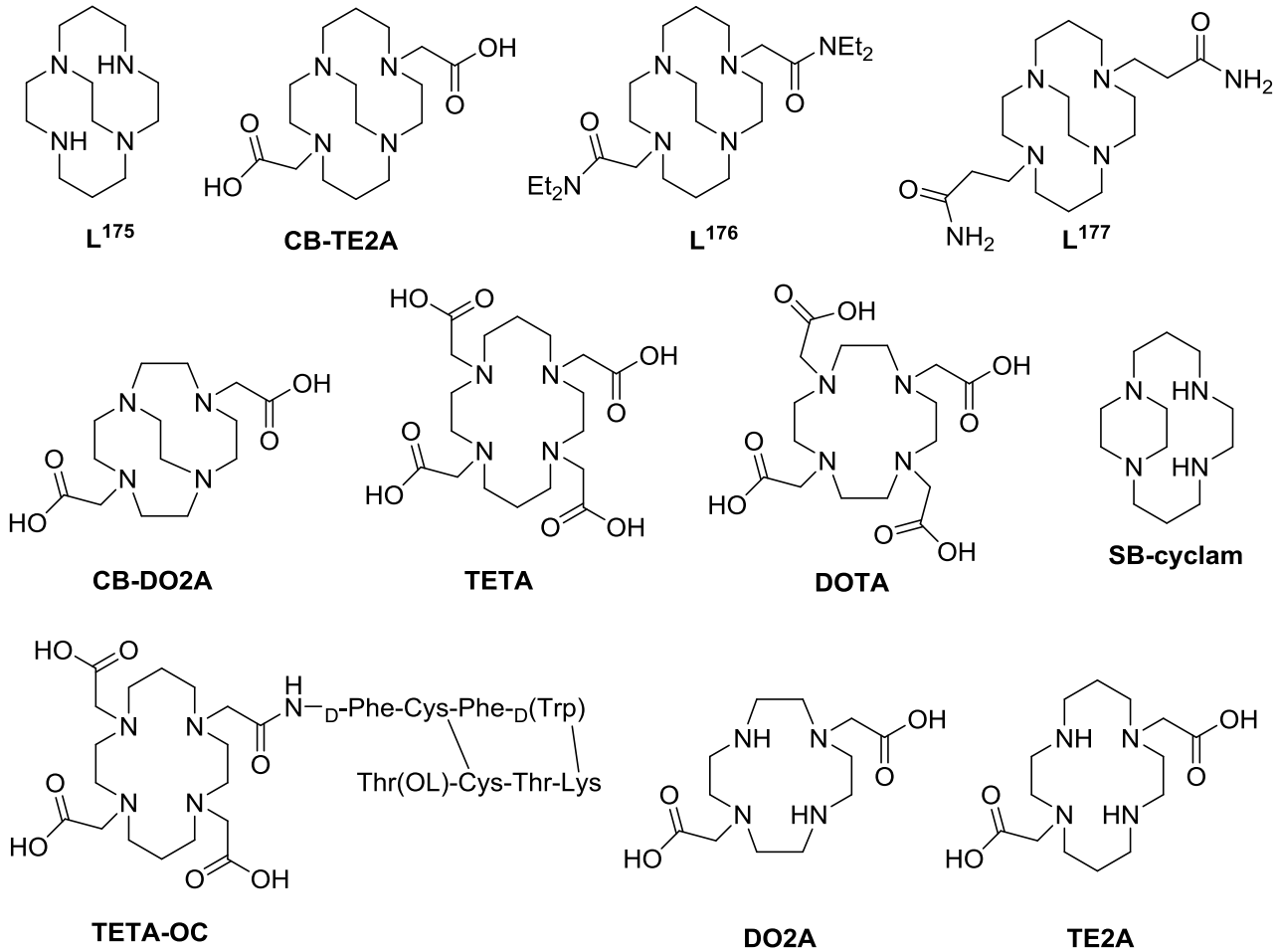

Figure 91 – Structures of ligands radiolabelled with ^{64}Cu

The preferred solvent for conducting ^{64}Cu radiolabelling reactions was EtOH; aqueous buffers such as ammonium acetate are also reported with the favoured pH being 5.5 but this is seen to vary between macrocycles. Sun *et al.* tested reactions using carriers to assist the radiolabelling of **L^{175}**, CB-TE2A, **L^{176}** and **L^{177}**, see Figure 91.[184b] Carriers are used to correct method performance in specific samples and contain known amounts of an isotope that will behave similarly to the radioactive one,

in this case ^{63}Cu. The group found that high RC purity was achieved for **L^{175}**, **L^{176}** and **L^{177}** regardless of whether a carrier was added. RC purity was significantly higher on addition of a carrier to CB-TE2A, going from 76% to >95%, see Table 9. Two species were observed prior to the addition of a carrier at a ratio of 3:1, but this converted to the single ^{64}Cu-CB-TE2A species with carrier. The group also explored the stabilities of the complexes in rat serum.[184b] All complexes, ^{64}Cu-**L^{175}**, ^{64}Cu-CB-TE2A, ^{64}Cu-**L^{176}** and ^{64}Cu-**L^{177}**, showed no decomposition after 24 h.

Jones-Wilson *et al.* outlined the thermodynamic stability constants of a series of Cu(II) macrocycles: cyclen, cyclam, SB-cyclam, DOTA, TETA and DO2A, see Figure 91.[175b] Cu(II)cyclam exhibited the highest log K, 28.1, whereas Cu(II)DO2A produced the lowest stability constant, 18.9. [175b, 268a-c] The trend in stability constants were: Cu(II)cyclam>Cu(II)SB-cyclam>cyclen>DOTA>TETA>DO2A. ^{64}Cu-SB-cyclam showed the slowest clearance and ^{64}Cu-TETA the fastest, ^{64}Cu-DOTA cleared the liver and kidneys faster than ^{64}Cu-cyclen.

Boswell *et al.* studied the stability of ^{64}Cu-CB-TE2A and ^{64}Cu-CB-DO2A, see Figure 91, and found that the size of the macrocycle ring significantly impacts the *in vivo* stability.[268d] The addition of the CB vastly improved the complexes *in vivo* stability, but ^{64}Cu-CB-TETA was found to be more stable than ^{64}Cu-CB-DO2A. ^{64}Cu-CB-DO2A was more resistant to transchelation compared with ^{64}Cu-DOTA. After 20 h ^{64}Cu-CB-TE2A was 24% dissociated in the liver and this was substantially better than ^{64}Cu-TETA which showed more than 90% dissociation after 20 h. On the other hand, dissociation of ^{64}Cu from TETA-OC was not observed in the work conducted by Bass *et al.*[268e]

Macrocycle	Reagents	Temperature / °C	Time / min	RC purity	Reference
Cyclen	20 mM water, pH 5.5	RT	10	98	Jones-Wilson *et al.*[175b]
Cyclam				97	
L[175]	EtOH (10 mM ligand), 5 µL 1 M NaOH (in EtOH)	75	60	99	Sun *et al.*[184b]
CB-TE2A				76	
	EtOH (10 mM ligand) Cu(II)/L: 1:100 to 1:1	75	240	>95	
	0.1M ammonium citrate, pH 6.5, Cu(II)/L: 1:100 to 1:1	75	240	>95	
	Cs_2CO_3, EtOH (30 min pre-incubation)	75	30	100	Boswell *et al.*[175a]
CB-DO2A				100	
L[176]	EtOH (10 mM ligand)	55	90	99	Sun *et al.*[184b]
L[177]	EtOH (5 mM ligand)	55	30	87	
TETA	20 mM water, pH 5.5	RT	30	100	Jones-Wilson *et al.*[175b]
DOTA	30 mM water, pH 5.5		45	95	
DO2A	10 mM water, pH 5.5		60	100	
SB-cyclam	5 mM water, pH 6.4		20	90	
TETA	0.1M ammonium acetate (5 mM ligand), pH 6.5	75	30	100	Boswell *et al.*[175a]
DOTA				100	
TETA-OC	0.1 M ammonium acetate (~7 µM ligand), pH 5.5	RT	60	>95	Bass *et al.*[268e]

Table 9 – Reaction conditions for radiolabelling macrocycles with ^{64}Cu

6.3 SYNTHESIS OF ^{64}Cu(II) RADIOLABELLED 1,7-BIS-[4-[[1,4,8,11-TETRAAZABICYCLO[10.2.2]HEXADECANE]METHYL]BENZYL]-1,4,7,10-TETRAAZABICYCLO[5.5.2]DODECANE ZINC(II) ACETATE [CuZn$_3$18]$^{6+}$ AND 1,8-BIS-[4-[[1,4,8,11-TETRAAZABICYCLO[10.2.2]HEXADECANE]METHYL]BENZYL]-1,4,8,11-TETRAAZABICYCLO [6.6.2]HEXADECANE [CuZn$_3$19]$^{6+}$

6.3.1 Cold Copper(II) Isotope Test Reaction

^{64}Cu is an attractive radioisotope due to its long half-life of 12.7 h, its increased use has called for the development of stable chelators, vital for *in vivo* applications.[175a] Macrocycles have renowned chelating abilities and have seen significant application in this field. The high stability of macrocycles compared to acyclic chelating agents has ensured extensive investigation with a variety of radioisotopes. The kinetic inertness of bridged macrocycles, in acidic media and physiological conditions, makes these chelators even more attractive.[184b] Structurally reinforced macrocycles bearing an ethylene bridge has resulted in optimal ligand design due to increased stability; bridged cyclam has shown more than 8 orders of magnitude higher kinetic stability compared to its non-bridged counterpart.[188, 269] Transchelation of ^{64}Cu from ^{64}Cu-labeled chelators during *in vivo* metabolism to 32 kDa proteins has been observed with the non-bridged macrocycle ^{64}Cu-TETA-OC, see Figure 92.[268e] Due to the stable nature of bridged macrocycles this is less likely to happen.[175, 220, 270]

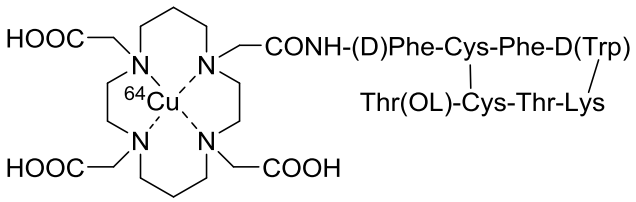

Figure 92 – Structure of non-bridged macrocycle ^{64}Cu-TETA-OC which causes loss of ^{64}Cu *in vivo*[268e]

Transmetalation was chosen as the route to introduce the radioisotope ^{64}Cu(II) as it was the easiest and meant the macrocycle did not require prior functionalisation. The tris-macrocycles, [Zn$_3$**18**]$^{6+}$ and [Zn$_3$**19**]$^{6+}$ see Figure 94, were selected for radiolabelling based on their high affinity at inhibiting the CXCR4 receptor in the displacement assay, see section 5.3.4. Radiolabelled, configurationally restricted macrocycles are likely to induce less toxic side effects than [^{64}Cu-AMD3100]$^{2+}$, through loss of ^{64}Cu(II), due to the increased stability of these complexes, which is crucial for *in vivo* delivery of ^{64}Cu for PET imaging.[71b, 175a, 184b, 188] Boswell *et al.* reported that ^{64}Cu-CB-TE2A was the most stable complex when compared to other ^{64}Cu-radiolabelled non-restricted macrocycles; H$_4$-TETA and H$_4$-DOTA, see Figure 93.[175a] Woodard *et al.* recently reported two ^{64}Cu(II)-CB-cyclam macrocycles RAD1-24 and RAD1-52, very similar structurally to AMD3465, see Figure 93.[271] The PET images revealed the mono-macrocycles showed specific uptake in CXCR4-expressing U87-subcutaneous brain tumour

xenografts, however when competed with AMD3465, uptake decreased by 85%-90% which suggests that the compounds bind in a similar manner to AMD3465. High accumulation of radioactivity was observed in the liver and kidneys for both compounds.

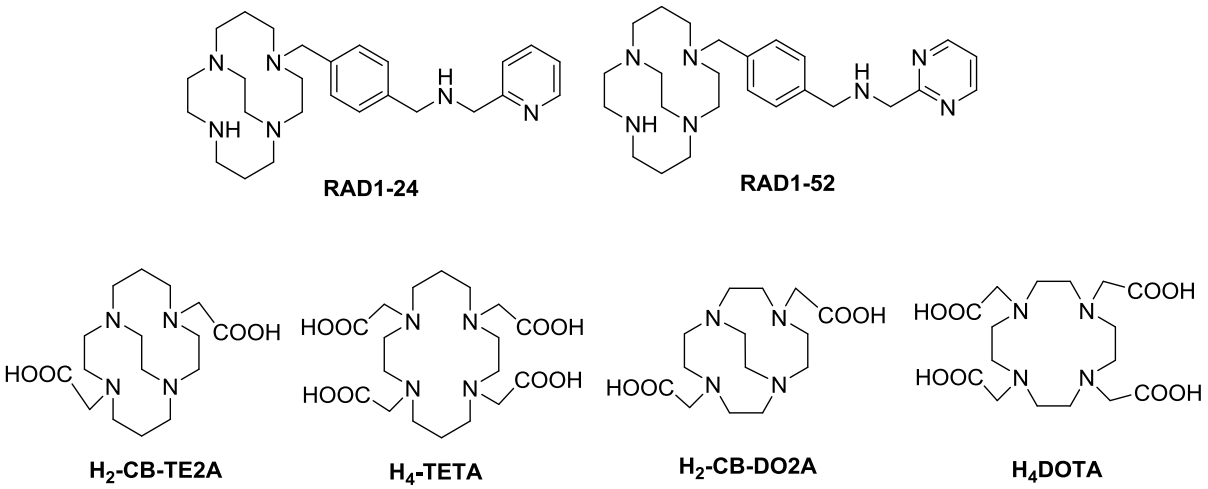

Figure 93 – Structures of mono-macrocycles radiolabelled by Boswell *et al.*[175a] and Woodard *et al.* [271]

Copper(II) should effectively undergo transmetalation with zinc(II) because the binding constant for $[Zn\text{-cyclam}]^{2+}$ is 11 orders of magnitude lower than that of $[Cu\text{-cyclam}]^{2+}$ thus the formation of $[Cu\text{-cyclam}]^{2+}$ is thermodynamically favoured.[72] Furthermore, the stability of copper(II) cyclam is higher than zinc(II) and the rate of complexation to cyclam is faster for copper(II) than zinc(II).[71a, 82a, 272] Displacement of zinc(II) by copper(II) was observed by Paisey *et al.*, initially zinc(II) bound to cyclam – when both metal ions were added to a solution of cyclam, however copper(II) displaced zinc(II) slowly at RT and 37°C.[82a] In this work, the cold copper(II) complex was synthesised by reacting $[Zn_3\mathbf{18}]^{6+}$ with a molar equivalence of copper(II)acetate monohydrate and heating at 60°C for 2 hours. This time was chosen as it was the standard literature procedure for incorporating a metal ion into a SB macrocycle.[61b, 160c] A molar equivalence was used because only one zinc(II) ion was to be replaced. The copper(II) ion most probably substituted one of the zinc(II) ions in the terminal SB-cyclam because higher energy is required to remove a metal ion from a CB-cyclam cavity as the structure is extremely stable.[63b] Furthermore, the flexibility of the CB structure is less than the SB therefore the SB is easier to introduce a metal ion into. On addition of the copper(II) acetate monohydrate methanolic solution the tris-macrocycle solution immediately turned deep blue. $[CuZn_2\mathbf{18}]^{6+}$ was purified by size exclusion chromatography using Sephadex LH20 to yield the blue product in 49% yield. The complexes, see Figure 94, were eluted in 95:5 water:MeOH on 'neutral alumina sheets' saturated with NaCl as a test for radiochemistry to monitor the progress of the reaction. These unusual conditions were selected as they enabled the macrocycle complex to travel

on the TLC plate and neutralised the charge of the macrocycle complex. The concentration of copper-64 ions is so low that it will be statistically impossible to replace more than one zinc centre.

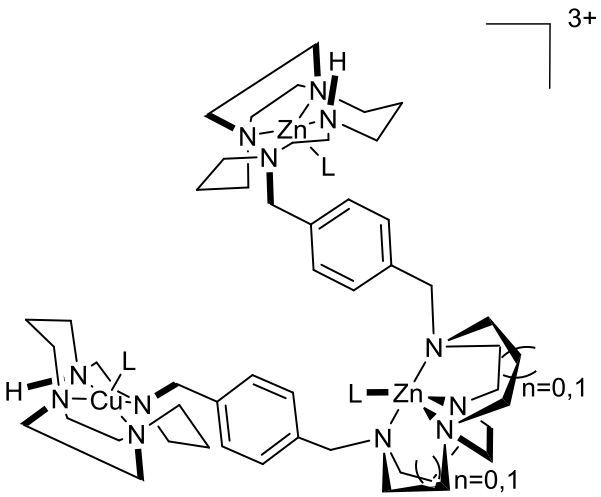

n=0 $[CuZn_2\mathbf{18}]^{6+}$

n=1 $[CuZn_2\mathbf{19}]^{6+}$

Figure 94 – Structure of radiolabelled tris-macrocycles $[Zn_3\mathbf{18}]^{6+}$ and $[Zn_3\mathbf{19}]^{6+}$

A displacement assay was conducted to test whether the substitution of one zinc(II) metal ion for a copper(II) ion in $[Zn_3\mathbf{18}]^{6+}$ had any negative effect on percentage inhibition as zinc(II) coordinated cyclam is known to show higher affinity towards the CXCR4 receptor than the corresponding copper(II) complex.[74] It can be seen in Table 10 that there is a significant difference between the free-ligand percentage of inhibition and the metal complexes, whereby the metal complexes show a stronger affinity for the CXCR4 receptor, this trend has been observed by Gerlach *et al.* and Woodard *et al.*[56a, 271] Importantly, the introduction of the copper(II) ion in place of a single zinc(II) ion has no negative effect on inhibition.

Sample	Average % inhibition
18	12
Cu_3[18]	100
Zn_3[18]	100
$CuZn_2$[18]	100

Table 10 – Percentage inhibition values of L^{19} and its metal complexes

6.3.2 Radiolabelling of $[Zn_3\mathbf{18}]^{6+}$ and $[Zn_3\mathbf{19}]^{6+}$

Following the successful cold transmetalation reaction of $[Zn_3\mathbf{18}]$, radioactive transmetalation was explored. Woodard *et al.* afforded their radiolabelled CB-cyclam analogues by dissolving the macrocycle in water, adding 0.1 M sodium acetate pH 8.0 before addition of $[^{64}Cu]Cu(II)Cl_2$ in HCl and heating at 95°C for 1 h.[271] This differed from the method outlined by Jacobson *et al.* who began by converting $[^{64}Cu]CuCl_2$ to $[^{64}Cu]Cu(II)(CH_3CO_2)_2$ by adding 0.4 M ammonium acetate buffer, pH 5.5, the buffer addition facilitated anion exchange.[263] The $[^{64}Cu]Cu(II)(CH_3CO_2)_2$ solution was added to

AMD3100 dissolved in 0.4 M ammonium acetate buffer pH 5.5 and stirred for 1 h at RT. Boswell *et al.* used a similar method to synthesise ^{64}Cu-SB-TE1A1P, see Figure 95, except [^{64}Cu]Cu(II)Cl_2 was added directly to the macrocycle in ammonium acetate buffer pH 7.5.[273] The method used in this work was comparable to Jacobson *et al.* although heat was introduced due to the transmetalation aspect of the reaction.

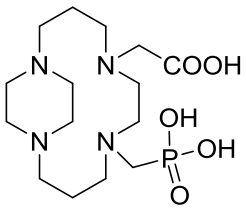

SB-TE1A1P

Figure 95 – Structure of SB-TE1A1P radiolabelled with ^{64}Cu(II)[273]

$^{64}CuZn_2$[**18**] and $^{64}CuZn_2$[**19**] were synthesised by making a solution of macrocycle and 0.4 M ammonium acetate buffer pH 5.5. This was added to a [^{64}Cu]Cu(II)Cl_2 solution, earlier incubated at 60^{o}C with 0.4 M ammonium acetate buffer pH 5.5, heated at 90^{o}C and the conversion of Zn_3[**18**] and Zn_3[**19**] to $^{64}CuZn_2$[**18**] and $^{64}CuZn_2$[**19**] was monitored via radio-TLC. HPLC was attempted but the sample smeared extensively down the column and interpretation was not possible, therefore true RCYs could not be calculated. The chromatograms obtained from the radio-TLCs, see Figure 97 for $^{64}CuZn_2$[**18**] and $^{64}CuZn_2$[**19**], see Figure 98, show the transmetalation of the zinc(II) complexes to the corresponding radiolabelled complex generated at each time point measured. The radiolabelled macrocycles were eluted with 95:5 water:MeOH, saturated with NaOH, which allowed reaction progress to be monitored. The chromatograms taken after 15 min were slightly noisy due to the reaction solution on the radio-TLC plates being too weak, this issue was overcome in subsequent chromatograms. The radio-TLC taken after 30 min for $^{64}CuZn_2$[**18**], see Figure 96, was anomalous as it depicted a significant decrease in the percentage converted to $^{64}CuZn_2$[**18**] and does not follow the overall trend in data as shown in Figure 99. The noise observed in the chromatogram indicates that insufficient reaction solution was added to the radio-TLC plate.

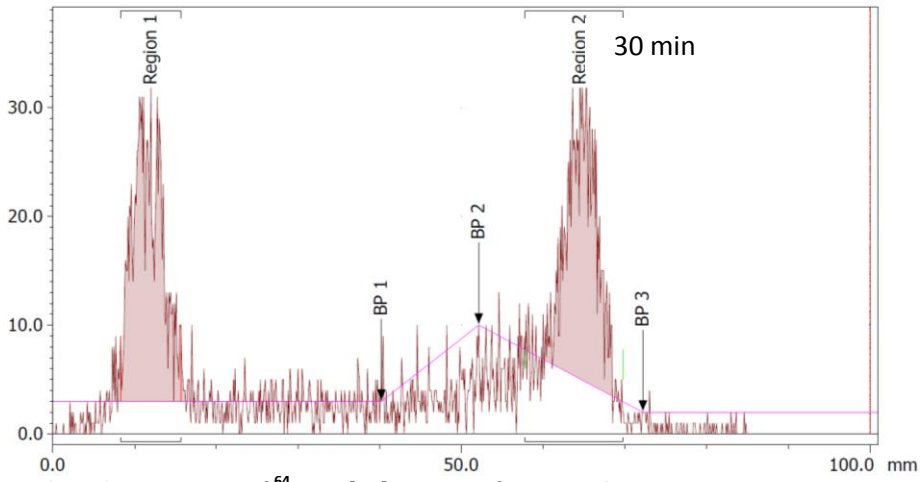

Figure 96 – Anomalous chromatogram of $^{64}CuZn_2$[18] at 30 min from a single run

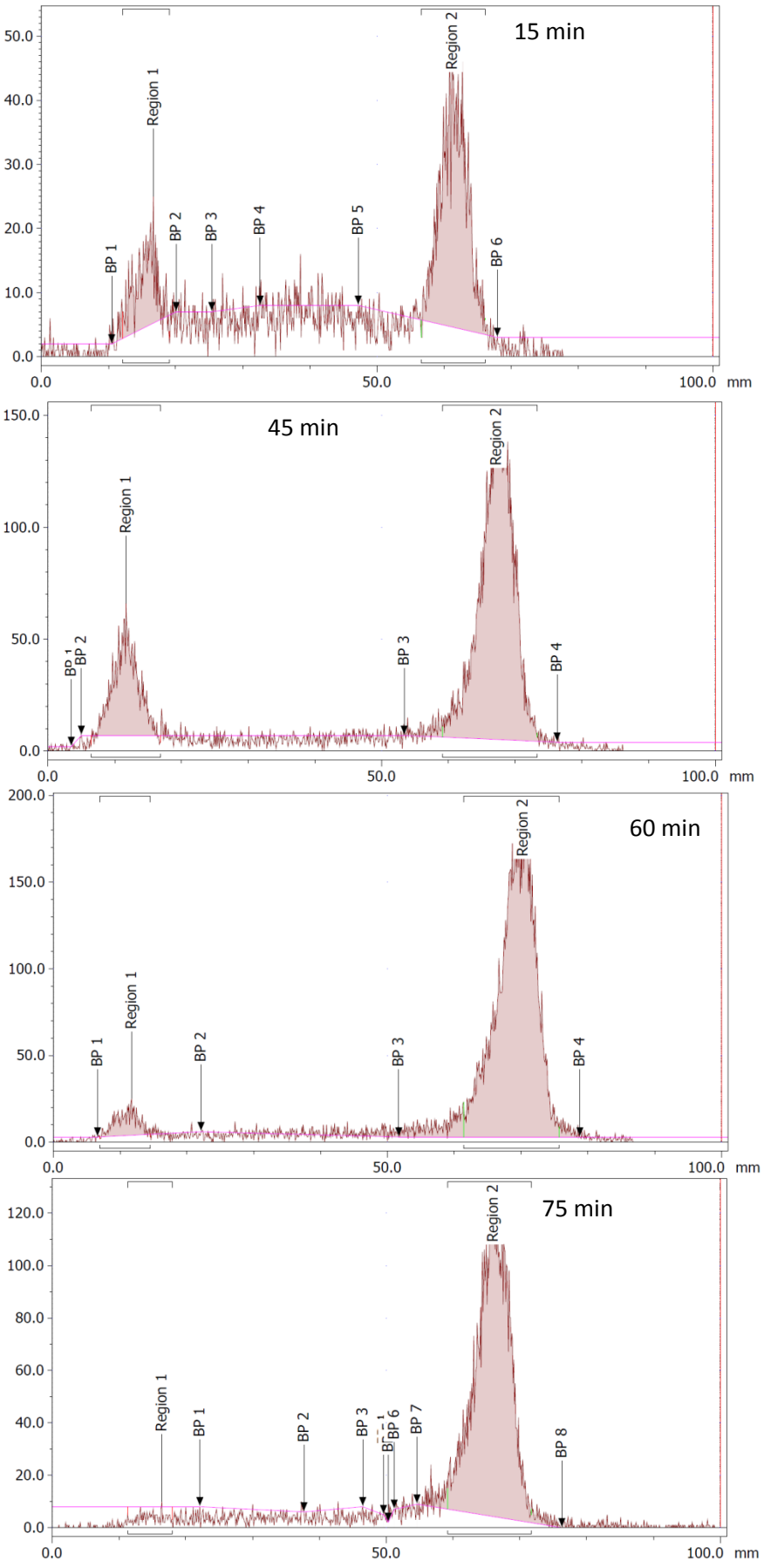

Figure 97 – Chromatograms of radio-TLCs of $^{64}CuZn_2$[18] over time from a single run

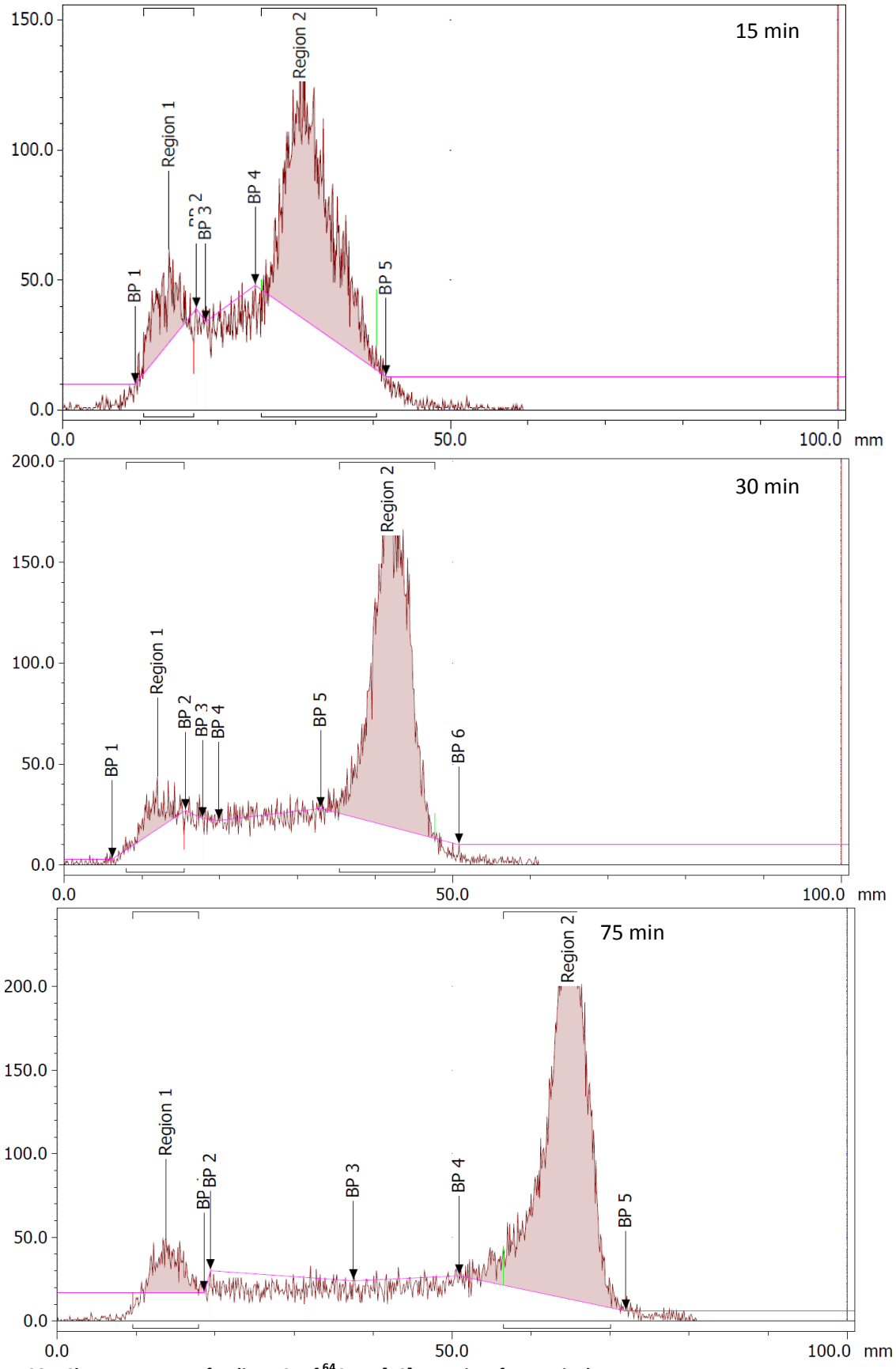

Figure 98 – Chromatograms of radio-TLCs of $^{64}CuZn_2$[19] over time from a single run

The chromatograms show that after just 15 minutes a considerable amount of ^{64}Cu was incorporated into the macrocyclic cavities of $^{64}CuZn_2$[**18**] and $^{64}CuZn_2$[**19**], 77% and 86% respectively see Figure 99. It was noted that conversion to $^{64}CuZn_2$[**19**] was initially quicker than $^{64}CuZn_2$[**18**]. A general trend observed for both macrocycle complexes was an increase in ^{64}Cu(II) incorporation over the course of the reaction, 75 min, see Figure 99. This was most obvious for $^{64}CuZn_2$[**18**] where a 25% increase in ^{64}Cu incorporation was seen over 75 min. For $^{64}CuZn_2$[**19**], it would be interesting to explore the level of ^{64}Cu incorporation achieved with a reaction time of less than 15 min as incorporation plateaus after 15 min. As a high percentage of ^{64}Cu incorporation was observed after a short length of time $^{64}CuZn_2$[**19**] may be the better PET imaging agent. After 75 min full incorporation of ^{64}Cu was observed for $^{64}CuZn_2$[**18**]. Complete conversion to $^{64}CuZn_2$[**19**] was not achieved but a yield of almost 93% was still acceptable. Whilst 75 min is a relatively long radiochemical reaction time the long half-life of ^{64}Cu(II), 12.7 h, provides more flexibility with regard to reaction times.[108] Considering the structures of the macrocycles were relatively similar, the only difference being the central macrocycle, the behaviour during radiolabelling was somewhat dissimilar. $^{64}CuZn_2$[**19**] consists of three bridged cyclam rings whereas $^{64}CuZn_2$[**19**] consists of two terminal bridged cyclam rings and one central bridged cyclen ring. The presence of the bridged cyclen ring appears to enable a high amount of ^{64}Cu incorporation quickly, whilst the central cyclam ring causes the same level of ^{64}Cu incorporation almost 45 min later. These are only preliminary results and more work and replications are required before accurate conclusions can be made, although it was an interesting observation to note.

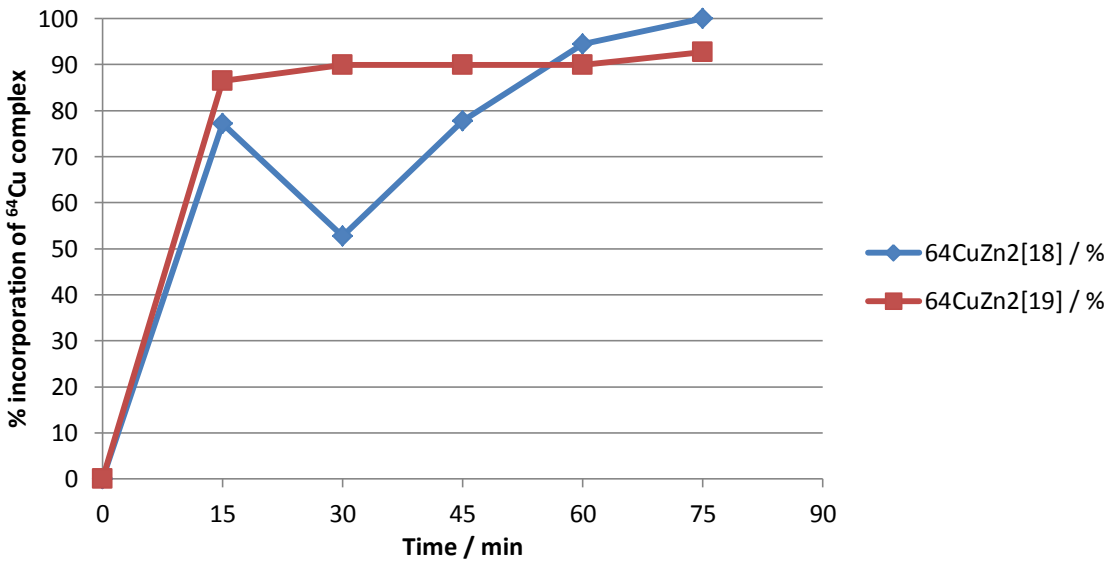

Figure 99 – Conversion of Zn_3[18/19] to $^{64}CuZn_2$[18/19] over time
The result after 30 min for $^{64}CuZn_2$[18] is anomalous

As a result of the true RCY not being able to be ascertained, crude RCYs were calculated. The crude-RCY was 79 % for $^{64}CuZn_2$[**18**] whilst a lower crude-RCY of 62 % was achieved for $^{64}CuZn_2$[**19**]. This

suggests that whilst $^{64}CuZn_2$[**19**] could potentially be radiolabelled quicker the best PET images would be generated with $^{64}CuZn_2$[**19**]. Rationalisation for this is specific activity because there would be a greater number of radiolabelled macrocycles to interact with the receptor as a higher percentage of macrocycle can be radiolabelled. In conclusion, important steps have been made in the quest to radiolabel targeted macrocyclic ligands and data suggests that $^{64}CuZn_2$[**18**] and $^{64}CuZn_2$[**19**] were successfully isolated but optimisation is needed.

6.3.3 Calculating the partition coefficient (LogP)

The partition coefficient (LogP) is a term used to describe how hydrophilic or hydrophobic a compound is.[274] As poor absorption and pharmacokinetics are the main reasons for drug candidates failing to progress in the drug development process, obtaining the physiochemical and pharmacokinetic drug properties as early as possible is highly advantageous.[275] Poor absorption is noted when drugs have a LogP of more than 5, solubility is known to be the limiting factor in terms of the absorption process which transports drugs across the gastrointestinal membrane in oral drugs.

LogP values were calculated for $^{64}CuZn_2$[**18**] and $^{64}CuZn_2$[**19**] to determine whether these macrocycles were hydrophilic or hydrophobic as this provides an insight into how the macrocycles will behave *in vivo*.[274-275] The general trend in LogP values of successfully launched oral drugs between 1965 and 2007 were between 1.5 to 3.5,[276] what's more between 1937 and 1997 the LogP value of drugs has not significantly changed. A rationalisation for this is that when lipophilicity is too high, observed in compounds with high LogP values, the chances of non-specific binding, toxicity, poor solubility and metabolic clearance are higher and these facts have long been established.[274-275, 277] There has been a general decline in the number of drugs released which have a molecular weight of less than 350 Da.[276a] A driving factor for this is that new biological targets are "less druggable" and require larger molecules to achieve high affinity binding, an example being antagonists for GPCRs. This contradicts the predictions of the rule of 5.[278]

The rule of 5 was originally outlined by Lipinksi in 1997 and is a well-accepted method for predicting likely drug candidates that will have desirable absorption and permeability properties.[278] The rules state that drugs should be less than 500 Da in molecular weight, have a LogP of less than 5, have less than 5 H-bond donors and less than 10 H-bond acceptors. One well known exception to this rule is AMD3100 which has a molecular weight of 794.46 Da, which is well above the general trend for successful drugs. However, the difference between standard drugs and AMD3100 is that it is administered via injection into subcutaneous tissue rather than given orally. This difference may provide the reason for the success of AMD3100 which breaks multiple 'rule of 5' guidelines. It also

provides strong evidence that other larger molecules which do not adhere to the rule of 5 can be developed as successful drugs. The LogP values for $^{64}CuZn_2$[**18**] and $^{64}CuZn_2$[**19**] were calculated by making a solution of 0.5 MBq macrocycle solution in 1 mL PBS:octanol 50:50. This mixture was then shaken for 5 min on a VV3 Vortex Mixer at 25^{o}C before being centrifuged for 5 min at 12,000 RPM at 25^{o}C. A small portion of each layer was taken and added to PBS, in triplicate, to give a final volume of 1 mL; 50 µL of the octanol layer and 5 µL of the PBS layer was taken. A larger volume of octanol was taken so that the instrument could detect a high enough reading of radioactivity because the hydrophilic nature of $^{64}CuZn_2$[**18**] and $^{64}CuZn_2$[**18**] meant that the majority of the sample would be in the aqueous layer, this higher value was taken into account when calculating the LogP values. The LogP values obtained for $^{64}CuZn_2$[**18**] and $^{64}CuZn_2$[**19**] were -3.69 and -2.2 respectively. The LogP of [^{64}Cu]AMD3100 was 0.52 which is much higher than the LogP values of $^{64}CuZn_2$[**18**] and $^{64}CuZn_2$[**19**].[112] These low values suggest that the macrocycles would not be suitable to image CXCR4 expression beyond the blood-brain barrier because they are too hydrophilic. It would be beneficial to repeat the process of calculating LogP for $^{64}CuZn_2$[**19**] as the PBS radioactivity readings varied widely so a more accurate LogP value can be generated. Nonetheless, [^{64}Cu]AMD3100 showed strong potential as a PET imaging agent therefore with the more optimal $^{64}CuZn_2$[**18**] and $^{64}CuZn_2$[**19**] structures it would be worth investigating these compounds further.

6.4 CONCLUSIONS

Two tris-macrocycles, Zn_3[**18**] and Zn_3[**19**], have been radiolabelled with ^{64}Cu via transmetalation to produce potential PET imaging agents to diagnose CXCR4 expressing cancers. These structurally rigidified complexes potentially offer ideal properties for PET imaging by preventing toxic side effects from ^{64}Cu transchelation *in vivo*, observed in non-bridged complexes, due to their enhanced stability.[71b, 175a, 184b, 188] LogP values for $^{64}CuZn_2$[**18**] and $^{64}CuZn_2$[**19**] were calculated and indicate that the macrocycles are more hydrophilic than [^{64}Cu]AMD3100. Nevertheless, based on the findings of [^{64}Cu]AMD3100, these compounds could be used to diagnose metastases which show increased accumulation of radioactivity.[112]

6.5 FUTURE WORK

Whilst it is anticipated that the rigidified $^{64}CuZn_2$[**18**] and $^{64}CuZn_2$[**19**] would be more stable than [^{64}Cu]AMD3100 a scope for further development would be to conduct stability tests and compare the findings with [^{64}Cu]AMD3100 to validate whether this predication is true.[71b, 175a, 184b, 188] Preliminary work into developing the first radiolabelled tris-macrocycles has been conducted, in order to expand on these foundations it would be logical to carry out additional runs to clarify anomalies, such as the sudden drop in ^{64}Cu incorporation in $^{64}CuZn_2$[**18**] after 30 min and the variations in radioactivity readings during the LogP calculations.

Radiochemistry disclosed in this chapter was accomplished for the most active tris-macrocycles and it would be interesting to investigate the properties of other tris-macrocycles synthesised in chapter 2. Once a range of tris-macrocycles had been radiolabelled stronger conclusions could then be made about the optimum structure for a PET imaging agent. An additional option to explore is the incorporation of a ^{64}Cu metal ion into the novel bis-macrocycles disclosed in chapter 3. The bis-macrocycles also offer the flexibility to include other radioisotopes such as ^{68}Ga if DOTA anhydride was successfully bound, or ^{18}F incorporation through click chemistry.

Finally, a long term goal would be to test the compounds *in vivo* to see whether positively charged macrocycles show a high accumulation in the liver and slow clearance as reported by Jones-Wilson *et al.*[175b] This could be overcome by incorporating a group onto the macrocycle to create an overall neutral or negative charge to determine whether this leads to clearance 24 h after injection.[175b, 219a]. A route to neutralising the tris-macrocycle metal complexes could be to incorporate a charge modifying group. A negatively charged group, such as a carboxylate group, could be attached to tris-macrocycles through C-functionalisation. Across the three macrocycles there is ample opportunity for C-functionalisation, the entire synthetic route would have to be re-structured to encompass this, but a fantastic opportunity to expand the initial findings of this chapter is provided.

A different method of achieving neutrality could be to include acetate arms onto pendant arms for coordination with the metal centre. Wong *et al.* synthesised a copper(II) coordinated CB-mono-macrocycle which contained two acetate groups to further increase the kinetic stability of the complex and to fully coordinate the copper(II) ion which neutralised the 2+ charge.[61b, 184b] Although, a neutral charge induced by acetate arms within the macrocycle structure could prevent interaction of metal ions with the surface of the CXCR4 receptor and have drastic effects on affinity. An alternative proposal would be to have two macrocycles linked with a *para*-xylyl linker and a third macrocycle linked with a different pendant arm which would contain one acetate group for bi-dentate interaction with the ^{64}Cu ion. This would lead to a reduced overall charge as well as a highly

stable imaging agent that could still interact strongly with the CXCR4 receptor through the zinc bound macrocycles. The synthetic route to these tris-macrocycles would need to be investigated and a novel pendant arm would need synthesising. A potential idea for the pendant arm is proposed in Figure 100. The ideal group for interaction with the metal ion would be an acetate group, although this would need protecting when initially reacting the linker group with the macrocycle. Potentially, an ester group would be best suited which could then be reduced to produce the acetate group. The exact carbon chain length would need to be optimised to ensure the acetate group could reach the metal ion because the tris-macrocycle structure is quite rigid and movement of the linker group to interact with the metal ion would be hindered. Prior to any radiochemistry the affinity of the distinctly different tris-macrocycles would need to be evaluated to assess whether the bulkier linker arm would have negative impact on affinity. A drop in affinity due to bulkier linker groups has been observed for non-reinforced bis-macrocycles.[74, 79]

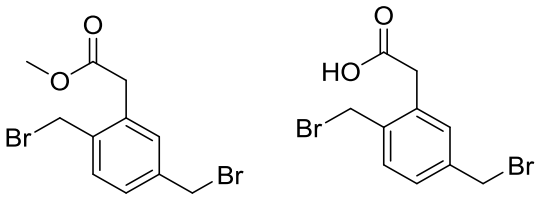

Figure 100 – Potential linker group for novel tris-macrocycles

CHAPTER SEVEN

CONCLUSIONS AND FUTURE WORK

7.1 CONCLUSIONS

7.1.1 Overview

This work highlights the synthesis of highly stable metal-containing multi-ring macrocycles for use as CXCR4 expressing cancer diagnosis and therapeutic agents. Macrocycles have been extensively used as chelating agents in the literature however transmetallation and toxicity has sometimes restricted their clinical application. The structural reinforcement present in the compounds discussed in this work can counteract this limitation. The development of PET imaging agents has received a lot of interest in recent years for a wide range of applications. The incorporation of ^{64}Cu(II) into the macrocycle cavity is attractive due to the long half-life of the radioisotope allowing longer radiochemistry reaction and purification times, and more importantly longer timescales for imaging studies to allow full clearance of the tracer from the bloodstream.

A further attractive option for new CXCR4 imaging agents is the use of ^{18}F as it is the most commonly used radioisotope for PET imaging and hence the clinical infrastructure is already available. The development of therapeutic agents for CXCR4 expressing cancers has also received considerable attention as a result of its connection to metastasis which is responsible for the majority of deaths in cancer patients. The well-reported strong interaction between macrocyclic ligands and the CXCR4 receptor has attracted many research groups and led to the development of novel CXCR4 antagonists. This work reported in this thesis outlines the synthesis of novel tris- and bis-macrocycles which were structurally reinforced and coordinated to transition metals to provide optimum interactions with the CXCR4 receptor. A series of novel tris- and bis-macrocycles and their metal complexes were biologically evaluated to determine their capability as CXCR4 antagonists for the diagnosis and therapy of CXCR4 expressing cancers. A set of novel SPR experiments were conducted in order to develop a method to determine macrocycle residence time on the CXCR4 receptor. Two high affinity, tris-macrocycle zinc(II) coordinated CXCR4 antagonists synthesised in this work were radiolabelled with ^{64}Cu(II) to produce a potential PET imaging agent for CXCR4 expressing cancer diagnosis. This work outlines progress towards the production of high affinity compounds for use in clinical applications.

7.1.2 Main Achievements

The successful synthesis of novel configurationally-restricted, linear tris-macrocycles has been completed. Configurational restriction to obtain SB and CB macrocycles was achieved by the introduction of an ethyl bridge between adjacent or opposite nitrogen atoms in the macrocycle respectively. Macrocycles were linked with two *para*-xylyl linkers previously reported to result in higher anti-HIV activity than *meta* or *para* substitutions in bis-macrocycles.[79] The coordination of the

SB-cyclen, SB-cyclam, CB-cyclen, CB-cyclam and TMC containing tris-macrocycles, **16**-**21**, to copper(II), nickel(II) and zinc(II) metal ions was carried out to enhance macrocycle interaction with the CXCR4 receptor by the formation of coordinate bonds as opposed to weaker hydrogen bonds.[56a] The synthesis of unsymmetrical tris-macrocycles has not been reported previously. Tris-macrocycles could potentially interact with multiple aspartate residues on the CXCR4 receptor thus enhancing the interaction with the CXCR4 receptor. Their ability to act as CXCR4 antagonists was evaluated through a number of biological assays such as displacement assays and calcium(II) signalling assays. The series of tris-macrocycle metal complexes synthesised all exhibited micromolar affinity with all but one complex being potent at nanomolar concentrations. Both the free ligands and metal complexes showed a measurable inhibitory response although the metal complexes were significantly higher. The most potent anti-HIV tris-macrocycle metal complexes were Zn_3[**19**], Zn_3[**21**] and Zn_3[**18**] which were significantly more potent than AMD3100 (IC_{50}: 1.9, 2.2 and 0.9 nM respectively *vs*. 12 nM). The general trend of anti-HIV activity in terms of the metal complexes was zinc(II)>nickel(II)>copper(II). Calcium(II) signalling studies revealed that Zn_3[**19**] and Zn_3[**21**] were the most potent complexes, IC_{50}: 2.90 and 1.55 nM respectively, and were up to six fold better at preventing calcium(II) flux than AMD3100, IC_{50}: 9.94 nM. All tris-macrocycles exhibited low toxicity and zinc(II) coordinated tris-macrocycles were seen to be the most potent CXCR4 antagonists with multiple tris-macrocycles outperforming AMD3100.

Two high affinity tris-macrocycles, Zn_3[**18**] and Zn_3[**19**], have been radiolabelled with ^{64}Cu via transmetalation to produce potential PET imaging agents to diagnose CXCR4 expressing cancers. These structurally rigidified complexes potentially offer ideal properties for PET imaging without the toxic side effects *in vivo* caused by free ^{64}Cu ions.[71b, 175a, 184b, 188] Transmetalation was achieved by heating the macrocycle in ammonium acetate buffer with $^{64}Cu(II)Cl_2$ for up to 75 min at 90^{o}C to yield crude-RCY of more than 60 %. LogP values for $^{64}CuZn_2$[**18**] and $^{64}CuZn_2$[**19**] were calculated and indicated that the macrocycles were more hydrophobic than [^{64}Cu]AMD3100..[112]

A novel route to synthesise a series of bis-macrocycles, **28**-**39**, containing a terminal pendant arm for functionalisation has been outlined. The synthesis of the novel N-functionalised bis-macrocycles provides the opportunity for applications in different imaging applications. The bis-macrocycles were isolated by reacting equimolar amounts of mono-substituted mono-macrocycle quaternary salts together before a lengthy (10 d) reduction with $NaBH_4$ to ascertain **28**-**33** in good yields (>45%). The terminal linker group was functionalised with nitro, nitrile, amine, azide and ester groups and the conjugation of imaging groups for use in PET imaging or optical imaging was explored. The synthesis of a macrocycle containing an azide group or an ester group has not been previously reported.

Zinc(II) and copper(II) complexes of the bis-macrocycles were synthesised to improve the interaction with the CXCR4 receptor and the biological profile of these complexes *in vitro* was determined. As symmetry is not required for high affinity these compounds may show improved interaction with the CXCR4 receptor.[79] Displacement assays showed that the free-ligands were significantly poorer (0% - 54% inhibition) at competing for the CXCR4 receptor, against a CXCR4 specific mAb, compared to the metal complexes which all showed >92% inhibition. The unusually high inhibition percentage generated by **37** is likely due to its amine functionalised pendant arm which provides an extra group to interact with the CXCR4 receptor. Poorer inhibition was generally observed for bis-macrocycles containing two bridged-cyclen macrocycles. Anti-HIV activity data revealed that Zn_2[**32**] was highly potent and more than three times more active than AMD3100. Further data is required to evaluate the remaining bis-macrocycle metal complexes completely.

Mono-macrocycles were utilised in a series of test reactions to determine how well functionalised groups could undergo conjugation reactions. Mono-macrocycles were selected due to the ease and speed at which they could be synthesised. The development of a novel pendant arm capable of undergoing click chemistry has been outlined. The alkyne pendant arm was achieved in good yield and was successfully conjugated to SB-cyclam, SB-cyclen and CB-cyclen. The functionalization of an azide pendant arm was achieved through hydrogenation of a nitro-group followed by triazotisation on SB-cyclam. This route was relatively quick and high yielding generating azido bearing macrocycles which could conjugate to a variety of different molecules through click reactions. This area requires subsequent investigation as all copper(I) catalysed reactions with the alkyne and nitro functionalised macrocycle were unsuccessful which meant that PET radioisotopes could not be conjugated to the macrocycles. An alternative route to incorporate a PET radioisotope was explored through the conjugation of DOTAGA anhydride to an amine functionalised mono-macrocycle however, whilst the product was isolated the reaction required optimisation to drive the reaction to completion. Efforts to utilise an ester functionalised macrocycle proved ineffective however, these test reactions provided insight as to the direction of subsequent work.

7.1.3 Overall Achievements in Relation to the Field

This work has focused on the development of high affinity CXCR4 antagonists for use as diagnostic and therapeutic agents in CXCR4 expressing cancers. Multiple novel mono-, bis- and tris-macrocycles have been synthesised. Mono- and bis-macrocycles bearing pendant arms have been functionalised in order to diversify the potential conjugatable groups. The bis- and tris- macrocycles have been optimised for CXCR4 receptor interaction through structural reinforcement to restrict the macrocycles to more active configurations as well as coordination to metal ions to create stronger

bonds with the receptor surface. These features have resulted in the production of a series of highly potent compounds.

An effective and reproducible synthetic route to yield novel SB-and CB-containing tris-macrocycles has been outlined in this work. This work reports a number of tris-macrocycle metal complexes that show nanomolar and sub-nanomolar anti-HIV activity which is a significant advancement in the development of a macrocycle with diagnostic and therapeutic applications and this extent of activity has not been previously reported by similar compounds in this field. This work reports the successful transmetalation of ^{64}Cu(II) into a tris-macrocycle to produce novel multi-metal containing compounds which can be applied to PET imaging.

The development of a novel SPR method for the calculation of macrocycle-CXCR4 receptor residence time proved challenging, however important progress has been made and subsequent work should lead to a successful method.

Significant steps towards a macrocycle capable of undergoing click reactions have been outlined in this work through functionalisation of pendant arms on mono- and bis-macrocycles. A number of novel unsymmetrical, configurationally restricted bis-macrocycles have been synthesised by a reliable and efficient route which greatly expands the number of reinforced bis-macrocycles reported in the literature. This work reports the first known example of an azide functionalised bis-macrocycle which avoids a synthetic route involving the handling of likely-explosive pendant arms. The azide functionalisation enables conjugation to a range of imaging groups which improve its applicability. Functionalisation of the bis-macrocycles with an amine group could enable the subsequent addition of fluorescent dye or DOTAGA-anhydride. Conjugation of bis-macrocycles to DOTAGA-anhydride was troublesome but initial progress has been made with mono-macrocycles towards a unique ^{68}Ga(III) radiolabelled bis-macrocycle for use in PET imaging. The collection of bis-macrocycles were coordinated to metal ions and the consequent complexes exhibited strong affinity for the CXCR4 receptor which also revealed that the terminal pendant arm did not have a detrimental impact. Furthermore, the different pendant arm functional groups did not interfere with the bis-macrocycles interaction with the CXCR4 receptor.

This work outlines the synthesis of a range of multi-ring macrocycles that disclose the importance of configurational restriction in combination with metal ion coordination in the development of high affinity CXCR4 antagonists. This work highlights the ease at which slight structural modifications can convert the macrocycle from a therapeutic agent to a diagnostic agent and pinpoints the adaptability of multi-ring macrocycles to desired applications. Incorporating a terminal pendant arm

increases the functionality of the bis-macrocycles and provides a large scope of potential applications. The development of CXCR4 diagnostic agents is a relatively new concept, the targeting of CXCR4 for therapy has been an area of interest for a number of years therefore the design of multi-functional and high affinity compounds is attractive. This work demonstrates a significant advancement in the synthesis of novel bis-macrocycles and reports the first reinforced tris-macrocycles to be applied as CXCR4 expressing cancer diagnosis and therapeutic agents.

7.2 FUTURE WORK

7.2.1 Short-Term Goals

A more in depth study to determine which aspartate residues the tris-macrocycle metal complexes interact with would be useful to acknowledge, specifically to determine 'new' aspartate residues were involved resulting in the high affinity observed. This could be achieved through mutagenesis studies as conducted previously by Gerlach *et al.* to ascertain how cyclam, AMD3100 and its metal complexes interacted with the receptor.[56a] It would also be beneficial to determine the crystal structures of the macrocycles to confirm their metal-complex structure instead of hypothesising based on similar structures.

It would be beneficial to repeat the method used to obtain **15** for the other tris-macrocycle quaternary salts to ascertain whether these alternate conditions, anhydrous DMF at RT for 14 d, would lead to higher yields.

In order to improve the characterisation of the tris-macrocycle metal complexes it would be favourable to synthesise all the chloride metal complexes which would enable better elemental analysis as the product would precipitate out of solution as a solid and consequently improve the attained yield as less product would be lost through purification.

Whilst it is anticipated that the rigidified $^{64}CuZn_2$[**18**] and $^{64}CuZn_2$[**19**] would be more stable than [^{64}Cu]AMD3100 a scope for further development would be to conduct stability tests and compare the findings with [^{64}Cu]AMD3100 to validate whether this predication is true.[71b, 175a, 184b, 188] As a few of the results contain anomalies, such as sudden drop in ^{64}Cu incorporation in $^{64}CuZn_2$[**18**] after 30 min and the variations in radioactivity readings during the LogP calculations, it would be strongly advised to repeat these experiments to rule out these issues and clarify the findings.

The radiochemistry in this work was limited to two tris-macrocycles therefore it would be interesting to radiolabel other tris-macrocycles. Once a range of tris-macrocycles had been radiolabelled stronger generalisations could then be made about the optimum structure for a PET imaging agent.

To complete the series of bis-macrocycles the zinc(II) and copper(II) complexes of azide functionalised bis-SB-cyclen-CB-cyclen macrocycle could be synthesised. Copper-free click reactions with these complexes, $[Zn_2\mathbf{39}]^{4+}$ and $[Cu_2\mathbf{39}]^{4+}$, could be conducted to determine whether they could be labelled with ^{18}F for use as PET imaging agents. The incorporation of ^{64}Cu into the novel bis-macrocycles could also be tested using the same method as for the tris-macrocycles.

Further investigations regarding azide functionalised mono- and bis-macrocycles and SPAAC reactions should be conducted to establish if this is an effective route to attach imaging groups.

Another copper-free click reaction that requires a more detailed evaluation is the synthesis of **42** to ascertain whether the tetrazine group was successfully isolated. This then provides an additional route to radiolabel the macrocycle with ^{18}F through a radiolabelled TCO group which selectively reacts with tetrazine.

The bis-macrocycles synthesised in this work were not coordinated to nickel(II) therefore it would be interesting to determine whether these or nickel(II) containing complexes exhibited high affinity as was observed for tris-macrocycle nickel(II) complexes.

It would be advantageous to repeat the nucleophilic substitution step in the synthesis of the azide containing pendant arm, **50**. Routes to achieve this could include substituting the solvent and driving the reaction by heating it.

Repetition of the pendant arm synthesis outlined in Scheme 32 would be beneficial in order to understand if a longer alkyl chain between the aromatic group and the alkyne would prevent pendant arm cleavage during formation of CB cyclam as observed with **57**. Another reaction to repeat would be the synthesis of **61** as it provides a quick route to functionalising the macrocycle with an alkyne, though the method by Silversides *et al.* should be followed.[160c] Click reactions with an azide group could then be explored.

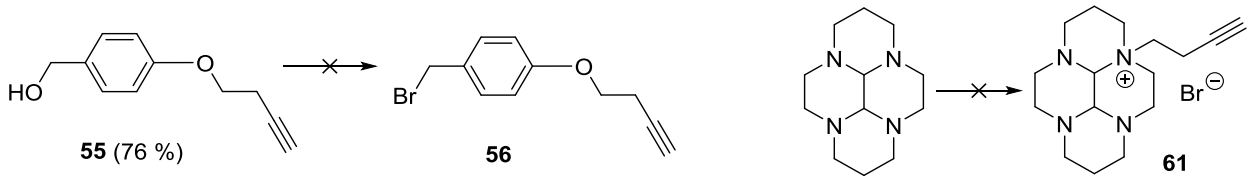

Scheme 32 – Synthesis to alkyne functionalised CB-cyclam

It is worth re-investigating the conjugation of ethylene diamine because minimal adaptation would be required to isolate **77**. One amine group in ethylene diamine could be BOC protected and then be reacted with **61** before deprotection with HCl to yield the desired product. The macrocycle could then be labelled with a fluorescent dye for use in optical imaging, once coordinated to a metal ion. The use of longer chain lengths may decrease the quenching effect that copper(II) can have on the dye's photophysical properties.

A final recommendation would be to retry the conjugation of DOTAGA anhydride to **62** with a fresh batch of DOTAGA anhydride because the subsequent macrocycle could be easily radiolabelled with ^{68}Ga, prior to metal complexation.

7.2.2 Long-Term Goals

7.2.2.1 Synthesis

It would be interesting to synthesise a series of tris-macrocycles containing formaldehyde cyclen, **76**, in the central position given that time constraints prevented this investigation, see Figure 101. Alternatively it would be interesting to determine whether a tris-macrocycle made up of three formaldehyde macrocycles, or tris-macrocycles containing TMC or tetramethylcyclen in the terminal positions, would have a drastic effect on affinity. Another collection to explore could be tris-CB macrocycles, see Figure 101. Combinations of the macrocycles could also be studied. It would be interesting to compare the activity of these to the activity of the metal complexes of **16**-**21**.

If the general trend is that bis-macrocycles are more active than mono-macrocycles and tris-macrocycles are more active than bis-macrocycles it is logical that tetrakis-macrocycles and pentakis-macrocycles may be even more active. It would certainly be interesting to synthesise these compounds and find out whether this is the case, however the molecular weight may become too high for these compounds to be used effectively *in vivo* especially when considering the metal complexes which would significantly increase the molecular weights. Still it would be interesting to test the theory and high molecular weight peptides have shown potential as anti-metastatic agents.[174]

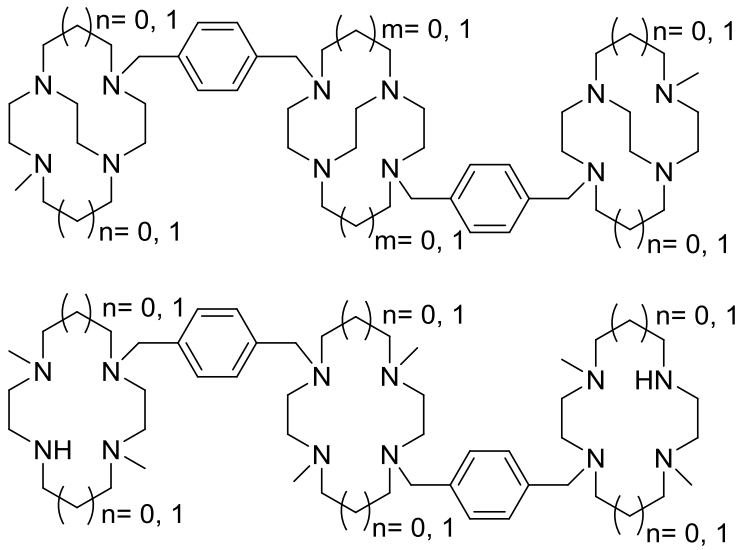

Figure 101 – Structure of potential tris-CB cyclam and tris-CB cyclen macrocycles

Once the radiolabelled macrocycles were evaluated *in vitro* they could be tested *in vivo* to see whether the positively charged macrocycles show a high accumulation in the liver and slow clearance as reported by Jones-Wilson *et al.*[175b] A way to prevent this would be to neutralise the macrocycles and increase their kinetic stability.[61b, 184b] A route to neutralising the tris-macrocycle metal complexes could be to incorporate a charge modifying group. A negatively charged group, such as a carboxylate group, could be attached to tris-macrocycles through C-functionalisation.

Across the three macrocycles there is ample opportunity for C-functionalisation, the entire synthetic route would have to be re-structured to encompass this, but a fantastic opportunity to expand initial findings is provided.

Alternatively, neutrality and increased kinetic stability could be achieved through development of a novel pendant arm to include acetate arms for coordination with a metal centre.[61b, 184b] Wong *et al.* synthesised a copper(II) coordinated CB-mono-macrocycle which contained two acetate groups to further increase the kinetic stability of the complex and to fully coordinate the copper(II) ion which neutralised the 2+ charge.[61b, 184b] Although, this could prevent interaction of zinc(II) ions with the surface of the CXCR4 receptor and have drastic effects on affinity. An alternative proposal would be linking two macrocycles with a *para*-xylyl linker to a third macrocycle linked with a different pendant arm, containing one acetate group for bi-dentate interaction with the ^{64}Cu ion, resulting in reduced overall charge and improved stability whilst allowing strong interactions with the CXCR4 receptor. The synthetic route to obtain these tris-macrocycles would need to be investigated and a novel pendant arm would need synthesising.

A potential idea for the pendant arm is proposed in Figure 102. The ideal group for interaction with the metal ion would be an acetate group, although this would need protecting when initially reacting the linker group with the macrocycle. Potentially, an ester group would be best suited and could then be reduced to produce an acetate group. The exact carbon chain length would need to be optimised to ensure the acetate group could reach the metal ion because the tris-macrocycle structure is quite rigid and movement of the linker group to interact with the metal ion would be hindered. Prior to any radiochemistry the affinity of the distinctly different tris-macrocycles would need to be evaluated to assess whether the bulkier linker arm would have negative impact on affinity. A drop in affinity due to bulkier linker groups has been observed for non-reinforced bis-macrocycles.[74, 79]

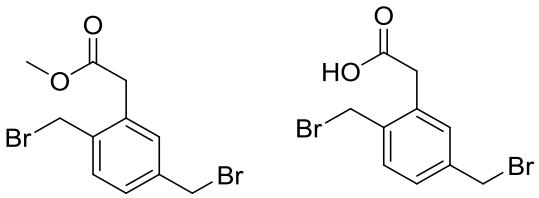

Figure 102 – Potential linker group for novel tris-macrocycles

Further pendant arm development involves the nucleophilic aromatic substitution of **64** which did not lead to the desired product because of the absence of an EWG. Scheme 30 highlights some potential synthetic routes to isolate a pendant arm capable of undergoing fluorination. Test reactions would be conducted with the pendant arm attached to mono-macrocycles first before

proceeding to synthesise bis-macrocycles. The second synthetic route shown in Scheme 30 would form an amide upon reaction with a macrocycle, it is unknown what effect this may have on the activity of the macrocycle but biological evaluation would clarify this.

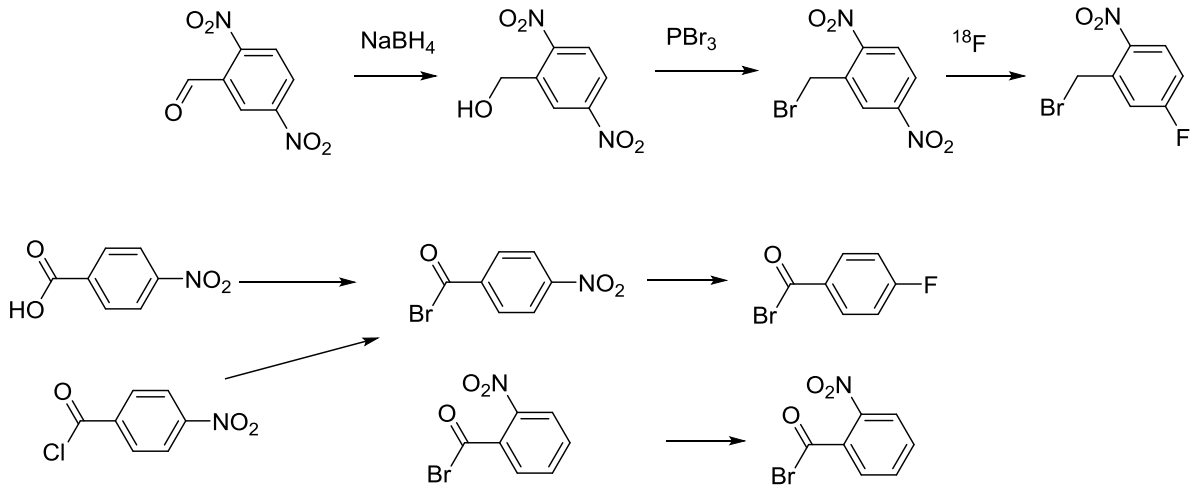

Scheme 33 – Proposed synthetic route to fluorinated pendant arms containing EWG in *ortho* or *para* position

Once the reaction conditions were determined for the conjugation of DOTAGA-anhydride to bis-macrocycles future studies could be conducted to improve the affinity of the ^{68}Ga(III) radiolabelled diagnostic agent. This could be achieved by the conjugation of multiple bis-macrocycles to the DOTAGA analogue, see Figure 103. The multiple bis-macrocycles may improve affinity based on previous findings from the literature whereby increasing numbers of CXCR4 targeting groups improved affinity of a radiolabelled group.[215] The DOTAGA analogue could be modified to enable the incorporation of up to four bis-macrocycles because only two acetate arms are needed for ^{68}Ga(III) encapsulation. It would be interesting to see what difference, one to four bis-macrocycles made to the compounds affinity. Once these groups where conjugated to their imaging group it would be worth pursuing biological evaluation to determine if the additional group had detrimental effects on the macrocycle's affinity for the CXCR4 receptor.

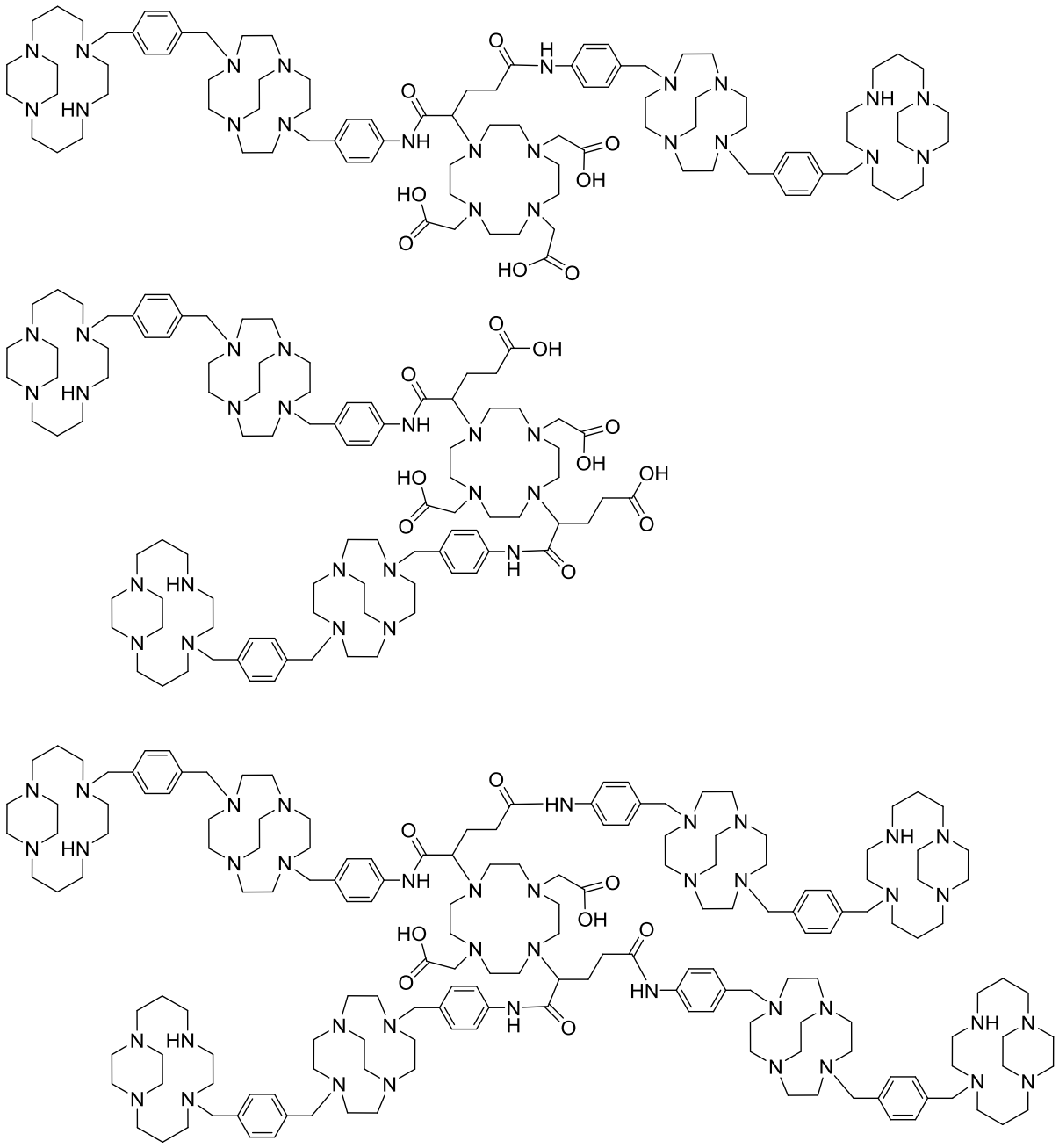

Figure 103 – Potential routes to improve the affinity of DOTAGA conjugated bis-macrocycles

7.2.2.2 Biological Studies

The development of a novel SPR method to efficiently evaluate the binding kinetics of macrocycles synthesised by the group is required. Initial steps have been made in this work but it is predicted that the production of a tagged CXCR4 expressing cell line will lead to the development of a successful method following the example set by Babcock *et al.* and Navratilova *et al.*[245, 261] The commonly used GST tag will be captured by the anti-GST Ab immobilised onto a sensor chip, as outlined in this work. The use of the anti-GST Ab is beneficial as it can recognise multiple epitopes on the GST tag which increases its ability to identify the GST tag and potentially improve the amount of

captured material on the sensor chip.[260] This in turn could lead to the generation of kinetic binding data.

To assess the suitability of radiolabelled macrocycles to diagnose CXCR4 expressing cancers *in vitro* and *in vivo* experiments could be conducted. Animal models using severe combined immunodeficient, SCID, mice implanted with U87, human glioblastoma cell line, and U87-stb-CXCR4, a U87 cell line stably transfected with human CXCR4, brain tumour cells could show macrocycles, disclosed in chapter 2, 3 and 6, interacting specifically with CXCR4 expressing tumours. PET imaging of the animal model would show locations of macrocycle uptake and blocking studies would ideally show reduction of radioactivity in tumours. A control injection of $^{64}Cu(II)Cl_2$ into a mouse would show specificity of the macrocycles because $^{64}Cu(II)Cl_2$ would show uniform distribution whereas macrocycles would show specific accumulation in CXCR4 expressing tissue.[112]

For breast tumour imaging, SCID mice inoculated with low CXCR4 expressing human breast cancer cell line, $CXCR4^{low}$ MDA-MB-231 and, high CXCR4 expressing human breast cancer cell line, $CXCR4^{high}$ DU4475 would result in tumour growth, grown to 100-200 mm^3 to minimise necrosis, and be used to identify whether macrocycles could differentiate low and high CXCR4 expressing tumours. Histological examinations, on organs and tumours collected prior to animal sacrifice, could be stained for the determination of CXCR4 expression and to quantify the degree of radiotracer uptake.[112]

In order to evaluate macrocycles as metastatic diagnostic and therapeutic agents metastatic mouse model studies, using MDA-MB-231 cell line in SCID mice, could be performed and compared to a control, SCID mice injected with saline solution. Multiple models would identify the best macrocycles, from this work, to diagnose and inhibit metastasis. To validate imaging and biodistribution results sacrificed animal tumour cells could be extracted from control and study mice and CXCR4 expression analysed by flow cytometry. An increase in CXCR4 expression would be expected in the metastasised cell lines.[112]

Biopsies from human tumours could be kept alive with microfluidic systems, macrocycles could be administered and tumour response monitored. Biopsy tissue from a tumour is an ideal model for drug testing because the tissue architecture is preserved and produces species relevant results. Kinetic modelling would enable the radioactivity in blood and other tissues to be quantified.[279]

Finally, first stage clinical trials could be conducted in normal healthy volunteers. In phase I trials, AMD3100 was well tolerated therefore it is likely that macrocycles outlined in this work would also

be, preliminary *in vitro* data supports this theory. PET imaging agents would be administered in very small doses that a biological reaction to radiolabelled macrocycles would be unexpected.

CHAPTER EIGHT

EXPERIMENTAL

8.1. GENERAL METHODS

8.1.1 General Notes

Bulk solvent was removed by rotary evaporation on a Buchi RE 111 evaporator equipped with a diaphragm vacuum pump, trace solvent was removed in a vacuum oven. Reactions were performed at room temperature (RT) unless otherwise stated. All metal containing compounds were purified *via* size exclusion chromatography using Sephadex LH20, which was pre-soaked in methanol for three hours before use.

8.1.2 NMR spectroscopy

^{1}H NMR and ^{13}C NMR spectra were obtained using a Jeol JNM-LA400 spectrometer at 400 MHz for ^{1}H and 100 MHz for ^{13}C. Solvents used for the analysis were referenced against standard internal TMS or residual non-deuterated solvent signal and were purchased from Goss chemicals Ltd or Cambridge Isotopes Ltd. Chemical shifts are reported in parts per million, ppm, for ^{1}H NMR and ^{13}C NMR spectra and coupling constants, J, reported in Hertz, Hz. Splitting patterns are assigned as *s*: singlet, *d*: doublet, *dt*: double triplet, *t*: triplet, *q*: quartet, *m*: multiplet, *td*: triple doublet and *br*: broad signal.

8.1.3 MS

Electrospray MS was performed at the University of Hull using a Finnegan MAT 900 XLT system. Accurate mass spectrometry measurements (HRMS) were recorded at the EPSRC National Mass Spectrometry Service Centre at the University of Swansea using a LQT Orbitrap XL. The EPSRC National Mass Spectrometry Service Centre have struggled to generate data for bis- and tris-macrocycles and their corresponding metal complexes. This could be due to degradation of the macrocycles during analysis at high temperatures or as a result of the macrocycles flying poorly in the instrument because of their molecular weight. MALDI analysis has also failed to generate useful data.

8.1.4 UV-vis

UV-vis spectra were obtained using a Varian Cary Bio UV-via spectrophotometer using optical glass cells.

8.1.5 Elemental Analysis

CHN analysis was performed using a CHN analyser EA1108 (Carlo Erba). Most compounds were within the limit of 0.4% of the expected ratios, however **6**, **9**, **12**, **16**, **17**, **18**, Ni_3**16**, Cu_3**18**, Ni_3**21**, **23**, **25**, **27**, **35**, **37**, Cu_2**28**, Cu_2**30**, **57**, **59** and **65** were within 0.5%. This higher limit is due to products being viscous oils which make elemental analysis challenging. For other products, higher solvent association or salt impurities are likely to cause the larger deviation from the predicted element values.

8.1.6 Radio-Thin layer chromatography (Radio-TLC)

Radio-TLCs were ran on 'neutral alumina sheets' (Merck USA), eluting with H_2O:MeOH (95:5) saturated with NaCl. Radio-TLC was carried out using a Lablogic Scan-Ram, equipped with a NaI detector at a speed of 10mm/min. Data was recorded using Lablogic Laura (version 4.1.7.70).

8.1.7 Materials

Reagents for chemical reactions were purchased from Sigma-Aldrich, Fisher, CheMatech, Acros, Strem, Click-Chemistry Tools, GE Healthcare, R&D Systems, ACRO Biosystems, and Avanti Polar Lipids Inc. Chemicals were used as received without further purification. Solvents used were of general purpose grade and used as received. Acetonitrile (MeCN), dichloromethane (DCM), tetrahydrofuran (THF), and methanol (MeOH) were dried over molecular sieves, following activation at 300^{o}C for 18 h, according to literature methods outlined by Bradley and co-workers.[280]

8.2. MACROCYCLE PRECURSORS

8.2.1 Synthesis of 1,4,8,11-tetraazacyclotetradodecane (1)

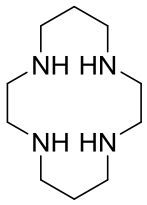

1

1,5,8,12-Tetraazadodecane (26.0 g, 0.15 mol) was added to a solution of nickel(II) perchlorate (54.7 g, 0.15 mol) in water (400 mL). The resulting red/brown solution was cooled to ~5°C and an aqueous solution of glyoxal (40% w/w, 25 mL, 0.15 mol) was added, the resulting solution was left to stand for 4 hours. The mixture was again cooled to ~5°C and treated with sodium borohydride (11.0 g, 0.30 mol) in small portions. The solution was heated to 90˚C for 20 min and filtered whilst hot. Sodium cyanide (29.0 g, 0.60 mol) was added to the filtrate which was heated to the point of reflux then left to cool overnight. Sodium hydroxide (15.0 g, 0.38 mol) was added and the resulting yellow-brown mixture was filtered through a pad of hyflo super cel. The solid was washed with chloroform (3 x 100 mL) and the aqueous layer was then extracted with chloroform (5 x 100 mL). The organic phases were dried (Na_2SO_4), filtered and the solvent removed *in vacuo*. The resulting yellow solid was recrystallised from chlorobenzene (150 mL), filtered and washed with ether (50 mL) to yield white needles (14.02 g, 47%).

^{1}H NMR (400 MHz, $CDCl_3$, δ): 1.72(*m*, N-α-CH_2, 4H), 2.19 (*br s*, NH, 4H), 2.68 (*s*, N-α-CH_2, 8H), 2.74 (*m*, N-α-CH_2, 8H). ^{13}C NMR (100 MHz, $CDCl_3$, δ): 29.56 (N-α-CH_2), 49.47 (N-α-CH_2), 50.78 (N-α-CH_2). MS (m/z): $[M + H]^+$ calcd for $C_{10}H_{25}N_4$, 201.34; found, 201.9. Anal. calcd for $C_{10}H_{25}N_4$: C, 59.96; H, 12.08; N, 27.97. Found: C, 59.82; H, 12.20; N, 28.11.

8.2.2 Synthesis of cis-13-1,4,7,10-tetraazatetracyclo[5.5.1.04,14010,13]tetradecane (2) and cis-3a,5a,8a,10a-tetraazaperhydropyrene (3)

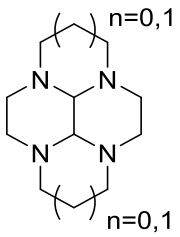

n=0 **2**
n=1 **3**

General procedure A

The macrocycle was dissolved in methanol and cooled to –10˚C. A cold (0˚C) aqueous solution of glyoxal was added dropwise over 90 min. The clear solution was stirred at –10˚C for 30 min then at RT for 3 hours. The solvent was removed *in vacuo* and the crude solid was redissolved in diethyl ether. The filtrate was dried ($MgSO_4$), filtered and solvent removed *in vacuo*.

***cis*-13-1,4,7,10-tetraazatetracyclo[5.5.1.$0^{4,14}0^{10,13}$]tetradecane (2)**

Amounts: 1,4,7,10-tetraazacyclododecane (3 g, 17.41 mmol), methanol (600 mL), aqueous glyoxal solution (40 % *w/w*, 2.53 g, 43.54 mmol), diethyl ether (200 mL). To yield a white solid (3.03 g, 90 %). ^{1}H NMR (400 MHz, $CDCl_3$, δ): 2.44-2.57 (*m,* N-α-CH_2, 8H), 2.81-2.90 (*m,* N-α-CH_2, 8H), 3.29-3.61 (*m,* H_{aminal}, 2H). ^{13}C NMR (100 MHz, $CDCl_3$, δ): 46.07 (N-α-CH_2), 50.43 (N-α-CH_2), 51.21 (N-α-CH_2), 63.50 (C_{aminal}), 67.93 (C_{aminal}). HRMS (*m/z*): $[M+H]^+$ calcd for $C_{10}H_{19}N_4$, 195.1604; found, 195.1600. Anal. calcd for $C_{10}H_{18}N_4$: C, 61.82; H, 9.34; N, 28.84. Found: C, 61.80; H, 9.55; N, 28.61.

***cis*-3a,5a,8a,10a-tetraazaperhydropyrene (3)**

Amounts: 1,4,8,11-tetraazacyclotetradodecane (3 g, 14.98mmol), methanol (600 mL), aqueous glyoxal solution (40 % w/w, 2.17 g, 37.45 mmol), diethyl ether (200 mL). To yield a white solid (2.88 g, 87 %).

^{1}H NMR (400 MHz, $CDCl_3$, δ): 1.20-1.24 (m, N-β-CH_2, 4H), 2.08-2.37 (m, N-α-CH_2, 8H), 2.68-2.75 (m, N-α-CH_2, 2H), 2.90-3.00 (m, N-α-CH_2, 4H), 3.08 (s, H_{aminal}, 2H), 3.50-3.56 (t, N-α-CH_2, 2H). ^{13}C NMR (100 MHz, $CDCl_3$, δ): 19.56 (N-β-CH_2), 44.73 (N-α-CH_2), 52.46 (N-α-CH_2), 54.33 (N-α-CH_2), 56.02 (C_{aminal}). HRMS (*m/z*): $[M+H]^+$ calcd for $C_{12}H_{23}N_4$, 223.1923; found, 223.1916. Anal. calcd for $C_{12}H_{22}N_4$: C, 64.83; H, 9.97; N, 25.20. Found: C, 64.59; H, 10.17; N, 25.00.

8.2.3 Synthesis of 1,4,8,11-tetraazatricyclo[9.3.1.1^{4,8}]hexadecane (4)

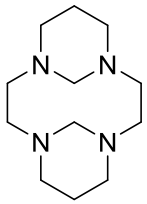

4

General procedure B

Cyclam (**1**) (2.00 g, 9.98 mmol) was suspended in acetonitrile (500 mL) and stirred at room temperature as aqueous formaldehyde (37% w/v, 2.50 mL,) was added in one portion. The solution was then stirred for 24 h. Following this, the solvent was then removed *in vacuo* and the crude yellow/orange product was dried overnight under high vacuum. The crude product was then purified by sublimation (50 µm Hg, 70^{o}C) to yield white crystals (1.97 g, 88 %) which were dried under high vacuum.

^{1}H NMR (400 MHz, $CDCl_3$, δ): 1.15-1.19 (*m*, N-β-CH_2, 4H), 2.20-2.33 (*m*, N-α-CH_2, 2H), 2.35-2.43 (*m*, N-α-CH_2, 2H), 2.59-2.66 (*m*, N-α-CH_2, 4H), 2.81-2.95 (*m*, N-α-CH_2, 4H), 3.10-3.19 (*m*, N-α-CH_2, 4H), 5.43-5.46 (*m*, N-α-CH_2, 4H). ^{13}C NMR: (100 MHz, $CDCl_3$, δ): 20.28 (N-β-CH_2), 49.44 (N-α-CH_2), 53.75 (N-α-CH_2), 68.95 (N-α-CH_2). MS (*m/z*): $[M+H]^+$ calcd for $C_{12}H_{25}N_4$, 225.2079; found, 225.2070. Anal. calcd. for $C_{12}H_{24}N_4$: C, 64.24; H, 10.78; N, 24.97. Found: C, 64.44; H, 11.00; N, 25.19.

8.2.4 Synthesis of 2a-[4-[bromomethyl]benzyl]-decahydro-2a,4a,6a,8a-tetraaza-pyrenium bromide (5), 2a-[4-nitrobenzyl]-decahydro-2a,4a,6a,8a-tetraaza-pyrenium bromide (6), 2a-[4-cyanobenzyl]-decahydro-2a,4a,6a,8a-tetraaza-pyrenium bromide (7) and 2a-[4-[methoxycarbonyl]benzyl]-decahydro-2a,4a,6a,8a-tetraaza-pyrenium bromide (8)

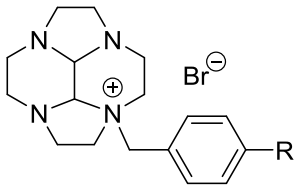

R=CH_2Br	**5**
R=NO_2	**6**
R=CN	**7**
R=COOMe	**8**

Method 1 – Attempted synthesis

2a-[4-[bromomethyl]benzyl]-decahydro-2a,4a,6a,8a-tetraaza-pyrenium bromide (5)

Amounts: *cis*-13-1,4,7,10-tetraazatetracyclo[5.5.1.$0^{4,14}0^{10,13}$]tetradecane (**2**) (1 g, 5.15 mmol), dry THF (100 mL), α-α'-dibromo-*p*-xylene (3.40 g, 12.89 mmol), dry THF (2 x 10 mL). To yield a white solid (2.05 g). The desired product was not isolated using this synthetic procedure. Analytical data indicates that the desired product was not obtained.

Method 2 – Attempted synthesis

Macrocycle was added to dry acetonitrile to this pendant arm was added and the solution stirred under argon for 3 d at RT. Following this the resulting precipitate was filtered and washed with acetonitrile and diethyl ether.

2a-[4-nitrobenzyl]-decahydro-2a,4a,6a,8a-tetraaza-pyrenium bromide (6)

Amounts: *cis*-13-1,4,7,10-tetraazatetracyclo[5.5.1.$0^{4,14}0^{10,13}$]tetradecane (**2**) (1.25 g, 6.43 mmol), dry acetonitrile (25 mL), 4-nitrobenzyl bromide (1.81 g, 8.36 mmol), dry acetonitrile (2 x 10 mL).To yield a white solid (3.75 g). The desired product was not isolated using this synthetic procedure. Analytical data indicates that the desired product was not obtained.

2a-[4-cyanobenzyl]-decahydro-2a,4a,6a,8a-tetraaza-pyrenium bromide (7)

Amounts: *cis*-13-1,4,7,10-tetraazatetracyclo[5.5.1.$0^{4,14}0^{10,13}$]tetradecane (**2**) (1.25 g, 6.43 mmol), dry acetonitrile (100 mL), 4-[bromomethyl]benzonitrile (3.15 g, 16.09 mmol), dry

acetonitrile (2 x 20 mL). To yield a white solid (2.47 g). The desired product was not isolated using this synthetic procedure. Analytical data indicates that the desired product was not obtained.

2a-[4-[methoxycarbonyl]benzyl]-decahydro-2a,4a,6a,8a-tetraaza-pyrenium bromide (8)

Amounts: *cis*-13-1,4,7,10-tetraazatetracyclo[5.5.1.$0^{4,14}0^{10,13}$]tetradecane (**2**) (1.25 g, 6.43 mmol), dry acetonitrile (100 mL), methyl 4-[bromomethyl]benzoate (3.69 g, 16.09 mmol), acetonitrile (2 x 20 mL). To yield a white solid (2.18 g). The desired product was not isolated using this synthetic procedure. Analytical data indicates that the desired product was not obtained.

Method 3 – Preferred route

General procedure C

The macrocycle was dissolved in dry THF, pendant arm was added and the solution was stirred under argon for 3 h at RT. The resulting precipitate was filtered and washed with dry THF.

2a-[4-[bromomethyl]benzyl]-decahydro-2a,4a,6a,8a-tetraaza-pyrenium bromide (5)

Amounts: *cis*-13-1,4,7,10-tetraazatetracyclo[5.5.1.$0^{4,14}0^{10,13}$]tetradecane (**2**) (900 mg, 4.63 mmol), dry THF (5 mL), α-α'-dibromo-*p*-xylene (1.22 g, 4.63 mmol), dry THF (2 x 10 mL). To yield a white solid (2.09 g, 99 %).

^{1}H NMR (400 MHz, D_2O, δ): 1.69-2.40 (*m,* N-α-CH_2, 2H), 2.68-3.19 (*m,* N-α-CH_2, 6H), 3.58-3.81 (*m,* N-α-CH_2, 6H), 4.14-4.32 (*m,* N-α-CH_2, 2H), 4.56-5.16 (*m,* CH_2-Ar, 4H), 5.20-5.53 (*m,* H_{aminal}, 2H), 7.45-7.99 (*m,* Ar-H, 4H). ^{13}C NMR (100 MHz, DMSO, δ): 35.85 (N-α-CH_2), 45.41 (N-α-CH_2), 50.20 (N-α-CH_2), 51.49 (N-α-CH_2), 54.24 (N-α-CH_2), 63.14 (CH_2-Br), 73.72 (C_{aminal}), 79.84 (C_{aminal}), 130.46 (Ar-H), 132.75 (Ar-C), 135.60 (Ar-C), 135.94 (Ar-H). 3 N-α-CH_2 peaks missing. MS (*m/z*): $[M-Br+H]^+$ calcd for $C_{18}H_{27}BrN_4$, 379.35; found, 379.1. HRMS (*m/z*): Pending data, see 8.1.3. Anal. calcd for $C_{18}H_{26}Br_2N_4.2.55H_2O$: C, 42.88; H, 6.22; N, 11.11. Found: C, 42.90; H, 6.39; N, 11.10.

2a-[4-nitrobenzyl]-decahydro-2a,4a,6a,8a-tetraaza-pyrenium bromide (6)

Amounts: *cis*-13-1,4,7,10-tetraazatetracyclo[5.5.1.$0^{4,14}0^{10,13}$]tetradecane (**2**) (2.00 g, 10.29 mmol), dry THF (8 mL), 4-nitrobenzyl bromide (2.22 g, 10.29 mmol), dry THF (3 x 20 mL).To yield a white solid (3.75 g, 89 %).

^{1}H NMR (400 MHz, D_2O, δ): 2.34-2.42 (*m,* N-α-CH_2, 2H), 2.59-2.81 (*m,* N-α-CH_2, 4H), 2.95-3.18 (*m,* N-α-CH_2, 5H), 3.33-3.50 (*m,* N-α-CH_2, 4H), 3.63 (*d,* J=2.7 Hz, N-α-CH_2, 1H), 3.93 (*d,* J=2.2 Hz, CH_2-Ar, 1H), 4.05-4.10 (*m,* CH_2-Ar, 1H), 4.68 (*s,* H_{aminal}, 1H), 4.88 (*d,* J=13.5 Hz, H_{aminal}, 1H), 7.66 (*d,* J=8.6 Hz, Ar-H,

2H), 8.18 (*d,* J=8.57 Hz, Ar-H, 2H). ^{13}C NMR (100 MHz, D_2O, δ): 43.74 (N-α-CH_2), 47.57 (*d,* J=3.8 Hz, N-α-CH_2), 47.54 (N-α-CH_2), 48.29 (N-α-CH_2), 51.30 (N-α-CH_2), 57.22 (N-α-CH_2), 60.17 (N-α-CH_2), 61.65 (N-α-CH_2), 71.64 (C_{aminal}), 83.30 (C_{aminal}), 124.53 (Ar-H), 133.78 (Ar-H), 133.82 (Ar-C), 149.09 (Ar-C). HRMS: (*m/z*): $[M\text{-}Br^-]^+$ calcd for $C_{17}H_{24}N_5O_2$, 330.1925; found, 330.1923. Anal. calcd for $C_{17}H_{24}BrN_5O_2$: C, 49.76; H, 5.90; N, 17.07. Found: C, 49.56; H, 5.90; N, 17.54.

2a-[4-cyanobenzyl]-decahydro-2a,4a,6a,8a-tetraaza-pyrenium bromide (7)

Amounts: *cis*-13-1,4,7,10-tetraazatetracyclo[5.5.1.$0^{4,14}0^{10,13}$]tetradecane (**2**) (1.68 g, 8.63 mmol), dry THF (7 mL), 4-[bromomethyl]benzonitrile (1.69 g, 8.63 mmol), dry THF (3 x 20 mL). To yield a white solid (2.95 g, 88 %).

^{1}H NMR (400 MHz, D_2O, δ): 2.35 (*d,* J=6.7 Hz, N-α-CH_2, 2H), 2.65-2.91 (*m,* N-α-CH_2, 6H), 2.98 (*t,* J=12.5 Hz, N-α-CH_2, 2H), 3.08-3.13 (*m,* N-α-CH_2, 2H), 3.31-3.41 (*m,* N-α-CH_2, 4H), 3.89 (*s,* CH_2-Ar, 1H), 4.04 (*t,* J=10.1 Hz, CH_2-Ar, 1H), 4.58 (*s,* H_{aminal}, 1H), 4.81 (*d,* J = 13.3 Hz, H_{aminal}, 1H), 7.59 (*d,* J=7.5 Hz, Ar-H, 2H), 7.75 (*d,* J=7.3 Hz, Ar-H, 2H). ^{13}C NMR (100 MHz, D_2O, δ): 42.94 (N-α-CH_2), 43.68 (N-α-CH_2), 47.54 (N-α-CH_2), 48.29 (N-α-CH_2), 51.28 (N-α-CH_2), 57.15 (N-α-CH_2), 60.47 (N-α-CH_2), 61.55 (N-α-CH_2), 71.62 (C_{aminal}), 83.27 (C_{aminal}), 113.81 (CN), 132.13 (Ar-C), 133.22 (Ar-C), 133.48 (Ar-H). HRMS (*m/z)*: $[M\text{-}Br^-]^+$ calcd for $C_{18}H_{24}N_5$, 310.2026, found, 310.2029. Anal. calcd for $C_{18}H_{24}BrN_5$: C, 55.39; H, 6.20; N, 17.94. Found: C, 55.14; H, 6.26; N, 18.02.

2a-[4-[methoxycarbonyl]benzyl]-decahydro-2a,4a,6a,8a-tetraaza-pyrenium bromide (8)

Amounts: *cis*-13-1,4,7,10-tetraazatetracyclo[5.5.1.$0^{4,14}0^{10,13}$]tetradecane (**2**) (890 mg, 4.62 mmol), dry THF (5 mL), methyl 4-[bromomethyl]benzoate (1.06 g, 4.62 mmol), dry THF (2 x 10 mL). To yield a white solid (1.84 g, 95 %).

^{1}H NMR (400 MHz, D_2O, δ): 2.36-2.42 (*m,* N-α-CH_2, 2H), 2.63-2.71 (*m,* N-α-CH_2, 3H), 2.78-2.83 (*m,* N-α-CH_2, 1H), 2.95-3.04 (*m,* N-α-CH_2, 2H), 3.10-3.20 (*m,* N-α-CH_2, 3H), 3.32-3.49 (*m,* N-α-CH_2, 4H), 3.64 (*d,* J=2.7 Hz, N-α-CH_2, 1H), 3.78 (*s,* CH_3-O, 3H), 3.92 (*d,* J=2.5 Hz, CH_2-Ar , 1H), 4.06-4.12 (*m,* CH_2-Ar, 1H), 4.61 (*s,* H_{aminal}, 1H), 4.82 (*d,* J=13.5 Hz, H_{aminal}, 1H), 7.56 (*d,* J=8.4 Hz, Ar-H, 2H), 7.97 (*d,* J=8.2 Hz, Ar-H, 2H). ^{13}C NMR (100 MHz, D_2O, δ): 43.79 (N-α-CH_2), 47.59 (N-α-CH_2), 47.61 (N-α-CH_2), 48.26 (N-α-CH_2), 51.30 (CH_3-O), 52.93 (N-α-CH_2), 57.24 (N-α-CH_2), 60.82 (N-α-CH_2), 61.59 (N-α-CH_2), 71.68 (C_{aminal}), 83.04 (C_{aminal}), 130.37 (Ar-H), 131.83 (Ar-C), 131.94 (Ar-C), 132.77 (Ar-H), 168.36 (C=O). HRMS (*m/z)*: $[M\text{-}Br^-]^+$ calcd for $C_{19}H_{27}N_4O_2$, 343.2134, found, 343.2131. Anal. calcd for $C_{19}H_{27}BrN_5O_2$.0.4H_2O.0.5THF: C, 54.06; H, 6.87; N, 12.01. Found: C, 54.06; H, 6.97; N, 12.08.

8.2.5 Synthesis of 3a-[4-[bromomethyl]benzyl]-decahydro-3a,5a,8a,10a-tetraaza-pyrenium bromide (9)

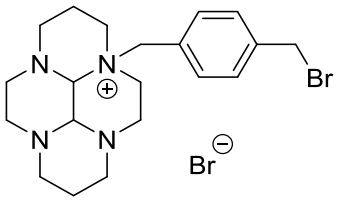

9

cis-3a,5a,8a,10a-tetraazaperhydropyrene (**3**) (3 g, 13.49 mmol) was dissolved in dry THF (50 mL), α-α'-dibromo-*p*-xylene (7.12 g, 26.99 mmol) was added and the mixture stirred at RT under argon for 3 d. The resulting precipitate was filtered and washed with dry THF (5 x 20 mL). To yield a white solid (6.44 g, 98 %).

^{1}H NMR (400 MHz, D_2O, δ): 1.14 (*s*, N-β-CH_2, 2H), 1.36-1.46 (*m*, N-β-CH_2, 2H), 1.76-3.75 (*br m*, N-α-CH_2, 16H), 4.34 (*s*, Ar-CH_2, 2H), 4.63 (*s*, CH_2-Br, 2H), 4.69 (*s*, H_{aminal}, 1H), 5.13-5.17 (*m*, H_{aminal}, 1H), 7.67 (*m*, Ar-H, 4H). ^{13}C NMR (100 MHz, D_2O, δ): 18.15 (N-β-CH_2), 18.55 (N-β-CH_2), 42.12 (CH_2-Br), 46.73 (N-α-CH_2), 51.51 (N-α-CH_2), 53.46 (N-α-CH_2), 54.12 (N-α-CH_2), 54.82 (N-α-CH_2), 60.28 (N-α-CH_2), 61.81 (N-α-CH_2), 69.73 (ArH2), 75.53 (C_{aminal}), 82.45 (C_{aminal}), 128.04 (Ar-H), 128.06 (Ar-H), 133.66 (Ar), 134.24 (Ar). HRMS (*m/z)*: $[M\text{-}Br\text{-}H]^+$ calcd for $C_{20}H_{30}BrN_4$, 405.1648; found, 405.1637. Anal. calcd for $C_{20}H_{30}Br_2N_4.2H_2O$: C, 45.99; H, 6.56; N, 10.73. Found C, 45.87; H, 7.02; N, 10.83.

8.3. TRIS-MACROCYCLES

8.3.1 Synthesis of 2a,6a-bis-[[4-[decahydro-2a,4a,6a,8a-tetraaza-pyrenium]methyl]benzyl]-decahydro-2a,4a,6a,8a-tetraaza-pyrenium tetrabromide(10), 3a,8a-bis-[[4-[decahydro-2a,4a,6a,8a-tetraaza-pyrenium]methyl]benzyl]-decahydro-3a,5a,8a,10a-tetraazaperhydro pyrene tetrabromide (11), 3a,8a-bis-[[4-[decahydro-3a,5a,8a,10a-tetraaza-pyrenium]methyl] benzyl]-decahydro-3a,5a,8a,10a-tetraazaperhydropyrene tetra bromide (12), 1,4-bis-[[4-[decahydro-2a,4a,6a,8a-tetraaza-pyrenium]methyl]benzyl]-1,4,8,11-tetraazatricyclo[9.3.1. $1^{4,8}$]hexadecane tetrabromide (13), 1,4-bis-[[4-[decahydro-3a,5a,8a,10a-tetraaza-pyrenium]methyl]benzyl]-1,4,8,11-tetraazatricyclo[9.3.1.$1^{4,8}$]hexa decane tetrabromide (14)

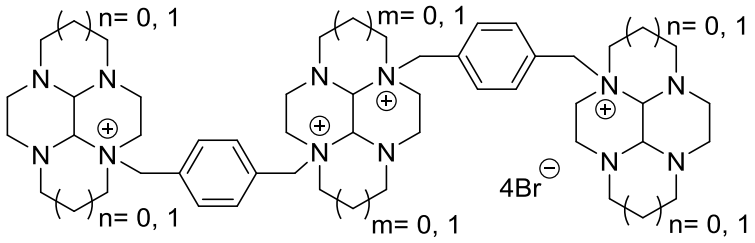

n=0, m=0 **10**
n=0, m=1 **11**
n=1, m=1 **12**

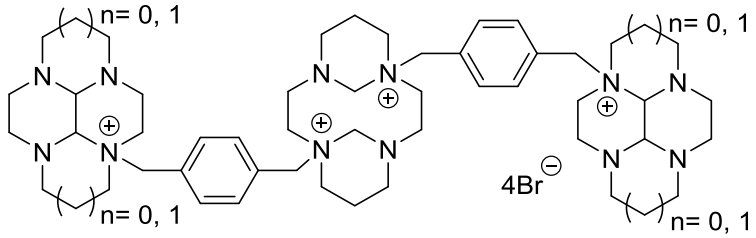

n=0 **13**
n=1 **14**

General procedure D

Macrocycle was dissolved in dry MeCN, to this mono-substituted macrocycle as a suspension of dry MeCN was added. The mixture was stirred at RT for 14 d under an atmosphere of argon after which the precipitate was filtered and washed with MeCN and diethyl ether.

2a,6a-bis-[[4-[decahydro-2a,4a,6a,8a-tetraaza-pyrenium]methyl]benzyl]- decahydro-2a,4a,6a,8a-tetraaza-pyrenium tetra bromide(10)

Amounts: *cis*-13-1,4,7,10-tetraazatetracyclo[5.5.1.$0^{4,14}0^{10,13}$]tetradecane (**2**) (212 mg, 1.09 mmol), dry acetonitrile (50 mL and 100 mL), 2a-[4-[bromomethyl]benzyl]-decahydro-2a,4a,6a,8a-tetraaza-pyrenium bromide (**5**) (1.00 g, 2.18 mmol), acetonitrile (2 x 20 mL), diethyl ether (2 x 20 mL). To yield a white solid (761 mg, 63 %).

^{1}H NMR (400 MHz,D_2O, δ): 2.36 (*m*, N-α-CH_2, 2H), 2.62-3.88 (*br m*, N-α-CH_2, 46H), 4.15 (*br s*, CH_2-Ar, 4H), 4.52 (*br s*, CH_2-Ar, 2H), 4.60 (*br s*, CH_2-Ar, 2H), 5.00 (*m*, H_{aminal}, 6H), 7.35-7.42 (*m*, Ar-H, 4H), 7.56-7.62 (*m*, Ar-H, 4H). MS: Pending data, see 8.1.3. Anal. calcd for $C_{46}H_{70}Br_4N_{12}.13.25H_2O$: C, 40.94; H, 7.21; N, 12.46. Found: C, 40.56; H, 6.84; N, 12.43.

3a,8a-bis-[[4-[decahydro-2a,4a,6a,8a-tetraaza-pyrenium]methyl]benzyl]-decahydro-3a,5a,8a,10a-tetraaza-pyrenium tetra bromide (11)

Amounts: *cis*-3a,5a,8a,10a-tetraazaperhydropyrene (**3**) (243 mg, 1.09 mmol), dry acetonitrile (50 mL and 100 mL), 2a-[4-[bromomethyl]benzyl]-decahydro-2a,4a,6a,8a-tetraaza-pyrenium bromide (**5**) (1.00 g, 2.18 mmol), acetonitrile (2 x 20 mL), diethyl ether (2 x 20 mL). To yield a white solid (608 mg, 49 %).

^{1}H NMR (400 MHz,D_2O, δ): 2.34 (*m*, N-β-CH_2, 2H), 2.68 (*m*, N-β-CH_2, 2H), 2.80 (*m*, N-α-CH_2, 2H), 3.03 (*m*, N-α-CH_2, 12H), 3.29 (*m*, N-α-CH_2, 8H), 3.45 (*m*, N-α-CH_2, 16H), 3.61 (*m*, N-α-CH_2, 1H), 3.73 (*m*, N-α-CH_2, 7H), 3.90 (*m*, N-α-CH_2, 2H), 4.18 (*m*, N-α-CH_2, 8H), 4.45-4.49 (*m*, H_{aminal}, 6H), 7.40-7.44 (*m*, Ar-H, 4H), 7.63 (*br s*, Ar-H, 4H). MS: Pending data, see 8.1.3.

3a,8a-bis-[[4-[decahydro-3a,5a,8a,10a-tetraaza-pyrenium]methyl]benzyl]-decahydro-3a,5a,8a,10a-tetraaza-pyrenium tetra bromide (12)

Amounts: *cis*-3a,5a,8a,10a-tetraazaperhydropyrene (**3**) (274 mg, 1.23 mmol), dry MeCN (100 mL), 3a-[4-[bromomethyl]benzyl]-decahydro-3a,5a,8a,10a-tetraaza-pyrenium bromide (**9**) (1.20 g, 2.47 mmol), dry MeCN (300 mL), MeCN (2 x 20 mL), diethyl ether (2 x 20 mL). To yield the product as a white solid (1.22 g, 83 %).

^{1}H NMR (400 MHz,D_2O, δ): 1.28-1.38 (*m*, N-β-CH_2, 3H), 1.62 (*d*, J=11.4 Hz, N-β-CH_2, 2H), 1.71-1.81 (*m*, N-β-CH_2, 2H), 1.99-2.06 (*m*, N-β-CH_2, 5H), 2.10-2.22 (*m*, N-α-CH_2, 3H), 2.30-2.37 (*m*, N-α-CH_2, 4H), 2.47-2.56 (*m*, N-α-CH_2, 4H), 2.63-2.73 (*m*, N-α-CH_2, 1H), 2.83-3.16 (*m*, N-α-CH_2, 24H), 3.19-3.33 (*m*, N-α-CH_2, 5H), 3.42-3.48 (*m*, N-α-CH_2, 3H), 3.48-3.65 (*m*, N-α-CH_2, 4H), 4.01-4.08 (*m*, CH_2-Ar, 2H), 4.26 (*s*, CH_2-Ar, 3H), 4.44-4.56 (*m*, CH_2-Ar, 3H), 4.66-4.75 (*m*, H_{aminal}, 2H), 4.93-4.96 (*m*, H_{aminal}, 1H), 5.05 (*d*, J=13.3 Hz, H_{aminal}, 1H), 5.13-5.24 (*m*, H_{aminal}, 2H), 7.21-7.40 (*m*, Ar-H, 2H), 7.43 (*d*, J=5.7 Hz, Ar-H, 2H), 7.53 (*s*, Ar-H, 2H), 7.56 (*s*, Ar-H, 1H), 7.60 (*d*, J=8.8 Hz, Ar-H, 1H). ^{13}C NMR (100 MHz, D_2O, δ): 17.72 (N-β-CH_2), 17.87 (N-β-CH_2), 18.15 (N-β-CH_2), 18.41 (N-β-CH_2), 37.02 (N-α-CH_2), 42.00 (N-α-CH_2), 42.54 (N-α-CH_2), 46.47 (N-α-CH_2), 46.71 (N-α-CH_2), 48.33 (N-α-CH_2), 50.61 (N-α-CH_2), 51.24 (N-α-CH_2), 51.92 (N-α-CH_2), 53.10 (N-α-CH_2), 53.84 (N-α-CH_2), 54.22 (N-α-CH_2), 59.90 (N-α-

CH_2), 60.17 (N-α-CH_2), 60.71 (N-α-CH_2), 61.44 (N-α-CH_2), 61.72 (N-α-CH_2), 62.11 (N-α-CH_2), 62.40 (N-α-CH_2), 63.20 (N-α-CH_2), 63.61 (N-α-CH_2), 69.63 (N-α-CH_2), 75.02 (C_{aminal}), 76.79 (C_{aminal}), 81.68 (C_{aminal}), 81.98 (C_{aminal}), 82.12 (C_{aminal}), 124.73 (Ar-C), 127.77 (Ar-C), 127.90 (Ar-H), 128.56 (Ar-H), 128.90 (Ar-H), 133.59 (Ar-H), 134.19 (Ar-H), 134.37 (Ar-H), 139.74 (Ar-C), 143.45 (Ar-C). MS: Pending data, see 8.1.3. Anal. calcd for $C_{52}H_{82}Br_4N_{12}.6H_2O$: C, 47.93; H, 7.27; N, 12.90. Found: C, 47.43; H, 7.70; N, 13.04.

1,4-bis-[[4-[decahydro-2a,4a,6a,8a-tetraaza-pyrenium]methyl]benzyl]-1,4,8,11-tetraazatricyclo[9.3.1.1^{4,8}]hexadecane tetrabromide (13)

Amounts**:** 1,4,8,11-tetraazatricyclo[9.3.1.1^{4,8}]hexadecane (**4**) (61 mg, 0.03 mmol), dry acetonitrile (50 mL and 100 mL), 2a-[4-[bromomethyl]benzyl]-decahydro-2a,4a,6a,8a-tetraaza-pyrenium bromide (**5**) (250 mg, 0.54 mmol), acetonitrile (2 x 10 mL), diethyl ether (2 x 10 mL). To Yield a white solid (214 mg, 69 %).

^{1}H NMR (400 MHz,D_2O, δ): 5.06-5.12 (m, 2H, N-β-CH_2), 5.52-5.58 (m, 2H, N-β-CH_2), 5.69-5.72 (m, 2H, N-α-CH_2), 5.82-5.93 (m, 3H, N-α-CH_2), 6.04-6.08 (m, 2H, N-α-CH_2), 6.10-6.13 (m, 2H, N-α-CH_2), 6.47-6.69 (br m, 10H, N-α-CH_2), 6.72-6.75 (m, 6H, N-α-CH_2), 6.79 (br s, 1H, N-α-CH_2), 6.83-7.00 (m, 16H, N-α-CH_2), 7.06 (br s, 1H, N-α-CH_2), 7.19-7.20 (m, 3H, N-α-CH_2), 7.24 (s, 5H, N-α-CH_2), 7.49-7.52 (m, 2H, H_{aminal}), 7.62-7.63 (m, 1H, H_{aminal}), 7.68 (d, 1H, J=13.1 Hz, H_{aminal}), 7.76 (d, 1H, J=13Hz, H_{aminal}), 7.96-7.99 (m, 1H, H_{aminal}), 8.05-8.08 (m, 1H, H_{aminal}), 8.15-8.18 (d, 1H, J=12.9Hz, H_{aminal}), 11.21 (s, 8H, Ar-H). MS: Pending data, see 8.1.3. Anal. calcd for $C_{48}H7_6N_{12}Br_4$ expected: C, 50.54; H, 6.72; N, 14.73. Found: C, 45.50; H, 7.50; N, 13.44 – contains impurity.

1,4-bis-[[4-[decahydro-3a,5a,8a,10a-tetraaza-pyrenium]methyl]benzyl]-1,4,8,11-tetraazatricyclo[9.3.1.1^{4,8}]hexadecane tetrabromide (14)

Amounts: 1,4,8,11-tetraazatricyclo[9.3.1.1^{4,8}]hexadecane (**4**) (80 mg, 0.35mmol), dry acetonitrile (50mL and 100 mL), 3a-[4-[bromomethyl]benzyl]-decahydro-3a,5a,8a,10a-tetraaza-pyrenium bromide (**9**) (350 mg, 0.7mmol), acetonitrile (2 x 10 mL), diethyl ether (2 x 10mL). To yield the product (200 mg, 48%).

^{1}H NMR: (400 MHz, DMSO, δ): 1.11-1.26 (*m*, N-β-CH_2, 2H), 1.60-2.05 (*m*, N-β-CH_2, 10H), 2.08-2.45 (*m*, N-α-CH_2, 11H), 2.55-2.70 (*m*, N-α-CH_2, 4H), 2.75-2.91 (*m*, N-α-CH_2, 16H), 2.98-3.15 (*m*, N-α-CH_2, 12H), 3.53-3.58 (*m*, N-α-CH_2, 5H), 3.64-3.95 (*m*, CH_2-Ar, 8H), 4.25-4.34 (*m*, H_{aminal}, 4H), 4.79-4.89 (*m*, H_{aminal}, 2H), 5.35-5.60 (*m*, H_{aminal}, 2H), 7.51 (*s*, Ar-H, 4H), 7.66 (*s*, Ar-H, 4H). ^{13}C NMR: (100 MHz, DMSO, δ):

18.72 (N-β-CH_2), 24.85 (N-β-CH_2), 42.12 (N-α-CH_2), 46.74 (N-α-CH_2), 47.12 (N-α-CH_2), 47.55 (N-α-CH_2), 50.15 (N-α-CH_2), 51.29 (N-α-CH_2), 52.42 (N-α-CH_2), 54.25 (N-α-CH_2), 54.37 (N-α-CH_2), 59.57 (N-α-CH_2), 60.33 (N-α-CH_2), 60.87 (N-α-CH_2), 69.65 (C_{aminal}), 83.17 (C_{aminal}), 129.73 (Ar-H), 130.89 (Ar-H), 133.57 (C-Ar), 134.22 (C-Ar). HRMS (*m/z*): $[M-2Br-2H]^{2+}$ calcd for $C_{52}H_{82}Br_2N_{12}$, 517.2564, found: 517.2541. Elemental analysis: (%) Calcd. for $C_{52}H_{84}Br_4N_{12}$: C, 46.86; H, 7.51; N, 13.09. Found: C, 46.65; H, 7.84; N, 13.09.

8.3.2 Synthesis of 3a,8a-bis-[[4-[decahydro-3a,5a,8a,10a-tetraaza-pyrenium]methyl]benzyl]-decahydro-2a,4a,6a,8a-tetraaza-pyrenium tetra bromide (15)

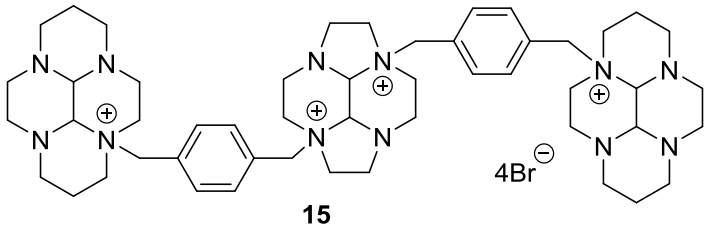

15

General procedure E

cis-13-1,4,7,10-tetraazatetracyclo[5.5.1.$0^{4,14}0^{10,13}$]tetradecane (400 mg, 2.06 mmol) was dissolved in dry DMF (20 mL) to this 3a-[4-[bromomethyl]benzyl]-decahydro-3a,5a,8a,10a-tetraaza-pyrenium bromide (**9**) (2.00 g, 4.11 mmol) was added. The mixture was stirred at RT for 14 d under an atmosphere of argon after which the precipitate was filtered and washed with diethyl ether (4 x 20 mL). To yield a white solid (1.05 g, 94 %).

^{1}H NMR (400 MHz,D_2O, δ): 1.30 (*d*, J=13.7 Hz, N-β-CH_2, 2H), 1.61 (*d*, J=13.7 Hz, N-β-CH_2, 2H), 1.74 (*d*, J=10.6 Hz, N-β-CH_2, 1H), 1.96-2.04 (*m*, N-β-CH_2, 3H), 2.07 (*d*, J=3.7 Hz, N-α-CH_2, 2H), 2.13-2.16 (*m*, N-α-CH_2, 3H), 2.31-2.33 (*m*, N-α-CH_2, 4H), 2.48-2.63 (*m*, N-α-CH_2, 5H), 2.72-2.77 (*m*, N-α-CH_2, 2H), 2.92-3.80 (*br m*, N-α-CH_2, 31H), 4.03-4.09 (*m*, CH_2-Ar/N-α-CH_2, 2H), 4.16 (*td*, J=11.0 Hz, CH_2-Ar, 1H), 4.25-4.61 (*m*, CH_2-Ar, 5H), 4.67-4.71 (*m*, CH_2-Ar, 1H), 4.73-4.77 (*m*, H_{aminal}, 1H), 4.92 (*d*, J=13.5 Hz, H_{aminal}, 1H), 4.59-5.13 (*m*, H_{aminal}, 3H), 5.20-5.25 (*m*, H_{aminal}, 1H), 7.34-7.43 (*m*, Ar-H, 1H), 7.51-7.66 (*m*, Ar-H, 1H). ^{13}C NMR (100 MHz, D_2O, δ): 17.69 (N-β-CH_2), 41.94 (N-α-CH_2), 42.56 (N-α-CH_2), 46.48 (N-α-CH_2), 46.65 (N-α-CH_2), 48.51 (N-α-CH_2), 50.56 (N-α-CH_2), 51.27 (N-α-CH_2), 51.87 (N-α-CH_2), 53.17 (N-α-CH_2), 53.89 (N-α-CH_2), 54.19 (N-α-CH_2), 54.84 (N-α-CH_2), 60.11 (N-α-CH_2), 60.95 (N-α-CH_2), 61.60 (N-α-CH_2), 69.58 (C_{aminal}), 82.16 (C_{aminal}), 127.74 (Ar-H), 128.62 (Ar-H), 128.87 (Ar-H), 129.09 (Ar-H), 133.31 (Ar-H), 134.09 (Ar-H), 134.51 (Ar-C), 140.68 (Ar-C). MS (*m/z*): [M-Br-H]$^{+}$ calcd for $C_{50}H_{77}Br_3N_{12}$, 1085.96; found, 1085.4. HRMS: Pending data, see 8.1.3. Anal. calcd for $C_{50}H_{78}Br_4N_{12}$ expected: C, 51.47; H, 6.74; Br, 27.39; N, 14.40. Found C, 46.33; H, 7.13; N, 12.36 – contains impurity.

8.3.3 Synthesis of 1,7-bis-[4-[[1,4,7,10-tetraazabicyclo[8.2.2]dodecane]methyl]benzyl]-1,4,7,10-tetraazabicyclo[5.5.2]dodecane (16), 1,8-bis-[4-[[1,4,7,10-tetraazabicyclo[8.2.2]dodecane] methyl]benzyl]-1,4,8,11-tetraazabicyclo[6.6.2]hexadecane (17), 1,7-bis-[4-[[1,4,8,11-tetraaza bicyclo[10.2.2]hexadecane]methyl]benzyl]-1,4,7,10-tetraazabicyclo[5.5.2]dodecane (18), 1,8-bis-[4-[[1,4,8,11-tetraazabicyclo[10.2.2]hexadecane]methyl]benzyl]-1,4,8,11-tetraazabicyclo [6.6.2]hexadecane (19)

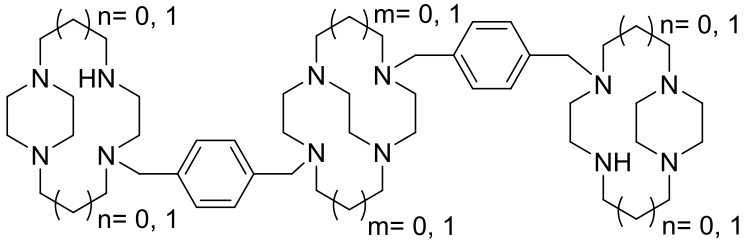

n=0, m=0 **16**
n=0, m=1 **17**
n=1, m=0 **18**
n=1, m=1 **19**

General procedure F

Macrocycle was added to ethanol and sodium borohydride was added in small portions over 1 h. The mixture was stirred for 10 days at RT. Aqueous hydrochloric acid (2 M) was added until pH 3-4 to decompose excess sodium borohydride and the solvents were removed *in vacuo*. The residue was taken up into water and made strongly basic (pH 14, KOH). The basic solution was extracted with dichloromethane, the combined organic extracts were dried ($MgSO_4$), filtered and solvent removed *in vacuo.*

1,7-bis-[4-[[1,4,7,10-tetraazabicyclo[8.2.2]dodecane]methyl]benzyl]-1,4,7,10-tetraazabicyclo[5.5.2]dodecane (16)

Method as outlined previously with the following:

Amounts: (**10**) (650 mg, 0.59 mmol), ethanol (300 mL), sodium borohydride (664 mg, 17.56 mmol) water (25 mL), dichloromethane (5 x 25 mL). To yield the product as a yellow oil (236 mg, 50 %).

^{1}H NMR (400 MHz, MeOH, δ): 2.34-3.15 (*br m,* N-α-CH_2*,* 60H), 3.58-3.68 (*m,* CH_2-Ar*,* 5H), 3.99-4.04 (*m,* CH_2-Ar*,* 3H), 4.57-4.61 (*m,* NH*,* 2H), 7.28 (*br s,* Ar-H*,* 3H), 7.40 (*m,* Ar-H*,* 4H), 7.48 (*br s,* Ar-H*,* 1H).

^{13}C NMR (100 MHz, MeOH, δ): 44.63 (N-α-CH_2), 46.69 (N-α-CH_2), 48.86 (N-α-CH_2), 49.78 (N-α-CH_2), 50.46 (N-α-CH_2), 50.94 (N-α-CH_2), 51.28 (N-α-CH_2), 52.16 (N-α-CH_2), 53.66 (N-α-CH_2), 55.75 (N-α-CH_2), 56.28 (N-α-CH_2), 56.75 (N-α-CH_2), 57.32 (N-α-CH_2), 58.35 (N-α-CH_2), 59.03 (N-α-CH_2), 59.60 (N-

α-CH_2), 61.47 (N-α-CH_2), 63.63 (N-α-CH_2), 126.68 (Ar-C), 126.98 (Ar-H), 128.82 (Ar-H), 128.98 (Ar-H), 129.24 (Ar-H), 137.15 (Ar-C), 138.70 (Ar-C), 139.60 (Ar-C). HRMS (*m/z*): $[M+H]^+$ calcd for $C_{46}H_{79}N_{12}$ 799.6545; found, 799.6544. Elemental analysis: % Calc'd for $C_{46}H_{78}N_{12}$ expected: C, 69.13; H, 9.84; N, 21.03. Found: C, 57.04; H, 8.51; N, 14.03 – contains impurity.

1,8-bis-[4-[[1,4,7,10-tetraazabicyclo[8.2.2]dodecane]methyl]benzyl]-1,4,8,11-tetraazabicyclo [6.6.2]hexadecane (**17**)

Amounts: (**11**) (500 mg, 0.44 mmol), ethanol (300 mL), sodium borohydride (498 mg, 13.17 mmol), water (25 mL), dichloromethane (5 x 25 mL). To yield a yellow oil (196 mg, 54 %).

^{1}H-NMR (400 MHz, MeOD, δ): 1.16-1.28 (*m*, N-β-CH_2, 1H), 1.71 (*m*, N-β-CH_2, 1H), 2.32-2.34 (*m*, N-β-CH_2, 2H), 2.42-2.91(m, N-α-CH_2, 38H), 3.06-3.15 (*m*, N-α-CH_2, 15H), 3.30 (*td*, J=3.1 Hz, N-α-CH_2, 2H), 3.48-3.71 (*m*, N-α-CH_2, 7H), 3.94-4.04 (*m*, N-α-CH_2, 5H), 4.57-4.62 (*m*, NH, 2H), 7.21-7.48 (*m*, Ar-H, 8H). ^{13}C-NMR (100 MHz, MeOD, δ): 19.17 (N-β-CH_2), 20.04 (N-β-CH_2), 44.64 (N-α-CH_2), 44.64 (N-α-CH_2), 44.64 (N-α-CH_2), 49.81 (N-α-CH_2), 51.30 (N-α-CH_2), 52.18 (N-α-CH_2), 53.68 (N-α-CH_2), 55.74 (N-α-CH_2), 56.30 (N-α-CH_2), 56.74 (N-α-CH_2), 57.32 (N-α-CH_2), 58.90 (N-α-CH_2), 59.08 (N-α-CH_2), 59.58 (N-α-CH_2), 61.49 (N-α-CH_2), 63.59 (N-α-CH_2), 76.57 (N-α-CH_2), 77.71 (N-α-CH_2), 78.03 (N-α-CH_2), 78.22 (N-α-CH_2), 126.69 (Ar-C), 126.99 (Ar-C), 127.95 (Ar-C), 128.83 (Ar-H), 129.03 (Ar-H), 129.24 (Ar-H). MS: (*m/z*): $[M+3K+H]^+$ calcd for $C_{48}H_{83}N_{12}K_3$, 945.57; found, 945.5. HRMS: Pending data, see 8.1.3.

1,7-bis-[4-[[1,4,8,11-tetraazabicyclo[10.2.2]hexadecane]methyl]benzyl]-1,4,7,10-tetraazabicyclo[5.5.2]dodecane (**18**)

Amounts: (**15**) (2.30 g, 1.97 mmol), ethanol (150 mL), sodium borohydride (2.24 g, 59.13 mmol), water (50 mL), dichloromethane (5 x 50 mL). To yield a yellow oil (662 mg, 39 %).

^{1}H NMR (400 MHz, MeOD, δ): 1.14-1.17 (*m,* N-β-CH_2, 2H), 1.48 (*m,* N-β-CH_2, 1H), 1.64-1.69 (*m,* N-β-CH_2, 5H), 2.16-3.23 (*br m,* N-α-CH_2, 57H), 3.47-4.11 (*br m,* N-α-CH_2, 11H), 4.25 (*m,* NH, 1H), 4.55 (*m,* NH, 1H), 7.11-7.25 (*m,* Ar-H, 7H), 8.05-8.07 (*m,* Ar-H, 1H). ^{13}C NMR (100 MHz, MeOD, δ): 19.19 (N-β-CH_2), 22.79 (N-β-CH_2), 23.83 (N-β-CH_2), 24.44 (N-β-CH_2), 39.59 (N-α-CH_2), 44.23 (N-α-CH_2), 50.19 (*d,* J=16.9 Hz, N-α-CH_2), 51.05 (N-α-CH_2), 51.47 (N-α-CH_2), 52.01 (N-α-C_2), 53.02 (N-α-CH_2), 53.72 (N-α-CH_2), 53.85 (N-α-CH_2), 54.66 (N-α-CH_2), 55.18 (N-α-CH_2), 55.62 (N-α-CH_2), 56.07 (N-α-CH_2), 56.30 (N-α-CH_2), 56.80 (N-α-CH_2), 57.06 (N-α-CH_2), 57.46 (N-α-CH_2), 58.07 (N-α-CH_2), 58.53 (N-α-CH_2), 61.46 (N-α-CH_2), 61.61 (N-α-CH_2), 123.04 (Ar-H), 123.30 (Ar-H), 126.66 (Ar-H), 126.84 (Ar-H), 128.97 (Ar-H), 129.74 (Ar-H), 129.90 (Ar-H), 129.97 (Ar-H), 130.07 (Ar-H), 131.29 (Ar-C), 136.11 (Ar-C), 136.60 (Ar-

C), 137.34 (Ar-C). HRMS (*m/z*): $[M+H]^+$ calcd for $C_{50}H_{87}N_{12}$ 855.7171; found, 855.7174. Anal. calc'd for $C_{50}H_{86}N_{12}$.6EtOH: expected: C, 65.80; H, 10.87; N, 14.85. Found: C, 65.96; H, 11.31; N, 15.07.

1,8-bis-[4-[[1,4,8,11-tetraazabicyclo[10.2.2]hexadecane]methyl]benzyl]-1,4,8,11-tetraazabicyclo [6.6.2]hexadecane (**19**)

Amounts: (**12**) (1.11 g, 0.92 mmol), ethanol (65 mL), sodium borohydride (1.05 g, 27.73 mmol), water (25 mL), dichloromethane (5 x 50 mL). To yield a yellow-brown solid (546 mg, 71 %).

^{1}H NMR (400 MHz, MeOD, δ): 1.78 (*br s*, N-β-CH_2, 12H), 2.07-2.12 (*m*, N-α-CH_2, 5H), 2.21-2.31 (*m*, N-α-CH_2, 2H), 2.34 (*s*, N-α-CH_2, 1H), 2.52-2.67(*m*, N-α-CH_2, 24H), 2.78-3.03 (*m*, N-α-CH_2, 21H), 3.37-3.65 (*m*, N-α-CH_2, 7H), 3.69-3.71 (*m*, Ar-CH_2, 2H), 3.83-3.86 (*m*, Ar-CH_2, 2H), 4.59-4.62 (*m*, NH, 2H), 5.11 (*s*, Ar-CH_2, 4H), 7.16 (*s*, Ar-H, 1H), 7.24-7.37 (*m*, Ar-H, 6H), 7.43-7.63 (*m*, Ar-H, 1H). ^{13}C NMR (100 MHz, MeOD, δ): 19.41 (N-β-CH_2), 20.36 (N-β-CH_2), 22.94 (N-β-CH_2), 23.97 (N-β-CH_2), 24.73 (N-β-CH_2), 25.65 (N-β-CH_2), 43.73 (N-α-CH_2), 44.40 (N-α-CH_2), 47.08 (N-α-CH_2), 49.58 (N-α-CH_2), 50.31 (*d,* J=16.14 Hz, N-α-CH_2), 51.49 (N-α-CH_2), 52.19 (N-α-CH_2), 52.37 (N-α-CH_2), 53.07 (N-α-CH_2), 53.92 (*d,* J=9.22 Hz, N-α-CH_2), 54.50 (N-α-CH_2), 54.74 (N-α-CH_2), 54.95 (N-α-CH_2), 55.27 (N-α-CH_2), 55.47 (N-α-CH_2), 55.67 (N-α-CH_2), 56.09 (N-α-CH_2), 56.42 (N-α-CH_2), 56.70 (N-α-CH_2), 57.58 (N-α-CH_2), 63.56 (N-α-CH_2), 63.65 (N-α-CH_2), 76.71 (CH_2-Ar), 126.28 (Ar-C), 126.68 (*d,* J=12.30 Hz, Ar-H), 128.78 (Ar-H), 129.27 (*d,* J=7.69 Hz, Ar-C), 129.80 (Ar-H), 130.13 (*d,* J=7.69 Hz, Ar-H), 130.45 (Ar-H), 133.11 (Ar-H), 133.98 (Ar-H), 136.15 (Ar-H), 136.73 (Ar-C), 141.09 (Ar-C). HRMS (*m/z*): $[M+H]^+$ calcd for $C_{52}H_{91}N_{12}$ 883.7484; found, 883.7471. Anal. calc'd for $C_{52}H_{90}N_{12}.6H_2O$: expected: C, 62.99; H, 10.37; N, 16.95. Found: C, 62.92; H, 10.25; N, 16.91.

8.3.4. Synthesis of 1,8-[dimethyl]-4,11-bis-[4-[[1,4,7,10-tetraazabicyclo[8.2.2]dodecane]methyl] benzyl]-1,4,8,11-tetraazacyclotetradecane (20), 1,8-[dimethyl]-4,11-bis-[4-[[1,4,8,11-tetraazabicyclo[10.2.2]hexadecane]methyl]benzyl]-1,4,8,11-tetraazacyclotetradecane (21)

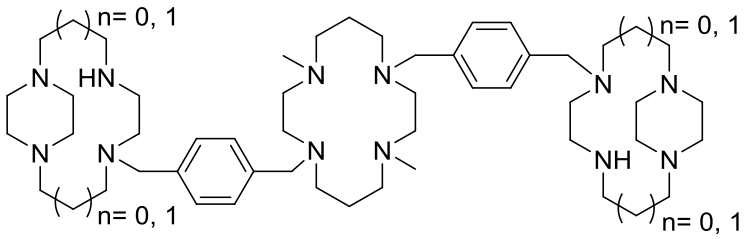

n=0 **20**
n=1 **21**

General procedure G

Macrocycle was added to ethanol, to this sodium borohydride was added slowly with stirring. The mixture was stirred at RT for 1 h and heated under reflux for 2 h. Once cooled to RT an aqueous solution of hydrochloric acid was added in one portion and the mixture concentrated *in vacuo*. The resulting residue was re-dissolved in water, made basic (KOH) and extracted with chloroform or dichloromethane. The combined organic phases were dried ($MgSO_4$) and concentrated *in vacuo.*

1,8-[dimethyl]-4,11-bis-[4-[[1,4,7,10-tetraazabicyclo[8.2.2]dodecane]methyl]benzyl]-1,4,8,11-tetraazacyclotetradecane (20)

Amounts: 1,4-bis-[[4-[decahydro-2a,4a,6a,8a-tetraaza-pyrenium]methyl]benzyl]-1,4,8,11-tetraaza tricyclo[9.3.1.1^{4,8}]hexadecane tetrabromide (**13**) (433 mg, 0.38 mmol), ethanol (100 mL), sodium borohydride (287 mg, 7.59 mmol), water (20 mL), dichloromethane (5 x 20 mL). To yield the product as a yellow oil (127 mg, 40 %).

^{1}H NMR (400 MHz, $CDCl_3$, δ): 1.19-1.24 (*m,* N-β-CH_2, 2H), 1.55-1.73 (*m,* N-β-CH_2, 2H), 1.83-1.84 (*m,* N-α-CH_2, 1H), 2.10-2.18 (*m,* N-α-CH_2, 2H), 2.29-2.94 (*br m,* N-α-CH_2, 43H), 2.98-3.17 (*m,* N-α-CH_2, 14H), 3.32-3.56 (*m,* CH_2-Ar, 7H), 3.63-3.67 (*m*, CH_3-N, 6H), 3.81 (*s,* CH_2-Ar, 1H), 3.91 (*s,* H_{aminal}, 1H), 4.62 (*m,* H_{aminal}, 1H), 7.22 (*d*, J=6.5 Hz, Ar-H, 2H), 7.23-7.24 (*m*, Ar-H, 1H), 7.29 (*m*, Ar-H, 4H), 7.49 (*d*, J=16.3 Hz, Ar-H, 1H). ^{13}C NMR (100 MHz, MeOD, δ): 25.27 (N-β-CH_2), 29.46 (N-β-CH_2), 32.07 (CH_3), 40.75 (N-α-CH_2), 42.06 (N-α-CH_2), 43.39 (N-α-CH_2), 43.73 (N-α-CH_2), 43.89 (N-α-CH_2), 44.60 (N-α-CH_2), 45.62 (N-α-CH_2), 46.46 (N-α-CH_2), 48.85 (N-α-CH_2), 49.72 (N-α-CH_2), 49.72 (N-α-CH_2), 50.11 (N-α-CH_2), 50.72 (N-α-CH_2), 50.88 (N-α-CH_2), 52.17 (N-α-CH_2), 52.65 (N-α-CH_2), 53.08 (N-α-CH_2), 53.98 (N-α-CH_2), 54.76 (N-α-CH_2), 55.84 (N-α-CH_2), 55.99 (N-α-CH_2), 56.72 (N-α-CH_2), 57.87 (N-α-CH_2), 58.09 (N-α-CH_2), 58.94 (N-α-CH_2), 59.45 (N-α-CH_2), 59.53 (N-α-CH_2), 59.61 (N-α-CH_2), 62.21 (N-α-CH_2), 63.53 (N-α-CH_2), 77.70 (H_{aminal}), 78.03 (H_{aminal}), 78.22 (H_{aminal}), 78.36 (H_{aminal}), 126.76 (Ar-H),

126.96 (Ar-H), 127.89 (Ar-H), 128.91 (Ar-H), 129.07 (Ar-H), 129.29 (Ar-H), 137.26 (Ar-H), 137.63 (Ar-C), 138.49 (Ar-C), 139.29 (Ar-C), 141.07 (Ar-C). MS: Pending data, see 8.1.3.

1,8-[dimethyl]-4,11-bis-[4-[[1,4,8,11-tetraazabicyclo[10.2.2]hexadecane]methyl]benzyl]-1,4,8,11-tetraazacyclotetradecane (21)

Amounts: 1,4-bis-[[4-[decahydro-3a,5a,8a,10a-tetraaza-pyrenium]methyl]benzyl]-1,4,8,11-tetraazatricyclo[9.3.1.1^{4,8}]hexadecane tetrabromide (**14**) (140 mg, 0.17 mmol), EtOH (50 mL), $NaBH_4$ (130 mg, 3.50 mmol), HCl (3M, 10 mL), water (30 mL), $CHCl_3$ (5 x 20 mL). To yield the product as a yellow oil (120 mg, 80 %).

^{1}H NMR (400 MHz, $CDCl_3$, δ): 1.17-1.67 (*m*, 12H, N-β-CH_2), 2.13 (s, 6H, CH_3), 2.29-2.78 (m, 50H, N-α-CH_2), 2.78 (m, 2H, NH), 3.50 (s, 8H, Ar-CH_2), 3.62 (s, 3H, N-α-CH_2), 4.62 (m, 3H, N-α-CH_2), 7.10 (m, 4H, Ar-H), 7.25 (m, 4H, Ar-H). ^{13}C NMR (100 MHz, $CDCl_3$, δ): 15.35 (N-β-CH_2), 21.18 (CH_3), 23.85 (N-β-CH_2), 25.10 (N-β-CH_2), 43.27 (N-α-CH_2), 47.52 (N-α-CH_2), 48.82 (N-α-CH_2), 50.80 (N-α-CH_2), 53.82 (N-α-CH_2), 55.11 (N-α-CH_2), 58.41 (N-α-CH_2), 59.17 (N-α-CH_2), 64.91 (Ar-CH_2), 65.91 (Ar-CH_2), 126.51 (Ar-H), 126.91 (Ar-H), 128.87 (Ar-H), 129.79 (Ar-H), 136.38 (Ar-C), 136.98 (Ar-C). HRMS (*m/z*): $[M+H]^+$ calcd for $C_{52}H_{93}N_{12}$ 885.7550; found, 885.7529.

8.4. TRIS-MACROCYCLE METAL COMPLEXES

8.4.1. Synthesis of metal complexes of ligands 1,7-bis-[4-[[1,4,7,10-tetraazabicyclo[8.2.2] dodecane]methyl]benzyl]-1,4,7,10-tetraazabicyclo[5.5.2]dodecane (16), 1,8-bis-[4-[[1,4,7,10-tetraazabicyclo[8.2.2]dodecane]methyl]benzyl]-1,4,8,11-tetraazabicyclo [6.6.2]hexadecane (17), 1,7-bis-[4-[[1,4,8,11-tetraazabicyclo[10.2.2]hexadecane]methyl]benzyl]-1,4,7,10-tetraaz abicyclo[5.5.2]dodecane (18), 1,8-bis-[4-[[1,4,8,11-tetraazabicyclo[10.2.2]hexadecane]methyl]benzyl]-1,4,8,11-tetraazabicyclo [6.6.2]hexadecane (19)

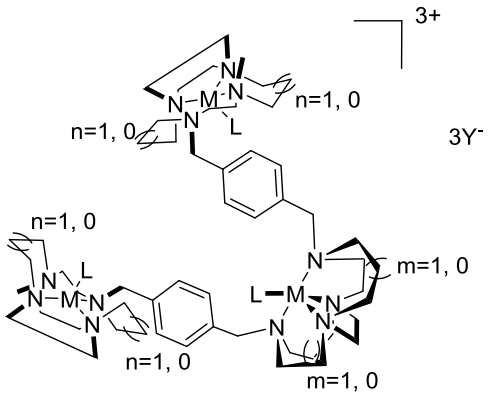

n=0				n=1			
$[Cu_3\mathbf{16}]^{6+}$	m=0,	$M^{2+}=Cu^{2+}$,	$Y^-=CH_3CO_2^-$	$[Cu_3\mathbf{18}]^{6+}$	m=0,	$M^{2+}=Cu^{2+}$,	$Y^-=CH_3CO_2^-$
$[Zn_3\mathbf{16}]^{6+}$	m=0,	$M^{2+}=Zn^{2+}$,	$Y^-=CH_3CO_2^-$	$[Zn_3\mathbf{18}]^{6+}$	m=0,	$M^{2+}=Zn^{2+}$,	$Y^-=CH_3CO_2^-$
$[Ni_3\mathbf{16}]^{6+}$	m=0,	$M^{2+}=Ni^{2+}$,	$Y^-=CH_3CO_2^-$	$[Ni_3\mathbf{18}]^{6+}$	m=0,	$M^{2+}=Ni^{2+}$,	$Y^-=CH_3CO_2^-$
n=0				n=1			
$[Cu_3\mathbf{17}]^{6+}$	m=1,	$M^{2+}=Cu^{2+}$,	$Y^-=CH_3CO_2^-$	$[Cu_3\mathbf{19}]^{6+}$	m=1,	$M^{2+}=Cu^{2+}$,	$Y^-=CH_3CO_2^-$
$[Zn_3\mathbf{17}]^{6+}$	m=1,	$M^{2+}=Zn^{2+}$,	$Y^-=CH_3CO_2^-$	$[Zn_3\mathbf{19}]^{6+}$	m=1,	$M^{2+}=Zn^{2+}$,	$Y^-=CH_3CO_2^-$
$[Ni_3\mathbf{17}]^{6+}$	m=1,	$M^{2+}=Ni^{2+}$,	$Y^-=CH_3CO_2^-$	$[Ni_3\mathbf{19}]^{6+}$	m=1,	$M^{2+}=Ni^{2+}$,	$Y^-=CH_3CO_2^-$

General procedure H

Macrocycle was dissolved in degassed dry methanol to this a dry methanolic solution of metal salt was added dropwise. The solution was heated at reflux overnight after which the solvent was reduced *in vacuo* ~5 mL and purified via size exclusion chromatography using a LH20 Sephadex column.

1,7-bis-[4-[[1,4,7,10-tetraazabicyclo[8.2.2]dodecane]methyl]benzyl]-1,4,7,10-tetraazabicyclo[5.5.2]dodecane copper(II) acetate $(Cu_3\mathbf{16})^{6+}$

Amounts: 1,7-bis-[4-[[1,4,7,10-tetraazabicyclo[8.2.2]dodecane]methyl]benzyl]-1,4,7,10-tetraazabicyclo[5.5.2]dodecane (**16**) (55 mg, 0.07 mmol), dry methanol (5 mL and 10 mL) copper(II) acetate monohydrate (46 mg, 0.23 mmol). To yield a blue solid (21 mg, 22%).

MS: Pending data, see 8.1.3. Anal. calc'd for $C_{58}H_{96}Cu_3N_{12}O_{12}..4H_2O$: expected: C, 49.19; H, 7.40; N, 11.87. Found: C, 49.31; H, 7.40; N, 11.01. UV-Vis (MeOH) λ_{max}, nm (ε): 665 (2 M^{-1} cm^{-1}).

1,7-bis-[4-[[1,4,7,10-tetraazabicyclo[8.2.2]dodecane]methyl]benzyl]-1,4,7,10-tetraazabicyclo[5.5.2]dodecane zinc(II) acetate ($Zn_3$16)$^{6+}$

Amounts: 1,7-bis-[4-[[1,4,7,10-tetraazabicyclo[8.2.2]dodecane]methyl]benzyl]-1,4,7,10-tetraazabicyclo[5.5.2]dodecane (**16**) (55 mg, 0.07 mmol), dry methanol (5 mL and 10 mL), zinc acetate (42 mg, 0.23 mmol). To yield a yellow solid (51 mg, 55%).

^{1}H NMR (400 MHz, MeOD, δ): 2.02 (*s*, CH_3-C, 12H), 2.68 (*s*, CH_3-C, 6H), 2.86-3.17 (*m*, N-α-CH_2, 34H), 3.30 (*s*, N-α-CH_2, 10H), 3.52 (*s*, N-α-CH_2, 4H), 3.69-3.71 (*m*, N-α-CH_2, 11H), 3.99-4.05 (*m*, N-α-CH_2, 9H), 4.63 (*m*, NH, 2H), 7.43-7.53 (*m*, Ar-H, 7H), 7.98 (*s*, Ar-H, 1H). ^{13}C NMR (100 MHz, MeOD, δ): 21.43 ($\underline{C}H_3$-C), 32.68 (N-α-CH_2), 41.46 (N-α-CH_2), 45.25 (N-α-CH_2), 51.85 (N-α-CH_2), 54.70 (N-α-CH_2), 54.85 (N-α-CH_2), 55.73 (N-α-CH_2), 57.12 (N-α-CH_2), 63.35 (CH_2-Ar), 126.96 (Ar-H), 129.10 (Ar-H), 130.60 (Ar-H), 130.83 (Ar-H), 180.33 (C=O), 179.88 (C=O). MS (*m/z*): [M-CH_3CO_2+2Na+H]$^+$ calcd for $C_{56}H_{94}N_{12}O_{10}Zn_3$ 1337.56; found, 1337.9. HRMS: Pending data, see 8.1.3. Anal. calc'd for $C_{58}H_{96}Zn_3N_{12}O_{12}$.2EtOH: expected: C, 51.65; H, 7.55; N, 11.66. Found: C, 51.16; H, 7.26; N, 10.90.

1,7-bis-[4-[[1,4,7,10-tetraazabicyclo[8.2.2]dodecane]methyl]benzyl]-1,4,7,10-tetraazabicyclo[5.5.2]dodecane nickel(II) acetate ($Ni_3$16)$^{6+}$

Amounts: Amounts: 1,7-bis-[4-[[1,4,7,10-tetraazabicyclo[8.2.2]dodecane]methyl]benzyl]-1,4,7,10-tetraazabicyclo[5.5.2]dodecane (**16**) (51 mg, 0.06 mmol), dry methanol (5 mL and 10 mL), nickel acetate tetrahydrate (52 mg, 0.21 mmol). To yield a yellow solid (51 mg, 87%).

MS (*m/z*): [M-2CH_3CO_2+3H]$^+$ calcd for $C_{54}H_{93}N_{12}Ni_3O_8$ 1214.50; found, 1214.8. HRMS: Pending data, see 8.1.3. Anal. calc'd for $C_{58}H_{96}Ni_3N_{12}O_{12}$ expected: C, 52.40; H, 7.28; N, 12.64. Found: C, 47.56; H, 6.98; N, 9.64 – contains impurity. UV-Vis: (MeOH) λ_{max}, nm (ε): 670 (28 M^{-1} cm^{-1}), 749 (20 M^{-1} cm^{-1}).

1,8-bis-[4-[[1,4,7,10-tetraazabicyclo[8.2.2]dodecane]methyl]benzyl]-1,4,8,11-tetraazabicyclo[6.6.2]hexadecane copper(II) acetate ($Cu_3$17)$^{6+}$

Amounts: 1,8-bis-[4-[[1,4,7,10-tetraazabicyclo[8.2.2]dodecane]methyl]benzyl]-1,4,8,11-tetraazabicyclo[6.6.2]hexadecane (**17**) (51 mg, 0.06 mmol), dry methanol (5 mL and 10 mL), copper(II) acetate monohydrate (41 mg, 0.20 mmol). To yield a blue solid (12 mg, 14 %).

MS (*m/z*): [M-2CH_3CO_2+3NH_4-H]$^+$ calcd for $C_{56}H_{105}Cu_3N_{15}O_8$ 1307.19; found, 1307.6. HRMS: Pending data, see 8.1.3. Anal. calc'd for $C_{60}H_{100}Cu_3N_{12}O_{12}$.1.25DCM.2.75MeCN: expected: C, 50.38; H, 7.02; N, 12.98. Found: C, 49.96; H, 7.51; N, 13.26. UV-Vis (MeOH) λ_{max}, nm (ε): 665 (182 M^{-1} cm^{-1}).

1,8-bis-[4-[[1,4,7,10-tetraazabicyclo[8.2.2]dodecane]methyl]benzyl]-1,4,8,11-tetraazabicyclo [6.6.2]hexadecane zinc(II) acetate ($Zn_3$17)$^{6+}$

Amounts: 1,8-bis-[4-[[1,4,7,10-tetraazabicyclo[8.2.2]dodecane]methyl]benzyl]-1,4,8,11-tetraazabicyclo[6.6.2]hexadecane (**17**) (50 mg, 0.06 mmol), dry methanol (5 mL and 10 mL), zinc(II) acetate (37 mg, 0.20 mmol). To yield a yellow solid (34 mg, 40 %).

^{1}H NMR (MeOD): δ 1.28 (*m*, N-β-CH_2, 4H), 1.99 (*s*, $\underline{C}H_3$-C, 18H), 2.14-2.35 (*m*, N-α-CH_2, 6H), 2.85-3.16 (*br m*, N-α-CH_2, 30H), 3.26-3.37 (*m*, N-α-CH_2, 4H), 3.47-3.94 (*br m*, N-α-CH_2, 18H), 4.01 (*d*, J=18.0 Hz, N-α-CH_2, 8H), 4.57-4.63 (*m*, N-α-CH_2, 2H), 4.82-4.86 (*m*, NH, 2H), 7.24 (*d*, J=7.3 Hz, Ar-H, 1H), 7.31-7.40 (*m*, Ar-H, 3H), 7.42 (*s*, Ar-H, 2H), 7.50-7.52 (*m*, Ar-H, 2H). ^{13}C NMR (100 MHz, MeOD, δ): 18.50 ($\underline{C}H_3$-C), 21.33 (N-β-CH_2), 46.01(N-α-CH_2), 46.34 (N-α-CH_2), 52.73 (N-α-CH_2), 54.66 (N-α-CH_2), 55.75 (N-α-CH_2),56.31 (N-α-CH_2), 63.26 (N-α-CH_2), 64.61 (N-α-CH_2), 126.95 (Ar-H), 128.39 (Ar-C), 130.59 (Ar-H), 132.15 (Ar-C), 138.15 (Ar-C), 140.24 (Ar-H), 141.03 (Ar-H), 145.12 (Ar-C), 151.68 (C=O). MS (*m/z*): [M-6CH_3CO_2+NH_4-H]$^+$ calcd for $C_{48}H_{85}N_{13}Zn_3$ 1040.44; found, 1040.7. HRMS: Pending data, see 8.1.3.

1,8-bis-[4-[[1,4,7,10-tetraazabicyclo[8.2.2]dodecane]methyl]benzyl]-1,4,8,11-tetraazabicyclo [6.6.2]hexadecane nickel(II) acetate ($Ni_3$17)$^{6+}$

Amounts: 1,8-bis-[4-[[1,4,7,10-tetraazabicyclo[8.2.2]dodecane]methyl]benzyl]-1,4,8,11-tetraazabicyclo[6.6.2]hexadecane (**17**) (51 mg, 0.06 mmol), dry methanol (5 mL and 10 mL), nickel(II) acetate tetrahydrate (51 mg, 0.20 mmol). To yield a green solid (70 mg, 83 %).

MS: Pending data, see 8.1.3. UV-Vis (MeOH) λ_{max}, nm (ε): 670 (12 M^{-1} cm^{-1}), 742 (10 M^{-1} cm^{-1}).

1,7-bis-[4-[[1,4,8,11-tetraazabicyclo[10.2.2]hexadecane]methyl]benzyl]-1,4,7,10-tetraazabicyclo[5.5.2]dodecane copper(II) acetate ($Cu_3$18)$^{6+}$

Amounts: 1,7-bis-[4-[[1,4,8,11-tetraazabicyclo[10.2.2]hexadecane]methyl]benzyl]-1,4,7,10-tetraazabicyclo[5.5.2]dodecane (**18**) (100 mg, 0.12 mmol), dry methanol (5 mL and 10 mL), copper(II) acetate monohydrate (77 mg, 0.39 mmol). To yield a blue solid (101 mg, 62 %).

HRMS (*m/z*): [M-5CH_3CO_2+Na+3H]$^{3+}$ calcd for $C_{52}H_{92}Cu_3N_{12}Na$: 376.8409, found: 376.8411. Anal. calc'd for $C_{62}H_{104}Cu_3N_{12}O_{12}$ expected: C, 53.18; H, 7.49; N, 12.00. Found: C, 48.70; H, 8.11; N, 10.47 – contains impurity. UV-Vis (MeOH) λ_{max}, nm (ε): 645 (815 M^{-1} cm^{-1}).

1,7-bis-[4-[[1,4,8,11-tetraazabicyclo[10.2.2]hexadecane]methyl]benzyl]-1,4,7,10-tetraazabicyclo[5.5.2]dodecane zinc(II) acetate ($Zn_3$18)$^{6+}$

Amounts: 1,7-bis-[4-[[1,4,8,11-tetraazabicyclo[10.2.2]hexadecane]methyl]benzyl]-1,4,7,10-tetraazabicyclo[5.5.2]dodecane (**18**) (100 mg, 0.12 mmol), dry methanol (5 mL and 8 mL), zinc(II) acetate (71 mg, 0.39 mmol). To yield a yellow solid (133 mg, 81 %).

^{1}H NMR ($CDCl_3$): δ 1.67(*s,* 2H, N-β-CH_2), 1.60-1.64 (*m,* 2H, N-β-CH_2), 1.79 (*d,* 4H, J=13.3 Hz, N-β-CH_2), 1.99 (*s,* 18H, CH_3), 2.15-2.25 (*m,* 7H, N-α-CH_2), 2.31 (*t,* 2H, J=10.0 Hz, N-α-CH_2), 2.48-3.26 (*m,* 42H, N-α-CH_2), 3.47-4.15 (*m,* 16H, N-α-CH_2), 4.19 (*d,* 1H, J=6.7 Hz, N-α-CH_2), 4.23 (*d,* 1H, J=6.9 Hz, N-α-CH_2), 4.54-4.62 (*m,* 2H, NH), 7.29 (*d,* 1H, J=7.8 Hz, Ar-H), 7.33 (*s,* 2H, Ar-H), 7.37 (*d,* 3H, J=8.0 Hz, Ar-H), 7.47-7.53 (*m,* 2H, Ar-H). ^{13}C NMR ($CDCl_3$): δ 19.10 (N-β-CH_2), 21.01 (CH_3-O), 21.82 (N-β-CH_2), 23.76 (N-β-CH_2), 24.30 (N-β-CH_2), 43.37 (N-α-CH_2), 44.48 (N-α-CH_2), 49.15 (N-α-CH_2), 49.15 (N-α-CH_2), 49.56 (N-α-CH_2), 51.43 (N-α-CH_2), 52.24 (N-α-CH_2), 52.30 (N-α-CH_2), 53.17 (N-α-CH_2), 53.95 (N-α-CH_2), 54.88 (N-α-CH_2), 55.72 (N-α-CH_2), 56.56 (N-α-CH_2), 57.20 (N-α-CH_2), 57.98 (N-α-CH_2), 123.28 (Ar-H), 126.61 (Ar-H), 126.79 (Ar-H), 129.92 (Ar-H), 130.48 (Ar-H), 130.98 (Ar-H), 131.32 (Ar-C), 131.91 (Ar-H), 132.23 (Ar-H), 135.14 (Ar-C), 145.96 (Ar-C), 147.03 (Ar-C), 179.86 (C=O). MS (*m/z*): [M-2H-6CH_3CO_2]$^+$ calcd for 1049.45; found, 1049.7. HRMS: Pending data, see 8.1.3. Anal. calc'd for $C_{62}H_{104}N_{12}O_{12}$ Zn_3: C, 52.97; H, 7.46; N, 11.96. Found: C, 47.49; H, 7.92; N, 9.52 – contains impurities.

1,7-bis-[4-[[1,4,8,11-tetraazabicyclo[10.2.2]hexadecane]methyl]benzyl]-1,4,7,10-tetraazabicyclo[5.5.2]dodecane nickel(II) acetate ($Ni_3$18)$^{6+}$

Amounts: 1,7-bis-[4-[[1,4,8,11-tetraazabicyclo[10.2.2]hexadecane]methyl]benzyl]-1,4,7,10-tetraazabicyclo[5.5.2]dodecane (**18**) (78 mg, 0.09 mmol), dry methanol (10 mL and 10 mL), nickel(II) acetate tetrahydrate (68 mg, 0.27 mmol). To yield a green solid (116 mg, 92 %).

MS (*m/z*): [M+2H-6CH_3CO_2+2Na+NH_4]$^+$ calcd for 1097.44; found, 1097.6. HRMS: Pending data, see 8.1.3. Anal. calc'd for $C_{62}H_{104}N_{12}Ni_3O_{12}$: C, 53.74; H, 7.57; N, 12.13. Found: C, 44.63; H, 7.36; N, 9.83 – contains impurities. UV-Vis (MeOH) λ_{max}, nm (ε): 440 (68 M^{-1} cm^{-1}), 590 (42 M^{-1} cm^{-1}).

1,8-bis-[4-[[1,4,8,11-tetraazabicyclo[10.2.2]hexadecane]methyl]benzyl]-1,4,8,11-tetraazabicyclo[6.6.2]hexadecane copper(II) acetate ($Cu_3$19)$^{6+}$

Amounts: 1,8-bis-[4-[[1,4,8,11-tetraazabicyclo[10.2.2]hexadecane]methyl]benzyl]-1,4,8,11-tetraazabicyclo[6.6.2]hexadecane (**19**) (100 mg, 0.11 mmol), dry methanol (5 mL and 10 mL), copper(II) acetate monohydrate (75 mg, 0.37 mmol). To yield a blue solid (136 mg, 84 %).

MS (*m/z*): $[M\text{-}4CH_3CO_2]^{3+}$ calcd for 396.86; found, 396.8473. HRMS: Pending data, see 8.1.3. Anal. calc'd for $C_{46}H_{110}Cu_3N_{12}O_{12}.9H_2O$: C, 48.33; H, 7.99; N, 10.57. Found: C, 48.76; H, 8.13; N, 10.63. UV-Vis (MeOH) λ_{max}, nm (ε): 645 (555 M^{-1} cm^{-1}).

1,8-bis-[4-[[1,4,8,11-tetraazabicyclo[10.2.2]hexadecane]methyl]benzyl]-1,4,8,11-tetraazabicyclo [6.6.2]hexadecane zinc(II) acetate ($Zn_3$19)$^{6+}$

Amounts: 1,8-bis-[4-[[1,4,8,11-tetraazabicyclo[10.2.2]hexadecane]methyl]benzyl]-1,4,8,11-tetraaza bicyclo [6.6.2]hexadecane (**19**) (100 mg, 0.11 mmol), dry methanol (5 mL and 10 mL), zinc(II) acetate (69 mg, 0.37 mmol). To yield a yellow solid (145 mg, 89 %).

^{1}H NMR (MeOD): δ 1.62 (*d,* J=16.3 Hz, N-β-CH_2, 4H), 1.79 (*d*, J=14.3Hz, N-β-CH_2, 8H), 1.98 (*s,* 18H, CH_3), 2.14-2.25 (*m,* N-α-CH_2, 7H), 2.29-2.33 (*m,* N-α-CH_2, 2H), 2.49-3.24 (*br m,* N-α-CH_2, 40H), 3.45-3.67 (*m,* N-α-CH_2, 6H), 3.75-3.84 (*m,* N-α-CH_2, 5H), 3.89-4.00 (*m,* CH_2-Ar, 4H), 4.15-4.26 (*m,* CH_2-Ar, 4H), 4.54-4.60 (*m,* 2H, NH), 7.24-7.30 (*m,* Ar-H*,* 3H), 7.36 (*m,* Ar-H, 2H), 7.44-7.49 (*m,* Ar-H, 2H), 7.56-7.58 (*m,* Ar-H, 1H). ^{13}C NMR (MeOD): δ 19.15 (N-β-CH_2), 19.94 (N-β-CH_2), 20.99 (N-β-CH_2), 22.15 ($\underline{C}H_3$-C), 24.28 ($\underline{C}H_3$-C), 43.35 (N-α-CH_2), 44.45 (N-α-CH_2), 48.58 (N-α-CH_2), 49.13 (N-α-CH_2), 49.55 (N-α-CH_2), 51.42 (N-α-CH_2), 52.22 (N-α-CH_2), 52.32 (N-α-CH_2), 53.15 (N-α-CH_2), 53.97 (N-α-CH_2), 54.92 (N-α-CH_2), 55.63 (N-α-CH_2), 56.56 (N-α-CH_2), 57.51 (N-α-CH_2), 57.99 (N-α-CH_2), 63.34 (N-α-CH_2), 126.62 (Ar-H), 127.21 (Ar-H), 128.82 (Ar-H), 129.39 (Ar-H), 129.74 (Ar-H), 130.98 (Ar-H), 131.75 (Ar-H), 131.91 (Ar-H), 132.75 (Ar-C), 133.06 (Ar-C), 138.47 (Ar-C), 142.25 (Ar-C), 179.69 (C=O). MS: Pending data, see 8.1.3.

1,8-bis-[4-[[1,4,8,11-tetraazabicyclo[10.2.2]hexadecane]methyl]benzyl]-1,4,8,11-tetraazabicyclo [6.6.2]hexadecane nickel(II) acetate ($Ni_3$19)$^{6+}$

Amounts: 1,8-bis-[4-[[1,4,8,11-tetraazabicyclo[10.2.2]hexadecane]methyl]benzyl]-1,4,8,11-tetraazab icyclo[6.6.2]hexadecane (**19**) (100 mg, 0.11 mmol), dry methanol (5 mL and 10 mL), nickel(II) acetate tetrahydrate (93 mg, 0.37 mmol). To yield a blue solid (144 mg, 90 %).

MS: Pending data, see 8.1.3. UV-Vis (MeOH) λ_{max}, nm (ε): 439 (54 M^{-1} cm^{-1}), 595 (33 M^{-1} cm^{-1}).

8.4.2. Synthesis of metal complexes of ligands 1,8-[dimethyl]-4,11-bis-[4-[[1,4,7,10-tetraazabicyclo[8.2.2]dodecane]methyl]benzyl]-1,4,8,11-tetraazacyclotetradecane (20), 1,8-[dimethyl]-4,11-bis-[4-[[1,4,8,11-tetraazabicyclo[10.2.2]hexadecane]methyl]benzyl]-1,4,8,11-tetraazacyclotetradecane (21)

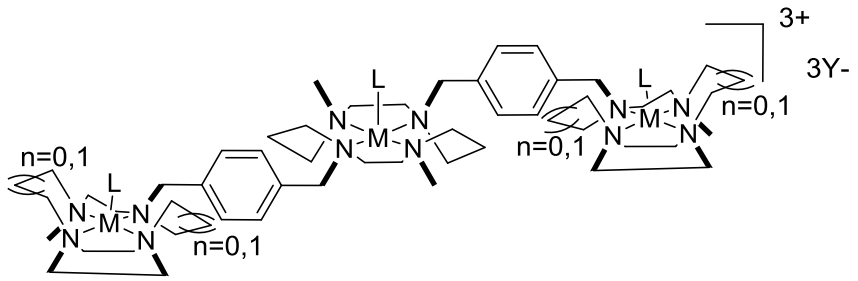

n=0

$[Cu_3\mathbf{20}]^{6+}$ $M^{2+}=Cu^{2+}$, $Y^-=CH_3CO_2^-$

$[Zn_3\mathbf{20}]^{6+}$ $M^{2+}=Zn^{2+}$, $Y^-=CH_3CO_2^-$

$[Ni_3\mathbf{20}]^{6+}$ $M^{2+}=Ni^{2+}$, $Y^-=CH_3CO_2^-$

n=1

$[Cu_3\mathbf{21}]^{6+}$ $M^{2+}=Cu^{2+}$, $Y^-=CH_3CO_2^-$

$[Zn_3\mathbf{21}]^{6+}$ $M^{2+}=Zn^{2+}$, $Y^-=CH_3CO_2^-$

$[Zn_3\mathbf{21}]^{6+}$ $M^{2+}=Zn^{2+}$, $Y^-=Cl^-$

$[Ni_3\mathbf{21}]^{6+}$ $M^{2+}=Ni^{2+}$, $Y^-=CH_3CO_2^-$

General procedure H Was followed

1,8-[dimethyl]-4,11-bis-[4-[[1,4,7,10-tetraazabicyclo[8.2.2]dodecane]methyl]benzyl]-1,4,8,11-tetraazacyclotetradecane copper(II) acetate $(Cu_3\mathbf{20})^{6+}$

Amounts: 1,8-[dimethyl]-4,11-bis-[4-[[1,4,7,10-tetraazabicyclo[8.2.2]dodecane]methyl]benzyl]-1,4,8,11-tetraazacyclotetradecane (**20**) (10 mg, 0.012 mmol), dry methanol (2 mL and 3 mL), copper(II) acetate monohydrate (8 mg, 0.040 mmol). To yield a blue solid (12 mg, 74 %).

MS: Pending data, see 8.1.3. UV-Vis (MeOH) λ_{max}, nm (ε): 655 (279 M^{-1} cm^{-1}).

1,8-[dimethyl]-4,11-bis-[4-[[1,4,7,10-tetraazabicyclo[8.2.2]dodecane]methyl]benzyl]-1,4,8,11-tetraazacyclotetradecane zinc(II) acetate $(Zn_3\mathbf{20})^{6+}$

Amounts: 1,8-[dimethyl]-4,11-bis-[4-[[1,4,7,10-tetraazabicyclo[8.2.2]dodecane]methyl]benzyl]-1,4,8,11-tetraazacyclotetradecane (**20**) (13 mg, 0.015 mmol), dry methanol (2 mL and 3 mL), zinc(II) acetate monohydrate (9 mg, 0.050 mmol). To yield a yellow solid (17 mg, 79%).

MS: Pending data, see 8.1.3.

1,8-[dimethyl]-4,11-bis-[4-[[1,4,7,10-tetraazabicyclo[8.2.2]dodecane]methyl]benzyl]-1,4,8,11-tetraazacyclotetradecane nickel(II) acetate ($Ni_3$20)$^{6+}$

Amounts: 1,8-[dimethyl]-4,11-bis-[4-[[1,4,7,10-tetraazabicyclo[8.2.2]dodecane]methyl]benzyl]-1,4,8,11-tetraazacyclotetradecane (**20**) (12 mg, 0.014 mmol), dry methanol (2 mL and 3 mL), nickel(II) acetate monohydrate (9 mg, 0.050 mmol). To yield a green solid (15 mg, 77 %).

MS: Pending data, see 8.1.3. UV-Vis (MeOH) λ_{max}, nm (ε): 388 (175 M^{-1} cm^{-1}), 660 (279 M^{-1} cm^{-1}).

1,8-[dimethyl]-4,11-bis-[4-[[1,4,8,11-tetraazabicyclo[10.2.2]hexadecane]methyl]benzyl]-1,4,8,11-tetraazacyclotetradecane copper(II) acetate ($Cu_3$21)$^{6+}$

Amounts: 1,8-[dimethyl]-4,11-bis-[4-[[1,4,8,11-tetraazabicyclo[10.2.2]hexadecane]methyl]benzyl]-1,4,8,11-tetraazacyclotetradecane (**21**) (50 mg, 0.05 mmol), dry methanol (5 mL and 10 mL), copper(II) acetate monohydrate (35 mg, 0.18 mmol). To yield a blue solid (90 mg, 75 %).

MS (*m/z*): $[M\text{-}2CH_3CO_2\text{+Na-2H}]^+$ calcd for $C_{60}H_{102}Cu_3N_{12}NaO_8$, 1333.18; found, 1333.5285. Anal. calc'd for $C_{64}H_{110}Cu_3N_{12}O_{12}$: C, 53.74; H, 7.75; Cu, 13.33; N, 11.75. Found: C, 58.17; H, 9.02; N, 9.60. – contains impurities. UV-Vis (MeOH) λ_{max}, nm (ε): 610 (297 M^{-1} cm^{-1}).

1,8-[dimethyl]-4,11-bis-[4-[[1,4,8,11-tetraazabicyclo[10.2.2]hexadecane]methyl]benzyl]-1,4,8,11-tetraazacyclotetradecane zinc(II) acetate ($Zn_3$21)$^{6+}$

Amounts: 1,8-[dimethyl]-4,11-bis-[4-[[1,4,8,11-tetraazabicyclo[10.2.2]hexadecane]methyl]benzyl]-1,4,8,11-tetraazacyclotetradecane (**21**) (150 mg, 0.17 mmol), dry methanol (10 mL and 10 mL), zinc(II) acetate (103 mg, 0.56 mmol). To yield the yellow oil (146 mg, 60 %).

^{1}H NMR (400 MHz, MeOH, δ): 1.28 (*m,* N-β-CH_2*,* 1H), 1.60-1.85 (*m,* N-β-CH_2*,* 11H), 1.98 (*s,* $\underline{C}H_3$-C*,* 18H), 2.21-2.38 (*m,* N-α-CH_2*,* 10H), 2.48-3.55 (*m,* CH_3-N*,* 6H), 2.58-2.69 (*m,* N-α-CH_2*,* 7H), 2.74-2.98 (*m,* N-α-CH_2*,* 18H), 3.07-3.12 (*m,* N-α-CH_2*,* 6H), 3.20-3.21 (*m,* N-α-CH_2*,* 6H), 3.45-3.70 (*m,* N-α-CH_2*,* 9H), 3.83-4.00 (*m,* CH_2-Ar*,* 4H), 4.20 (*d,* J=14.3 Hz, CH_2-Ar*,* 4H), 4.33-4.65 (*m,* NH*,* 2H), 7.30-7.33 (*m,* Ar-H*,* 8H). ^{13}C NMR (100 MHz, MeOH, δ): 19.13 (N-β-CH_2), 20.97 (N-β-CH_2), 22.24 (N-β-CH_2), 24.28 ($\underline{C}H_3$-C), 27.35 ($\underline{C}H_3$-C), 42.24 (CH_3-N), 43.31 (N-α-CH_2), 44.03 44.46 (N-α-CH_2), 44.46 (N-α-CH_2), 44.67 (N-α-CH_2), 45.12 (N-α-CH_2), 46.27 (N-α-CH_2), 48.84 (N-α-CH_2), 49.14 (N-α-CH_2), 49.51 (N-α-CH_2), 49.78 (N-α-CH_2), 50.12 (N-α-CH_2), 50.29 (N-α-CH_2), 51.43 (N-α-CH_2), 52.26 (N-α-CH_2), 53.58 (N-α-CH_2), 55.54 (N-α-CH_2), 56.57 (N-α-CH_2), 58.00 (N-α-CH_2), 59.94 (N-α-CH_2), 126.63 (Ar-H), 130.63 (Ar-H), 130.88 (Ar-H), 130.95 (Ar-H), 131.13 (Ar-C), 131.37 (Ar-H), 131.51 (Ar-C), 131.65 (Ar-C), 131.77 (Ar-H), 131.93 (Ar-H), 132.05 (Ar-C), 179.74 (C=O). MS (*m/z*): $[M\text{-}CH_3CO_2\text{+H}]^+$ calcd for $C_{62}H_{108}N_{12}O_{10}Zn_3$, 1377.76; found, 1377.9. HRMS: Pending data, see 8.1.3.

1,8-[dimethyl]-4,11-bis-[4-[[1,4,8,11-tetraazabicyclo[10.2.2]hexadecane]methyl]benzyl]-1,4,8,11-tetraazacyclotetradecane zinc(II) chloride ($Zn_3$21)$^{6+}$

Amounts: 1,8-[dimethyl]-4,11-bis-[4-[[1,4,8,11-tetraazabicyclo[10.2.2]hexadecane]methyl]benzyl]-1,4,8,11-tetraazacyclotetradecane (**21**) (100 mg, 0.11 mmol), dry methanol (7 mL and 10 mL), zinc(II) chloride (51 mg, 0.37 mmol). To yield the white solid (70 mg, 57 %).

MS (*m/z*): $[M-H]^+$ calcd for $C_{52}H_{91}Cl_6N_{12}Zn_3$, 1293.23; found, 1293.3. HRMS: Pending data, see 8.1.3. Anal. calc'd for $C_{52}H_{92}Cl_6N_{12}Zn_3$: C, 48.26; H, 7.17; N, 12.99. Found: C, 40.16; H, 6.09; N, 9.80.

1,8-[dimethyl]-4,11-bis-[4-[[1,4,8,11-tetraazabicyclo[10.2.2]hexadecane]methyl]benzyl]-1,4,8,11-tetraazacyclotetradecane nickel(II) acetate ($Ni_3$21)$^{6+}$

Amounts: 1,8-[dimethyl]-4,11-bis-[4-[[1,4,8,11-tetraazabicyclo[10.2.2]hexadecane]methyl]benzyl]-1,4,8,11-tetraazacyclotetradecane (**21**) (160 mg, 0.18 mmol), dry methanol (10 mL and 10 mL), nickel(II) acetate (150 mg, 0.60 mmol). To yield the yellow solid (160 mg, 67%).

HRMS (*m/z*): $[M-2CH_3CO_2+NH_4]^+$ calcd for $C_{60}H_{112}N_{14}Ni_3O_8$, 1333.5273; found, 1333.5273. MS (*m/z*): $[M-4CH_3CO_2+NH_4+H]^+$ calcd for $C_{56}H_{107}N_{14}Ni_3O_4$, 1216.65; found, 1216.6. Anal. calc'd for $C_{64}H_{110}N_{12}Ni_3O_{12}$: C, 54.30; H, 7.83; N, 11.87. Found: C, 49.17; H, 8.31; N, 13.16 – contains impurities. UV-Vis (MeOH) λ_{max}, nm (ε): 431 (3 M^{-1} cm^{-1}), 585 (12 M^{-1} cm^{-1}).

8.4.3. Transmetalation of 1,7-bis-[4-[[1,4,8,11-tetraazabicyclo[10.2.2]hexadecane]methyl]benzyl]-1,4,7,10-tetraazabicyclo[5.5.2]dodecane zinc(II) acetate with copper(II) acetate ($CuZn_2$18)$^{6+}$

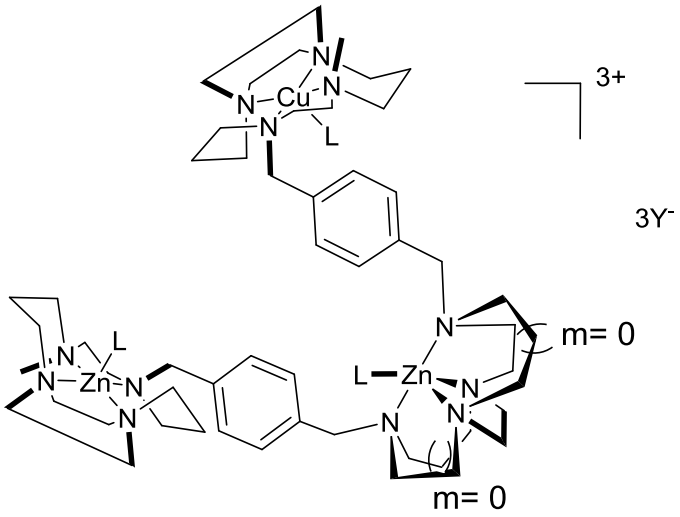

[$CuZn_2$**18**]$^{6+}$ Y^- and L =$CH_3CO_2^-$

1,7-bis-[4-[[1,4,8,11-tetraazabicyclo[10.2.2]hexadecane]methyl]benzyl]-1,4,7,10-tetraazabicyclo[5.5.2]dodecane zinc(II) acetate (Zn_3**18**)$^{6+}$ (10 mg, 7.11 µmol) was added to dry methanol (1 mL), to this a methanolic solution of copper(II) acetate monohydrdate (1.42 mg, 7.11 µmol) in dry methanol (500 µL) was added dropwise and the solution heated to 60^{o}C for 2 h. The solution was reduced *in vacuo* and purified via size exclusion chromatography (Sephadex LH20). To yield a blue solid (5 mg, 49 %).

MS: Pending data, see 8.1.3. UV-Vis (MeOH) λ_{max}, nm (ε): 630 (9 M^{-1} cm^{-1}).

8.4.4. Transmetalation of 1,7-bis-[4-[[1,4,8,11-tetraazabicyclo[10.2.2]hexadecane]methyl] benzyl]-1,4,7,10-tetraazabicyclo[5.5.2]dodecane zinc(II) acetate with 64-copper(II) acetate ($^{64}CuZn_2$18)$^{6+}$ and 1,8-bis-[4-[[1,4,8,11-tetraazabicyclo[10.2.2]hexadecane]methyl]benzyl]-1,4,8,11-tetraazabicyc lo [6.6.2]hexadecane zinc(II) acetate with 64-copper(II) acetate ($^{64}CuZn_2$19)^{6}

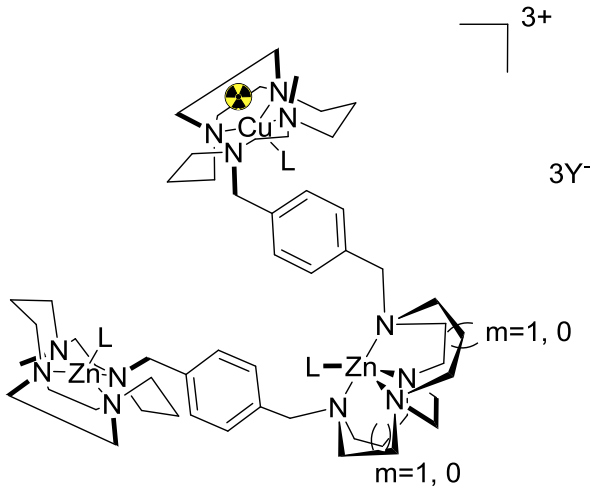

[$^{64}CuZn_2$**18**]$^{6+}$ m=0, Y^- and L =$CH_3CO_2^-$
[$^{64}CuZn_2$**19**]$^{6+}$ m=1, Y^- and L =$CH_3CO_2^-$

General procedure I

Ammonium acetate buffer was added to 64-copper(II) chloride and incubated for 10 min at 60°C. A stock solution of macrocycle was made by dissolving in ammonium acetate buffer. A portion of the macrocycle ammonium acetate buffer solution was added to the 64-copper(II) chloride ammonium acetate buffer solution and incubated at 90°C for up to 75 min.

Transmetalation of 1,7-bis-[4-[[1,4,8,11-tetraazabicyclo[10.2.2]hexadecane]methyl]benzyl]-1,4,7,10-tetraazabicyclo[5.5.2]dodecane zinc(II) acetate with 64-copper(II) acetate ($^{64}CuZn_2$18)$^{6+}$

Amounts: ammonium acetate buffer (400 mM, pH 5.5, 230 µL), 64-copper(II) chloride (3 MBq), 1,7-bis-[4-[[1,4,8,11-tetraazabicyclo[10.2.2]hexadecane]methyl]benzyl]-1,4,7,10-tetraazabicyclo[5.5.2] dodecane zinc(II) acetate (Zn_3**18**)$^{6+}$ (1.00 mg, 0.71 µmol), ammonium acetate buffer (400 mM, pH 5.5, 250 µL), 1,7-bis-[4-[[1,4,8,11-tetraazabicyclo[10.2.2]hexadecane]methyl]ben zyl]-1,4,7,10-tetraazabicyclo[5.5.2]dodecane zinc(II) acetate (Zn_3**18**)$^{6+}$ ammonium acetate buffer solution (2.8 mM, 12.5 µL).

Radio-TLC	Conversion / %
Time / min	2.8 mM
15	77.16
30	52.72
45	77.73
60	94.46
75	99.55

Crude RCY: 79 %

1,8-bis-[4-[[1,4,8,11-tetraazabicyclo[10.2.2]hexadecane]methyl]benzyl]-1,4,8,11-tetraazabicyclo [6.6.2]hexadecane zinc(II) acetate with 64-copper(II) acetate ($^{64}CuZn_2$19**$)^{6+}$**

Ammonium acetate buffer (400 mM, pH 5.5, 70 µL), 64-copper(II) chloride (19 MBq), 1,8-bis-[4-[[1,4,8,11-tetraazabicyclo[10.2.2]hexadecane]methyl]benzyl]-1,4,8,11-tetraazabicyclo[6.6.2]hexadecane zinc(II) acetate (Zn_3**19**$)^{6+}$ (0.80 mg, 0.56 µmol), ammonium acetate buffer (400 mM, pH 5.5, 200 µL), 1,8-bis-[4-[[1,4,8,11-tetraazabicyclo[10.2.2]hexadecane]methyl]ben zyl]-1,4,8,11-tetraazabicyclo [6.6.2]hexadecane zinc(II) acetate (Zn_3**19**$)^{6+}$ ammonium acetate buffer solution (2.8 mM, 12.5 µL).

Radio-TLC	Conversion / %
Time / min	2.8 mM
15	87
30	89.88
75	89.67

Crude RCY: 62%

8.5. BIS-MACROCYCLES

8.5.1. Attempted synthesis of 2a-[4-cyanobenzyl]-6a-[4-[[decahydro-2a,4a,6a,8a-tetraaza-pyren-2a-ium]methyl]benzyl]-decahydro-2a,4a,6a,8a-tetraaza-pyrenium tribromide (22) and 2a-[4-nitrobenzyl]-6a-[4-[[decahydro-2a,4a,6a,8a-tetraaza-pyren-2a-ium]methyl]benzyl]-decahydro-2a,4a,6a,8a-tetraaza-pyrenium tribromide (23)

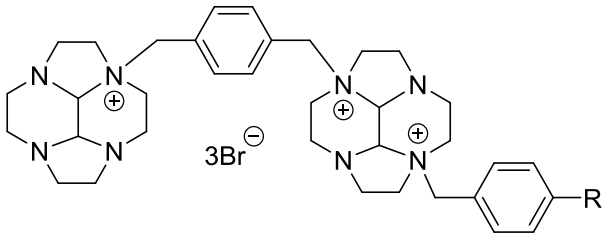

R=CN **22**

$R=NO_2$ **23**

2a-[4-cyanobenzyl]-6a-[4-[[decahydro-2a,4a,6a,8a-tetraaza-pyren-2a-ium]methyl]benzyl]-decahydro-2a,4a,6a,8a-tetraaza-pyrenium tribromide (22)

To a solution of 2a-[4-[bromomethyl]benzyl]-decahydro-2a,4a,6a,8a-tetraaza-pyrenium bromide (**5**) (0.29 g, 0.64 mmol) in dry dimethyl formamide (25 mL), 2a-[4-cyanobenzyl]-decahydro-2a,4a,6a,8a-tetraaza-pyrenium bromide (**7**) (0.25 g, 0.64 mmol) in dry dimethyl formamide (250 mL) was added slowly and the mixture stirred at RT for 10 d under an inert atmosphere. Any precipitate was filtered off and the filtrate concentrated *in vacuo* and washed with diethyl ether (3 x 10 mL). To yield a pale brown solid (1.09 g). Analytical data indicates that the desired product was not obtained.

2a-[4-nitrobenzyl]-6a-[4-[[decahydro-2a,4a,6a,8a-tetraaza-pyren-2a-ium]methyl]benzyl]-decahydro-2a,4a,6a,8a-tetraaza-pyrenium tribromide (23)

To a solution of 2a-[4-[bromomethyl]benzyl]-decahydro-2a,4a,6a,8a-tetraaza-pyrenium bromide (**5**) (0.28 g, 0.61 mmol) in dry dimethyl formamide (50 mL), 2a-[4-nitrobenzyl]-decahydro-2a,4a,6a,8a-tetraaza-pyrenium bromide (**6**) (0.25 g, 0.61 mmol) in dry dimethyl formamide (50 mL) was added slowly and the mixture stirred at RT for 10 d under an inert atmosphere. Any precipitate was filtered off and the filtrate concentrated *in vacuo* and washed with diethyl ether (3 x 10 mL). To yield a pale brown solid (0.85 g). Analytical data indicates that the desired product was not obtained.

8.5.2. Synthesis of 2a-[4-cyanobenzyl]-6a-[4-[[decahydro-2a,4a,6a,8a-tetraaza-pyren-2a-ium] methyl]benzyl]-decahydro-2a,4a,6a,8a-tetraaza-pyrenium tribromide (22), 2a-[4-nitrobenzyl]-6a-[4-[[decahydro-2a,4a,6a,8a-tetraaza-pyren-2a-ium]methyl]benzyl]-decahydro-2a,4a,6a,8a-tetraaza-pyrenium tribromide (23), 2a-[4-[methoxycarbonyl]benzyl]-6a-[4-[[decahydro-2a,4a,6a,8a-tetraaza-pyren-2a-ium]methyl]benzyl]-decahydro-2a,4a,6a,8a-tetraaza-pyrenium tribromide (24), 2a-[4-cyanobenzyl]-6a-[4-[[decahydro-3a,5a,8a,10a-tetraaza-pyren-3a-ium]methyl]benzyl]-decahydro-2a,4a,6a,8a-tetraaza-pyrenium tribromide (25), 2a-[4-nitrobenzyl]-6a-[4-[[decahydro-3a,5a,8a,10a-tetraaza-pyren-3a-ium]methyl]benzyl]-decahydro-2a,4a,6a,8a-tetraaza-pyrenium tribromide (26) and 2a-[4-[methoxycarbonyl]benzyl]-6a-[4-[[decahydro-3a,5a,8a,10a-tetraaza-pyren-3a-ium]methyl]benzyl]-decahydro-2a,4a,6a,8a-tetraaza-pyrenium tribromide (27)

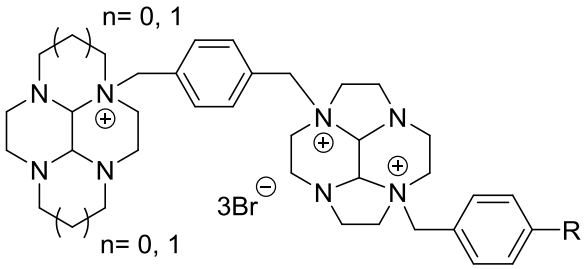

n=0		n=1	
R=CN	**22**	R=CN	**25**
$R=NO_2$	**23**	$R=NO_2$	**26**
R=COOMe	**24**	R=COOMe	**27**

General procedure E was followed

2a-[4-cyanobenzyl]-6a-[4-[[decahydro-2a,4a,6a,8a-tetraaza-pyren-2a-ium]methyl]benzyl]-decahydro-2a,4a,6a,8a-tetraaza-pyrenium tribromide (22)

Amounts: 2a-[4-[bromomethyl]benzyl]-decahydro-2a,4a,6a,8a-tetraaza-pyrenium bromide (**5**) (1 g, 2.18 mmol), dry acetonitrile (100 mL and 100 mL), 2a-[4-cyanobenzyl]-decahydro-2a,4a,6a,8a-tetraaza-pyrenium bromide (**7**) (850 mg, 2.18 mmol), diethyl ether (4 x 20 mL). To yield a white solid (1.41 g, 76 %).

^{1}H NMR (400 MHz,D_2O, δ): 2.01 (*s,* N-α-CH_2, 1H), 2.34-2.40 (*m,* N-α-CH_2, 2H), 2.62-2.85 (*m,* N-α-CH_2, 5H), 2.92-3.53 (*br m,* N-α-CH_2, 23H), 3.67 (*s,* N-α-CH_2, 1H), 3.69-3.77 (*m,* CH_2-Ar, 2H), 3.90 (*s,* CH_2-Ar, 1H), 3.99-4.14 (*m,* CH_2-Ar, 2H), 4.44-4.60 (*m,* CH_2-Ar, 2H), 4.65-4.71 (*m,* H_{aminal}, 2H), 4.74-4.89 (*m,* H_{aminal}, 2H), 7.33-7.45 (*m,* Ar-H, 1H), 7.54-7.59 (*m,* Ar-H, 5H), 7.72-7.76 (*m,* Ar-H, 2H). ^{13}C NMR (100 MHz, D_2O, δ): 30.19 (N-α-CH_2), 42.50 (N-α-CH_2), 43.53 (N-α-CH_2), 45.94 (N-α-CH_2), 47.37 (N-α-CH_2), 47.41 (N-α-CH_2), 48.44 (N-α-CH_2), 51.42 (N-α-CH_2), 56.93 (N-α-CH_2), 60.49 (N-α-CH_2), 61.11 (N-α-CH_2), 71.46 (C_{aminal}), 71.52 C_{aminal}),

78.12 C_{aminal}), 118.41 (CN), 129.93 (Ar-C), 131.32 (Ar-C), 131.91 (Ar-C), 133.04 (Ar-H), 133.10 (Ar-H), 133.44 (Ar-H), 133.54 (Ar-H), 133.65 (Ar-C). LRMS (*m/z*): $[M\text{-}3Br\text{-}3H]^+$calcd for $C_{36}H_{47}N_9$, 605.83; found, 605.5. HRMS: Pending data, see 8.1.3. Anal. calcd for $C_{36}H_{50}Br_3N_9$ expected: C, 50.96; H, 5.94; N, 14.76. Found: C, 50.77; H, 6.14; N, 14.87.

2a-[4-nitrobenzyl]-6a-[4-[[decahydro-2a,4a,6a,8a-tetraaza-pyren-2a-ium]methyl]benzyl]-decahydro-2a,4a,6a,8a-tetraaza-pyrenium tribromide (23)

Amounts: 2a-[4-[bromomethyl]benzyl]-decahydro-2a,4a,6a,8a-tetraaza-pyrenium bromide (**5**) (1.00 g, 2.18 mmol), dry acetonitrile (100 mL and 100 mL), 2a-[4-nitrobenzyl]-decahydro-2a,4a,6a,8a-tetraaza-pyrenium bromide (**6**) (895 mg, 2.18 mmol), diethyl ether (4 x 20 mL). To yield a pale brown solid (1.16g, 61 %).

^{1}H-NMR (400 MHz, D_2O, δ): 2.42-2.47 (*m,* N-α-CH_2, 3H), 2.70-2.79 (*m,* N-α-CH_2, 5H), 2.86-2.86 (*m,* N-α-CH_2, 2H), 3.01-3.58 (*br m,* N-α-CH_2, 22H), 3.67-3.72 (*m,* CH_2-Ar, 1H), 3.76 (*s,* CH_2-Ar, 1H), 3.86-3.87 (*m,* CH_2-Ar, 2H), 3.99 (*s,* CH_2-Ar, 2H), 4.07-4.16 (*m,* H_{aminal}, 2H), 4.67-4.70 (*m,* H_{aminal}, 1H), 4.90 (*d,* J=13.3 Hz, H_{aminal}, 1H), 7.37-7.44 (*m,* Ar-H, 1H), 7.69 (*d,* J=8.6 Hz, Ar-H, 2H), 7.75 (*s,* Ar-H, 1H), 7.99-8.08 (*m,* Ar-H, 2H), 8.21 (*d,* J=8.6 Hz, Ar-H, 2H). ^{13}C NMR (100 MHz, D_2O, δ): 41.34 (N-α-CH_2), 42.59 (N-α-CH_2), 43.26 (N-α-CH_2), 43.60 (N-α-CH_2), 46.31 (N-α-CH_2), 47.47 (N-α-CH_2), 47.83 (N-α-CH_2), 48.52 (N-α-CH_2), 49.42 (N-α-CH_2), 51.27 (N-α-CH_2), 51.51 (N-α-CH_2), 57.05 (N-α-CH_2), 60.16 (N-α-CH_2), 61.64 (N-α-CH_2), 69.89 (C_{aminal}), 71.52 (C_{aminal}), 73.52 (C_{aminal}), 82.88 (C_{aminal}), 123.46 (Ar-H), 123.94 (Ar-H), 124.55 (Ar-H), 130.28 (Ar-C), 131.62 (Ar-C), 133.74 (Ar-H), 133.79 (Ar-H), 149.12 (Ar-C). LRMS (*m/z*): $[M\text{-}3Br^-\text{+}H]^+$ calc for $C_{35}H_{51}N_9O_2$, 629.85; found, 629.3. HRMS: Pending data, see 8.1.3. Anal. calcd for $C_{35}H_{50}Br_3N_9$.3MeOH: C, 43.69; H, 5.98; N, 12.07. Found: C, 43.28; H, 6.37; N, 11.53.

2a-[4-[methoxycarbonyl]benzyl]-6a-[4-[[decahydro-2a,4a,6a,8a-tetraaza-pyren-2a-ium]methyl]benzyl]-decahydro-2a,4a,6a,8a-tetraaza-pyrenium tribromide (24)

Amounts: 2a-[4-[bromomethyl]benzyl]-decahydro-2a,4a,6a,8a-tetraaza-pyrenium bromide (**5**) (758 mg, 1.65 mmol), dry MeCN (20 mL), 2a-[4-[methoxycarbonyl]benzyl]-decahydro-2a,4a,6a,8a-tetraaza-pyrenium bromide (**8**) (700 mg, 1.65 mmol), dry MeCN (40 mL), diethyl ether (2 x 20 mL). To yield a white solid (867 mg, 60 %).

^{1}H-NMR (400 MHz, DMSO, δ): 2.33 (*s,* N-α-CH_2, 2H), 2.68-2.89 (*m,* N-α-CH_2, 4H), 2.99-3.17 (*m,* N-α-CH_2, 10H), 3.47-3.57 (*m,* N-α-CH_2, 6H), 3.69-3.82 (*m,* N-α-CH_2, 10H), 3.90 (*s,* CH_3-O,

3H), 4.30-4.32 (*m,* CH_2-Ar, 3H), 4.96-5.03 (*m,* CH_2-Ar, 3H), 5.08-5.11 (*m,* H_{aminal}, 2H), 5.17-5.20 (*m,* H_{aminal}, 2H), 7.78-7.95 (*m,* Ar-H, 7H), 8.12 (*d,* J=7.8 Hz, Ar-H, 1H). ^{13}C-NMR (400 MHz, DMSO, δ): 41.27 (N-α-CH_2), 41.59 (N-α-CH_2), 42.81 (N-α-CH_2), 46.77 (N-α-CH_2), 46.92 (N-α-CH_2), 48.13 (N-α-CH_2), 49.44 (N-α-CH_2), 52.21 (N-α-CH_2), 53.11 (CH_3-O), 55.32 (N-α-CH_2), 56.31 (N-α-CH_2), 56.73 (N-α-CH_2), 57.68 (N-α-CH_2), 59.49 (N-α-CH_2), 59.60 (N-α-CH_2), 61.28 (N-α-CH_2), 75.79 (C_{aminal}), 77.24 (C_{aminal}), 83.24 (C_{aminal}), 127.26 (Ar-H), 129.22 (Ar-H), 130.07 (Ar-H), 130.48 (Ar-H), 131.05 (Ar-C), 132.37 (Ar-C), 133.75 (Ar-H), 134.00 (Ar-H), 140.99 (Ar-C), 142.86 (Ar-C), 161.91 (C=O). MS (*m/z)*: $[M\text{-}3Br^{-}+Na\text{-}2H]^{+}$ calcd for $C_{37}H_{51}N_8O_2$, 662.86; found, 662.9. HRMS: Pending data, see 8.1.3. Anal. calcd for $C_{37}H_{53}Br_3N_8O_2.2EtOH$: C, 46.74; H, 6.22; N, 10.64. Found: C, 47.29; H, 6.56; N, 11.13.

2a-[4-cyanobenzyl]-6a-[4-[[decahydro-3a,5a,8a,10a-tetraaza-pyren-3a-ium]methyl]benzyl]-decahydro-2a,4a,6a,8a-tetraaza-pyrenium tribromide (25)

Amounts: 3a-[4-[bromomethyl]benzyl]-decahydro-3a,5a,8a,10a-tetraaza-pyrenium bromide **(9)** (750 mg, 1.54 mmol), dry acetonitrile (40 mL and 20 mL), 2a-[4-cyanobenzyl]-decahydro-2a,4a,6a,8a-tetraaza-pyrenium bromide (**7**) (602 mg, 1.54 mmol), diethyl ether (4 x 20 mL). To yield a white solid (1.05 g, 77 %).

^{1}H NMR (400 MHz, D_2O, δ): 1.08 (*t*, J=7.04 Hz, N-β-CH_2, 1H), 1.45 (*d*, J=13.87 Hz, N-β-CH_2, 1H), 1.72 (*d*, J=14.5 Hz, N-β-CH_2, 1H), 1.80 (*s*, H, N-β-CH_2, 1H), 2.12-2.19 (*m*, N-α-CH_2, 2H), 2.31 (*t*, N-α-CH_2, 1H), 2.44-2.50 (*m*, N-α-CH_2, 2H), 2.73-2.79 (*m*, N-α-CH_2, 1H), 2.94-3.01 (*m*, N-α-CH_2, 2H), 3.13 (*m*, N-α-CH_2, 4H), 3.35-3.38 (*m*, N-α-CH_2, 4H), 3.41-3.48 (*m*, N-α-CH_2, 5H), 3.52-3.70 (*m*, N-α-CH_2, 6H), 3.78-3.86 (*m*, N-α-CH_2, 2H), 4.15-4.27 (*m*, N-α-CH_2, 3H), 4.52 (*s*, H_{aminal}, 1H), 4.73 (*d*, J=13.5 Hz, Ar-CH_2, 2H), 4.79-4.86 (*m*, Ar-CH_2, 4H), 4.93-5.05 (*m*, H_{aminal}, 2H), 5.15 (*d*, J=13.06 Hz, H_{aminal}, 1H), 7.64-7.71 (*m*, Ar-H, 4H), 7.74 (*d*, J=8.0 Hz, Ar-H, 2H), 7.87 (*d*, J=7.5Hz, Ar-H, 2H). ^{13}C NMR (100 MHz, D_2O, δ): 17.81 (N-β-CH_2), 18.44 (N-β-CH_2), 42.10 (CH_2-Br), 42.65 (N-α-CH_2), 46.12 (N-α-CH_2), 46.44 (N-α-CH_2), 48.22 (N-α-CH_2), 51.28 (N-α-CH_2), 51.89 (N-α-CH_2), 53.01 (N-α-CH_2), 53.89 (N-α-CH_2), 54.94 (N-α-CH_2), 60.13 (N-α-CH_2), 60.34 (N-α-CH_2), 61.06 (N-α-CH_2), 61.30 (N-α-CH_2), 61.81 (N-α-CH_2), 66.08 (N-α-CH_2), 69.89 (N-α-CH_2), 77.74 (C_{aminal}), 78.24 (C_{aminal}), 82.10 (C_{aminal}), 114.10 (C≡N), 118.67 (Ar-C), 128.79 (Ar-H), 129.26 (Ar-H), 131.61 (Ar-C), 133.32 (Ar-H), 133.49 (Ar-H), 133.76 (Ar-H), 134.67 (Ar-C). MS (*m/z)*: $[M\text{-}Br^{-}]^{+}$ calcd for $C_{38}H_{54}N_9$, 796.72; found, 796.3. HRMS: Pending data, see 8.1.3. Anal. calcd for $C_{38}H_{54}Br_3N_9.5H_2O$: C, 47.21; H, 6.67; N, 13.04. Found C, 47.02; H, 5.97; N, 12.62.

2a-[4-nitrobenzyl]-6a-[4-[[decahydro-3a,5a,8a,10a-tetraaza-pyren-3a-ium]methyl]benzyl] tribromide (26)

Amounts: 3a-[4-[bromomethyl]benzyl]-decahydro-3a,5a,8a,10a-tetraaza-pyrenium bromide **(9)** (750 mg, 1.54 mmol), dry acetonitrile (40 mL and 20 mL), 2a-[4-cyanobenzyl]-decahydro-2a,4a,6a,8a-tetraaza-pyrenium bromide (**6**) (633 mg, 1.54 mmol), diethyl ether (4 x 20 mL). To yield a white solid (1.111 g, 80 %).

^{1}H NMR (400 MHz, D_2O, δ): 1.00 (*t*, J=7.0 Hz, N-β-CH_2, 1H), 1.38 (*d*, J=13.7 Hz, N-β-CH_2, 1H), 1.64 (*d*, J=14.5 Hz, N-β-CH_2, 1H), 2.03 (*d*, J=14.5 Hz, N-α-CH_2, 1H), 2.10 (*d*, J=12.2 Hz, N-α-CH_2, 1H), 2.22 (*t*, J=11.9 Hz, N-α-CH_2, 1H), 2.36-2.43 (*m*, N-α-CH_2, 2H), 2.66 (*t*, J=12.3 Hz, N-α-CH_2, 1H), 2.87-3.05 (*m*, N-α-CH_2, 10H), 3.26-3.34 (*m*, N-α-CH_2, 2H), 3.69 (*s*, N-α-CH_2, 1H), 3.79 (*t*, J=11.3 Hz, N-α-CH_2, 2H), 4.11 (*m*, CH_2-Ar, 1H), 4.18 (*m*, CH_2-Ar, 1H), 4.45 (*s*, H_{aminal}, 1H), 4.76-4.79 (*m*, CH_2-Ar, 4H), 4.91 (*d*, J=13.3 Hz, H_{aminal}, 1H), 5.00-5.09 (*m*, H_{aminal}, 2H), 7.56-7.63 (*m*, Ar-H, 4H), 7.73 (*d*, J=7.8 Hz, Ar-H, 2H), 8.23 (*d*, J=7.6 Hz, Ar-H, 2H). ^{13}C NMR (100 MHz, D_2O, δ): 17.70 (N-β-CH_2), 18.33 (N-β-CH_2), 41.99 (N-α-CH_2), 42.58 (N-α-CH_2), 46.02 (N-α-CH_2), 46.37 (N-α-CH_2), 48.20 (N-α-CH_2), 51.19 (N-α-CH_2), 51.82 (N-α-CH_2), 52.94 (N-α-CH_2), 53.82 (N-α-CH_2), 54.86 (N-α-CH_2), 59.65 (N-α-CH_2), 60.15 (N-α-CH_2), 60.98 (N-α-CH_2), 61.26 (N-α-CH_2), 61.75 (N-α-CH_2), 66.05 (N-α-CH_2), 69.79 (N-α-CH_2), 77.70 (C_{aminal}), 81.98 (C_{aminal}), 124.67 (Ar-H), 128.72 (Ar-C), 129.17 (Ar-C), 133.14 (Ar-C), 133.38 (Ar-H), 133.77 (Ar-H), 134.56 (Ar-H), 149.28 (Ar-NO_2). MS (*m/z)*: $[M\text{-}Br^-]^+$ calcd for $C_{37}H_{54}N_9O_2$, 816.71; found, 816.3. HRMS: Pending data, see 8.1.3. Anal. calcd for $C_{38}H_{54}Br_3N_9$: C, 45.51; H, 5.57; N, 12.91. Found C, 46.05; H, 6.22; N, 12.85.

2a-[4-[methoxycarbonyl]benzyl]-6a-[4-[[decahydro-3a,5a,8a,10a-tetraaza-pyren-3a-ium]methyl] benzyl]-decahydro-2a,4a,6a,8a-tetraaza-pyrenium tribromide (27)

Amounts: 3a-[4-[bromomethyl]benzyl]-decahydro-3a,5a,8a,10a-tetraaza-pyrenium bromide (**9**) (486 mg, 1.65 mmol), dry acetonitrile (20 mL and 40 mL), 2a-[4-[methoxycarbonyl]benzyl]-decahydro-2a,4a,6a,8a-tetraaza-pyrenium bromide (**8**) (700 mg, 1.65 mmol), dry acetonitrile (2 x 20 mL), diethyl ether (4 x 20 mL). To yield a white solid (633 g, 42 %).

^{1}H NMR (400 MHz, D_2O, δ): 1.30 (*m*, N-β-CH_2, 2H), 1.64 (*m*, N-β-CH_2, 2H), 1.88 (*m*, N-α-CH_2, 2H), 2.03-2.49 (*br m*, N-α-CH_2, 7H), 2.89-3.56 (*br m*, N-α-CH_2, 22H), 3.77 (*s*, O-CH_3, 3H), 4.05 (*m*, N-α-CH_2, 1H), 4.21 (*m*, CH_2-Ar, 2H), 4.71-4.77 (*m*, N-α-CH_2, 4H), 4.88-4.92 (*m*, H_{aminal}, 2H), 5.03 (*d*, J=12.9 Hz, H_{aminal}, 2H), 7.60 (*br s*, Ar-H, 6H), 7.97 (*br s*, Ar-H, 2H). ^{13}C NMR (100 MHz, D_2O, δ): 18.01 (N-β-CH_2), 18.44 (N-β-CH_2), 41.98 (N-α-CH_2), 42.66 (N-α-CH_2), 46.06 (N-α-CH_2), 46.59 (N-α-CH_2), 48.64 (N-α-CH_2), 51.35 (N-α-CH_2), 51.92 (N-α-CH_2), 53.01 (O-CH_3), 53.29 (N-α-CH_2), 53.94 (N-α-CH_2), 54.88 (N-α-CH_2), 60.12 (N-α-CH_2), 60.29 (N-α-CH_2), 61.09 (N-α-CH_2), 61.19 (N-α-CH_2), 61.63 (N-α-CH_2), 69.55 (N-α-CH_2), 77.77 (C_{aminal}),

78.01 (C_{aminal}), 82.31 (C_{aminal}), 128.94 (Ar-C), 129.09 (Ar-C), 130.51 (Ar-H), 131.29 (Ar-C), 132.07 (Ar-C), 132.76 (Ar-H), 133.36 (Ar-H), 134.56 (Ar-H), 168.34 (C=O). HRMS (*m/z)*: $[M-Br]^+$ calcd for $C_{39}H_{57}N_8O_2Br_2$, 829.2949; found, 829.2949. Anal. calcd for $C_{39}H_{57}Br_3N_8O_2$.MeCN.$4H_2O$: C, 44.66; H, 6.22; N, 11.43. Found C, 44.12; H, 6.34; N, 11.39.

8.5.3. Synthesis of 1-[4-cyanobenzyl]-7-[4-[[1,4,7,10-tetraazabicyclo[8.2.2]dodecane] methyl] benzyl]-1,4,7,10-tetraazabicyclo[5.5.2]dodecane (28), 1-[4-nitrobenzyl]-7-[4-[[1,4,7,10-tetraaza bicyclo[8.2.2]dodecane]methyl]benzyl]-1,4,7,10-tetraazabicyclo [5.5.2]dodecane (29), 1-[4-[methoxycarbonyl]benzyl-7-[4-[[1,4,7,10-tetraazabicyclo [8.2.2]dodecane]methyl] benzyl]-1,4,7,10-tetraazabicyclo[5.5.2]dodecane (30), 1-[4-cyanobenzyl]-7-[4-[[1,4,8,11-tetraazabicyclo [10.2.2] hexadecane]methyl]benzyl]-1,4,7,10-tetraazabicyclo[5.5.2]dodecane (31), 1-[4-nitrobenzyl]-7-[4-[[1,4,8,11-tetraazabicyclo [10.2.2]hexadecane]methyl]benzyl]-1,4, 7,10-tetraazabicyclo[5.5.2]dedecane (32) and attempted synthesis of 1-[4-[methoxocarbonyl]benzyl-7-[4-[[1,4,8,11-tetraazabicyclo [10.2.2]hexadecane]methyl]benzyl] -1,4,7,10-tetraazabicyclo [5.5.2]dodecane (33)

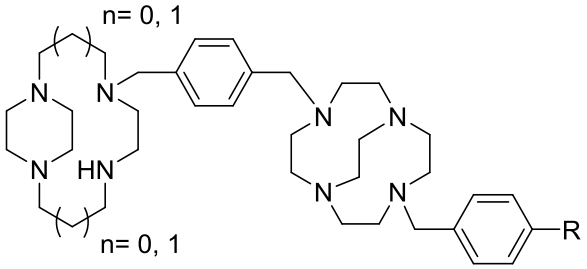

n=0		n=1	
R=CN	**28**	R=CN	**31**
$R=NO_2$	**29**	$R=NO_2$	**32**
R=COOMe	**30**	R=COOMe	**33**

General procedure F was followed

1-[4-cyanobenzyl]-7-[4-[[1,4,7,10-tetraazabicyclo[8.2.2]dodecane]methyl]benzyl]-1,4,7,10-tetraazabicyclo[5.5.2]dodecane (28)

Amounts: 2a-[4-cyanobenzyl]-6a-[4-[[decahydro-2a,4a,6a,8a-tetraaza-pyren-2a-ium]methyl]benzyl]-decahydro-2a,4a,6a,8a-tetraaza-pyrenium tribromide (**22**) (1.24 g, 1.46 mmol), ethanol (65 mL), sodium borohydride (1.66 g, 43.84 mmol), aqueous hydrochloric acid (2 M, 18 mL), water (60 mL), dichoromethane (5 x 50 mL). To yield a yellow oil (557 mg, 62 %).

^{1}H NMR (400 MHz, $CDCl_3$, δ): 2.20-3.12 (*br m,* N-α-CH_2, 38H), 3.20-3.38 (*m,* N-α-CH_2, 2H), 3.48-3.77 (*m,* CH_2-Ar, 6H), 3.85-4.00 (*m,* NH, 1H), 7.17-7.21 (*m,* Ar-H, 3H), 7.24 (*m,* Ar-H, 1H), 7.35 (*d,* J=7.8 Hz, Ar-H, 2H), 7.5 (*d,* J=8.8 Hz, Ar-H, 2H). ^{13}C NMR (100 MHz, $CDCl_3$, δ): 41.04 (N-α-CH_2), 43.13 (N-α-CH_2), 45.72 (N-α-CH_2), 46.90 (N-α-CH_2), 48.48 (N-α-CH_2), 49.10 (N-α-CH_2), 49.65 (N-α-CH_2), 50.37 (N-α-CH_2), 51.51 (N-α-CH_2), 52.64 (N-α-CH_2), 53.08 (N-α-CH_2), 53.56 (N-α-CH_2), 54.45 (N-α-CH_2), 56.30 (N-α-CH_2), 56.58 (N-α-CH_2), 57.06 (N-α-CH_2), 57.35 (N-α-CH_2), 57.80 (N-α-CH_2), 58.26 (N-α-CH_2), 59.97 (N-α-CH_2), 60.78 (N-α-CH_2), 110.48 (CN), 119.12 (Ar-C), 128.77 (Ar-H), 129.39 (Ar-H), 132.09 (Ar-H), 132.51 (Ar-H), 137.97 (Ar-C), 138.74 (Ar-C), 146.40 (Ar-C). MS (*m/z*): $[M+NH_4-3H]^+$ calcd for $C_{36}H_{56}N_{10}$

628.92; found, 628.6, $[M+NH_4-3H]^+$, $[M+NH_4-3H]^+$ calcd for $C_{36}H_{54}K_3N_9$ 730.19; found, 730.6. HRMS: Pending data, see 8.1.3.

1-[4-nitrobenzyl]-7-[4-[[1,4,7,10-tetraazabicyclo[8.2.2]dodecane]methyl]benzyl]-1,4,7,10-tetraazabicyclo[5.5.2]dodecane (29)

Amounts: 2a-[4-nitrobenzyl]-6a-[4-[[decahydro-2a,4a,6a,8a-tetraaza-pyren-2a-ium]methyl]benzyl]-decahydro-2a,4a,6a,8a-tetraaza-pyrenium tribromide (**23**) (599 mg, 0.69 mmol), ethanol (35 mL), sodium borohydride (783 mg, 20.70 mmol), aqueous hydrochloric acid (2 M, 10 mL), water (20 mL), dichoromethane (5 x 20 mL). To yield a yellow oil (300 mg, 69 %).

^{1}H NMR (400 MHz, MeOD, δ): 2.29-2.65 (*br m,* N-α-CH_2, 15H), 2.68-2.76 (*m,* N-α-CH_2, 5H), 2.90-3.19 (*m,* N-α-CH_2, 20H), 3.36-3.60 (*m,* CH_2-Ar, 3H), 3.68-3.84 (*m,* CH_2-Ar, 2H), 3.79-4.05 (*m,* CH_2-Ar, 1H), 4.16-4.19 (*m,* NH*,* 1H), 7.20-7.28 (*m,* Ar-H, 2H), 7.32-7.69 (*m,* Ar-H, 4H), 8.15-8.28 (*m,* Ar-H, 2H). ^{13}C NMR (100 MHz, MeOD, δ): 39.32 (N-α-CH_2), 42.81 (N-α-CH_2), 44.70 (N-α-CH_2), 46.72 (N-α-CH_2), 48.87 (N-α-CH_2), 49.33 (N-α-CH_2), 49.89 (N-α-CH_2), 51.05 (N-α-CH_2), 51.29 (N-α-CH_2), 52.24 (N-α-CH_2), 53.14 (N-α-CH_2), 53.39 (N-α-CH_2), 53.77 (N-α-CH_2), 56.22 (N-α-CH_2), 57.27 (N-α-CH_2), 58.25 (N-α-CH_2), 59.07 (N-α-CH_2), 59.58 (N-α-CH_2), 60.37 (N-α-CH_2), 63.08 (N-α-CH_2), 123.20 (Ar-H), 123.49 (Ar-H), 127.01 (Ar-H), 128.84 (Ar-H), 129.10 (Ar-H), 129.41 (Ar-H), 129.67 (Ar-H), 138.14 (Ar-H), 138.60 (Ar-H), 138.91 (Ar-C), 146.53 (Ar-C), 147.05 (Ar-C), 147.35 (Ar-C). MS (*m/*z): $[M-H]^+$ calcd for $C_{35}H_{54}N_9O_2$, 632.88; found, 632.2. HRMS: Pending data, see 8.1.3. Anal. calcd for $C_{35}H_{55}N_9O_2$.2.5EtOH: C, 64.49; H, 9.57; N, 16.51. Found: C, 64.41; H, 9.19; N, 16.49.

1-[4-[methoxycarbonyl]benzyl]-7-[4-[[1,4,7,10-tetraazabicyclo[8.2.2]dodecane]methyl]benzyl]-1,4,7,10-tetraazabicyclo[5.5.2]dodecane (30)

Amounts: 2a-[4-[methoxycarbonyl]benzyl]-6a-[4-[[decahydro-2a,4a,6a,8a-tetraaza-pyren-2a-ium]methyl]benzyl]-decahydro-2a,4a,6a,8a-tetraaza-pyrenium tribromide (**24**) (790 mg, 0.90 mmol), ethanol (50 mL), sodium borohydride (1.02 mg, 26.87 mmol), aqueous hydrochloric acid (2 M, 10 mL), water (30 mL), dichoromethane (5 x 25 mL). To yield a yellow oil (260 mg, 45 %).

^{1}H NMR (400 MHz, $CDCl_3$, δ): 2.21-2.40 (*m,* N-α-CH_2, 4H), 2.47 (*br s,* N-α-CH_2, 2H), 2.62-2.83 (*br m,* N-α-CH_2, 26H), 3.02-3.08 (*m,* N-α-CH_2, 8H), 3.12-3.19 (*m,* CH_2-Ar, 2H), 3.49-3.54 (*m,* CH_2-Ar, 1H), 3.61 (*s,* CH_2-Ar, 1H), 3.66 (*s,* CH_3-O, 3H), 3.73 (*s,* CH_2-Ar, 1H), 3.86 (*s,* CH_2-Ar, 1H), 4.30-4.35 (*m,* NH*,* 1H), 7.19-7.22 (*m,* Ar-H, 6H), 7.34 (*d,* J=8.2 Hz, Ar-H, 1H), 7.95 (*d,* J=8.2 Hz, Ar-H, 1H). ^{13}C NMR (100 MHz, $CDCl_3$, δ): 45.70 (N-α-CH_2), 47.32 (N-α-CH_2), 48.61 (N-α-CH_2), 48.99 (N-α-CH_2), 49.06 (N-α-CH_2), 50.17 (N-α-CH_2), 50.49 (N-α-CH_2), 51.88 (CH_3-O), 52.06 (N-α-CH_2), 52.24 (N-α-CH_2), 56.31 (N-α-CH_2), 57.51

(N-α-CH_2), 57.67 (N-α-CH_2), 57.81 (N-α-CH_2), 59.76 (N-α-CH_2), 59.97 (N-α-CH_2), 59.97 (N-α-CH_2), 60.87 (N-α-CH_2), 60.97 (N-α-CH_2), 126.81 (Ar-H), 128.74 (Ar-H), 128.89 (Ar-H), 129.55 (Ar-H), 138.28 (Ar-C), 138.78 (Ar-C), 139.04 (Ar-C), 145.95 (Ar-C), 166.69 (C=O). HRMS (*m/*z): $[M+H^+]^+$calcd for $C_{37}H_{59}N_8O_2$, 647.4755; found, 647.4754.

1-[4-cyanobenzyl]-7-[4-[[1,4,8,11-tetraazabicyclo[10.2.2]hexadecane]methyl]benzyl]-1,4,7,10-tetraazabicyclo[5.5.2]dodecane (31)

Amounts: 2a-[4-cyanobenzyl]-6a-[4-[[decahydro-3a,5a,8a,10a-tetraaza-pyren-3a-ium]methyl]benzyl]-decahydro-2a,4a,6a,8a-tetraaza-pyrenium tribromide (**25**) (2.00 g, 2.28 mmol), ethanol (120 mL), sodium borohydride (2.59 g, 68.44 mmol), 2 M aqueous hydrochloric acid (40 mL), water (40 mL), dichoromethane (5 x 25 mL). To yield a yellow oil (999 mg, 68 %).

^{1}H NMR (400 MHz, MeOD, δ): 1.40-1.72 (*m,* N-β-CH_2, 4H), 2.58-3.13 (*m,* N-β-CH_2, 36H), 3.29-3.58 (*m,* N-α-CH_2, 1H), 3.74-3.79 (*m,* N-α-CH_2, 1H), 3.97-4.00 (*m,* N-α-CH_2, 1H), 4.07-4.12 (*m,* N-α-CH_2, 1H), 4.54-4.62 (*br s,* NH, 1H), 4.86-4.91 (*m,* CH_2-Ar, 6H), 7.30 (*m,* Ar-H, 3H), 7.43-7.50 (*m,* Ar-H, 1H), 7.56-7.70 (*m,* Ar-H, 4H). ^{13}C NMR (100 MHz, MeOD, δ): 22.96 (N-β-CH_2), 25.33 (N-β-CH_2), 46.70 (N-α-CH_2), 48.90 (N-α-CH_2), 50.06 (*d,* J=13.1 Hz, N-α-CH_2), 50.50 (N-α-CH_2), 50.78 (N-α-CH_2), 51.23 (*d,* J=7.7 Hz, N-α-CH_2), 51.62 (N-α-CH_2), 53.30 (N-α-CH_2), 54.77 (N-α-CH_2), 55.11 (N-α-CH_2), 55.47 (N-α-CH_2), 55.80 (N-α-CH_2), 56.02 (N-α-CH_2), 56.41 (N-α-CH_2), 56.58 (N-α-CH_2), 56.68 (N-α-CH_2), 57.08 (*d,* J=14.6 Hz, N-α-CH_2), 57.45 (N-α-CH_2), 58.54 (N-α-CH_2), 58.54 (N-α-CH_2), 59.38 (N-α-CH_2), 60.63 (N-α-CH_2), 118.54 (C≡N), 126.83 (Ar-H), 129.02 (Ar-H), 129.51 (Ar-H), 129.70 (Ar-H), 129.97 (Ar-H), 130.26 (Ar-H), 130.42 (Ar-C), 131.97 (Ar-H), 132.28 (Ar-H), 137.08 (Ar-C), 144.35 (Ar-C), 146.35 (Ar-C). HRMS (*m/z*): $[M+H^+]^+$ calcd for $C_{38}H_{60}N_9$, 642.4966; found, 642.4957. Anal. calcd for $C_{38}H_{59}N_9.4H_2O$: C, 63.92; H, 9.46; N, 17.66. Found: C, 63.42; H, 8.94; N, 16.84.

1-[4-nitrobenzyl]-7-[4-[[1,4,8,11-tetraazabicyclo[10.2.2]hexadecane]methyl]benzyl]-1,4,7,10-tetraazabicyclo[5.5.2]dodecane (32)

Amounts: 2a-[4-nitrobenzyl]-6a-[4-[[decahydro-3a,5a,8a,10a-tetraaza-pyren-3a-ium]methyl]benzyl]-decahydro-2a,4a,6a,8a-tetraaza-pyrenium tribromide (**26**) (1.84 g, 2.05 mmol), ethanol (100 mL), sodium borohydride (2.32 g, 61.56 mmol), aqueous hydrochloric acid (2 M, 25 mL), water (20 mL), dichloromethane (5 x 50 mL). To yield a yellow oil (1.082 g, 80 %).

^{1}H NMR (400 MHz, MeOD, δ): 1.26-1.73 (*m,* N-β-CH_2, 4H), 2.02-3.26 (*br m,* N-α-CH_2, 40H), 3.51-4.04 (*m,* CH_2-Ar, 6H), 4.14-4.18 (*m,* NH, 1H), 7.16-7.43 (*m,* Ar-H, 4H), 7.51-7.68 (*m,* Ar-H, 2H), 8.14-8.26 (*m,* Ar-H, 2H). ^{13}C NMR (100 MHz, MeOD, δ): 19.19 (N-β-CH_2), 20.05 (N-β-CH_2), 21.97 (N-β-CH_2),

22.97 (N-β-CH_2), 25.18 (N-β-CH_2), 25.34 (N-β-CH_2), 46.65 (N-α-CH_2), 50.04 (N-α-CH_2), 50.55 (N-α-CH_2), 50.81 (N-α-CH_2), 51.07 (N-α-CH_2), 51.48 (N-α-CH_2), 53.66 (N-α-CH_2), 55.14 (N-α-CH_2), 55.81 (N-α-CH_2), 55.95 (N-α-CH_2), 56.07 (N-α-CH_2), 56.17 (N-α-CH_2), 56.65 (N-α-CH_2), 56.96 (N-α-CH_2), 57.18 (N-α-CH_2), 57.33 (N-α-CH_2), 58.97 (N-α-CH_2), 60.18 (N-α-CH_2), 61.49 (N-α-CH_2), 62.72 (N-α-CH_2), 123.17 (Ar-H), 123.17 (Ar-H), 123.48 (Ar-H), 126.97 (Ar-H), 129.04 (Ar-H), 129.26 (Ar-C), 129.62 (Ar-H), 129.98 (Ar-H), 139.05 (Ar-C), 146.44 (Ar-H), 147.04 (Ar-H), 147.38 (Ar-C), 148.41 (Ar-C). HRMS (*m/z*): $[M+H^+]^+$ calcd for $C_{37}H_{60}N_9O_2$, 662.4864; found: 662.4851. Anal. calcd for $C_{37}H_{59}N_9O_2$: C, 67.14; H, 8.98; N, 19.04. Found: C, 54.49; H, 8.37; N, 15.42 – contains impurity.

1-[4-[methoxycarbonyl]benzyl]-7-[4-[[1,4,8,11-tetraazabicyclo[10.2.2]hexadecane]methyl]benzyl]-1,4,7,10-tetraazabicyclo[5.5.2]dodecane (33)

Amounts: 2a-[4-[methoxycarbonyl]benzyl]-6a-[4-[[decahydro-3a,5a,8a,10a-tetraaza-pyren-3a-ium] methyl]benzyl]-decahydro-2a,4a,6a,8a-tetraaza-pyrenium tribromide (**27**) (1 g, 1.10 mmol), ethanol (100 mL), sodium borohydride (1.25 g, 32.98 mmol), aqueous hydrochloric acid (2 M, 25 mL), water (100 mL), dichloromethane (5 x 50 mL). To yield a yellow oil (502 mg). Analytical data indicates that the desired product was not obtained.

^{1}H NMR (400 MHz, $CDCl_3$, δ): 1.12-1.17 (*m,* CH_3, 3H), 1.47-1.54 (*m,* N-β-CH_2, 4H), 1.98-2.00 (*m,* N-α-CH_2, 2H), 2.08-2.11 (*m,* N-α-CH_2, 1H), 2.17-2.22 (*m,* N-α-CH_2, 2H), 2.30-2.46 (*m,* N-α-CH_2, 13H), 2.55-2.70 (*m,* N-α-CH_2, 7H), 2.78-3.06 (*m,* N-α-CH_2, 13H), 3.11-15 (*m,* N-α-CH_2, 3H), 3.26-3.52 (*m,* Ar-H, 4H), 3.74-3.82 (*m,* Ar-H, 2H), 4.08-4.15 (*m,* NH, 1H), 5.08 (*s,* CH_2-O, 2H), 6.92-7.14 (*m,* Ar-H, 5H), 7.23-7.25 (*m,* Ar-H, 1H), 7.73-7.75 (*m,* Ar-H, 1H), 7.80 (*d,* J=8.2 Hz, Ar-H, 1H). ^{13}C NMR (100 MHz, $CDCl_3$, δ): 14.29 (CH_3), 26.02 (N-β-CH_2), 28.04 (N-β-CH_2), 44.82 (N-α-CH_2), 48.12 (N-α-CH_2), 50.65 (N-α-CH_2), 50.96 (CH_2-O), 52.06 (N-α-CH_2), 52.54 (N-α-CH_2), 54.41 (N-α-CH_2), 54.79 (N-α-CH_2), 54.89 (N-α-CH_2), 54.96 (N-α-CH_2), 55.36 (N-α-CH_2), 55.45 (N-α-CH_2), 55.54 (N-α-CH_2), 55.61 (N-α-CH_2), 56.12 (N-α-CH_2), 56.57 (N-α-CH_2), 57.00 (N-α-CH_2), 57.41 (N-α-CH_2), 57.87 (N-α-CH_2), 59.72 (N-α-CH_2), 60.84 (N-α-CH_2), 126.52 (Ar-H), 126.74 (Ar-H), 126.90 (Ar-H), 127.86 (Ar-H), 128.72 (Ar-H), 129.01 (Ar-C), 129.52 (Ar-H), 129.64 (Ar-C), 136.50 (Ar-C), 145.86 (Ar-CO), 166.61 (C=O). HRMS (*m/z*): $[M+H^+]^+$ calcd for $C_{40}H_{65}N_8O_2$, 689.5225; found: 689.5223 Anal. calcd for $C_{40}H_{64}N_8O_2.2EtOH.4H_2O$: C, 61.55; H, 9.85; N, 13.35. Found: C, 61.39; H, 9.93; N, 13.86.

8.5.4. Synthesis of 1-[4-[aminomethyl]benzyl]-7-[4-[[1,4,7,10-tetraazabicyclo[8.2.2]dodecane] methyl]benzyl]-1,4,7,10-tetraazabicyclo[5.5.2]dodecane (34) and 1-[4-[aminomethyl]benzyl]-7-[4-[[1,4,8,11-tetraazabicyclo[10.2.2]hexadecane]methyl]benzyl]-1,4,7,10-tetraazabicyclo [5.5.2]dodecane (35)

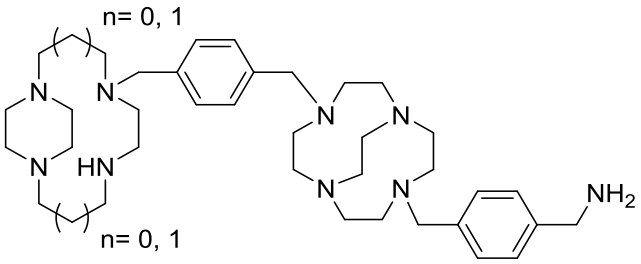

n=0 **34**
n=1 **35**

General procedure J

Macrocycle in dry tetrahydrofuran was added to a suspension of lithium aluminium hydride in dry tetrahydrofuran at 0°C. Once completely added the mixture was stirred for 30 min and then heated at reflux for 3 h. The reaction was cooled in an ice bath and portions of water, 15 % sodium hydroxide solution and water were added respectively dropwise. The resulting white precipitate was filtered, washed with tetrahydrofuran and water before being made strongly basic (KOH, pH 14). The aqueous layer was extracted with tetrahydrofuran, the organic phase dried (Na_2SO_4), filtered and concentrated *in vacuo*.

1-[4-[aminomethyl]benzyl]-7-[4-[[1,4,7,10-tetraazabicyclo[8.2.2]dodecane]methyl]benzyl]-1,4,7,10-tetraazabicyclo[5.5.2]dodecane (34)

Amounts: 1-[4-cyanobenzyl]-7-[4-[[1,4,7,10-tetraazabicyclo[8.2.2]dodecane]methyl]benzyl]-1,4,7,10-tetraazabicyclo[5.5.2]dodecane (**28**) (91 mg, 0.15 mmol), dry tetrahydrofuran (3 mL and 1 mL), lithium aluminium hydride (14 mg, 0.37 mmol), water (14.5 μL and 43 μL), 15 % sodium hydroxide solution (14.5 μL). To yield a yellow oil (6 mg, 7 %).

^{1}H NMR (400 MHz, MeOD, δ): 2.07-2.17 (*m,* N-α-CH_2, 1H), 2.42-3.16 (*br m,* N-α-CH_2, 44H), 3.57-3.58 (*m,* N-α-CH_2, 3H), 3.79-3.91 (*m,* NH_2, 2H), 4.00-4.05 (*m,* NH, 1H), 7.28-7.41 (*m,* Ar-H, 8H). ^{13}C NMR (100 MHz, MeOD, δ): 42.74 (N-α-CH_2), 43.73 (N-α-CH_2), 44.13 (N-α-CH_2), 44.57 (N-α-CH_2), 45.15 (N-α-CH_2), 45.62 (N-α-CH_2), 45.94 (N-α-CH_2), 46.71 (N-α-CH_2), 48.81 (N-α-CH_2), 49.78 (N-α-CH_2), 50.58 (N-α-CH_2), 50.91 (N-α-CH_2), 51.16 (N-α-CH_2), 52.20 (N-α-CH_2), 53.59 (N-α-CH_2), 53.78 (N-α-CH_2), 55.71 (N-α-CH_2), 56.15 (N-α-CH_2), 57.19 (N-α-CH_2), 58.68 (N-α-CH_2), 59.53 (N-α-CH_2), 61.49 (N-α-CH_2), 63.67 (N-α-CH_2), 124.84 (Ar-H), 127.08 (Ar-H), 127.42 (Ar-H), 128.13 (Ar-H), 128.98 (Ar-H), 129.03 (Ar-H), 129.17 (Ar-H), 136.88 (Ar-H), 137.94 (Ar-C), 138.36 (Ar-C), 141.34 (Ar-C), 141.88 (Ar-C). MS

(*m/z*): $[M+H]^+$ calcd for $C_{36}H_{60}N_9$, 618.94; found, 618.70. HRMS (*m/z*): $[M-NH_2]^+$ calcd for $C_{36}H_{57}N_8$, 601.4701; found, 601.4696.

1-[4-[aminomethyl]benzyl]-7-[4-[[1,4,8,11-tetraazabicyclo[10.2.2]hexadecane]methyl]benzyl]-1,4,7,10-tetraazabicyclo[5.5.2]dodecane (35)

Amounts: 1-[4-cyanobenzyl]-7-[4-[[1,4,8,11-tetraazabicyclo[10.2.2]hexadecane]methyl]benzyl]-1,4,7,10-tetraazabicyclo[5.5.2]dodecane (**31**) (852 mg, 0.91 mmol), dry tetrahydrofuran (15 mL and 5 mL), lithium aluminium hydride (56 mg, 2.26 mmol), water (65 μL and 195 μL), 15 % sodium hydroxide solution (65 μL). To yield a yellow oil (272 mg, 46 %).

^{1}H NMR (400 MHz, MeOD, δ) 1.73 (*br s,* N-β-CH_2, 4H), 2.13-3.26 (*br m,* N-α-CH_2, 44H), 3.48-3.65 (*m,* N-α-CH_2, 3H), 3.79-3.83 (*m,* N-α-CH_2, 1H), 3.99-4.05 (*m,* NH_2, 2H), 4.76 (*m,* NH, 1H), 7.21-7.32 (*m,* Ar-H, 5H), 7.39-7.41 (*m,* Ar-H, 2H), 7.72-7.85 (*m,* Ar-H, 1H). ^{13}C NMR (100 MHz, MeOD, δ): 22.95 (N-β-CH_2), 28.61 (N-β-CH_2), 45.16 (N-α-CH_2), 46.62 (N-α-CH_2), 49.99 (N-α-CH_2), 50.55 (N-α-CH_2), 51.21 (N-α-CH_2), 53.60 (N-α-CH_2), 54.77 (N-α-CH_2), 55.05 (N-α-CH_2), 55.18 (N-α-CH_2), 55.33 (N-α-CH_2), 56.17 (N-α-CH_2), 56.64 (N-α-CH_2), 56.76 (N-α-CH_2), 57.28 (N-α-CH_2), 57.37 (N-α-CH_2), 59.54 (N-α-CH_2), 61.43 (N-α-CH_2), 64.21 (N-α-CH_2), 124.82 (Ar-H), 127.01 (Ar-H), 127.80 (Ar-H), 128.19 (Ar-H), 128.85 (Ar-H), 129.19 (Ar-H), 129.29 (Ar-H), 129.48 (Ar-H), 129.90 (Ar-H), 136.59 (Ar-H), 137.25 (Ar-C), 137.96 (Ar-C), 139.07 (Ar-C), 144.79 (Ar-C). MS (*m/z*): $[M]^+$ calcd for $C_{38}H_{64}N_9$, 645.99; found, 645.60. HRMS (*m/z*): $[M+H]^+$ calcd for $C_{38}H_{64}N_9$, 646.5279; found, 646.5268, $[M]^+$ calcd for $C_{38}H_{63}N_9$, 645.5201; found, 645.4953.

8.5.5. Synthesis of 1-[4-aminobenzyl]-7-[4-[[1,4,7,10-tetraazabicyclo[8.2.2]dodecane]methyl] benzyl]-1,4,7,10-tetraazabicyclo[5.5.2]dodecane (36) and 1-[4-aminobenzyl]-7-[4-[[1,4,8,11-tetraazabicyclo[10.2.2]hexadecane]methyl]benzyl]-1,4,7,10-tetraazabicyclo[5.5.2]dodecane (37)

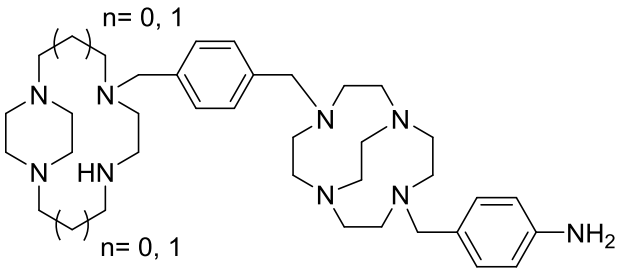

n=0 **36**
n=1 **37**

Method 1 – Attempted synthesis of 36

General procedure K

Macrocycle was dissolved in ethanol and 10 % palladium on carbon was added. The solution was hydrogenated for 4 h after which the solution was filtered through high flow super cell and washed with ethanol. The solvent was then removed *in vacuo*.

1-[4-aminobenzyl]-7-[4-[[1,4,7,10-tetraazabicyclo[8.2.2]dodecane]methyl]benzyl]-1,4,7,10-tetraazabicyclo[5.5.2]dodecane (36)

Amounts: 1-[4-[aminomethyl]benzyl]-7-[4-[[1,4,7,10-tetraazabicyclo[8.2.2]dodecane]methyl]benzyl]-1,4,7,10-tetraazabicyclo[5.5.2]dodecane (**29**), ethanol (200 mL), (934 mg, 1.47 mmol), 10% palladium on activated carbon (471 mg, 4.43 mmol), ethanol (8 x 20 mL). To yield a yellow oil (641 mg). Analytical data indicates that the desired product was not obtained.

1-[4-aminobenzyl]-7-[4-[[1,4,8,11-tetraazabicyclo[10.2.2]hexadecane]methyl]benzyl]-1,4,7,10-tetraazabicyclo[5.5.2]dodecane (37)

Amounts: 1-[4-nitrobenzyl]-7-[4-[[1,4,8,11-tetraazabicyclo[10.2.2]hexadecane]methyl]benzyl]-1,4,7,10-tetraazabicyclo[5.5.2]dodecane (**32**) (684 mg, 1.033 mmol), ethanol (120 mL), 10 % palladium on carbon (330 mg 10 %), ethanol (8 x 20 mL). To yield a yellow oil (629 mg, 96 %).

^{1}H NMR (400 MHz, MeOD, δ): 1.74 (*br s,* N-β-CH_2, 4H), 2.03-3.12 (*br m,* N-α-CH_2, 40H), 3.71-3.93 (*m,* CH_2-Ar, 6H), 3.99-4.11 (*m,* NH_2, 2H), 4.43-4.61 (*m,* NH, 1H), 6.62-6.75 (*m,* Ar-H, 1H), 7.08 (*d,* J=8.0 Hz, Ar-H, 1H) 7.16-7.47 (*m,* Ar-H, 5H), 7.59-7.65 (*m,* Ar-H, 1H). ^{13}C NMR (100 MHz, MeOD, δ): 22.88 (N-β-CH_2), 25.26 (N-β-CH_2), 45.08 (N-α-CH_2), 46.69 (N-α-CH_2), 49.96 (N-α-CH_2), 50.48 (N-α-CH_2), 51.42 (N-α-CH_2), 52.95 (N-α-CH_2), 52.95 (N-α-CH_2), 54.44 (N-α-CH_2), 55.07 (N-α-CH_2), 56.18 (N-α-CH_2), 57.00 (N-α-CH_2), 58.71 (N-α-CH_2), 115.02 (Ar-H), 125.63 (Ar-C), 129.27 (Ar-H), 130.11 (Ar-H), 147.35 (Ar-C). HRMS (*m/z*): $[M+H]^+$ calcd for $C_{37}H_{62}N_9$, 632.5123; found, 632.5135.

Method 2 – Preferred route

General procedure L

Macrocycle was dissolved in ethanol and 10 % palladium on carbon was added. The solution was placed under an atmosphere of hydrogen for 4 h after which the solution was filtered through high flow super cell and washed with ethanol. The solvent was then removed *in vacuo*.

1-[4-aminobenzyl]-7-[4-[[1,4,7,10-tetraazabicyclo[8.2.2]dodecane]methyl]benzyl]-1,4,7,10-tetraazabicyclo[5.5.2]dodecane (36)

Amounts: 1-[4-[aminomethyl]benzyl]-7-[4-[[1,4,7,10-tetraazabicyclo[8.2.2]dodecane]methyl]benzyl]-1,4,7,10-tetraazabicyclo[5.5.2]dodecane (**29**), ethanol (50 mL), (189 mg, 0.30 mmol), 10% palladium on activated carbon (95 mg, 0.90 mmol), ethanol (8 x 20 mL). To yield a yellow oil (135 mg, 73 %).

^{1}H NMR (400 MHz, MeOD, δ): 1.76-1.88 (*m,* N-α-CH_2, 1H), 2.21-3.14 (*br m,* N-α-CH_2, 32H), 3.30 (*m,* N-α-CH_2, 2H), 3.49 (*m,* N-α-CH_2, 3H), 4.61-4.01 (*m,* N-α-CH_2, 10H), 4.42-4.59 (*m,* NH_2, 2H), 6.73 (m, Ar-H, 1H), 7.40 (*m*, Ar-H, 7H). - Missing one NH proton. ^{13}C NMR (100 MHz, MeOD, δ): 44.07 (N-α-CH_2), 45.08 (N-α-CH_2), 45.36 (N-α-CH_2), 46.76 (N-α-CH_2), 50.21 (N-α-CH_2), 51.20 (N-α-CH_2), 53.93 (N-α-CH_2), 54.76 (N-α-CH_2), 56.19 (N-α-CH_2), 58.38 (N-α-CH_2), 61.80 (N-α-CH_2), 63.51 (N-α-CH_2), 126.98 (Ar-H), 129.09 (Ar-H), 129.32 (Ar-H), 130.04 (Ar-H), 137.77 (Ar-C), 138.31 (Ar-C), 141.06 (Ar-C).
HRMS (*m/z*): $[M+2Na-2H]^+$ calcd for $C_{35}H_{55}N_9Na_2$, 647.4376; found, 647.5112.

8.5.6. Synthesis of 1-[4-azidobenzyl]-7-[4-[[1,4,7,10-tetraazabicyclo[8.2.2]dodecane]methyl]benzyl]-1,4,7,10-tetraazabicyclo[5.5.2]dodecane (38) and 1-[4-azidobenzyl]-7-[4-[[1,4,8,11-tetraazabicyclo[10.2.2]hexadecane]methyl]benzyl]-1,4,7,10-tetraazabicyclo[5.5.2]dodecane (39)

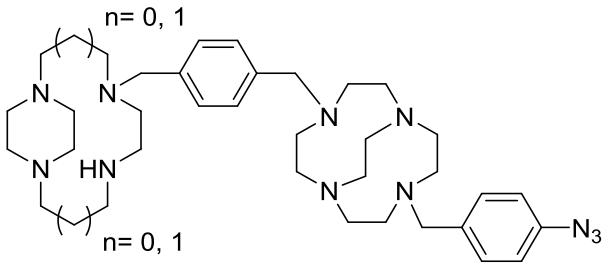

n=0 **38** n=1 **39**

General procedure M

A solution of sodium nitrite in water was slowly added to a solution of macrocycle in concentracted hydrochloric acid cooled to 0-5^{o}C. The solution was stirred at 0-5^{o}C for 1 h before sodium azide in water was slowly added at 0-5^{o}C. The solvent was removed *in vacuo,* the residue taken up in water, made basic (KOH, pH 14) and extracted with dichloromethane. The combined organic layers were dried (Na_2SO_4) and the solvent removed *in vacuo*.

1-[4-azidobenzyl]-7-[4-[[1,4,7,10-tetraazabicyclo[8.2.2]dodecane]methyl]benzyl]-1,4,7,10-tetraazabicyclo[5.5.2]dodecane (38)

1-[4-aminobenzyl]-7-[4-[[1,4,7,10-tetraazabicyclo[8.2.2]dodecane]methyl]benzyl]-1,4,7,10-tetraazabicyclo[5.5.2]dodecane (**36**) (61 mg, 0.10 mmol), concentrated hydrochloric acid (1 mL), sodium nitrite (8 mg, 0.10 mmol), water (1.5 mL and 1 mL), sodium azide (7 mg, 0.10 mmol), dichloromethane (5 x 5 mL). To yield a yellow solid (16 mg, 25 %).

^{1}H NMR (400 MHz, $CDCl_3$, δ): 1.69-1.73 (*m,* N-α-CH_2, 2H), 2.17-3.59 (*br m,* N-α-CH_2, 38H), 3.61-4.12 (*br m,* CH_2-Ar, 6H), 4.64 (*m,* NH, 1H), 6.95-7.22 (*m,* Ar-H, 5H), 7.28-7.52 (*m,* Ar-H, 3H). ^{13}C NMR (100 MHz, $CDCl_3$, δ): 44.91 (N-α-CH_2), 48.18 (N-α-CH_2), 49.02 (N-α-CH_2), 50.64 (N-α-CH_2), 51.31 (N-α-CH_2), 52.63 (N-α-CH_2), 53.51 (N-α-CH_2), 54.31 (N-α-CH_2), 54.51 (N-α-CH_2), 55.57 (N-α-CH_2), 56.20 (N-α-CH_2), 56.32 (N-α-CH_2), 57.09 (N-α-CH_2), 58.08 (N-α-CH_2), 59.58 (N-α-CH_2), 61.10 (N-α-CH_2), 62.94 (N-α-CH_2), 119.00 (Ar-H), 126.96 (Ar-C), 128.77 (Ar-H), 128.88 (Ar-H), 129.13 (Ar-H), 129.35 (Ar-H), 129.52 (Ar-H), 130.12 (Ar-C), 130.35 (Ar-C). HRMS (*m/z*): $[M+H^+]^+$ calcd for $C_{35}H_{59}N_{12}$, 647.4986; found, 647.5109.

1-[4-azidobenzyl]-7-[4-[[1,4,8,11-tetraazabicyclo[10.2.2]hexadecane]methyl]benzyl]-1,4,7,10-tetraazabicyclo[5.5.2]dodecane (39)

Amounts: sodium nitrite (33 mg, 0.47 mmol), water (4 mL), 1-[4-aminobenzyl]-7-[4-[[1,4,8,11-tetraazabicyclo[10.2.2]hexadecane]methyl]benzyl]-1,4,7,10-tetraazabicyclo[5.5.2]dodecane (**37**) (300 mg, 0.47 mmol), concentrated hydrochloric acid (2 mL), sodium azide (31 mg, 0.47 mmol), water (4 mL), water (10 mL), dichloromethane (5 x 10 mL). To yield a yellow oil (73 mg, 23 %).

^{1}H NMR (400 MHz, MeOH, δ): 1.28 (*br s*, N-β-CH_2, 2H), 1.75 (*br s*, N-β-CH_2, 2H), 2.18-2.23 (*m,* N-α-CH_2, 2H), 2.33-2.75 (*br m,* N-α-CH_2, 17H), 2.93-3.25 (*br m,* N-α-CH_2, 16H), 3.44-4.13 (*m,* N-α-CH_2, 16H), 4.44-4.59 (*m,* NH, 2H), 7.03-7.14 (*m,* Ar-H, 2H), 7.31-7.71 (*m,* Ar-H, 2H). ^{13}C NMR (100 MHz, MeOD, δ): 22.92 (N-β-CH_2), 25.28 (N-β-CH_2), 46.76 (N-α-CH_2), 49.87 (N-α-CH_2), 50.47 (N-α-CH_2), 51.13 (N-α-CH_2), 51.52 (N-α-CH_2), 53.76 (N-α-CH_2), 54.04 (N-α-CH_2), 54.73 (N-α-CH_2), 54.99 (N-α-CH_2), 55.14 (N-α-CH_2), 55.34 (N-α-CH_2), 56.10 (N-α-CH_2), 56.60 (N-α-CH_2), 56.79 (N-α-CH_2), 125.66 (Ar-H), 128.50 (Ar-H), 128.83 (Ar-H), 128.83 (Ar-H), 129.04 (Ar-H), 129.48 (Ar-H), 129.90 (Ar-H), 130.58 (Ar-C), 135.21 (Ar-C), 137.31 (Ar-C). HRMS (*m/z*): $[M+H^+]^+$ calcd for $C_{37}H_{60}N_{11}$, 658.5028; found, 658.5026.

8.5.7. Attempted conjugation of 1-[4-azidobenzyl]-7-[4-[[1,4,8,11-tetraazabicyclo [10.2.2]hexa decane]methyl]benzyl]-1,4,7,10-tetraazabicyclo[5.5.2]dodecane (39) to carboxyrhodamine 110 dibenzocyclooctyl (40)

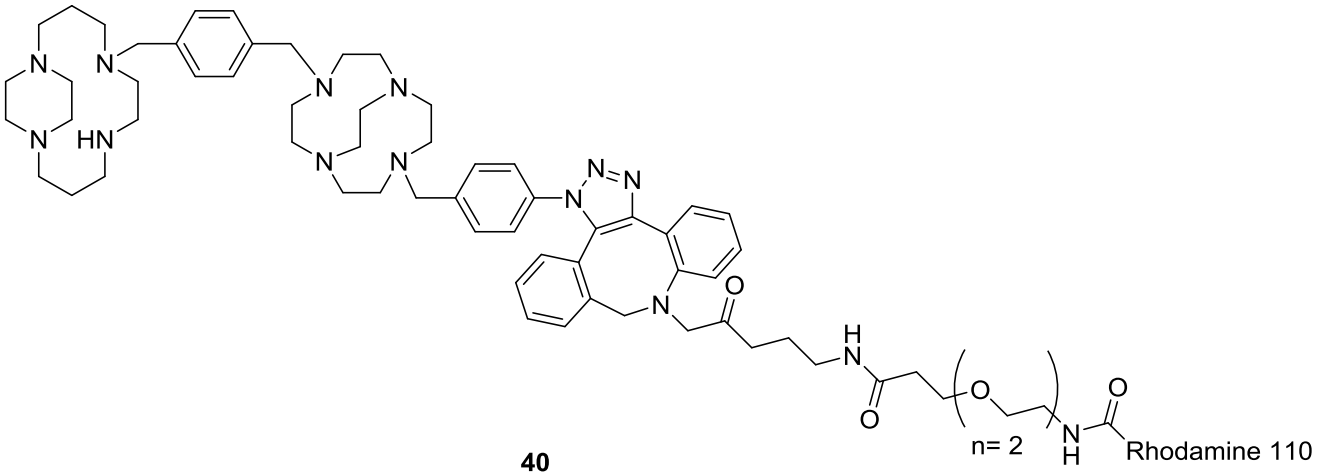

40

General procedure N

To a solution of 1-[4-azidobenzyl]-7-[4-[[1,4,8,11-tetraazabicyclo[10.2.2]hexadecane]methyl]benzyl]-1,4,7,10-tetraazabicyclo[5.5.2]dodecane (**39**) (0.56 mg, 0.08 µmol) in methanol (100 µL), carboxyrhodamine 110 dibenzocyclooctyl (0.50 mg, 0.06 µmol) in methanol (175 µL) was added. The solution was incubated in the dark for 1 h and the solvent was removed *in vacuo*. Analytical data did not confirm the isolation of this product.

8.5.8. Conjugation of 1-[4-[aminomethyl]benzyl]-7-[4-[[1,4,7,10-tetraazabicyclo[8.2.2]dodecane] methyl]benzyl]-1,4,7,10-tetraazabicyclo[5.5.2]dodecane (34) and 1-[4-[aminomethyl]benzyl]-7-[4-[[1,4,8,11-tetraazabicyclo[10.2.2]hexadecane]methyl]benzyl]-1,4,7,10-tetraazabicyclo [5.5.2]dodecane (35) with tetrazine-PEG4-NHS

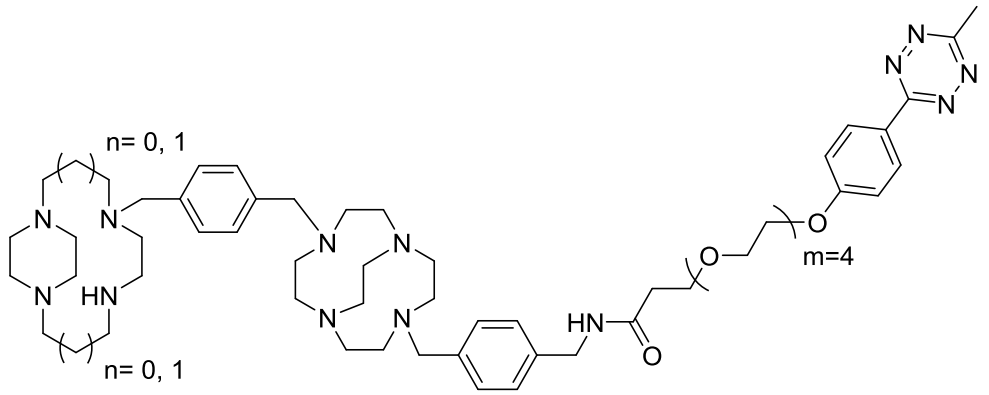

n=0 **41** n=1 **42**

General procedure O

An immediately prepared tetrazine-PEG4-NHS in dimethylsulfoxide solution was added to macrocycle in PBS buffer. The solution was incubated at RT for 1 h. After this the reaction was stopped by quenching with tris-HCl buffer and incubated for a further 5 min at RT. The product was purified through a desalting column (Sephadex PD-10).

1-[4-[[4-[2-[2-[2-[2[2-[4-[6-methyl-1,2,4,5-tetrazin-3-yl]phenoxy]ethoxy]ethoxy]ethoxy]ethoxy] ethyl]-aminocarbonyl]methyl]benzyl]-7-[4-[[1,4,7,10-tetraazabicyclo[8.2.2]dodecane]methyl] benzyl]-1,4,7,10-tetraazabicyclo[5.5.2]dodecane (41)

Amounts: tetrazine-PEG4-NHS in dimethylsulfoxide solution (10 mM, 183 µL), 1-[4-[aminomethyl]benzyl]-7-[4-[[1,4,7,10-tetraazabicyclo[8.2.2]dodecane]methyl]benzyl]-1,4,7,10-tetraazabicyclo[5.5.2]dodecane (**34**) (0.06 mg, 0.09 µmol), PBS buffer (1.62 mM, 57 µL, pH 7.5), tris-HCl buffer (1 M, pH 8.0, 2.160 mL).

MS (*m/z*): $[M]^+$ calcd for $C_{56}H_{85}N_{13}O_6$, 1036.38; found, 1036.9.

1-[4-[[4-[2-[2-[2-[2[2-[4-[6-methyl-1,2,4,5-tetrazin-3-yl]phenoxy]ethoxy]ethoxy]ethoxy]ethoxy]ethyl]-aminocarbonyl]methyl]benzyl]-7-[4-[[1,4,8,11-tetraazabicyclo[10.2.2]hexadecane]methyl]benzyl]-1,4,7,10-tetraazabicyclo[5.5.2]dodecane (42)

Amounts: tetrazine-PEG4-NHS in dimethylsulfoxide solution (10 mM, 183 µL), 1-[4-[aminomethyl]benzyl]-7-[4-[[1,4,7,10-tetraazabicyclo[8.2.2]dodecane]methyl]benzyl]-1,4,7,10-

tetraazabicyclo[5.5.2]dodecane (**34**) (0.06 mg, 0.09 µmol), PBS buffer (1.55 mM, 61 µL, pH 7.5), tris-HCl buffer (1 M, pH 8.0, 2.160 mL).

MS (*m/z*): $[M+2H]^+$ calcd for $C_{58}H_{91}N_{13}O_6$, 1066.45; found, 1066.4.

8.5.9. Attempted conjugation of 1-[4-[aminomethyl]benzyl]-7-[4-[[1,4,8,11-tetraazabicyclo[10.2.2]hexadecane]methyl]benzyl]-1,4,7,10-tetraazabicyclo[5.5.2]dodecane (35) with DOTAGA anhydride

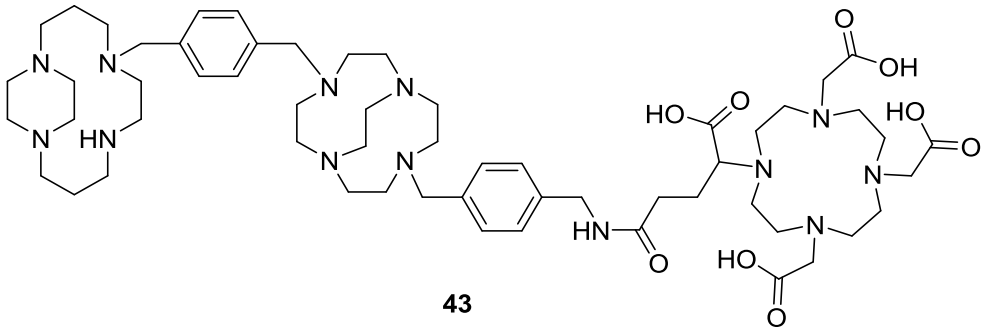

43

1-[4-[aminomethyl]benzyl]-7-[4-[[1,4,8,11-tetraazabicyclo[10.2.2]hexadecane]methyl]benzyl]-1,4,7,10-tetraazabicyclo[5.5.2]dodecane (**35**) (14 mg, 0.02 mmol), was added to dry tetrahydrofuran (1 mL) to this triethylamine (6 µL) and DOTAGA anhydride (15 mg, 0.03 mmol) were added and the solution stirred at RT under argon for 24 h. The solvent was removed *in vacuo.* To yield a pale yellow solid (20 mg). Analytical data indicates that the desired product was not obtained.

8.6. BIS-MACROCYCLE METAL COMPLEXES

8.6.1. Synthesis of metal complexes of bis-macrocycle ligands (28), (29), (30), (34), (36), (31), (32), (33), (35), (37) and (39)

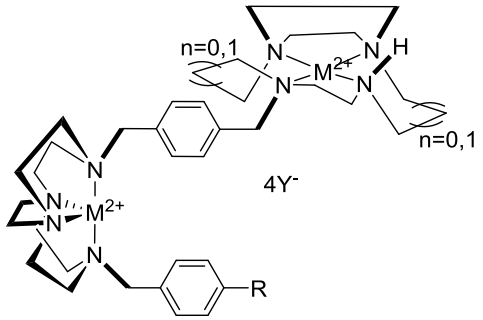

n=0

$[Cu_2\mathbf{28}]^{4+}$	R=CN,	$M^{2+}=Cu^{2+}$,	$Y^-=CH_3CO_2^-$
$[Zn_2\mathbf{28}]^{4+}$	R=CN,	$M^{2+}=Zn^{2+}$,	$Y^-=CH_3CO_2^-$
$[Cu_2\mathbf{29}]^{4+}$	$R=NO_2$,	$M^{2+}=Cu^{2+}$,	$Y^-=CH_3CO_2^-$
$[Zn_2\mathbf{29}]^{4+}$	$R=NO_2$,	$M^{2+}=Zn^{2+}$,	$Y^-=CH_3CO_2^-$
$[Cu_2\mathbf{30}]^{4+}$	R=COOMe,	$M^{2+}=Cu^{2+}$,	$Y^-=CH_3CO_2^-$
$[Zn_2\mathbf{30}]^{4+}$	R=COOMe,	$M^{2+}=Zn^{2+}$,	$Y^-=CH_3CO_2^-$
$[Cu_2\mathbf{34}]^{4+}$	$R=CH_2NH_2$,	$M^{2+}=Cu^{2+}$,	$Y^-=CH_3CO_2^-$
$[Zn_2\mathbf{34}]^{4+}$	$R=CH_2NH_2$,	$M^{2+}=Zn^{2+}$,	$Y^-=CH_3CO_2^-$
$[Cu_2\mathbf{36}]^{4+}$	$R=NH_2$,	$M^{2+}=Cu^{2+}$,	$Y^-=CH_3CO_2^-$
$[Zn_2\mathbf{36}]^{4+}$	$R=NH_2$,	$M^{2+}=Zn^{2+}$,	$Y^-=CH_3CO_2^-$

n=1

$[Cu_2\mathbf{31}]^{4+}$	R=CN,	$M^{2+}=Cu^{2+}$,	$Y^-=CH_3CO_2^-$
$[Zn_2\mathbf{31}]^{4+}$	R=CN,	$M^{2+}=Zn^{2+}$,	$Y^-=CH_3CO_2^-$
$[Cu_2\mathbf{32}]^{4+}$	$R=NO_2$,	$M^{2+}=Cu^{2+}$,	$Y^-=CH_3CO_2^-$
$[Zn_2\mathbf{32}]^{4+}$	$R=NO_2$,	$M^{2+}=Zn^{2+}$,	$Y^-=CH_3CO_2^-$
$[Cu_2\mathbf{33}]^{4+}$	R=COOMe,	$M^{2+}=Cu^{2+}$,	$Y^-=CH_3CO_2^-$
$[Zn_2\mathbf{33}]^{4+}$	R=COOMe,	$M^{2+}=Zn^{2+}$,	$Y^-=CH_3CO_2^-$
$[Cu_2\mathbf{35}]^{4+}$	$R=CH_2NH_2$,	$M^{2+}=Cu^{2+}$,	$Y^-=CH_3CO_2^-$
$[Zn_2\mathbf{35}]^{4+}$	$R=CH_2NH_2$,	$M^{2+}=Zn^{2+}$,	$Y^-=CH_3CO_2^-$
$[Cu_2\mathbf{37}]^{4+}$	$R=NH_2$,	$M^{2+}=Cu^{2+}$,	$Y^-=CH_3CO_2^-$
$[Zn_2\mathbf{37}]^{4+}$	$R=NH_2$,	$M^{2+}=Zn^{2+}$,	$Y^-=CH_3CO_2^-$
$[Cu_2\mathbf{39}]^{4+}$	$R=N_3$,	$M^{2+}=Cu^{2+}$,	$Y^-=CH_3CO_2^-$
$[Zn_2\mathbf{39}]^{4+}$	$R=N_3$,	$M^{2+}=Zn^{2+}$,	$Y^-=CH_3CO_2^-$

General procedure H was followed

1-[4-cyanobenzyl]-7-[4-[[1,4,7,10-tetraazabicyclo[8.2.2]dodecane]methyl]benzyl]-1,4,7,10-tetraazabicyclo[5.5.2]dodecane copper(II) acetate $(Cu_2\mathbf{28})^{4+}$

Amounts: 1-[4-cyanobenzyl-7-[4-[[1,4,7,10-tetraazabicyclo[8.2.2]dodecane]methyl]benzyl]-1,4,7,10-tetraazabicyclo[5.5.2]dodecane (**28**) (133 mg, 0.22 mmol), dry methanol (10 mL), copper(II) acetate monohydrate (95 mg, 0.48 mmol), dry methanol (7 mL). To yield a blue solid (134 mg, 63 %).

MS (*m/z*): $[M\text{-}4CH_3CO_2\text{-}2H\text{-}Cu]^+$ calcd for $C_{36}H_{53}CuN_9$, 675.43; found, 678.8, $[M+3CH_3CO_2+3NH_4]^+$ calcd for $C_{58}H_{91}N_{13}O_6$, 854.15; found, 854.2. HRMS (*m/z*): Pending data, see 8.1.3. Anal. calcd for $C_{44}H_{67}Cu_2N_9O_8$: C, 54.08; H, 6.91; N, 12.90. Found: C, 46.26; H, 7.09; N, 11.87 – contains impurities. UV-vis (MeOH) λmax, nm (ε): 649.9 (508 M-1 cm-1).

1-[4-cyanobenzyl]-7-[4-[[1,4,7,10-tetraazabicyclo[8.2.2]dodecane]methyl]benzyl]-1,4,7,10-tetraazabicyclo[5.5.2]dodecane zinc(II) acetate $(Zn_2\mathbf{28})^{4+}$

Amounts: 1-[4-cyanobenzyl-7-[4-[[1,4,7,10-tetraazabicyclo[8.2.2]dodecane]methyl]benzyl]-1,4,7,10-tetraazabicyclo[5.5.2]dodecane (**28**) (133 mg, 0.22 mmol), dry methanol (10 mL), zinc(II) acetate (87 mg, 0.48 mmol), dry methanol (7 mL). To yield a yellow-brown solid (174 mg, 84 %).

^{1}H NMR (400 MHz, MeOD δ): 1.92-1.99 (*m,* CH_3-C, 12H), 2.20-3.28 (*br m,* N-α-CH_2, 33H), 3.36-4.63 (*br m,* N-α-CH_2, 13H), 4.80 (*m,* NH*,* 1H), 7.33-7.45 (*m,* Ar-H, 2H), 7.54-7.81 (*m,* Ar-H, 6H). ^{13}C NMR (100 MHz, MeOD, δ): 22.26 (CH_3-O), 43.03 (N-α-CH_2), 43.63 (N-α-CH_2), 43.86 (N-α-CH_2), 44.64 (N-α-CH_2), 45.14 (N-α-CH_2), 46.64 (N-α-CH_2), 49.18 (N-α-CH_2), 49.62 (N-α-CH_2), 49.85 (N-α-CH_2), 50.59 (N-α-CH_2), 50.94 (N-α-CH_2), 51.64 (N-α-CH_2), 52.54 (N-α-CH_2), 54.21 (N-α-CH_2), 55.05 (N-α-CH_2), 55.76 (N-α-CH_2), 57.54 (N-α-CH_2), 58.94 (N-α-CH_2), 59.16 (N-α-CH_2), 62.80 (N-α-CH_2), 110.97 (C≡N), 119.00 (Ar-C), 129.62 (Ar-H), 130.04 (Ar-H), 132.20 (Ar-H), 132.32 (Ar-H), 132.32 (Ar-H), 144.30 (Ar-C), 144.59 (Ar-C), 179.67 (C=O). MS (*m/z*): $[M\text{-}CH_3CO_2+NH_4]^+$ calcd for $C_{42}H_{68}N_{10}O_6Zn_2$, 939.83; found, 939.3. HRMS (*m/z*): Pending data, see 8.1.3. Anal. calcd for $C_{44}H_{67}N_9O_8Zn_2.5H_2O$.MeCN: C, 49.69; H, 7.25; N, 12.60. Found: C, 49.28; H, 6.92; N, 12.80.

1-[4-nitrobenzyl]-7-[4-[[1,4,7,10-tetraazabicyclo[8.2.2]dodecane]methyl]benzyl]-1,4,7,10-tetraazabicyclo[5.5.2]dodecane copper(II) acetate ($Cu_2$29)$^{4+}$

Amounts: 1-[4-nitrobenzyl]-7-[4-[[1,4,7,10-tetraazabicyclo[8.2.2]dodecane]methyl]benzyl]-1,4,7,10-tetraazabicyclo[5.5.2]dodecane (**29**) (39 mg, 0.06 mmol), dry methanol (4 mL), copper(II) acetate tetrahydrate (34 mg, 0.13 mmol), dry MeOH (10 mL). To yield a blue solid (18 mg, 28 %).

MS (*m/z*): Pending data, see 8.1.3. UV-vis (MeOH) λmax, nm (ε): 610.0 (467 M-1 cm-1).

1-[4-nitrobenzyl]-7-[4-[[1,4,7,10-tetraazabicyclo[8.2.2]dodecane]methyl]benzyl]-1,4,7,10-tetraazabicyclo[5.5.2]dodecane zinc(II) acetate ($Zn_2$29)$^{4+}$

Amounts: 1-[4-nitrobenzyl]-7-[4-[[1,4,7,10-tetraazabicyclo[8.2.2]dodecane]methyl]benzyl]-1,4,7,10-tetraazabicyclo[5.5.2]dodecane (**29**) (41 mg, 0.08 mmol), dry methanol (4 mL), zinc(II) acetate (31 mg, 0.17 mmol), dry MeOH (5 mL). To yield a yellow solid (44 mg, 70%).

^{1}H NMR (400 MHz, MeOD, δ): 1.97 (*s,* CH_3-C, 12H), 2.42-3.28 (*br m,* N-α-CH_2, 30H), 3.39-3.83 (*br m,* N-α-CH_2, 10H), 3.88-4.41 (*m,* CH_2-Ar, 6H), 4.50-4.73 (*m,* NH*,* 1H), 7.32-7.79 (*m,* Ar-H, 4H), 7.99-8.39 (*m,* Ar-H, 4H). ^{13}C NMR (100 MHz, MeOD, δ): 21.52 (CH_3-C), 42.24 (N-α-CH_2), 43.71 (N-α-CH_2), 44.37 (N-α-CH_2), 44.59 (N-α-CH_2), 45.03 (N-α-CH_2), 46.90 (N-α-CH_2), 49.26 (N-α-CH_2), 49.43 (N-α-CH_2), 49.65 (N-α-CH_2), 49.81 (N-α-CH_2), 50.40 (N-α-CH_2), 52.65 (N-α-CH_2), 54.18 (N-α-CH_2), 55.18 (N-α-CH_2), 57.72 (N-α-CH_2), 58.13 (N-α-CH_2), 60.01 (N-α-CH_2), 123.26 (Ar-H), 128.53 (Ar-C), 130.02 (Ar-H), 131.02 (Ar-H), 132.07 (Ar-H), 148.44 (Ar-C), 149.51 (Ar-C), 179.72 (C=O). MS (*m/z*): Pending data, see 8.1.3.

1-[4-[methoxycarbonyl]benzyl]-7-[4-[[1,4,7,10-tetraazabicyclo[8.2.2]dodecane]methyl]benzyl]-1,4,7,10-tetraazabicyclo[5.5.2]dodecane copper(II) acetate ($Cu_2$30)$^{4+}$

Amounts: 1-[4-[methoxycarbonyl]benzyl]-7-[4-[[1,4,7,10-tetraazabicyclo[8.2.2]dodecane]methyl]benzyl]-1,4,7,10-tetraazabicyclo[5.5.2]dodecane (**30**) (52.20 mg, 0.08 mmol), dry MeOH (5 mL and 5 mL), copper(II) acetate monohydrate (36.00 mg, 0.18 mmol). To yield a blue solid (44.60 mg, 55 %).

MS(*m/z*): $[M+K+H]^+$ calcd for $C_{45}H_{71}Cu_2KN_8O_{10}$, 1050.30; found, 1050.7. HRMS (*m/z*): Pending data, see 8.1.3. UV-vis (MeOH) λmax, nm (ε): 649 (356 M-1 cm-1).

1-[4-[methoxycarbonyl]benzyl]-7-[4-[[1,4,7,10-tetraazabicyclo[8.2.2]dodecane]methyl]benzyl]-1,4,7,10-tetraazabicyclo[5.5.2]dodecane zinc(II) acetate ($Zn_2$30)$^{4+}$

Amounts: 1-[4-[methoxycarbonyl]benzyl]-7-[4-[[1,4,7,10-tetraazabicyclo[8.2.2]dodecane]methyl]benzyl]-1,4,7,10-tetraazabicyclo[5.5.2]dodecane (**30**) (41.30 mg, 0.06 mmol), dry methanol (5 mL and 5 mL), zinc(II) acetate (26.00 mg, 0.14 mmol). To yield a yellow solid (35 mg, 54 %).

^{1}H NMR (400 MHz, MeOD, δ): 1.99 (*s,* CH_3-C, 12H), 2.32-2.47 (*m,* N-α-CH_2, 2H), 2.55-2.58 (*m,* N-α-CH_2, 1H), 2.68-2.73 (*m,* N-α-CH_2, 3H), 2.81-3.08 (*br m,* N-α-CH_2, 26H), 3.12-3.19 (*m,* N-α-CH_2, 8H), 3.43-3.49 (*m,* N-α-CH_2, 2H), 3.68-3.70 (*m,* N-α-CH_2, 3H), 3.77-3.80 (*m,* CH_2-Ar, 1H), 3.92 (*s,* CH_3-O, 3H), 4.00-4.10 (*m,* CH_2-Ar, 5H), 4.63 (*m,* NH, 1H), 7.41-7.52 (*m,* Ar-H, 6H), 7.55-7.58 (*m,* Ar-H, 1H), 8.07 (*d,* J=8.2 Hz, Ar-H, 1H). ^{13}C NMR (100 MHz, MeOD, δ): 21.95 (CH_3-C), 44.50 (N-α-CH_2), 45.60 (N-α-CH_2), 46.62 (N-α-CH_2), 48.78 (N-α-CH_2), 49.17 (N-α-CH_2), 49.63 (N-α-CH_2), 51.02 (N-α-CH_2), 51.44 (N-α-CH_2), 54.23 (N-α-CH_2), 54.77 (N-α-CH_2), 54.87 (N-α-CH_2), 55.01 (N-α-CH_2), 55.71 (N-α-CH_2), 56.15 (N-α-CH_2), 57.32 (N-α-CH_2), 59.29 (N-α-CH_2), 59.43 (N-α-CH_2), 126.96 (Ar-H), 129.07 (Ar-H), 129.18 (Ar-H), 129.50 (Ar-H), 129.97 (Ar-C), 130.35 (Ar-C), 130.76 (Ar-H), 135.57 (Ar-C), 166.80 (C=O), 180.29 (C=O). MS (*m/z*): Pending data, see 8.1.3.

1-[4-[Aminomethyl]benzyl]-7-[4-[[1,4,7,10-tetraazabicyclo[8.2.2]dodecane]methyl]benzyl]-1,4,7,10-tetraazabicyclo[5.5.2]dodecane copper(II) acetate ($Cu_2$34)$^{4+}$

Amounts: 1-[4-[Aminomethyl]benzyl]-7-[4-[[1,4,7,10-tetraazabicyclo[8.2.2]dodecane]methyl] benzyl] -1,4,7,10-tetraazabicyclo[5.5.2]dodecane (**34**) (14.50 mg, 0.02 mmol), dry methanol (3 mL and 5 mL), copper(II) acetatate monohydrate (10.30 mg, 0.05 mmol). To yield a blue solid (14.10 mg, 61 %).

MS (*m/z*): Pending data, see 8.1.3. UV-vis (MeOH) λmax, nm (ε): 650 (494 M-1 cm-1).

1-[4-[aminomethyl]benzyl]-7-[4-[[1,4,7,10-tetraazabicyclo[8.2.2]dodecane]methyl]benzyl]-1,4,7,10-tetraazabicyclo[5.5.2]dodecane zinc(II) acetate ($Zn_2$34)$^{4+}$

Amounts: 1-[4-[aminomethyl]benzyl]-7-[4-[[1,4,7,10-tetraazabicyclo[8.2.2]dodecane]methyl]benzyl]-1,4,7,10-tetraazabicyclo[5.5.2]dodecane (**34**) (14.50 mg, 0.02 mmol), dry methanol (3 mL and 5 mL), zinc(II) acetatate (9.50 mg, 0.05 mmol). To yield a yellow solid (15.70 mg, 68 %).

^{1}H NMR (400 MHz, MeOD, δ): 1.95 (*s,* CH_3-C, 12H), 2.21-2.33 (*m,* N-α-CH_2, 2H), 2.43-3.27 (*br m,* N-α-CH_2, 32H), 3.36-2.82 (*m,* N-α-CH_2, 6H), 3.86-4.10 (*m,* CH_2-Ar, 7H), 4.48-4.63 (*m,* CH_2-Ar, 1H), 4.82-4.84 (*m,* NH, 1H), 4.94-5.00 (*m,* NH_2, 2H), 7.28-7.62 (*m,* Ar-H, 8H).^{13}C NMR (100 MHz, MeOD, δ): 22.01 ($\underline{C}H_3$-C), 43.75 (N-α-CH_2), 44.37 (N-α-CH_2), 44.64 (N-α-CH_2), 46.06 (N-α-CH_2), 46.61 (N-α-CH_2), 49.15 (N-α-CH_2), 49.62 (N-α-CH_2), 49.70 (N-α-CH_2), 51.17 (N-α-CH_2), 51.49 (N-α-CH_2), 53.76 (N-α-CH_2), 54.25 (N-α-CH_2), 54.87 (N-α-CH_2), 55.30 (N-α-CH_2), 55.73 (N-α-CH_2), 55.89 (N-α-CH_2), 127.95 (Ar-H), 128.14 (Ar-C), 129.03 (Ar-C), 129.61 (Ar-H), 131.25 (Ar-H), 131.38 (Ar-H), 131.58 (Ar-H), 132.32 (Ar-H), 139.56 (Ar-C), 141.30 (Ar-C), 179.51 (C=O). MS (*m/z*): Pending data, see 8.1.3.

1-[4-Aminobenzyl]-7-[4-[[1,4,7,10-tetraazabicyclo[8.2.2]dodecane]methyl]benzyl]-1,4,7,10-tetraazabicyclo[5.5.2]dodecane copper(II) acetate ($Cu_2$36)$^{4+}$

Amounts: 1-[4-Aminobenzyl]-7-[4-[[1,4,7,10-tetraazabicyclo[8.2.2]dodecane]methyl]benzyl]-1,4,7,10-tetraazabicyclo[5.5.2]dodecane (**36**) (11.10 mg, 0.02 mmol), dry methanol (3 mL and 3 mL), copper(II) acetatate monohydrate (8.00 mg, 0.04 mmol). To yield a blue solid (8.58 mg, 48 %).

MS (*m/z*): Pending data, see 8.1.3. UV-vis (MeOH) λmax, nm (ε): 655 (236 M-1 cm-1).

1-[4-Aminobenzyl]-7-[4-[[1,4,7,10-tetraazabicyclo[8.2.2]dodecane]methyl]benzyl]-1,4,7,10-tetraazabicyclo[5.5.2]dodecane zinc(II) acetate ($Zn_2$36)$^{4+}$

Amounts: 1-[4-Aminobenzyl]-7-[4-[[1,4,7,10-tetraazabicyclo[8.2.2]dodecane]methyl]benzyl]-1,4,7,10-tetraazabicyclo[5.5.2]dodecane (**36**) (11.10 mg, 0.02 mmol), dry methanol (3 mL and 2 mL), zinc(II) acetatate (7.00 mg, 0.04 mmol). To yield a yellow solid (8 mg, 45%).

MS (*m/z*): Pending data, see 8.1.3.

1-[4-Cyanobenzyl]-7-[4-[[1,4,8,11-tetraazabicyclo[10.2.2]hexadecane]methyl]benzyl]-1,4,7,10-tetraazabicyclo[5.5.2]dodecane copper(II) acetate ($Cu_2$31)$^{4+}$

Amounts: 1-[4-Cyanobenzyl-7-[4-[[1,4,8,11-tetraazabicyclo[10.2.2]hexadecane]methyl]benzyl]-1,4,7,10-tetraazabicyclo[5.5.2]dodecane (**31**) (101.00 mg, 0.16 mmol), dry methanol (10 mL and 5 mL), copper(II) acetate monohydrate (69.00 mg, 0.35 mmol). To yield a blue solid (137 mg, 86 %).

MS (*m/z*): $[M-2CH_3CO_2+ H]^+$ calcd for $C_{42}H_{64}Cu_2N_9O_4$, 886.13; found, 886.3. UV-vis (MeOH) λmax, nm (ε): 670.0 (185.5 M-1 cm-1).

1-[4-Cyanobenzyl]-7-[4-[[1,4,8,11-tetraazabicyclo[10.2.2]hexadecane]methyl]benzyl]-1,4,7,10-tetraazabicyclo[5.5.2]dodecane zinc(II) acetate ($Zn_2$31)$^{4+}$

Amounts: 1-[4-Cyanobenzyl-7-[4-[[1,4,8,11-tetraazabicyclo[10.2.2]hexadecane]methyl]benzyl]-1,4,7, 10-tetraazabicyclo[5.5.2]dodecane (**31**) (100 mg, 0.16 mmol), dry methanol (10 mL and 5 mL), zinc(II) acetate (63 mg, 0.34 mmol). To yield a yellow-brown solid (130 mg, 83 %).

^{1}H NMR (400 MHz, MeOD, δ): 1.63 (*d,* J=16.3 Hz, N-β-CH_2, 1H), 1.80 (*d,* J=12.6 Hz, N-β-CH_2, 2H), 2.00 (*br s*, C̲H3-C, 12H), 2.21-2.24 (*m,* N-β-CH_2, 1H), 2.29-2.34 (*m,* N-α-CH_2, 1H), 2.48-2.58 (*m,* N-α-CH_2, 3H), 2.63 (*d*, J=11.6 Hz, N-α-CH_2, 2H), 2.73 (*dd,* J=14.2 Hz, N-α-CH_2, 2H), 2.80-3.25 (*br m,* N-α-CH_2, 24H), 3.41-3.52 (*m,* N-α-CH_2, 2H), 3.59-3.73 (*m,* N-α-CH_2, 6H), 3.82-3.98 (*m,* CH_2-Ar, 2H), 4.02-4.12 (*m,* CH_2-Ar, 2H), 4.16-4.23 (*m,* CH_2-Ar, 2H), 4.54-4.64 (*m,* NH, 1H), 7.30-7.37 (*m,* Ar-H, 2H), 7.44-7.56 (*m,* Ar-H, 2H), 7.59-7.66 (*m,* Ar-H, 2H), 7.71-7.79 (*m,* Ar-H, 2H). ^{13}C NMR (100 MHz, MeOD, δ): 21.02 (C̲H_3-C), 22.12 (N-β-CH_2), 24.33 (N-β-CH_2), 43.38 (N-α-CH_2), 44.52 (N-α-CH_2), 48.58 (N-α-CH_2), 48.94 (N-α-CH_2), 49.15 (N-α-CH_2), 49.29 (N-α-CH_2), 49.55 (N-α-CH_2), 51.23 (N-α-CH_2), 51.40 (N-α-CH_2), 52.28 (N-α-CH_2), 54.99 (N-α-CH_2), 55.65 (N-α-CH_2), 56.57 (N-α-CH_2), 57.48 (N-α-CH_2), 57.99 (N-α-CH_2), 111.62 (CN), 118.18 (Ar-C), 129.04 (Ar-H), 129.62 (Ar-H), 130.51 (Ar-H), 131.07 (Ar-H), 131.91 (Ar-C), 132.21 (Ar-H), 140.63 (Ar-C), 180.22 (C=O). MS (*m/z*): $[M-2CH_3CO_2+2NH_4]^+$ calcd for $C_{42}H_{73}N_{11}O_4Zn_2$, 926.88; found, 926.5. HRMS (*m/z*): Pending data, see 8.1.3.

1-[4-Nitrobenzyl]-7-[4-[[1,4,8,11-tetraazabicyclo[10.2.2]hexadecane]methyl]benzyl]-1,4,7,10-tetraazabicyclo[5.5.2]dodecane copper(II) acetate ($Cu_2$32)$^{4+}$

Amounts: 1-[4-Nitrobenzyl]-7-[4-[[1,4,8,11-tetraazabicyclo[10.2.2]hexadecane]methyl]benzyl]-1,4,7, 10-tetraazabicyclo[5.5.2]dodecane (**32**) (100 mg, 0.15 mmol), dry methanol (10 mL and 5 mL), copper(II)acetate monohydrate (66 mg, 0.33 mmol). To yield a blue solid (133 mg, 86 %).

MS (*m/z*): $[M-4CH_3CO_2+Na+2H]^+$ calcd for $C_{37}H_{61}Cu_2N_9NaO_2$, 814.04; found, 814.7. HRMS (*m/z*): Pending data, see 8.1.3.UV-vis (MeOH) λmax, nm (ε): 650 (285 M-1 cm-1).

1-[4-Nitrobenzyl]-7-[4-[[1,4,8,11-tetraazabicyclo[10.2.2]hexadecane]methyl]benzyl]-1,4,7,10-tetraazabicyclo[5.5.2]dodecane zinc(II) acetate ($Zn_2$32)$^{4+}$

Amounts: 1-[4-Nitrobenzyl]-7-[4-[[1,4,8,11-tetraazabicyclo[10.2.2]hexadecane]methyl]benzyl]-1,4,7,10-tetraazabicyclo[5.5.2]dodecane (**32**) (100 mg, 0.15 mmol), dry methanol (10 mL and 5 mL), zinc(II)acetate (61 mg, 0.33 mmol). To yield a blue solid (130 mg, 84 %).

^{1}H NMR (400 MHz, MeOD, δ): 1.63 (*d,* J=16.7 Hz, N-β-CH_2, 1H), 1.81 (*d,* J=16.7 Hz, N-β-CH_2, 2H), 1.99 (*br s,* $\underline{C}H_3$-C, 12 H), 2.15-2.19 (*m,* N-β-CH_2, 1H), 2.22-2.26 (*m,* N-α-CH_2, 1H), 2.30-3.35 (*m,* N-α-CH_2, 1H), 2.46-2.55 (*m,* N-α-CH_2, 2H), 2.59-2.76 (*m,* N-α-CH_2, 4H), 2.80-2.88 (*m,* N-α-CH_2, 3H), 2.91-3.17 (*m,* N-α-CH_2, 18H), 3.19-3.26 (*m,* N-α-CH_2, 4H), 3.46-3.48 (*m,* N-α-CH_2, 1H), 3.53-3.58 (*m,* N-α-CH_2, 2H), 3.63-3.70 (*m,* N-α-CH_2, 4H), 3.93-4.11 (*m,* CH_2-Ar, 4H), 4.44 (*br s,* NH, 1H), 7.32-7.40 (*m,* Ar-H, 2H), 7.45-7.50 (*m,* Ar-H, 2H), 7.63-7.68 (*m,* Ar-H, 1H), 7.71 (*d,* J=8.6 Hz, Ar-H, 1H), 8.29 (*d*, J=8.8 Hz, Ar-H, 2H). ^{13}C NMR (100 MHz, MeOD, δ): 20.97 ($\underline{C}H_3$-C), 21.87 (N-β-CH_2), 24.30 (N-β-CH_2), 43.30 (N-α-CH_2), 44.47 (N-α-CH_2), 48.75 (N-α-CH_2), 49.15 (N-α-CH_2), 49.49 (N-α-CH_2), 51.40 (N-α-CH_2), 52.19 (N-α-CH_2), 52.30 (N-α-CH_2), 54.86 (N-α-CH_2), 55.11 (N-α-CH_2), 55.48 (N-α-CH_2), 55.70 (N-α-CH_2), 56.54 (N-α-CH_2), 56.80 (N-α-CH_2), 57.96 (N-α-CH_2), 123.34 (Ar-H), 128.99 (Ar-C), 129.64 (Ar-C), 130.48 (Ar-H), 131.11 (Ar-H), 132.23 (Ar-H), 132.36 (Ar-C), 142.40 (Ar-C), 180.19 (C=O). MS (*m/z*): [M-2CH_3CO_2+NH_4-2H]$^+$ calcd for $C_{41}H_{67}N_{10}O_6Zn_2$, 926.81; found, 926.4. HRMS (*m/z*): Pending data, see 8.1.3.

1-[4-[methoxycarbonyl]benzyl]-7-[4-[[1,4,8,11-tetraazabicyclo[10.2.2]hexadecane]methyl]benzyl]-1,4,7,10-tetraazabicyclo[5.5.2]dodecane copper(II) acetate ($Cu_2$33)$^{4+}$

Amounts: 1-[4-[Methoxycarbonyl]benzyl]-7-[4-[[1,4,8,11-tetraazabicyclo[10.2.2]hexadecane]methyl]benzyl]-1,4,7,10-tetraazabicyclo[5.5.2]dodecane (**33**) (50 mg, 0.07 mmol), dry methanol (5 mL and 5 mL), copper(II) acetate monohydrate (33 mg, 0.16 mmol). To yield a blue solid (49 mg, 64 %).

MS (*m/z*): [M-4CH_3CO_2+K-H]$^+$ calcd for $C_{39}H_{61}Cu_2N_8O_2$, 840.16; found, 840.5. HRMS (*m/z*): Pending data, see 8.1.3. UV-vis (MeOH) λmax, nm (ε): 650 (345 M-1 cm-1).

1-[4-[Methoxycarbonyl]benzyl]-7-[4-[[1,4,8,11-tetraazabicyclo[10.2.2]hexadecane]methyl]benzyl]-1,4,7,10-tetraazabicyclo[5.5.2]dodecane zinc(II) acetate ($Zn_2$33)$^{4+}$

Amounts: 1-[4-[Methoxycarbonyl]benzyl]-7-[4-[[1,4,8,11-tetraazabicyclo[10.2.2]hexadecane]methyl]benzyl]-1,4,7,10-tetraazabicyclo[5.5.2]dodecane (**33**) (91 mg, 0.14 mmol), dry methanol (10 mL and 5 mL), zinc(II) acetate (54 mg, 0.30 mmol). To yield a yellow solid (119 mg, 85 %).

^{1}H NMR (400 MHz, MeOD, δ): 1.39-1.41 (*m*, CH_3-CH_2, 3H), 1.64 (*d,* J=16.3 Hz, N-β-CH_2, 1H), 1.80 (*d,* J=15.9 Hz, N-β-CH_2, 2H), 2.01 (*br s,* CH_3-C, 12 H), 2.10 (*m,* N-β-CH_2, 1H), 2.17-2.26 (*m,* N-α-CH_2, 2H), 2.30-3.35 (*m,* N-α-CH_2, 1H), 2.48-2.65 (*m,* N-α-CH_2, 5H), 2.72-2.85 (*m,* N-α-CH_2, 3H), 2.91-3.17 (*m,* N-α-CH_2, 19H), 3.22-3.28 (*m,* N-α-CH_2, 3H), 3.45-3.50 (*m,* N-α-CH_2, 1H), 3.57-3.74 (*m,* N-α-CH_2, 6H), 3.91 (*m,* CH_2-O, 2H), 3.99-4.12 (*m,* CH_2-Ar, 4H), 4.20-4.23 (*m,* CH_2-Ar, 1H), 4.35-4.40 (*m,* CH_2-Ar, 1H), 4.49-4.51 (*m,* NH, 1H), 7.33-7.42 (*m,* Ar-H, 2H), 7.45-7.53 (*m,* Ar-H, 2H), 7.58 (*d,* J=8.2 Hz, Ar-H, 2H), 8.04-8.07 (*m*, Ar-H, 2H). ^{13}C NMR (100 MHz, MeOD, δ): 13.36 (CH_3-CH_2), 21.04 (CH_3-C), 21.72 (N-β-CH_2), 24.31 (N-β-CH_2), 43.40 (N-α-CH_2), 44.47 (N-α-CH_2), 49.08 (N-α-CH_2), 49.17 (N-α-CH_2), 49.58 (N-α-CH_2), 51.42 (N-α-CH_2), 51.52 (N-α-CH_2), 52.24 (N-α-CH_2), 52.34 (N-α-CH_2), 54.95 (N-α-CH_2), 55.11 (N-α-CH_2), 55.63 (N-α-CH_2), 56.12 (N-α-CH_2), 56.57 (N-α-CH_2), 57.59 (N-α-CH_2), 57.69 (N-α-CH_2), 57.98 (N-α-CH_2), 61.04 (N-α-CH_2), 126.97 (Ar-H), 128.99 (Ar-H), 129.51 (Ar-H), 129.74 (Ar-C), 130.05 (Ar-C), 130.40 (Ar-H), 132.24 (Ar-H), 135.20 (Ar-H), 140.19 (Ar-C), 140.27 (Ar-C), 166.89 (C=O), 180.16 (C=O). HRMS (*m/z*): Pending data, see 8.1.3.

1-[4-[Aminomethyl]benzyl]-7-[4-[[1,4,8,11-tetraazabicyclo[10.2.2]hexadecane]methyl]benzyl]-1,4,7,10-tetraazabicyclo[5.5.2]dodecane copper(II) acetate ($Cu_2$35)$^{4+}$

Amounts: 1-[4-[Aminomethyl]benzyl]-7-[4-[[1,4,8,11-tetraazabicyclo[10.2.2]hexadecane]methyl]benzyl]-1,4,7,10-tetraazabicyclo[5.5.2]dodecane (**35**) (77 mg, 0.12 mmol), dry methanol (10 mL and 5 mL), copper(II)acetate monohydrate (52 mg, 0.26 mmol). To yield a blue solid (115 mg, 96 %).

MS (*m/z*): [M-3CH_3CO_2-3H+2NH_4]$^{+}$ calcd for $C_{40}H_{71}Cu_2N_{11}O_2$, 865.18; found, 865.8. HRMS (*m/z*): Pending data, see 8.1.3. UV-vis (MeOH) λmax, nm (ε): 660.0 (210.5 M-1 cm-1).

1-[4-[Aminomethyl]benzyl]-7-[4-[[1,4,8,11-tetraazabicyclo[10.2.2]hexadecane]methyl]benzyl]-1,4,7,10-tetraazabicyclo[5.5.2]dodecane zinc(II) acetate ($Zn_2$35)$^{4+}$

Amounts: 1-[4-[Aminomethyl]benzyl]-7-[4-[[1,4,8,11-tetraazabicyclo[10.2.2]hexadecane]methyl]benzyl]-1,4,7,10-tetraazabicyclo[5.5.2]dodecane (**35**) (79 mg, 0.12 mmol), dry methanol (10 mL and 5 mL), zinc(II)acetate (49 mg, 0.27 mmol). To yield a yellow solid (91 mg, 74 %).

^{1}H NMR (400 MHz, MeOD, δ): 1.63 (*d,* J=16.5 Hz, N-β-CH_2, 1H), 1.81 (*d,* J=15.7 Hz, N-β-CH_2, 2H), 2.11-2.15 (*m,* N-β-CH_2, 1H), 2.19-2.38 (*m,* N-α-CH_2, 3H), 2.46-2.55 (*m,* N-α-CH_2, 2H), 2.59-2.72 (*m,* N-α-CH_2, 5H), 2.80-2.84 (*m,* N-α-CH_2, 2H), 2.94-3.14 (*br m,* N-α-CH_2, 19H), 3.20-3.28 (*m,* N-α-CH_2, 5H), 3.46-3.57 (*m,* N-α-CH_2, 2H), 3.68 (*m,* N-α-CH_2, 4H), 3.81-3.93 (*m,* CH_2-Ar, 2H), 3.97-4.07 (*m,* CH_2-Ar, 4H), 4.17-4.24 (*m,* NH_2, 1H), 4.41-4.43 (*m,* NH_2, 1H), 4.83-4.88 (*m,* NH, 1H), 7.29-7.38 (*m,* Ar-H, 2H), 7.42-7.50 (*m,* Ar-H, 4H), 7.56 (*d,* J=7.8 Hz, Ar-H, 1H), 7.86 (*d,* J=8.0 Hz, Ar-H, 1H). ^{13}C NMR (100 MHz,

MeOD, δ): 20.95 (CH_3-COOH), 22.09 (N-β-CH_2), 28.58 (N-β-CH_2), 43.28 (CH_2-NH_2), 44.48 (N-α-CH_2), 44.59 (N-α-CH_2), 48.57 (N-α-CH_2), 48.85 (N-α-CH_2), 49.14 (N-α-CH_2), 49.49 (N-α-CH_2), 51.43 (N-α-CH_2), 52.21 (N-α-CH_2), 52.28 (N-α-CH_2), 54.86 (N-α-CH_2), 54.74 (N-α-CH_2), 54.93 (N-α-CH_2), 55.48 (N-α-CH_2), 55.70 (N-α-CH_2), 56.56 (N-α-CH_2), 57.35 (N-α-CH_2), 58.00 (N-α-CH_2), 63.37 (N-α-CH_2), 64.07 (N-α-CH_2), 124.84 (Ar-H), 126.96 (Ar-H), 128.25 (Ar-H), 128.43 (Ar-H), 130.47 (Ar-H), 130.59 (Ar-H), 130.82 (Ar-H), 131.92 (Ar-C), 132.23 (Ar-H), 135.15 (Ar-C), 137.96 (Ar-C), 144.54 (Ar-C), 180.07 (C=O). MS (*m/z*): $[M\text{-}CH_3CO_2+K]^+$ calcd for $C_{44}H_{72}KN_9O_6\ Zn_2$, 992.98; found, 992.20. HRMS (*m/z*): Pending data, see 8.1.3.

1-[4-Aminobenzyl]-7-[4-[[1,4,8,11-tetraazabicyclo[10.2.2]hexadecane]methyl]benzyl]-1,4,7,10-tetraazabicyclo[5.5.2]dodecane copper(II) acetate ($Cu_2$37)$^{4+}$

Amounts: 1-[4-Aminobenzyl]-7-[4-[[1,4,8,11-tetraazabicyclo[10.2.2]hexadecane]methyl]benzyl]-1,4,7,10-tetraazabicyclo[5.5.2]dodecane (**37**) (50 mg, 0.08 mmol), dry methanol (5 mL and 6 mL), copper(II) acetate monohydrate (35 mg, 0.18 mmol). To yield a blue solid (65 mg, 82 %).

MS (*m/z*): Pending data, see 8.1.3. UV-vis (MeOH) λmax, nm (ε): 645 (230 M^{-1} cm^{-1}).

1-[4-Aminobenzyl]-7-[4-[[1,4,8,11-tetraazabicyclo[10.2.2]hexadecane]methyl]benzyl]-1,4,7,10-tetraazabicyclo[5.5.2]dodecane zinc(II) acetate ($Zn_2$37)$^{4+}$

Amounts: 1-[4-Aminobenzyl]-7-[4-[[1,4,8,11-tetraazabicyclo[10.2.2]hexadecane]methyl]benzyl]-1,4,7,10-tetraazabicyclo[5.5.2]dodecane (**37**) (51 mg, 0.08 mmol), dry methanol (5 mL and 5 mL), zinc(II) acetate (32 mg, 0.18 mmol). To yield a yellow solid (59 mg, 73 %).

^{1}H NMR (400 MHz, MeOD, δ): 1.62-1.83 (*m,* N-β-CH_2, 2H), 1.99 (*br s,* CH_3-C, 12 H), 2.14-2.24 (*m,* N-β-CH_2, 1H), 2.22-2.36 (*m,* N-α-CH_2, 1H), 2.51-2.57 (*m,* N-α-CH_2, 3H), 2.64 (*d,* J=10.0 Hz, N-α-CH_2, 3H), 2.75-2.83 (*m,* N-α-CH_2, 3H), 2.91-3.17 (*br m,* N-α-CH_2, 19H), 3.21-3.26 (*m,* N-α-CH_2, 3H), 3.39-3.53 (*m,* N-α-CH_2, 4H), 3.61-3.71 (*m,* N-α-CH_2, 4H), 3.81-3.85 (*m,* CH_2-Ar, 1H), 3.90-4.04 (*m,* CH_2-Ar, 3H), 4.09-4.12 (*m,* CH_2-Ar, 1H), 4.15-4.24 (*m,* CH_2-Ar, 1H), 4.36 (*m,* CH_2-Ar, 1H), 4.59-4.64 (*m,* NH, 1H), 4.94 (*m,* NH_2, 2H), 6.73 (*d,* J=8.4 Hz, Ar-H, 1H), 7.16 (*d,* J=8.4 Hz, Ar-H, 1H), 7.33-7.38 (*m,* Ar-H, 2H), 7.47-7.53 (*m,* Ar-H, 1H), 7.61-7.70 (*m,* Ar-H, 1H), 8.24 (*d,* J=8.6 Hz, Ar-H, 1H), 8.38 (*d,* J=8.8 Hz, Ar-H, 1H). ^{13}C NMR (100 MHz, MeOD, δ): 20.95 (CH_3-COOH), 22.16 (N-β-CH_2), 24.30 (N-β-CH_2), 41.69 (N-α-CH_2), 43.28 (N-α-CH_2), 44.46 (N-α-CH_2), 49.48 (N-α-CH_2), 51.39 (N-α-CH_2), 52.30 (N-α-CH_2), 54.39 (N-α-CH_2), 54.86 (N-α-CH_2), 55.73 (N-α-CH_2), 56.53 (N-α-CH_2), 57.28 (N-α-CH_2), 57.93 (N-α-CH_2), 114.95 (Ar-H), 122.27 (Ar-H), 125.45 (Ar-C), 129.14 (Ar-H), 129.90 (Ar-H), 130.81 (Ar-H), 131.92 (Ar-H), 132.23 (Ar-H), 139.59 (Ar-C), 179.98 (C=O). MS (*m/z*): Pending data, see 8.1.3.

1-[4-Azidobenzyl]-7-[4-[[1,4,8,11-tetraazabicyclo[10.2.2]hexadecane]methyl]benzyl]-1,4,7,10-tetraazabicyclo[5.5.2]dodecane copper(II) acetate ($Cu_2$39)$^{4+}$

Amounts: 1-[4-Azidobenzyl]-7-[4-[[1,4,8,11-tetraazabicyclo[10.2.2]hexadecane]methyl]benzyl]-1,4,7,10-tetraazabicyclo[5.5.2]dodecane (**39**) (31 mg, 0.05 mmol), dry methanol (5 mL and 5 mL), copper(II)acetate monohydrate (21 mg, 0.10 mmol). To yield a blue solid (30 mg, 61 %).

MS (*m/z*): $[M+2Na+NH_4+2H]^+$ calcd for $C_{45}H_{77}Cu_2N_{12}Na_2O_8$, 1087.26; found, 1087.1. HRMS (*m/z*): Pending data, see 8.1.3. UV-vis (MeOH) λmax, nm (ε): 645.0 (286.0 M-1 cm-1).

1-[4-Azidobenzyl]-7-[4-[[1,4,8,11-tetraazabicyclo[10.2.2]hexadecane]methyl]benzyl]-1,4,7,10-tetraazabicyclo[5.5.2]dodecane zinc(II) acetate ($Zn_2$39)$^{4+}$

Amounts: 1-[4-Azidobenzyl]-7-[4-[[1,4,8,11-tetraazabicyclo[10.2.2]hexadecane]methyl]benzyl]-1,4,7,10-tetraazabicyclo[5.5.2]dodecane (**39**) (18 mg, 0.03 mmol), dry methanol (5 mL and 5 mL), zinc(II)acetate (11 mg, 0.06 mmol). To yield a blue solid (26 mg, 91 %).

^{1}H NMR (400 MHz, MeOD, δ): 1.63 (*d,* J=14.5 Hz, N-β-CH_2, 1H), 1.81 (*d,* J=15.3 Hz, N-β-CH_2, 2H), 1.99 (*br s,* CH_3-C, 12 H), 2.13-2.16 (*m,* N-β-CH_2, 1H), 2.20-2.26 (*m,* N-α-CH_2, 1H), 2.30-2.36 (*m,* N-α-CH_2, 1H), 2.46-2.56 (*m,* N-α-CH_2, 3H), 2.63 (*d,* J=10.8 Hz, N-α-CH_2, 3H), 2.80-2.83 (*m,* N-α-CH_2, 3H), 2.91-3.18 (*br m,* N-α-CH_2, 19H), 3.20-3.27 (*m*, N-α-CH_2, 3H), 3.45-3.53 (*m,* N-α-CH_2, 3H), 3.65-3.67 (*m,* N-α-CH_2, 4H), 3.78-3.85 (*m,* CH_2-Ar, 1H), 3.92-4.00 (*m,* CH_2-Ar, 3H), 4.17-4.22 (*m,* CH_2-Ar, 1H), 4.36 (*m,* CH_2-Ar, 1H), 4.58-4.64 (*m,* NH*,* 1H), 6.72-6.81 (*m,* Ar-H, 1H), 7.11-7.18 (*m,* Ar-H, 1H), 7.33-7.40 (*m,* Ar-H, 3H), 7.45-7.52 (*m,* Ar-H, 2H), 7.58-7.70 (*m,* Ar-H, 1H). ^{13}C NMR (100 MHz, MeOD, δ): 18.95 (CH_3-C), 20.91 (N-β-CH_2), 24.28 (N-β-CH_2), 43.25 (N-α-CH_2), 44.44 (N-α-CH_2), 44.60 (N-α-CH_2), 48.77 (N-α-CH_2), 49.13 (N-α-CH_2), 49.44 (N-α-CH_2), 51.41 (N-α-CH_2), 52.17 (N-α-CH_2), 52.27 (N-α-CH_2), 54.59 (N-α-CH_2), 54.82 (N-α-CH_2), 55.47 (N-α-CH_2), 55.72 (N-α-CH_2), 56.53 (N-α-CH_2), 57.93 (N-α-CH_2), 122.58 (Ar-H), 122.98 (Ar-H), 130.41 (Ar-H), 130.59 (Ar-H), 131.01 (Ar-C), 131.92 (Ar-H), 132.22 (Ar-H), 132.67 (Ar-C), 139.64 (Ar-C), 144.01 (Ar-C), 182.86 (C=O). MS (*m/z*): Pending data, see 8.1.3.

8.6.2 Attempted conjugation of 1-[4-azidobenzyl]-7-[4-[[1,4,8,11-tetraazabicyclo[10.2.2]hexadecane]methyl]benzyl]-1,4,7,10-tetraazabicyclo[5.5.2]dodecane copper(II) acetate (39) to 1-(bromomethyl)-4-(prop-2-yn-1-yloxy)benzene (51)

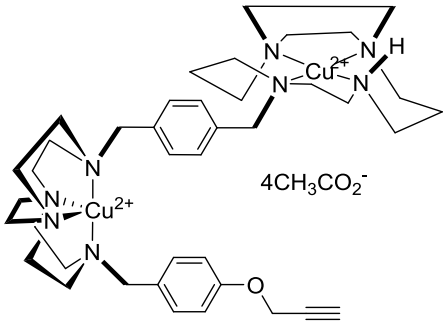

$[Cu_2\mathbf{44}]^{4+}$

Method 1

1-[4-Azidobenzyl]-7-[4-[[1,4,8,11-tetraazabicyclo[10.2.2]hexadecane]methyl]benzyl]-1,4,7,10-tetraazabicyclo[5.5.2]dodecane copper(II) acetate (**39**) (5 mg, 4.8 µmol), 1-(bromomethyl)-4-(prop-2-yn-1-yloxy)benzene (**51**) (1.1 mg, 5.0 µmol) and copper(I) iodide (47 µg, 0.20 µmol) were added to dry acetonitrile (1.6 mL) and triethylamine (0.2 M, 400 µL). The solution was heated at 100^{o}C for 30 min in the microwave in the microwave and the solvent removed *in vacuo*. To yield the brown solution (10 mg). The desired product was not isolated using this synthetic procedure. Analytical data indicates that the desired product was not obtained.

Method 2

1-[4-Azidobenzyl]-7-[4-[[1,4,8,11-tetraazabicyclo[10.2.2]hexadecane]methyl]benzyl]-1,4,7,10-tetraazabicyclo[5.5.2]dodecane copper(II) acetate (**39**) (3 mg, 2.9 µmol), 1-(bromomethyl)-4-(prop-2-yn-1-yloxy)benzene (**51**) (0.7 mg, 3.0 µmol) and copper(I) iodide (0.56 mg, 2.9 µmol) were added to dry acetonitrile (1.6 mL) and triethylamine (0.2 M, 400 µL). The solution was heated at 100^{o}C for 30 min in the microwave in the microwave and the solvent removed *in vacuo*. To yield the brown solution (10 mg). The desired product was not isolated using this synthetic procedure. Analytical data indicates that the desired product was not obtained.

8.6.3. Conjugation of metal complexes of 1-[4-[aminomethyl]benzyl]-7-[4-[[1,4,7,10-tetraaza bicyclo[8.2.2]dodecane]methyl]benzyl]-1,4,7,10-tetraazabicyclo[5.5.2]dodecane (34) and 1-[4-[aminomethyl]benzyl]-7-[4-[[1,4,8,11-tetraazabicyclo[10.2.2]hexadecane] methyl] benzyl]-1,4,7,10-tetraazabicyclo[5.5.2]dodecane (35) with tetrazine-PEG4-NHS

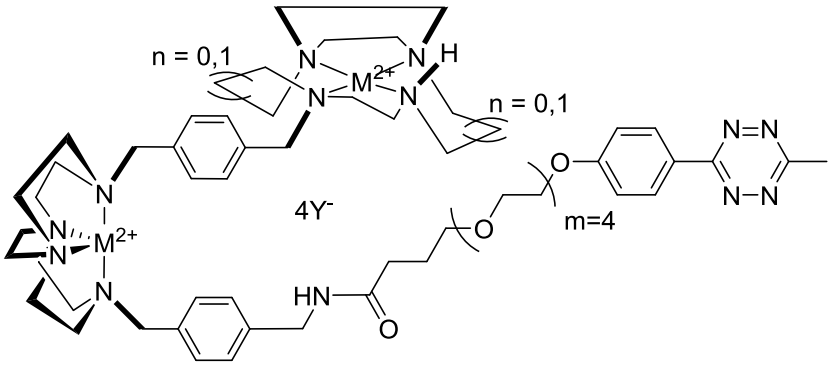

n=0

$[Cu_2\mathbf{41}]^{4+}$ $M^{2+}=Cu^{2+}$, $Y^-=CH_3CO_2^-$

$[Zn_2\mathbf{41}]^{4+}$ $M^{2+}=Zn^{2+}$, $Y^-=CH_3CO_2^-$

n=1

$[Cu_2\mathbf{42}]^{4+}$ $M^{2+}=Cu^{2+}$, $Y^-=CH_3CO_2^-$

$[Zn_2\mathbf{42}]^{4+}$ $M^{2+}=Zn^{2+}$, $Y^-=CH_3CO_2^-$

General procedure O was followed

An immediately prepared tetrazine-PEG4-NHS in dimethylsulfoxide solution was added to macrocycle in PBS buffer. The solution was incubated at RT for 1 h. After this the reaction was stopped by quenching with tris-HCl buffer and incubated for a further 5 min at RT. The product was purified through a desalting column (Sephadex PD-10).

Conjugation with 1-[4-[[4-[2-[2-[2-[2[2-[4-[6-methyl-1,2,4,5-tetrazin-3-yl]phenoxy]ethoxy]ethoxy] ethoxy]ethoxy]ethyl]-aminocarbonyl]methyl]benzyl]-7-[4-[[1,4,7,10-tetraazabicyclo[8.2.2]dodeca ne]methyl]benzyl]-1,4,7,10-tetraazabicyclo[5.5.2]dodecane copper(II) acetate ($[Cu_2\mathbf{41}]^{4+}$)

Amounts: Tetrazine-PEG4-NHS in dimethylsulfoxide solution (10 mM, 183 µL), 1-[4-[aminomethyl]benzyl]-7-[4-[[1,4,7,10-tetraazabicyclo[8.2.2]dodecane]methyl]benzyl]-1,4,7,10-tetraazabicyclo[5.5.2]dodecane copper(II) acetate ($[Cu_2\mathbf{41}]^{4+}$) (0.09 mg, 0.09 µmol), PBS buffer (1 mg/mL, 92 µL, pH 7.5), tris-HCl buffer (1 M, pH 8.0, 2.475 mL). To yield a crude, pink solid (~0.1 mg).

MS (*m/z*): $[M\text{-}2Cu\text{-}4CH_3CO_2\text{-}2H+NH_4]^+$ calcd for $C_{57}H_{89}N_{14}O_6$, 1066.43; found, 1066.3, $[M\text{-}2CH_3CO_2+3Na+NH_4]^+$ calcd for $C_{61}H_{97}Cu_2N_{14}O_{10}$, 1382.60; found, 1382.5.

Conjugation with 1-[4-[[4-[2-[2-[2-[2[2-[4-[6-methyl-1,2,4,5-tetrazin-3-yl]phenoxy]ethoxy]ethoxy]ethoxy]ethoxy]ethyl]-aminocarbonyl]methyl]benzyl]-7-[4-[[1,4,7,10-tetraazabicyclo[8.2.2]dodecane]methyl]benzyl]-1,4,7,10-tetraazabicyclo[5.5.2]dodecane zinc(II) acetate ($[Zn_2$41**$]^{4+}$)**

Amounts: Tetrazine-PEG4-NHS in dimethylsulfoxide solution (10 mM, 183 µL), 1-[4-[aminomethyl]benzyl]-7-[4-[[1,4,7,10-tetraazabicyclo[8.2.2]dodecane]methyl]benzyl]-1,4,7,10-tetraazabicyclo[5.5.2]dodecane zinc(II) acetate ($[Zn_2$**41**$]^{4+}$) (0.09 mg, 0.09 µmol), PBS buffer (1 mg/mL, 92 µL, pH 7.5), tris-HCl buffer (1 M, pH 8.0, 2.475 mL). To yield a crude, pink solid (~0.1 mg).

MS (*m/z*): $[M\text{-}2Zn\text{-}4CH_3CO_2\text{-}2H+NH_4]^+$ calcd for $C_{57}H_{89}N_{14}O_6$, 1066.43; found, 1066.3.

Conjugation with 1-[4-[[4-[2-[2-[2-[2[2-[4-[6-methyl-1,2,4,5-tetrazin-3-yl]phenoxy]ethoxy]ethoxy]ethoxy]ethoxy]ethyl]-aminocarbonyl]methyl]benzyl]-7-[4-[[1,4,8,11-tetraazabicyclo[10.2.2]hexadecane]methyl]benzyl]-1,4,7,10-tetraazabicyclo[5.5.2]dodecane copper(II) acetate ($[Cu_2$42**$]^{4+}$)**

Amounts: Tetrazine-PEG4-NHS in dimethylsulfoxide solution (10 mM, 183 µL), 1-[4-[aminomethyl]benzyl]-7-[4-[[1,4,8,11-tetraazabicyclo[10.2.2]hexadecane]methyl]benzyl]-1,4,7,10-tetraazabicyclo[5.5.2]dodecane copper(II) acetate ($[Cu_2$**42**$]^{4+}$) (0.10 mg, 0.09 µmol), PBS buffer (1 mg/mL, 95 µL, pH 7.5), tris-HCl buffer (1 M, pH 8.0, 2.502 mL). To yield a pink, crude solid (~0.1 mg).

MS (*m/z*): $[M\text{-}2CH_3CO_2+4NH_4]^+$ calcd for $C_{62}H_{111}Cu_2N_{17}O_{10}$, 1381.77; found, 1381.7.

Conjugation with 1-[4-[[4-[2-[2-[2-[2[2-[4-[6-methyl-1,2,4,5-tetrazin-3-yl]phenoxy]ethoxy]ethoxy]ethoxy]ethoxy]ethyl]-aminocarbonyl]methyl]benzyl]-7-[4-[[1,4,8,11-tetraazabicyclo[10.2.2]hexadecane]methyl]benzyl]-1,4,7,10-tetraazabicyclo[5.5.2]dodecane zinc(II) acetate ($[Zn_2$42**$]^{4+}$)**

Amounts: Tetrazine-PEG4-NHS in dimethylsulfoxide solution (10 mM, 183 µL), 1-[4-[aminomethyl]benzyl]-7-[4-[[1,4,8,11-tetraazabicyclo[10.2.2]hexadecane]methyl]benzyl]-1,4,7,10-tetraazabicyclo[5.5.2]dodecane zinc(II) acetate ($[Zn_2$**42**$]^{4+}$) (0.10 mg, 0.09 µmol), PBS buffer (1 mg/mL, 95 µL, pH 7.5), tris-HCl buffer (1 M, pH 8.0, 2.502 mL). To yield a pink, crude solid (~0.1 mg).

MS (*m/z*): $[M\text{-}2CH_3CO_2+3Na]^+$ calcd for $C_{62}H_{95}Na_3N_{13}O_{10}Zn_2$, 1382.25; found, 1382.2.

8.6.4. Attempted conjugation of metal complexes of 1-[4-azidobenzyl]-7-[4-[[1,4,8,11-tetraazabicyclo[10.2.2]hexadecane]methyl]benzyl]-1,4,7,10-tetraazabicyclo[5.5.2]dodecane (39) to carboxyrhodamine 110 dibenzocyclooctyl

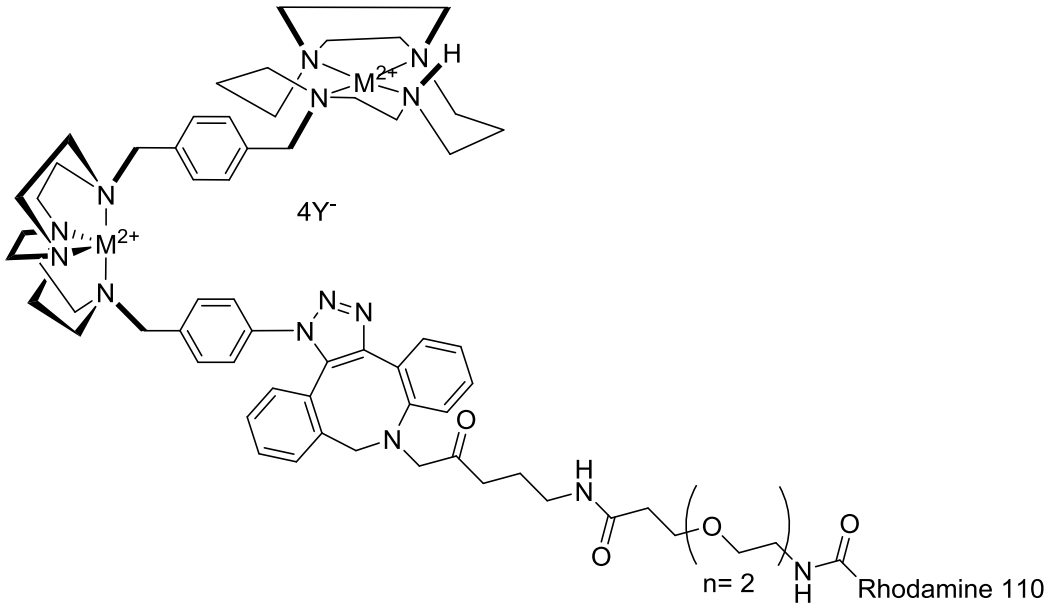

$[Cu_2\mathbf{40}]^{4+}$ $M^{2+}=Cu^{2+}$, $Y^-=CH_3CO_2^-$
$[Zn_2\mathbf{40}]^{4+}$ $M^{2+}=Zn^{2+}$, $Y^-=CH_3CO_2^-$

General procedure N was followed

Conjugation with 1-[4-azidobenzyl]-7-[4-[[1,4,8,11-tetraazabicyclo[10.2.2]hexadecane]methyl]benzyl]-1,4,7,10-tetraazabicyclo[5.5.2]dodecane copper(II) acetate $(Cu_2\mathbf{40})^{4+}$

Amounts: 1-[4-azidobenzyl]-7-[4-[[1,4,8,11-tetraazabicyclo[10.2.2]hexadecane]methyl]benzyl]-1,4,7,10-tetraazabicyclo[5.5.2]dodecane copper(II) acetate $(Cu_2\mathbf{39})^{4+}$ (0.87 mg, 0.08 µmol), carboxyrhodamine 110 dibenzocyclooctyl (0.50 mg, 0.06 µmol), methanol (100 µL and 175 µL). To yield a pink solid (~ 1 mg). Analytical data indicates that the desired product was not obtained.

Conjugation with 1-[4-azidobenzyl]-7-[4-[[1,4,8,11-tetraazabicyclo[10.2.2]hexadecane]methyl]benzyl]-1,4,7,10-tetraazabicyclo[5.5.2]dodecane zinc(II) acetate $(Zn_2\mathbf{40})^{4+}$

Amounts: 1-[4-azidobenzyl]-7-[4-[[1,4,8,11-tetraazabicyclo[10.2.2]hexadecane]methyl]benzyl]-1,4,7,10-tetraazabicyclo[5.5.2]dodecane zinc(II) acetate $(Zn_2\mathbf{39})^{4+}$ (0.87 mg, 0.08 µmol), carboxyrhodamine 110 dibenzocyclooctyl (0.50 mg, 0.06 µmol), methanol (100 µL and 175 µL). To yield a crude, pink solid (~ 1 mg). Analytical data indicates the desired product was not obtained.

8.7. SYNTHESIS OF PENDANT ARM WITH CLICK REACTION FUNCTIONALITY

8.7.1. Attempted synthesis of 1-(bromomethyl)-4-(prop-2-yn-1-yloxy)benzene (45)

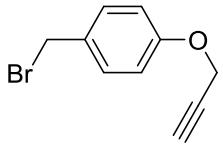

45

Method 1 – Attempted Synthesis

Propargyl alcohol (6 mL, 103.07 mmol) was added in small portions to a suspension of sodium hydride (60% in mineral oil, 4.54 g, 113.37 mmol) in dry dimethylformamide (200 mL) at 0^{o}C. After 30 min α-α'-dibromo-*p*-xylene (29.93 g, 113.37 mmol) in dry dimethylformamide (100 mL) was added and the resulting mixture stirred at RT overnight. A small amount of methanol was added to kill off any un-reacted sodium hydride, the mixture was diluted with ethyl acetate (400 mL) and washed with aqueous hydrochloric acid (1 M, 2x200 mL). The organic layer was dried ($MgSO_4$) and the bulk solvent removed *in vacuo* to yield an oil. Column chromatography (30:70-50:50-80:20, dichloromethane:hexane-10:90 methanol:dichloromethane) was conducted to yield a pale yellow solid (2.4 g). The desired product was not isolated using this synthetic procedure. Analytical data indicates that the desired product was not obtained.

Method 2 – Attempted Synthesis

Propargyl alcohol (3 mL, 51.54 mmol) was added in small portions to a suspension of sodium hydride (60% in mineral oil, 2.26 g, 56.69 mmol) in dry dimethylformamide (100 mL) at 0^{o}C. After 30 min α-α'-dibromo-*p*-xylene (29.93 g, 113.37 mmol) in dry dimethylformamide (100 mL) was added and the resulting mixture stirred at RT overnight. A small amount of methanol was added to kill off any un-reacted sodium hydride and the solvent was removed *in vacuo*. The solid was dissolved in ethyl acetate (200 mL) and washed with aqueous hydrochloric acid (1 M, 2x200 mL). The organic layer was dried ($MgSO_4$) and the bulk solvent removed *in vacuo* to yield an oil. Column chromatography (50:50, ethyl acetate:hexane) was conducted to yield a pale yellow solid (2.98 g). The desired product was not isolated using this synthetic procedure. Analytical data indicates that the desired product was not obtained.

8.7.2. Synthesis of methyl 4-(prop-2-yn-1-yloxy)benzoate (46)

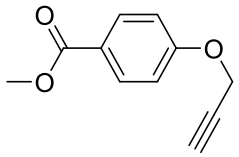

46

General procedure P

Methyl-4-hydroxybenzoate (6.00 g, 39.44 mmol) was dissolved in acetone (degassed, 300 mL) and propargyl bromide (80% toluene, 4.08 mL, 47.32 mmol) added. The mixture was stirred for 10 min and the potassium carbonate (38.15 g, 276.04 mmol) added. The mixture was heated at reflux overnight and the solvent was removed *in vacuo*. The residue was re-dissolved in dichloromethane (200 mL), dried ($MgSO_4$), filtered and the solvent was removed *in vacuo*. To yield a pale yellow solid (7.34 g, 98%).

^{1}H NMR (400 MHz, $CDCl_3$, δ): 2.56 (*t*, J=2.3 Hz, C≡CH, 1H), 3.87 (*s*, CH_3-O, 3H), 4.75 (*s*, CH_2-O, 2H), 6.96-7.00 (*m*, Ar-H, 2H), 7.98-8.01 (*m*, Ar-H, 2H). ^{13}C NMR (100 MHz, $CDCl_3$, δ): 52.02 (CH_3-O), 55.90 (CH_2-O), 76.18 (C≡CH), 77.90 (C≡CH), 114.56 (Ar-CH), 123.53 (Ar-C), 131.65 (Ar-H), 161.23 (Ar-C), 166.79 (C=O). HRMS (*m/z*): $[M+H]^+$ calcd for $C_{11}H_{10}O_3$, 191.0703; found, 191.0702. Anal. calcd for $C_{11}H_{10}O_3$: C, 69.46; H, 5.30. Found: C, 69.19; H, 5.04.

8.7.3. Attempted synthesis of 1-(azidomethyl)-4-(bromomethyl)benzene (47)

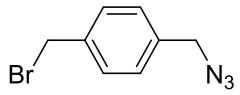

47

Method 1 – Attempted Synthesis

α- α'-dibromo-*p*-xylene (1.00 mg, 3.79 mmol) was added to dry dimethyl formamide (50 mL), to this sodium azide (246 mg, 3.79 mmol) was added. The solution was stirred at RT for 16 h under argon after which the bulk solvent was removed *in vacuo*. To yield a white solid. The desired product was not isolated using this synthetic procedure. Analytical data indicates that the desired product was not obtained.

8.7.4. Synthesis of (4-(bromomethyl)phenyl)methanol (48) and (4-(prop-2-yn-1-yloxy)phenyl)methanol (49)

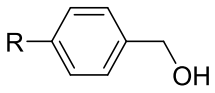

R =  **48**

R = 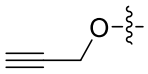 **49**

General procedure Q

Lithium aluminium hydride was added in one portion to dry tetrahydrofuran and the suspension cooled to 0°C. To this a dry solution of ester in dry tetrahydrofuran was added dropwise. The solution was stirred at 0°C under nitrogen for 1 h and then at RT overnight under nitrogen. The lithium aluminium hydride was neutralised with water, 15 % sodium hydroxide solution and washed with copious amounts of water to yield a white precipitate. This was filtered off and washed with a copious amount of dichloromethane until the precipitate was completely white and fine. The organic layers were washed with water, dried ($MgSO_4$) and the solvent removed *in vacuo*.

(4-(bromomethyl)phenyl)methanol (48)

Amounts: Lithium aluminium hydride (4.94 g, 0.13 mol), dry tetrahydrofuran (50 mL), methyl-4-(bromomethyl)benzoate (3.02 g, 0.013 mol), dry tetrahydrofuran (30 mL), water (1 mL), 15 % sodium hydroxide solution (1 mL), water (30 mL). To yield a white crystalline solid (0.87 g, 33%).

^{1}H NMR (400 MHz, $CDCl_3$, δ): 2.72 (*s*, CH_2-Br, 2H), 4.24 (*s*, OH, 1H), 4.58 (*s*, CH_2-OH, 2H), 7.22-7.54 (*m*, Ar-H, 4H). ^{13}C NMR (100 MHz, $CDCl_3$, δ): 20.73 (CH_2-Br), 64.07 (CH_2-OH), 126.75 (Ar-H), 128.68 (Ar-H), 136.49 (Ar-C), 137.70 (Ar-C). HRMS (m/z): $[M\text{-}Br]^+$ calcd for C_8H_9O 121.0648; found, 121.0645.

(4-(prop-2-yn-1-yloxy)phenyl)methanol (49)

Lithium aluminium hydride (14.38 g, 0.38 mol), dry tetrahydrofuran (150 mL), methyl-4-(prop-2-yn-1-yloxy)benzoate (**46**) (7.21 g, 0.04 mol), dry tetrahydrofuran (50 mL), water (1 mL), 15 % sodium hydroxide solution (1 mL), water (50 mL). To yield a yellow solid (5.32 g, 86%).

^{1}H NMR (400 MHz, $CDCl_3$, δ): 2.53 (*s*, C≡CH, 1H), 3.30 (*s*, OH, 1H), 4.63 (*s*, CH_2-Br, 2H), 4.81 (*s*, CH_2-OH, 2H), 6.87-6.89 (*m*, Ar-H, 2H), 7.19-7.21 (*m*, Ar-H, 2H). ^{13}C NMR (100 MHz, $CDCl_3$, δ): 49.42 (CH_2-

Br), 55.86 (CH_2-O), 64.44 (C≡CH), 75.76 (C≡CH), 114.91 (Ar-H), 128.57 (Ar-H), 134.33 (Ar-C), 156.97 (Ar-O). HRMS(m/z): $[M+H]^+$ calcd for $C_{10}H_9O_2$, 161.0597; found, 161.0595.

8.7.5. Synthesis of (4-(azidomethyl)phenyl)methanol (50)

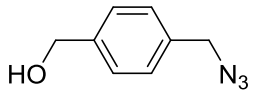

50

Method 1 – Attempted Synthesis

(4-(Bromomethyl)phenyl)methanol (**48**) (672 mg, 3.34 mmol) and sodium azide (283 mg, 4.35 mmol) were added to water (10 mL) and stirred at RT for 3d. After this the reaction mixture was extracted with diethyl ether (3 x 10 mL) and dried (Na_2SO_4) before being reduced *in vacuo* to yield a white solid (131 mg). The desired product was not isolated using this synthetic procedure. Analytical data indicates that the desired product was not obtained.

Method 2 – Attempted Synthesis

(4-(Bromomethyl)phenyl)methanol (**48**) (329 mg, 1.64 mmol) was dissolved in dry dimethyl formamide (10 mL), sodium azide (160 mg, 2.46 mmol) was added. The solution was stirred at 65^{o}C overnight under argon before being diluted with water (10 mL) and extracted with diethyl ether (3 x 10 mL) and dried ($MgSO_4$). The solvent was removed *in vacuo* to yield an oil (224 mg). The desired product was not isolated using this synthetic procedure. Analytical data indicates that the desired product was not obtained.

Method 3 – Attempted Synthesis

(4-(Bromomethyl)phenyl)methanol (**48**) (50 mg, 0.25 mmol) was dissolved in dry dimethylformamide (10 mL), to this sodium azide (32 mg, 0.50 mmol) was added and the mixture stirred at RT under argon overnight. Subsequently the solvent was removed *in vacuo* to yield an oil (93 mg). The desired product was not isolated using this synthetic procedure. Analytical data indicates that the desired product was not obtained.

8.7.6. Synthesis of 1-(bromomethyl)-4-(prop-2-yn-1-yloxy)benzene (51)

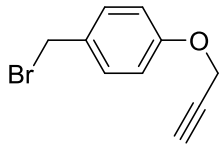

51

(4-(Prop-2-yn-1-yloxy)phenyl)methanol (**49**) (1.92 g, 7.12 mmol) and phosphorus tribromide (2.30 mL, 24.18 mmol) were dissolved in dry dichloromethane (100 mL) and stirred under argon for 18 h at RT. Water (50 mL) was added to kill off any remaining phosphorus tribromide and the water layer extracted with dichloromethane (5 x 25 mL). The organic layer was dried ($MgSO_4$) and the solvent removed *in vacuo.* The crude product was purified with a plug column (55:45, hexane:dichloromethane). To yield a yellow crystalline solid (2.71 g, 46 %).

^{1}H NMR (400 MHz, $CDCl_3$, δ): 2.53 (*s*, C≡CH, 1H), 4.54 (*s*, CH_2-Br, 2H), 4.69 (*s*, CH_2-O, 2H), 6.93-6.96 (*m*, Ar-H, 2H), 7.25-7.35 (*m*, Ar-H, 2H). ^{13}C NMR (100 MHz, $CDCl_3$, δ): 33.76 (CH_2-Br), 55.91 (CH_2-O), 75.86 (C≡CH), 78.38 (C≡CH), 115.24 (Ar-H), 130.55 (Ar-H), 130.98 (Ar-C), 157.66 (Ar-O). HRMS (*m/z*): $[M+H]^+$ calcd for $C_{10}H_{10}BrO$, 224.9910; found, 224.9910. Anal. calcd for $C_{10}H_9BrO$: C, 53.36; H, 4.03. Found: C, 44.34; H, 4.56 – contains impurity.

8.7.7. Attempted synthesis of methyl 4-(but-3-yn-1-yloxy)benzoate (52)

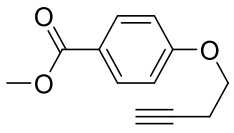

52

Method 1 - General procedure P was followed

Amounts: Methyl-4-hydroxybenzoate (5.33 g, 35.03 mmol), 4-bromo-1-butyne (5.00 g, 42.03 mmol), potassium carbonate (33.89 g, 245.21 mmol). To yield an orange liquid (10.33 g). Analytical data indicates that the desired product was not obtained.

Method 2

Methyl-4-hydroxybenzoate (5.33 g, 35.03 mmol) was dissolved in acetone (degassed, 300 mL) and 4-bromo-1-butyne (5.00 g, 42.03 mmol) was added. The mixture was stirred for 15 min and potassium carbonate (33.89 g, 245.21 mmol) was added. The mixture was heated at reflux for 3 d, the solvent removed *in vacuo* and the residue re-dissolved in dichloromethane. The solution was dried over $MgSO_4$, filtered and the solvent removed *in vacuo* to yield an orange liquid (10.33 g). Analytical data indicates that the desired product was not obtained.

8.7.8. Synthesis of but-3-yn-1-yl 4-methylbenzenesulfonate (53)

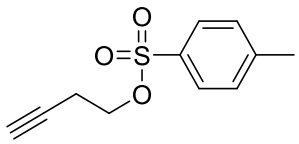

53

General procedure R

3-butyn-1-ol (4.00 g, 57.07 mmol) was dissolved in dichloromethane (100 mL) and triethylamine (9.55 mL, 68.48 mmol). The solution was stirred at 0°C and p-toluenesulfonyl chloride (11.42 g, 59.92 mmol). The reaction was allowed to warm to room over a period of 1 hour and stirring was continued overnight. Thin layer chromatography (TLC) analysis (hexanes/ethyl acetate (EtOAc) 6: 1) after 20 hours of reaction showed a complete consumption of 3-butyn-1-ol. The precipitated triethylamine hydrochloride was filtered off and the filtrate washed with water (2 x 30 mL) and brine (2 x 30 mL). The organic layer was dried over Na_2SO_4 and the solvent evaporated. To yield a light-yellow oil (8.27 g, 72 %).

^{1}H NMR (400 MHz, $CDCl_3$, δ): 1.96 (*m*, C≡CH, 1H), 2.44 (*s*, CH_3-Ar, 3H), 2.54 (*td*, J=7.0 Hz, $\underline{C}H_2$-C, 2H), 4.08 (*t*, J=7.0 Hz, CH_2-O, 2H), 7.34 (*dd*, J=8.6 Hz, Ar-H, 2H), 7.77-7.80 (*m*, Ar-H, 2H). ^{13}C NMR (100 MHz, $CDCl_3$, δ): 19.51 ($\underline{C}H_2$-Ar), 21.75 ($\underline{C}H_2$-C), 67.55 (CH_2-O), 70.88 (C≡$\underline{C}$H), 78.48 ($\underline{C}$≡CH), 127.10 (Ar-H), 128.06 (Ar-H), 129.70 (Ar-H), 130.01 (Ar-H), 132.81 (Ar-C), 145.15 (Ar-C). MS (m/z): $[M]^+$ calcd for $C_{11}H_{12}O_3S$, 224.27; found, 224.2.

8.7.9. Synthesis of 4-(but-3-yn-1-yloxy)benzaldehyde (54)

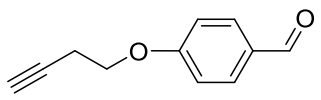

54

General procedure S

A suspension of 4-hydroxybenzaldehyde (**53**) (0.66 g, 5.40 mmol), **1** (7.5 g, 33 mmol), potassium carbonate (1.78, 16.20 mmol), and sodium iodide (81 mg, 0.54 mmol) in acetonitrile (150 mL) was refluxed for 16 h. The solution was concentrated *in vacuo* and treated with ethyl acetate/water (50 mL) and the aqueous layer was extracted with ethyl acetate (5 x 25 mL). The combined organic layers were washed with water (25 mL) and brine (25 mL), dried over $MgSO_4$ and concentrated to dryness. To yield a colourless solid (0.39 g, 52 %).

^{1}H NMR (400 MHz, $CDCl_3$, δ): 2.06 (*m*, C≡CH, 1H), 2.73 (*td*, J=6.9 Hz, $\underline{C}H_2$-C, 2H), 4.18 (*t*, J=6.9 Hz, CH_2-O, 2H), 7.01-7.04 (*m*, Ar-H, 2H), 7.84-7.87 (*m*, Ar-H, 2H), 9.88 (*s,* HC=O, 1H). ^{13}C NMR (100 MHz, $CDCl_3$, δ): 19.52 ($\underline{C}H_2$-C), 66.31 (CH_2-O), 70.39 (C≡$\underline{C}$H), 76.55 ($\underline{C}$≡CH), 114.98 (Ar-H), 132.30 (Ar-C), 132.65 (Ar-H), 162.36 (Ar-O), 191.39 (C=O). MS (m/z): $[M]^+$ calcd for $C_{11}H_{10}O_2$, 174.20; found, 174.3.

8.7.10. Synthesis of (4-(but-3-yn-1-yloxy)phenyl)methanol (55)

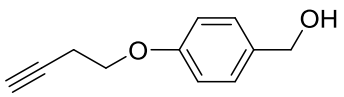

55

General procedure T

At 0^{o}C sodium borohydride (1.33 g, 0.36 mol) was slowly added to a cooled solution of 4-(but-3-yn-1-yloxy)benzaldehyde (**54**) (1.2 g, 6 mmol) in dry THF (150 mL). After 30 min the reaction mixture was treated with water (20 mL) and extracted with ethyl acetate (5 x 50 mL). The combined organic layers were washed with water (50 mL) and brine (50 mL), dried over $MgSO_4$ and concentrated *in vacuo*. The crude product was used without further purification. To yield an oil (2.46 g, 76 %).

^{1}H NMR (400 MHz, $CDCl_3$, δ): 2.32 (*m*, C≡CH, 1H), 2.62 (*td*, J=6.7 Hz, $\underline{C}H_2$-C, 2H), 4.05 (*t*, J=6.7 Hz, CH_2-O, 2H), 4.48 (*s*, CH_2-OH, 2H), 4.52 (*s*, OH, 1H), 6.74-6.76 (*m*, Ar-H, 2H), 7.15-7.17 (*m*, Ar-H, 2H). ^{13}C NMR (100 MHz, $CDCl_3$, δ): 18.90 ($\underline{C}H_2$-C), 63.79 (CH_2-OH), 66.05 (CH_2-O), 69.56 (C≡$\underline{C}$H), 80.20 ($\underline{C}$≡CH), 114.76 (Ar-H), 128.52 (Ar-H), 129.50 (Ar-H), 132.16 (Ar-H), 133.81 (Ar-C), 156.59 (Ar-O). MS (m/z): $[M]^+$ calcd for $C_{11}H_{12}O_2$, 176.22; found, 176.2.

8.7.11. Attempted synthesis of 1-(bromomethyl)-4-(but-3-yn-1-yloxy)benzene (56)

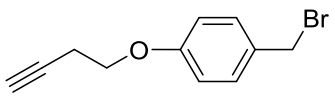

56

(4-(But-3-yn-1-yloxy)phenyl)methanol (**55**) (2.30 g, 13.10 mmol) was dissolved in dry dichloromethane (75 mL) to this phosphorus tribromide (1.24 mL, 13.10 mmol) was added in one portion. The mixture was stirred at RT for 24 h under argon. Water (45 mL) was added to kill off any remaining phosphorus tribromide and the aqueous layer extracted with dichloromethane (3 x 20 mL). The combined organic layers were dried with $MgSO_4$ and the solvent removed *in vacuo*. To yield the product as a red solid (1.81 g). Analytical data indicates that the desired product was not obtained.

8.8. MONO-MACROCYCLES

8.8.1. Synthesis of 2a-[4-[prop-2-yn-1-yloxy]benzyl]-decahydro-2a,4a,6a,8a-tetraaza-pyrenium bromide (57)

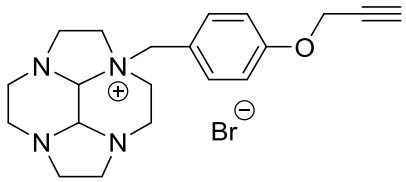

57

Method 1 – Attempted synthesis

2a-[4-[bromomethyl]benzyl]-decahydro-2a,4a,6a,8a-tetraaza-pyrenium bromide (5)

Amounts: *cis*-13-1,4,7,10-tetraazatetracyclo[5.5.1.04,14010,13]tetradecane (2) (1 g, 5.15 mmol), dry THF (100 mL), α-α'-dibromo-p-xylene (3.40 g, 12.89 mmol), dry THF (2 x 10 mL). To yield a white solid (2.05 g). The desired product was not isolated using this synthetic procedure. Analytical data indicates that the desired product was not obtained.

Method 2 – Attempted synthesis

Macrocycle was added to dry acetonitrile to this pendant arm was added and the solution stirred under argon for 3 d at RT. Following this the resulting precipitate was filtered and washed with acetonitrile and diethyl ether.

2a-[4-nitrobenzyl]-decahydro-2a,4a,6a,8a-tetraaza-pyrenium bromide (6)

Amounts: *cis*-13-1,4,7,10-tetraazatetracyclo[5.5.1.04,14010,13]tetradecane (2) (1.25 g, 6.43 mmol), dry acetonitrile (25 mL), 4-nitrobenzyl bromide (1.81 g, 8.36 mmol), dry acetonitrile (2 x 10 mL).To yield a white solid (3.75 g). The desired product was not isolated using this synthetic procedure. Analytical data indicates that the desired product was not obtained.

2a-[4-cyanobenzyl]-decahydro-2a,4a,6a,8a-tetraaza-pyrenium bromide (7)

Amounts: *cis*-13-1,4,7,10-tetraazatetracyclo[5.5.1.04,14010,13]tetradecane (2) (1.25 g, 6.43 mmol), dry acetonitrile (100 mL), 4-[bromomethyl]benzonitrile (3.15 g, 16.09 mmol), dry acetonitrile (2 x 20 mL). To yield a white solid (2.47 g). The desired product was not isolated using this synthetic procedure. Analytical data indicates that the desired product was not obtained.

2a-[4-[methoxycarbonyl]benzyl]-decahydro-2a,4a,6a,8a-tetraaza-pyrenium bromide (8)

Amounts: *cis*-13-1,4,7,10-tetraazatetracyclo[5.5.1.04,14010,13]tetradecane (2) (1.25 g, 6.43 mmol), dry acetonitrile (100 mL), methyl 4-[bromomethyl]benzoate (3.69 g, 16.09 mmol), acetonitrile (2 x 20 mL). To yield a white solid (2.18 g). The desired product was not isolated using this synthetic procedure. Analytical data indicates that the desired product was not obtained.

Method 3 – Preferred route**Method** 1 – Attempted synthesis

2a-[4-[bromomethyl**]benzyl]-decahydro-2a,4a,6a,8a-tetraaza-pyrenium bromide (5)**

Amounts: *cis-13-1,4,7,10-tetraazatetracyclo*[5.5.1.04,14010,13]tetradecane (**2**) (1 g, 5.15 mmol), dry THF (100 mL), α-α'-dibromo-p-xylene (3.40 g, 12.89 mmol), dry THF (2 x 10 mL). To yield a white solid (2.05 g). The desired product was not isolated using this synthetic procedure. Analytical data indicates that the desired product was not obtained.

Method 2 – Attempted synthesis

Macrocycle was added to dry acetonitrile to this pendant arm was added and the solution stirred under argon for 3 d at RT. Following this the resulting precipitate was filtered and washed with acetonitrile and diethyl ether.

2a-[4-nitrobenzyl]-decahydro-2a,4a,6a,8a-tetraaza-pyrenium bromide (6)

Amounts: *cis-13-1,4,7,10-tetraazatetracyclo*[5.5.1.04,14010,13]tetradecane (**2**) (1.25 g, 6.43 mmol), dry acetonitrile (25 mL), 4-nitrobenzyl bromide (1.81 g, 8.36 mmol), dry acetonitrile (2 x 10 mL).To yield a white solid (3.75 g). The desired product was not isolated using this synthetic procedure. Analytical data indicates that the desired product was not obtained.

2a-[4-cyanobenzyl]-decahydro-2a,4a,6a,8a-tetraaza-pyrenium bromide (7)

Amounts: *cis-13-1,4,7,10-tetraazatetracyclo*[5.5.1.04,14010,13]tetradecane (**2**) (1.25 g, 6.43 mmol), dry acetonitrile (100 mL), 4-[bromomethyl]benzonitrile (3.15 g, 16.09 mmol), dry acetonitrile (2 x 20 mL). To yield a white solid (2.47 g). The desired product was not isolated using this synthetic procedure. Analytical data indicates that the desired product was not obtained.

2a-[4-[methoxycarbonyl]benzyl]-decahydro-2a,4a,6a,8a-tetraaza-pyrenium bromide (8)

Amounts: *cis-13-1,4,7,10-tetraazatetracyclo*[5.5.1.04,14010,13]tetradecane (**2**) (1.25 g, 6.43 mmol), dry acetonitrile (100 mL), methyl 4-[bromomethyl]benzoate (3.69 g, 16.09 mmol), acetonitrile (2 x 20 mL). To yield a white solid (2.18 g). The desired product was not isolated using this synthetic procedure. Analytical data indicates that the desired product was not obtained.

Method 3 – Preferred route

General procedure C was followed

Amounts: *cis*-13-1,4,7,10-Tetraazatetracyclo[5.5.1.04,14010,13]tetradecane (**2**) (100 mg, 0.51 mmol), dry THF (0.5 mL), 1-(bromomethyl)-4-(prop-2-yn-1-yloxy)benzene (**51**) (116 mg, 0.51 mmol), diethyl ether (3 x 10 mL), dichloromethane (1 x 10 mL). To yield a cream solid (163 mg, 75 %).

^{1}H NMR (400 MHz, DMSO, δ): 2.30-2.35 (*m*, N-α-CH_2, 1H), 2.38-2.43 (*m*, N-α-CH_2, 1H), 2.61 (*d*, J=10.4 Hz, N-α-CH_2, 1H), 2.68 (*d*, J=9.0 Hz, N-α-CH_2, 1H), 2.71-2.80 (*m*, N-α-CH_2, 2H), 2.90 (*s*, C≡CH, 1H), 3.02-3.14 (*m*, N-α-CH_2, 4H), 3.18-3.22 (*m*, N-α-CH_2, 1H), 3.26 (*d*, J=13.1 Hz, N-α-CH_2, 1H), 3.42-3.44 (*m*, N-α-CH_2, 1H), 3.48-3.55 (*m*, N-α-CH_2, 1H), 3.61 (*m*, N-α-CH_2, 1H), 3.64-3.65 (*m*, N-α-CH_2, 1H), 3.97 (*m*, CH_2-Ar, 1H), 4.13-4.18 (*m*, CH_2-Ar, 1H), 4.73 (*d*, J=13.1 Hz, H_{aminal}, 1H), 4.87-4.88 (*m*, CH_2-O, 2H), 4.89-4.90 (*m*, Hz, H_{aminal}, 1H), 7.12 (*d*, J=8.4 Hz, Ar-H, 2H), 7.59 (*d*, J=8.4 Hz, Ar-H, 2H). ^{13}C NMR (100 MHz, DMSO, δ): 43.42 (N-α-CH_2), 48.28 (N-α-CH_2), 48.75 (N-α-CH_2), 49.37 (N-α-CH_2), 52.13 (N-α-CH_2), 56.13 (CH_2-O), 57.42 (N-α-CH_2), 59.87 (N-α-CH_2), 60.91 (N-α-CH_2), 71.90 (C≡$\underline{C}$H), 79.19 ($\underline{C}$≡CH), 79.47 (C_{aminal}), 83.12 (C_{aminal}), 115.92 (Ar-H), 121.26 (Ar-C), 134.60 (Ar-H), 159.13 (Ar-C). HRMS (*m/z*): [M-Br]$^{+}$ calcd for $C_{20}H_{27}N_4O$, 339.2179; found, 339.2177. Anal. calcd for $C_{20}H_{27}N_4O.MeOH.H_2O$: C 53.73, H 7.09, N 11.94; found C 53.30, H 6.22, N 11.52.

8.8.2. Synthesis of 3a-[4-[prop-2-yn-1-yloxy]benzyl]-dodecahydro-3a,5a,8a,10a-tetraazapyrenium bromide (58), 3a-[4-nitrobenzyl]-decahydro-3a,5a,8a,10a-tetraazapyrenium bromide (59) and 3a-[4-[methoxycarbonyl]benzyl]-decahydro-3a,5a,8a,10a-tetraazapyrenium bromide (60)

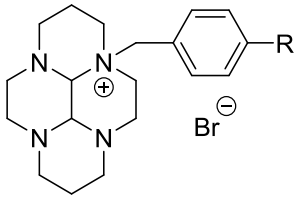

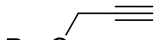

R= O **58**
R=NO_2 **59**
R=COOMe **60**

General procedure U

Macrocycle was added to dry acetonitrile to this pendant arm was added and the solution stirred under argon for 3 d at RT. Following this the resulting precipitate was filtered and washed with acetonitrile and diethyl ether.

3a-[4-[prop-2-yn-1-yloxy]benzyl]-decahydro-3a,5a,8a,10a-tetraazapyrenium bromide (58)

Amounts: *cis*-3a,5a,8a,10a-tetraazaperhydropyrene (**3**) (1.00 g, 4.50 mmol), dry acetonitrile (25 mL), 1-(bromomethyl)-4-(prop-2-yn-1-yloxy)benzene (**51**) (2.02 g, 9.00 mmol), acetonitrile (2 x 20 mL), diethyl ether (2 x 20 mL). To yield a white solid (2.01g, 100 %).

^{1}H NMR (400 MHz, D_2O, δ): 1.27 (*d*, J=13.5 Hz, N-β-CH_2, 1H), 1.59 (*d*, J=14.9 Hz, N-β-CH_2, 1H), 1.87 (*s*, N-β-CH_2, 1H), 1.93-2.03 (*m*, N-β-CH_2, 1H), 2.05-2.11 (*m*, N-α-CH_2, 1H), 2.24-2.31 (*m*, N-α-CH_2, 2H), 2.42 (*td*, J=12.0 Hz, C≡C-H, 1H), 2.77-2.92 (*m*, N-α-CH_2, 8H), 3.03 (*t*, J=13.6 Hz, N-α-CH_2, 1H), 3.12-3.15 (*d,* J=11.8 Hz, N-α-CH_2, 1H), 3.27-3.36 (*m*, N-α-CH_2, 2H), 3.45 (*s,* N-α-CH_2, 1H), 3.94-4.01 (*m*, CH_2-Ar, 1H), 4.15 (*s*, CH_2-Ar, 1H), 4.53-4.57 (*d*, J=13.5 Hz, H_{aminal}, 1H), 4.67 (*s,* CH_2-O, 2H), 4.81-4.84 (*d*, J=13.5 Hz, H_{aminal}, 1H), 6.97-6.99 (*m*, Ar-H, 2H), 7.30-7.32 (*m*, Ar-H, 2H). ^{13}C NMR (100 MHz, DMSO, δ): 14.96 (N-β-CH_2), 17.89 (N-β-CH_2), 30.91 (N-α-CH_2), 50.40 (N-α-CH_2), 52.14 (N-α-CH_2), 59.50 (CH_2-O), 62.90 (N-α-CH_2), 67.64 (CH_2-Ar), 71.68 (C≡C-H), 72.19 (C≡C-CH_2), 118.22 (H_{aminal}), 127.75 (H_{aminal}), 134.83 (Ar-H), 145.12 (Ar-C), 146.34 (Ar-H), 151.06 (Ar-H). HRMS (*m/z*): $[M-Br]^+$ calcd for $C_{22}H_{31}N_4O$, 367.2492; found, 367.2493. Anal. calcd for $C_{22}H_{31}N_4O$: C 59.06, H 6.98, N 12.52; found C 59.27, H 7.05, N 12.36.

3a-[4-nitrobenzyl]-decahydro-3a,5a,8a,10a-tetraazapyrenium bromide (59)

Amounts: *cis*-3a,5a,8a,10a-tetraazaperhydropyrene (**3**) (2.00 g, 9.00 mmol), dry acetonitrile (25 mL), 4-nitrobenzyl bromide (4.85 g, 22.49 mmol), acetonitrile (2 x 20 mL), diethyl ether (2 x 20 mL). To yield a yellow precipitate (3.84 g, 97 %).

^{1}H NMR (400 MHz, DMSO, δ): 1.24-1.28 (*m,* N-β-CH_2, 3H), 1.68 (*d,* J=14.1 Hz, N-β-CH_2, 1H), 2.24-2.3 (*m,* N-α-CH_2, 2H), 2.40 (*d,* J=10.8 Hz, N-α-CH_2, 1H), 2.66 (*d,* J=10.9 Hz, N-α-CH_2, 1H), 2.86-3.01 (*m,* N-α-CH_2, 6H), 3.16-3.23 (*m,* N-α-CH_2, 3H), 3.55-3.58 (*m,* N-α-CH_2, 1H), 3.69 (*t,* J=11.4 Hz, N-α-CH_2, 1H), 3.83 (*s,* N-α-CH_2, 1H), 4.18-4.27 (*m,* CH_2-Ar, 1H), 4.83 (*s,* CH_2-Ar, 1H), 4.98 (*d,* J=13.1 Hz, NH, 1H), 5.44 (*d,* J=13.1 Hz, NH, 1H), 7.89 (*d,* J=7.3 Hz, Ar-H, 2H), 8.35 (*d,* J=7.5 Hz, Ar-H, 2H). ^{13}C NMR (100 MHz, DMSO, δ): 32.50 (N-β-CH_2), 42.72 (N-α-CH_2), 46.65 (N-α-CH_2), 48.85 (N-α-CH_2), 52.41 (N-α-CH_2), 54.20 (N-α-CH_2), 54.34 (N-α-CH_2), 69.62 (C_{aminal}), 83.08 (C_{aminal}), 118.37 (Ar-H), 124.24 (Ar-H), 131.10 (Ar-H), 134.97 (Ar-C), 135.47 (Ar-H), 149.11 (Ar-NO_2). HRMS (*m/z*): $[M\text{-}Br]^+$ calcd for $C_{19}H_{28}N_5O_2$, 358.2238; found, 358.2238.

3a-[4-[methoxycarbonyl]benzyl]-decahydro-3a,5a,8a,10a-tetraazapyrenium bromide (60)

Amounts: *cis*-3a,5a,8a,10a-tetraazaperhydropyrene (**3**) (2.50 g, 11.24 mmol), dry acetonitrile (50 mL), methyl-4-(bromomethyl)benzoate (5.51 g, 22.49 mmol), acetonitrile (2 x 20 mL), diethyl ether (2 x 20 mL). To yield a yellow precipitate (4.53 g, 89 %).

^{1}H NMR (400 MHz, D_2O, δ): 1.28 (*d,* J=14.1 Hz, N-β-CH_2, 1H), 1.59 (*d,* J=14.9 Hz, N-β-CH_2, 1H), 1.97-2.06 (*m,* N-β-CH_2, 2H), 2.28-2.14 (*m,* N-α-CH_2, 1H), 2.27-2.33 (*m,* N-α-CH_2, 2H), 2.44 (*td,* J=12.3 Hz, N-α-CH_2, 1H), 2.81-2.98 (*m,* N-α-CH_2, 7H), 3.05-3.18 (*m,* N-α-CH_2, 2H), 3.28-3.43 (*m,* N-α-CH_2, 2H), 3.52 (*s,* N-α-CH_2, 1H), 3.77 (*s,* CH_3-O, 3H), 4.04 (*td,* J=13.1 Hz, CH_2-Ar, 1H), 4.17 (*s,* CH_2-Ar, 1H), 4.61 (*s,* H_{aminal}, 1H), 5.00 (*d,* J=13.3 Hz, H_{aminal}, 1H), 7.48 (*d,* J=8.4 Hz, Ar-H, 2H), 7.95 (*d,* J=8.2 Hz, Ar-H, 2H). ^{13}C NMR (100 MHz, D_2O, δ)*:* 17.93 (N-β-CH_2), 18.32 (N-β-CH_2), 41.89 (N-α-CH_2), 46.56 (N-α-CH_2), 48.57 (N-α-CH_2), 51.28 (N-α-CH_2), 51.89 (N-α-CH_2), 52.87 (N-α-CH_2), 53.25 (N-α-CH_2), 53.89 (N-α-CH_2), 60.07 (N-α-CH_2), 61.70 (N-α-CH_2), 69.49 (C_{aminal}), 82.30 (C_{aminal}), 130.01 (Ar-H), 130.81 (Ar-C), 131.80 (Ar-C), 133.49 (Ar-H), 168.41 (C=O). HRMS (*m/z*): $[M\text{-}Br]^+$ calcd for $C_{21}H_{31}N_4O_2$, 371.2447; found, 371.2438. Anal. calcd for $C_{21}H_{31}N_4O_2Br$: C, 55.88; H, 6.92; N, 12.41. Found: C, 56.01; H, 6.99; N, 12.40.

8.8.3. Attempted synthesis of 3a-[but-3-yn-1-yl]-dodecahydro-3a,5a,8a,10a-tetraazapyrenium bromide (61)

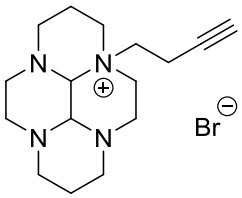

61

Cis-3a,5a,8a,10a-tetraazaperhydropyrene (**3**) (1.67 g, 7.51 mmol) was dissolved in dry tetrahydrofuran (10 mL), to this 4-bromo-1-butyne (2.00 g, 15.02 mmol) was added and the solution stirred at RT for 3 d under an atmosphere of argon. Precipitation was not observed and the reaction was allowed to stir for a total of 10 d. The solvent was removed *in vacuo* and washed with diethyl ether (2 x 20 mL) to yield a pale yellow residue (200 mg). Analytical data indicates that the desired product was not obtained.

8.8.4. Synthesis of 2a-[methyl]-6a-[4-[prop-2-yn-1-yloxy]benzyl]-decahydro-2a,4a,6a,8a-tetraaza-pyrenium bromide (62)

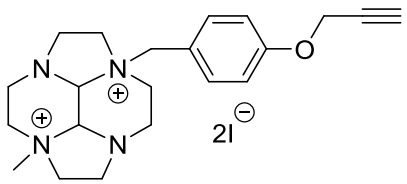

62

2a-[4-[prop-2-yn-1-yloxy]benzyl]-decahydro-2a,4a,6a,8a-tetraaza-pyrenium bromide (**57**) (50 mg, 0.12 mmol) was suspended in dry MeCN (15 mL) under nitrogen, to this iodomethane (0.61 mL, 9.78 mmol) was added dropwise. The white suspension was left to stir for 10 d, after 5 d a second portion of iodomethane (0.31 mL, 4.89 mmol) was added. Excess iodomethane was removed by flowing nitrogen through the suspension for 30 min. The solution was filtered, washed with diethyl ether (2 x 10 mL) and dried *in vacuo*. To yield the product as a white solid (25 mg, 35 %).

^{1}H NMR (400 MHz, D_2O, δ): 1.91 (*br s,* CH_3-N, 3H), 2.77 (*br s*, C≡CH, 1H), 2.83 (*br s,* N-α-CH_2, 1H), 2.94-3.03 (*m,* N-α-CH_2, 3H), 3.16 (*br s,* N-α-CH_2, 1H), 3.25-3.29 (*m,* N-α-CH_2, 6H), 3.71-3.78 (*m,* N-α-CH_2, 2H), 3.91 (*br s,* N-α-CH_2, 2H), 4.09 (*br s,* CH_2-Ar, 1H), 4.34 (*br s,* CH_2-Ar, 1H), 4.47 (*m,* H_{aminal}, 2H), 4.71 (*br s,* CH_2-O, 2H), 7.04 (*br s,* Ar-H, 2H), 7.43 (*br s,* Ar-H, 2H). ^{13}C NMR (100 MHz, D_2O, δ): 42.86 (N-α-CH_2), 46.36 (N-α-CH_2), 46.95 (N-α-CH_2), 48.00 (N-α-CH_2), 49.41 (N-α-CH_2), 51.16 (N-α-CH_2), 56.19 (CH_2-O), 60.02 (N-α-CH_2), 60.54 (N-α-CH_2), 64.40 (N-α-CH_2), 75.94 (C≡<u>C</u>H), 76.90 (<u>C</u>≡CH), 79.26 (C_{aminal}), 79.45 (C_{aminal}), 116.10 (Ar-H), 120.30 (Ar-C), 134.77 (Ar-H), 159.42 (Ar-C). HRMS (*m/z*): $[M\text{-}I]^+$ calcd for $C_{21}H_{30}IN_4O$, 481.1459; found, 481.1452. Anal. calcd for $C_{21}H_{30}N_4OI_2.2H_2O$: C 39.15, H 5.32, N 8.70; found C 38.57, H 4.87, N 8.58.

8.8.5. Attempted synthesis of 3a-[methyl]-8a-[4-[prop-2-yn-1-yloxy]benzyl]-dodecahydro-3a,5a,8a,10a-tetraazapyrenium bromide (63)

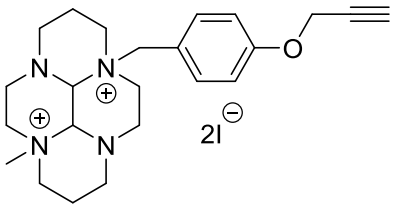

63

3a-[4-[prop-2-yn-1-yloxy]benzyl]-decahydro-3a,5a,8a,10a-tetraazapyrenium bromide (**58**) (1.50 g, 3.35 mmol) was suspended in dry MeCN (50 mL) under nitrogen, to this iodomethane (17.11 mL, 274.70 mmol) was added dropwise. The white suspension was left to stir for 10 d, after 5 d a second portion of iodomethane (8.56 mL, 137.35 mmol) was added. Excess iodomethane was removed by flowing nitrogen through the suspension for 30 min. The solution was filtered, washed with diethyl ether (2 x 50 mL) and dried *in vacuo*. To yield a white solid (1.52 g). The desired product was not isolated using this synthetic procedure. Analytical data indicates that the desired product was not obtained.

8.8.6. Synthesis of 1-[4-[prop-2-yn-1-yloxy]benzyl]-1,4,7,10-tetraazabicyclo[8.2.2]dodecane (64), 1-[4-[prop-2-yn-1-yloxy]benzyl]-1,4,8,11-tetraazabicyclo[10.2.2]hexadecane (65), 1-[4-nitro benzyl]-1,4,8,11-tetraazabicyclo[10.2.2]hexadecane (66) and 1-[4-[methoxycarbonyl]benzyl]-1,4,8,11-tetraazabicyclo[10.2.2]hexadecane (67)

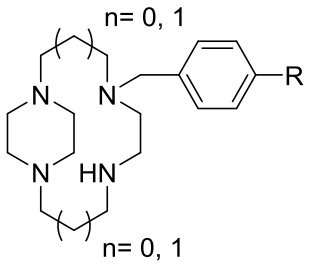

n=0

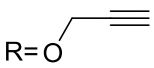

64

n=1

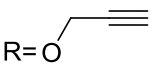

65

$R=NO_2$ **66**

R=COOMe **67**

General procedure G was followed

1-[4-[prop-2-yn-1-yloxy]benzyl]-1,4,7,10-tetraazabicyclo[8.2.2]dodecane (64)

Amounts: 2a-[4-[prop-2-yn-1-yloxy]benzyl]-decahydro-2a,4a,6a,8a-tetraaza-pyrenium bromide (**57**) (360 mg, 0.86 mmol), ethanol (75 mL), sodium borohydride (975 mg, 25.76 mmol), aqueous hydrochloric acid (2M, 10 mL), water (100 mL), dichloromethane (5 x 25 mL). To yield a yellow oil (242 mg, 82 %).

^{1}H NMR (400 MHz, $CDCl_3$, δ): 2.32-2.34 (*m*, N-α-CH_2, 2H), 2.48-2.50 (*m*, N-α-CH_2, 2H), 2.57-2.59 (*m*, HC≡C, 1H), 2.63-2.69 (*m*, N-α-CH_2, 1H), 2.71-3.22 (*m*, N-α-CH_2, 14H), 3.48-3.55 (*m*, N-α-CH_2, 1H), 3.65 (*s*, CH_2-Ar, 2H), 4.69-4.73 (*m*, NH, 1H), 4.91 (*br s*, CH_2-O, 2H), 6.92-7.02 (*m*, Ar-H, 2H), 7.24-7.37 (*m*, Ar-H, 2H). ^{13}C NMR (100 MHz, $CDCl_3$, δ): 45.93 (N-α-CH_2), 49.64 (N-α-CH_2), 50.02 (N-α-CH_2), 50.28 (N-α-CH_2), 51.17 (N-α-CH_2), 55.60 (N-α-CH_2), 56.26 (N-α-CH_2), 58.35 (N-α-CH_2), 59.23 (N-α-CH_2), 63.49 (CH_2-Ar), 68.49 (CH_2-O), 75.54 (C≡CH), 78.16 (C≡CH), 114.66 (Ar-H), 129.94 (Ar-C), 130.19 (Ar-H), 131.93 (Ar-H), 157.18 (Ar-O). HRMS (*m/z*): $[M+H]^+$ calcd for $C_{20}H_{31}N_4O$, 343.2492; found, 343.2493.

1-[4-[prop-2-yn-1-yloxy]benzyl]-1,4,8,11-tetraazabicyclo[10.2.2]hexadecane (65)

Amounts: 3a-[4-[prop-2-yn-1-yloxy]benzyl]-dodecahydro-3a,5a,8a,10a-tetraazapyrenium bromide (**58**) (717 mg, 1.60 mmol), ethanol (100 mL), sodium borohydride (1.82 g, 48.07 mmol), water (200 mL), dichloromethane (5 x 50 mL). To yield a yellow oil (497 mg, 84 %).

^{1}H NMR (400 MHz, $CDCl_3$, δ): 1.16-1.20 (*t*, J=7 Hz, N-β-CH_2, 1H), 1.73 (*m*, N-β-CH_2, 3H), 2.11-2.42 (*m*, N-α-CH_2, 2H), 2.50-2.54 (*m*, N-α-CH_2, 4H), 2.60 (*m*, N-α-CH_2, 1H), 2.62 (*br s*, C≡CH, 1H), 2.64-2.67 (*m*, N-α-CH_2, 3H), 2.79-2.86 (*m*, N-α-CH_2, 1H), 2.89-3.04 (*m*, N-α-CH_2, 4H), 2.08 (*s*, N-α-CH_2, 1H), 3.21-3.31 (*m*, N-α-CH_2, 2H), 3.42-3.53 (*m*, N-α-CH_2, 1H), 3.61-3.63 (*m*, N-α-CH_2, 2H), 3.67-3.79 (*m*, N-α-CH_2, 1H), 4.71 (*m*, NH, 1H), 5.01 (*s*, CH_2-O, 2H), 6.90-6.99 (*m*, Ar-H, 2H), 7.15-7.26 (*m*, Ar-H, 2H). ^{13}C NMR (100 MHz, $CDCl_3$, δ): 23.47 (N-β-CH_2), 26.15 (N-β-CH_2), 48.17 (N-α-CH_2), 50.66 (N-α-CH_2), 51.20 (N-α-CH_2), 54.82 (N-α-CH_2), 55.55 (N-α-CH_2), 55.90 (N-α-CH_2), 56.01 (N-α-CH_2), 57.03 (N-α-CH_2), 57.61 (CH_2-Ar), 59.39 (CH_2-O), 75.59 (C≡CH), 78.67 (C≡CH), 114.49 (Ar-H), 130.03 (Ar-C), 130.78 (Ar-H), 156.63 (Ar-C). HRMS (*m/z*): $[M+H]^+$ calcd for $C_{22}H_{35}N_4O$, 371.2805; found, 371.2804.

1-[4-nitrobenzyl]-1,4,8,11-tetraazabicyclo[10.2.2]hexadecane (66)

Amounts: 3a-[4-nitrobenzyl]-decahydro-3a,5a,8a,10a-tetraazapyrenium bromide (**59**) (1.00 g, 2.28 mmol), ethanol (100 mL), sodium borohydride (2.59 g, 68.44 mmol), water (50 mL), dichloromethane (5 x 30 mL). To yield a yellow oil (800 mg, 97 %).

^{1}H NMR (400 MHz, $CDCl_3$, δ): 1.50-1.62 (*m,* N-β-CH_2, 4H), 2.04-2.27 (*m,* N-α-CH_2, 3H), 2.33-2.68 (*m,* N-α-CH_2, 13H), 2.86-2.87 (*m,* N-α-CH_2, 2H), 2.97-3.04 (*m,* N-α-CH_2, 2H), 3.46-3.47 (*m,* NH, 1H), 3.53-3.59 (*m,* CH_2-Ar, 2H), 7.07-7.15 (*d,* J=8.6 Hz, Ar-H, 2H), 7.96-7.99 (*m,* Ar-H, 2H). ^{13}C NMR (100 MHz, $CDCl_3$, δ): 23.52 (N-β-CH_2), 25.71 (N-β-CH_2), 44.77 (N-α-CH_2), 48.31 (N-α-CH_2), 50.04 (N-α-CH_2), 51.21 (N-α-CH_2), 54.45 (N-α-CH_2), 54.79 (N-α-CH_2), 55.15 (N-α-CH_2), 56.68 (N-α-CH_2), 57.31 (N-α-CH_2), 59.40 (N-α-CH_2), 62.82 (N-α-CH_2), 123.21 (Ar-H), 126.71 (Ar-H), 129.29 (Ar-H),129.76 (Ar-H), 130.36 (Ar-C), 146.79 (Ar-C). HRMS (*m/z*): $[M-2H]^+$ calcd for $C_{19}H_{28}N_5O_2$, 358.2238; found, 358.2240. Anal. calcd for $C_{19}H_{31}N_5O_2$.0.55DCM.0.9MeOH: C, 63.13; H, 8.64; N, 19.37. Found C, 56.19; H, 8.26; N, 16.14 – contains impurity.

1-[4-[methoxycarbonyl]benzyl]-1,4,8,11-tetraazabicyclo[10.2.2]hexadecane (67)

Amounts: 3a-[4-nitrobenzyl]-decahydro-3a,5a,8a,10a-tetraazapyrenium bromide (**60**) (324 mg, 0.72 mmol), ethanol (50 mL), sodium borohydride (816 mg, 21.56 mmol), water (50 mL), chloroform (5 x 20 mL). To yield a colourless oil (269 mg, 99 %).

^{1}H NMR (400 MHz, MeOD, δ): 1.85-1.87 (*m*, N-β-CH_2, 4H), 2.28-2.34 (*m,* N-α-CH_2, 2H), 2.54-2.75 (*br m*, N-α-CH_2, 9H), 2.83-2.91 (*m*, N-α-CH_2, 5H), 2.99-3.09 (*m*, N-α-CH_2, 4H), 3.37 (*m*, CH_2-Ar, 2H), 3.75-3.79 (*m*, CH_3-O, 3H), 4.61 (*s*, NH, 1H), 7.29-7.31 (*m*, Ar-H, 2H), 7.93 (*d*, J=8.2 Hz, 2H, Ar-H). ^{13}C NMR (100 MHz, MeOD, δ): 22.46 (N-β-CH_2), 22.71 (N-β-CH_2), 45.95 (N-α-CH_2), 47.11 (N-α-CH_2), 49.66 (N-α-CH_2), 50.23 (CH_3-O), 52.30 (N-α-CH_2), 52.49 (N-α-CH_2), 54.72 (N-α-CH_2), 55.15 (N-α-CH_2), 55.59 (N-α-

CH_2), 60.91 (N-α-CH_2), 63.53 (N-α-CH_2), 126.82 (Ar-H), 129.15 (Ar-H), 129.96 (Ar-H), 135.14 (Ar-H), 137.14 (Ar-C), 138.83 (Ar-C), 173.68 (C=O). HRMS (*m/z*): Pending data, see 8.1.3.

8.8.7. Synthesis of 1-[4-aminobenzyl]-1,4,8,11-tetraazabicyclo[10.2.2]hexadecane (68)

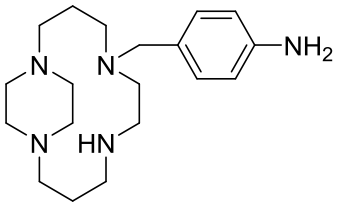

68

General procedure V

1-[4-Nitrobenzyl]-1,4,8,11-tetraazabicyclo[10.2.2]hexadecane (**66**) (400 mg, 1.11 mmol) and palladium on carbon (10 %, 353 mg, 3.32 mmol) were added to ethanol (75 mL). The solution was placed under an atmosphere of hydrogen overnight. The solution was filtered through Hyflo super cell, washed with ethanol (10 x 20 mL) and concentrated *in vacuo*. To yield a yellow solid (186 mg, 51 %).

^{1}H NMR (400 MHz, MeOD, δ): 1.86-1.90 (*m,* N-β-CH_2, 4H), 2.14-2.18 (*m,* N-α-CH_2, 1H), 2.27-2.36 (*m,* N-α-CH_2, 2H), 2.61-2.67 (*m,* N-α-CH_2, 6H), 2.61-2.67 (*m,* N-α-CH_2, 6H), 2.76 (*m,* N-α-CH_2, 2H), 2.87 (*m,* N-α-CH_2, 1H), 2.95-2.97 (*m,* N-α-CH_2, 3H), 3.01-3.14 (*m,* N-α-CH_2, 5H), 3.30-3.38 (*m,* CH_2-Ar, 2H), 3.46-3.47 (*m,* NH, 1H), 3.66-3.71 (*m,* NH_2, 2H), 6.64 (*d,* J=8.2 Hz, Ar-H, 2H), 7.00 (*d*, J=8.16 Hz, Ar-H, 2H). ^{13}C NMR (100 MHz, MeOD, δ): 22.18 (N-β-CH_2), 23.01 (N-β-CH_2), 45.41 (N-α-CH_2), 46.59 (N-α-CH_2), 49.26 (N-α-CH_2), 50.07 (N-α-CH_2), 51.71 (N-α-CH_2), 53.89 (N-α-CH_2), 54.71 (N-α-CH_2), 55.36 (N-α-CH_2), 55.60 (N-α-CH_2), 55.94 (N-α-CH_2), 114.94 (Ar-H), 115.55 (Ar-H), 123.68 (Ar-H), 129.32 (Ar-C), 131.12 (Ar-H), 147.67 (Ar-C). MS (*m/z*): $[M+H]^+$ calcd for $C_{19}H_{33}N_5$, 332.51; found, 332.4.

8.8.8. Synthesis of 1-[4-azidobenzyl]-1,4,8,11-tetraazabicyclo[10.2.2]hexadecane (69)

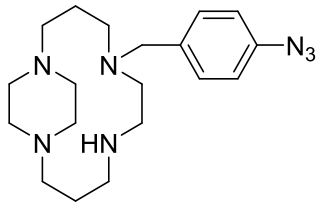

69

General procedure M was followed

A solution of sodium nitrite (10 mg, 0.15 mmol) in water (2 mL) was slowly added to a solution of 1-[4-aminobenzyl]-1,4,8,11-tetraazabicyclo[10.2.2]hexadecane (**68**) (50 mg, 0.15 mmol) and concentrated hydrochloric acid (1 mL) at a temperature of 0-5^{o}C. The solution was stirred at 0-5^{o}C for 1 h before sodium azide (10 mg, 0.15 mmol) in water (2 mL) was slowly added. After full generation of nitrogen under stirring at 0-5^{o}C the solvent was removed *in vacuo*. The resulting residue was dissolved in water (5 mL) and extracted with dichloromethane (3 x 5 mL). The combined organic phases were dried (Na_2SO_4) and reduced *in vacuo*. To yield a yellow solid (11 mg, 20 %).

MS (*m/z*): $[M+H]^+$ calcd for $C_{19}H_{31}N_7$, 358.51; found, 358.4.

8.8.9. Synthesis of 1-[methyl]-7-[4-[[1,4,7,10-tetraazabicyclo[8.2.2]dodecane]methyl]benzyl]-1,4,7,10-tetraazabicyclo[5.5.2]dodecane (70)

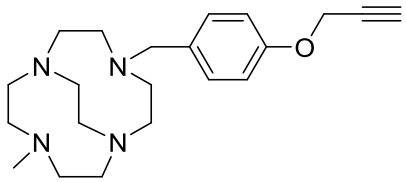

70

General procedure F was followed

Amounts: 2a-[methyl]-6a-[4-[prop-2-yn-1-yloxy]benzyl]-decahydro-2a,4a,6a,8a-tetraaza-pyrenium bromide (**62**) (23 mg, 0.04 mmol), EtOH (5 mL), $NaBH_4$ (42 mg, 1.11 mmol), water (5 mL), dichloromethane (6 x 5 mL). To yield a yellow oil (4 mg, 30 %).

^{1}H NMR (400 MHz, $CDCl_3$, δ): 2.54 (*m,* C≡CH, 1H), 2.64 (*s*, CH_3-N, 3H), 2.67-2.69 (*m*, N-α-CH_2, 1H), 2.76 (*dt*, J=14.1 Hz, N-α-CH_2, 2H), 2.81-2.88 (*m*, N-α-CH_2, 2H), 2.90-2.94 (*m*, N-α-CH_2, 1H), 2.95-3.07 (*m*, N-α-CH_2, 7H), 3.15 (*t*, J=3.3 Hz, N-α-CH_2, 1H), 3.18 (*t*, J=3.4 Hz, N-α-CH_2, 1H), 3.21-3.23 (*m*, N-α-CH_2, 1H), 3.25 (*t*, J=3.5 Hz, N-α-CH_2, 1H), 3.44 (*s*, N-α-CH_2, 2H), 3.37 (*br s*, N-α-CH_2, 1H), 3.76-3.77 (*m*, CH_2-Ar, 1H), 3.86-3.87 (*m*, CH_2-Ar, 1H), 4.69 (*d*, J=2.2 Hz, CH_2-O, 2H), 6.91-6.98 (*m,* Ar-H, 2H), 7.21-7.24 (*m,* Ar-H, 1H), 7.29-7.32 (*m,* Ar-H, 1H). ^{13}C NMR (400 MHz, $CDCl_3$, δ): 23.78 (CH_2-N), 44.21 (N-α-CH_2), 47.64 (N-α-CH_2), 48.49 (N-α-CH_2), 50.25 (N-α-CH_2), 52.12 (N-α-CH_2), 52.68 (N-α-CH_2), 53.14 (N-α-CH_2), 53.34 (N-α-CH_2), 55.73 (N-α-CH_2), 55.97 (N-α-CH_2), 56.32 (N-α-CH_2), 60.38 (CH_2-O), 75.87 (C≡CH), 78.38 (C≡CH), 115.03 (Ar-H), 115.18 (Ar-H), 130.29 (Ar-H), 131.60 (Ar-H), 133.48 (Ar-C), 162.99 (Ar-C). HRMS (*m/z*): $[M+H]^+$ calcd for $C_{21}H_{33}N_4O$, 357.2649; found, 357.2649.

8.8.10. Attempted synthesis of 3a-[4-carboxybenzyl]-dodecahydro-3a,5a,8a,10a-tetraazapyrenium bromide (71)

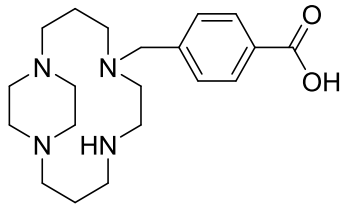

71

Method 1

1-[4-[Methoxycarbonyl]benzyl]-1,4,8,11-tetraazabicyclo[10.2.2]hexadecane (**67**) (187 mg, 0.52 mmol) was added to NaOH (10 % solution, 30 mL) and heated at reflux for 1 h. Subsequently, the reaction was cooled in ice water and acidified with concentrated HCl until pH 1. A white ppt formed and was filtered off and washed with a small amount of ice-cold water (~3 mL) to yield the white solid crude product (681 mg). Re-crystallization was attempted but did not isolate the desired product. Analytical data indicates that the desired product was not obtained.

8.8.11. Attempted synthesis of 1-[4-fluorobenzyl]-1,4,8,11-tetraazabicyclo[10.2.2]hexadecane (72)

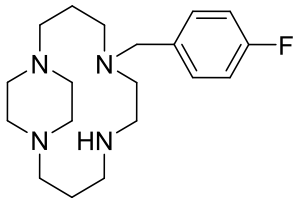

72

Method 1

1-[4-Nitrobenzyl]-1,4,8,11-tetraazabicyclo[10.2.2]hexadecane (**66**) (5 mg, 0.014 mmol) and potassium fluoride (2 mg, 0.042 mmol) were added to acetonitrile (8 mL) and heated to 85^{o}C for 30 min in the microwave. The solvent was removed *in vacuo*. To yield a golden yellow solid (3 mg). The desired product was not isolated with this synthetic procedure. Analytical data indicates that the desired product was not obtained.

Method 2

1-[4-Nitrobenzyl]-1,4,8,11-tetraazabicyclo[10.2.2]hexadecane (**66**) (5 mg, 0.014 mmol) and potassium fluoride (2 mg, 0.042 mmol) were added to acetonitrile (8 mL) and heated to 100^{o}C for 30 min in the microwave. The solvent was removed *in vacuo*. To yield a golden yellow solid (7 mg). The desired product was not isolated with this synthetic procedure. Analytical data indicates that the desired product was not obtained.

Method 3

1-[4-Nitrobenzyl]-1,4,8,11-tetraazabicyclo[10.2.2]hexadecane (**66**) (5 mg, 0.014 mmol) and potassium fluoride (2 mg, 0.042 mmol) were added to acetonitrile (8 mL) and heated to 130^{o}C for 15 min in the microwave. The solvent was removed *in vacuo*. To yield a golden yellow solid (1 mg). The desired product was not isolated with this synthetic procedure. Analytical data indicates that the desired product was not obtained.

Method 4

1-[4-Nitrobenzyl]-1,4,8,11-tetraazabicyclo[10.2.2]hexadecane (**66**) (5 mg, 0.014 mmol) and potassium fluoride (2 mg, 0.042 mmol) were added to DMSO (8 mL) and heated to 130^{o}C for 10 min in the microwave. The mixture was cooled and diluted with water (10 mL) and extracted with dichloromethane (5 x 10 mL). The organic layers were dried ($MgSO_4$) and reduced *in vacuo*. To yield a brown solid (7 mg). The desired product was not isolated with this synthetic procedure. Analytical data indicates that the desired product was not obtained.

Method 5

1-[4-Nitrobenzyl]-1,4,8,11-tetraazabicyclo[10.2.2]hexadecane (**66**) (5 mg, 0.014 mmol) and potassium fluoride (2 mg, 0.042 mmol) were added to DMSO (8 mL) and heated to 130^{o}C for 15 min in the microwave. The mixture was cooled and diluted with water (10 mL) and extracted with dichloromethane (5 x 10 mL). The organic layers were dried ($MgSO_4$) and reduced *in vacuo*. To yield a brown solid (7 mg). The desired product was not isolated with this synthetic procedure. Analytical data indicates that the desired product was not obtained.

Method 6

1-[4-Nitrobenzyl]-1,4,8,11-tetraazabicyclo[10.2.2]hexadecane (**66**) (10 mg, 0.03 mmol) and tetra-n-butyl ammonium fluoride in dry tetrahydrofuran (1.0 M, 83 µL, 0.083 mmol) were added to acetonitrile (2 mL) and heated to 100^{o}C for 5 min in the microwave. The solvent was removed *in vacuo*. To yield a brown solid (10 mg). The desired product was not isolated with this synthetic procedure. Analytical data indicates that the desired product was not obtained.

Method 7

1-[4-Nitrobenzyl]-1,4,8,11-tetraazabicyclo[10.2.2]hexadecane (**66**) (10 mg, 0.03 mmol) and tetra-n-butyl ammonium fluoride in dry tetrahydrofuran (1.0 M, 83 µL, 0.083 mmol) were added to dry DMSO (2 mL) and heated to 130^{o}C for 10 min in the microwave. The solvent was removed *in vacuo*. To yield a brown solid (10 mg). The desired product was not isolated with this synthetic procedure. Analytical data indicates that the desired product was not obtained.

Method 8

1-[4-Nitrobenzyl]-1,4,8,11-tetraazabicyclo[10.2.2]hexadecane (**66**) (10 mg, 0.03 mmol) and tetra-n-butyl ammonium fluoride in dry tetrahydrofuran (1.0 M, 83 µL, 0.083 mmol) were added to dry DMSO (2 mL) and heated to 160^{o}C for 10 min in the microwave. The solvent was removed *in vacuo*. To yield a brown solid (10 mg). The desired product was not isolated with this synthetic procedure. Analytical data indicates that the desired product was not obtained.

8.8.12. Attempted conjugation of zinc-5-[4-[azido]phenyl]-10,15,20-tris-[phenyl]porphyrin with 1-[4-[prop-2-yn-1-yloxy]benzyl]-1,4,8,11-tetraazabicyclo[10.2.2]hexadecane (73)

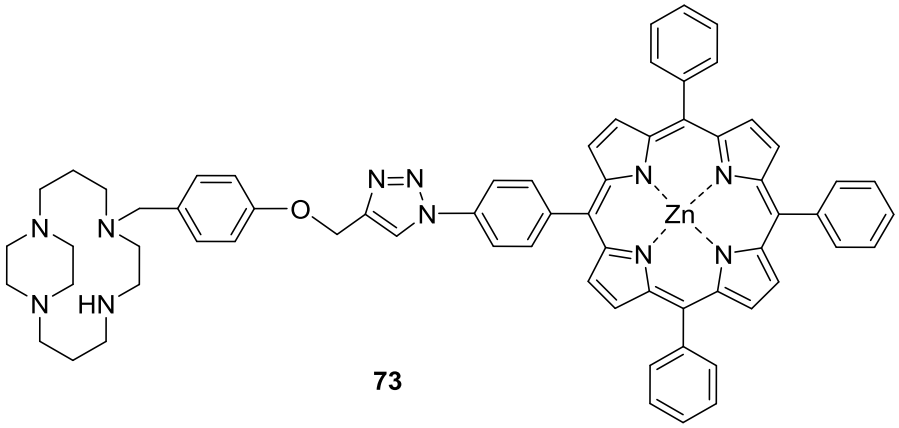

73

General procedure W

Zinc-5-[4-[azido]phenyl]-10,15,20-tris-[phenyl]porphyrin (**83**) (10 mg, 0.01 mmol) was dissolved in water (4 mL) to this 1-(4-(prop-2-yn-1-yloxy)benzyl)-1,4,8,11-tetraazabicyclo[10.2.2]hexadecane (**59**) (4 mg, 0.01 mmol) in MeOH (4 mL). Copper(II) sulfate pentahydrate (5 mg, 0.02 mmol) and sodium-L-ascorbate (5 mg, 0.03 mmol) were added to the solution and then heated at 80^{o}C for 40 min in a microwave. To yield a dark brown solid (15mg). The desired product was not isolated using this synthetic procedure.

8.8.13. Attempted conjugation of zinc-5-[4-[[2-[2-[2-azidoethoxy]ethoxy]ethane]aminocarbonyl) benzyl]-10,15,20-tris-[4-*N*-methylpyridinium]porphyrin trichloride with 1-[4-[prop-2-yn-1-yloxy]benzyl]-1,4,8,11-tetraazabicyclo[10.2.2]hexadecane (74)

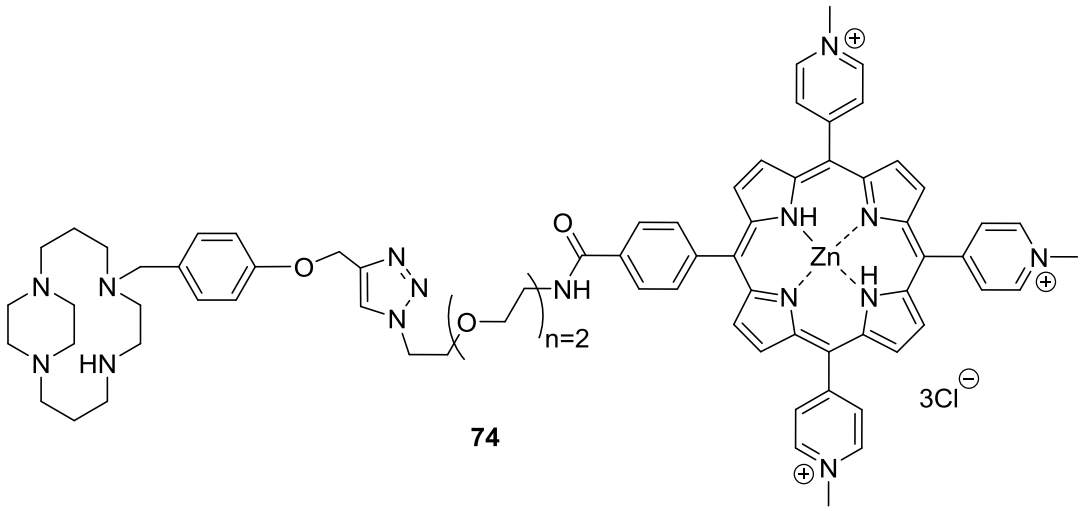

74

General procedure X

Zinc-5-[4-[[2-[2-[2-azidoethoxy]ethoxy]ethane]aminocarbonyl)benzyl]-10,15,20-tris-(4-*N*-methylpyridinium)porphyrin trichloride (**84**) (10 mg, 0.01 mmol) was dissolved in water (8 mL), to this 1-(4-(prop-2-yn-1-yloxy)benzyl)-1,4,8,11-tetraazabicyclo[10.2.2]hexadecane (**59**) (4 mg, 0.01 mmol) was added. Copper(II) sulfate pentahydrate (5 mg, 0.02 mmol) and sodium-L-ascorbate (5 mg, 0.03 mmol) were then added and the solution heated at 45^{o}C for 20 min in a microwave. To yield a dark brown solid (14 mg). The desired product was not isolated using this synthetic procedure.

8.8.14. Conjugation of 1-[4-aminobenzyl]-1,4,8,11-tetraazabicyclo[10.2.2]hexadecane with DOTAGA anhydride (75)

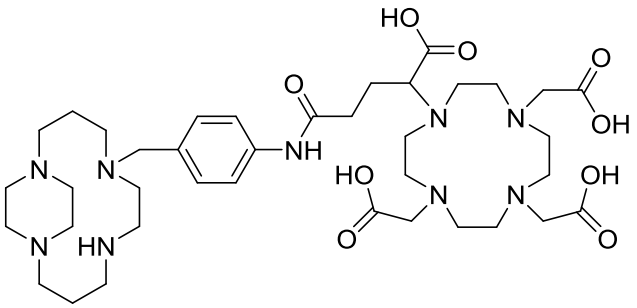

75

Method 1

1-[4-Aminobenzyl]-1,4,8,11-tetraazabicyclo[10.2.2]hexadecane (**68**) (13 mg, 0.04 mmol) was added to pyridine (2 mL), to this DOTAGA anhydride (23 mg, 0.05 mmol) was added. The solution was heated at 45°C for 2 h before the solvent was removed *in vacuo*. To yield the crude as a cream solid (~40 mg).

^{1}H NMR (400 MHz, MeOD, δ): 1.95-1.99 (*m,* N-β-CH_2, 4H), 2.04-2.15 (*m,* C$\underline{H}_2$-CH_2, 2H), 2.28-2.37 (*m,* CH_2-C$\underline{H}_2$-COOH, 1H), 2.46-2.53 (*m,* CH_2-C$\underline{H}_2$-COOH, 1H), 2.59-2.70 (*m,* N-α-CH_2, 4H), 2.80-2.86 (*m,* N-α-CH_2, 7H), 3.00-3.27 (*br m,* N-α-CH_2, 17H), 3.52-3.55 (*m,* N-α-CH_2, 3H), 3.66 (*s,* C$\underline{H}_2$-C=O, 6H), 3.71 (*m,* N-α-CH_2, 1H), 3.76-3.81 (*m,* N-α-CH_2, 4H), 3.98 (*m,* CH_2-Ar, 2H), 4.06 (*t*, J=6.5 Hz, C$\underline{H}$-C=ONH, 1H), 4.39 (*s,* NH, 1H), 6.81 (*m,* Ar-H, 1H), 7.02-7.19 (*m,* Ar-H, 2H), 7.23-7.30 (*m,* Ar-H, 1H), 7.45 (*d*, J=8.2 Hz, Ar-H, 1H), 7.59-7.63 (*m,* Ar-H, 1H), 8.61-8.63 (*m,* NH-C=O, 1H), – Missing 4 protons from OH peaks. ^{13}C NMR (100 MHz, MeOH, δ): 18.35 (N-β-CH_2), 20.03 (N-β-CH_2), 21.79 (C$\underline{H}_2$-CH_2COOH), 32.98 (CH_2-COOH), 43.10 (N-α-CH_2), 44.54 (N-α-CH_2), 49.06 (N-α-CH_2), 50.56 (N-α-CH_2), 51.73 (N-α-CH_2), 52.29 (N-α-CH_2), 53.05 (N-α-CH_2), 55.09 (N-α-CH_2), 55.72 (N-α-CH_2), 56.05 (N-α-CH_2), 56.65 (N-α-CH_2), 61.33 (N-α-CH_2), 62.24 (N-α-CH), 120.04 (Ar-H), 129.06 (Ar-C), 131.23 (Ar-H), 138.58 (Ar-C), 168.94 (C=ONH). – Missing 2 peaks from C=OOH and N-α-C=OOH. HRMS (*m/z*): $[M-H]^-$ calcd for $C_{38}H_{62}N_9O_9$, 788.4676; found, 788.4661. MS (*m/z*): $[M+Na-2H]^-$ calcd for $C_{38}H_{61}N_9O_9Na$, 810.4495; found, 810.4473.

Method 2 – preferred route

General procedure Y

1-[4-Aminobenzyl]-1,4,8,11-tetraazabicyclo[10.2.2]hexadecane (**68**) (13 mg, 0.04 mmol) was added to dry THF (1 mL), to this triethylamine (11 µL 0.08 mmol) and DOTAGA anhydride (25 mg, 0.06 mmol) were added. The solution was stirred for 24 h before the solvent was removed *in vacuo*. To yield the crude as a cream solid (~40 mg).

^{1}H NMR (400 MHz, MeOD, δ): 1.96 (*m,* N-β-CH_2, 4H), 2.05 (*m,* C<u>H</u>$_2$-CH_2, 2H), 2.15-2.37 (*m,* CH_2-C<u>H</u>$_2$-COOH, 2H), 2.44-2.46 (*m,* N-α-CH_2, 2H), 2.49-2.81 (*br m,* N-α-CH_2, 13H), 3.00-3.13 (*m,* N-α-CH_2, 12H), 3.48 (*m,* N-α-CH_2, 3H), 3.52 (*m,* N-α-CH_2, 2H), 3.57 (*m,* N-α-CH_2, 4H), 3.65 (*m,* CH_2-Ar, 2H), 3.72 (*m,* C<u>H</u>$_2$-C=O, 6H), 4.06 (*t*, J=6.5 Hz, C<u>H</u>-C=ONH, 1H), 4.70-4.76 (*m,* NH, 1H), 6.92-7.17 (*m,* Ar-H, 2H), 7.45 (*d*, J=8.6 Hz, Ar-H, 1H), 7.66 (*m,* Ar-H, 2H), 7.80 (*d*, J=8.6 Hz, Ar-H, 1H), – Missing 5 protons from, NH-C=O and OH peaks. ^{13}C NMR (100 MHz, MeOH, δ): 18.10 (N-β-CH_2), 20.29 (N-β-CH_2), 21.56 (<u>C</u>H$_2$-CH_2COOH), 31.17 (CH_2-COOH), 43.10 (N-α-CH_2), 42.73 (N-α-CH_2), 45.38 (N-α-CH_2), 46.32 (N-α-CH_2), 49.27 (N-α-CH_2), 50.29 (N-α-CH_2), 50.85 (N-α-CH_2), 52.30 (N-α-CH_2), 52.76 (N-α-CH_2), 54.44 (N-α-CH_2), 55.58 (N-α-CH_2), 56.46 (N-α-CH_2), 59.27 (N-α-CH), 126.19 (Ar-H), 129.08 (Ar-H), 131.71 (Ar-C), 144.52 (Ar-C), 177.70 (C=ONH), 177.70 (C=OOH), 179.84 (N-α-C=OOH). HRMS (*m/z*): $[M-H]^-$ calcd for $C_{38}H_{62}N_9O_9$, 788.4676; found, 788.4661.

8.8.15. Synthesis of 1,4,8,11-tetraazatricyclo[9.3.1.1^{4,8}]hexadecane (76)

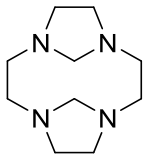

76

Method 1 – Attempted synthesis

General procedure Z was followed

Amounts: Cyclen (100 mg, 9.98 mmol), acetonitrile (200 mL) aqueous formaldehyde (37% w/v, 200 µL, 1.76 mmol). To yield a clear oil (98 mg). The desired product was not isolated using this synthetic procedure.

Method 2

Cyclen (1 g, 5.00 mmol) was dissolved in DCM (100 mL) which was then added to an aqueous solution of sodium hydroxide (30.00 g in 100 mL water) and stirred for 36 h. The two phases were separated and the aqueous layer extracted (5 x 20 mL) DCM. The combined organic phases were dried ($MgSO_4$) and concentrated *in vacuo*. To yield a clear colourless solid (30 mg). The desired product was not isolated using this synthetic procedure.

Method 3

General procedure AA

Cyclen (1.00 g, 5.00 mmol) was dissolved in DCM (100 mL) which was then added to an aqueous solution of NaOH (30.00 g in 100 mL water) and the stirred mixture was heated at reflux for 5 d. The two phases were separated and the aqueous layer extracted (5 x 20 mL) DCM. The combined organic phases were dried ($MgSO_4$) and concentrated *in vacuo*. To yield an orange-brown oil which was unsuccessfully re-crystallised with THF/water (103 mg, 9 %).

^{1}H NMR (400 MHz, $CDCl_3$, δ): 2.36-2.58 (*m*, N-α-CH_2, 3H), 2.75-2.83 (*m*, N-α-CH_2, 3H), 2.90-3.28 (*m*, N-α-CH_2, 7H), 3.38-3.60 (*m*, H_{aminal}, 3H), 3.93-3.96 (*m*, H_{aminal}, 1H). ^{13}C NMR (100 MHz, $CDCl_3$, δ): 42.74 (N-α-CH_2), 44.76 (N-α-CH_2), 45.51 (N-α-CH_2), 46.23 (N-α-CH_2), 48.57 (N-α-CH_2), 50.31 (N-α-CH_2), 51.57 (N-α-CH_2), 52.33 (N-α-CH_2), 70.14 (C_{aminal}), 73.37 (C_{aminal}). MS (*m/z*): $[M+H]^+$ calcd for $C_{10}H_{21}N_4$, 197.31; found, 197.2.

8.8.16. Attempted synthesis of 1,4,8,11-tetraazatricyclo[9.3.1.1^{4,8}]hexadecane (77)

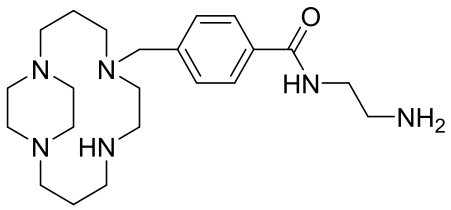

77

1-[4-[Methoxycarbonyl]benzyl]-1,4,8,11-tetraazabicyclo[10.2.2]hexadecane (**67**) (34 mg, 0.09 mmol) was dissolved in dry ethanol (10 mL) to this stirred solution ethylene diamine (23 µL, 0.36 mmol) was added. The mixture was then heated at 80^{o}C under an atmosphere of argon for 7 d after which the solvent was removed *in vacuo*. To yield an oil (50 mg). The desired product was not isolated using this synthetic procedure.

8.9. MONO-MACROCYCLE METAL COMPLEXES

8.9.1. Synthesis of 1-[4-[prop-2-yn-1-yloxy]benzyl]-1,4,8,11-tetraazabicyclo[10.2.2]hexadecane copper(II) acetate $[Cu65]^{2+}$ and 1-[4-[aminobenzyl]-1,4,8,11-tetraazabicyclo[10.2.2]hexadecane zinc(II) acetate $[Zn68]^{2+}$

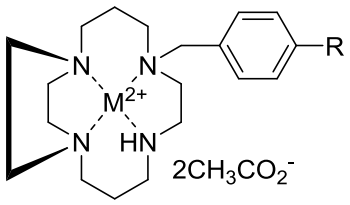

M= Cu^{2+}, R = O  $[Cu\mathbf{65}]^{2+}$

M= Zn^{2+}, R = NH_2 $[Zn\mathbf{68}]^{2+}$

General procedure H was followed

1-[4-[Prop-2-yn-1-yloxy]benzyl]-1,4,8,11-tetraazabicyclo[10.2.2]hexadecane copper(II) acetate $[Cu_2\mathbf{65}]^{2+}$

Amounts: 1-(4-(Prop-2-yn-1-yloxy)benzyl)-1,4,8,11-tetraazabicyclo[10.2.2]hexadecane (**65**) (50 mg, 0.14 mmol), methanol (2 mL), copper(II) acetate tetrahydrate (38 mg, 0.15 mmol), methanol (7 mL). To yield a blue solid (56 mg, 74 %).

HRMS (*m/z*): $[M\text{-}2CH_3CO_2+H]^+$ calcd for $C_{22}H_{35}CuN_4O$, 434.2094; found, 434.2101. Anal. calcd for $C_{20}H_{30}CuN_4O.2CH_3CO_2.2.5H_2O$: C, 52.29; H, 7.60; N, 9.38. Found: C, 51.91; H, 7.53; N, 9.78. UV-vis (MeOH) λmax, nm (ε): 622.8 (173.8 M^{-1} cm^{-1}).

1-[4-[Aminobenzyl]]-1,4,8,11-tetraazabicyclo[10.2.2]hexadecane zinc(II) acetate $[Zn68]^{2+}$

Amounts: 1-[4-[Aminobenzyl]-1,4,8,11-tetraazabicyclo[10.2.2]hexadecane (**68**) (46 mg, 0.14 mmol), methanol (5 mL), zinc(II) acetate (28 mg, 0.15 mmol), methanol (5 mL). To yield a yellow solid (47 mg, 66 %).

^{1}H NMR (400 MHz, MeOD, δ): 1.26-1.28 (*m*, N-β-CH_2, 1H), 1.62 (*d*, J=16.7 Hz, N-β-CH_2, 1H), 1.79 (*d*, J=16.1 Hz, N-β-CH_2, 2H), 2.00 (*br s*, CH_3, 6H), 2.12-2.24 (*m,* N-α-CH_2, 2H), 2.29-2.38 (*m,* N-α-CH_2, 2H), 2.42-2.54 (*m,* N-α-CH_2, 2H), 2.60-2.66 (*m,* N-α-CH_2, 3H), 2.77-2.85 (*m,* N-α-CH_2, 2H), 2.90-2.96 (*m,* N-α-CH_2, 3H), 3.06-3.12 (*m,* N-α-CH_2, 2H), 3.19-3.22 (*m,* N-α-CH_2, 2H), 3.42-3.46 (*m,* N-α-CH_2, 1H), 3.53-3.59 (*m,* N-α-CH_2, 1H), 3.63-3.70 (*m,* CH_2-Ar, 1H), 3.79 (*d*, J=14.5 Hz, CH_2-Ar, 1H), 4.04 (*d*, J=14.5 Hz, NH, 1H), 4.14 (*s*, NH_2, 1H), 4.38 (*br s*, NH, 1H), 6.69 (*d,* J=8.6 Hz, Ar-H, 2H), 6.98 (*d*, J=8.4 Hz, Ar-H, 2H). ^{13}C NMR (100 MHz, MeOD, δ): 19.12 (CH_3), 21.01 (N-β-CH_2), 24.36 (N-β-CH_2), 43.37 (N-α-CH_2), 44.65 (N-α-CH_2), 49.23 (N-α-CH_2), 49.54 (N-α-CH_2), 50.13 (N-α-CH_2), 51.37 (N-α-CH_2), 52.19 (N-α-CH_2), 52.23 (N-α-CH_2), 54.61 (N-α-CH_2), 56.62 (N-α-CH_2), 57.76 (N-α-CH_2), 114.56 (Ar-H), 115.41 (Ar-

H), 189.06 (Ar-H), 130.12 (Ar-C), 132.61 (Ar-H), 148.31 (Ar-C), 179.59 (C=O). MS (*m/z*): [M-2CH_3CO_2+2Na-2H]$^+$ calcd for $C_{19}H_{31}N_5Na_2Zn$, 440.85; found, 440.3. HRMS (*m/z*): Pending data, see 8.1.3.

8.9.2. Attempted conjugation of 1-[4-[aminobenzyl]]-1,4,8,11-tetraazabicyclo[10.2.2]hexadecane zinc(II) acetate (Zn68)$^{2+}$ to DOTAGA anhydride

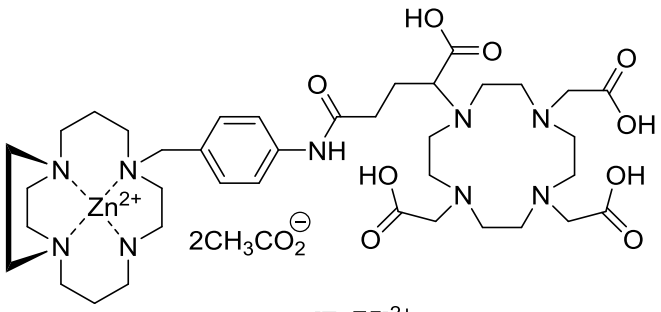

[Zn**75**]$^{2+}$

General procedure Y was followed

Amounts: 1-[4-Aminobenzyl]-1,4,8,11-tetraazabicyclo[10.2.2]hexadecane zinc(II) acetate (Zn**68**)$^{2+}$ (11 mg, 0.02 mmol) was added to dry THF (1 mL), to this triethylamine (6 µL, 0.04 mmol) and DOTAGA anhydride (15 mg, 0.03 mmol) were added. The solution was stirred for 24 h before the solvent was removed *in vacuo*. To yield the crude as a cream solid (46 mg). The desired product was not isolated using this synthetic procedure. Analytical data indicates that the desired product was not obtained.

8.9.3. Attempted Synthesis of gallium(III) complexation with 1-[1-[4-methyl]phenylaminocarbonyl-3-[DOTAGA]-3-[hydroxycarbonyl]propane]-1,4,8,11-tetraazabicyclo[10.2.2]hexadecane zinc(II) acetate ([Zn75]$^{2+}$)

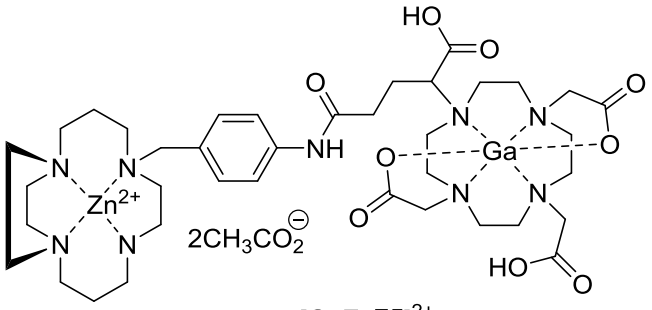

[GaZn**75**]$^{2+}$

1-[1-[4-Methyl]phenylaminocarbonyl-3-[DOTAGA]-3-[hydroxycarbonyl]propane]-1,4,8,11-tetraazabicyclo[10.2.2]hexadecane zinc(II) acetate ([Zn**75**]$^{2+}$) (14.25 mg, 14.60 µmol) was dissolved in ammonium acetate buffer (200 mM, pH 5.0, 2 mL) and added to gallium(III)chloride (30 mg/mL, 3.87 mg, 21.96 µmol) in ammonium acetate buffer (200 mM, pH 5.0, 2 mL). The solution was heated to 37^{o}C for 1 h and the solvent was removed by flowing a stream of nitrogen through the solution. The solution was then taken up in methanol (1 mL) and purified via size exclusion chromatography. To yield a solid (~18 mg, %).

8.9.4. Attempted conjugation of zinc-5-[4-[azido]phenyl]-10,15,20-tris-[phenyl]porphyrin with 1-1-[4-[prop-2-yn-1-yloxy]benzyl]-1,4,8,11-tetraazabicyclo[10.2.2]hexadecane copper(II) acetate (Cu65)$^{2+}$

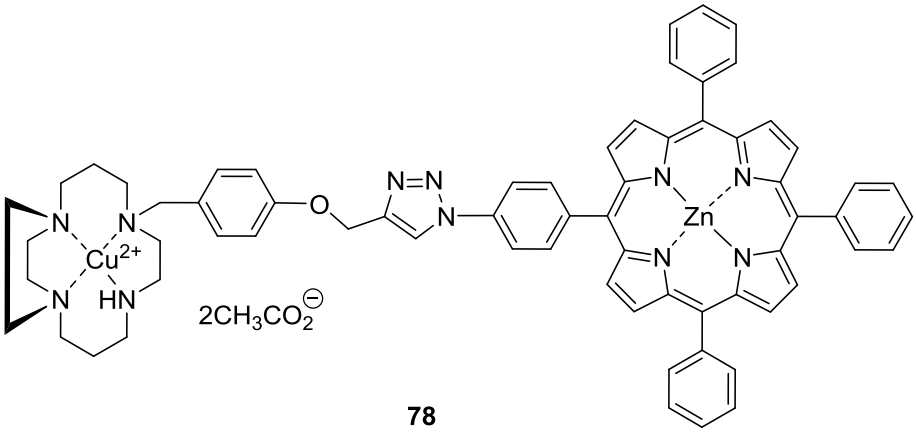

78

General procedure W was followed

Amounts: Zinc-5-[4-[azido]phenyl]-10,15,20-tris-[phenyl]porphyrin (**83**) (5 mg, 0.01 mmol), water (4 mL), 1-(4-(prop-2-yn-1-yloxy)benzyl)-1,4,8,11-tetraazabicyclo[10.2.2]hexadecane copper(II) acetate (Cu**65**)$^{2+}$ (4 mg, 0.01 mmol), MeOH (4 mL), copper sulfate pentahydrate (5 mg, 0.02 mmol), sodium-L-ascorbate (5 mg, 0.03 mmol). To yield a dark brown solid (15mg). The desired product was not isolated using this synthetic procedure.

8.9.5. Attempted conjugation of zinc- zinc-5-[4-[[2-[2-[2-azidoethoxy]ethoxy]ethane]aminocarbonyl)benzyl]-10,15,20-tris-(4-*N*-methylpyridinium)porphyrin trichloride with 1-(4-(prop-2-yn-1-yloxy)benzyl)-1,4,8,11-tetraazabicyclo[10.2.2]hexadecane copper(II) acetate (Cu65)$^{2+}$

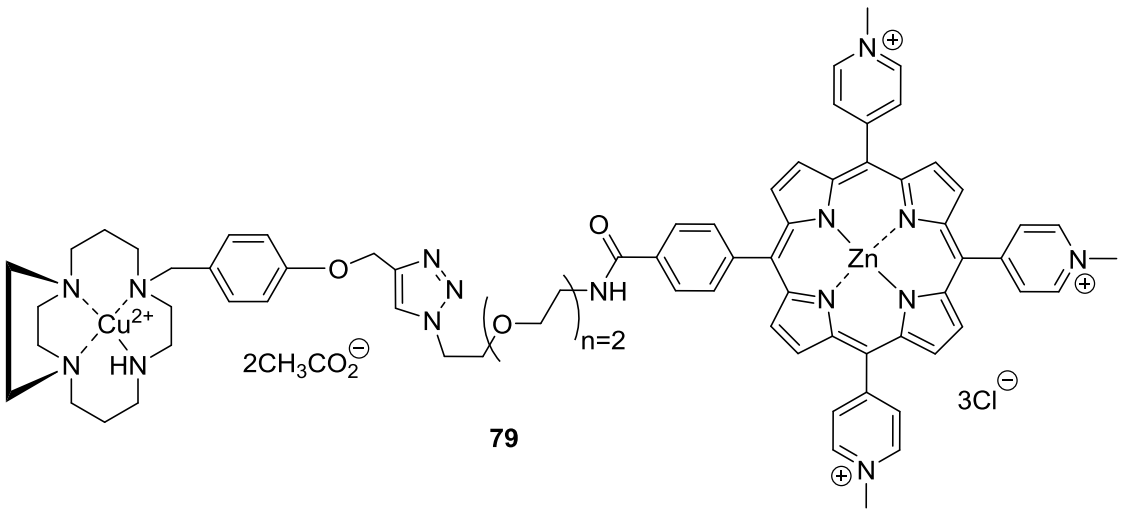

79

General procedure X was followed

Amounts: Zinc-5-[4-[[2-[2-[2-azidoethoxy]ethoxy]ethane]aminocarbonyl)benzyl]-10,15,20-tris-[4-*N*-methylpyridinium]porphyrin trichloride (**84**) (5 mg, 0.01 mmol), water (8 mL), 1-(4-[prop-2-yn-1-yloxy]benzyl]-1,4,8,11-tetraazabicyclo[10.2.2]hexadecane copper(II) acetate (Cu**65**)$^{2+}$ (3 mg, 0.01 mmol), copper(II) sulfate pentahydrate (5 mg, 0.02 mmol), sodium-L-ascorbate (5 mg, 0.03 mmol). To yield a dark red solid (10 mg). The desired product was not isolated using this synthetic procedure.

8.9.6. Attempted conjugation of 4-azidobenzoic acid with 1-(4-(prop-2-yn-1-yloxy)benzyl)-1,4,8,11-tetraazabicyclo[10.2.2]hexadecane copper(II) acetate (Cu65)$^{2+}$

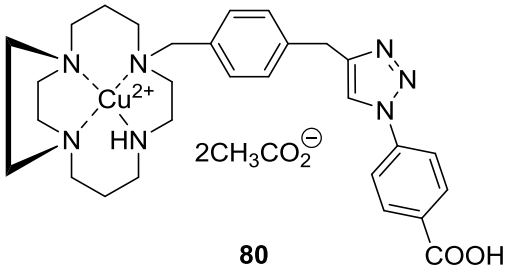

80

Method 1

1-(4-(Prop-2-yn-1-yloxy)benzyl)-1,4,8,11-tetraazabicyclo[10.2.2]hexadecane copper(II) acetate (Cu**65**)$^{2+}$ (4 mg, 0.009 mmol), 4-azidobenzoic acid (**85**) (2 mg, 0.01 mmol) and Cu(I)I (86 µg, 0.5 µmol) were suspended in acetonitrile (7.774 mL) and diisopropylamine (0.2 M, 226 µL). The solution was heated at 100^{o}C for 30 min in a microwave. To yield a green solid (10 mg). The desired product was not isolated using this synthetic procedure.

Method 2

1-(4-(Prop-2-yn-1-yloxy)benzyl)-1,4,8,11-tetraazabicyclo[10.2.2]hexadecane copper(II) acetate (Cu**65**)$^{2+}$ (4 mg, 0.009 mmol), 4-azidobenzoic acid (2 mg, 0.01 mmol) and Cu(I)I (172 µg, 0.001 mmol) were suspended in acetonitrile (7.548 mL) and diisopropylamine (0.4 M, 452 µL). The solution was heated at 100^{o}C for 30 min in a microwave. To yield a green solid (10 mg). The desired product was not isolated using this synthetic procedure.

8.10. BIOLOGICAL EXPERIMENTS

8.10.1. Experimental for competition binding assays

8.10.1.1. General methods and preparation of cell cultures

Human leukaemia T cell lymphoblast cells (Jurkat E6.1) were purchased from the ECACC. RPMI 1640 media (Invitro technologies, UK) containing 10% (v/v) heat inactivated FBS (Biowest, France), 1 % glutamate (2 mM), 1 % (v/v) penicillin and streptomycin (100 units/mL) antibiotics were used to maintain the cells. The cell cultures were stored at 37 °C in a humidified, CO_2 (5 %) controlled atmosphere and passaged every 2-3 days. Aseptic techniques were conducted when handling cells in a Class II microbiological safety cabinet fitted with a UV sterilising lamp. All glassware and heat stable solutions were autoclaved prior to use at 121°C for 10 min, disposable equipment and all solutions were of sterile tissue culture grade.

8.10.1.2. Antibodies and fluorescent dyes

Unconjugated mouse anti-human CXCR4 mAb clone 44717.111, 44716.111 and 44708.111 were purchased from R & D systems Europe, Abingdon, UK. Secondary FITC conjugated rabbit anti-mouse IgG antibody was purchased from Serotec, UK. PE conjugated Human CXCR4 Phycoerythrin mAb clone 12G5 and mouse IgG1 isotype control clone 11711 were purchased from R & D systems Europe, Abingdon, UK. Dilutions of mAbs were prepared using PBS supplemented with 0.25 % (v/v) BSA and sodium azide (1.00 mM). All reagents, antibodies and fluorescent dyes were reconstituted and stored according to the manufacturer's instructions unless otherwise stated.

8.10.1.3. Cell counting

The number of cells per flask was determined using a Neubauer hematocytometer. Cells in suspension were diluted 1:1 with 0.2% (v/v) Trypan blue stain. This dilution was placed into a hematocytometer chamber and the cell density was determined using light microscopy by counting the number of viable cells. The equation below was used to calculate the concentration of cells.

Equation 1: Cell concentration (cells / mL) = Averaged cell count x 2 (dilution factor) x 10^4 (volume of chamber)

8.10.1.4. Antibody binding and subsequent fluorescent tagging for flow cytometry

Passage flasks containing the Jurkat cell culture were centrifuged (180 x g for 3 min), the media was decanted and the cell pellet resuspended in PBS (10 mL). The solution was centrifuged (180 x g for 3 min) and the supernatant removed. The cell pellet was resuspended in a volume of PBS to give a cell density of ~200,000 cells per 50 µL PBS. Cells in PBS (50 µL) were aliquoted into polypropylene FACS

tubes (Falcon 2054 tubes), and then incubated with the compound under study (small molecule antagonist) in PBS (10 µL, 20 µM) for 1 hour 4°C in the dark. Each compound was run in duplicate alongside a positive and negative control. Cells were then washed with PBS (1.00 mL), centrifuged (180 x g for 3 min) and the supernatant removed. CXCR4 mAb (10 µL) was added to all samples except the negative control to which was added mouse IgG1 isotype control and incubated for 1 h at 4°C in the dark. Cells were washed with PBS (1.00 mL), centrifuged (180 x g for 3 min) and the supernatant was removed. All samples were resuspended in PBS (300 µL) and analysed on a FACScan flow cytometer (BD Biosciences Europe, Erembodegem, Belgium). Data were acquired and analysed with CellQuest software (Becton Dickinson). For assays using unconjugated mAb a third incubation was conducted with secondary fluorescently tagged antibody (10 µl, 1:100 solution in PBS) for 30 min at 4°C in the dark. The samples were washed with PBS (1.00 mL), centrifuged (180 x g for 3 min), the supernatant removed and resuspended in PBS (300 µL) before being analysed. The positive control provides a reading for 100 % antibody binding and the negative control provides a 0 % reading.

8.10.2. Experimental for calcium signalling assays

8.10.2.1. Cell cultures

U87.CD4.CXCR4 cells were obtained from the ATCC (Rockville, MD) and cultured in RPMI-1640 medium (Gibco BRL, Gaithersburg, MD) supplemented with 10% heat-inactivated FBS and 1% glutamine (Gibco BRL). The cell cultures were maintained at 37°C in a humidified CO_2 (5 %) controlled atmosphere. Passaging was completed every 2-3 days and cells were used in assays when in the stationary growth phase (3 days after two thirds passaging).

8.10.2.2. Loading of the cells with the Ca^{2+} indicator Fluo-3

A detailed experimental is provided by Princen *et al.* but briefly,[255] a 2 mM stock solution of Fluo-3 acetoxymethylester (Fluo-3/AM; Molecular Probes, Leiden, The Netherlands) was prepared with anhydrous dimethylsulfoxide.[255] The acetoxymethyl ester bound to Fluo-3 masks the negative charges in the indicator molecule and makes it hydrophobic and, hence, cell membrane permeable. Once inside the cell, the acetoxymethyl group is hydrolyzed by cytosol esterases, and the Ca^{2+} sensitive polycarboxylate form of the indicator is formed (λ_{ex} = 488 nm, λ_{em} = 530 nm). A 20 % w/v stock solution of the detergent Pluronic acid F-127 (Molecular Probes) was also prepared in dimethylsulfoxide. An equal volume of Pluronic acid stock was added to the dye stock, just before use, to increase Fluo-3/AM solubility and improve dye loading into the cells. Cells were centrifuged and resuspended in RPMI-1640 medium supplemented with 2 % FBS, for a final Fluo-3/AM

concentration of 4 µM. After incubation for 45 min at room temperature, cells were washed two times at room temperature in Ca^{2+} flux assay buffer (Hank's balanced salt solution containing 20 mM HEPES and 0.2 % BSA, pH 7.4) to remove extracellular dye. After the second wash, cells were incubated for 10 min at room temperature. In the meantime, cells were counted with the use of trypan blue staining to determine the percentage of dead cells (blue cells). Then cells were centrifuged and resuspended at a density of 3 x 10^6 cells/mL.

8.10.2.3. Measurement of intracellular Ca^{2+} mobilization and evaluation of receptor antagonists by the Fluorometric Imaging Plate Reader (FLIPR)

The CXC chemokine CXCL12 was provided by Dr. I. Clark-Lewis (University of British Columbia, Vancouver, BC, Canada). After loading with Fluo-3, the cells were seeded (at a density of 0.3 x 10^6 cells/mL) in a black-wall microplate (Costar, Cambridge, UK) that already contained 50 µL of the CXCR4 antagonist. To form a uniform monolayer of cells on the bottom of the wells, the microplate was gently centrifuged for 3 min with low acceleration and without break. After a 10 min incubation in the FLIPR test chamber, which was maintained at 37 °C, fluorescence was recorded over a 4 min period, with measurements every 2 s during the first 2 min and subsequently every 6 s. At the beginning of a data run, a "signal test" is performed to check the background fluorescence and the basal fluorescence signal from the cells. Background fluorescence is produced by autofluorescence of the cells and by the test plate and tips. The autofluorescence of plates and tips is already very low Ca^{2+} because the black-wall microplate and black tips are used to avoid this. The basal fluorescence of the cells or the green fluorescence of unstimulated cells should be in the range of 8,000–10,000 counts (saturation of the camera occurs at 65,000 counts). Acceptable basal fluorescence values can be obtained by adjusting the exposure length of the CCD camera and/or increasing or decreasing the laser power, but the latter should be weaker than 0.150 W and no stronger than 0.800 W during the assay. After a 20 s baseline monitoring, 50 µL of chemokine CXCL12, diluted in Ca^{2+} flux assay buffer at four times the final concentration was transferred to the test plate from a second 96 well microplate (Sero-wel, Sterilin Ltd, Stone, Staffs, UK). For each condition, the average of four identical microplate wells was measured. The data was expressed as fluorescence units versus time and was analysed using the Softmax PRO 4.0 program (Molecular Devices) and IC50 values were calculated using the GraphPad Prism 4.0 software (San Diego, CA).

8.10.3. Experimental for anti-HIV assays

The anti-HIV activity and cytotoxicity of the compounds were evaluated against wild-type HIV-1 strain IIIB in MT-4 and U87.CD4.CXCR4 cell cultures using the MTT method as described in depth by

Pauwels *et al.*[253] Anti-HIV activity and cytotoxicity measurements in MT-4 and U87.CD4.CXCR4 cells were based on the viability of the cells that had been infected or not infected with HIV-1 IIIB and exposed to various concentrations of the test compound.[252] After the cells were allowed to proliferate for 5 days, the number of viable cells was quantified.[122, 253] PBMCs were purified and infected with HIV as described in detail by Schols *et al.*[254]

8.11. SURFACE PLASMON RESONANCE EXPERIMENTS

8.11.1. Intact Cell Immobilisation Method

8.11.1.1. Cell Immobilisation

Method 1:

Jurkat cells were immobilised onto a CM5 chip using aldehyde coupling chemistry and tris buffer (20 mM, pH 7.4) as the running buffer on a Biacore T200. Cells were prepared from a passage flask by centrifuging (180 x g, 3 min), removing supernatant and washing with PBS (10 mL). The solution was then centrifuged (1500 rpm, 3 min) and resuspended in PBS (500 µL), to this sodium acetate buffer (10 mM, pH 4.0, 500 µL) was added. A new CM5 sensor chip was allowed to equilibrate to RT for 30 min prior to use. The carboxymethyl dextran surface was primed twice and activated with a 3 min injection of a 1:1 ratio of 0.40 M EDC:0.1M NHS, followed by a 7 min injection of hydrazine (5 mM). Remaining activated groups were blocked with a 7 min injection of 1.00 M ethanolamine (pH 8.5). The cells, in PBS:sodium acetate buffer (1 mL), were coupled to the surface with a 10 min injection at a flow rate of 2 µL/min and at a temperature of 37 °C and a 20 min injection of 0.10 M cyanoborohydride in sodium acetate (0.10 M, pH 4.0) stabilised the coupling bond. All solutions and buffers were filtered through a 0.22 µm filter with the exception of the solution containing the cells. A cell surface density of approximately 5,500 RU was obtained.

Method 1 Repeat:

Method 1 was followed but a cell surface density of approximately 10,000 RU was achieved.

8.11.1.2. Testing Surface Interactions

Method 1:

Samples of CXCR4 conformation specific mAb with differing concentrations were made up including a replicate and three blank samples for reference. Binding analysis was run in tris buffer (20 mM, pH 7.4) against a control surface using the Assay wizard on the Biacore T200 software. The reaction was conducted at 37^{o}C at a flow rate of 10 µL/min. No binding was observed.

Sample concentrations: mAb 44708: 0.184 mM, 0.092 mM, 0.046 mM 0.023 mM, 0.0115 mM, 0.0055 mM, 0.0027 mM, 0.00135 mM, 0.000675 mM, 0.000336 mM, replicate was 0.0115 mM.

Method 2:

Method 1 was followed but higher concentrations of mAb were used. No binding was observed.

Sample concentrations: mAb 44708: 2.94 mM, 1.47 mM, 0.735 mM, 0.368 mM, 0.184 mM, 0.092 mM, 0.046 mM 0.023 mM, 0.0115 mM, 0.0055 mM, replicate was 0.184 mM.

8.11.2. Intact Cell Capture Method

8.11.2.1. mAb Immobilisation pH Scouting

A new CM5 sensor chip was allowed to equilibrate to RT for 30 min prior to use and two primes were conducted prior to the start of the experiment. Immobilisation pH scouting for PE-12G5 mAb was achieved using a contact time of 180 s with a flow rate of 10 µL/min. A running buffer of PBS (0.01 M, pH 7.4) was used and the experiment was carried out at 25 °C. PE-12G5 mAb (100 µg/mL in PBS) was diluted 50:50 with 0.01 M sodium acetate buffer at pH 5.5, 5.0, 4.5 and 4.0. The optimum sodium acetate buffer for binding was pH 4.5, no binding was observed at any other pHs.

8.11.2.2. mAb Immobilisation

PE-12G5 mAb was immobilised onto a CM5 chip using amine coupling chemistry and PBS buffer (10 mM, pH 7.4) as the running buffer on a Biacore T200. PE-12G5 mAb (100 µg/mL in PBS) was diluted 50:50 with 0.01 M sodium acetate buffer (pH 4.5). The carboxymethyl dextran surface was primed twice and activated with a 7 min injection of a 1:1 ratio of 0.40 M EDC:0.1M NHS. Remaining activated groups were blocked with a 7 min injection of 1.00 M ethanolamine (pH 8.5). PE-12G5 mAb was coupled to the surface using the "*Aim for immobilised level*" option with a target of 10,000 RU at a flow rate of 5 µL/min, a contact time of 2 min and at a temperature of 25 °C. All solutions and buffers were filtered through a 0.22 µm filter. The immobilised target level was reached. Immobilisation was conducted on FC 3 and 4 with a mAb surface density of approximately 10,000 RU on each.

8.11.2.3. Intact Cell Capture

Method 1:

Manual run was selected on a Biacore T200 to capture the Jurkat cells on the PE-12G5 mAb surface. The surface was primed twice prior to the start of the experiment.Cells from a passage flask were centrifuged (180 x g, 3 min), the supernatant removed and the cell pellet washed with PBS (2.00 mL). The cells were centrifuged (180 x g, 3 min) and re-suspended in PBS (700 µL). The temperature was set to 37^{o}C on the Biacore T200 and the cells in PBS were injected for 960 s at a flow rate of 2 µL/min.

A further injection was conducted for 960 s at a flow rate of 2 µL/min after the baseline had stabilised. Capture of between 50-100 RU was observed but the baseline was not stable enough to conduct further experiments.

Method 2:

The surface generated in method 1 was used but capture was conducted at 25^{o}C. Three cell solution injections of 960 s at a flow rate of 2 µL/min were conducted after the baseline had been monitored for 1.70 h. The baseline was allowed to stabilise in between injections. Cell capture was observed, a total response of 53 RU was achieved following all three injections. This level of capture was to low to conduct further experiments on.

8.11.3. CXCR4 Receptor Capture Method

8.11.3.1. Anti-GST Ab Immobilisation

Anti-GST pAb was immobilised onto a CM4 chip using amine coupling chemistry and HBS-P buffer (10 mM Hepes, 0.15 M NaCl, 0.005 % v/v P20, pH 7.4) as the running buffer on a Biacore T200. Anti-GST pAb (30 µg/mL) was diluted 5:95 with 0.01 M sodium acetate buffer (pH 5.5). A new CM4 sensor chip was allowed to equilibrate to RT for 30 min prior to use and two primes were conducted prior to the start of the experiment. The carboxymethyl dextran surface was activated with a 7 min injection of a 1:1 ratio of 0.40 M EDC:0.1M NHS. Remaining activated groups were blocked with a 7 min injection of 1.00 M ethanolamine (pH 8.5). Anti-GST pAb was coupled to the surface using the "*Specify contact time and flow rate*" option where a flow rate of 10 µL/min and a contact time of 420 s was selected. The experiment was carried out at 25 °C and all solutions and buffers were filtered through a 0.22 µm filter. Immobilisation was conducted on FC 1 and 2 with a pAb surface density of 7361 RU and 6506 RU respectively.

The method was repeated on FC 3 and 4 where a response of 6213 RU and 7356 RU was achieved respectively.

8.11.3.2. CXCR4 Receptor Capture

8.11.3.2.1. CXCR4 Receptor Capture – Method 1

Manual run was selected on a Biacore T200 to capture the reconstituted CXCR4 receptor on the anti-GST pAb surface. CXCR4 receptor (ACRO Biosystems, Delaware, USA) was reconstituted in tris buffer (20 mM, pH 7.0) containing 0.10 M $(NH_4)_2SO_4$, 10 % glycerol, 0.07 % CHS, 0.33 % DOM, 0.33 % Chaps, 0.23 mM DOPC, 1.00 mM calcium chloride and 5.00 mM magnesium chloride, the buffer was also the running buffer. The surface was primed twice prior to the start of the experiment and receptor solution was injected onto FC 2 for 180 s at a flow rate of 10 µL/min. The temperature was set at 25^{o}C and capture of 638 RU was achieved.

The method was repeated on FC 3 and 4 where a response of 973 RU was achieved.

Subsequent injections of receptor solution to FC 2 at 2 mg/mL for 180 s at a flow rate of 10 µL/min, a repeat of the first injection, and 10 mg/mL for 180 s at a flow rate of 10 µL/min increased the response to 722 RU and 826 RU respectively.

8.11.3.2.2. CXCR4 Receptor Capture – Method 2

Manual run was selected on a Biacore T200 to capture the reconstituted CXCR4 receptor on the anti-GST pAb surface. CXCR4 receptor (ACRO Biosystems, Delaware, USA) was reconstituted in tris buffer (20 mM, pH 7.0) containing 0.10 M $(NH_4)_2SO_4$, 10 % glycerol, 0.07 % CHS, 0.33 % DOM, 0.33 % Chaps,

0.23 mM DOPC, 1.00 mM calcium chloride and 5.00 mM magnesium chloride, the buffer was also the running buffer. Lipids and detergents were prepared by dissolving in chloroform and rotating the test-tube while evaporating the chloroform with a stream on nitrogen. Remaining chloroform was removed by drying under vacuum overnight. 1.00 mL of buffer (20 mM tris (pH 7.0) containing 0.10 M $(NH_4)_2SO_4$, 10 % glycerol) was added to each test tube and frozen. Once frozen the samples were allowed to thaw and vortexed. This was repeated four times before uniform liposomes were prepared by extrusion through a 100 nm polycarbonate filter using an Avanti mini-extruder kit. The samples were then added to the buffer. The surface was primed twice prior to the start of the experiment and receptor solution was injected onto FC 2 for 240 s at a flow rate of 10 µL/min. The temperature was set at 25^{o}C and capture of 800 RU was achieved.

8.11.3.2.3. CXCR4 Receptor Capture – Method 3

Manual run was selected on a Biacore T200 to capture the reconstituted CXCR4 receptor on the anti-GST pAb surface. CXCR4 receptor (ACRO Biosystems, Delaware, USA) was reconstituted in tris buffer (20 mM, pH 7.0) containing 0.10 M $(NH_4)_2SO_4$, 10 % glycerol, 0.07 % CHS, 0.33 % DOM, 0.33 % Chaps, 0.23 mM DOPC, 1.00 mM calcium chloride and 5mM magnesium chloride, the buffer was also the running buffer. Lipids and detergents were prepared by dissolving in chloroform and rotating the test-tube while evaporating the chloroform with a stream on nitrogen. Remaining chloroform was removed by drying under vacuum overnight. 1 mL of buffer (20 mM tris (pH 7.0) containing 0.1 M $(NH_4)_2SO_4$, 10 % glycerol) was added to each test tube and frozen. Once frozen the samples were allowed to thaw and vortexed. This was repeated four times before uniform liposomes were prepared by extrusion through a 100 nm polycarbonate filter using an Avanti mini-extruder kit. The samples were then added to the buffer. The surface was primed twice prior to the start of the experiment and receptor solution was injected onto FC 2 for 600 s at a flow rate of 10 µL/min. The temperature was set at 25^{o}C and capture of 1800 RU was achieved.

8.11.3.2.4. CXCR4 Receptor Capture – Method 4

Manual run was selected on a Biacore T200 to capture the reconstituted CXCR4 receptor on the anti-GST pAb surface. CXCR4 receptor (ACRO Biosystems, Delaware, USA) was reconstituted in tris buffer (20 mM, pH 8.5) containing 0.10 M $(NH_4)_2SO_4$, 10 % glycerol, 1.00 % Chapso. A 2.5 mg aliquot of POPC in chloroform (100 µL) was transferred into a glass test tube and a thin film was formed by rotating the tube and evaporating the chloroform with a stream of nitrogen gas. Any remaining chloroform was removed under vacuum for at least 1 h. To this dry aliquot 1.00 mL HBS-N (10 mM HBS-N, pH 7.4) supplemented with 5.00 mM Chapso was added and the mixture was frozen, thawed,

and vortexed three times and uniform liposomes were produced by extrusion through a 100 nm polycarbonate filter using an Avanti mini-extruder kit. The samples were then added to the buffer. The surface was primed twice prior to the start of the experiment with 10 mM HBS-N (pH 7.4, 10 mM HEPES, 0.15M NaCl) containing 5.00 mM Chapso. The receptor solution was injected onto FC 2 for 600 s at a flow rate of 10 μL/min followed immediately by an injection of the 3.30 mM POPC and 5 mM Chapso HBS-N solution for 20 min at 10 μL/min. The temperature was set at 25^{o}C and capture of 1800 RU was achieved.

8.11.3.2.4. CXCR4 Receptor Capture – Method 5

Manual run was selected on a Biacore T200 to capture the reconstituted CXCR4 receptor on the anti-GST pAb surface. CXCR4 receptor (ACRO Biosystems, Delaware, USA) was reconstituted in tris buffer (20 mM, pH 8.5) containing 0.10 M $(NH_4)_2SO_4$, 10 % glycerol, 1.00 % Chapso. A 2.5 mg aliquot of POPC in chloroform (100 μL) was transferred into a glass test tube and a thin film was formed by rotating the tube and evaporating the chloroform with a stream of nitrogen gas. Any remaining chloroform was removed under vacuum for at least 1 h. To this dry aliquot 1.00 mL HBS-N (10 mM HBS-N, pH 7.4) supplemented with 5.00 mM Chapso was added and the mixture was frozen, thawed, and vortexed three times and uniform liposomes were produced by extrusion through a 100 nm polycarbonate filter using an Avanti mini-extruder kit. The samples were then added to the buffer. The surface was primed twice prior to the start of the experiment with 10 mM HBS-N (pH 7.4, 10 mM HEPES, 0.15M NaCl) containing 5.00 mM Chapso. The receptor solution was injected onto FC 2 for 900 s at a flow rate of 10 μL/min followed immediately by an injection of the 3.30 mM POPC and 5 mM Chapso HBS-N solution for 20 min at 10 μL/min. The temperature was set at 25^{o}C and capture of 1800 RU was achieved.

8.11.3.3. Regeneration of the Captured Surface

On manual run the surface was regenerated using a single 120 s "*Regeneration injection*" of 10 mM glycine-HCl (pH 2.1) at a flow rate of 10 μL/min with a HBS-P running buffer (10 mM Hepes, 0.15 M NaCl, 0.005 % v/v P20, pH 7.4). The surface of FC2 and 4 were successfully regenerated.
This was repeated on multiple occasions and was reproducible.

8.11.3.3.1. Testing Surface Interactions – Method 1

On manual run the surface was primed twice with the 50 mM Hepes (pH 7.0) containing 150 mM NaCl, 0.02 % CHS, 0.1 % DOM, 0.1 % Chaps and 50 nM DOPC/DOPS (7:3), 5 mM $MgCl_2$, 1 mM $CaCl_2$

and 0.1 mg/mL BSA running buffer. CXCR4 conformation specific mAb PE-12G5 in running buffer (120 µL, 200 nM) was injected over 120 s at 20 µL/min. No binding was observed.

8.11.3.3.2. Testing Surface Interactions – Method 2

Using the "*Binding assay*" wizard run the surface was primed twice with the 50 mM Hepes (pH 7.0) containing 150 mM NaCl, 0.02 % CHS, 0.1 % DOM, 0.1 % Chaps and 50 nM DOPC/DOPS (7:3), 5 mM $MgCl_2$, 1 mM $CaCl_2$ and 0.1 mg/mL BSA running buffer. Lipids and detergents were prepared by dissolving in chloroform and rotating the test-tube while evaporating the chloroform with a stream on nitrogen. Remaining chloroform was removed by drying under vacuum overnight. 1 mL of buffer (20 mM tris (pH 7.0) containing 0.1 M $(NH_4)_2SO_4$, 10 % glycerol) was added to each test tube and frozen. Once frozen the samples were allowed to thaw and vortexed. This was repeated four times before uniform liposomes were prepared by extrusion through a 100 nm polycarbonate filter using an Avanti mini-extruder kit. The samples were then added to the buffer. CXCR4 conformation specific mAb PE-12G5 in running buffer (200 nM and 50 nM) were injected over 60 s at 20 µL/min. No binding was observed.

8.11.3.3.3. Testing Surface Interactions – Method 3

On manual run the surface was primed twice with the 50 mM Hepes (pH 7.0) containing 150 mM sodium chloride, 0.02 % CHS, 0.10 % DOM, 0.10 % Chaps and 50 nM DOPC/DOPS (7:3), 5.00 mM magnesium chloride, 1.00 mM calcium chloride and 0.10 mg/mL BSA running buffer. Lipids and detergents were prepared by dissolving in chloroform and rotating the test-tube while evaporating the chloroform with a stream on nitrogen. Remaining chloroform was removed by drying under vacuum overnight. 1.00 mL of tris buffer (20 mM, pH 7.0) containing 0.10 M $(NH_4)_2SO_4$, 10 % glycerol) was added to each test tube and frozen. Once frozen the samples were allowed to thaw and vortexed. This was repeated four times before uniform liposomes were prepared by extrusion through a 100 nm polycarbonate filter using an Avanti mini-extruder kit. The samples were then added to the buffer. CXCR4 conformation specific mAb PE-12G5 in running buffer (120 µL, 200 nM) was injected over 120 s at 20 µL/min. No binding was observed. A second injection of mAb PE-12G5 in running buffer (120 µL, 200 nM) was injected over 120 s at 10 µL/min. No binding was observed. A further injection of mAb PE-12G5 in running buffer (100 µL, 600 nM) was conducted for 120 s at 20 µL/min. No binding was observed.

8.11.3.3.4. Testing Surface Interactions – Method 4

On manual run the surface was primed twice with the 50 mM Hepes (pH 7.5) containing 5 % dialysed FBS, 5.00 mM magnesium chloride, 1.00 mM calcium chloride and 5.00 mg/mL BSA running buffer.

CXCR4 conformation specific mAb PE-12G5 in running buffer (120 µL, 400 nM) was injected for 60 s at 20 µL/min. No binding was observed. This method was repeated following CXCR4 capture Method 5 but no binding was observed.

8.11.4. Binding of biotinylated macrocycle with streptavidin

A new SA sensor chip was allowed to equilibrate at RT for 30 min prior to use. Manual run was used to test the interactions between a biotinylated macrocycle and a streptavidin surface compared to an unlabelled macrocycle. PBS running buffer (10 mM, pH 7.5) was used to prime the SA sensor chip. Three 60 s injections of 1.00 M NaCl in 50 mM NaOH at a flow rate of 10 µL/min were conducted to condition the sensor chip. 100 nM solutions of **74**, **75** and (5-([(N-(Biotinoyl)amino)hexanoyl]-amino)pentylamine trifluoroacetate salt were made up in running buffer and filtered through 0.22 µm filter. **74** acted as a negative control to produce a reading for 0 % binding and (5-([(N-(Biotinoyl)amino)hexanoyl]-amino)pentylamine trifluoroacetate salt was used as a positive control to produce a reading for 100 % binding. Samples were injected with a contact time of 60 s at a flow rate of 10 µL/min. **74** was injected onto FC 1 followed by (5-([(N-(Biotinoyl)amino)hexanoyl]-amino)pentylamine trifluoroacetate salt. Subsequently **74** was injected onto FC 2 followed by **75**.

Following this the samples were flowed over the cells with a contact time of 60 s at a flow rate of 10 µL/min. RS409, the zero sample, was flowed over flow cell 1 followed by (5-([(N-(Biotinoyl)amino)hexanoyl]-amino)pentylamine trifluoroacetate salt, the 100 % sample. **75** was flowed over FC 2 subsequent to **74**.

The responses in resonance units (RU) of all samples were taken and divided by the sample molecular weight to give the results per molecule binding:

Negative control (**74**): $\frac{24.35}{919.11} x\ 100 = 2.6\ \%$

Positive control: $\frac{136}{555.65} x\ 100 = 24.6\ \%$

75: $\frac{296.5}{1145.41} x\ 100 = 25.9\ \%$

From this experiment it can be concluded that **75** binds 100 % to streptavidin.

9. REFERENCES

1. Lichty, J.; Allen, S. M.; Grillo, A. I.; Archibald, S. J.; Hubin, T. J., Synthesis and characterization of the cobalt(III) complexes of two pendant-arm cross-bridged cyclams. *Inorg. Chim. Acta* **2004,** *357* (2), 615-618.
2. Teicher, B. A.; Fricker, S. P., CXCL12 (SDF-1)/CXCR4 pathway in cancer. *Clin. Cancer Res.* **2010,** *16* (11), 2927-2931.
3. Zlotnik, A., The Chemokine Super family revisited. *Immunity* **2012,** *36*, 705-716.
4. Zlotnik, A.; Yoshie, O., Chemokines: A New Classification System and Their Role in Immunity. *Immunity* **2000,** *12* (2), 121-127.
5. Onuffer, J. J.; Horuk, R., Chemokines, chemokine receptors and small-molecule antagonists: recent developments. *Trends Pharmacol. Sci.* **2002,** *23* (10), 459-467.
6. Vicari, A. P.; Caux, C., Chemokines in cancer. *Cytokine Growth F. R.* **2002,** *13*, 143-154.
7. Zlotnik, A.; Yoshie, O.; Nomiyama, H., The chemokine and chemokine receptor superfamilies and their molecular evolution. *Genome Biol.* **2006,** *7* (12), 243.
8. Kohidai, L. Structure of chemokine families. http://commons.wikimedia.org/wiki/File:ChtxChemokineStruct.png (accessed 15/12/2014).
9. (a) Cheng, F.; Hope, C. N.; Archibald, S. J.; Bradley, J. S.; Clark, S.; Francesconi, M. G.; Kelly, S. M.; Young, N. A.; Lefebvre, F., Preparation, Structural Characterization, and Thermal Ammonolysis of Two Novel Dimeric Transition Silylamide Complexes. *Int. J. Appl. Ceram. Tec.* **2011,** *8* (2), 467-481; (b) Yu, M.; Price, J. R.; Jensen, P.; Lovitt, C. J.; Shelper, T.; Duffy, S.; Windus, L. C.; Avery, V. M.; Rutledge, P. J.; Todd, M. H., Copper, nickel, and zinc cyclam-amino acid and cyclam-peptide complexes may be synthesized with "click" chemistry and are noncytotoxic. *Inorg. Chem.* **2011,** *50* (24), 12823-35; (c) Muller, A., <Involvement of chemokine receptors in breast cancer metastasis.pdf>. **2001**.
10. Tanaka, T.; Bai, Z.; Srinoulprasert, Y.; Yang, B. G.; Hayasaka, H.; Miyasaka, M., Chemokines in tumor progression and metastasis. *Cancer Sci.* **2005,** *96* (6), 317-22.
11. Flower, D. R., Modelling G-protein-coupled receptors for drug design. *BBA.-Rev. Biomembranes* **1999,** *1422* (3), 207-234.
12. Ji, T. H.; Grossman, M.; Ji, I., G Protein-coupled Receptors I. Diversity of receptor-ligand interactions. *J. Biol. Chem.* **1998,** *273* (28), 17299–17302.
13. Bokoch, M. P.; Zou, Y.; Rasmussen, S. G. F.; Liu, C. W.; Nygaard, R.; Rosenbaum, D. M.; Fung, J. J.; Choi, H.-J.; Thian, F. S.; Kobilka, T. S.; Puglisi, J. D.; Weis, W. I.; Pardo, L.; Prosser, R. S.; Mueller, L.; Kobilka, B. K., Ligand-specific regulation of the extracellular surface of a G-protein-coupled receptor. *Nature* **2010,** *463* (7277), 108-112.
14. Teller, D. C.; Okada, T.; Behnke, C. A.; Palczewski, K.; Stenkamp, R. E., Advances in determination of a high-resolution three-dimensional structure of rhodopsin, a model of G-protein-coupled receptors (GPCRs). *Biochemistry* **2001,** *40* (26), 7761-7772.
15. (a) Khan, A.; Greenman, J.; Archibald, S. J., Small molecule CXCR4 chemokine receptor antagonists: Developing drug candidates. *Curr. Med. Chem.* **2007,** *14*, 2257-2277; (b) Furusato, B. a. R., J. S., *Chemokine Receptors in Cancer*. Humana Press: New York, 2009.
16. Tanegashima, K.; Suzuki, K.; Nakayama, Y.; Tsuji, K.; Shigenaga, A.; Otaka, A.; Hara, T., CXCL14 is a natural inhibitor of the CXCL12-CXCR4 signaling axis. *FEBS Lett.* **2013,** *587* (12), 1731-1735.
17. Fruehauf, S., Rosenkilde, M. M., Steen, A., and Zeller, J. W., *Novel Developments in Stem Cell Mobilizations: Focus on CXCR4*. Springer: London, 2012.
18. De Clercq, E., The bicyclam AMD3100 story. *Nat. Rev. Drug Discov.* **2003,** *2*, 581-587.
19. Fricker, S. P.; Anastassov, V.; Cox, J.; Darkes, M. C.; Grujic, O.; Idzan, S. R.; Labrecque, J.; Lau, G.; Mosi, R. M.; Nelson, K. L.; Qin, L.; Santucci, Z.; Wong, R. S., Characterization of the molecular pharmacology of AMD3100: a specific antagonist of the G-protein coupled chemokine receptor, CXCR4. *Biochem. Pharmacol.* **2006,** *72* (5), 588-96.

20. Dittmar, T., Kassmer, S. H., Kasenda, B., Niggermann, B., Seidel, J. and Zänker, K. S., *Stem Cell Biology in Health and Diesease*. Springer: New York, 2009.
21. Unutmaz, D.; Littman, D. R., Expression pattern of HIV-1 coreceptors on T cells: Implications for viral transmission and lymphocyte homing. *P. Natl. Acad. Sci. USA.* **1997,** *94* (5), 1615-1618.
22. Zlotnik, A., Chemokines and cancer. *Int. J. Cancer* **2006,** *119* (9), 2026-2029.
23. Balkwill, F., The significance of cancer cell expression of the chemokine receptor CXCR4. *Semin. Cancer Biol.* **2004,** *14* (3), 171-9.
24. Zou, Y.-R.; Kottmann, A. H.; Kuroda, M.; Taniuchi, I.; Littman, D. R., Function of the chemokine receptor CXCR4 in haematopoiesis and in cerebellar development. *Nature* **1998,** *393* (6685), 595-599.
25. Nagasawa, T.; Hirota, S.; Tachibana, K.; Takakura, N.; Nishikawa, S.-I.; Kitamura, Y.; Yoshida, N.; Kikutani, H.; Kishimoto, T., Defects of B-cell lymphopoiesis and bone-marrow myelopoiesis in mice lacking the CXC chemokine PBSF/SDF-1. *Nature* **1996,** *382* (6592), 635-638.
26. De La Luz Sierra, M.; Yang, F.; Narazaki, M.; Salvucci, O.; Davis, D.; Yarchoan, R.; Zhang, H. H.; Fales, H.; Tosato, G., Differential processing of stromal-derived factor-1α and stromal-derived factor-1β explains functional diversity. *Blood* **2004,** *103* (7), 2452-2459.
27. Sun, X.; Cheng, G.; Hao, M.; Zheng, J.; Zhou, X.; Zhang, J.; Taichman, R. S.; Pienta, K. J.; Wang, J., CXCL12 / CXCR4 / CXCR7 chemokine axis and cancer progression. *Cancer metastasis reviews* **2010,** *29* (4), 709-22.
28. Roussos, E. T.; Condeelis, J. S.; Patsialou, A., Chemotaxis in cancer. *Nature reviews. Cancer* **2011,** *11* (8), 573-87.
29. (a) Hatse, S.; Princen, K.; De Clercq, E.; Rosenkilde, M. M.; Schwartz, T. W.; Hernandez-Abad, P. E.; Skerlj, R. T.; Bridger, G. J.; Schols, D., AMD3465, a monomacrocyclic CXCR4 antagonist and potent HIV entry inhibitor. *Biochem. Pharmacol.* **2005,** *70* (5), 752-61; (b) Ling, X.; Spaeth, E.; Chen, Y.; Shi, Y.; Zhang, W.; Schober, W.; Hail Jr, N.; Konopleva, M.; Andreeff, M., The CXCR4 Antagonist AMD3465 Regulates Oncogenic Signaling and Invasiveness In Vitro and Prevents Breast Cancer Growth and Metastasis In Vivo. *PLOS ONE* **2013,** *8* (3).
30. Balkwill, F., The significance of cancer cell expression of the chemokine receptor CXCR4. *Seminars in Cancer Biology* **2004,** *14* (3), 171-179.
31. al, B. W. e., Structures of the CXCR4 chemokine GPCR with small molecule and cyclic peptide antagonists. *Science* **2010,** *330*, 1066-1071.
32. (a) Muller, A.; Homey, B.; Soto, H.; Ge, N.; Catron, D.; Buchanan, M. E.; McClanahan, T.; Murphey, E.; Yuan, W.; Wagner, S. N.; Barrera, J. L.; Mohar, A.; Verastegui, E.; Zlotnik, A., Involvement of chemokine receptors in breast cancer metastasis. *Nature* **2001,** *410*, 50-56; (b) Li, Y. M.; Pan, Y.; Wei, Y.; Cheng, X.; Zhou, B. P.; Tan, M.; Zhou, X.; Xia, W.; Hortobagyi, G. N.; Yu, D.; Hung, M. C., Upregulation of CXCR4 is essential for HER2-mediated tumor metastasis. *Cancer Cell* **2004,** *6* (5), 459-469.
33. Milliken, D.; Scotton, C.; Raju, S.; Balkwill, F.; Wilson, J., Analysis of chemokines and chemokine receptor expression in ovarian cancer ascites. *Clin. Cancer Res.* **2002,** *8* (4), 1108-1114.
34. Darash-Yahana, M.; Pikarsky, E.; Abramovitch, R.; Zeira, E.; Pal, B.; Karplus, R.; Beider, K.; Avniel, S.; Kasem, S.; Galun, E.; Peled, A., Role of high expression levels of CXCR4 in tumor growth, vascularization, and metastasis. *Faseb J.* **2004,** *18* (9), 1240-+.
35. Marchesi, F.; Monti, P.; Leone, B. E.; Zerbi, A.; Vecchi, A.; Piemonti, L.; Mantovani, A.; Allavena, P., Increased survival, proliferation, and migration in metastatic human pancreatic tumor cells expressing functional CXCR4. *Cancer Res.* **2004,** *64* (22), 8420-8427.
36. (a) Muller, A.; Sonkoly, E.; Eulert, C.; Gerber, P. A.; Kubitza, R.; Schirlau, K.; Franken-Kunkel, P.; Poremba, C.; Snyderman, C.; Klotz, L. O.; Ruzicka, T.; Bier, H.; Zlotnik, A.; Whiteside, T. L.; Homey, B.; Hoffmann, T. K., Chemokine receptors in head and neck cancer: association with metastatic spread and regulation during chemotherapy. *Int. J. Cancer* **2006,** *118* (9), 2147-2157; (b) Letsch, A.; Keilholz, U.; Schadendorf, D.; Assfalg, G.; Asemissen, A. M.; Thiel, E.; Scheibenbogen, C., Functional CCR9 expression is associated with small intestinal metastasis.

J. Invest. Dermatol. **2004,** *122* (3), 685-690; (c) Scala, S.; Ottaiano, A.; Ascierto, P. A.; Cavalli, M.; Simeone, E.; Giuliano, P.; Napolitano, M.; Franco, R.; Botti, G.; Castello, G., Expression of CXCR4 predicts poor prognosis in patients with malignant melanoma. *Clin. Cancer Res.* **2005,** *11* (5), 1835-1841.

37. (a) Kaifi, J. T.; Yekebas, E. F.; Schurr, P.; Obonyo, D.; Wachowiak, R.; Busch, P.; Heinecke, A.; Pantel, K.; Izbicki, J. R., Tumor-cell homing to lymph nodes and bone marrow and CXCR4 expression in esophageal cancer. *J. Natl. Cancer I.* **2005,** *97* (24), 1840-1847; (b) Ding, Y. Z.; Shimada, Y.; Maeda, M.; Kawabe, A.; Kaganoi, J.; Komoto, I.; Hashimoto, Y.; Miyake, M.; Hashida, H.; Imamura, M., Association of CC chemokine receptor 7 with lymph node metastasis of esophageal squamous cell carcinoma. *Clin. Cancer Res.* **2003,** *9* (9), 3406-3412.
38. (a) Phillips, R. J.; Burdick, M. D.; Lutz, M.; Belperio, J. A.; Keane, M. P.; Strieter, R. M., The stromal derived factor-1/CXCL12-CXC chemokine receptor 4 biological axis in non-small cell lung cancer metastases. *Am. J. Resp. Crit. Care* **2003,** *167* (12), 1676-1686; (b) Takanami, I., Overexpression of CCR7 mRNA in nonsmall cell lung cancer: Correlation with lymph node metastasis. *Int. J. Cancer* **2003,** *105* (2), 186-189.
39. Katayama, A.; Ogino, T.; Bandoh, N.; Nonaka, S.; Harabuchi, Y., Expression of CXCR4 and its down-regulation by IFN-gamma in head and neck squamous cell carcinoma. *Clin. Cancer Res.* **2005,** *11* (8), 2937-2946.
40. Eisenhardt, A.; Frey, U.; Tack, M.; Rosskopf, D.; Lummen, G.; Rubben, H.; Siffert, W., Expression analysis and potential functional role of the CXCR4 chernokine receptor in bladder cancer. *Eur. Urol.* **2005,** *47* (1), 111-117.
41. (a) Kim, J.; Takeuchi, H.; Lam, S. T.; Turner, R. R.; Wang, H. J.; Kuo, C.; Foshag, L.; Bilchik, A. J.; Hoon, D. S., Chemokine receptor CXCR4 expression in colorectal cancer patients increases the risk for recurrence and for poor survival. *J. Clin. Oncol.* **2005,** *23* (12), 2744-53; (b) Gunther, K.; Leier, J.; Henning, G.; Dimmler, A.; Weissbach, R.; Hohenberger, W.; Forster, R., Prediction of lymph node metastasis in colorectal carcinoma by expression of chemokine receptor CCR7. *Int. J. Cancer* **2005,** *116* (5), 726-733; (c) Schimanski, C. C.; Schwald, S.; Simiantonaki, N.; Jayasinghe, C.; Gonner, U.; Wilsberg, V.; Junginger, T.; Berger, M. R.; Galle, P. R.; Moehler, M., Effect of chemokine receptors CXCR4 and CCR7 on the metastatic behavior of human colorectal cancer. *Clin. Cancer Res.* **2005,** *11* (5), 1743-1750.
42. Laverdiere, C.; Hoang, B. H.; Yang, R.; Sowers, R.; Qin, J.; Meyers, P. A.; Huvos, A. G.; Healey, J. H.; Gorlick, R., Messenger RNA expression levels of CXCR4 correlate with metastatic behavior and outcome in patients with osteosarcoma. *Clin. Cancer Res.* **2005,** *11* (7), 2561-2567.
43. Russell, H. V.; Hicks, J.; Okcu, M. F.; Nuchtern, J. G., CXCR4 expression in neuroblastoma primary tumors is associated with clinical presentation of bone and bone marrow metastases. *J. Pediatr. Surg.* **2004,** *39* (10), 1506-1511.
44. Corcione, A.; Arduino, N.; Ferretti, E.; Pistorio, A.; Spinelli, M.; Ottonello, L.; Dallegri, F.; Basso, G.; Pistoia, V., Chemokine receptor expression and function in childhood acute lymphoblastic leukemia of B-lineage. *Leukemia Res.* **2006,** *30* (4), 365-372.
45. (a) Burger, J. A.; Kipps, T. J., Chemokine receptors and stromal cells in the homing and homeostasis of chronic lymphocytic leukemia B cells. *Leukemia Lymphoma* **2002,** *43* (3), 461-466; (b) Trentin, L.; Cabrelle, A.; Facco, M.; Carollo, D.; Miorin, M.; Tosoni, A.; Pizzo, P.; Binotto, G.; Nicolardi, L.; Zambello, R.; Adami, F.; Agostini, C.; Semenzato, G., Homeostatic chemokines drive migration of malignant B cells in patients with non-Hodgkin lymphomas. *Blood* **2004,** *104* (2), 502-508.
46. Lambert, D. G., Drugs and receptors. *CEACCP* **2004,** *4* (6), 181-184.
47. De Clercq, E., The AMD3100 story: the path to the discovery of a stem cell mobilizer (Mozobil). *Biochem. Pharmacol.* **2009,** *77* (11), 1655-64.
48. (a) De Clercq, E., Inhibition of HIV infection by bicyclams, highly potent and specific CXCR4 antagonists. *Mol. Pharmacol.* **2000,** *57*, 833-839; (b) Schols, D.; Struyf, S.; Van Damme, J.; Este, J. A.; Henson, G.; De Clercq, E., Inhibition of T-tropic HIV strains by selective antagonization of

the chemokine receptor CXCR4. *J. Exp. Med.* **1997,** *186*, 1383-1388; (c) Donzella, G. A.; Schols, D.; Lin, S. W.; Este, J. A.; Nagashima, K. A.; Maddon, P. J., AMD3100, a small molecule inhibitor of HIV-1 entry via the CXCR4 co-receptor. *Nat. Med.* **1998,** *4*, 72-77.

49. Berridge, M. J.; Lipp, P.; Bootman, M. D., The versatility and universality of calcium signalling. *Nat. Rev. Mol. Cell Bio.* **2000,** *1* (1), 11-21.
50. Calandra, G.; McCarty, J.; McGuirk, J.; Tricot, G.; Crocker, S.-A.; Badel, K., AMD3100 plus G-CSF can successfully mobilize CD34+ cells from non-Hodgkin's lymphoma, Hodgkin's disease and multiple myeloma patients previously failing mobilization with chemotherapy and/or cytokine treatment: compassionate use data. *Bone Marrow Transpl.* **2008,** *41*, 331-338.
51. (a) Gazitt, Y.; Freytes, C. O.; Akay, C.; Badel, K.; Calandra, G., Improved mobilization of peripheral blood CD34+ cells and dendritic cells by AMD3100 plus granulocyte-colony-stimulating factor in non-Hodgkin's lymphoma patients. *Stem Cells Dev.* **2007,** *16*, 657-666; (b) Flomenberg, N.; DiPersio, J.; Calandra, G., Role of CXCR4 chemokine receptor blockade using AMD3100 for mobilization of autologous hematopoietic progenitor cells. *Acta Haematol.-Basel* **2005,** *114*, 198-205; (c) Devine, S.; Gazitt, Y.; Calandra, G., Clinical use of AMD3100 to mobilize CD34+ cells in patients affected by non-Hodgkin's lymphoma or multiple myeloma. *J. Clin. Oncol.* **2005,** *23*, 3872-3873.
52. De Falco, V.; Guarino, V.; Avilla, E.; Castellone, M. D.; Salerno, P.; Salvatore, G., Biological role and potential therapeutic targeting of the chemokine receptor CXCR4 in undifferentiated thyroid cancer. *Cancer Res.* **2007,** *67*, 11821-11829.
53. Rubin, J. B.; Kung, A. L.; Klein, R. S.; Chan, J. A.; Sun, Y.; Schmidt, K., A small-molecule antagonist of CXCR4 inhibits intracranial growth of primary brain tumors. *P. Natl. Acad. Sci. USA.* **2003,** *100*, 13513–13518.
54. Li, J. K.; Yu, L.; Shen, Y.; Zhou, L. S.; Wang, Y. C.; Zhang, J. H., Inhibition of CXCR4 activity with AMD3100 decreases invasion of human colorectal cancer cells in vitro. *World J. Gastroentero.* **2008,** *14* (15), 2308-13.
55. (a) De Clercq, E., Recent advances on the use of the CXCR4 antagonist plerixafor (AMD3100, Mozobil™) and potential of other CXCR4 antagonists as stem cell mobilizers. *Pharmacology & Therapeutics* **2010,** *128* (3), 509-518; (b) Peled, A.; Wald, O.; Burger, J., Development of novel CXCR4-based therapeutics. *Expert Opin. Inv. Drug.* **2012,** *21* (3), 341-353.
56. (a) Gerlach, L. O.; Jakobsen, J. S.; Jensen, K. P.; Rosenkilde, M. R.; Skerlj, R. T.; Ryde, U.; Bridger, G. J.; Schwartz, T. W., Metal Ion Enhanced Binding of AMD3100 to Asp262 in the CXCR4 Receptor. *Biochemistry* **2003,** *42*, 710-717; (b) Fruehauf, S.; Rosenkilde, M. M.; Steen, A.; Zeller, J. W., *Novel Developments in Stem Cell Mobilizations: Focus on CXCR4*. Springer: London, 2012.
57. (a) Gerlach, L. O.; Skerlj, R. T.; Bridger, G. J.; Schwartz, T. W., Molecular interactions of cyclam and bicyclam non-peptide antagonists with the CXCR4 chemokine receptor. *J. Biol. Chem.* **2001,** *276* (17), 14153-60; (b) Vinader, V.; Ahmet, D. S.; Ahmed, M. S.; Patterson, L. H.; Afarinkia, K., Discovery and computer aided potency optimization of a novel class of small molecule CXCR4 antagonists. *PLoS One* **2013,** *8* (10), e78744; (c) Wong, R. S.; Bodart, V.; Metz, M.; Labrecque, J.; Bridger, G.; Fricker, S. P., Comparison of the potential multiple binding modes of bicyclam, monocylam, and noncyclam small-molecule CXC chemokine receptor 4 inhibitors. *Mol Pharmacol* **2008,** *74* (6), 1485-95; (d) Bridger, G. J.; Skerlj, R. T.; Hernandez-Abad, P. E.; Bogucki, D. E.; Wang, Z.; Zhou, Y.; Nan, S.; Boehringer, E. M.; Wilson, T.; Crawford, J.; Metz, M.; Hatse, S.; Princen, K.; De Clercq, E.; Schols, D., Synthesis and structure-activity relationships of azamacrocyclic C-X-C chemokine receptor 4 antagonists: Analogues containing a single azamacrocyclic ring are potent inhibitors of T-cell tropic (X4) HIV-1 replication. *J. Med. Chem.* **2010,** *53* (3), 1250-1260.
58. Shriver, D. F.; Atkins, P. W.; Overton, T. L.; Rourke, J. P.; Weller, M. T.; Armstrong, F. A., *Inorganic Chemistry*. Fourth ed.; Oxford University Press: Oxford, 2006.

59. Cabbiness, D. K.; Margerum, D. W., Macrocyclic effect on the stability of copper(II) tetramine complexes [36]. *J. Am. Chem. Soc.* **1969,** *91* (23), 6540-6541.
60. (a) Wainwright, K. P., Bridging alkylation of saturated polyaza macrocycles: A means for imparting structural rigidity. *Inorg. Chem.* **1980,** *19* (5), 1396-1398; (b) Hancock, R. D.; Dobson, S. M.; Evers, A.; Wade, P. W.; Ngwenya, M. P.; Boeyens, J. C. A.; Wainwright, K. P., More rigid macrocyclic ligands that show metal ion size-based selectivity. A crystallographic, molecular mechanics, and formation constant study of the complexes of bridged cyclen. *J. Am. Chem. Soc.* **1988,** *110* (9), 2788-2794.
61. (a) Weisman, G. R.; Rogers, M. E.; Wong, E. H.; Jasinski, J. P.; Paight, E. S., Cross-bridged cyclam. Protonation and complexation of Li+in a diamond lattice cleft. *J. Am. Chem. Soc.* **1990,** *112*, 8604-8605; (b) Wong, E. H.; Weisman, G. R.; Hill, D. C.; Reed, D. P.; Rogers, M. E.; Condon, J. S.; Fagan, M. A.; Calabrese, J. C.; Lam, K.-C.; Guzei, I. A.; Rheingold, A. L., Synthesis and Characterization of Cross-Bridged Cyclams and Pendant-Armed Derivatives and Structural Studies of Their Copper(II) Complexes. *J. Am. Chem. Soc.* **2000,** *122*, 10561-10572.
62. Hancock, R. D.; Pattrick, G.; Wade, P. W.; Hosken, G. D., Structurally reinforced macrocyclic ligands. *pac* **1993,** *65* (3), 473.
63. (a) Pandya, D. N.; Bhatt, N.; An, G. I.; Ha, Y. S.; Soni, N.; Lee, H.; Lee, Y. J.; Kim, J. Y.; Lee, W. H.; Ahn, H.; Yoo, J., Propylene cross-bridged macrocyclic bifunctional chelator: a new design for facile bioconjugation and robust 64Cu-complex stability. *J. Med. Chem.* **2014**; (b) Pandya, D. N.; Dale, A. V.; Kim, J. Y.; Lee, H.; Ha, Y. S.; An, G. I.; Yoo, J., New Macrobicyclic Chelator for the Development of Ultrastable 64Cu-Radiolabeled Bioconjugate. *Bioconjugate Chem.* **2012,** *23* (3), 330-335.
64. Pais, M.; Rattle, M. M. G.; Sarfati, R.; Jarreau, F.-X., L'homaline, nouveau type d'alcaloide isolé d'un Homalium sp. africain (Flacourtiacées). *C. R. Acad. Sc.* **1968,** *266*, 37.
65. (a) Liang, X.; Parkinson, J. A.; Weishaupl, M.; Gould, R. O.; Paisey, S. J.; Park, H. S.; Hunter, T. M.; Blindauer, C. A.; Parsons, S.; Sadler, P. J., Structure and dynamics of metallomacrocycles: recognition of zinc xylyl-bicyclam by an HIV coreceptor. *J. Am. Chem. Soc.* **2002,** *124* (31), 9105-12; (b) Liang, X.; Weishäupl, M.; Parkinson, J. A.; Parsons, S.; McGregor, P. A.; Sadler, P. J., Selective Recognition of Configurational Substates of Zinc Cyclam by Carboxylates: Implications for the Design and Mechanism of Action of Anti-HIV Agents. *Chem.-Eur. J.* **2003,** *9* (19), 4709-4717.
66. Hunter, T. M.; McNae, I. W.; Simpson, D. P.; Smith, A. M.; Moggach, S.; White, F.; Walkinshaw, M. D.; Parsons, S.; Sadler, P. J., Configurations of nickel-cyclam antiviral complexes and protein recognition. *Chem.-Eur. J.* **2007,** *13* (1), 40-50.
67. Smith, R.; Huskens, D.; Daelemans, D.; Mewis, R. E.; Garcia, C. D.; Cain, A. N.; Freeman, T. N. C.; Pannecouque, C.; Clercq, E. D.; Schols, D.; Hubin, T. J.; Archibald, S. J., CXCR4 chemokine receptor antagonists: Nickel(ii) complexes of configurationally restricted macrocycles. *Dalton Trans.* **2012,** *41* (37), 11369-11377.
68. (a) Li, Z.; Ding, H.; Wu, S.; Liu, H.; Su, H.; Sun, J.; Zheng, D.; Huo, Q.; Guan, J.; Kan, Q., Tetraazamacrocycle complexes of Cu(II) and VO(IV) exchanged in the interlayers of montmorillonite clay: Heterogeneous catalysts for the aerobic oxidation of styrene. *Mater. Res. Bull.* **2013,** *48* (5), 1920-1926; (b) Islam, M. J.; Miller, E. J.; Gordner, J. S.; Patel, D.; Wang, Z., Effective synthesis of bis-bispidinone and facile difunctionalization of highly rigid macrocyclic tetramines. *Tetrahedron Lett.* **2013,** *54* (17), 2133-2136; (c) Khoshro, H.; Zare, H. R.; Gorji, A.; Namazian, M., A study of the catalytic activity of symmetric and unsymmetric macrocyclic [N42−] coordinated nickel complexes for electrochemical reduction of carbon dioxide. *Electrochimica Acta* **2014,** *117* (0), 62-67; (d) Kang, S.-G.; Lee, Y.-T.; Chun, H.; Kim, K., Synthesis of new structurally constrained tetraaza macropolycyclic compounds containing two rigid bridges: Crystal structure and chemical properties of a copper(II) complex. *Inorg. Chim. Acta* **2014,** *409, Part B* (0), 315-319; (e) Piro, N. A.; Robinson, J. R.; Walsh, P. J.; Schelter, E. J.,

The electrochemical behavior of cerium(III/IV) complexes: Thermodynamics, kinetics and applications in synthesis. *Coord. Chem. Rev.* **2014,** *260* (0), 21-36.
69. Gano, L.; Marques, F.; Campbello, M. P.; Balbina, M.; Lacerda, S.; Santos, I., Radiolanthanide complexes with tetraazamacrocycles bearing methylphosphonate pendant arms as bone seeking agents. *Q. J. Nucl. Med. Mol. Im.* **2007,** *51* (1), 6-15.
70. Cao, J.; Geng, Z.; Ma, X.; Wen, J.; Yin, Y.; Wang, Z., Evidence for inhibition of HIF-1α prolyl hydroxylase 3 activity by four biologically active tetraazamacrocycles. *Org. Biomol. Chem.* **2012,** *10* (19), 3913-3923.
71. (a) Liang, X.; Sadler, P. J., Cyclam complexes and their applications in medicine. *Chem. Soc. Rev.* **2004,** *33* (4), 246-266; (b) Valks, G. C.; McRobbie, G.; Lewis, E. A.; Hubin, T. J.; Hunter, T. M.; Sadler, P. J.; Pannecouque, C.; De Clercq, E.; Archibald, S. J., Configurationally Restricted Bismacrocyclic CXCR4 Receptor Antagonists. *J. Med. Chem.* **2006,** *49*, 6162-6165; (c) Kimura, E., Macrocyclic polyamines with intelligent functions. *Tetrahedron* **1992,** *48* (30), 6175-6217; (d) Khan, A. e. a., Small molecules CXCR4 chemokine receptor antagonists: developing drug candidates. *Curr. Medic. Chem.* **2007,** *14*, 2257-2277.
72. Dabrowiak, J. C., Vanadium, Copper and Zinc in Medicine. In *Metals in Medicine*, John Wiley & Sons, Ltd: 2009; pp 219-249.
73. Ronconi, L.; Sadler, P. J., Using coordination chemistry to design new medicines. *Coordination Chemistry Reviews* **2007,** *251* (13-14 SPEC. ISS.), 1633-1648.
74. Esté, J. A.; Cabrera, C.; De Clercq, E.; Struyf, S.; Van Damme, J.; Bridger, G.; Skerlj, R. T.; Abrams, M. J.; Henson, G.; Gutierrez, A.; Clotet, B.; Schols, D., Activity of different bicyclam derivatives against human immunodeficiency virus depends on their interaction with the CXCR4 chemokine receptor. *Mol. Pharmacol.* **1999,** *55* (1), 67-73.
75. (a) Berthon, G., *Handbook of Metal-Ligand Interactions in Biological Fluids: Bioinorganic Medicine Volume 2 (In Two Volumes)*. Taylor & Francis: 1995; (b) Kodama, M.; Kimura, E., Equilibria and kinetics of complex formation between zinc(II), lead(II), and cadmium(II), and 12-, 13-, 14-, and 15-membered macrocyclic tetra-amines. *J. Chem. Soc. Dalton* **1977,** (22), 2269-2276.
76. Subhan, M. A.; Choi, J.-H., X-ray structure and spectroscopy of novel trans-[Ni(L)(NO3)2] and [Ni(L)](ClO4)2·2H2O complexes. *Spectrochim. Acta A* **2014,** *123* (0), 410-415.
77. Silversides, J. D.; Burke, B. P.; Archibald, S. J., Rapid synthesis of cross-bridged cyclam chelators for copper(II) complex formation. *Comptes Rendus Chimie* **2013,** *16* (6), 524-530.
78. Timmons, J. C.; Hubin, T. J., Preparations and applications of synthetic linked azamacrocycle ligands and complexes. *Coord. Chem. Rev.* **2010,** *254* (15-16), 1661-1685.
79. Bridger, G. J.; T., S. R.; Thornton, D.; Padmanabhan, S.; Martellucci, S. A.; W., H. G.; Abrams, M. J.; Yamamoto, N.; De Vreese, K.; Pauwels, R.; E., D. C., Synthesis and Structure - Activity Relationships of Phenylenebis (methylene) Linked Bis-Tetraazamacrocycles That Inhibit HIV Replication. Effects of Macrocyclic Ring Size and Substituents on the Aromatic Linker. *J. Med. Chem.* **1995,** *38*, 366-378.
80. Tanaka, T.; Narumi, T.; Ozaki, T.; Sohma, A.; Ohashi, N.; Hashimoto, C.; Itotani, K.; Nomura, W.; Murakami, T.; Yamamoto, N.; Tamamura, H., Azamacrocyclic metal complexes as CXCR4 antagonists. *ChemMedChem* **2011,** *6* (5), 834-839.
81. McRobbie, G.; Valks, G. C.; Empson, C. J.; Khan, A.; Silversides, J. D.; Pannecouque, C.; De Clercq, E.; Fiddy, S. G.; Bridgeman, A. J.; Young, N. A.; Archibald, S. J., Probing key coordination interactions: Configurationally restricted metal activated CXCR4 antagonists. *Dalton Trans.* **2007,** (43), 5008-5018.
82. (a) Paisey, S. J.; Sadler, P. J., Anti-viral cyclam macrocycles : rapid zinc uptake at physiological pH. *Chem. Commun.* **2004,** (3), 306-307; (b) Roeper, J. R.; Elias, H., Kinetic studies of nickel(II) and copper(II) complexes with N4 macrocycles of the cyclam type. 1. Kinetics and mechanism of complex formation with different N-methylated 1,4,8,11-tetraazacyclotetradecanes. *Inorg. Chem.* **1992,** *31* (7), 1202-1210.

83. Valks, G. C.; McRobbie, G.; Lewis, E. A.; Hubin, T. J.; Hunter, T. M.; Sadler, P. J.; Pannecouque, C.; De Clercq, E.; Archibald, S. J., Configurationally restricted bismacrocyclic CXCR4 receptor antagonists. *Journal of Medicinal Chemistry* **2006,** *49* (21), 6162-6165.
84. McRobbie, G.; Valks, G. C.; Empson, C. J.; Khan, A.; Silversides, J. D.; Pannecouque, C.; De Clercq, E.; Fiddy, S. G.; Bridgeman, A. J.; Young, N. A.; Archibald, S. J., Probing key coordination interactions: configurationally restricted metal activated CXCR4 antagonists. *Dalton transactions* **2007,** (43), 5008-18.
85. Khan, A.; Nicholson, G.; Greenman, J.; Madden, L.; McRobbie, G.; Pannecouque, C.; De Clercq, E.; Ullom, R.; Maples, D. L.; Maples, R. D.; Silversides, J. D.; Hubin, T. J.; Archibald, S. J., Binding optimization through coordination chemistry CXCR4 chemokine receptor antagonists from ultrarigid metal complexes. *J. Am. Chem. Soc.* **2009,** *131*, 3416–3417.
86. Ross, A.; Soares, D. C.; Covelli, D.; Pannecouque, C.; Budd, L.; Collins, A.; Robertson, N.; Parsons, S.; De Clercq, E.; Kennepohl, P.; Sadler, P. J., Oxovanadium(IV) cyclam and bicyclam complexes: potential CXCR4 receptor antagonists. *Inorg. Chem.* **2010,** *49* (3), 1122-32.
87. Chartres, J. D.; Lindoy, L. F.; Meehan, G. V., Transition and post-transition metal systems incorporating linked synthetic macrocycles as structural elements. *Coord. Chem. Rev.* **2001,** *216-217* (0), 249–286.
88. Koike, T.; Takashige, M.; Kimura, E.; Fujioka, H.; Shiro, M., Bis(ZnII-cyclen) Complex as a Novel Receptor of Barbiturates in Aqueous Solution. *Chem.-Eur. J.* **1996,** *2*, 617.
89. Kimura E, K. M., Kitamura H, Koike T, *Chem. Eur. J.* **1999,** *5*, 3113.
90. Bencini, A.; Biagini, S.; Giorgi, C.; Handel, H.; Le Baccon, M.; Mariani, P.; Paoletti, P.; Paoli, P.; Rossi, P.; Tripier, R.; Valtancoli, B., A Tris-Macrocycle with Proton Sponge Characteristics as Efficient Receptor for Inorganic Phosphate and Nucleotide Anions. *Eur. J. Org. Chem.* **2009,** *2009* (32), 5610-5621.
91. Sun, S.; Saltmarsh, J.; Mallik, S.; Thomasson, K., *J. Chem. Soc. Chem. Comm.* **1998**, 519.
92. Choy, G.; Choyke, P.; Libutti, S. K., Current advances in molecular imaging: noninvasive in vivo bioluminescent and fluorescent optical imaging in cancer research. *Mol. Imaging* **2003,** *2* (4), 303-12.
93. Hellebust, A.; Richards-Kortum, R., Advances in molecular imaging: targeted optical contrast agents for cancer diagnostics. *Nanomedicine-UK* **2012,** *7* (3), 429-45.
94. Zanetti-Domingues, L. C.; Tynan, C. J.; Rolfe, D. J.; Clarke, D. T.; Martin-Fernandez, M., Hydrophobic Fluorescent Probes Introduce Artifacts into Single Molecule Tracking Experiments Due to Non-Specific Binding. *PLOS ONE* **2013,** *8* (9), e74200.
95. Hanninen, P.; Harma, H.; Ala-Kleme, T.; Bunzli, J.-C. G.; Bazin, H.; Eliseeva, S. V.; Faulkner, S.; Hemmilä, I.; Hyppanen, I.; Kankare, J.; Kulmala, S.; Kuusisto, A.; Laitala, V.; Mathis, G.; Nann, T.; Schaferling, M.; Soukka, T.; Spangler, C.; Stenman, U.-H.; Suomi, J.; Sykes, D.; Tanke, H. J.; Tanner, P. A.; Wang, H.-Q.; Werts, M. H. V., *Lanthanide Luminescence*. Springer Berlin Heidelberg: Germany, 2011.
96. Faulkner, S.; Pope, S. J. A.; Burton-Pye, B. P., Lanthanide complexes for luminescence imaging applications. *Appl. Spectrosc. Rev.* **2005,** *40* (1), 1-31.
97. Bunzli, J.-C. G.; Piguet, C., Taking advantage of luminescent lanthanide ions. *Chem. Soc. Rev.* **2005,** *34* (12), 1048-1077.
98. (a) Bornhop, D. J.; Griffin, J. M. M.; Goebel, T. S.; Sudduth, M. R.; Bell, B.; Motamedi, M., Luminescent Lanthanide Chelate Contrast Agents and Detection of Lesions in the Hamster Oral Cancer Model. *Appl. Spectrosc.* **2003,** *57* (10), 1216-1222; (b) Gunnlaugsson, T.; Leonard, J. P., Responsive lanthanide luminescent cyclen complexes: From switching/sensing to supramolecular architectures. *Chem. Commun.* **2005,** (25), 3114-3131.
99. Kuil, J.; Buckle, T.; Yuan, H.; Van Den Berg, N. S.; Oishi, S.; Fujii, N.; Josephson, L.; Van Leeuwen, F. W., Synthesis and evaluation of a bimodal CXCR4 antagonistic peptide. *Bioconjugate Chem.* **2011,** *22* (5), 859-64.

100. Rosenthal, E. L.; Zinn, K. R., Putting Numbers to Fluorescent Guided Surgery. *Molecular imaging and biology : MIB : the official publication of the Academy of Molecular Imaging* **2013**, 1-2.
101. Dar, A.; Goichberg, P.; Shinder, V.; Kalinkovich, A.; Kollet, O.; Netzer, N.; Margalit, R.; Zsak, M.; Nagler, A.; Hardan, I.; Resnick, I.; Rot, A.; Lapidot, T., Chemokine receptor CXCR4-dependent internalization and resecretion of functional chemokine SDF-1 by bone marrow endothelial and stromal cells. *Nat. Immun.* **2005,** *6* (10), 1038-1046.
102. Khan, A.; Silversides, J. D.; Madden, L.; Greenman, J.; Archibald, S. J., Fluorescent CXCR4 chemokine receptor antagonists: Metal activated binding. *Chem. Commun.* **2007,** (4), 416-418.
103. Fabbrizzi, L.; Licchelli, M.; Mascheroni, S.; Poggi, A.; Sacchi, D.; Zema, M., Water soluble molecular switches of fluorescence based on the NiIII/NiII redox change. *Inorg. Chem.* **2002,** *41* (23), 6129-6136.
104. Knight, J. C.; Hallett, A. J.; Brancale, A.; Paisey, S. J.; Clarkson, R. W. E.; Edwards, P. G., Evaluation of a fluorescent derivative of AMD3100 and its interaction with the CXCR4 chemokine receptor. *ChemBioChem* **2011,** *12* (17), 2692-2698.
105. Oltmanns, D.; Zitzmann-Kolbe, S.; Mueller, A.; Bauder-Wuest, U.; Schaefer, M.; Eder, M.; Haberkorn, U.; Eisenhut, M., Zn(II)-bis(cyclen) Complexes and the imaging of apoptosis/necrosis. *Bioconjugate Chem.* **2011,** *22* (12), 2611-2624.
106. Oishi, S.; Masuda, R.; Evans, B.; Ueda, S.; Goto, Y.; Ohno, H.; Hirasawa, A.; Tsujimoto, G.; Wang, Z.; Peiper, S. C.; Naito, T.; Kodama, E.; Matsuoka, M.; Fujii, N., Synthesis and application of fluorescein- and biotin-labeled molecular probes for the chemokine receptor CXCR4. *ChemBioChem* **2008,** *9* (7), 1154-1158.
107. Nishizawa, K.; Nishiyama, H.; Oishi, S.; Tanahara, N.; Kotani, H.; Mikami, Y.; Toda, Y.; Evans, B. J.; Peiper, S. C.; Saito, R.; Watanabe, J.; Fujii, N.; Ogawa, O., Fluorescent imaging of high-grade bladder cancer using a specific antagonist for chemokine receptor CXCR4. *Int. J. Cancer* **2010,** *127* (5), 1180-1187.
108. Wernick, M. N.; Lalush, D. S., *Emission Tomography: The Fundamentals of PET and SPECT*. Elsevier Academic Press: London, 2004.
109. Paans, A. M. J.; Van Waarde, A.; Elsinga, P. H.; Willemsen, A. T. M.; Vaalburg, W., Positron emission tomography: The conceptual idea using a multidisciplinary approach. *Methods* **2002,** *27* (3), 195-207.
110. Vallabhajosula, S., *Molecular Imaging: Radiopharmaceuticals for PET and SPECT*. Springer Science & Business Media: Germany, 2009; p 392.
111. Knight, J. C.; Wuest, F. R., Nuclear (PET/SPECT) and optical imaging probes targeting the CXCR4 chemokine receptor. *MedChemComm* **2012,** *3* (9), 1039-1053.
112. Nimmagadda, S.; Pullambhatla, M.; Stone, K.; Green, G.; Bhujwalla, Z. M.; Pomper, M. G., Molecular imaging of CXCR4 receptor expression in human cancer xenografts with [64Cu]AMD3100 positron emission tomography. *Cancer Res.* **2010,** *70* (10), 3935-44.
113. Nimmagadda, S.; Pullambhatla, M.; Pomper, M. G., Immunoimaging of CXCR4 expression in brain tumor xenografts using SPECT/CT. *J. Nucl. Med.* **2009,** *50* (7), 1124-1130.
114. Macey, M. G., *Flow Cytometry Principles and Applications*. Humana Press: Totowa, 2007.
115. OptoIQ Semiconductor lasers shed new light on flow cytometry. http://www.optoiq.com/index/photonics-technologies-applications/lfw-display/lfw-article-display/209783/articles/laser-focus-world/volume-40/issue-8/features/optoelectronic-applications-drug-discovery/semiconductor-lasers-shed-new-light-on-flow-cytometry (accessed 15 August 2014).
116. Darzynkiewicz, Z.; Holden, E.; Pozarowski, P.; Kaur, D.; Rew, D.; Woltmann, G., *Cell Imaging Techniques Method and Protocols*. Humana Press: Totowa, 2006; Vol. 319.

117. Waller, A.; Pipkorn, D.; Sutton, K. L.; Linderman, J. J.; Omann, G. M., Validation of flow cytometric competitive binding protocols and characterization of fluorescently labeled ligands. *Cytometry* **2001,** *45* (2), 102-14.
118. Findlay, J. W. A.; Khan, M. N., Ligand-Binding Assays in Drug Development: Introduction and Historical Perspective. In *Ligand-Binding Assays*, John Wiley & Sons, Inc.: 2009; pp 1-13.
119. (a) Berson, S. A.; Yalow, R. S., Correction of sample absorption of radioactivity. *Science* **1960,** *131* (3400), 606; (b) Berson, S. A.; Yalow, R. S., K42-tagged red blood cells in blood volume determinations. *Meth. Med. Res.* **1960,** *8*, 76-80; (c) Yalow, R. S.; Berson, S. A., Plasma insulin concentrations in nondiabetic and early diabetic subjects. Determinations by a new sensitive immuno-assay technic. *Diabetes* **1960,** *9*, 254-260; (d) Yalow, R. S.; Berson, S. A., Plasma insulin in man. *Am. J. Med.* **1960,** *29* (1), 1-8; (e) Yalow, R. S.; Berson, S. A., Immunoassay of endogenous plasma insulin in man. *J. Clin. Invest.* **1960,** *39*, 1157-1175; (f) Yalow, R. S.; Black, H.; Villazon, M.; Berson, S. A., Comparison of plasma insulin levels following administration of tolbutamide and glucose. *Diabetes* **1960,** *9*, 356-362.
120. Khan, M. N.; Dass, P. D.; Leete, J. H.; Schuman, R. F.; Gunsior, M.; Sadhu, C., Development of Ligand-Binding Assays for Drug Development Support. In *Ligand-Binding Assays*, John Wiley & Sons, Inc.: 2009; pp 39-79.
121. Van Meerloo, J.; Kaspers, G. J.; Cloos, J., Cell sensitivity assays: the MTT assay. *Methods. Mol. Biol.* **2011,** *731*, 237-45.
122. Pannecouque, C.; Daelemans, D.; De Clercq, E., Tetrazolium-based colorimetric assay for the detection of HIV replication inhibitors: revisited 20 years later. *Nature Protocols* **2008,** *3* (3), 427-434.
123. Domanska, U. M.; Kruizinga, R. C.; Nagengast, W. B.; Timmer-Bosscha, H.; Huls, G.; De Vries, E. G. E.; Walenkamp, A. M. E., A review on CXCR4/CXCL12 axis in oncology: No place to hide. *Eur. J. Cancer* **2013,** *49* (1), 219-230.
124. Princen, K.; Hatse, S.; Vermeire, K.; De Clercq, E.; Schols, D., Evaluation of SDF-1/CXCR4-induced Ca2+ signaling by fluorometric imaging plate reader (FLIPR) and flow cytometry. *Cytometry. Part A : the journal of the International Society for Analytical Cytology* **2003,** *51* (1), 35-45.
125. De Mol, N. J.; Fishcher, M. J. E., *Surface Plasmon Resonance Methods and Protocols*. Humana Press: New York, 2010; p 286.
126. Wood, R. W., On a remarkable case of uneven distribution of light ina diffraction grating spectrum. *Philos. Mag.* **1902,** *4*, 396-402.
127. (a) Kretschmann, E.; Raether, H., Radiative decay of non-radiative surface plasmons excited by light. *Z. Naturforsch.* **1968,** *23A*, 2135-2136; (b) Otto, A., Excitation of surface plasma waves in silver by the method of frustrated total reflection. *Z. Phys.* **1968,** *216*, 398-410.
128. (a) Liedberg, B.; Nylander, C.; Lundström, I., Biosensing with surface plasmon resonance — how it all started. *Biosensors & bioelectronics* **1995,** *10* (8), i-ix; (b) Liedberg, B.; Nylander, C.; Lunström, I., Surface plasmon resonance for gas detection and biosensing. *Sensor. Actuator.* **1983,** *4* (0), 299-304.
129. Rich, R. L.; Myszka, D. G., Advances in surface plasmon resonance biosensor analysis. *Curr. Opin. Biotech.* **2000,** *11*, 54-61.
130. Healthcare, G., *Biacore Sensor Surface Handbook*. Sweden, 2005.
131. Dale, D. AMD3100 for Treatment of Myelokathexis. https://clinicaltrials.gov/ct2/show/NCT01058993?term=CXCR4&rank=5 (accessed 26th August 2014).
132. Wen, P. Y. Plerixafor (AMD3100) and Bevacizumab for recurrent high-grade glioma. https://clinicaltrials.gov/ct2/show/NCT01339039?term=Plerixafor&rank=1 (accessed 26th August 2014).
133. Ghobrial, I. Combination Plerixafor (AMD3100)and Bortezomib in relapsed or relapsed/refractory multiple myeloma.

https://clinicaltrials.gov/ct2/show/NCT00903968?term=Plerixafor&rank=4 (accessed 26th August 2014).
134. Mestastatix, I. MSX-122 administered orally in patients with refractory metastatic or locally advanced solid tumors. https://clinicaltrials.gov/ct2/show/NCT00591682?term=CXCR4&rank=22 (accessed 26th August 2014).
135. Diseases, N. I. o. A. a. I. Safety of AMD070 when administered alone or boosted with low-dose ritonavir in HIV uninfected men. https://clinicaltrials.gov/ct2/show/NCT00063804?term=CXCR4&rank=32 (accessed 26th August 2014).
136. Moyle, G.; Dejesus, E.; Boffito, M. A.; Wong, R. S.; Gibney, C.; Badel, K.; MacFarland, R.; Calandra, G.; Bridger, G.; Becker, S., Proof of activity with AMD11070, an orally bioavailable inhibitor of CXCR4-tropic HIV type 1. *Clin. Infect. Dis.* **2009,** *48* (6), 798-805.
137. Wong, D.; Korz, W., Translating an antagonist of chemokine receptor CXCR4: From bench to bedside. *Clin. Cancer Res.* **2008,** *14* (24), 7975-7980.
138. Polyphor, L. Safety and efficacy of POL6326 for mobilization/transplant of sibling donor in patients with hematologic malignancies. https://clinicaltrials.gov/ct2/show/NCT01413568?term=POL6326&rank=2 (accessed 26th August 2014).
139. Polyphor, L. Dose escalation of POL6326 in combination with Eribulin in patients with metastatic breast Cancer. https://clinicaltrials.gov/ct2/show/NCT01837095?term=POL6326&rank=1 (accessed 26th August 2014).
140. Mewis, R. E.; Archibald, S. J., Biomedical applications of macrocyclic ligand complexes. *Coord. Chem. Rev.* **2010,** *254* (15-16), 1686-1712.
141. Bazzicalupi, C.; Bencini, A.; Berni, E.; Bianchi, A.; Ciattini, S.; Giorgi, C.; Maoggi, S.; Paoletti, P.; Valtancoli, B., Synthesis of new tren-based tris-macrocycles. Anion cluster assembling inside the cavity generated by a bowl-shaped receptor. *J. Org. Chem.* **2002,** *67* (25), 9107-9110.
142. Kimura, E.; Kikuchi, M.; Kitamura, H.; Koike, T., Selective and efficient recognition of thymidylylthymidine (TpT) by bis(ZnII-cyclen) and thymidylylthymidylylthymidine (TpTpT) by tris(ZnII-cyclen) at neutral pH in aqueous solution. *Chem.-Eur. J.* **1999,** *5* (11), 3113-3123.
143. Ramasubbu, A.; Wainwright, K. P., Structurally reinforced cyclen: A rigidly trans-co-ordinating twelve-membered macrocycle. *J. Chem. Soc. Chem. Comm.* **1982,** (5), 277-278.
144. Bencini, A.; Bazzicalupi, C.; Ciampolini, M.; Fusi, V.; Micheloni, M.; Nardi, N.; Paoli, P.; Valtancoli, B., Proton inclusion properties of a new azamacrocycle. Synthesis, characterization and crystal structure of [H3L][Cl]3.2H2O (L = 4,10-dimethyl-1,4,7,10-tetraazabicyclo[5.5.2]tetradecane). *Supramol. Chem.* **1994,** *3*, 141-146.
145. Luengo, J.; Price, A. T.; Shaw, A.; Wiggall, K. CXCR-4 receptor antagonists - thrombopoietin mimetics. WO/2000/066112, 2000.
146. Dong, Y.; Lindoy, L. F., A three-ring, linked cyclam derivative and its interaction with selected transition and post-transition metal ions. *Coord. Chem. Rev.* **2003,** *245* (1–2), 11-16.
147. Sun, S.; Thomasson, K., Molecular recognition of a tris(histidine) ligand. *Chem. Commun.* **1998,** (4), 519-520.
148. Dong, Y.; Lindoy, L. F., New macrocyclic ligands. XIII single-ring and tri-linked macrocyclic systems derived from selectively protected cyclam. *Aust. J. Chem.* **2001,** *54* (5), 291-297.
149. Chartres, J. D.; Lindoy, L. F.; Meehan, G. V., Transition and post-transition metal systems incorporating linked synthetic macrocycles as structural elements. *Coord. Chem. Rev.* **2001,** *216-217* (0), 249-286.
150. Dong, Y.; Lindoy, L. F.; Turner, P.; Wei, G., Three-ring, branched cyclam derivatives and their interaction with nickel(ii), copper(ii), zinc(ii) and cadmium(ii). *Dalton Trans.* **2004,** (8), 1264-1270.

151. Comba, P.; Lampeka, Y. D.; Nazarenko, A. Y.; Prikhod'ko, A. I.; Pritzkow, H., Interactions between copper(II) complexes of mono-, bis-, and tris(macrocyclic) ligands and inorganic or organic guests. *Eur. J. Inorg. Chem.* **2002,** (6), 1464-1474.
152. Ramli, M.; Smith, S. V.; Lindoy, L. F., Investigation of novel bis- and tris-tetraazamacrocycles for use in the copper-64 (64Cu) radiolabeling of antibodies with potential to increase the therapeutic index for drug targeting. *Bioconjugate Chem.* **2009,** *20* (5), 868-876.
153. M. Ramli, M. D., L.F. Lindoy, S.V. Smith, J.G. Wilson, *J. Heterocycl. Chem.* **2008,** *42*, 77.
154. Silversides, J. D.; Smith, R.; Archibald, S. J., Challenges in chelating positron emitting copper isotopes: Tailored synthesis of unsymmetric chelators to form ultra stable complexes. *Dalton Trans.* **2011,** *40* (23), 6289-6297.
155. K, B. E.; F, W.; W, H. A.; R, D. A., *Inorg Synth* **1976,** *16*, 220-225.
156. Le Baccon, M.; Chuburu, F.; Toupet, L.; Handel, H.; Soibinet, M.; De'champs-Olivier, I.; Barbier, J.-P.; Aplincourt, M., Bis-aminals: efficient tools for bis-macrocycle synthesis. *New J. Chem.* **2001,** *25* (9), 1168-1174.
157. Alder, R. W.; Heilbronner, E.; Honegger, E.; McEwen, A. B.; Moss, R. E.; Olefirowicz, E.; Petillo, P. A.; Sessions, R. B.; Weisman, G. R.; White, J. M.; Yang, Z. Z., The out,out to out,in transition for 1,(n+2)-diazabicyclo[n.3.1]alkanes. *J. Am. Chem. Soc.* **1993,** *115* (15), 6580-6591.
158. Royal, G.; Dahaoui-Gindreyb, V.; Dahaouib, S.; Tabarda, A.; Guilard, R.; Pullumbic, P.; Lecomte, C., New Synthesis of trans-Disubstituted Cyclam Macrocycles – Elucidation of the Disubstitution Mechanism on the Basis of X-ray Data and Molecular Modeling. *Eur. J.Org. Chem.* **1998**, 1971-1975.
159. Gluzinski, P.; Krajewski, J. W.; Urbanczyk-Lipkowska, Z., Structures of isomeric 10b,10c-*cis*-and 10b,10c-*trans*-3a,5a,8a,10a-tetraazaperhydropyrene. *Acta Crystallogr.* **1982,** *B38*, 3038-3041.
160. (a) Kolinski, R. A., Synthesis of Piperazinocyclams by Reductive Ring Cleavage of mono-Quaternary Salts of cis-Perhydro-3a,5a,8a,10a-tetraazapyrene. *Pol. J. Chem.* **1995,** *69*, 1039-1045; (b) Valks G C, M. G., Lewis E A, Hubin T J, Hunter T M, Sadler P J, Pannecouque C, De Clercq E, Archibald S J, Configurationally restricted bismacrocyclic CXCR4 receptor antagonists. *J Med Chem* **2006,** *49*, 6162-6165; (c) Silversides, J. D.; Allan, C. C.; Archibald, S. J., Copper(II) cyclam-based complexes for radiopharmaceutical applications: Synthesis and structural analysis. *Dalton Trans.* **2007,** (9), 971-978.
161. Del Mundo, I. M. A.; Siters, K. E.; Fountain, M. A.; Morrow, J. R., Structural Basis for Bifunctional Zinc(II) Macrocyclic Complex Recognition of Thymine Bulges in DNA. *Inorg. Chem.* **2012,** *51* (9), 5444-5457.
162. Archibald, S. J.; Lewis, E. A.; Hubin, T. J. Novel antiviral macrocycle derivatives and metal complexes incorporating bridged macrocycles. WO2005/121109 A2, 2005.
163. Gridley, B., The University of Hull: 2009.
164. Bernier, N.; Esteves, C. V.; Delgado, R., Heteroditopic receptor based on crown ether and cyclen units for the recognition of zwitterionic amino acids. *Tetrahedron* **2012,** *68* (24), 4860-4868.
165. (a) Tasker, P. A.; Sklar, L., Crystal and molecular structure of di(perchlorato)(1,4,8,11-tetraazacyclotetradecane)copper (II). Cu(cyclam) (ClO4)2. *J. Cryst. Mol. Struct.* **1975,** *5* (5), 329-344; (b) Endicott, J. F.; Lilie, J.; Kuszaj, J. M.; Ramaswamy, B. S.; Schmonsees, W. G.; Simic, M. G.; Glick, M. D.; Rillema, D. P., The trans-influence and axial interactions in low spin, tetragonal cobalt(II) complexes containing macrocyclic and/or cyano ligands. Pulse radiolytic studies in fluid solution, electron paramagnetic resonance spectra at 77 K, and single-crystal x-ray structures. *J. Am. Chem. Soc.* **1977,** *99* (2), 429-439.
166. Alcock, N. W.; Curson, E. H.; Herron, N.; Moore, P., Structural and dynamic behaviour of cadmium(II) and mercury(II) complexes of 1,4,8,11-tetra-azacyclotetradecane and 1,4,8,11-tetramethyl-1,4,8,11-tetra-azacyclotetradecane. *J. Chem. Soc. Dalton* **1979,** (12), 1987-1993.
167. Bosnich, B.; Poon, C. K.; Tobe, M. L., Complexes of cobalt(III) with a cyclic tetradentate secondary amine. *Inorg. Chem.* **1965,** *4* (8), 1102-1108.

168. Gerlach L O, J. J. S., Jensen, K P, Rosenkilde M R, Skerlj R T, Ryde U, Bridger G J and Schwartz T W, Metal Ion Enhanced Binding of AMD3100 to Asp262 in the CXCR4 Receptor. *Biochemistry* **2003,** *42*, 710-717.
169. Glusker, J. P., Structural aspects of metal liganding to functional groups in proteins. *Adv. Protein Chem.* **1991,** *42*, 1-76.
170. Khan, A.; Nicholson, G.; Greenman, J.; Madden, L.; McRobbie, G.; Pannecouque, C.; De Clercq, E.; Ullom, R.; Maples, D. L.; Maples, R. D.; Silversides, J. D.; Hubin, T. J.; Archibald, S. J., Binding Optimization through Coordination Chemistry: CXCR4 Chemokine Receptor Antagonists from Ultrarigid Metal Complexes. *J. Am. Chem. Soc.* **2009,** *131*, 3416–3417.
171. Ferdani, R.; Stigers, D. J.; Fiamengo, A. L.; Wei, L.; Li, B. T. Y.; Golen, J. A.; Rheingold, A. L.; Weisman, G. R.; Wong, E. H.; Anderson, C. J., Synthesis, Cu(ii) complexation, 64Cu-labeling and biological evaluation of cross-bridged cyclam chelators with phosphonate pendant arms. *Dalton Trans.* **2012,** *41* (7), 1938-1950.
172. Elias, H., Kinetics and mechanism of metal complex formation with N4-donor macrocycles of the cyclam type. *Coord. Chem. Rev.* **1999,** *187* (1), 37-73.
173. Schönherr, T.; Weber, E.; Seichter, W., Copper complexes of dicarboxy-functionalized tetramethylcyclam. Crystal structures of complexes with the axial ligands perchlorate, chloride, and iodide. *Z. Anorg. Allg. Chem.* **2001,** *627* (10), 2420-2424.
174. Huang, E. H.; Singh, B.; Cristofanilli, M.; Gelovani, J.; Wei, C.; Vincent, L.; Cook, K. R.; Lucci, A., A CXCR4 Antagonist CTCE-9908 Inhibits Primary Tumor Growth and Metastasis of Breast Cancer. *J. Surg. Res.* **2009,** *155* (2), 231-236.
175. (a) Boswell, C. A.; Sun, X.; Niu, W.; Weisman, G. R.; Wong, E. H.; Rheingold, A. L.; Anderson, C. J., Comparative in vivo stability of copper-64-labeled cross-bridged and conventional tetraazamacrocyclic complexes. *J. Med. Chem.* **2004,** *47* (6), 1465-74; (b) Jones-Wilson, T. M.; Deal, K. A.; Anderson, C. J.; McCarthy, D. W.; Kovacs, Z.; Motekaitis, R. J.; Sherry, A. D.; Martell, A. E.; Welch, M. J., The in vivo behavior of copper-64-labeled azamacrocyclic complexes. *Nucl. Med. Biol.* **1998,** *25* (6), 523-530.
176. Joao, H. C.; De Vreese, K.; Pauwels, R.; De Clercq, E.; Henson, G. W.; Bridger, G. J., Quantitative structural activity relationship study of bis-tetraazacyclic compounds. A novel series of HIV-1 and HIV-2 inhibitors. *J. Med. Chem.* **1995,** *38* (19), 3865-3873.
177. McAuley, A.; Subramanian, S.; Whitcombe, T. W., Synthesis and X-ray crystal structure of a C-spiro-bi-[cyclam nickel(II)] complex (cyclam = 1,4,8,11-tetra-azacyclotetradecane). *J. Chem. Soc. Chem. Comm.* **1987,** (8), 539-541.
178. (a) Bridger, G.; Skerlj, R. T.; Henson, G. W.; Abrams, M. J.; C., J. H.; Witvrouw, M.; De Vreese, K.; Pauwels, R.; De Clercq, E., Synthesis and Structure-Activity Relationships of Phenylenebis(methylene)-Linked Bis-tetraazamacrocycles That Inhibit Human Immunodeficiency Virus Replication. 2. Effect of Heteroaromatic Linkers on the Activity of Bicyclams. *J. Med. Chem.* **1996,** *39*, 109-119; (b) Hediger, M.; Kaden, T. A., Metal complexes with macrocyclic ligands, XVII. Synthesis of two key intermediates for the preparation of mono-N-functionalized tetraazamacrocycles and their metal complexes. *Helv. Chim. Acta* **1983,** *66* (3), 861-870; (c) Gunnlaugsson, T.; Leonard, J. P.; Mulready, S.; Nieuwenhuyzen, M., Three step vs one pot synthesis and X-ray crystallographic investigation of heptadentate triamide cyclen (1,4,7,10-tetraazacyclododecane) based ligands and some of their lanthanide ion complexes. *Tetrahedron* **2004,** *60* (1), 105-113; (d) Pope, S. J. A.; Kenwright, A. M.; Boote, V. A.; Faulkner, S., Synthesis and luminescence properties of dinuclear lanthanide complexes derived from covalently linked macrocyclic ligands. *J. Chem. Soc. Dalton* **2003,** (19), 3780-3784; (e) Bridger, G. J.; Skerlj, R. T.; Padmanabhan, S.; Martellucci, S. A.; Henson, G. W.; Struyf, S.; Witvrouw, M.; Schols, D.; De Clercq, E., Synthesis and Structure-Activity Relationships of Phenylenebis(methylene)-Linked Bis-azamacrocycles That Inhibit HIV-1 and HIV-2 Replication by Antagonism of the Chemokine Receptor CXCR4. *J. Med. Chem.* **1999,** *42*, 3971-3981.

179. (a) Schneider, R.; Riesen, A.; Kaden, T. A., Metal complexes with macrocyclic ligands. Part XXII. Synthesis two of bis-tetraaza-macrocycles and study of the structures, electrochemistry, VIS and EPR spectra of their binuclear Cu2+ and Ni2+ complexes. *Helv. Chim. Acta* **1986,** *69* (1), 53-61; (b) Ciampolini, M.; Fabbrizzi, L.; Perotti, A.; Poggi, A.; Seghi, B.; Zanobini, F., Dinickel and dicopper complexes with N,N-linked bis(cyclam) ligands. An ideal system for the investigation of electrostatic effects on the redox behavior of pairs of metal ions. *Inorg. Chem.* **1987,** *26* (21), 3527-3533.
180. (a) Izatt, R. M.; Pawlak, K.; Bradshaw, J. S.; Bruening, R. L., Thermodynamic and kinetic data for macrocycle interaction with cations and anions. *Chem. Rev.* **1991,** *91* (8), 1721-2085; (b) Smith, R. M.; Martell, A. E.; Motekaitis, R. J.; Technology, N. I. o. S., NIST critical stability constants of metal complexes database. U.S. Dept. of Commerce, Technology Administration, National Institute of Standards and Technology, Standard Reference Data Program: Gaithersburg, MD, 1993.
181. Costa, J.; Balogh, E.; Turcry, V.; Tripier, R.; Le Baccon, M.; Chuburu, F.; Handel, H.; Helm, L.; Tóth, É.; Merbach, A. E., Unexpected aggregation of neutral, xylene-cored dinuclear GdIII chelates in aqueous solution. *Chem.-Eur. J.* **2006,** *12* (26), 6841-6851.
182. Barefield, E. K.; Wagner, F.; Herlinger, A. W.; Dahl, A. R., *(1,4,8,11-Tetraazacyclotetradecane)Nickel(II) Perchlorate and 1,4,8,11-Tetraazacyclotetradecane*. Wiley: USA, 1976; Vol. 16, p 220-225.
183. Bernier, N.; Allali, M.; Tripier, R.; Conan, F.; Patinec, V.; Develay, S.; Le Baccon, M.; Handel, H., New side-bridged bismacrocycles and cross-bridged macrotricycles. Syntheses and Cu(ii) complexation study. *New J. Chem.* **2006,** *30* (3), 435.
184. (a) Bernier, N.; Tripier, R.; Patinec, V.; Le Baccon, M.; Handel, H., Proton-sponge behaviour of new pendant armed cross-bridged bis-cyclens: Synthesis, NMR, X-ray, and potentiometric investigations. *C. R. Chimie* **2007,** *10* (9), 832-838; (b) Sun, X.; Wuest, M.; Weisman, G. R.; Wong, E. H.; Reed, D. P.; Boswell, C. A.; Motekaitis, R.; Martell, A. E.; Welch, M. J.; Anderson, C. J., Radiolabeling and In Vivo Behavior of Copper-64-Labeled Cross-Bridged Cyclam Ligands. *J. Med. Chem.* **2002,** *45*, 469-477.
185. (a) Hancock, R. D., *Toward More Preorganized Macrocycles*. VCH: New York, 1992; (b) Kowallick, R.; Neuburger, M.; Zehnder, M.; Kaden, T. A., Metal Complexes with Macrocyclic Ligands: Part XLV - Axial Coordination Tendency in Reinforced Tetraazamacrocyclic Complexes. *Helv. Chim. Acta* **1997,** *80* (3), 948-959.
186. Weisman, G. R.; Wong, E. H.; Hill, D. C.; Rogers, M. E.; Reed, D. P.; Calabrese, J. C., Synthesis and transition-metal complexes of new cross-bridged tetraamine ligands. *Chem. Commun.* **1996,** (8), 947.
187. (a) Kimura, E.; Kotake, Y.; Koike, T.; Shionoya, M.; Shiro, M., A novel cyclam appended with 3-hydroxypyridine. An ambident donor ligand comprising a pyridyl N and a pyridinolate O-donor. *Inorg. Chem.* **1990,** *29* (24), 4991-4996; (b) McLaren, F.; Moore, P.; Wynn, A. M., Rates and mechanism of co-ordination of labile transition metal ions with tri- and tetra-azamacrocycles functionalised with a single pendent co-ordinating 2,2'-bipyridyl-6-yl-methyl arm: Evidence for two-stage reactions with initial co-ordination of the pendent bipyridyl group. *J. Chem. Soc. Chem. Comm.* **1989,** (12), 798-800; (c) Takenouchi, K.; Tabe, M.; Watanabe, K.; Hazato, A.; Kato, Y.; Shionoya, M.; Koike, T.; Kimura, E., Novel pendant-type macrocyclic bifunctional chelating agents: (Carboxymethyl)amino derivatives of 2-(4-nitrobenzyl)-1,4,7,10-tetraazacyclododecane-N,N',N",N'"- tetraacetic acid and their complex formation with yttrium(III). *J. Org. Chem.* **1993,** *58* (24), 6895-6899.
188. Hubin, T. J.; McCormick, J. M.; Collinson, S. R.; Alcock, N. W.; Busch, D. H., Ultra rigid cross-bridged tetraazamacrocycles as ligands—the challenge and the solution. *Chem. Commun.* **1998**, 1675-1676.

189. Costamagna, J.; Ferraudi, G.; Matsuhiro, B.; Campos-Vallette, M.; Canales, J.; Villagrán, M.; Vargas, J.; Aguirre, M. J., Complexes of macrocycles with pendant arms as models for biological molecules. *Coord. Chem. Rev.* **2000,** *196* (1), 125-164.
190. (a) Lewis, E. A.; Boyle, R. W.; Archibald, S. J., Ultrastable complexes for in vivo use: a bifunctional chelator incorporating a cross-bridged macrocycle. *Chem. Commun.* **2004,** (19), 2212-3; (b) Lewis, E. A.; Allan, C. C.; Boyle, R. W.; Archibald, S. J., Efficient N- and C-functionalisation of cyclam macrocycles utilising bisaminal methodology. *Tetrahedron Lett.* **2004,** *45* (15), 3059-3062.
191. Plutnar, J.; Havlíčková, J.; Kotek, J.; Hermann, P.; Lukeš, I., Unsymmetrically substituted side-bridged cyclam derivatives and their Cu(ii) and Zn(ii) complexes. *New J. Chem.* **2008,** *32* (3), 496.
192. Rohovec, J.; Gyepes, R.; Císařová, I.; Rudovský, J.; Lukeš, I., Nucleophilic reactivity of perhydro-3,6,9,12-tetraazacyclopenteno[1,3- f,g]acenaphthylene. A unified approach to N-monosubstituted and N,N''- disubstituted cyclene derivatives. *Tetrahedron Lett.* **2000,** *41* (8), 1249-1253.
193. Sereda, G.; Pothula, S.; Dreessen, J., Sodium Borohydride–Mediated Transesterification. *Synthetic Commun.* **2010,** *40* (9), 1312-1321.
194. Zhu, H.-J.; Pittman Jr, C. U., Reductions of Carboxylic Acids and Esters with NaBH4 in Diglyme at 1628C. *Synthetic Commun.* **2003,** *33* (10), 1733-1750.
195. Smith, R. Towards the synthesis of Multifunctional Constructs: Coupling PET and PDT for the Targeted Diagnosis and Therapy of CXCR4 Expressing Tumours. The University of Hull, Hull, 2012.
196. Kaye, I. A.; Burlant, W. J.; Price, L., Thiocyanation of p-Dialkylaminoalkoxyanilines. *J. Org. Chem.* **1951,** *16* (9), 1421-1426.
197. Sun, R.; Wang, Z.; Li, Y.; Xiong, L.; Liu, Y.; Wang, Q., Design, Synthesis, and Insecticidal Evaluation of New Benzoylureas Containing Amide and Sulfonate Groups Based on the Sulfonylurea Receptor Protein Binding Site for Diflubenzuron and Glibenclamide. *J. Agr. Food Chem.* **2013,** *61* (3), 517-522.
198. Liu, Q.; Tor, Y., Simple conversion of aromatic amines into azides. *Org. Lett.* **2003,** *5* (14), 2571-2572.
199. Griffin, R. J.; Evers, E.; Davison, R.; Gibson, A. E.; Layton, D.; Irwin, W. J., The 4-azidobenzyloxycarbonyl function; application as a novel protecting group and potential prodrug modification for amines. *J. Chem. Soc. Perk. T. 1* **1996,** (11), 1205-1211.
200. Belkheira, M.; El Abed, D.; Pons, J. M.; Bressy, C., Organocatalytic synthesis of 1,2,3-triazoles from unactivated ketones and arylazides. *Chem.-Eur. J.* **2011,** *17* (46), 12917-12921.
201. Wijtmans, M.; Verzijl, D.; Van Dam, C. M. E.; Bosch, L.; Smit, M. J.; Leurs, R.; De Esch, I. J. P., Exploring a pocket for polycycloaliphatic groups in the CXCR3 receptor with the aid of a modular synthetic strategy. *Bioorg. Med. Chem. Lett.* **2009,** *19* (8), 2252-2257.
202. Gubbens, J.; Ruijter, E.; De Fays, L. E. V.; Damen, J. M. A.; De Kruijff, B.; Slijper, M.; Rijkers, D. T. S.; Liskamp, R. M. J.; de Kroon, A. I. P. M., Photocrosslinking and Click Chemistry Enable the Specific Detection of Proteins Interacting with Phospholipids at the Membrane Interface. *Chem. Biol.* **2009,** *16* (1), 3-14.
203. Barral, K.; Moorhouse, A. D.; Moses, J. E., Efficient Conversion of Aromatic Amines into Azides: A One-Pot Synthesis of Triazole Linkages. *Org. Lett.* **2007,** *9* (9), 1809-1811.
204. Kolb, H. C.; Finn, M. G.; Sharpless, K. B., Click Chemistry: Diverse Chemical Function from a Few Good Reactions. *Angew. Chem. Int. Ed.* **2001,** *40* (11), 2004-2021.
205. Kappe, C. O.; Van Der Eycken, E., Click chemistry under non-classical reaction conditions. *Chem. Soc. Rev.* **2010,** *39* (4), 1280-1290.
206. Huisgen, R., 1,3-Dipolar Cycloadditions. Past and Future. *Angew. Chem. Int. Ed.* **1963,** *2* (10), 565-598.

207. (a) Calvo-Flores, F. G.; Isac-García, J.; Hernández-Mateo, F.; Pérez-Balderas, F.; Calvo-Asín, J. A.; Sanchéz-Vaquero, E.; Santoyo-González, F., 1,3-dipolar cycloadditions as a tool for the preparation of multivalent structures. *Org. Lett.* **2000,** *2* (16), 2499-2502; (b) Pérez-Balderas, F.; Ortega-Muñoz, M.; Morales-Sanfrutos, J.; Hernández-Mateo, F.; Calvo-Flores, F. G.; Calvo-Asín, J. A.; Isac-García, J.; Santoyo-González, F., Multivalent neoglycoconjugates by regiospecific cycloaddition of alkynes and azides using organic-soluble copper catalysts. *Org. Lett.* **2003,** *5* (11), 1951-1954; (c) Lewis, W. G.; Green, L. G.; Grynszpan, F.; Radić, Z.; Carlier, P. R.; Taylor, P.; Finn, M. G.; Sharpless, K. B., Click chemistry in situ: Acetylcholinesterase as a reaction vessel for the selective assembly of a femtomolar inhibitor from an array of building blocks. *Angew. Chem. Int. Ed.* **2002,** *41* (6), 1053-1057; (d) Brik, A.; Muldoon, J.; Lin, Y. C.; Elder, J. H.; Goodsell, D. S.; Olson, A. J.; Fokin, V. V.; Sharpless, K. B.; Wong, C. H., Rapid Diversity-Oriented Synthesis in Microtiter Plates for in Situ Screening of HIV Protease Inhibitors. *ChemBioChem* **2003,** *4* (11), 1246-1248; (e) Whiting, M.; Fokin, V. V., Copper-catalyzed reaction cascade: Direct conversion of alkynes into N-sulfonylazetidin-2-imines. *Angew. Chem. Int. Ed.* **2006,** *45* (19), 3157-3161; (f) Whiting, M.; Muldoon, J.; Lin, Y. C.; Silverman, S. M.; Lindstrom, W.; Olson, A. J.; Kolb, H. C.; Finn, M. G.; Sharpless, K. B.; Elder, J. H.; Fokin, V. V., Inhibitors of HIV-1 protease by using in situ click chemistry. *Angew. Chem. Int. Ed.* **2006,** *45* (9), 1435-1439.

208. Nwe, K.; Brechbiel, M. W., Growing applications of "click chemistry" for bioconjugation in contemporary biomedical research. *Cancer Biother. Radio.* **2009,** *24* (3), 289-302.

209. Himo, F.; Lovell, T.; Hilgraf, R.; Rostovtsev, V. V.; Noodleman, L.; Sharpless, K. B.; Fokin, V. V., Copper(I)-catalyzed synthesis of azoles. DFT study predicts unprecedented reactivity and intermediates. *J. Am. Chem. Soc.* **2005,** *127* (1), 210-216.

210. (a) Bock, V. D.; Hiemstra, H.; Van Maarseveen, J. H., Cu I-catalyzed alkyne-azide "click" cycloadditions from a mechanistic and synthetic perspective. *Eur. J. Org. Chem.* **2006,** (1), 51-68; (b) Hein, C. D.; Liu, X. M.; Wang, D., Click chemistry, a powerful tool for pharmaceutical sciences. *Pharm. Res.* **2008,** *25* (10), 2216-2230.

211. (a) Szíjjártó, C.; Pershagen, E.; Borbas, K. E., Functionalisation of lanthanide complexes via microwave-enhanced Cu(i)-catalysed azide-alkyne cycloaddition. *Dalton Trans.* **2012,** *41* (25), 7660-7669; (b) Aucagne, V.; Berná, J.; Crowley, J. D.; Goldup, S. M.; Hänni, K. D.; Leigh, D. A.; Lusby, P. J.; Ronaldson, V. E.; Slawin, A. M. Z.; Viterisi, A.; Walker, D. B., Catalytic "active-metal" template synthesis of [2]rotaxanes, [3]rotaxanes, and molecular shuttles, and some observations on the mechanism of the Cu(I)-catalyzed azide-alkyne 1,3-cycloaddition. *J. Am. Chem. Soc.* **2007,** *129* (39), 11950-11963.

212. Tamanini, E.; Katewa, A.; Sedger, L. M.; Todd, M. H.; Watkinson, M., A Synthetically Simple, Click-Generated Cyclam-Based Zinc(II) Sensor. *Inorg. Chem.* **2008,** *48* (1), 319-324.

213. (a) Sletten, E. M.; Bertozzi, C. R., Bioorthogonal chemistry: fishing for selectivity in a sea of functionality. *Angewandte Chemie* **2009,** *48* (38), 6974-98; (b) Prescher, J. A.; Dube, D. H.; Bertozzi, C. R., Chemical remodelling of cell surfaces in living animals. *Nature* **2004,** *430* (7002), 873-877; (c) Sletten, E. M.; Bertozzi, C. R., From Mechanism to Mouse: A Tale of Two Bioorthogonal Reactions. *Accounts Chem. Res.* **2011,** *44* (9), 666-676.

214. Sunil, D. A.; Nikunj, S. M. Toll-like receptor-7 and -8 modulatory 1H imidazoquinoline derived compounds. 2012.

215. Sano, K.; Masuda, R.; Hisada, H.; Oishi, S.; Shimokawa, K.; Ono, M.; Fujii, N.; Saji, H.; Mukai, T., A radiogallium–DOTA-based bivalent peptidic ligand targeting a chemokine receptor, CXCR4, for tumor imaging. *Bioorg. Med. Chem. Lett.* **2014,** *24* (5), 1386-1388.

216. Silversides, J. D.; Burke, B. P.; Archibald, S. J., Rapid synthesis of cross-bridged cyclam chelators for copper(II) complex formation. *C. R. Chimie* **2013,** *16* (6), 524-530.

217. Edlin, C. D.; Faulkner, S.; Parker, D.; Wilkinson, M. P., An efficient metal-templated route to C-functionalised derivatives of [12]aneN4. *Chem. Commun.* **1996,** (10), 1249-1250.

218. Boschetti, F.; Denat, F.; Espinosa, E.; Lagrange, J. M.; Guilard, R., A powerful route to C-functionalised tetraazamacrocycles. *Chem. Commun.* **2004,** *10* (5), 588-589.
219. (a) Cutler, C. S.; Wuest, M.; Anderson, C. J.; Reichert, D. E.; Sun, Y.; Martell, A. E.; Wekh, M. J., Labeling and in vivo evaluation of novel copper(II) dioxotetraazamacrocyclic complexes. *Nucl. Med. Biol.* **2000,** *27* (4), 375-380; (b) Slocik, J. M.; Ward, M. S.; Shepherd, R. E., Synthesis and characterization of meso-[Ru(NO)Cl(dioxocyclam)] and the 1H NMR comparison with [MII(dioxocyclam)] complexes (MII = NiII and PdII) (dioxocyclam = 1,4,8,11-tetraazacyclotetradecane-5,7-dione). *Inorg. Chim. Acta* **2001,** *317* (1-2), 290-303; (c) Goeta, A. E.; Howard, J. A. K.; Maffeo, D.; Puschmann, H.; Williams, G. J. A.; Yufit, D. S., Copper(n) complexes of the isomeric tetraazamacrocyclic ligands 1,11- And l,8-bis(2-pyridylmethyl)-l,4,8,ll-tetraazacyclotetradecane and of the 1,4,8,1 l-tetraazacyclotetradecane-5,12-dione analogue at neutral and basic pH. *J. Chem. Soc. Dalton* **2000,** (12), 1873-1880.
220. Heroux, K. J.; Woodin, K. S.; Tranchemontagne, D. J.; Widger, P. C.; Southwick, E.; Wong, E. H.; Weisman, G. R.; Tomellini, S. A.; Wadas, T. J.; Anderson, C. J.; Kassel, S.; Golen, J. A.; Rheingold, A. L., The long and short of it: the influence of N-carboxyethyl versusN-carboxymethyl pendant arms on in vitro and in vivo behavior of copper complexes of cross-bridged tetraamine macrocycles. *Dalton Trans.* **2007,** (21), 2150-62.
221. Bräse, S.; Gil, C.; Knepper, K.; Zimmermann, V., Organic azides: An exploding diversity of a unique class of compounds. *Angew. Chem. Int. Ed.* **2005,** *44* (33), 5188-5240.
222. Ju, Y.; Kumar, D.; Varma, R. S., Revisiting nucleophilic substitution reactions Microwave assisted synthesis of azides, thiocyanates, and sulfones in an aqueous medium. *J. Org. Chem.* **2006**.
223. Luehr, G. W.; Sundaram, A.; Jaishankar, P.; Bhakta, C.; Druzgala, P. Agonists of peroxisome proliferator activated receptor-a. 2010.
224. (a) Maury, J.; Feray, L.; Bertrand, M. P.; Kapat, A.; Renaud, P., Unexpected conversion of alkyl azides to alkyl iodides and of aryl azides to N-tert-butyl anilines. *Tetrahedron* **2012,** *68* (47), 9606-9611; (b) Lee, J. H.; Gupta, S.; Jeong, W.; Rhee, Y. H.; Park, J., Characterization and utility of N-unsubstituted imines synthesized from alkyl azides by ruthenium catalysis. *Angew. Chem. Int. Ed.* **2012,** *51* (43), 10851-10855.
225. Farran, D.; Slawin, A. M. Z.; Kirsch, P.; O'Hagan, D., Diastereoselective synthesis of 2,3,4,5,6-pentafluoroheptanes. *J. Org. Chem.* **2009,** *74* (18), 7168-7171.
226. Streitwieser, W., Stereochemistry of the Primary Carbon. V. Optically Active Benzyl-α-d Alcohol. *J. Am. Chem. Soc.* **1959,** *81*, 4912,4914.
227. Anda, C.; Bencini, A.; Berni, E.; Ciattini, S.; Chuburu, F.; Danesi, A.; Giorgi, C.; Handel, H.; Le Baccon, M.; Paoletti, P.; Tripier, R.; Turcry, V.; Valtancoli, B., Mono- and dinuclear CuII and ZnII complexes of cyclen-based Bis(macrocycles) containing two aminoalkyl pendant arms of different lengths. *Eur. J. Inorg. Chem.* **2005,** (11), 2044-2053.
228. Bryden, F. M. Synthesis of water-soluble prophyrin-dendron conjugated for targeted photodynamic therapy. University of Hull, Hull, 2013.
229. Battenberg, O. A.; Nodwell, M. B.; Sieber, S. A., Evaluation of α-Pyrones and Pyrimidones as Photoaffinity Probes for Affinity-Based Protein Profiling. *J. Org. Chem.* **2011,** *76* (15), 6075-6087.
230. (a) LaBeaume, P.; Placzek, M.; Daniels, M.; Kendrick, I.; Ng, P.; McNeel, M.; Afroze, R.; Alexander, A.; Thomas, R.; Kallmerten, A. E.; Jones, G. B., Microwave-accelerated fluorodenitrations and nitrodehalogenations: expeditious routes to labeled PET ligands and fluoropharmaceuticals. *Tetrahedron Lett.* **2010,** *51* (14), 1906-1909; (b) Burke, B. P.; Archibald, S. J., Macrocyclic coordination chemistry. *Annu. Rep. Prog. Chem. A* **2013,** *109*, 232-253.
231. (a) Smith, S. V., Molecular imaging with copper-64. *J. Inorg. Biochem.* **2004,** *98* (11), 1874-901; (b) Smith, S. V., Molecular imaging with copper-64 in the drug discovery and development area. *Expert Opin. Drug Dis.* **2007,** *2* (5), 659-672; (c) Wadas, T. J.; Wong, E. H.; Weisman, G. R.;

Anderson, C. J., Coordinating Radiometals of Copper, Gallium, Indium, Yttrium, and Zirconium for PET and SPECT Imaging of Disease. *Chem. Rev.* **2010,** *110*, 2858–2902.

232. (a) Shen, B.; Löffler, D.; Reischl, G.; Machulla, H.-J.; Zeller, K.-P., Nucleophilic [18F]Fluorination and subsequent decarbonylation of methoxy-substituted nitro- and halogen-benzenes activated by one or two formyl groups. *J. Labelled Compd. Rad.* **2010,** *53* (3), 113-119; (b) Vanbrocklin, H. F.; O'Neil, J. P.; Hom, D. L.; Gibbs, A. R., Synthesis of [18F]fluoroanilines: Precursors to [18F]fluoroanilinoquinazolines. *J. Labelled Compd. Rad.* **2001,** *44* (S1), S880-S882; (c) Sun, H.; DiMagno, S. G., Room-temperature nucleophilic aromatic fluorination: experimental and theoretical studies. *Angew. Chem. Int. Ed.* **2006,** *45* (17), 2720-2725; (d) Li, Y.; Xu, Y.; Zhang, L.; Liu, Y.; Shi, L. Preparations of 18F-labeling precursors and their applications for labeling amino acids and polypeptides. CN102126985A, 2011; (e) Kim, D. W.; Jeong, H.-J.; Lim, S. T.; Sohn, M.-H., Facile nucleophilic fluorination of primary alkyl halides using tetrabutylammonium fluoride in a tert-alcohol medium. *Tetrahedron Lett.* **2010,** *51* (2), 432-434; (f) Hu, Y. F.; Luo, J.; Lu, C. X., A mild and efficient method for nucleophilic aromatic fluorination using tetrabutylammonium fluoride as fluorinating reagent. *Chinese Chem. Lett.* **2010,** *21* (2), 151-154.
233. (a) Cai, L.; Lu, S.; Pike, V. W., Chemistry with [18F]fluoride ion. *Eur. J. Org. Chem.* **2008,** (17), 2853-2873; (b) Wagner, H. N.; Szabo, Z., Research and Clinical Application of Neuroreceptor Imaging. In *Handbook of Radiopharmaceuticals*, John Wiley & Sons, Ltd: 2002; pp 581-602.
234. Becaud, J.; Mu, L.; Karramkam, M.; Schubiger, P. A.; Ametamey, S. M.; Graham, K.; Stellfeld, T.; Lehmann, L.; Borkowski, S.; Berndorff, D.; Dinkelborg, L.; Srinivasan, A.; Smits, R.; Koksch, B., Direct one-step 18F-labeling of peptides via nucleophilic aromatic substitution. *Bioconjugate Chem.* **2009,** *20* (12), 2254-61.
235. Miller, P. W.; Long, N. J.; Vilar, R.; Gee, A. D., Synthesis of 11C, 18F, 15O, and 13N radiolabels for positron emission tomography. *Angewandte Chemie* **2008,** *47* (47), 8998-9033.
236. Nicholson, K. L., 22 Month Report: Synthesis and evaluation of CXCR4 antagonists. University of Hull: Hull, 2013.
237. Lopez-Prados, J.; Cuevas, F.; Reichardt, N.-C.; de Paz, J.-L.; Morales, E. Q.; Martin-Lomas, M., Design and synthesis of inositolphosphoglycan putative insulin mediators. *Org. Biomol. Chem.* **2005,** *3* (5), 764-786.
238. Collman, J. P.; Yan, Y.-L.; Lei, J.; Dinolfo, P. H., Efficient Synthesis of Trisimidazole and Glutaric Acid Bearing Porphyrins: Ligands for Active-Site Models of Bacterial Nitric Oxide Reductase. *Org. Lett.* **2006,** *8* (5), 923-926.
239. (a) Fumio, I.; Hiroyuki, K.; Hideki, I.; Tomohiro, K.; Mitsuru, S.; Shuji, K. Jnk Inhibitor. EP1348700 A2, 2004; (b) Ito, M.; Sakaguchi, A.; Kobayashi, C.; Ikariya, T., Chemoselective Hydrogenation of Imides Catalyzed by Cp*Ru(PN) Complexes and Its Application to the Asymmetric Synthesis of Paroxetine. *J. Am. Chem. Soc.* **2006,** *129* (2), 290-291.
240. De Clercq, E.; Yamamoto, N.; Pauwels, R.; Baba, M.; Schols, D.; Nakashima, H.; Balzarini, J.; Debyser, Z.; Murrer, B. A.; Schwartz, D.; et al., Potent and selective inhibition of human immunodeficiency virus (HIV)-1 and HIV-2 replication by a class of bicyclams interacting with a viral uncoating event. *P. Natl. Acad. Sci. USA.* **1992,** *89* (12), 5286-90.
241. De Clercq, E.; Yamamoto, N.; Pauwels, R.; Balzarini, J.; Witvrouw, M.; De Vreese, K.; Debyser, Z.; Rosenwirth, B.; Peichl, P.; Datema, R.; Thornton, D.; Skerlj, R.; Gaul, F.; Padmanabhan, S.; Bridger, G.; Henson, G.; Abrams, M., Highly potent and selective inhibition of human immunodeficiency virus by the bicyclam derivative JM3100. *Antimicrob. Agents Ch.* **1994,** *38* (4), 668-674.
242. Bridger, G. J.; Skerlj, R. T.; Hernandez-Abad, P. E.; Bogucki, D. E.; Wang, Z.; Zhou, Y.; Nan, S.; Boehringer, E. M.; Wilson, T.; Crawford, J.; Metz, M.; Hatse, S.; Princen, K.; De Clercq, E.; Schols, D., Synthesis and structure-activity relationships of azamacrocyclic C-X-C chemokine receptor 4 antagonists: analogues containing a single azamacrocyclic ring are potent inhibitors of T-cell tropic (X4) HIV-1 replication. *J Med Chem* **2010,** *53* (3), 1250-60.

243. Vega, B.; Munoz, L. M.; Holgado, B. L.; Lucas, P.; Rodriguez-Frade, J. M.; Calle, A.; Rodriguez-Fernandez, J. L.; Lechuga, L. M.; Rodriguez, J. F.; Gutierrez-Gallego, R.; Mellado, M., Technical Advance: Surface plasmon resonance-based analysis of CXCL12 binding using immobilized lentiviral particles. *Journal of leukocyte biology* **2011**.
244. Hoffman, T. L.; Canziani, G.; Jia, L.; Rucker, J.; Doms, R. W., A biosensor assay for studying ligand-membrane receptor interactions: binding of antibodies and HIV-1 Env to chemokine receptors. *P. Natl. Acad. Sci. USA.* **2000,** *97* (21), 11215-20.
245. Navratilova, I.; Sodroski, J.; Myszka, D. G., Solubilization, stabilization, and purification of chemokine receptors using biosensor technology. *Anal. Biochem.* **2005,** *339* (2), 271-81.
246. Mizuguchi, T.; Uchimura, H.; Kataoka, H.; Akaji, K.; Kiso, Y.; Saito, K., Intact-cell-based surface plasmon resonance measurements for ligand affinity evaluation of a membrane receptor. *Anal. Biochem.* **2012,** *420* (2), 185-187.
247. Vega, B.; Calle, A.; Sánchez, A.; Lechuga, L. M.; Ortiz, A. M.; Armelles, G.; Rodríguez-Frade, J. M.; Mellado, M., Real-time detection of the chemokine CXCL12 in urine samples by surface plasmon resonance. *Talanta* **2013**.
248. Stenlund, P.; Babcock, G. J.; Sodroski, J.; Myszka, D. G., Capture and reconstitution of G protein-coupled receptors on a biosensor surface. *Anal. Biochem.* **2003,** *316* (2), 243-250.
249. Navratilova, I.; Dioszegi, M.; Myszka, D. G., Analyzing ligand and small molecule binding activity of solubilized GPCRs using biosensor technology. *Anal. Biochem.* **2006,** *355* (1), 132-9.
250. Navratilova, I.; Besnard, J.; Hopkins, A. L., Screening for GPCR Ligands Using Surface Plasmon Resonance. *ACS Med. Chem. Lett.* **2011,** *2* (7), 549-554.
251. Rich, R. L.; Errey, J.; Marshall, F.; Myszka, D. G., Biacore analysis with stabilized G-protein-coupled receptors. *Anal. Biochem.* **2011,** *409* (2), 267-272.
252. Harada, S.; Koyanagi, Y.; Yamamoto, N., Infection of HTLV-III/LAV in HTLV-I-carrying cells MT-2 and MT-4 and application in a plaque assay. *Science* **1985,** *229* (4713), 563-566.
253. Pauwels, R.; Balzarini, J.; Baba, M.; Snoeck, R.; Schols, D.; Herdewijn, P.; Desmyter, J.; De Clercq, E., Rapid and automated tetrazolium-based colorimetric assay for the detection of anti-HIV compounds. *J. Virol. Methods* **1988,** *20* (4), 309-21.
254. Schols, D.; Struyf, S.; Van Damme, J.; Este, J. A.; Henson, G.; De Clercq, E., Inhibition of T-tropic HIV strains by selective antagonization of the chemokine receptor CXCR4. *J Exp Med* **1997,** *186* (8), 1383-8.
255. Princen, K.; Hatse, S.; Vermeire, K.; De Clercq, E.; Schols, D., Evaluation of SDF-1/CXCR4-Induced Ca2+ Signaling by Fluorometric Imaging Plate Reader (FLIPR) and Flow Cytometry. *Cytometry A* **2003,** *51* (1), 35-45.
256. Hunter, T. M.; Paisey, S. J.; Park, H. S.; Cleghorn, L.; Parkin, A.; Parsons, S.; Sadler, P. J., Configurations of metallocyclams and relevance to anti-HIV activity. *J. Inorg. Biochem.* **2004,** *98* (5), 713-719.
257. Jin, G. B.; Unfricht, D. W.; Fernandez, S. M.; Lynes, M. A., Cytometry on a chip: cellular phenotypic and functional analysis using grating-coupled surface plasmon resonance. *Biosensors & bioelectronics* **2006,** *22* (2), 200-6.
258. Lang, K.; Hatt, H.; Niggemann, B.; Zaenker, K. S.; Entschladen, F., A Novel Function for Chemokines: Downregulation of Neutrophil Migration. *Scand. J. Immunol.* **2003,** *57* (4), 350-361.
259. Navratilova, I.; Pancera, M.; Wyatt, R. T.; Myszka, D. G., A biosensor-based approach toward purification and crystallization of G protein-coupled receptors. *Anal. Biochem.* **2006,** *353* (2), 278-283.
260. Healthcare, G., GST Capture Kit. General Electrical Company: Sweden, 2013; pp 1-6.
261. Babcock, G. J.; Mirzabekov, T.; Wojtowicz, W.; Sodroski, J., Ligand Binding Characteristics of CXCR4 Incorporated into Paramagnetic Proteoliposomes. *J. Biol. Chem.* **2001,** *276* (42), 38433-38440.

262. (a) Phelps, M. E., PET: A Biological Imaging Technique. *Neurochemical Res.* **1991,** *16*, 929-940; (b) Phelps, M. E., Positron emission tomography provides molecular imaging of biological processes. *P. Natl. Acad. Sci. USA.* **2000,** *97*, 9226–9233.
263. Jacobson, O.; Weiss, I. D.; Szajek, L.; Farber, J. M.; Kiesewetter, D. O., 64Cu-AMD3100--a novel imaging agent for targeting chemokine receptor CXCR4. *Bioorganic & medicinal chemistry* **2009,** *17* (4), 1486-93.
264. Weiss, I. D.; Jacobson, O.; Kiesewetter, D. O.; Jacobus, J. P.; Szajek, L. P.; Chen, X.; Farber, J. M., Positron emission tomography imaging of tumors expressing the human chemokine receptor CXCR4 in mice with the use of 64Cu-AMD3100. *Molecular imaging and biology : MIB : the official publication of the Academy of Molecular Imaging* **2012,** *14* (1), 106-14.
265. De Silva, R. A.; Peyre, K.; Pullambhatla, M.; Fox, J. J.; Pomper, M. G.; Nimmagadda, S., Imaging CXCR4 expression in human cancer xenografts: Evaluation of monocyclam64Cu-AMD3465. *J. Nucl. Med.* **2011,** *52* (6), 986-993.
266. (a) Zhu, A.; Zhan, W.; Liang, Z.; Yoon, Y.; Yang, H.; Grossniklaus, H. E.; Xu, J.; Rojas, M.; Lockwood, M.; Snyder, J. P.; Liotta, D. C.; Shim, H., Dipyrimidine amines: a novel class of chemokine receptor type 4 antagonists with high specificity. *J. Med. Chem.* **2010,** *53* (24), 8556-8568; (b) Shim, H.; Liotta, D. C.; Zhu, A.; Goodman, M. CXCR4 antagonists for imaging of cancer and inflammatory disorders. 2011.
267. Zhang, J. M.; Tian, J. H.; Li, T. R.; Guo, H. Y.; Shen, L., 99mTc–AMD3100: A novel potential receptor-targeting radiopharmaceutical for tumor imaging. *Chinese Chem. Lett.* **2010,** *21* (4), 461-463.
268. (a) Clarke, E. T.; Martell, A. E., Stabilities of the alkaline earth and divalent transition metal complexes of the tetraazamacrocyclic tetraacetic acid ligands. *Inorg. Chim. Acta* **1991,** *190* (1), 27-36; (b) Martell, A. E.; Smith, R. M., *Critical stability constants*. Plenum Press: New York, 1982; (c) Motekaitis, R. J.; Rogers, B. E.; Reichert, D. E.; Martell, A. E.; Welch, M. J., Stability and structure of activated macrocycles. Ligands with biological applications. *Inorg. Chem.* **1996,** *35* (13), 3821-3827; (d) Boswell, C. A.; Regino, C. A.; Baidoo, K. E.; Wong, K. J.; Bumb, A.; Xu, H.; Milenic, D. E.; Kelley, J. A.; Lai, C. C.; Brechbiel, M. W., Synthesis of a cross-bridged cyclam derivative for peptide conjugation and 64Cu radiolabeling. *Bioconjugate Chem.* **2008,** *19* (7), 1476-84; (e) Bass, L. A.; Wang, M.; Welch, M. J.; Anderson, C. J., In Vivo Transchelation of Copper-64 from TETA-Octreotide to Superoxide Dismutase in Rat Liver. *Biconjugate Chem.* **2000,** *11*, 527-532.
269. (a) Hubin, T. J.; McCormick, J. M.; Alcock, N. W.; Clase, H. J.; Busch, D. H., Crystallographic Characterization of Stepwise Changes in Ligand Conformations as their Internal Topology Changes and Two Novel Cross-Bridged Tetraazamacrocyclic Copper(II) Complexes. *Inorg. Chem.* **1999,** *38*, 4435-4446; (b) Hubin, T. J.; McCormick, J. M.; Collinson, S. R.; Buchalova, M.; Perkins, C. M.; Alcock, N. W.; Kahol, P. K.; Raghunathan, A.; Busch, D. H., New Iron(II) and Manganese(II) Complexes of Two Ultra-Rigid, Cross-Bridged Tetraazamacrocycles for Catalysis and Biomimicry. *J. Am. Chem. Soc.* **2000,** *122*, 2512-2522; (c) Hubin, T. J.; Alcock, N. W.; Busch, D. H., Copper(I) and copper(II) complexes of an ethylene cross-bridged cyclam. *Acta Crystallogr. C* **2000,** *56* (1), 37-39.
270. Jiang, M.; Ferdani, R.; Shokeen, M.; Anderson, C. J., Comparison of two cross-bridged macrocyclic chelators for the evaluation of 64Cu-labeled-LLP2A, a peptidomimetic ligand targeting VLA-4-positive tumors. *Nucl. Med. Biol.* **2013,** *40* (2), 245-251.
271. Woodard, L. E.; De Silva, R. A.; Behnam Azad, B.; Lisok, A.; Pullambhatla, M.; G. Lesniak, W.; Mease, R. C.; Pomper, M. G.; Nimmagadda, S., Bridged cyclams as imaging agents for chemokine receptor 4 (CXCR4). *Nucl. Med. Biol.* **2014,** *41* (7), 552-561.
272. Leugger, A. P.; Hertli, L.; Kaden, T. A., Metal complexes with macrocyclic ligands. 11. Ring size effect on the complexation rates with transition metal ions. *Helv. Chim. Acta* **1978,** *61* (7), 2296–2306.

273. Boswell, C. A.; Regino, C. A.; Baidoo, K. E.; Wong, K. J.; Milenic, D. E.; Kelley, J. A.; Lai, C. C.; Brechbiel, M. W., A novel side-bridged hybrid phosphonate/acetate pendant cyclam: synthesis, characterization, and 64Cu small animal PET imaging. *Bioorganic & medicinal chemistry* **2009,** *17* (2), 548-52.
274. Mannhold, R.; Van De Waterbeemd, H., Substructure and whole molecule approaches for calculating log P. *J. Comput. Aid. Mol. Des.* **2001,** *15* (4), 337-354.
275. Van De Waterbeemd, H.; Smith, D. A.; Beaumont, K.; Walker, D. K., Property-based design: Optimization of drug absorption and pharmacokinetics. *J. Med. Chem.* **2001,** *44* (9), 1313-1333.
276. (a) Leeson, P. D.; Springthorpe, B., The influence of drug-like concepts on decision-making in medicinal chemistry. *Nat. Rev. Drug Discov.* **2007,** *6* (11), 881-890; (b) Proudfoot, J. R., The evolution of synthetic oral drug properties. *Bioorg. Med. Chem. Lett.* **2005,** *15* (4), 1087-1090.
277. (a) Hansch, C., A quantitative approach to biochemical structure-activity relationships. *Accounts Chem. Res.* **1969,** *2* (8), 232-239; (b) Tute, M. S., *Principles and practice of Hansch analysis: a guide to structure-activity correlation for the medicinal chemist*. 1971; Vol. 6, p 1-77; (c) Kubinyi, H., Lipophilicity and drug activity. *Prog. Drug Res.* **1979,** *23*, 97-198; (d) Kubinyi, H., Lipophilicity and biological acitivity. Drug transport and drug distribution in model systems and in biological systems. *Arzneimittel-Forsch.* **1979,** *29* (8), 1067-1080; (e) Cronin, M. T. D., The role of hydrophobicity in toxicity prediction. *Curr. Comput. Aided Drug Des.* **2006,** *2* (4), 405-413.
278. (a) Lipinski, C. A.; Lombardo, F.; Dominy, B. W.; Feeney, P. J., Experimental and computational approaches to estimate solubility and permeability in drug discovery and development settings. *Adv. Drug Deliver. Rev.* **2001,** *46* (1–3), 3-26; (b) Lipinski, C. A.; Lombardo, F.; Dominy, B. W.; Feeney, P. J., Experimental and computational approaches to estimate solubility and permeability in drug discovery and development settings. *Adv. Drug Deliver. Rev.* **1997,** *23* (1–3), 3-25.
279. Serdons, K.; Verbruggen, A.; Bormans, G. M., Developing new molecular imaging probes for PET. *Methods* **2009,** *48* (2), 104-11.
280. Williams, D. B. G.; Lawton, M., Drying of Organic Solvents: Quantitative Evaluation of the Efficiency of Several Desiccants. *J. Org. Chem.* **2010,** *75* (24), 8351-8354.